MYOFILAMENT FUNCTION IN HEALTH AND DISEASE

EDITED BY: Julien Ochala
PUBLISHED IN: Frontiers in Physiology

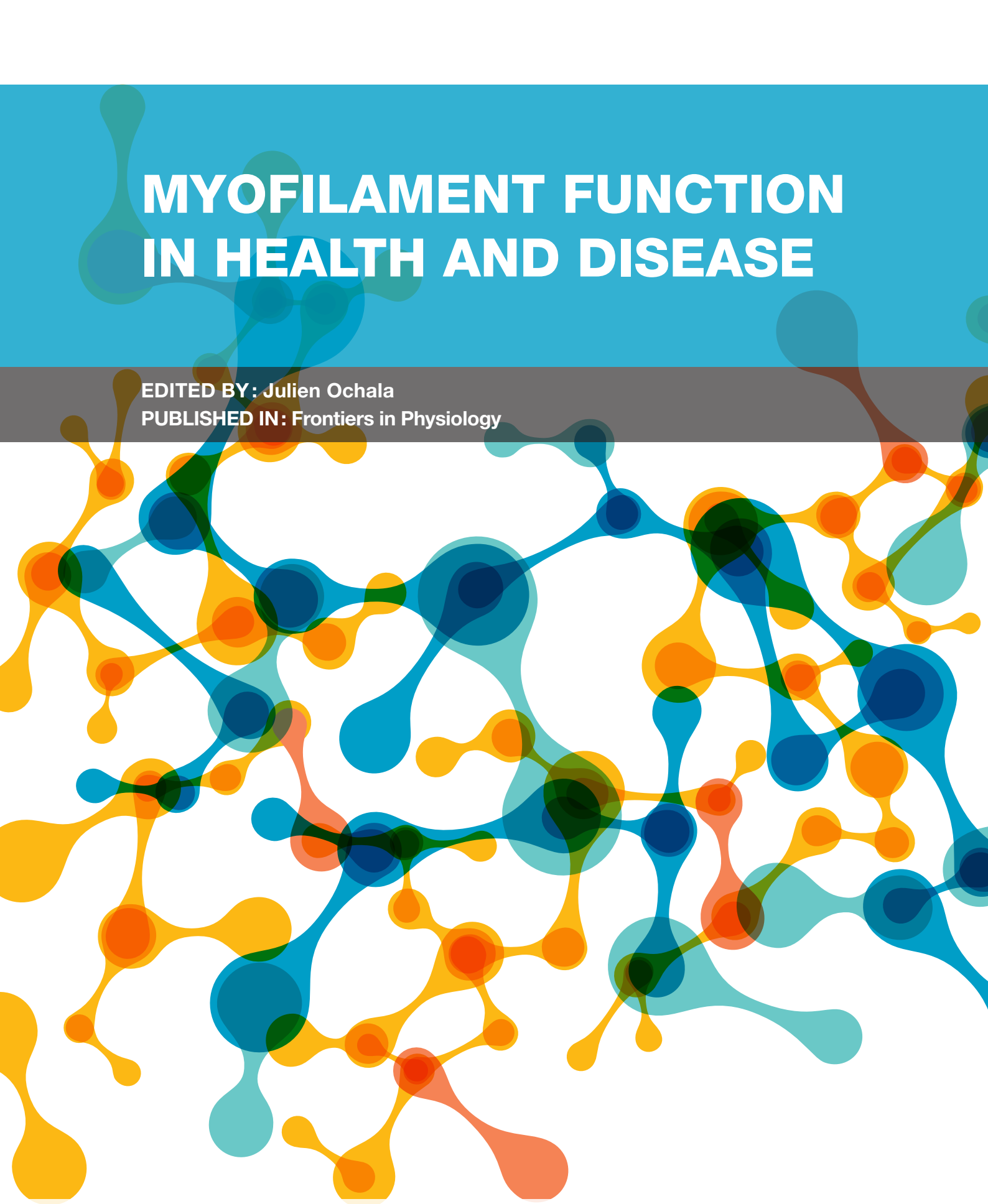

frontiers Research Topics

frontiers

Frontiers Copyright Statement

© Copyright 2007-2017 Frontiers Media SA. All rights reserved.

All content included on this site, such as text, graphics, logos, button icons, images, video/audio clips, downloads, data compilations and software, is the property of or is licensed to Frontiers Media SA ("Frontiers") or its licensees and/or subcontractors. The copyright in the text of individual articles is the property of their respective authors, subject to a license granted to Frontiers.

The compilation of articles constituting this e-book, wherever published, as well as the compilation of all other content on this site, is the exclusive property of Frontiers. For the conditions for downloading and copying of e-books from Frontiers' website, please see the Terms for Website Use. If purchasing Frontiers e-books from other websites or sources, the conditions of the website concerned apply.

Images and graphics not forming part of user-contributed materials may not be downloaded or copied without permission.

Individual articles may be downloaded and reproduced in accordance with the principles of the CC-BY licence subject to any copyright or other notices. They may not be re-sold as an e-book.

As author or other contributor you grant a CC-BY licence to others to reproduce your articles, including any graphics and third-party materials supplied by you, in accordance with the Conditions for Website Use and subject to any copyright notices which you include in connection with your articles and materials.

All copyright, and all rights therein, are protected by national and international copyright laws.

The above represents a summary only. For the full conditions see the Conditions for Authors and the Conditions for Website Use.

ISSN 1664-8714
ISBN 978-2-88945-186-9
DOI 10.3389/978-2-88945-186-9

About Frontiers

Frontiers is more than just an open-access publisher of scholarly articles: it is a pioneering approach to the world of academia, radically improving the way scholarly research is managed. The grand vision of Frontiers is a world where all people have an equal opportunity to seek, share and generate knowledge. Frontiers provides immediate and permanent online open access to all its publications, but this alone is not enough to realize our grand goals.

Frontiers Journal Series

The Frontiers Journal Series is a multi-tier and interdisciplinary set of open-access, online journals, promising a paradigm shift from the current review, selection and dissemination processes in academic publishing. All Frontiers journals are driven by researchers for researchers; therefore, they constitute a service to the scholarly community. At the same time, the Frontiers Journal Series operates on a revolutionary invention, the tiered publishing system, initially addressing specific communities of scholars, and gradually climbing up to broader public understanding, thus serving the interests of the lay society, too.

Dedication to Quality

Each Frontiers article is a landmark of the highest quality, thanks to genuinely collaborative interactions between authors and review editors, who include some of the world's best academicians. Research must be certified by peers before entering a stream of knowledge that may eventually reach the public - and shape society; therefore, Frontiers only applies the most rigorous and unbiased reviews.
Frontiers revolutionizes research publishing by freely delivering the most outstanding research, evaluated with no bias from both the academic and social point of view.
By applying the most advanced information technologies, Frontiers is catapulting scholarly publishing into a new generation.

What are Frontiers Research Topics?

Frontiers Research Topics are very popular trademarks of the Frontiers Journals Series: they are collections of at least ten articles, all centered on a particular subject. With their unique mix of varied contributions from Original Research to Review Articles, Frontiers Research Topics unify the most influential researchers, the latest key findings and historical advances in a hot research area! Find out more on how to host your own Frontiers Research Topic or contribute to one as an author by contacting the Frontiers Editorial Office: **researchtopics@frontiersin.org**

MYOFILAMENT FUNCTION IN HEALTH AND DISEASE

Topic Editor:
Julien Ochala, King's College London, UK

The present E-book, consisting of a compilation of original articles and reviews, presents how myofilaments are regulated in cardiac and skeletal muscles and trigger contraction. Additionally, this E-book gives insights into their dysregulation in a number of muscle disorders.

Citation: Ochala, J., ed. (2017). Myofilament Function in Health and Disease. Lausanne: Frontiers Media. doi: 10.3389/978-2-88945-186-9

Table of Contents

frontiers in Physiology

REVIEW
published: 10 June 2015
doi: 10.3389/fphys.2015.00174

A new paradigm for muscle contraction

*Walter Herzog *, Krysta Powers, Kaleena Johnston and Mike Duvall*

Faculty of Kinesiology, Engineering, Medicine and Veterinary Medicine, University of Calgary, Calgary, AB, Canada

For the past 60 years, muscle contraction had been thought to be governed exclusively by the contractile filaments, actin, and myosin. This thinking explained most observations for concentric and isometric, but not for eccentric muscle contractions. Just over a decade ago, we discovered that eccentric contractions were associated with a force that could not be assigned to actin and myosin, but was at least in part associated with the filamentous protein titin. Titin was found to bind calcium upon activation, thereby increasing its structural stability, and thus its stiffness and force. Furthermore, there is increasing evidence that the proximal part of titin binds to actin in an activation- and force-dependent manner, thereby shortening its free length, thus increasing its stiffness and force. Therefore, we propose that muscle contraction involves three filaments, actin, myosin and titin, and that titin regulates force by binding calcium and by shortening its spring length by binding to actin.

Keywords: titin, actin, myosin, crossbridge theory, muscle contraction, eccentric, muscle stretching, force enhancement

OPEN ACCESS

Edited by:
Julien Ochala,
King's College London, UK

Reviewed by:
Samantha P. Harris,
University of Arizona, USA
Bill Baltzopoulos,
Brunel University, UK

****Correspondence:***
Walter Herzog,
Faculty of Kinesiology, Engineering, Medicine and Veterinary Medicine, University of Calgary, Calgary, AB T2N 1N4, Canada
walter@kin.ucalgary.ca

Specialty section:
This article was submitted to Striated Muscle Physiology, a section of the journal Frontiers in Physiology

Received: *27 August 2014*
Accepted: *21 May 2015*
Published: *10 June 2015*

Citation:
Herzog W, Powers K, Johnston K and Duvall M (2015) A new paradigm for muscle contraction. Front. Physiol. 6:174. doi: 10.3389/fphys.2015.00174

Introduction and Background

Muscle contraction has fascinated lay people and scientists for centuries. However, a good understanding of how muscle contraction occurs seemed only possible once microscopy techniques had evolved to a level where basic structural features, such as the regular cross striation patterns of fibers, could be observed in the late 19th century. In the early 20th century, a stimulated muscle was simply considered a new elastic body (Gasser and Hill, 1924). Shortening and work production took place with a fixed amount of energy that was stored in this body and evolved elastically through stimulation. However, this notion was proven false when Wallace Fenn demonstrated that muscle produced an increasing amount of total energy when increasing its mechanical work output; an observation that was in contradiction with Hill's elastic body theory (Fenn, 1923, 1924). Specifically, Fenn, who worked in the laboratory of Hill and measured heat and work production in frog muscles, found that a muscle allowed to shorten liberated more energy than a muscle held isometrically or a muscle that was stretched. This has become known as the Fenn effect in muscle physiology.

Prior to the 1950s, muscle contraction and force production were thought to be caused by the folding of long protein chains visible in the middle of the sarcomere. This shortening had been thought to be caused by lactic acid, but this theory was refuted by experiments demonstrating that contractions could be obtained in the absence of lactic acid in muscles poisoned with iodoacetic acid (Lundsgaard, 1930). The role of lactic acid was then replaced briefly with phosphorylcreatine breakdown, until it was discovered that this reaction merely served to re-phosphorylate ADP into ATP. Thereafter, filament shortening became associated with the hydrolysis of ATP into ADP and inorganic phosphate.

In the early 1950s, careful analysis of A-band dimensions revealed that myosin filaments were not substantially shortening under a variety of contractile conditions, and thus, could not account for muscle contraction, force production and the large length changes that muscle tissue can undergo (Huxley, 1953). In two seminal papers, arrived at independently, Hugh Huxley and Andrew Huxley proposed that muscle contraction occurred not by shortening of the myosin filaments, but by the relative sliding of two sets of filaments, actin, and myosin (Huxley and Hanson, 1954; Huxley and Niedergerke, 1954). In 1957, Andrew Huxley proposed how this relative sliding might occur, and provided a mathematical framework for what is now known as the cross-bridge theory of muscle contraction (Huxley, 1957). This paper, which has been cited over 3000 times (Google Scholar, June 2014), outlines in broad strokes how we think about muscle contraction today. The success of this paper is insofar surprising as Huxley never intended to publish it, and thought of the mathematical formulation of the cross-bridge theory merely as a preliminary idea (Huxley, personal communication, August 1999). He sent the paper to his friend and editor of *Biophysics and biophysical Chemistry*, who, to Huxley's surprise, suggested publishing it.

Unaccounted Observations

The initial two state model of the cross-bridge theory published in 1957 underwent several reformulations, although the basic premise remained unchanged. Briefly, in the cross-bridge model, contraction and force production is achieved by extensions (cross-bridges) from the thick (myosin) filaments that interact cyclically with the thin (actin) filaments and exert force between these two sets of filaments to produce shortening. Each cycle of attachment and detachment of a cross-bridge is associated with the hydrolysis of one molecule of ATP. Therefore, the regulation of force is governed exclusively by the contractile proteins actin and myosin, while structural proteins provide passive forces upon muscle elongation that are determined exclusively by their viscoelastic properties.

In 1969, the cross-bridge theory was amended with the idea that cross-bridges produce force and shortening through rotation requiring multiple attached states (Huxley, 1969; Huxley and Simmons, 1971), and in 1993, a detailed description of the atomic structure of cross-bridges and the corresponding actin attachment sites revealed a cross-bridge stroke that included rotation of the cross-bridge around a fixed element of the cross-bridge head that attached uniquely to the actin attachment site (**Figure 1**) (Rayment et al., 1993).

In his original description of the cross-bridge theory, Huxley (1957) was able to predict forces for concentric contractions accurately. Specifically, Huxley derived a set of rate constants for the attachment/detachment kinetics of cross-bridges that accurately predicted "the best available data at the time," the concentric force-velocity relationship of striated muscles (Hill, 1938). Furthermore, the cross-bridge theory also explained beautifully the isometric force as a function of fiber and sarcomere lengths (Gordon et al., 1966). However, the forces

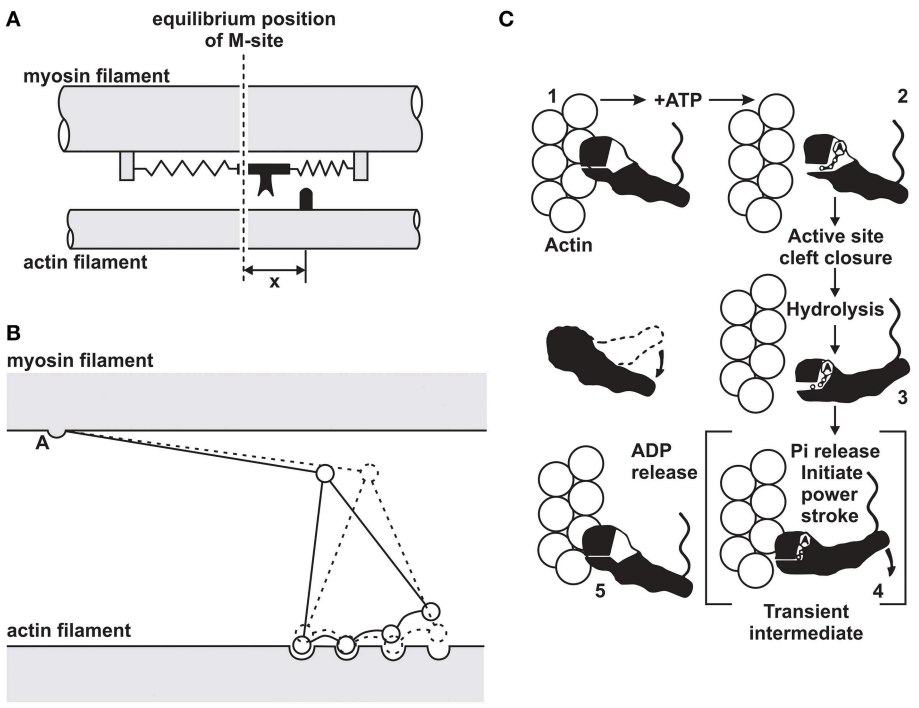

FIGURE 1 | Evolution of the cross-bridge model of muscle contraction. (A) Original 2-state model proposed by Huxley (1957). **(B)** Multi-state cross-bridge model with rotating head as proposed initially by Huxley (1969) and mathematically described by Huxley and Simmons (1971). **(C)** Multi-state model based on the atomic structure of cross-bridges and actin attachment sites as proposed by Rayment et al. (1993).

and energetics for eccentric contractions (actively stretched muscles), were not predicted accurately: they were much too big (Huxley, 1957). Also, the well-known results on residual force enhancement following active stretching of muscles (Abbott and Aubert, 1952; Edman et al., 1982) could not be predicted conceptually (Walcott and Herzog, 2008) or numerically (Herzog et al., 2012a,b; Herzog, 2014).

Residual force enhancement is an acknowledged property of skeletal muscle (Edman et al., 1982). It describes the increase in steady-state isometric force following an active muscle stretch, compared to the corresponding purely isometric force at the same length and same activation (**Figure 2**). Residual force enhancement has been observed in whole muscle preparations, activated voluntarily (Oskouei and Herzog, 2005) or through electrical stimulation (Lee and Herzog, 2002), in single intact and skinned fibers (Edman et al., 1978, 1982; Sugi and Tsuchiya, 1988; Rassier et al., 2003c; Peterson et al., 2004; Lee and Herzog, 2008; Joumaa and Herzog, 2013), in myofibrils (Rassier et al., 2003a; Joumaa et al., 2008) and in single, mechanically isolated sarcomeres (Leonard et al., 2010) and half sarcomeres (Joumaa et al., 2008). Residual force enhancement cannot be predicted using the cross-bridge theory (Walcott and Herzog, 2008), because the rate constants of cross-bridge attachment/detachment do not depend on time but only on the relative location of the cross-bridge's equilibrium position relative to its nearest attachment site on actin (Huxley, 1957). Therefore, an explanation for residual force enhancement needed to be found that would not undermine the cross-bridge theory. Thus, for more than half a century, residual force enhancement was explained conceptually, albeit not numerically, with the idea of instability of sarcomeres on the descending limb of the force-length relationship (Hill, 1953) and the associated development of large sarcomere lengths non-uniformities (Morgan, 1990, 1994).

Explanation of Residual Force Enhancement (Using Sarcomere Length Non-Uniformity)

According to the sarcomere length non-uniformity theory, sarcomeres on the descending limb of the force-length relationship are unstable (Hill, 1953; Allinger et al., 1996; Zahalak, 1997). This instability is thought to be caused by a "weakening" behavior of sarcomeres (negative stiffness). Therefore, for a perturbation, such as active stretching of muscle on the descending limb of the force-length relationship, sarcomeres were thought to be destabilized, causing a quick, uncontrolled over-stretching (popping) of some sarcomeres at the expense of others that only stretch slightly, not at all, or might even shorten by a small amount. The popped sarcomeres were thought to achieve force equilibrium with the short (active) sarcomeres through passive forces that become high at long lengths. Force enhancement was then explained with the idea that isometric contractions on the descending limb do not produce a sufficient perturbation to sarcomeres, thus sarcomeres remain relatively uniform and thus produce a force in accordance with actin-myosin filament overlap (Gordon et al., 1966). In contrast, a muscle that is stretched actively was thought to produce perturbations that result in instabilities and large sarcomere length non-uniformities that give rise to two distinct sets of sarcomere lengths. The steady-state force following active stretch was then thought to be greater than the purely isometric force because the active sarcomeres are shorter following active stretch compared to the purely isometric contraction (and thus can produce more force), and the passive sarcomeres are pulled to such lengths that their passive forces match the forces of the short, active sarcomeres (**Figure 3**).

In the following, we would like to identify predictions that are direct outcomes of the mathematical formulation of

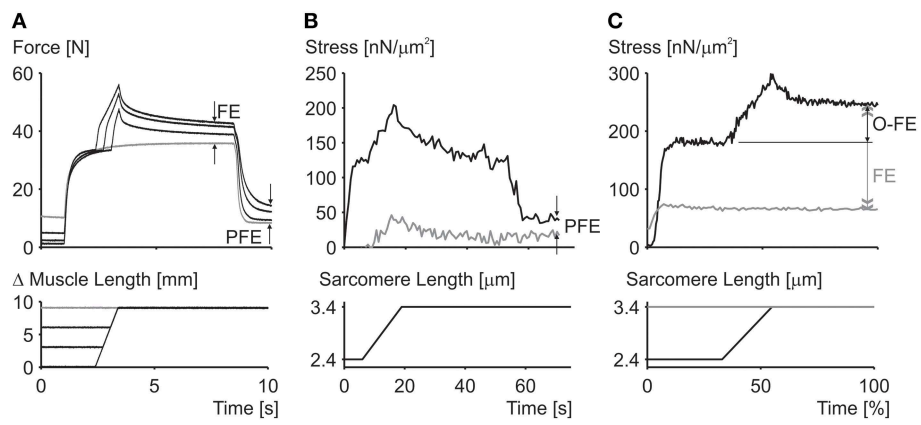

FIGURE 2 | Residual force enhancement in skeletal muscles. (A) Residual force enhancement (FE) and passive force enhancement (PFE) in a whole muscle preparation (cat soleus at 37°C). **(B)** Passive force enhancement (PFE) in a single myofibril preparation (rabbit psoas at 21°C). **(C)** Force enhancement (FE) and force above the isometric plateau (O-FE) in a single sarcomere preparation (rabbit psoas at 21°C). The gray line in **(A)** represents the isometric reference contraction while the black lines represent active stretch contractions followed by an isometric contraction. The gray line in **(B)** represents passive force during myofibril stretching and the black line the corresponding active force; deactivation occurred at about 55 s. The gray line in **(C)** represents the isometric reference force while the black line represents the experimentally enhanced force following an active stretch.

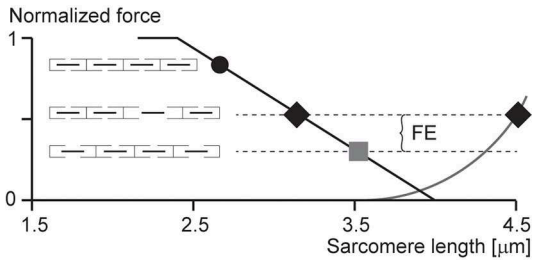

FIGURE 3 | Force enhancement (FE) based on the sarcomere length non-uniformity theory. Isometric contractions of muscles on the descending limb of the force-length relationship are thought to occur with sarcomeres of uniform lengths (black circle and gray square). However, if a muscle is stretched from a short length (black circle) to a long length (gray square), some sarcomeres are thought to become overstretched (popped—right black diamond) while others are thought to be stretched only minimally (left black diamond), thus producing an average sarcomere length the same as that of the long isometric contraction (gray square), but producing more force because of the more favorable position of the short sarcomeres (left black diamond) and the passive forces of the overstretched sarcomeres (right black diamond).

the sarcomere length non-uniformity theory. We will discuss these theoretical predictions in view of existing experimental evidence, and then will attempt to draw conclusions about the appropriateness of this theory.

Predictions Based on the Sarcomere length Non-Uniformity Theory

The theoretical models of the sarcomere length non-uniformity theory provide uniquely testable predictions (Zahalak, 1997; Campbell, 2009). Some of the primary predictions have been identified and discussed by proponents and opponents of this theory (Morgan et al., 2000; Herzog and Leonard, 2006, 2013; Herzog et al., 2006; Morgan and Proske, 2006; Edman, 2012). However, other equally obvious predictions, have received less attention, possibly because of the difficulties in testing them.

The primary predictions of the sarcomere length non-uniformity theory that have been discussed in previous works might be summarized as follows:

1. Sarcomeres are unstable on the descending limb of the force-length relationship following active stretching (Morgan, 1990, 1994).
2. Instability of sarcomere lengths, and thus the development of sarcomere length non-uniformities (and associated force enhancement) can only occur on the unstable descending limb but not the stable ascending limb of the force-length relationship (Allinger et al., 1996; Zahalak, 1997).
3. Forces in the force enhanced state cannot exceed the purely isometric forces at the plateau of the force-length relationship (Edman et al., 1982; Rassier et al., 2003c).
4. Force enhancement cannot occur in a single sarcomere preparation (Leonard et al., 2010).

Secondary predictions that follow directly from the mathematical framework and conceptual thinking of the sarcomere length non-uniformity theory that have received less, or no attention, may be summarized as follows:

5. Isometric contractions on the descending limb of the force-length relationship are associated with sarcomeres of essentially uniform length (Morgan, 1990, 1994).
6. Sarcomere length non-uniformities increase when a muscle is actively stretched compared to the corresponding purely isometric contractions (Morgan, 1990, 1994; Allinger et al., 1996).
7. Sarcomere lengths following active muscle stretching will have two distinct values (Allinger et al., 1996; Walcott and Herzog, 2008).

The primary predictions (1–4) of the sarcomere length non-uniformity theory have been discussed extensively (Herzog et al., 2006, 2012a,b; Edman, 2012; Herzog, 2014) but for completeness are summarized here briefly.

1. **Instability of sarcomeres on the descending limb of the force-length relationship:** More than 30 years ago, when first reading about sarcomere length instability on the descending limb of the force-length relationship, I asked myself the question: why would nature evolve a universal motor for contraction that was unstable and would tear itself apart, over more than half of its potential working range? After developing a setup for single myofibril testing, it was the first question I wanted to be answered. Stretching of serially arranged sarcomeres onto the descending limb of the force-length relationship did not produce sarcomere length instabilities (Rassier et al., 2003b); i.e., there was no quick, uncontrolled popping of the "weakest" sarcomeres, as predicted by the theory (Morgan, 1990, 1994). Rather, sarcomeres were perfectly stable at vastly differing lengths on the descending limb of the force-length relationship (**Figure 4A**), an observation that still needs satisfactory explanation. Frequently, sarcomeres that were shorter compared to other sarcomeres prior to active stretching, were longer after stretching (**Figure 4B**), a finding that is incompatible with the sarcomere length non-uniformity and cross-bridge theories.
2. **Force enhancement on the ascending limb of the force-length relationship:** The ascending limb of the force-length relationship has a positive slope, and thus strengthening character which produces inherent sarcomere length stability (Epstein and Herzog, 1998). Therefore, according to the sarcomere length non-uniformity theory, there should be no force enhancement on the ascending limb of the force-length relationship. However, in the very first systematic analysis of force enhancement, Abbott and Aubert (1952) reported force enhancement on the ascending limb of isolated muscle preparations. This initial finding was supported by further observations on whole muscles (Morgan et al., 2000), and single fibers (Peterson et al., 2004). However, force enhancement on the ascending limb tends to be small compared to the descending limb, and thus, although consistently observed, may not always be acknowledged (Morgan et al., 2000; Edman, 2012).

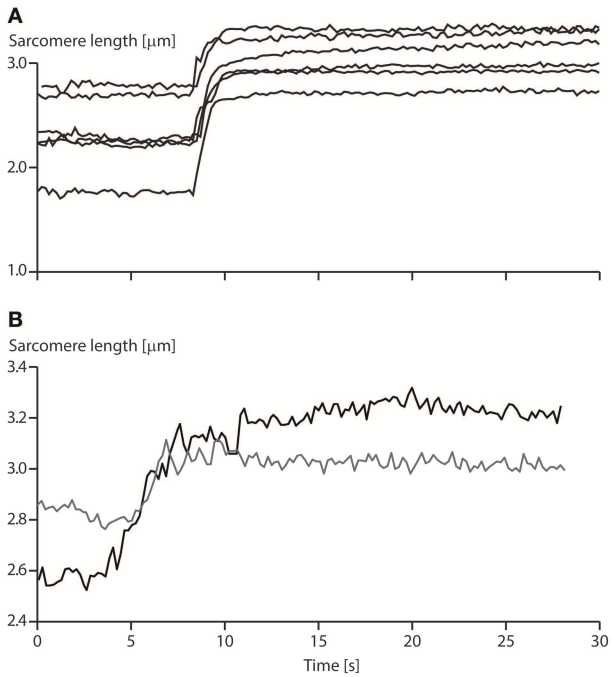

FIGURE 4 | Sarcomere length stability on the descending limb of the force-length relationship. (A) Sarcomere lengths as a function of time for a six sarcomere myofibril stretched on the descending limb of the force-length relationship. Note that none of the sarcomeres is rapidly stretched beyond actin-myosin filament overlap (popped approximately 4.0 μm), but that they stay relatively constant in length for a 20 s period following active stretching. **(B)** Sarcomere lengths of two specific sarcomeres from a single myofibril. Note, when the myofibril is stretched, the initially short sarcomere becomes the long sarcomere and vice versa.

3. **Enhanced force above the isometric plateau forces:** In the sarcomere length non-uniformity theory, the steady-state isometric forces, independent of the history of contraction, cannot exceed the isometric forces obtained at the plateau of the force-length relationship. Since, the short sarcomeres in this theory are the active force producers, and since they must be within a region of actin-myosin filament overlap, the maximal force they can produce is that obtained at optimal sarcomere length represented by the plateau of the force-length relationship (Gordon et al., 1966). However, forces in the enhanced state exceeding those of purely isometric contractions at optimal lengths have been observed as early as 1978 (Edman et al., 1978), although these authors later revised their results. However, enhanced forces clearly exceeding the isometric plateau forces were found in a series of subsequent studies on whole muscles (Schachar et al., 2004), single fibers (Rassier et al., 2003c; Lee and Herzog, 2008), and most importantly, in single myofibrils and single, mechanically isolated sarcomeres (Leonard et al., 2010) (**Figure 2**). In conclusion, isometric steady-state forces following active muscle stretch can exceed the purely isometric forces at optimal length by a substantial amount.
4. **Force enhancement in a single sarcomere:** Obviously, if force enhancement requires the development of sarcomere length non-uniformities, as indicated in **Figure 3**, then force enhancement should never occur in a single sarcomere. The classic work by Tim Leonard was the first published research on force enhancement in a mechanically isolated single sarcomere preparation (Leonard et al., 2010). In that study, 10 single sarcomeres were isolated and stretched from optimal length (2.4 μm) to a length of 3.4 μm, and compared to the steady-state forces obtained for purely isometric contractions. Force enhancement was 190% on average and the enhanced forces exceeded the purely isometric forces at optimal length by an average of 37%. It has been suggested that these results might have been obtained due to the development of half-sarcomere length non-uniformities in this single sarcomere preparation. However, if so, the question remains how a single half-sarcomere can produce forces in excess of its isometric force at optimal length. Needless to say that one must be careful of results from a single study that have not been repeated in other laboratories, but for lack of evidence to the contrary, we accept that force enhancement is a sarcomeric property, and can occur in the absence of multiple sarcomeres of vastly different lengths.

The secondary predictions (5–7) of the sarcomere lengths non-uniformity theory have received much less, or no attention in the past, but seem equally relevant and will be discussed in the following.

5. **Uniform sarcomere lengths for isometric contractions:** For the sarcomere length non-uniformity theory to work, specifically for it to account for the residual force enhancement property of skeletal muscle, it is necessary that sarcomeres are essentially uniform for isometric contractions. Active stretching is then thought to be the stimulus that produces sarcomere length instability and associated length non-uniformities. There have been extensive reports that sarcomere lengths in muscle fibers are highly non-uniform (Huxley and Peachey, 1961), thus requiring specialized approaches when studying sarcomere force-length properties (Gordon et al., 1966). Sarcomere length non-uniformities have been primarily observed as average sarcomere length variations across single fibers, but more recently have been demonstrated for single sarcomeres in whole muscles (Llewellyn et al., 2008), and in single myofibrils (**Figure 4**). When quantifying sarcomere lengths in passive and active human muscles, Llewellyn et al. (2008) noticed variations in sarcomere lengths of 20% in a radius as small as 25 μm, while we found peak sarcomere length non-uniformities for purely isometric contractions of 37% in isolated myofibril preparations. Sarcomere lengths variations have been shown to range from 1.7 to 3.5 μm in frog semitendinosus fibers at rest (Huxley and Peachey, 1961). Taken together, these results suggest that sarcomere lengths non-uniformities are a natural occurrence of resting and activated muscle preparations at all structural levels. Thus, observing sarcomere length non-uniformities after stretch or shortening contractions should not imply that the dynamics of muscle contraction produced these non-uniformities, nor should these non-uniformities be thought to be the cause

of specific mechanical properties of muscle without careful analyses.

6. **Increase in sarcomere length non-uniformity with active stretching of muscle:** One of the tenets of the sarcomere length non-uniformity theory in explaining force enhancement is the idea that sarcomere lengths become non-uniform during active stretching on the descending limb of the force length relationship, while they remain uniform with passive stretching and subsequent isometric contraction. If sarcomere lengths are indeed more non-uniform in the force enhanced compared to the isometric reference state has never been tested systematically. Initial work on this topic was done by stretching active single fibers or whole muscle preparations, and fixing them quickly following the stretch. These "stretched" preparations were then compared histologically to corresponding preparations that were activated isometrically or were allowed to actively shorten (Julian and Morgan, 1979; Morgan et al., 1982). These experiments typically showed an increased number of overstretched (popped) sarcomeres in the actively stretched muscles compared to those not undergoing active lengthening. These experiments have the advantage that they are performed in intact preparations, but have the disadvantage that overstretching of the sarcomeres cannot be accounted for by instability, rather than, for example, pre-existing structural damage of the muscle, and that only a tiny fraction of the whole muscle was analyzed for overstretched sarcomeres, thus making generalization difficult.

Reports of stability or sarcomere lengths non-uniformities after active stretching suggest that, if anything at all, sarcomeres are more stable (Edman et al., 1982), and sarcomere lengths are more uniform following active muscle stretching compared to the corresponding purely isometric reference contractions (Joumaa et al., 2008). Ongoing work in our lab has focused on measuring sarcomere length non-uniformities in isolated myofibril preparations in the force enhanced and normal isometric reference states. Preliminary results suggest that there is no systematic increase in sarcomere length non-uniformity, as quantified by the range and variance of sarcomere lengths following eccentric contractions on the descending limb of the force-length relationship compared to the corresponding purely isometric reference contractions.

7. **Two distinct sarcomere lengths following active muscle stretching:** In a muscle or fiber preparation, sarcomeres are not only connected serially but also in parallel. Therefore, force transmission by a sarcomere is not only determined by the force it exerts, but also by the forces acting on it in series and in parallel. However, in an idealized preparation, as typically modeled theoretically, sarcomeres are assumed to be perfectly in series. Such an idealization is achieved experimentally when using single myofibril preparations, which makes this preparation uniquely attractive to study sarcomeric properties. According to the sarcomere length non-uniformity theory, sarcomeres in series (in a myofibril) should be separated into two distinct groups with two distinct lengths when actively stretched. One group representing the sarcomeres that were not or only slightly stretched, the other representing the overstretched (popped) sarcomeres. Quantification of sarcomere lengths from a variety of published studies suggest that sarcomere lengths do not fall into two distinct lengths categories, but rather, are distributed over a range of lengths (e.g., **Figure 4**). Careful analysis of the sarcomere lengths of twelve myofibrils did not reveal a single one of them having two distinct sarcomere lengths in the force enhanced state thus defying this specific prediction.

Further Considerations

Force-Length Relationship

One of the most puzzling results of muscle physiology is the different shapes of the descending limbs of the force-length relationships for so-called "fixed-end" and "segment-clamped" conditions (**Figure 5**). In fixed-end experiments, the two ends of a fiber are fixed to a motor and a force transducer, respectively, and measurements of isometric force are made as a function of fiber lengths (Pollack, 1990). In segment-clamped experiments, a small mid-section of a fiber with relatively uniform sarcomeres is identified and marked, and its length is kept constant using length feedback by carefully adjusting the entire fiber length. Isometric forces are then expressed as a function of the sarcomere lengths in the fixed section of the fiber. For the fixed-end contractions, sarcomeres are allowed to take on their "normal" non-uniform length distribution (Pollack, 1990), while in the segment-clamped approach, sarcomere lengths are kept constant for the clamped segment (Gordon et al., 1966). Isometric forces on the descending limb of the force-length relationship in the fixed-end contractions have been reported to be substantially greater than those obtained in the corresponding segment-clamped experiments. Therefore, it appears that allowing sarcomeres

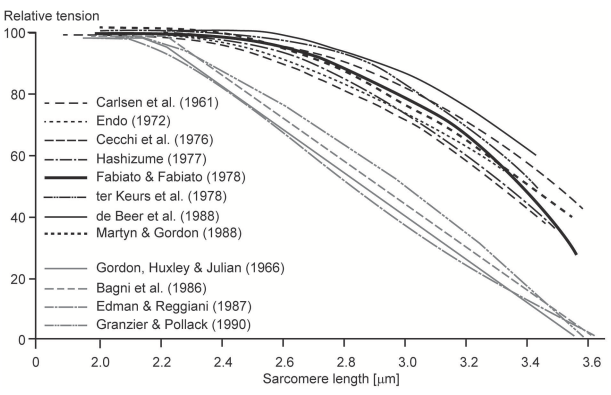

FIGURE 5 | Descending limb of the sarcomere force-length relationship. Relative tension as a function of sarcomere lengths obtained from fixed end contractions (black lines) and from segment-clamped experiments (gray lines). Note that when the natural development of sarcomere length non-uniformities is prevented by segment clamping, the isometric forces are severely decreased (Pollack, 1990).

to attain their natural non-uniform length distribution during purely isometric contraction enhances force, while attempting to keep sarcomere lengths artificially uniform results in a substantial loss of isometric force. We may conclude from these results that even during isometric contractions, sarcomere length non-uniformities develop naturally, they do not depend on active stretching on the descending limb of the force-length relationship, and they, in some unknown way, contribute to increased isometric force.

Theoretical Force-Length Relationship of Single Sarcomeres

When it was first demonstrated that force enhancement could be observed in a single sarcomere preparation (Leonard et al., 2010), critics were quick to point out the possibility that force enhancement could have been caused by the development of half-sarcomere non-uniformities. Although this argument sounds appealing on the surface, its acceptance leads quickly to a variety of unlikely consequences. Only one of these shall be discussed here.

Imagine we have a single sarcomere just at the edge of the plateau leading to the descending limb of the force-length relationship (**Figure 6**) and we now stretch this sarcomere. For the sake of argument, let's also assume that at this initial length, there is no passive force (or if there was, we could subtract it from the initial considerations without affecting the following argument). Imagine now that we stretch this sarcomere, so its total length is ¼down, then ½down, and then at the full length down on the descending limb of the force-length relationship. If we now assume that one half of the sarcomere remains at its initial short length, then the other half would have to elongate twice the stretch magnitude of the whole sarcomere (**Figure 6**), and, for force equilibrium's sake, its force has to be equal to that of the half sarcomere that remained at its initial length. For this to occur, the passive force would have to start at the beginning (left hand side) of the descending limb of the force-length relationship, it would have to be a straight line, and its slope would have to be the same as that of the descending limb, except with opposite sign (positive instead of negative). Then, when the half sarcomere loses actin-myosin filament overlap, the passive force would have to remain constant. Needless to say, such a passive force has never been observed, and even if it had, it still could not explain the results by Leonard et al. (2010), where forces in the enhanced state clearly exceeded the isometric plateau forces in a single sarcomere preparation. This example illustrates how one has to be careful when making a proposal, or stating a critique, without thinking through the associated implications.

A-Band Shifts and Force Enhancement

In a recent study, A-band shifts, which indicate the degree of half-sarcomere length non-uniformities, were argued to "significantly increase the level of force enhancement (Rassier, 2012)." The argument was based on observed correlations of "stretch-induced" A-band shifts with residual force enhancement in single myofibril preparations (**Figure 7**). Here, a maximal A-band shift of approximately 72 nm was associated with an enhanced force

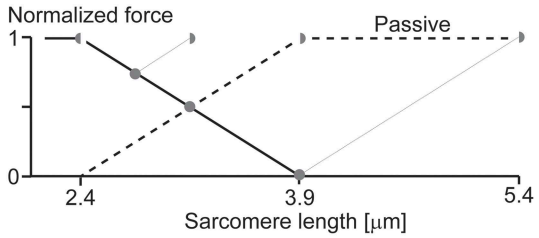

FIGURE 6 | Theoretical force-length relationship of a single sarcomere. If we assume that force enhancement in a single sarcomere, as observed in the literature (Leonard et al., 2010), is caused by half-sarcomere length non-uniformities, and that active force is proportional to actin-myosin filament overlap, then the passive force would have to look as indicated in the figure (thick black dashed line). Such a passive force has never been observed and seems to contradict anything known about passive forces in skeletal muscles. Therefore, the notion that substantial force enhancement in a single sarcomere can be explained with the development of half-sarcomere length non-uniformities seems far-fetched, not to say impossible. Full circles indicate an entire sarcomere on the descending limb of the force-length relationship, as expected during an isometric contraction with equal half sarcomeres. Half-circles indicate the corresponding half-sarcomeres expected after an active stretch in the force enhanced state of a single sarcomere. Black line = descending limb of the active force-length relationship. Dashed black line = passive force required for the overextended half-sarcomere to match the force of the other, active, half sarcomere.

of about 55%. However, a 72 nm shift would explain a 10% increase in force at best, thus most of the enhanced force remains unexplained. In a similar figure on single sarcomere experiments, with an implied spatial resolution of less than 0.5 nm, force enhancement for a 12 nm A-band shift was approximately 20%. A 12 nm shift explains a 1.5% increase in force leaving 92.5% of the observed force enhancement unexplained.

Moreover, experiments with no A-band shifts were found to have peak force enhancements of up to 16% (**Figure 7**). Finally, and probably most telling, half-sarcomere length non-uniformities for the isometric reference contractions, although not systematically evaluated in this study, were greater (their **Figure 5C**) or equal (their **Figure 6C**) to the non-uniformities of the actively stretched experimental contractions, thus it is hard to support the authors' claim that the force enhancement was associated with "stretch-induced" non-uniformities of half sarcomere lengths. Albeit not systematically evaluated, in studies where half-sarcomere length non-uniformities were compared for isometric reference and experimental stretch contractions, half-sarcomere lengths tended to be more uniform after stretch compared to reference contractions (Joumaa et al., 2007). Combined, these results provide little support that stretch-induced half-sarcomere non-uniformities contribute to the residual force enhancement in skeletal muscles.

Conclusions and Future Directions

Ever since the emergence of the cross-bridge theory, properties of actively stretched muscles could not be predicted properly (Huxley, 1957). Forces and energy consumption were much too big compared to experimental results (Huxley, 1957), and

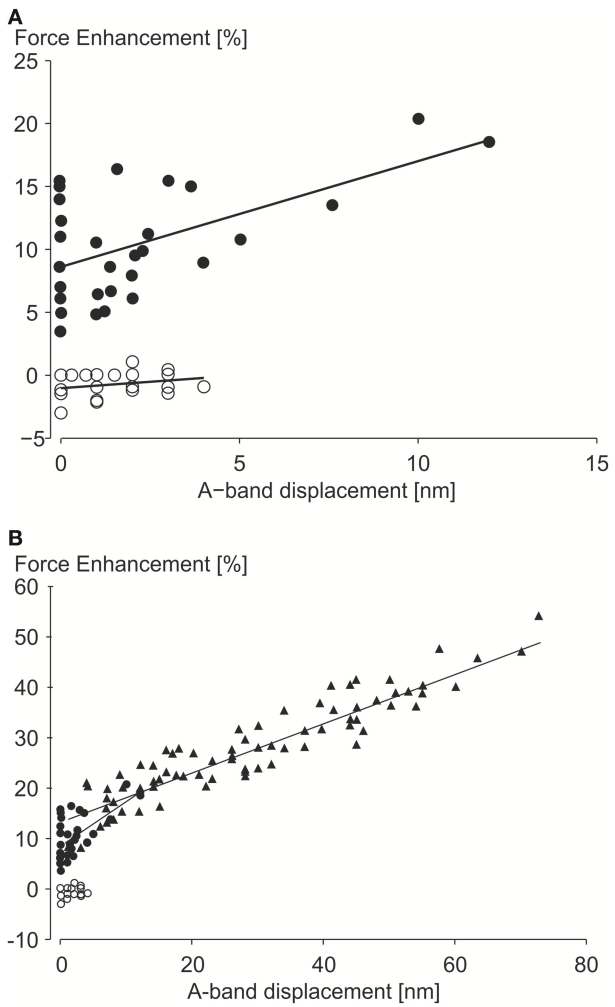

FIGURE 7 | Force enhancement as a function of half-sarcomere length non-uniformities. (A) Force enhancement as a function of A-band displacements (equivalent to half sarcomere length non-uniformities) in single sarcomere preparations, and **(B)** in single myofibril preparations with multiple serial sarcomeres. Note that the small A-band shifts in the single sarcomere and the single myofibril only explain approximately 7 and 18% of the total force enhancement observed, assuming that the isometric reference contractions have perfectly identical half- and sarcomere length. However, since the isometric reference contractions have similar A-band shifts as the experimental active stretch contractions, none of the enhanced forces seems explained by stretch-induced half-sarcomere length non-uniformities from Rassier (2012) with permission.

residual force enhancement could not be predicted conceptually, as steady-state forces in the cross-bridge theory are independent of the history of contraction (Huxley, 1957; Huxley and Simmons, 1971; Walcott and Herzog, 2008). This shortcoming of the cross-bridge theory had been addressed by assuming that muscle segments (Hill, 1953) and sarcomeres (Morgan, 1990, 1994) were unstable on the descending limb of the force-length relationship, and small perturbations would cause great non-uniformities in sarcomere lengths. Active lengthening of muscles (eccentric contraction) was thought to be such a perturbation. It is interesting to note that the sarcomere length instability and associated stretch-induced development of sarcomere length non-uniformity theory has survived for such a long time, and in many circles is still unquestionably accepted, despite lack of direct evidence, and despite experimental results from the very beginning that were not in agreement with the predictions of the theory. For example, Abbott and Aubert (1952) had strong evidence of force enhancement on the ascending and plateau regions of the force-length relationship more than half a century ago, predating the formulation of the cross-bridge theory itself.

The refinement of mechanical experiments on single myofibrils (Bartoo et al., 1993; Rassier et al., 2003a; Joumaa et al., 2008; Leonard et al., 2010; Leonard and Herzog, 2010) and mechanically isolated sarcomeres (Leonard et al., 2010) has allowed for direct testing of many of the predictions of the sarcomere length non-uniformity theory. Among these rejected predictions (see discussion above), the ones most damaging to the non-uniformity thinking were the following:

1. The evidence that sarcomeres of vastly different length could reside side by side on the descending limb of the force-length relationship without appreciable length changes over periods of 30 s, thereby demonstrating stability;
2. That substantial force enhancement could occur in a single, mechanically isolated sarcomere;
3. And that the enhanced forces in single sarcomeres could exceed the purely isometric reference forces obtained at optimal sarcomere length by a substantial amount.

There is no doubt that sarcomeres in the force enhanced state are non-uniform. However, sarcomeres in muscles (Llewellyn et al., 2008), fibers (Huxley and Peachey, 1961) and myofibrils (Rassier et al., 2003a; Joumaa et al., 2008; Leonard and Herzog, 2010; Leonard et al., 2010) are also non-uniform for purely isometric contractions. Whether, or not these sarcomere length-non-uniformities increase with stretching has not been systematically elucidated, but pilot results, and isolated findings from unrelated studies, suggest that, if anything at all, sarcomeres following active muscle stretching are more stable (Edman et al., 1982) and have equal or less sarcomere length-non-uniformity compared to the corresponding isometric reference contractions (Joumaa et al., 2008; Rassier, 2012).

From these results, and evidence in the literature, we propose that sarcomere length non-uniformities are a normal associate of muscle contraction on all structural levels. They are not an occurrence exclusive to active muscle stretching (eccentric contractions) on the descending limb of the force-length relationship, and they are not a primary cause for the enhanced forces observed in skeletal muscles after active stretching.

If not the development of stretch-induced sarcomere length non-uniformities, how else can we explain residual force enhancement? A little over a decade ago, we discovered the existence of a passive component of residual force enhancement (Herzog and Leonard, 2002). Evidence accumulated over the past decade strongly suggests that the structural protein titin causes this passive force enhancement (Herzog et al., 2006). The idea was that titin, which acts as a molecular spring in the I-band region of sarcomeres, alters its spring stiffness when a muscle is activated. In principle, titin's stiffness can be changed in two ways:

(i) by changing its material properties, or (ii) by changing its free spring length. Recent findings support the idea that both these mechanisms are at work in actively stretched skeletal muscles (**Figure 8**).

Titin is known to increase its stiffness upon muscle activation by binding calcium to specialized sites (Labeit et al., 2003; Joumaa et al., 2007). Labeit et al. (2003) identified the glutamate rich-region of the so-called PEVK segment of titin as a binding site for calcium, and Duvall et al. (2012) showed that calcium binds to specific Immunoglobulin (Ig) domains of titin and by doing so makes titin stiffer. There might be other calcium binding sites on titin that have yet to be identified.

Titin is also thought to change its free spring length by binding its proximal region to actin upon activation and muscle force production. Leonard and Herzog (2010) demonstrated that actively stretched sarcomeres and myofibrils produced about 3–4 times greater forces than passively stretched myofibrils in regions where actin-myosin filament overlap had been lost, and thus active forces were zero. Similarly, early findings on labeled titin segments in myofibrils indicate that during passive stretching, all I-band segments of titin elongate, as expected, while during active stretching, some proximal segments in the I-band region do not elongate, suggesting that they may be bound to a rigid backbone, for example the actin filament. In *mdm* knockout mice, where part of the N2A region of titin, thought to be critical for attachment of titin to actin, is eliminated, the difference between passive forces in actively and passively stretched myofibrils is small (about 15%) and can readily be explained with calcium binding to the titin segments identified above.

These results point to titin as a force regulating protein in muscle contraction; specifically in eccentric contractions and in the force enhanced state. Corresponding conceptual models of such a three filament force regulating sarcomere (**Figure 8**) have been discussed elsewhere in detail (Herzog et al., 2012a,b; Herzog, 2014) and a corresponding mathematical model has been developed and recently published (Schappacher-Tilp et al., 2015).

Independent of the ultimate explanation for residual force enhancement in skeletal muscles, the proposed substitution of

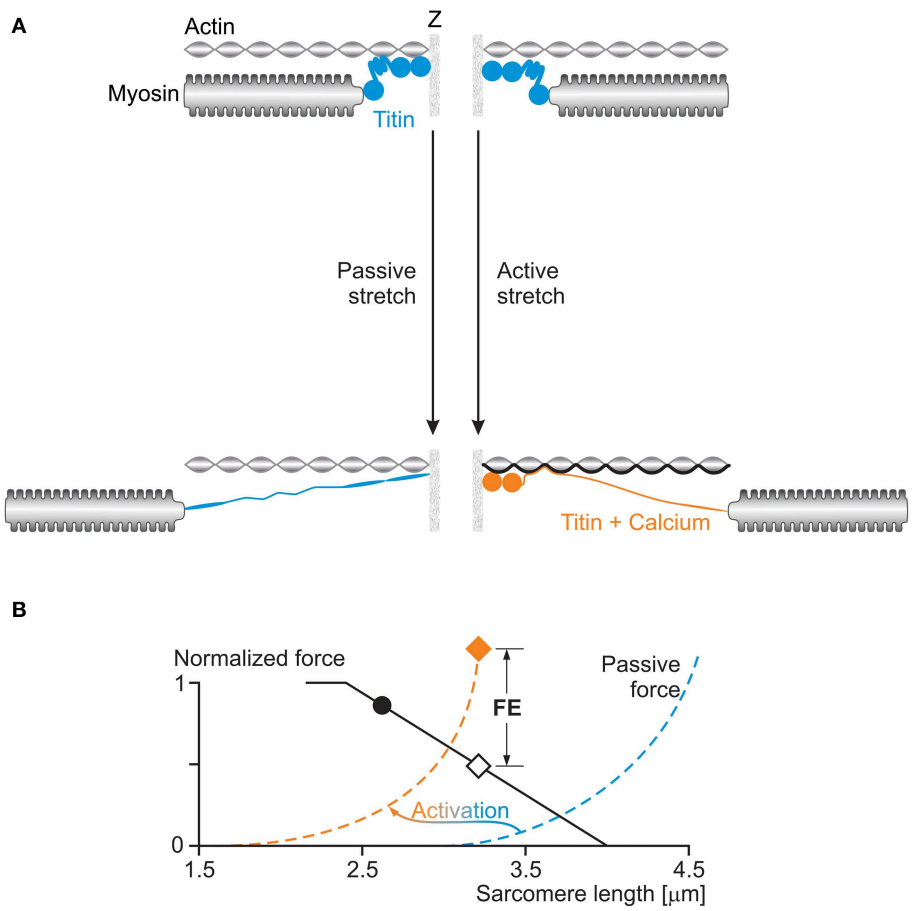

FIGURE 8 | (A) Titin-induced force enhancement: a half-sarcomere is stretched passively (left) and actively (right). During passive stretching, titin elongates according to its normal spring properties. During active stretching, calcium binds to titin and titin's proximal region binds to actin: both of these events increase titin's stiffness and thus its force when actively stretched compared to when passively stretched. **(B)** The effects of activation on titin's force (passive force) are illustrated schematically in the force-length graph with a shift of the passive force to the left of the sarcomere length scale, and an increase in stiffness at a given sarcomere length.

the two filament (actin and myosin) with a three filament (actin, myosin, and titin) sarcomere model for force production has a variety of advantages over the sarcomere length non-uniformity theory, not the least of which is that it can explain all isometric and concentric force properties of the traditional cross-bridge model, but can also predict the increased force during eccentric contractions, the efficiency of eccentric contractions and the active and passive force enhancement following active muscle stretching.

But not only that, the three filament model of muscle force production has some intuitively appealing properties, including:

i. The passive structures of muscles are soft and compliant when passively stretched but become hard and stiff during active stretching, thus providing additional force at negligible energetic cost.
ii. Titin forces increase when actin-myosin forces decrease, thereby providing a mechanism preventing damage in muscles stretched actively to long lengths.
iii. Titin provides stability for sarcomeres on the descending limb of the force-length relationship and for myosin filaments in the middle of the sarcomere. When titin is eliminated, all passive, and active force transmission across sarcomeres is lost (Leonard and Herzog, 2010).

Acknowledgments

The Canadian Institutes of Health Research (CIHR), the Natural Sciences and Engineering Research Council of Canada (NSERC), the Killam Foundation, and the Canada Research Chair Program for Molecular and Cellular Biomechanics.

References

Abbott, B. C., and Aubert, X. M. (1952). The force exerted by active striated muscle during and after change of length. *J. Physiol.* 117, 77–86.

Allinger, T. L., Epstein, M., and Herzog, W. (1996). Stability of muscle fibers on the descending limb of the force- length relation. A theoretical consideration. *J. Biomech.* 29, 627–633. doi: 10.1016/0021-9290(95)00087-9

Bartoo, M. L., Popov, V. I., Fearn, L. A., and Pollack, G. H. (1993). Active tension generation in isolated skeletal myofibrils. *J. Muscle Res. Cell Motil.* 14, 498–510. doi: 10.1007/BF00297212

Campbell, K. S. (2009). Interactions between connected half-sarcomeres produce emergent mechanical behavior in a mathematical model of muscle. *PLoS Comput. Biol. Nov.* 5:e1000560. doi: 10.1371/journal.pcbi.1000560

Duvall, M. M., Gifford, J. L., Amrein, M., and Herzog, W. (2012). Altered mechanical properties of titin immunoglobulin domain 27 in the presence of calcium. *Eur. Biophys. J.* 42, 301–307. doi: 10.1007/s00249-012-0875-8

Edman, K. A. (2012). Residual force enhancement after stretch in striated muscle. A consequence of increased myofilament overlap? *J. Physiol.* 590(Pt 6), 1339–1345. doi: 10.1113/jphysiol.2011.222729

Edman, K. A. P., Elzinga, G., and Noble, M. I. M. (1978). Enhancement of mechanical performance by stretch during tetanic contractions of vertebrate skeletal muscle fibres. *J. Physiol.* 281, 139–155. doi: 10.1113/jphysiol.1978.sp012413

Edman, K. A. P., Elzinga, G., and Noble, M. I. M. (1982). Residual force enhancement after stretch of contracting frog single muscle fibers. *J. Gen. Physiol.* 80, 769–784. doi: 10.1085/jgp.80.5.769

Epstein, M., and Herzog, W. (1998). *Theoretical Models of Skeletal Muscle:Biological and Mathematical Considerations*. New York, NY: John Wiley & Sons Ltd.

Fenn, W. O. (1923). A quantitative comparison between the energy liberated and the work performed by the isolated sartorius of the frog. *J. Physiol.* 58, 175–205. doi: 10.1113/jphysiol.1923.sp002115

Fenn, W. O. (1924). The relation between the work performed and the energy liberated in muscular contraction. *J. Physiol.* 58, 373–395. doi: 10.1113/jphysiol.1924.sp002141

Gasser, H. S., and Hill, A. V. (1924). The dynamics of muscular contraction. *Proc. R. Soc. Lond. B Biol. Sci.* 96, 398–437. doi: 10.1098/rspb.1924.0035

Gordon, A. M., Huxley, A. F., and Julian, F. J. (1966). The variation in isometric tension with sarcomere length in vertebrate muscle fibres. *J. Physiol.* 184, 170–192. doi: 10.1113/jphysiol.1966.sp007909

Herzog, W. (2014). Mechanisms of enhanced force production in lengthening (eccentric) muscle contractions. *J. Appl. Physiol. (1985)* 116, 1407–1417.

Herzog, W., Duvall, M., and Leonard, T. R. (2012a). Molecular mechanisms of muscle force regulation: a role for titin? *Exerc. Sport Sci. Rev.* 40, 50–57. doi: 10.1097/JES.0b013e31823cd75b

Herzog, W., Lee, E. J., and Rassier, D. E. (2006). Residual force enhancement in skeletal muscle. *J. Physiol.* 574, 635–642. doi: 10.1113/jphysiol.2006.107748

Herzog, W., Leonard, T., Joumaa, V., Duvall, M., and Panchangam, A. (2012b). The three filament model of skeletal muscle stability and force production. *Mol. Cell. Biomech.* 9, 175–191.

Herzog, W., and Leonard, T. R. (2002). Force enhancement following stretching of skeletal muscle: a new mechanism. *J. Exp. Biol.* 205, 1275–1283.

Herzog, W., and Leonard, T. R. (2006). Response to the (Morgan and Proske) Letter to the Editor by Walter Herzog and Tim Leonard (on behalf of the authors). *J. Physiol* 578(Pt 2), 617–620. doi: 10.1113/jphysiol.2006.125443

Herzog, W., and Leonard, T. R. (2013). Residual force enhancement: the neglected property of striated muscle contraction. *J. Physiol.* 591(Pt 8), 2221. doi: 10.1113/jphysiol.2012.248450

Hill, A. V. (1938). The heat of shortening and the dynamic constants of muscle. *Proc. R. Soc. Lond. B Biol. Sci.* 126, 136–195. doi: 10.1098/rspb.1938.0050

Hill, A. V. (1953). The mechanics of active muscle. *Proc. R. Soc. Lond. B Biol. Sci.* 141, 104–117. doi: 10.1098/rspb.1953.0027

Huxley, A. F. (1957). Muscle structure and theories of contraction. *Prog. Biophys. Biophys. Chem.* 7, 255–318.

Huxley, A. F., and Niedergerke, R. (1954). Structural changes in muscle during contraction. Interference microscopy of living muscle fibres. *Nature* 173, 971–973. doi: 10.1038/173971a0

Huxley, A. F., and Peachey, L. D. (1961). The maximum length for contraction in vertebrate striated muscle. *J. Physiol.* 156, 150–165. doi: 10.1113/jphysiol.1961.sp006665

Huxley, A. F., and Simmons, R. M. (1971). Proposed mechanism of force generation in striated muscle. *Nature* 233, 533–538. doi: 10.1038/233533a0

Huxley, H. E. (1953). Electron microscope studies of the organization of the filaments in striated muscle. *Biochim. Biophys. Acta* 12, 387–394. doi: 10.1016/0006-3002(53)90156-5

Huxley, H. E. (1969). The mechanism of muscular contraction. *Science* 164, 1356–1366. doi: 10.1126/science.164.3886.1356

Huxley, H. E., and Hanson, J. (1954). Changes in cross-striations of muscle during contraction and stretch and their structural implications. *Nature* 173, 973–976. doi: 10.1038/173973a0

Joumaa, V., and Herzog, W. (2013). Energy cost of force production is reduced after active stretch in skinned muscle fibres. *J. Biomech.* 46, 1135–1139. doi: 10.1016/j.jbiomech.2013.01.008

Joumaa, V., Leonard, T. R., and Herzog, W. (2008). Residual force enhancement in myofibrils and sarcomeres. *Proc. Biol. Sci.* 275, 1411–1419. doi: 10.1098/rspb.2008.0142

Joumaa, V., Rassier, D. E., Leonard, T. R., and Herzog, W. (2007). Passive force enhancement in single myofibrils. *Pflügers Arch* 455, 367–371. doi: 10.1007/s00424-007-0287-2

Julian, F. J., and Morgan, D. L. (1979). The effects of tension on non-uniform distribution of length changes applied to frog muscle fibres. *J. Physiol.* 293, 379–392. doi: 10.1113/jphysiol.1979.sp012895

Labeit, D., Watanabe, K., Witt, C., Fujita, H., Wu, Y., Lahmers, S., et al. (2003). Calcium-dependent molecular spring elements in the giant protein titin. *Proc. Natl. Acad. Sci. U.S.A.* 100, 13716–13721. doi: 10.1073/pnas.2235652100

Lee, E. J., and Herzog, W. (2008). Residual force enhancement exceeds the isometric force at optimal sarcomere length for optimized stretch conditions. *J. Appl. Physiol.* 105, 457–462. doi: 10.1152/japplphysiol.01109.2006

Lee, H. D., and Herzog, W. (2002). Force enhancement following muscle stretch of electrically and voluntarily activated human adductor pollicis. *J. Physiol.* 545, 321–330. doi: 10.1113/jphysiol.2002.018010

Leonard, T. R., Duvall, M., and Herzog, W. (2010). Force enhancement following stretch in a single sarcomere. *Am. J. Physiol. Cell. Physiol.* 299, C1398–C1401. doi: 10.1152/ajpcell.00222.2010

Leonard, T. R., and Herzog, W. (2010). Regulation of muscle force in the absence of actin-myosin based cross-bridge interaction. *Am. J. Physiol. Cell. Physiol.* 299, C14–C20. doi: 10.1152/ajpcell.00049.2010

Llewellyn, M. E., Barretto, R. P. J., Delp, S. L., and Schnitzer, M. J. (2008). Minimally invasive high-speed imaging of sarcomere contractile dynamics in mice and humans. *Nature* 454, 784–788. doi: 10.1038/nature07104

Lundsgaard, E. (1930). Untersuchungen über Muskelkontraktionen ohne Milchsäurebildung. *Biochem. Z.* 217, 162–177.

Morgan, D. L. (1990). New insights into the behavior of muscle during active lengthening. *Biophys. J.* 57, 209–221. doi: 10.1016/S0006-3495(90)82524-8

Morgan, D. L. (1994). An explanation for residual increased tension in striated muscle after stretch during contraction. *Exp. Physiol.* 79, 831–838. doi: 10.1113/expphysiol.1994.sp003811

Morgan, D. L., Mochon, S., and Julian, F. J. (1982). A quantitative model of intersarcomere dynamics during fixed-end contractions of single frog muscle fibres. *Biophys. J.* 39, 189–196. doi: 10.1016/S0006-3495(82)84507-4

Morgan, D. L., and Proske, U. (2006). Can all residual force enhancement be explained by sarcomere non-uniformities? *J. Physiol.* 578(Pt 2), 613–615. doi: 10.1113/jphysiol.2006.125039

Morgan, D. L., Whitehead, N. P., Wise, A. K., Gregory, J. E., and Proske, U. (2000). Tension changes in the cat soleus muscle following slow stretch or shortening of the contracting muscle. *J. Physiol.* 522(Pt 3), 503–513. doi: 10.1111/j.1469-7793.2000.t01-2-00503.x

Oskouei, A. E., and Herzog, W. (2005). Observations on force enhancement in sub-maximal voluntary contractions of human adductor pollicis muscle. *J. Appl. Physiol.* 98, 2087–2095. doi: 10.1152/japplphysiol.01217.2004

Peterson, D., Rassier, D. E., and Herzog, W. (2004). Force enhancement in single skeletal muscle fibres on the ascending limb of the force-length relationship. *J. Exp. Biol.* 207, 2787–2791. doi: 10.1242/jeb.01095

Pollack, G. H. (1990). *Muscles & Molecules - Uncovering the Principles of Biological Motion*. Seattle, WA: Ebner and Sons.

Rassier, D. E. (2012). Residual force enhancement in skeletal muscles: one sarcomere after the other. *J. Muscle Res. Cell. Motil.* 33, 155–165. doi: 10.1007/s10974-012-9308-7

Rassier, D. E., Herzog, W., and Pollack, G. H. (2003a). Dynamics of individual sarcomeres during and after stretch in activated single myofibrils. *Proc. Biol. Sci.* 270, 1735–1740. doi: 10.1098/rspb.2003.2418

Rassier, D. E., Herzog, W., and Pollack, G. H. (2003b). Stretch-induced force enhancement and stability of skeletal muscle myofibrils. *Adv. Exp. Med. Biol.* 538, 501–515. doi: 10.1007/978-1-4419-9029-7_45

Rassier, D. E., Herzog, W., Wakeling, J. M., and Syme, D. (2003c). Stretch-induced, steady-state force enhancement in single skeletal muscle fibers exceeds the isometric force at optimal fibre length. *J. Biomech.* 36, 1309–1316.

Rayment, I., Holden, H. M., Whittaker, M., Yohn, C. B., Lorenz, M., Holmes, K. C., et al. (1993). Structure of the actin-myosin complex and its implications for muscle contraction. *Science* 261, 58–65. doi: 10.1126/science.8316858

Schachar, R., Herzog, W., and Leonard, T. R. (2004). The effects of muscle stretching and shortening on isometric forces on the descending limb of the force-length relationship. *J. Biomech.* 37, 917–926. doi: 10.1016/j.jbiomech.2003.10.006

Schappacher-Tilp, G., Leonard, T., Desch, G., and Herzog, W., (2015). A novel three-filament model of force generation in eccentric contraction of skeletal muscles. *PLoS. One* 10:e0117634. doi: 10.1371/journal.pone.0117634

Sugi, H., and Tsuchiya, T. (1988). Stiffness changes during enhancement and deficit of isometric force by slow length changes in frog skeletal muscle fibres. *J. Physiol.* 407, 215–229. doi: 10.1113/jphysiol.1988.sp017411

Walcott, S., and Herzog, W. (2008). Modeling residual force enhancement with generic cross-bridge models. *Math. Biosci.* 216, 172–186. doi: 10.1016/j.mbs.2008.10.005

Zahalak, G. I. (1997). Can muscle fibers be stable on the descending limbs of their sarcomere length-tension relations? *J. Biomech.* 30, 1179–1182.

Conflict of Interest Statement: The authors declare that the research was conducted in the absence of any commercial or financial relationships that could be construed as a potential conflict of interest.

Copyright © 2015 Herzog, Powers, Johnston and Duvall. This is an open-access article distributed under the terms of the Creative Commons Attribution License (CC BY). The use, distribution or reproduction in other forums is permitted, provided the original author(s) or licensor are credited and that the original publication in this journal is cited, in accordance with accepted academic practice. No use, distribution or reproduction is permitted which does not comply with these terms.

frontiers in PHYSIOLOGY

HYPOTHESIS AND THEORY ARTICLE
published: 15 September 2014
doi: 10.3389/fphys.2014.00350

Hypothesis and theory: mechanical instabilities and non-uniformities in hereditary sarcomere myopathies

Alf Månsson*

Department of Chemistry and Biomedical Sciences, Linnaeus University, Kalmar, Sweden

Edited by:
Julien Ochala, KIng's College London, UK

Reviewed by:
Leonardo F. Ferreira, University of Florida, USA
Charles S. Chung, University of Kentucky, USA

****Correspondence:***
Alf Månsson, Department of Chemistry and Biomedical Sciences, Linnaeus University, Norra vägen 49, Kalmar, SE-391 82, Sweden
e-mail: alf.mansson@lnu.se

Familial hypertrophic cardiomyopathy (HCM), due to point mutations in genes for sarcomere proteins such as myosin, occurs in 1/500 people and is the most common cause of sudden death in young individuals. Similar mutations in skeletal muscle, e.g., in the *MYH7* gene for slow myosin found in both the cardiac ventricle and slow skeletal muscle, may also cause severe disease but the severity and the morphological changes are often different. In HCM, the modified protein function leads, over years to decades, to secondary remodeling with substantial morphological changes, such as hypertrophy, myofibrillar disarray, and extensive fibrosis associated with severe functional deterioration. Despite intense studies, it is unclear how the moderate mutation-induced changes in protein function cause the long-term effects. In hypertrophy of the heart due to pressure overload (e.g., hypertension), mechanical stress in the myocyte is believed to be major initiating stimulus for activation of relevant cell signaling cascades. Here it is considered how expression of mutated proteins, such as myosin or regulatory proteins, could have similar consequences through one or both of the following mechanisms: (1) contractile instabilities within each sarcomere (with more than one stable velocity for a given load), (2) different tension generating capacities of cells in series. These mechanisms would have the potential to cause increased tension and/or stretch of certain cells during parts of the cardiac cycle. Modeling studies are used to illustrate these ideas and experimental tests are proposed. The applicability of similar ideas to skeletal muscle is also postulated, and differences between heart and skeletal muscle are discussed.

Keywords: myopathy, striated muscle, force-velocity relationship, actomyosin, heart, skeletal muscle

INTRODUCTION

Hereditary heart diseases, cardiomyopathies, with mutations in genes for key proteins in the muscle sarcomere (**Figure 1**) occur in as many as 1/500 people and are the most common cause of sudden death in young individuals (Harvey and Leinwand, 2011; Teekakirikul et al., 2012). Some of the most commonly affected proteins include ventricular β-myosin heavy chains, myosin binding protein C, troponin I, troponin T, tropomyosin, and myosin regulatory light chains (Xu et al., 2010). While much attention has been directed to sarcomere myopathies in the heart, the insight into their genetic basis (Geisterfer-Lowrance et al., 1990) triggered interest into related skeletal muscle diseases (Cuda et al., 1993; Martinsson et al., 2000). The consequences of these skeletal muscle sarcomere myopathies may be equally severe with, grave disability, respiratory failure and death at a young age (Laing and Nowak, 2005b; Laing, 2007; Ochala, 2008; Tajsharghi and Oldfors, 2013). Interestingly, however, a large majority of the myosin mutations that cause severe cardiomyopathy, only cause mild skeletal muscle disease (Oldfors, 2007). Severe disease in skeletal muscle is generally associated with mutations in thin filament proteins such as nebulin (not present in heart), actin, or the regulatory troponin-tropomyosin complex (Ochala, 2008).

Importantly, both in heart and skeletal muscle, severe disease often does not develop until adolescence or adulthood (Frey et al., 2012). This offers a time window that should be useful for therapeutic interventions. However, such options are currently hampered by lack of insight into the mechanisms whereby the minor, primary disturbances in the sarcomere proteins are transformed into disease with appreciable morphological changes (Laing and Nowak, 2005a; Ochala, 2008; Frey et al., 2012; Teekakirikul et al., 2012). In the heart there is, for instance, severe hypertrophy with increased wall thickness and cell volume (hypertrophic cardiomyopathy-HCM) or dilation with elongated cells and larger ventricular cavities (dilated cardiomyopathy-DCM). The changes in HCM are associated with myofibrillar disarray and fibrosis throughout the myocardium (Ashrafian et al., 2011; Frey et al., 2012; Teekakirikul et al., 2012) but also with microvascular disease and defects in the mitral valves (Ashrafian et al., 2011). In skeletal muscle, the picture in myopathies is diverse both clinically and morphologically (Laing and Nowak, 2005a; Oldfors, 2007; Ochala, 2008; Marston et al., 2013; Tajsharghi and Oldfors, 2013). Here, the focus will be primarily on hereditary HCM due to appreciably higher prevalence than hereditary DCM. The developed ideas will also be considered in relation to hereditary skeletal muscle diseases with mutations in sarcomeric proteins. It is important to note that the term "HCM" will only refer to hereditary disease. It is not used to denote acquired diseases associated with cardiac hypertrophy, for example in pressure overload.

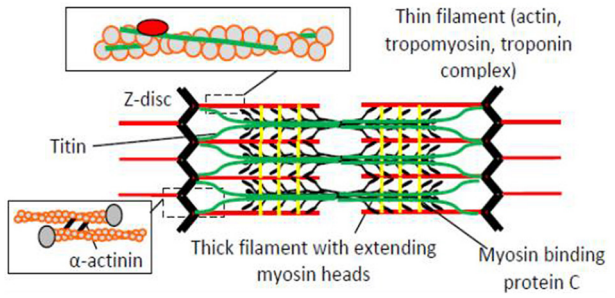

FIGURE 1 | The sarcomere, the highly ordered functional unit of striated muscle with key protein components schematically illustrated. The resting length of the sarcomere is approximately 2.0 μm in the human heart and 2.5 μm in human skeletal muscle.

One major reason why the mechanisms underlying HCM and skeletal muscle myopathies remain elusive is the appreciable multidimensional complexity in spite of a simple primary defect in the form of a point mutation. First of all, the time dependent secondary changes most likely start already during embryonic development (Olivotto et al., 2009). These changes continue throughout life, while being modulated by a range of environmental, genetic and epigenetic factors that may modify disease penetrance and where each is likely to vary with time (Cooper et al., 2013). This time dependence and variability in clinical course has contributed to the difficulty of obtaining a clear and comprehensive picture of the pathogenesis even for a given point mutation. The picture is further blurred by the additional dimension that the path from a given isolated mutation to full-blown disease seems to vary between humans and typical experimental animals, e.g., transgenic mice (Lowey et al., 2008, 2013; Spudich, 2014). Adding further to the complexity, recent studies have also suggested that the proportional expression of wild-type and mutated protein may vary between cells in the same individual (Kirschner et al., 2005), and that there is allelic imbalances with different proportional expression of the mutated protein in different heterozygous individuals (Casadonte et al., 2006; Tripathi et al., 2011; Di Domenico et al., 2012). Considering all the above, it is not surprising that it is highly challenging to arrive at a clear understanding of the pathogenesis of the sarcomere myopathies. Indeed, there are even conflicting views on how a given myosin mutation affects the actomyosin cross-bridge function and whether it leads to gain or loss of function (Wang et al., 2003; Lowey et al., 2008, 2013; Sommese et al., 2013b) (reviewed by Spudich, 2014). Part of the reason for the discrepancies seems to be that a given myosin mutation has different effects depending on the myosin isoform background, a property that varies between species due to differences in dominant ventricular isoform (Lowey et al., 2008, 2013). Recent insights gained using expression of wild-type and mutated proteins from both humans and key experimental animals seem to suggest that there is a tendency (Kohler et al., 2003; Marston, 2011; Teekakirikul et al., 2012; Bai et al., 2013; Spudich, 2014), although with exceptions (Greenberg et al., 2010), for HCM mutations in myosin and regulatory proteins to cause increased rather than reduced power output and/or increased rather than reduced Ca-sensitivity. There is also some evidence for early hypercontractility on the whole organ level (Teekakirikul et al., 2012) although the evidence is not unequivocal (Witjas-Paalberends et al., 2013). The association between increased diastolic pressure (related to, so called, diastolic heart failure) in HCM and an increased Ca-sensitivity (Ferrantini et al., 2009; Ashrafian et al., 2011; Harvey and Leinwand, 2011; Marston, 2011; Frey et al., 2012; Lovelock et al., 2012; Teekakirikul et al., 2012; Bai et al., 2013; Memo and Marston, 2013; Witjas-Paalberends et al., 2013; Sommese et al., 2013a; Spudich, 2014) seems to have gained more general, although not universal (Kirschner et al., 2005), acceptance. However, in this connection it should be mentioned that diastolic dysfunction can also be caused by changes in titin function. This has been demonstrated in mouse models where shortening of the titin spring region (Chung et al., 2013) caused increased ventricular wall stiffness. Moreover, in clinical studies (Borbely et al., 2009) hypophosphorylation of a specific titin isoform increased resting tension with possible implications for diastolic dysfunction in cardiomyocytes from failing human myocardioum.

A majority of the secondary remodeling effects in hereditary HCM are reminiscent of those in pressure overload such as caused by hypertension and aortic stenosis. This includes hypertrophy and fibrosis as well as changes in gene expression profile to a more fetal pattern (cf. Bernardo et al., 2010; Harvey and Leinwand, 2011). A difference is the often more patchy and regional appearance of the secondary changes in HCM due to sarcomeric protein mutation. In cardiac hypertrophy due to pressure overload, mechanical stimuli affecting the myocytes are believed to be major initiators of changes in cell signaling that lead to hypertrophy (Bernardo et al., 2010).

An important question that remains to be answered is why similar signaling pathways as in pressure overload would be activated in HCM (Ferrantini et al., 2009; Olivotto et al., 2009; Ashrafian et al., 2011; Harvey and Leinwand, 2011; Frey et al., 2012; Moore et al., 2012; Teekakirikul et al., 2012). Here, I hypothesize that the initiating stimuli in HCM are similar as in pressure overload but more localized, i.e., they involve increased mechanical stress that only affects a limited fraction of the cardiomyocytes. I further use model studies for initial tests as to whether this hypothesis is consistent with either or both of the following ideas: (i) that altered kinetics of the actomyosin interaction causes critical instabilities in the force-velocity (F-V) relation at the sarcomere level (Julicher and Prost, 1995; Vilfan et al., 1999; Mansson, 2010) and/or (ii) that certain cells in the heart or segments of skeletal muscle fibers are stretched during overall isometric/isovolumetric contraction due to non-uniformity in force-generating capacity between cells (Kirschner et al., 2005).

CELL SIGNALING AND PHENOTYPE IN PRESSURE OVERLOAD AND IN HCM—SIMILARITIES AND DIFFERENCES

Stimulation of angiotensin II (AT-II) receptors appears to be central in the signaling pathways that lead to hypertrophy, fibrosis etc. in HCM, as well as in pressure overload and, at least

in, pressure overload, it seems clear that this signaling is initiated by mechanical stress (Lijnen and Petrov, 1999; Lim et al., 2001; Amedeo Modesti et al., 2002; Zou et al., 2004; Bernardo et al., 2010; Ashrafian et al., 2011; Harvey and Leinwand, 2011; Weeks and McMullen, 2011; Teekakirikul et al., 2012; Luo et al., 2013). The down-stream effects are enhanced or complemented by the action of noradrenaline and endothelin on other G-protein coupled receptors and possibly by paracrine substances released from non-cardiomyocyte cells (Teekakirikul et al., 2012; Cilvik et al., 2013). These effects involve calcium dependent calcium/calmodulin kinase and calcineurin as well as a range of transcription factors ultimately leading to marked changes in protein expression (Bernardo et al., 2010; Harvey and Leinwand, 2011). Importantly, these pathologic pathways largely differ from those in physiologic hypertrophy ("athletes heart") which seem to mainly involve activation of the Akt-mTOR pathway (Bernardo et al., 2010; Weeks and McMullen, 2011).

The similarities in phenotype (hypertrophy associated with fibrosis and similar changes in protein expression pattern) between HCM and pressure overload as well as the involvement of similar signaling systems in the two cases seems undisputed on the basis of a survey of the literature. However, whereas the mechanical stimulus that initiates such signaling seems quite straightforward in pressure overload the initiating mechanism is less evident in HCM. It has been suggested that reduced energy efficiency of contraction is of importance in this regard but it is not clear how (Jung et al., 1998; Sweeney et al., 1998; Crilley et al., 2003; Frey et al., 2006; Luedde et al., 2009; Harvey and Leinwand, 2011; Marston, 2011; Frey et al., 2012; Teekakirikul et al., 2012). Another possibility that has also been widely considered is that disturbances in Ca-homeostasis, as a result of the mutations, could be a triggering factor (Ferrantini et al., 2009; Ashrafian et al., 2011; Harvey and Leinwand, 2011; Marston, 2011; Frey et al., 2012; Teekakirikul et al., 2012). The latter disturbances may be secondary to inefficient energy usage which may reduce calcium pumping by the sarcoplasmic reticulum ATPase. They may also be understood more directly for mutations that alter the Ca-affinity of troponin (Marston, 2011) thereby not only affecting the Ca-sensitivity of contraction but also changing the calcium buffering capacity.

STATEMENT OF HYPOTHESIS

I propose here an alternative hypothesis with the aims of supplementing existing ideas (cf. above) and stimulating new experiments and modeling studies. To the best of my knowledge this hypothesis has not been considered previously, at least not explicitly, but it has been stimulated by recent findings (Kirschner et al., 2005; Mansson, 2010) (see below for details).

I hypothesize that in HCM: (1) similar signaling pathways (associated with AT-II) operate as in pressure overload, but less homogeneously over the ventricular wall and (2) that the dominant initiating stimulus that activates these pathways is similar to that in pressure overload, i.e., increased cellular stress/stretch. The major distinguishing feature, compared to pressure overload, is the idea that the mechanical effects act locally on subpopulations of the cells, rather than globally on all ventricular cells.

INITIATION OF PATHOLOGIC SIGNAL TRANSDUCTION IN HCM

Two mechanisms are considered (see sub-sections below) that may mediate mechanical initiation of pathologic signal transduction. The major components of the overall hypothesis and the two mechanisms are summarized in **Figure 2**. The possible relation to skeletal muscle myopathies is discussed in a separate section at the end of the paper but is also considered briefly in other sections.

INSTABILITY ON SARCOMERE LEVEL

Model studies (Julicher and Prost, 1995; Vilfan and Frey, 2005; Mansson, 2010) have suggested that certain combinations of parameter values that govern the actomyosin interactions may produce mechanical instabilities. These are characterized by anomalous load-velocity (F-V) relationships of the muscle with more than one stable velocity for a given load. This is illustrated in **Figure 3** for a model similar to that in (Mansson, 2010). Here, the black curve simulates a "normal" F-V relationship based on the parameter values in Table S1 whereas the red curve simulates a relationship with instability at loads close to the isometric (see below and legend of **Figure 3** for details).

As pointed out previously (Mansson, 2010), regions of positive or infinite derivative of velocity with respect to force dV/dF (**Figure 3**) may be deleterious for normal muscle function with unpredictable effects and potential difficulties of regulation. The effect may be critical if sarcomeric units in series have different force-generating capacity. This is observed physiologically (see below) and it is proposed here, that the phenomenon is enhanced in myopathies.

The normally low magnitude of the negative slope |dV/dF| of the F-V relationship for lengthening and in the high-force region for shortening is probably important in order to reduce sarcomere-length redistribution during contractions where isometric or almost isometric tension is developed (Edman et al., 1997). This stabilizing effect follows from appreciable drop in tension-generating capability with a small increase in shortening velocity of the strongest fiber segments (the ones that shorten) and a high increase in resistance to stretch of elongating segments. Without such an inherent stabilization, the weakest segments may become severely overstretched with potential damage to the cell or strong local stimulation of hypertrophic signaling. The latter would be expected because stretch of a weak cell during activity will cause stretch of titin in this cell as well as high tension in the individual filaments and Z-lines, structures known to be associated with tension-, and strain-sensing (Luther, 2009; Linke and Kruger, 2010; Ottenheijm et al., 2011; Raskin et al., 2012).

A recently reported loss of the Frank-Starling mechanism in HCM (Sequeira et al., 2013) may also contribute to sarcomere instability similar to that seen with an anomalous F-V relationship. Thus, in normal cardiac muscle, the Frank-Starling mechanism immediately (Mateja and De Tombe, 2012) increases Ca-sensitivity of contraction upon increased sarcomere length, i.e., the strength of any weak segments that undergo stretch is increased, counteracting excessive sarcomere redistributions. It was suggested that the lost capacity to respond to increased

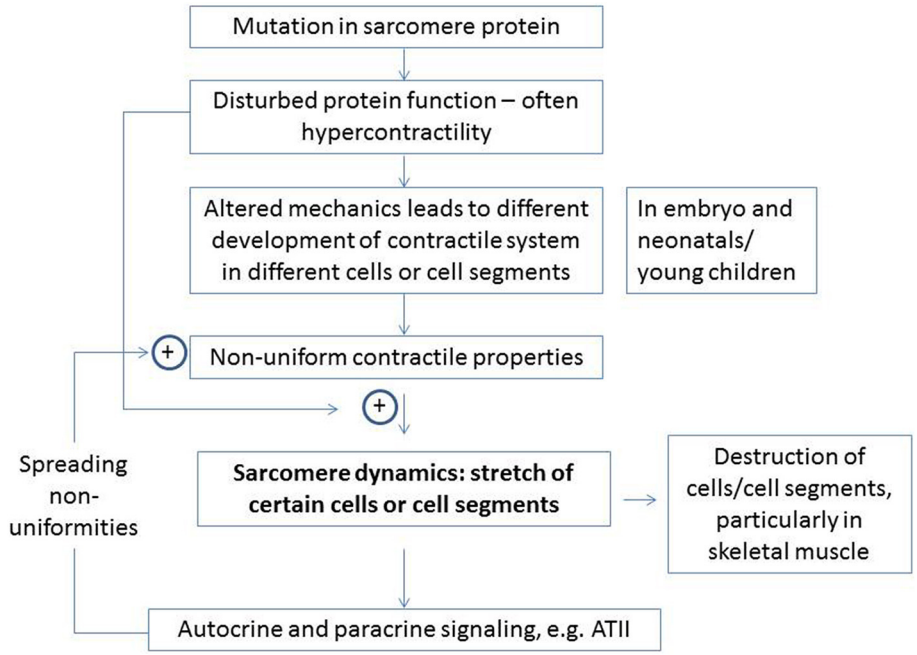

FIGURE 2 | Major elements of proposed hypothesis for development of HCM and related diseases in skeletal muscle. The enhancement of certain effects by specific elements is indicated by plus signs. Details are considered in the text.

filling pressure in HCM in the case of a blunted Frank-Starling mechanism might, in itself, initiate compensatory hypertrophy (Sequeira et al., 2013). On the other hand, the phenomenon would clearly also contribute to the mechanism proposed here and it may be important in pathogenesis if the Frank-Starling mechanism is blunted not only in HCM patients but also in healthy mutation carriers. As mentioned above, a range of HCM mutations cause rather subtle changes in the kinetics and mechanical properties of the actomyosin cross-bridges. In order to investigate whether such effects may cause instabilities in the F-V relationship, as described above, we performed a number of simulations using a model developed from recent work (Albet-Torres et al., 2009; Mansson, 2010; Persson et al., 2013) (Supporting Information). First, we found that isolated changes in only a limited number of the parameter values (Tables S1, S2) could reproduce instabilities in the F-V curve of the type illustrated in **Figure 3**, with only small simultaneous changes in maximal tension and maximal velocity, typically seen in HCM. Of particular interest in this connection was an isolated increase (∼40%) in cross-bridge stiffness that causes an anomalous F-V relationship (red, **Figure 3A**) with regions of positive slope and the mentioned type of instability with more than one stable velocity for a given load. This effect is due to the fact that the cross-bridge, after attachment, has to overcome an increased free-energy barrier (Figure S1), as result of increased stiffness, in stretching the elastic element before entering into the main force-generating state. This energy barrier is lowered by the reduced cross-bridge strain during shortening which explains why force can be as high or higher during slow shortening (red, **Figure 3A**) than in isometric contraction.

NON-UNIFORMITY BETWEEN CARDIAC MUSCLE CELLS OR ALONG SKELETAL MUSCLE FIBERS

Non-uniformity in strength of contraction between different cardiac muscle cells in series or along a skeletal muscle fiber, for whatever reason, will inevitably lead to shortening and elongation of the strongest and weakest segments, respectively if the muscle as a whole undergoes isometric contraction. The phenomenon exists physiologically along skeletal muscle fibers where it has been studied in appreciable detail (Gordon et al., 1966; Julian and Morgan, 1979; Edman and Reggiani, 1984; Edman et al., 1985, 1988). It has also been studied in mammalian myofibrils from heart and skeletal muscle (Stehle et al., 2002; Poggesi et al., 2005). Furthermore, two populations of cells differing with respect to certain contractile properties have been observed among porcine cardiomyocytes (McDonald et al., 2012).

The non-uniformity in contractile properties between different cardiac myocytes and along a skeletal muscle fiber has important physiological roles. This includes effects to speed up relaxation after an isometric contraction (Edman and Flitney, 1982; Poggesi et al., 2005) and to contribute to some aspects of the resistance to stretch (Campbell et al., 2011; Edman, 2012; Rassier, 2012). However, excessive stretch of some muscle segments associated with non-uniformities may also be the basis of cellular damage (Macpherson et al., 1997).

Interestingly, increased variability in calcium sensitivity (reported as pCa) was observed (Kirschner et al., 2005) between different skeletal muscle fibers of a given patient either affected by an Arg723Gly, Arg719Trp, or an Ile736Thr mutation in the β-cardiac/slow myosin gene (MYH7). In the discussion they (Kirschner et al., 2005) stated: "the variability in pCa(50) from

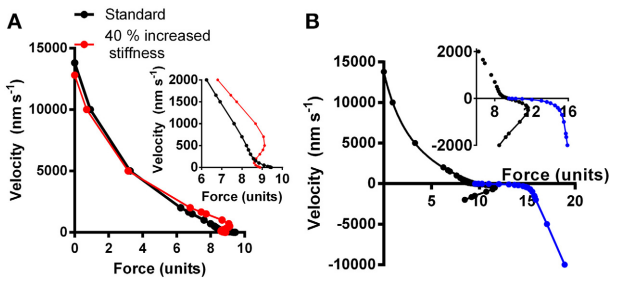

FIGURE 3 | Simulated relationship between force and shortening (positive) and lengthening velocity (negative). (A) Black symbols and connecting lines: standard parameter values (Table S1; corresponding to normal healthy fast skeletal muscle). Red symbols and connecting lines: standard parameter values but cross-bridge stiffness increased by 40% without further changes in parameter values. Inset: simulated force-velocity data in the high force region shown in greater detail. **(B)** The force-velocity relationship for the standard conditions in **(A)** re-plotted together with simulated lengthening part of the relationship either assuming same attachment rate as during shortening and isometric contraction (Equation S4a; black symbols) or assuming increased attachment rate with increased velocity of lengthening (Equation S4b; blue symbols). The latter data are reasonably consistent with experimental data (Lombardi and Piazzesi, 1990) whereas the former are not.

fiber to fiber is likely to cause imbalances in force generation and be the primary cause for contractile dysfunction and development of disarray in the myocardium."

One factor contributing to non-uniform contractile properties between different muscle segments under physiological conditions is differential expression of different myosin isoforms. For instance, different myosin isoform composition has been observed along the length of individual skeletal muscle fibers associated with the protein expression control by different nuclei of these multinuclear cells (Edman et al., 1988; Rosser and Bandman, 2003).

Related to this observation, Kirschner et al. (2005) also considered whether the non-uniformities in pCa between cells may be attributed to different content of mutated protein. Such effects may occur in heterozygous individuals with HCM if there is different fractional expression of mutated and wild-type protein in different cardiac cells or along a given skeletal muscle fiber (as used by Kirschner et al., 2005). However, it is not straightforward to reconcile the idea with findings (Fatkin et al., 1999; Ho et al., 2000; Richard et al., 2000; Nanni et al., 2003) that patients and experimental animals, who are homozygous for a given mutation, exhibit a more severe phenotype than those who are heterozygous. This finding suggests that the amount of mutated protein *per se*, is the critical factor. This idea is also consistent with positive correlation (Casadonte et al., 2006; Tripathi et al., 2011; Di Domenico et al., 2012) between the phenotype severity and the fractional expression of mutated protein in heterozygous individuals, although other interpretations (Tripathi et al., 2011) are possible. The increased severity with increased fraction of mutated protein also seems to accord with recent findings that RNA interference based inhibition of the expression of mutated myosin prevents development of HCM upon just 25% reduction in the level of the mutant transcripts (Jiang et al., 2013).

Of course, in spite of the above findings, one cannot exclude the possibility that non-uniform expression of mutated and wild-type myosin in different cells may affect disease severity in heterozygous individuals or that the pathogenic mechanisms differ between the homozygous and heterozygous cases. However, if it will be possible to conclusively demonstrate that the effect of non-uniform expression is negligible and that it is the overall amount of mutated protein that is important, the findings of Kirschner et al. (Kirschner et al., 2005) of inter-cellular variability must be explained by another mechanism. One may here consider overall changes in cytoarchitecture that give variations in force between cells or between cell segments, consistent with a developmental origin (Olivotto et al., 2009). Another, basis for the effect may be related to the myofibrillar disarray observed upon incorporation of myosin with HCM mutations into embryonic chicken myocytes (Wang et al., 2003), or upon drug induced (instead of mutation induced) modifications of contraction kinetics of embryonic myocytes (Rodriguez et al., 2013). Similar myofibrillar disarray in human cardiomyocytes during embryonic development in the presence of HCM mutations may account for the variability if different cells or cell segments are affected by disarray to different degree. Irrespective of the reason for variability between cells, the weakest cells or cell segments will be stretched by the remaining cells during isovolumetric/isometric contraction, an effect that might be worsened by changes to the load-velocity relationship as indicated in **Figure 3**. Such stretch would be sensed by tension-, and strain-sensing systems in the sarcomeres (Luther, 2009; Linke and Kruger, 2010; Ottenheijm et al., 2011) (see above) and elsewhere, e.g., in the cell membrane (Bernardo et al., 2010) with initiation of hypertrophic signaling. Areas with mechanical non-uniformity and local activation of such signaling pathways may then function as foci from which areas of hypertrophy, fibrosis and disarray on the myocyte level spread (**Figure 2**). This course of events is consistent with focal areas of abnormal strain and fibrosis seen within the limited resolution of cardiac imaging in patients with fully developed HCM (Nagakura et al., 2007; Ghio et al., 2009; Maron et al., 2009). Of even greater interest, regional and patchy irregularities in morphology (Germans et al., 2006) (without hypertrophy) and ventricular wall strain during both systole and diastole have also been observed (Cardim et al., 2002; Yiu et al., 2012; Forsey et al., 2013) in mutation carriers. These changes have particularly been seen in those regions of the ventricle where hypertrophy and fibrosis is most severe late in the course of the disease.

A simplified model (Supplementary Material) was used in order to elucidate the effect of non-uniform contractile properties between cardiac myocytes ($\sim$100 μm long) in series or along several cm long skeletal muscle fibers. Here we approximated this complex arrangement by assuming that two sarcomeres with different contractile properties act in series.

Figure 4 illustrates the effect of different force-generating capacity of the two sarcomeres (corresponding to cells or cell-segments) in series and the effect under these conditions of instability in the F-V relationship (red symbols in **Figure 3**). In **Figure 4A**, the tension and length changes of the two cells were simulated assuming that one of the sarcomeres develops 30% higher maximum force than the other, e.g., corresponding to

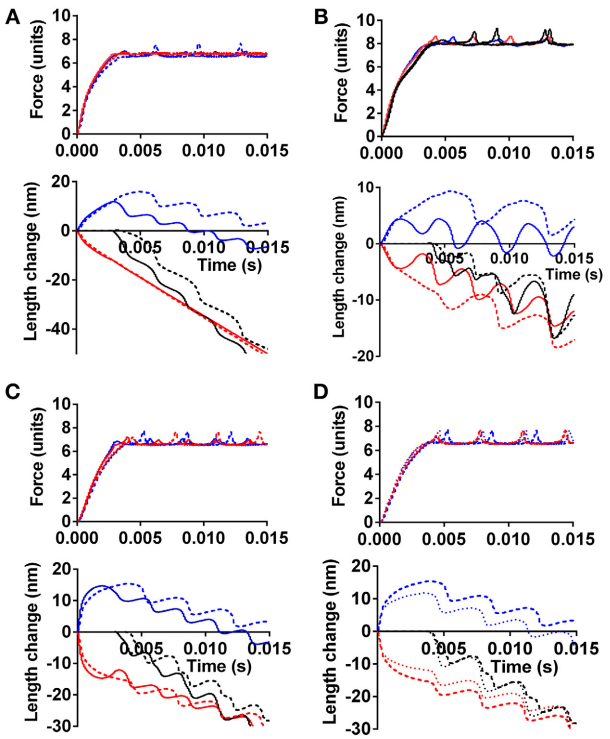

FIGURE 4 | The effect of different force-generating capacity or calcium sensitivity of two cells in series on simulated tension and length response. (A) Effect of 30% higher maximum tension of one cell. Force clamped to 70% of maximum isometric force of weaker cell. Full lines: Force-velocity curve as black symbols in **Figure 3**. Dashed lines: Force-velocity curve as red symbols in **Figure 3**. Blue: response of cell with lowest tension-generating capacity. Red: response of strongest cell. Black in length-time plot: sum of length change for both cells in series. **(B)** Similar to **(A)**, but only 10% higher maximum tension of one cell and force clamped to 85% of maximum isometric force of weaker cell. Line formats and color codes as in **(A)**. Full calcium activation assumed from onset of simulation. **(C)** Simulated time course including activation process with higher calcium sensitivity of contractile system in one cell (red) but similar maximum isometric tension in both cells. Line formats as in other panels. **(D)** Dashed lines, same as dashed lines in **(C)**. Dotted lines, same as in **(C)** but velocity-dependent increase in attachment rate during stretch as described in text.

more myofibrils in parallel or more correctly oriented myofibrils on the cellular level. The results are shown for both cases with a stable (black line in **Figure 3**) and instable (red line in **Figure 3**) F-V relationship of both sarcomeres. In **Figure 4B** similar results are shown as in **Figure 4A** but with only 10% higher force development of one sarcomere compared to the other, and with clamping of the force to 85% (instead of 70% in **Figure 4A**) of the maximum isometric force of the weakest sarcomere. It can be seen in both **Figures 4A,B** that the stronger sarcomere shortens, stretching the sarcomere in series during the overall isometric phase of contraction. It can also be seen that this effect is enhanced with the anomalous F-V curve (red curve in **Figure 3**), particularly when the load is clamped to the higher level and when the difference in maximum force-generating capacity is small (**Figure 4B**).

Effects of calcium-activation are included in the simulations in **Figure 4C**, for cases with a stable (black line in **Figure 3**) and instable (red line in **Figure 3**) F-V relationship. As expected, the sarcomere with highest calcium-sensitivity shortens during the isometric phase (corresponding to isovolumetric phase in the heart), stretching the sarcomere in series, in spite of the same maximum isometric tension in the two sarcomeres. Here, the instability of the F-V relationship only had a small enhancing effect on the amount of stretch of the weak sarcomere during the overall isometric phase of the contraction. This may be due to reduced instability at low level of activation, due to assumed calcium dependence of the attachment rate constant in these simulations. Importantly, not all models of activation include this assumption (Cecchi et al., 1981).

In the simulations above, it was assumed that the rate of myosin head attachment was not increased by stretch. If, instead, the attachment rate was assumed to increase with lengthening velocity, a type of effect found necessary in previous models (Lombardi and Piazzesi, 1990; Mansson, 2010) (see also **Figure 3**), the sarcomere length redistribution was reduced in amplitude as illustrated in **Figure 4D**.

IMPLICATIONS, LIMITATIONS, AND POTENTIALS OF MODEL STUDIES

The present model-simulations merely aim to illustrate the type of effects that may be seen due to sarcomere instabilities and non-uniform contractile properties between myocardial cells, or along a skeletal muscle fiber rather than simulating the exact behavior of human muscle. This limitation in scope is largely due to the limited availability of experimental data for full definition of the models under physiological conditions. This particularly applies to human cardiac muscle but also to an appreciable extent to mammalians skeletal muscle (Supporting Information). Thus, whereas model studies at present have certain limitations, ongoing developments are likely to increase their usefulness. In particular, kinetic and elastic properties of both wild-type and mutated cardiac myosins are in the process of being elucidated in similar detail to fast skeletal muscle myosin (Deacon et al., 2012; Bloemink et al., 2013; Sommese et al., 2013b). Similar developments are underway (Bai et al., 2013) for the contractile effects of e.g., regulatory thin filament proteins.

Clearly, to refine the model in order to critically evaluate the current idea that some sarcomeres are stretched by others, it will be essential to increase of the understanding of the lengthening part of the load-velocity relationship and establish whether cardiomyopathy mutations might affect this part (cf. **Figures 4C,D**).

Better models based on more complete experimental data should give further insights into the effect of the myopathy mutations in otherwise normal cells, before they are affected by remodeling. The models would allow extrapolation from single molecule results to ensemble function and also allow the incorporation of effects on higher level of hierarchial organization than that of sarcomeres and half-sarcomeres.

SUGGESTED EXPERIMENTAL TESTS

In studies of cardiomyopathies, using isolated proteins, limited effort has, so far, been devoted to the detailed shape of the load-velocity relationship for shortening as well as lengthening. Studies of F-V data have mainly utilized semi-quantitative methods with

so called loaded motility assays, where actin-binding proteins impose a frictional load between the surface and actin filaments (Bing et al., 2000; Sommese et al., 2013b). Whereas this technique detects gross changes in maximum power output it seems less likely that it will detect more subtle changes in shape of the force velocity relationship such as exemplified in **Figure 3**. In order to detect the types of instabilities considered here, high-resolution studies will be required to obtain F-V data from small ensembles of contractile proteins. The use of small ensembles is important because the F-V relationship is a property of an ensemble of actomyosin motors (Huxley, 1957; Eisenberg and Hill, 1978; Vilfan et al., 1999).

An interesting question, in terms of non-uniformities between cardiomyocuytes, is whether there is allelic expression of myosin so that some cells express the wild type and some the mutant or whether there is variable expression of both within one cell (Kirschner et al., 2005). However, whatever the cause of non-uniformities between cells, it is clear from the simulations that they would lead to increased lengthening of some cells and shortening of others during overall isovolumetric/isometric contraction. One would thus expect increased non-uniformity in strain during systole in the whole heart of healthy human mutation carriers, (cf. Ghio et al., 2009). Further insight in this regard relies on further improvements of methods for cardiac imaging. Increased non-uniformity of sarcomere behavior during contraction should also be possible to detect in cardiac ventricular strips from experimental animals and between segments along a skeletal muscle fiber. Another interesting test would be if a given degree of expression of a mutated myosin in e.g., a transfected embryonic cardiomyocyte (Wang et al., 2003) leads to increased variability in the degree of myofibrillar disarray indicating the possibility of non-uniformities developing embryologically.

One may also consider attempts to probe how activation of signal transduction systems is spatially and temporally distributed over the cardiac ventricle in experimental animals with HCM causing mutations. Finally, it may be of interest to consider the option to control the process in greater detail by actually inducing local non-uniformities in contractile function *in situ*, perhaps by localized adeno-associated virus (AAV) based transfection of relevant genes. The animals should then be followed up with regard to the presence of non-uniform contraction, localized AT-II signaling and, finally, development of a HCM phenotype.

SKELETAL MUSCLE MYOPATHIES

Skeletal muscle sarcomere myopathies are due to mutations in similar genes as cardiomyopathies but the mutations that predominantly cause severe disease differ. Whereas myosin and myosin-binding protein C are mainly affected in HCM (see above) it is mainly thin filament proteins such as nebulin (not present in heart), actin, tropomyosin, troponin T and troponin I that are affected in severe sarcomere myopathies in skeletal muscle (Laing, 2007; Ochala, 2008). It is particularly puzzling that that even malignant HCM-mutations e.g., in the MYH7 gene, with modified ventricular β-myosin heavy chain, identical to the slow skeletal muscle myosin heavy chain, often give a mild skeletal muscle phenotype (Oldfors, 2007). One may speculate about reasons for this, from differences in signaling cascades that are activated by the mutation over different loading conditions of the different muscles to different compensatory mechanisms, i.e., involving altered state of phosphorylation of a range of regulatory proteins in the heart and compensatory use of non-slow motor units in skeletal muscle. These are interesting questions that may teach us lessons about the pathogenesis but they are not a major focus here.

The most common among the rare skeletal muscle sarcomere myopathies with bewildering morphological and clinical consequences are denoted nemaline myopathy and distal arthrogryposis. These are caused by a range of mutations in the thin filament proteins. The nemaline myopathies, in addition to being characterized by specific morphological changes late in the course of the disease, with so called nemaline bodies (Ochala, 2008), containing actin and sarcomere Z-line proteins seem to exhibit reduced Ca-sensitivity and hypocontractility (Ochala, 2008; Ochala et al., 2012; Memo and Marston, 2013). In contrast, distal arthrogryoposis is characterized by increased Ca-sensitivity and hypercontractility (Robinson et al., 2007; Ochala, 2008; Memo and Marston, 2013), e.g., with contractures in distal muscles. For other skeletal muscle diseases, the reader is referred to a number of comprehensive recent reviews (Laing and Nowak, 2005a; Laing, 2007; Oldfors, 2007; Ochala, 2008; Wallgren-Pettersson et al., 2011; Tajsharghi and Oldfors, 2013).

In spite of the differences from cardiomyopathies, I postulate that the basic mechanisms for muscle destruction in several skeletal muscle diseases, caused by mutations in sarcomere proteins, are similar to the hypertrophy response in heart, i.e., instabilities on the sarcomere level and non-uniformities along the length of the muscle. This is consistent with the fact that the results of Kirschner et al. (2005), on basis of which they proposed that non-uniformities are important in cardiomyopathies, were actually derived using slow skeletal muscle preparations.

If there are increased differences in force-generating capability along skeletal muscle fibers with sarcomere myopathy mutations one would expect increased sarcomere re-distributions within the fiber with the risk that some segments are overstretched (see above for mechanisms). In skeletal muscle fibers it is also known that stretch could stimulate hypertrophy (Roig et al., 2009). On the other hand, extensive non-uniform stretch, possibly facilitated by instabilities of the F-V relationship may lead to cell damage. Indeed, cell damage, rather than hypertrophy may be even more likely in skeletal muscle than in the heart as the Frank-Starling mechanism, giving increased Ca-sensitivity with stretch, may counteract the stretch in heart muscle but is not present in skeletal muscle.

CONCLUSIONS

The present paper has analyzed a hypothesis according to which the early compensatory changes in HCM occur due to local stimulation of cell-signaling mechanisms similar to those in pressure-overload. According to this hypothesis, locally increased mechanical stress on the cardiomyocytes is of key importance as an initiating factor and may be brought about by one or both of two different mechanisms: (1) contractile instabilities within each sarcomere (with more than one stable velocity for a given load)

under certain loading conditions and (2) non-uniform mechanical properties (strength) of different cells leading to a tendency for inhomogeneous stretch of certain regions of the ventricle wall during parts of the cardiac cycle.

One common denominator of the proposed mechanisms is that they are not readily detected in studies using conventional preparations such as isolated proteins or cells already affected by secondary compensatory changes. What is required, in general, are studies on higher organizational levels using cells, tissues, whole hearts or sarcomere like ensembles that contain mutated proteins but that are unaffected by compensatory changes. Furthermore, for any form of mechanical studies to detect the ensemble effects it will be critical to explore the range of loads experienced during the cardiac cycle. The hypothesis, with slight modifications, may also be relevant in the pathogenesis of skeletal muscle myopathies.

ACKNOWLEDGMENTS

The paper was conceived and a major part of it was written when the author was at sabbatical leave in the lab of J. A. Spudich at Stanford University. I am grateful to P. M. Bennet, J. A. Spudich, M. Kawana, M. Persson, and S. Tågerud for valuable scientific comments and suggestions and I am indebted to P. M. Bennet and M. Lard for suggested language editing. Funding from the Wenner-Gren Foundation and the Faculty of Health and Life Sciences at the Linnaeus University is gratefully acknowledged.

SUPPLEMENTARY MATERIAL

The Supplementary Material for this article can be found online at: http://www.frontiersin.org/journal/10.3389/fphys.2014.00350/abstract

REFERENCES

Albet-Torres, N., Bloemink, M. J., Barman, T., Candau, R., Frölander, K., Geeves, M. A., et al. (2009). Drug effect unveils inter-head cooperativity and strain-dependent ADP release in fast skeletal actomyosin. *J. Biol. Chem.* 284, 22926–22937. doi: 10.1074/jbc.M109.019232

Amedeo Modesti, P., Zecchi-Orlandini, S., Vanni, S., Polidori, G., Bertolozzi, I., Perna, A. M., et al. (2002). Release of preformed Ang II from myocytes mediates angiotensinogen and ET-1 gene overexpression *in vivo* via AT1 receptor. *J. Mol. Cell. Cardiol.* 34, 1491–1500. doi: 10.1006/jmcc.2002.2095

Ashrafian, H., McKenna, W. J., and Watkins, H. (2011). Disease pathways and novel therapeutic targets in hypertrophic cardiomyopathy. *Circ. Res.* 109, 86–96. doi: 10.1161/CIRCRESAHA.111.242974

Bai, F., Wang, L., and Kawai, M. (2013). A study of tropomyosin's role in cardiac function and disease using thin-filament reconstituted myocardium. *J. Muscle Res. Cell Motil.* 34, 295–310. doi: 10.1007/s10974-013-9343-z

Bernardo, B. C., Weeks, K. L., Pretorius, L., and McMullen, J. R. (2010). Molecular distinction between physiological and pathological cardiac hypertrophy: experimental findings and therapeutic strategies. *Pharmacol. Ther.* 128, 191–227. doi: 10.1016/j.pharmthera.2010.04.005

Bing, W., Knott, A., and Marston, S. B. (2000). A simple method for measuring the relative force exerted by myosin on actin filaments in the *in vitro* motility assay: evidence that tropomyosin and troponin increase force in single thin filaments. *Biochem. J.* 350 Pt 3, 693–699. doi: 10.1042/0264-6021:3500693

Bloemink, M., Deacon, J., Langer, S., Vera, C., Combs, A., Leinwand, L., et al. (2013). The hypertrophic cardiomyopathy myosin mutation R453C alters ATP-binding and hydrolysis of human cardiac beta-myosin. *J. Biol. Chem.* 289, 5158–5167. doi: 10.1074/jbc.M113.511204

Borbely, A., Falcao-Pires, I., Van Heerebeek, L., Hamdani, N., Edes, I., Gavina, C., et al. (2009). Hypophosphorylation of the Stiff N2B titin isoform raises cardiomyocyte resting tension in failing human myocardium. *Circ. Res.* 104, 780–786. doi: 10.1161/CIRCRESAHA.108.193326

Campbell, S. G., Hatfield, P. C., and Campbell, K. S. (2011). A mathematical model of muscle containing heterogeneous half-sarcomeres exhibits residual force enhancement. *PLoS Comput. Biol.* 7:e1002156. doi: 10.1371/journal.pcbi.1002156

Cardim, N., Perrot, A., Ferreira, T., Pereira, A., Osterziel, K. J., Reis, R. P., et al. (2002). Usefulness of Doppler myocardial imaging for identification of mutation carriers of familial hypertrophic cardiomyopathy. *Am. J. Cardiol.* 90, 128–132. doi: 10.1016/S0002-9149(02)02434-7

Casadonte, R., Perticone, F., Costanzo, F., and Cuda, G. (2006). Betamyosin mutations and phenotypic heterogeneity in hypertrophic cardiomyopathy. *Int. J. Cardiol.* 110, 119–121. doi: 10.1016/j.ijcard.2005.05.069

Cecchi, G., Colomo, F., and Lombardi, V. (1981). Force-velocity relation in deuterium oxide-treated frog single muscle fibres during the rise of tension in an isometric tetanus. *J. Physiol. (Lond.)* 317, 207–221.

Chung, C. S., Hutchinson, K. R., Methawasin, M., Saripalli, C., Smith, J. E. 3rd, Hidalgo, C. G., et al. (2013). Shortening of the elastic tandem immunoglobulin segment of titin leads to diastolic dysfunction. *Circulation* 128, 19–28. doi: 10.1161/CIRCULATIONAHA.112.001268

Cilvik, S. N., Wang, J. I., Lavine, K. J., Uchida, K., Castro, A., Gierasch, C. M., et al. (2013). Fibroblast growth factor receptor 1 signaling in adult cardiomyocytes increases contractility and results in a hypertrophic cardiomyopathy. *PLoS ONE* 8:e82979. doi: 10.1371/journal.pone.0082979

Cooper, D. N., Krawczak, M., Polychronakos, C., Tyler-Smith, C., and Kehrer-Sawatzki, H. (2013). Where genotype is not predictive of phenotype: towards an understanding of the molecular basis of reduced penetrance in human inherited disease. *Hum. Genet.* 132, 1077–1130. doi: 10.1007/s00439-013-1331-2

Crilley, J. G., Boehm, E. A., Blair, E., Rajagopalan, B., Blamire, A. M., Styles, P., et al. (2003). Hypertrophic cardiomyopathy due to sarcomeric gene mutations is characterized by impaired energy metabolism irrespective of the degree of hypertrophy. *J. Am. Coll. Cardiol.* 41, 1776–1782. doi: 10.1016/S0735-1097(02)03009-7

Cuda, G., Fananapazir, L., Zhu, W. S., Sellers, J. R., and Epstein, N. D. (1993). Skeletal muscle expression and abnormal function of beta-myosin in hypertrophic cardiomyopathy. *J. Clin. Invest.* 91, 2861–2865. doi: 10.1172/JCI116530

Deacon, J. C., Bloemink, M. J., Rezavandi, H., Geeves, M. A., and Leinwand, L. A. (2012). Identification of functional differences between recombinant human alpha and beta cardiac myosin motors. *Cell. Mol. Life Sci.* 69, 2261–2277. doi: 10.1007/s00018-012-0927-3

Di Domenico, M., Casadonte, R., Ricci, P., Santini, M., Frati, G., Rizzo, A., et al. (2012). Cardiac and skeletal muscle expression of mutant beta-myosin heavy chains, degree of functional impairment and phenotypic heterogeneity in hypertrophic cardiomyopathy. *J. Cell. Physiol.* 227, 3471–3476. doi: 10.1002/jcp.24047

Edman, K. A. (2012). Residual force enhancement after stretch in striated muscle. A consequence of increased myofilament overlap? *J. Physiol.* 590, 1339–1345. doi: 10.1113/jphysiol.2011.222729

Edman, K. A., and Flitney, F. W. (1982). Laser diffraction studies of sarcomere dynamics during 'isometric' relaxation in isolated muscle fibres of the frog. *J. Physiol. (Lond.)* 329, 1–20.

Edman, K. A., Mansson, A., and Caputo, C. (1997). The biphasic force-velocity relationship in frog muscle fibres and its evaluation in terms of cross-bridge function [published erratum appears in J Physiol (Lond) 1997 Nov 1; 504(Pt 3):763]. *J. Physiol. (Lond.)* 503, 141–156. doi: 10.1111/j.1469-7793.1997.141bi.x

Edman, K. A., and Reggiani, C. (1984). Redistribution of sarcomere length during isometric contraction of frog muscle fibres and its relation to tension creep. *J. Physiol. (Lond).* 351, 169–198.

Edman, K. A., Reggiani, C., Schiaffino, S., and Te Kronnie, G. (1988). Maximum velocity of shortening related to myosin isoform composition in frog skeletal muscle fibres. *J. Physiol. (Lond).* 395, 679–694.

Edman, K. A., Reggiani, C., and Te Kronnie, G. (1985). Differences in maximum velocity of shortening along single muscle fibres of the frog. *J. Physiol. (Lond).* 365, 147–163.

Eisenberg, E., and Hill, T. L. (1978). A cross-bridge model of muscle contraction. *Prog. Biophys. Mol. Biol.* 33, 55–82. doi: 10.1016/0079-6107(79)90025-7

Fatkin, D., Christe, M. E., Aristizabal, O., McConnell, B. K., Srinivasan, S., Schoen, F. J., et al. (1999). Neonatal cardiomyopathy in mice homozygous for the Arg403Gln mutation in the alpha cardiac myosin heavy chain gene. *J. Clin. Invest.* 103, 147–153. doi: 10.1172/JCI4631

Ferrantini, C., Belus, A., Piroddi, N., Scellini, B., Tesi, C., and Poggesi, C. (2009). Mechanical and energetic consequences of HCM-causing mutations. *J. Cardiovasc. Transl. Res.* 2, 441–451. doi: 10.1007/s12265-009-9131-8

Forsey, J., Benson, L., Rozenblyum, E., Friedberg, M. K., and Mertens, L. (2013). Early changes in apical rotation in genotype positive children with hypertrophic cardiomyopathy mutations without hypertrophic changes on two-dimensional imaging. *J. Am. Soc. Echocardiogr.* 27, 215–221. doi: 10.1016/j.echo.2013.10.012

Frey, N., Brixius, K., Schwinger, R. H., Benis, T., Karpowski, A., Lorenzen, H. P., et al. (2006). Alterations of tension-dependent ATP utilization in a transgenic rat model of hypertrophic cardiomyopathy. *J. Biol. Chem.* 281, 29575–29582. doi: 10.1074/jbc.M507740200

Frey, N., Luedde, M., and Katus, H. A. (2012). Mechanisms of disease: hypertrophic cardiomyopathy. *Nat. Rev. Cardiol.* 9, 91–100. doi: 10.1038/nrcardio.2011.159

Geisterfer-Lowrance, A. A., Kass, S., Tanigawa, G., Vosberg, H. P., McKenna, W., Seidman, C. E., et al. (1990). A molecular basis for familial hypertrophic cardiomyopathy: a beta cardiac myosin heavy chain gene missense mutation. *Cell* 62, 999–1006. doi: 10.1016/0092-8674(90)90274-I

Germans, T., Wilde, A. A., Dijkmans, P. A., Chai, W., Kamp, O., Pinto, Y. M., et al. (2006). Structural abnormalities of the inferoseptal left ventricular wall detected by cardiac magnetic resonance imaging in carriers of hypertrophic cardiomyopathy mutations. *J. Am. Coll. Cardiol.* 48, 2518–2523. doi: 10.1016/j.jacc.2006.08.036

Ghio, S., Revera, M., Mori, F., Klersy, C., Raisaro, A., Raineri, C., et al. (2009). Regional abnormalities of myocardial deformation in patients with hypertrophic cardiomyopathy: correlations with delayed enhancement in cardiac magnetic resonance. *Eur. J. Heart Fail.* 11, 952–957. doi: 10.1093/eurjhf/hfp122

Gordon, A. M., Huxley, A. F., and Julian, F. J. (1966). The variation in isometric tension with sarcomere length in vertebrate muscle fibres. *J. Physiol. (Lond.)* 184, 170–192.

Greenberg, M. J., Kazmierczak, K., Szczesna-Cordary, D., and Moore, J. R. (2010). Cardiomyopathy-linked myosin regulatory light chain mutations disrupt myosin strain-dependent biochemistry. *Proc. Natl. Acad. Sci. U.S.A.* 107, 17403–17408. doi: 10.1073/pnas.1009619107

Harvey, P. A., and Leinwand, L. A. (2011). The cell biology of disease: cellular mechanisms of cardiomyopathy. *J. Cell Biol.* 194, 355–365. doi: 10.1083/jcb.201101100

Ho, C. Y., Lever, H. M., Desanctis, R., Farver, C. F., Seidman, J. G., and Seidman, C. E. (2000). Homozygous mutation in cardiac troponin T: implications for hypertrophic cardiomyopathy. *Circulation* 102, 1950–1955. doi: 10.1161/01.CIR.102.16.1950

Huxley, A. F. (1957). Muscle structure and theories of contraction. *Prog. Biophys. Biophys. Chem.* 7, 255–318.

Jiang, J., Wakimoto, H., Seidman, J. G., and Seidman, C. E. (2013). Allele-specific silencing of mutant Myh6 transcripts in mice suppresses hypertrophic cardiomyopathy. *Science* 342, 111–114. doi: 10.1126/science.1236921

Julian, F. J., and Morgan, D. L. (1979). Intersarcomere dynamics during fixed-end tetanic contractions of frog muscle fibres. *J. Physiol. (Lond.)* 293, 365–378.

Julicher, F., and Prost, J. (1995). Cooperative molecular motors. *Phys. Rev. Lett.* 75, 2618–2621. doi: 10.1103/PhysRevLett.75.2618

Jung, W. I., Sieverding, L., Breuer, J., Hoess, T., Widmaier, S., Schmidt, O., et al. (1998). 31P NMR spectroscopy detects metabolic abnormalities in asymptomatic patients with hypertrophic cardiomyopathy. *Circulation* 97, 2536–2542. doi: 10.1161/01.CIR.97.25.2536

Kirschner, S. E., Becker, E., Antognozzi, M., Kubis, H. P., Francino, A., Navarro-Lopez, F., et al. (2005). Hypertrophic cardiomyopathy-related beta-myosin mutations cause highly variable calcium sensitivity with functional imbalances among individual muscle cells. *Am. J. Physiol. Heart Circ. Physiol.* 288, H1242–H1251. doi: 10.1152/ajpheart.00686.2004

Kohler, J., Chen, Y., Brenner, B., Gordon, A. M., Kraft, T., Martyn, D. A., et al. (2003). Familial hypertrophic cardiomyopathy mutations in troponin I (K183D, G203S, K206Q) enhance filament sliding. *Physiol. Genomics* 14, 117–128. doi: 10.1152/physiolgenomics.00101.2002

Laing, N. G. (2007). Congenital myopathies. *Curr. Opin. Neurol.* 20, 583–589. doi: 10.1097/WCO.0b013e3282ef6e69

Laing, N. G., and Nowak, K. J. (2005a). When contractile proteins go bad: the sarcomere and skeletal muscle disease. *Bioessays* 27, 809–822. doi: 10.1002/bies.20269

Laing, N. G., and Nowak, K. J. (2005b). When contractile proteins go bad: the sarcomere and skeletal muscle disease. *Bioessays* 27, 809–822. doi: 10.1002/bies.20269

Lijnen, P., and Petrov, V. (1999). Renin-angiotensin system, hypertrophy and gene expression in cardiac myocytes. *J. Mol. Cell. Cardiol.* 31, 949–970. doi: 10.1006/jmcc.1999.0934

Lim, D. S., Lutucuta, S., Bachireddy, P., Youker, K., Evans, A., Entman, M., et al. (2001). Angiotensin II blockade reverses myocardial fibrosis in a transgenic mouse model of human hypertrophic cardiomyopathy. *Circulation* 103, 789–791. doi: 10.1161/01.CIR.103.6.789

Linke, W. A., and Kruger, M. (2010). The giant protein titin as an integrator of myocyte signaling pathways. *Physiology* 25, 186–198. doi: 10.1152/physiol.00005.2010

Lombardi, V., and Piazzesi, G. (1990). The contractile response during steady lengthening of stimulated frog muscle fibres. *J. Physiol. (Lond.)* 431, 141–171.

Lovelock, J. D., Monasky, M. M., Jeong, E. M., Lardin, H. A., Liu, H., Patel, B. G., et al. (2012). Ranolazine improves cardiac diastolic dysfunction through modulation of myofilament calcium sensitivity. *Circ. Res.* 110, 841–850. doi: 10.1161/CIRCRESAHA.111.258251

Lowey, S., Bretton, V., Gulick, J., Robbins, J., and Trybus, K. M. (2013). Transgenic mouse alpha- and beta-cardiac myosins containing the R403Q mutation show isoform-dependent transient kinetic differences. *J. Biol. Chem.* 288, 14780–14787. doi: 10.1074/jbc.M113.450668

Lowey, S., Lesko, L. M., Rovner, A. S., Hodges, A. R., White, S. L., Low, R. B., et al. (2008). Functional effects of the hypertrophic cardiomyopathy R403Q mutation are different in an alpha- or beta-myosin heavy chain backbone. *J. Biol. Chem.* 283, 20579–20589. doi: 10.1074/jbc.M800554200

Luedde, M., Flogel, U., Knorr, M., Grundt, C., Hippe, H. J., Brors, B., et al. (2009). Decreased contractility due to energy deprivation in a transgenic rat model of hypertrophic cardiomyopathy. *J. Mol. Med.* 87, 411–422. doi: 10.1007/s00109-008-0436-x

Luo, R., Li, X., Wang, Y., Li, Y., Deng, Y., Wan, Y., et al. (2013). The influence of Angiotensin converting enzyme and angiotensinogen gene polymorphisms on hypertrophic cardiomyopathy. *PLoS ONE* 8:e77030. doi: 10.1371/journal.pone.0077030

Luther, P. K. (2009). The vertebrate muscle Z-disc: sarcomere anchor for structure and signalling. *J. Muscle Res. Cell Motil.* 30, 171–185. doi: 10.1007/s10974-009-9189-6

Macpherson, P. C., Dennis, R. G., and Faulkner, J. A. (1997). Sarcomere dynamics and contraction-induced injury to maximally activated single muscle fibres from soleus muscles of rats. *J. Physiol. (Lond).* 500(Pt 2), 523–533.

Mansson, A. (2010). Actomyosin-ADP states, inter-head cooperativity and the force-velocity relation of skeletal muscle. *Biophys. J.* 98, 1237–1246. doi: 10.1016/j.bpj.2009.12.4285

Maron, M. S., Maron, B. J., Harrigan, C., Buros, J., Gibson, C. M., Olivotto, I., et al. (2009). Hypertrophic cardiomyopathy phenotype revisited after 50 years with cardiovascular magnetic resonance. *J. Am. Coll. Cardiol.* 54, 220–228. doi: 10.1016/j.jacc.2009.05.006

Marston, S. B. (2011). How do mutations in contractile proteins cause the primary familial cardiomyopathies? *J. Cardiovasc. Transl. Res.* 4, 245–255. doi: 10.1007/s12265-011-9266-2

Marston, S., Memo, M., Messer, A., Papadaki, M., Nowak, K., McNamara, E., et al. (2013). Mutations in repeating structural motifs of tropomyosin cause gain of function in skeletal muscle myopathy patients. *Hum. Mol. Genet.* 22, 4978–4987. doi: 10.1093/hmg/ddt345

Martinsson, T., Oldfors, A., Darin, N., Berg, K., Tajsharghi, H., Kyllerman, M., et al. (2000). Autosomal dominant myopathy: missense mutation (Glu-706 --> Lys) in the myosin heavy chain IIa gene. *Proc. Natl. Acad. Sci. U.S.A.* 97, 14614–14619. doi: 10.1073/pnas.250289597

Mateja, R. D., and De Tombe, P. P. (2012). Myofilament length-dependent activation develops within 5 ms in guinea-pig myocardium. *Biophys. J.* 103, L13–L15. doi: 10.1016/j.bpj.2012.05.034

McDonald, K. S., Hanft, L. M., Domeier, T. L., and Emter, C. A. (2012). Length and PKA dependence of force generation and loaded shortening in porcine cardiac myocytes. *Biochem. Res. Int.* 2012:371415. doi: 10.1155/2012/371415

Memo, M., and Marston, S. (2013). Skeletal muscle myopathy mutations at the actin tropomyosin interface that cause gain- or loss-of-function. *J. Muscle Res. Cell Motil.* 34, 165–169. doi: 10.1007/s10974-013-9344-y

Moore, J. R., Leinwand, L., and Warshaw, D. M. (2012). Understanding cardiomyopathy phenotypes based on the functional impact of mutations in the myosin motor. *Circ. Res.* 111, 375–385. doi: 10.1161/CIRCRESAHA.110.223842

Nagakura, T., Takeuchi, M., Yoshitani, H., Nakai, H., Nishikage, T., Kokumai, M., et al. (2007). Hypertrophic cardiomyopathy is associated with more severe

left ventricular dyssynchrony than is hypertensive left ventricular hypertrophy. *Echocardiography* 24, 677–684. doi: 10.1111/j.1540-8175.2007.00458.x

Nanni, L., Pieroni, M., Chimenti, C., Simionati, B., Zimbello, R., Maseri, A., et al. (2003). Hypertrophic cardiomyopathy: two homozygous cases with "typical" hypertrophic cardiomyopathy and three new mutations in cases with progression to dilated cardiomyopathy. *Biochem. Biophys. Res. Commun.* 309, 391–398. doi: 10.1016/j.bbrc.2003.08.014

Ochala, J. (2008). Thin filament proteins mutations associated with skeletal myopathies: defective regulation of muscle contraction. *J. Mol. Med.* 86, 1197–1204. doi: 10.1007/s00109-008-0380-9

Ochala, J., Gokhin, D. S., Penisson-Besnier, I., Quijano-Roy, S., Monnier, N., Lunardi, J., et al. (2012). Congenital myopathy-causing tropomyosin mutations induce thin filament dysfunction via distinct physiological mechanisms. *Hum. Mol. Genet.* 21, 4473–4485. doi: 10.1093/hmg/dds289

Oldfors, A. (2007). Hereditary myosin myopathies. *Neuromuscul. Disord.* 17, 355–367. doi: 10.1016/j.nmd.2007.02.008

Olivotto, I., Cecchi, F., Poggesi, C., and Yacoub, M. H. (2009). Developmental origins of hypertrophic cardiomyopathy phenotypes: a unifying hypothesis. *Nat. Rev. Cardiol* 6, 317–321. doi: 10.1038/nrcardio.2009.9

Ottenheijm, C. A., Van Hees, H. W., Heunks, L. M., and Granzier, H. (2011). Titin-based mechanosensing and signaling: role in diaphragm atrophy during unloading? *Am. J. Physiol. Lung Cell Mol. Physiol.* 300, L161–L166. doi: 10.1152/ajplung.00288.2010

Persson, M., Bengtsson, E., Ten Siethoff, L., and Mansson, A. (2013). Nonlinear cross-bridge elasticity and post-power-stroke events in fast skeletal muscle actomyosin. *Biophys. J.* 105, 1871–1881. doi: 10.1016/j.bpj.2013.08.044

Poggesi, C., Tesi, C., and Stehle, R. (2005). Sarcomeric determinants of striated muscle relaxation kinetics. *Pflugers Arch.* 449, 505–517. doi: 10.1007/s00424-004-1363-5

Raskin, A., Lange, S., Banares, K., Lyon, R. C., Zieseniss, A., Lee, L. K., et al. (2012). A novel mechanism involving four-and-a-half LIM domain protein-1 and extracellular signal-regulated kinase-2 regulates titin phosphorylation and mechanics. *J. Biol. Chem.* 287, 29273–29284. doi: 10.1074/jbc.M112.372839

Rassier, D. E. (2012). The mechanisms of the residual force enhancement after stretch of skeletal muscle: non-uniformity in half-sarcomeres and stiffness of titin. *Proc. Biol. Sci.* 279, 2705–2713. doi: 10.1098/rspb.2012.0467

Richard, P., Charron, P., Leclercq, C., Ledeuil, C., Carrier, L., Dubourg, O., et al. (2000). Homozygotes for a R869G mutation in the beta -myosin heavy chain gene have a severe form of familial hypertrophic cardiomyopathy. *J. Mol. Cell. Cardiol.* 32, 1575–1583. doi: 10.1006/jmcc.2000.1193

Robinson, P., Lipscomb, S., Preston, L. C., Altin, E., Watkins, H., Ashley, C. C., et al. (2007). Mutations in fast skeletal troponin I, troponin T, and beta-tropomyosin that cause distal arthrogryposis all increase contractile function. *FASEB J.* 21, 896–905. doi: 10.1096/fj.06-6899com

Rodriguez, A. G., Rodriguez, M. L., Han, S. J., Sniadecki, N. J., and Regnier, M. (2013). Enhanced contractility with 2-deoxy-ATP and EMD 57033 is correlated with reduced myofibril structure and twitch power in neonatal cardiomyocytes. *Integr. Biol.* 5, 1366–1373. doi: 10.1039/c3ib40135a

Roig, M., O'Brien, K., Kirk, G., Murray, R., McKinnon, P., Shadgan, B., et al. (2009). The effects of eccentric versus concentric resistance training on muscle strength and mass in healthy adults: a systematic review with meta-analysis. *Br. J. Sports Med.* 43, 556–568. doi: 10.1136/bjsm.2008.051417

Rosser, B. W. C., and Bandman, E. (2003). Heterogeneity of protein expression within muscle fibers. *J. Anim. Sci.* 81, E94–E101.

Sequeira, V., Wijnker, P. J., Nijenkamp, L. L., Kuster, D. W., Najafi, A., Witjas-Paalberends, E. R., et al. (2013). Perturbed length-dependent activation in human hypertrophic cardiomyopathy with missense sarcomeric gene mutations. *Circ. Res.* 112, 1491–1505. doi: 10.1161/CIRCRESAHA.111.300436

Sommese, R. F., Nag, S., Sutton, S., Miller, S. M., Spudich, J. A., and Ruppel, K. M. (2013a). Effects of troponin T cardiomyopathy mutations on the calcium sensitivity of the regulated thin filament and the actomyosin cross-bridge kinetics of human beta-cardiac myosin. *PLoS ONE* 8:e83403. doi: 10.1371/journal.pone.0083403

Sommese, R. F., Sung, J., Nag, S., Sutton, S., Deacon, J. C., Choe, E., et al. (2013b). Molecular consequences of the R453C hypertrophic cardiomyopathy mutation on human beta-cardiac myosin motor function. *Proc. Natl. Acad. Sci. U.S.A.* 110, 12607–12612. doi: 10.1073/pnas.1309493110

Spudich, J. A. (2014). Hypertrophic and dilated cardiomyopathy: four decades of basic research on muscle lead to potential therapeutic approaches to these devastating genetic diseases. *Biophys. J.* 106, 1236–1249. doi: 10.1016/j.bpj.2014.02.011

Stehle, R., Kruger, M., and Pfitzer, G. (2002). Force kinetics and individual sarcomere dynamics in cardiac myofibrils after rapid ca(2+) changes. *Biophys. J.* 83, 2152–2161. doi: 10.1016/S0006-3495(02)73975-1

Sweeney, H. L., Feng, H. S., Yang, Z., and Watkins, H. (1998). Functional analyses of troponin T mutations that cause hypertrophic cardiomyopathy: insights into disease pathogenesis and troponin function. *Proc. Natl. Acad. Sci. U.S.A.* 95, 14406–14410. doi: 10.1073/pnas.95.24.14406

Tajsharghi, H., and Oldfors, A. (2013). Myosinopathies: pathology and mechanisms. *Acta Neuropathol.* 125, 3–18. doi: 10.1007/s00401-012-1024-2

Teekakirikul, P., Padera, R. F., Seidman, J. G., and Seidman, C. E. (2012). Hypertrophic cardiomyopathy: translating cellular cross talk into therapeutics. *J. Cell Biol.* 199, 417–421. doi: 10.1083/jcb.201207033

Tripathi, S., Schultz, I., Becker, E., Montag, J., Borchert, B., Francino, A., et al. (2011). Unequal allelic expression of wild-type and mutated beta-myosin in familial hypertrophic cardiomyopathy. *Basic Res. Cardiol.* 106, 1041–1055. doi: 10.1007/s00395-011-0205-9

Vilfan, A., and Frey, E. (2005). Oscillations in molecular motor assemblies. *J. Phys. Condens. Matter* 17, S3901–S3911. doi: 10.1088/0953-8984/17/47/018

Vilfan, A., Frey, E., and Schwabl, F. (1999). Force-velocity relations of a two-state crossbridge model for molecular motors. *Europhys. Lett.* 45, 283–289. doi: 10.1209/epl/i1999-00160-3

Wallgren-Pettersson, C., Sewry, C. A., Nowak, K. J., and Laing, N. G. (2011). Nemaline myopathies. *Semin. Pediatr. Neurol.* 18, 230–238. doi: 10.1016/j.spen.2011.10.004

Wang, Q., Moncman, C. L., and Winkelmann, D. A. (2003). Mutations in the motor domain modulate myosin activity and myofibril organization. *J. Cell Sci.* 116, 4227–4238. doi: 10.1242/jcs.00709

Weeks, K. L., and McMullen, J. R. (2011). The athlete's heart vs. the failing heart: can signaling explain the two distinct outcomes? *Physiology* 26, 97–105. doi: 10.1152/physiol.00043.2010

Witjas-Paalberends, E. R., Piroddi, N., Stam, K., Van Dijk, S. J., Oliviera, V. S., Ferrara, C., et al. (2013). Mutations in MYH7 reduce the force generating capacity of sarcomeres in human familial hypertrophic cardiomyopathy. *Cardiovasc. Res.* 99, 432–441. doi: 10.1093/cvr/cvt119

Xu, Q., Dewey, S., Nguyen, S., and Gomes, A. V. (2010). Malignant and benign mutations in familial cardiomyopathies: insights into mutations linked to complex cardiovascular phenotypes. *J. Mol. Cell. Cardiol.* 48, 899–909. doi: 10.1016/j.yjmcc.2010.03.005

Yiu, K. H., Atsma, D. E., Delgado, V., Ng, A. C., Witkowski, T. G., Ewe, S. H., et al. (2012). Myocardial structural alteration and systolic dysfunction in preclinical hypertrophic cardiomyopathy mutation carriers. *PLoS ONE* 7:e36115. doi: 10.1371/journal.pone.0036115

Zou, Y., Akazawa, H., Qin, Y., Sano, M., Takano, H., Minamino, T., et al. (2004). Mechanical stress activates angiotensin II type 1 receptor without the involvement of angiotensin II. *Nat. Cell Biol.* 6, 499–506. doi: 10.1038/ncb1137

Conflict of Interest Statement: The author declares that the research was conducted in the absence of any commercial or financial relationships that could be construed as a potential conflict of interest.

Received: 13 June 2014; accepted: 26 August 2014; published online: 15 September 2014.

*Citation: Månsson A (2014) Hypothesis and theory: mechanical instabilities and non-uniformities in hereditary sarcomere myopathies. Front. Physiol. **5**:350. doi: 10.3389/fphys.2014.00350*

This article was submitted to Striated Muscle Physiology, a section of the journal Frontiers in Physiology.

Copyright © 2014 Månsson. This is an open-access article distributed under the terms of the Creative Commons Attribution License (CC BY). The use, distribution or reproduction in other forums is permitted, provided the original author(s) or licensor are credited and that the original publication in this journal is cited, in accordance with accepted academic practice. No use, distribution or reproduction is permitted which does not comply with these terms.

frontiers in PHYSIOLOGY

ORIGINAL RESEARCH ARTICLE
published: 20 November 2014
doi: 10.3389/fphys.2014.00449

Acute exercise modifies titin phosphorylation and increases cardiac myofilament stiffness

Anna E. Müller[1†], Matthias Kreiner[1†], Sebastian Kötter[1†], Philipp Lassak[1], Wilhelm Bloch[2], Frank Suhr[2]* and Martina Krüger[1]*

[1] Department of Cardiovascular Physiology, Heinrich Heine University Düsseldorf, Düsseldorf, Germany
[2] Department of Molecular and Cellular Sport Medicine, Institute of Cardiovascular Research and Sport Medicine, German Sport University Cologne, Cologne, Germany

Edited by:
Julien Ochala, King's College London, UK

Reviewed by:
Henk Granzier, University of Arizona, USA
Marion Lewis Greaser, University of Wisconsin-Madison, USA

***Correspondence:**
Martina Krüger, Department of Cardiovascular Physiology, Heinrich Heine University Düsseldorf, Universitätsstr. 1, 22.03 U1, D- 40225 Düsseldorf, Germany
e-mail: martina.krueger@uni-duesseldorf.de;
Frank Suhr, Department of Molecular and Cellular Sport Medicine, Institute of Cardiovascular Research and Sport Medicine, Am Sportpark Muengersdorf 6, building I, 9th floor, Köln, Germany
e-mail: suhr@dshs-koeln.de

† These authors have contributed equally to this work.

Titin-based myofilament stiffness is largely modulated by phosphorylation of its elastic I-band regions N2-Bus (decreases passive stiffness, PT) and PEVK (increases PT). Here, we tested the hypothesis that acute exercise changes titin phosphorylation and modifies myofilament stiffness. Adult rats were exercised on a treadmill for 15 min, untrained animals served as controls. Titin phosphorylation was determined by Western blot analysis using phosphospecific antibodies to Ser4099 and Ser4010 in the N2-Bus region (PKG and PKA-dependent. respectively), and to Ser11878 and Ser 12022 in the PEVK region (PKCα and CaMKIIδ-dependent, respectively). Passive tension was determined by step-wise stretching of isolated skinned cardiomyocytes to sarcomere length (SL) ranging from 1.9 to 2.4 μm and showed a significantly increased PT from exercised samples, compared to controls. In cardiac samples titin N2-Bus phosphorylation was significantly decreased by 40% at Ser4099, however, no significant changes were observed at Ser4010. PEVK phosphorylation at Ser11878 was significantly increased, which is probably mediated by the observed exercise-induced increase in PKCα activity. Interestingly, relative phosphorylation of Ser12022 was substantially decreased in the exercised samples. Surprisingly, in skeletal samples from acutely exercised animals we detected a significant decrease in PEVK phosphorylation at Ser11878 and an increase in Ser12022 phosphorylation; however, PKCα activity remained unchanged. In summary, our data show that a single exercise bout of 15 min affects titin domain phosphorylation and titin-based myocyte stiffness with obviously divergent effects in cardiac and skeletal muscle tissues. The observed changes in titin stiffness could play an important role in adapting the passive and active properties of the myocardium and the skeletal muscle to increased physical activity.

Keywords: passive tension, cardiac muscle, connectin, skeletal muscle, posttranslational modification, exercise

INTRODUCTION

The beneficial effect of regular physical activity on the cardiovascular system has been generally accepted. Not only in healthy humans, but particularly in the setting of cardiovascular diseases, such as heart failure (HF), regular exercise training has been shown to improve cardiac outcome (reviewed in Leosco et al., 2013). HF or impaired cardiovascular reserves in aging subjects are often associated with cardiac β-adrenergic receptor (β-AR) dysfunction and over-activity of the sympathetic nervous system (SNS) (Bristow et al., 1986). According to the current hypotheses regular exercise at least partly restores the normal SNS activity and thereby improves cardiac function (Leosco et al., 2013). In aged subjects this exercise-induced improvement has been shown to be mediated by an enhanced left ventricular inotropic response to Ca^{2+} (Ehsani et al., 1991; Spina et al., 1998).

Recent evidence suggests that changes in the passive titin-based myofilament stiffness may also contribute to the beneficial effects of physical training. Titin stiffness is closely associated with ventricular function and it has been shown that increased titin compliance improves diastolic function (reviewed in Linke and Hamdani, 2014). In contrast, titin stiffening may support the length-dependent activation involved in the Frank Starling mechanism of the heart, which is responsible for the elevated cardiac output in response to increased preload (Methawasin et al., 2014).

The giant protein titin is expressed in all striated muscles and is encoded by a single titin gene. Differential splicing of this gene is the basis for numerous species- and muscle-specific titin isoforms with molecular weights ranging from 3.0 to 3.7 MDa allowing the protein to span a half sarcomere from the Z-disc to the M-line. Due to its gigantic size, its central position in the sarcomere and its elastic I-band domains titin is a scaffold protein important for sarcomere assembly, and serves as a molecular spring that defines myofilament distensibility (for review see Krüger and Linke, 2011). Skeletal muscles express an isoform type called N2A titin (3.3–3.7 MDa) with

many muscle-specific splice variants (Freiburg et al., 2000; Prado et al., 2005). In mammalian heart titin is expressed as two main isoform types: the shorter and stiffer N2B isoform (3.0 MDa), and longer and more compliant N2BA isoforms (3.2–3.7 MDa). Titin-based passive myofilament stiffness is largely determined by the expression ratio of the N2BA and N2B titin isoforms (Cazorla et al., 2000). In rat heart the short N2B isoform predominates with approximately 90% of total titin, whereas in healthy human heart the expression ratio is about 40% N2BA:60% N2B. In comparison, the different isoform composition results in stiffer myofilaments in rat hearts compared to human hearts (Krüger and Linke, 2011). More dynamically titin stiffness is modulated via posttranslational modification of the elastic I-band regions N2-B and PEVK. To date, more than 28 phosphorylation sites within these regions have been identified by *in vitro* kinase assays or mass spectrometry (Linke and Hamdani, 2014). Among the characterized phosphorylation motifs are Ser4010 (targeted by PKA and ERK1/2) and Ser4099 (targeted by PKG) in the N2-Bus (Krüger et al., 2009; Raskin et al., 2012), and Ser11878 and Ser12022 (targeted by PKCα and CaMKIIδ) in the PEVK region (Hidalgo et al., 2009; Hamdani et al., 2013). Importantly, phosphorylation of the cardiac specific N2-Bus by cAMP- and cGMP-dependent protein kinases PKA and PKG (Yamasaki et al., 2002; Krüger and Linke, 2006; Krüger et al., 2009), and Ca^{2+}/calmodulin-dependent protein kinase II δ (CaMKIIδ) decreases titin-based passive myofilament stiffness (Hamdani et al., 2013), whereas phosphorylation of the PEVK domain by Ca^{2+}-dependent protein kinase alpha (PKCα) increases it (Hidalgo et al., 2009).

Changes in titin phosphorylation are a critical hallmark of many cardiac diseases (Linke and Hamdani, 2014), and physical exercise is a promising tool to improve cardiac performance (Brenner et al., 2001; Malfatto et al., 2009). This raises the hypothesis that exercise might alter titin properties. In a recent study performed on cardiac tissue from adult mice exercised for a period of 3 weeks significant changes in the posttranslational modification of the two titin domains N2-Bus and PEVK (Hidalgo et al., 2014) were detected. These changes suggest an exercise-induced increase in cardiac titin compliance, which may help diastolic filling and thereby improve cardiac output in the trained animals. In contrast, the changes in titin modification detected in trained skeletal muscles suggest an increase in titin stiffness, which may help to maintain the structural integrity of the exercised muscle tissue (Hidalgo et al., 2014).

To understand titin's posttranslational modifications induced by exercise training, it is important to study titin properties and biochemistry after acute exercise as a stimulus that activates related signaling pathways. In our present study we therefore investigated effects of a single acute exercise bout on posttranslational modification of titin in cardiac as well as skeletal muscle, and made a first attempt to relate the observed changes to altered protein kinase activation. Our results indicate that acute exercise has different effects on titin stiffness than regular exercise, as it rapidly increases titin-based myofilament stiffness and may therefore support the positive inotropic response of the heart to the elevated physical activity.

MATERIALS AND METHODS

ANIMALS AND EXERCISE REGIME

Rats were exercised as previously described (Hamann et al., 2013, 2014). Briefly, adult female Sprague Dawley rats were exercised using a treadmill (20 m/min) for a single 15 min level running bout. The group tested for eccentric downhill exercise conducted the running bout on a treadmill with an angle of −20°. All animals were euthanized directly after finishing the training bout. The control groups were not exercised. Muscle samples were dissected from the left ventricle of the heart and the Musculus vastus lateralis (LAT). Samples were deep-frozen in liquid nitrogen immediately after preparation and stored at −80°C until use. Previous tests from our group confirmed that this procedure effectively preserves the phosphorylation status of titin. We tested cardiac tissue samples from 6 control animals and 3 level running animals of the exercised group. For the skeletal muscle samples, 10 control and 6 level running LAT tissue samples were obtained from both groups. All animal experiments were in accordance with the institutional and the national guidelines and regulations. The experimental procedures were approved by the local animal health and care unit.

ISOLATION OF RAT CARDIOMYOCYTES AND PASSIVE FORCE MEASUREMENTS

For isolation of single rat cardiomyocytes, small samples (3–6 mg) were obtained from the left ventricular muscle strips and transferred into relaxing solution (7.8 mM ATP, 20 mM creatine phosphate, 20 mM imidazole, 4 mM EGTA, 12 mM Mg-propionate, 97.6 mM K-propionate, pH 7.0, freshly supplemented with 30 mM 2,3-butanedione monoxime (BDM), 1 mM dithiothreitol (DTT), 1:100 Protease Inhibitor Cocktail (P8340, Sigma), and 1:200 Phosphatase Inhibitor Cocktail (P0044, Sigma). Samples were then repeatedly homogenized with an ultrathurrax at 750 rpm. The myocyte suspension was then centrifuged with 1000 rpm for 3 min., resuspended and permeabilized for 3 min in the relaxing solution additionally supplemented with 3% Triton-X-100. Myocytes were washed in 3–5 centrifugation steps at 4°C and 2000 rpm using relaxing solution. After each centrifugation step the supernatant was discarded and the myocyte pellet was resuspended in fresh relaxing solution without Triton-X-100. The final myocyte suspension was kept on ice until further experimental use.

For passive force measurements a few microliters of the cardiomyocyte suspension were transferred to a cover slip mounted on an inverse phase contrast microscope (Nicon eclipse Ti). One single cell was selected and fixed between a piezoelectric motor and a force transducer (403A, Aurora Scientific) both covered with a mixture (ratio 2:1) of silicone glues (Dow Corning Glue 3140 and 3145-transparent). Cells were then stretched from slack SL (average, 1.9 μm) in five steps to a maximum sarcomere length (SL) of 2.4 μm. In between the stretches a 5 s holding period was performed to wait for stress relaxation. Following the last stretch-hold, cardiomyocytes were released back to slack SL to test for possible shifts of baseline force. During the stretch protocol SL was recorded using an IMPERX (CCD) camera (Aurora Scientific). From the recordings we analyzed the force at the end of each hold period (near steady-state force). Passive forces of

each cell were calculated considering their individual length and depth at initial SL before tightening.

SODIUM DODECYL SULFATE POLYACRYLAMIDE GEL ELECTROPHORESIS (SDS-PAGE)

For titin analyses cardiac and skeletal muscle tissue was homogenized in modified Laemmli buffer (Warren et al., 2003) and proteins were separated by agarose-strengthened 2.1% SDS PAGE as previously described (Opitz et al., 2004; Kötter et al., 2013). Similar protein concentrations were used for each sample and protein bands were visualized by Coomassie stain. The gels were scanned using a Fusion SOLO imager (Vilber) and analyzed densitometrically with Multi Gauge V3.2 software. Average titin-isoform composition was calculated from a minimum of $n = 3$ bands per experimental condition. For PKCα expression level analysis, tissue samples were homogenized in modified Laemmli buffer. Standard 10 and 12.5% SDS-PAGE gels were performed according to standard protocols (Krüger et al., 2009).

WESTERN BLOT ANALYSIS AND PHOSPHOSPECIFIC ANTIBODIES

Titin isoforms were separated by agarose-strengthened 2.1% SDS-PAGE, and were analyzed using two different protein concentrations (15 and 20 μg). Proteins were then transferred onto a PVDF-membrane by semi-dry Western blot technique using the Biorad turbo blot system (1.5A for 25 min with 20 V). Transfer efficiency was checked using Coomassie-based PVDF-stain, and only membranes showing good transfer of titin were used for further analysis. Titin phosphorylation status was tested using phospho-site directed antibodies generated for pSer4010 (VRIEEGKpSLRFPC) and pSer4099 (QANLFpSEWLRNID) in the titin N2-Bus region (peptide nomenclature refers to human cardiac titin; UniProtKB: Q8WZ42), and pSer11878 (CEVVLKpSVLRKR) and pSer12022 (KLRPGpSGGEKP) in the PEVK-region. Antibodies to pSer 4010, pSer4099, and Ser11878 had been generated by Eurogentech (Belgium) as previously described (Kötter et al., 2013). Antibodies to pSer12022 were kindly provided by Henk Granzier (University of Arizona) (Hudson et al., 2011). Incubation of primary antibodies was performed overnight at 4°C for primary and for 2 h at room temperature for secondary antibodies. Goat anti-rabbit IgG conjugated with horseradish peroxidase served as secondary antibody. Signal intensity was analyzed densitometrically (Multi Gauge V3.2 and ImageJ). To detect differences in titin phosphorylation levels we determined, for each sample, the signal intensity of phospho-titin and total-titin. The ratio of phospho:total titin was then used to normalize the phosphorylation status of exercised heart samples to that of untrained controls.

For phospho-PKCα and phospho-Phospholamban analysis, proteins were separated by 10 and 15% SDS-PAGE. Similar protein concentrations were used for each sample and a pre-stained protein ladder (Page Ruler # 26616 from Thermo Scientific) was used as a size standard. Proteins were then transferred onto a PVDF-membrane by semi-dry Western blot technique using the Biorad turbo blot system (1.3A for 7 min with 20V). To determine the expression levels antibodies were used against Phospho-PKCα (phospho-T497, Abcam), (Total-) PKCα (Cell Signaling Technology) and Phospho-Phospholamban (phospho-S16, Badrilla). Mouse and anti-rabbit IgG conjugated with horseradish peroxidase served as secondary antibody. All antibodies were diluted in standard TBST solution supplemented with 0.5–3% BSA or 0.5–3% milk powder. Signal intensity was analyzed densitometrically with ImageJ software. The signal intensity for phosphospecific PKCα or Phospholamban-signal was related to the respective PKCα-total or GAPDH-signal. Afterwards the ratio of phospho:total/GAPDH was used to normalize the status of phosphorylation of exercised muscle samples to the control samples.

DATA ANALYSIS

Unpaired Student's *t*-test and Mann-Whitney *U*-test was used to test for statistically significant differences. *P*-values <0.05 and $P_{(\text{exact})} \leq 0.001$ were taken as an indication of significant differences and, if not noted otherwise, are represented in figures by asterisks.

RESULTS

EXERCISE ACUTELY CHANGES CARDIAC TITIN PHOSPHORYLATION

In order to characterize the effects of acute physical exercise on cardiac passive myofilament stiffness we determined the I-band phosphorylation status of titin using phosphosite-directed antibodies to Ser4010 (PKA-targeted) and Ser4099 (PKG-targeted) in the cardiac-specific N2-Bus region, and to Ser11878 and Ser12022 (PKCα and CaMKIIδ-targeted) in the ubiquitously expressed part of the PEVK region.

As indicated by the large standard errors phosphorylation of residue Ser4010 in the N2-Bus differed largely among the analyzed exercise samples, and with a mean relative phosphorylation of 1.26 ± 0.72 compared to the control group the observed changes were not statistically significantly different (**Figure 1A**). In contrast, relative phosphorylation of Ser4099 in the N2-Bus was significantly reduced in the cardiac tissue of exercised animals to 0.59 ± 0.03 of the control levels (**Figure 1B**).

We further tested for changes in phosphorylation at Ser11878 and Ser12022 in the PEVK region of titin. The Western blot analyses demonstrated that relative phosphorylation of Ser11878 was significantly increased in the exercised samples to 2.15 ± 0.16 compared to control samples, whereas relative phosphorylation of Ser12022 was significantly decreased to 0.62 ± 0.04 of the control levels (**Figures 1C,D**).

EXERCISE INCREASES PASSIVE CARDIAC MYOFILAMENT STIFFNESS

To determine the effects of altered titin phosphorylation on the passive properties of the cardiac myofilaments we mechanically isolated single cardiomyocytes and measured PT in relation to SL. For this purpose, cardiomyocytes were stretched in five steps to SLs ranging from 1.9 to 2.4 μm and passive forces were recorded for each step. The results demonstrate that PT was significantly higher in cardiomyocytes isolated from acutely exercised animals, compared to controls (**Figure 2A**). PT was increased 2.78 ± 0.35-fold at SL = 2.0 μm, 1.91 ± 0.10-fold at SL = 2.2 μm, and 1.62 ± 0.17-fold at SL = 2.4 μm compared to cardiomyocytes isolated from sedentary control animals (**Figure 2B**).

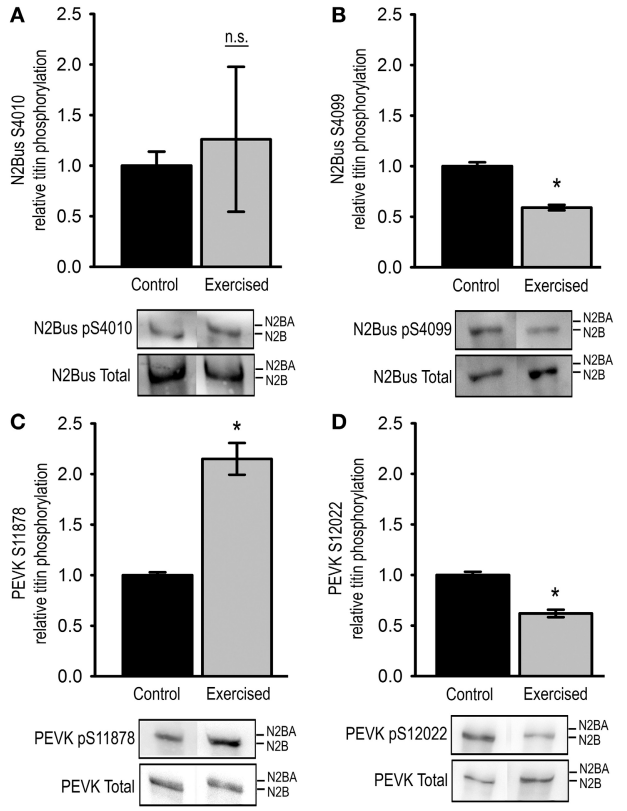

FIGURE 1 | Titin phosphorylation in cardiac tissue from exercised (Exercised, $n = 7$) and sedentary (Control, $n = 7$) animals. Bar graphs show statistical data from Western blot analysis using antibodies recognizing **(A)** pSer4010, **(B)** pSer4099, **(C)** pSer11878, or **(D)** pSer12022. Representative images of the Western blots are shown in the lower panel. Graphs show mean ± s.e.m. of a minimum of 3 individual experiments per sample. Asterisks indicate statistically significant differences ($P < 0.05$ in Student's *t*-test and Mann–Whitney *U*-test $P_{(exact)} = <0.001$, n.s. not significant).

EXERCISE ACUTELY MODIFIES SKELETAL TITIN PHOSPHORYLATION

We further investigated the effects of a single exercise bout on skeletal titin phosphorylation by analyzing the relative phosphorylation of Ser11878 and Ser12022 in the PEVK region of titin from the Musculus vastus lateralis (LAT). In order to determine putative differences in the response to concentric and eccentric exercise we analyzed LAT samples from animals after acute level and downhill running, respectively. Interestingly, unlike in cardiac tissue, Western blot analysis of the level-exercised skeletal muscles showed that the relative titin phosphorylation at Ser11878 was significantly reduced to 0.13 ± 0.02 compared to sedentary controls (**Figure 3A**). At the same time relative phosphorylation of Ser12022 was significantly increased to 1.84 ± 0.06 of the control levels (**Figure 3B**). Similar results were obtained from LAT muscles of downhill-exercised animals, in which relative titin phosphorylation at Ser11878 was also significantly reduced to 0.21 ± 0.08 (**Figure 3C**), whereas relative titin phosphorylation at Ser12022 was not significantly changed (**Figure 3D**).

EXERCISE INCREASES PKCα PHOSPHORYLATION AT THr497 IN CARDIAC BUT NOT IN SKELETAL MUSCLE

It has previously been shown that threonine 497 (Thr497) is a critical site for permissive activation of protein kinase Cα (Cazaubon et al., 1994). In a first attempt to investigate the signaling cascades responsible for increased titin PEVK phosphorylation after acute exercise we tested for changes in PKCα activity by determining the relative phosphorylation of Thr497 in cardiac and skeletal samples from exercised and non-exercised animals.

In cardiac tissue relative Thr497 phosphorylation significantly increased 3.23 ± 0.43-fold in exercised animals compared to sedentary controls (**Figure 4A**). To test for exercise-induced activation of PKA we determined the relative PKA-mediated phosphorylation of phospholamban (PLB) at position Ser16 using Western blot, and thereby detected a significantly increased activity of PKA in the exercised samples compared to sedentary controls (**Figure 4B**).

In skeletal muscle tissue relative phosphorylation of Thr497 was not significantly changed with a relative Thr497 phosphorylation of 1.29 ± 0.10 in LAT muscles after level running exercise, and 1.24 ± 0.09 in LAT muscles after downhill exercise compared to sedentary controls (**Figures 4C,D**).

DISCUSSION

In our present study we investigated the effects of an acute exercise bout on titin-based myofilament stiffness in cardiac and skeletal muscle tissue from adult rats. The main finding of our study is the observation that in cardiac tissue 15 min. of treadmill running induces a significant increase in passive myocyte tension. Western blot analyses of cardiac samples from acutely exercised rats suggest that this increase is mainly caused by altered titin modification. Our analysis revealed a significant decrease in the relative phosphorylation of residue Ser4099 (PKG-targeted) in the cardiac-specific N2-Bus region, and a significantly increased phosphorylation of residue Ser11878 (PKCα-targeted) in the PEVK-region of titin. Decreased N2-Bus phosphorylation as well as increased PEVK phosphorylation have previously been shown to increase titin-based myofilament stiffness (Hidalgo et al., 2009; Krüger et al., 2009; Kötter et al., 2013). The increased phosphorylation of Ser11878 in response to acute exercise is probably due to a substantial activation of PKCα, indicated by an increased phosphorylation of Thr497 in the activation loop of the kinase (Cazaubon et al., 1994). In this respect, our findings are in accordance with previous reports demonstrating that acute exercise increased cardiac total phospho-PKC epsilon (pSer729), PKC alpha (pSer657) and PKC delta (pThr507) levels (Carson and Korzick, 2003). To date it has been demonstrated that PKCα targets the PEVK-region of titin at Ser11878 and Ser12022 (Hidalgo et al., 2009). Interestingly, in the cardiac samples from exercised animals we observed a significantly lower phosphorylation level of Ser12022 compared to sedentary controls, which is in contrast to the concomitantly observed increase in PKCα activation. However, previous studies suggested that based on differences in the amino acid composition around the PKC phosphorylation motifs within the PEVK region PKCα has a lower affinity to Ser12022 than to Ser11878 (Hidalgo et al., 2009). Since the expression levels of PKCα were not changed within the 15 min.

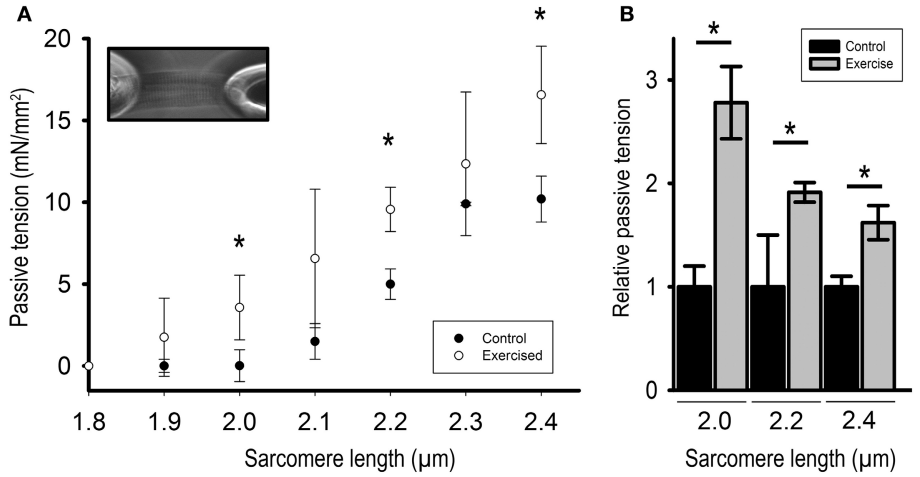

FIGURE 2 | Passive tension of isolated cardiomyocytes from exercised (Exercised, $n = 7$) and sedentary (Control, $n = 7$) animals in relation to sarcomere length. (A) Force extension curve showing passive tension (mN/mm²) of exercised compared to control cardiomyocytes. Inset: Image of a single cardiomyocyte fixed between a silicon-coated force transducer and a piezo-controlled length driver. **(B)** Bar graphs highlight the statistically significant differences in passive tension at sarcomere lengths (SL) 2.0, 2.2, and 2.4 μm. Graphs show mean ± s.e.m. of a minimum of 3 individual experiments per sample. Asterisks indicate statistically significant differences (* $P < 0.05$ in Student's *t*-test and Mann–Whitney *U*-test $P_{(exact)} = <0.001$).

exercise bout the increased activity may be sufficient to increase the phosphorylation status of the high-affinity site Ser11878, but not that of the lower-affinity site Ser12022 (Hidalgo et al., 2014).

Importantly, Ser12022 has also been shown to be targeted by CaMKIIδ, whereas CaMKIIδ-induced phosphorylation of Ser11878 is still under debate (Hamdani et al., 2013; Hidalgo et al., 2013). Hence, the adverse phosphorylation status of the two phosphorylation sites in the PEVK-region may be caused by differences in PKCα as well as CaMKIIδ activity. Nonetheless, PT of single cardiomyocytes was increased in acutely exercised compared to sedentary animals. We therefore assume that the detected decrease in Ser12022 phosphorylation seems to be overruled by the altered titin modification at Ser11878 and at Ser4099 in the N2-Bus region, which is targeted by PKG (Kötter et al., 2013). The reduced phosphorylation of Ser4099 suggests an exercise-induced decrease in ventricular PKG-activity. However, data on cardiac PKG activity in response to acute exercise are not available to date.

It is generally accepted (in humans) that acute exercise is accompanied by activation of the beta-adrenergic system, followed by activation of cAMP-dependent protein kinase A (PKA) (Chasiotis, 1983; Leosco et al., 2013). We therefore determined titin phosphorylation at position Ser4010 in the N2-Bus, which is targeted by PKA (Kötter et al., 2013). Interestingly, relative phosphorylation of this site varied substantially among the analyzed samples and therefore remained statistically unchanged by the 15 min. level exercise bout. To test for exercise-induced activation of PKA we determined the relative PKA-mediated phosphorylation of PLB at position Ser16, and thereby confirmed a significantly increased activity of PKA in the exercised samples compared to sedentary controls. Apparently, under the conditions investigated in our study, this increase does not influence phosphorylation of the PKA-sensitive site Ser4010.

Titin stiffness is closely associated with ventricular function and it is generally accepted that increased titin compliance improves diastolic function (reviewed in Linke and Hamdani, 2014). However, increased titin stiffness may support the length-dependent activation involved in the Frank Starling Mechanism of cardiac muscle (Methawasin et al., 2014), and thus contribute to improved cardiac output in response to acute exercise. To address the question of titin's phosphorylation state in the heart after chronic training, Hidalgo et al. (2014) investigated titin phosphorylation at Ser11878 and Ser12022 in animals trained for a period of 3 weeks and showed significantly decreased Ser12022 phosphorylation, while the phosphorylation of Ser11878 remained unchanged. Based on their results the authors concluded that chronic exercise lowers titin-based stiffness through altered PEVK phosphorylation at Ser12022 and thus improve diastolic function of chronically trained hearts. These data are in contrast to our findings, as we demonstrate acute exercise to increase PEVK-Ser11878 phosphorylation, but to lower PEVK-Ser12022 phosphorylation pointing to increased titin stiffness. Overall, the present results and those from Hidalgo et al. (2014) rise the hypothesis that acute and chronic exercise interventions determine critically different titin phosphorylation states and thus PT in cardiac muscles.

Beside cardiac titin regulation after acute exercise we also focused on skeletal muscle titin regulation in dependence on the primary muscle contraction mode (concentric vs. eccentric). This question is of great interest, since mechanical strains differ between concentric and eccentric muscle work with the consequence of muscle damage specifically after eccentric muscle contractions (Armstrong et al., 1983; Fridén et al., 1984; Fridén and Lieber, 1992). In this context it is known that eccentric exercise has no influence on titin isoform composition in skeletal muscle (Ochi et al., 2007). But surprisingly and due to its central role as an intrasarcomeric mechanosensor in skeletal muscles (Ottenheijm et al., 2011), titin's posttranslational modifications in the PEVK region have never been studied after these

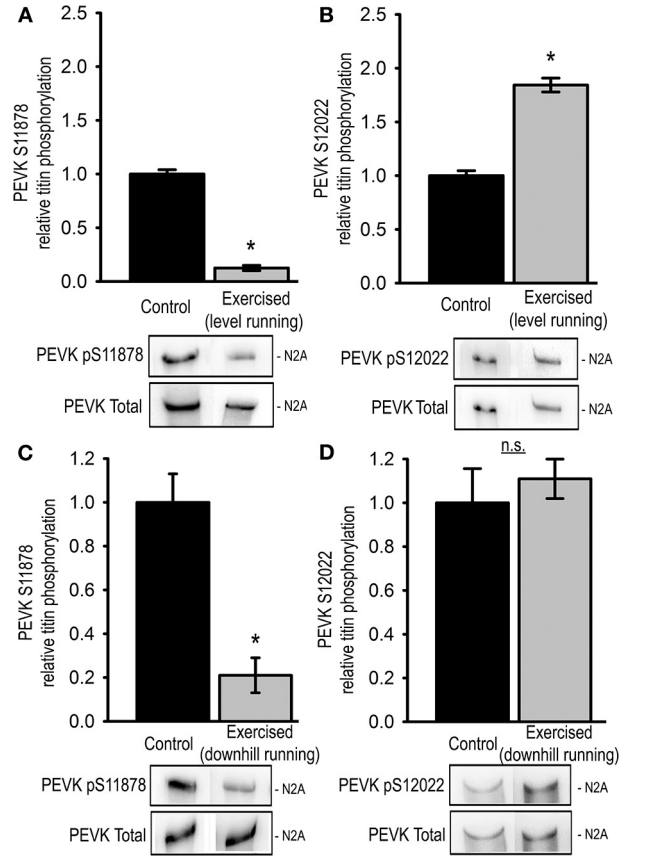

FIGURE 3 | Exercise-induced changes in skeletal muscle (musculus vastus lateralis) titin phosphorylation. Bar graphs show statistical data from Western blot analysis from level exercised (Exercised, level running, $n = 7$) and sedentary (Control, $n = 7$) animals using antibodies recognizing **(A)** pSer11878 or **(B)** pSer12022 and from downhill exercised (Exercised, downhill running, $n = 5$) and sedentary (Control, $n = 5$) animals using antibodies recognizing **(C)** pSer11878 or **(D)** pSer12022 in the PEVK region of titin. Bar graphs show mean ± s.e.m. of a minimum of 3 individual experiments per sample. Asterisks indicate statistically significant differences (*$P < 0.05$ in Student's *t*-test and Mann–Whitney *U*-test $P_{(exact)} = <0.001$).

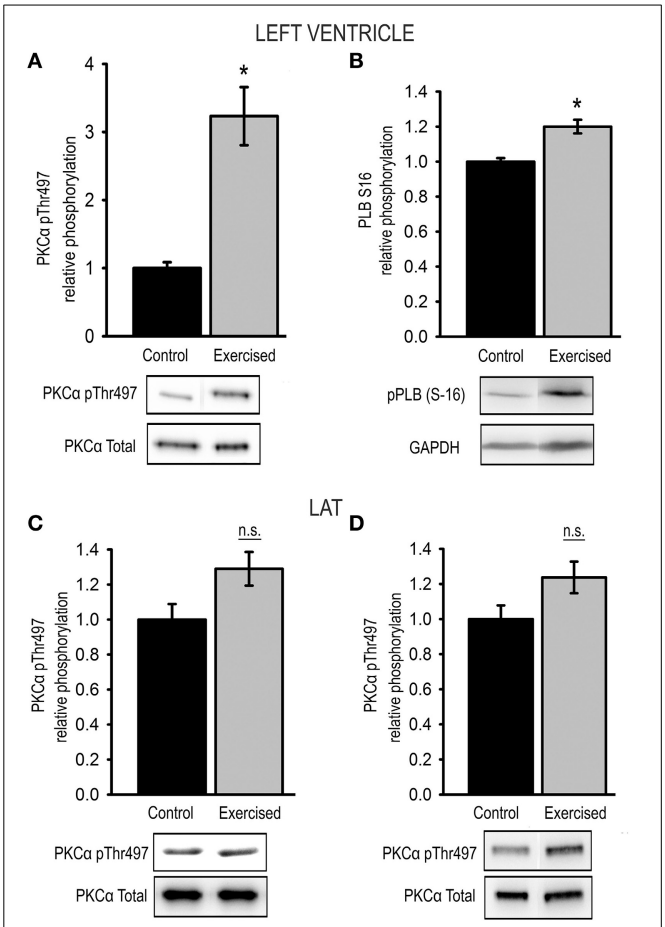

FIGURE 4 | Exercise-induced changes in kinase activity. Relative phosphorylation of **(A)** PKCα at Thr497 and **(B)** of the PKA-target phospholamban (pPLB S16) in cardiac muscle tissue from sedentary (control) and exercised (exercised) animals. Relative phosphorylation of PKCα at Thr497 in skeletal LAT muscle tissue from animals after **(C)** level exercise (level running) and **(D)** eccentric downhill exercise (downhill running) compared to sedentary controls (control). Bar graphs show mean ± s.e.m. of a minimum of 3 individual experiments, representative images of the Western blots are shown in the lower panel. Asterisks indicate statistically significant differences (*$P < 0.05$ in Student's *t*-test and Mann–Whitney *U*-test $P_{(exact)} = <0.001$, n.s., not significant).

two dominant contraction modes. Therefore, we addressed this question and found that both acute concentric and acute eccentric muscle contractions induce similar titin posttranslational modifications, specifically decreased Ser11878 levels in the PEVK region. PKCα activation at Thr497 was unchanged in both concentrically and eccentrically exercised animals compared to sedentary controls. This finding is in contrast to previous reports demonstrating that in skeletal muscle acute exercise bouts increase PKC activity within few minutes after onset of exercise (Rose et al., 2004). However, like in cardiac titin, Ser12022 in skeletal muscle can be phosphorylated also by CaMKIIδ, whose activity had previously been demonstrated to be increased in skeletal muscles upon acute exercise (Rose and Hargreaves, 2003). Therefore, the substantial increase in skeletal muscle titin phosphorylation at Ser12022 after acute running could possibly arise from altered CaMKIIδ activity in the LAT samples. We presume that compared to cardiac tissue the reduced relative phosphorylation of one serine residue (here Ser11878) is likely overruled by the substantial increase in the relative phosphorylation of another serine residue (here Ser12022), and will result in an overall increase in titin-based myofilament stiffness of exercised skeletal muscle tissue. It was surprising to find that, although they induce divergent mechanical strains, acute concentric and eccentric muscle contractions induce similar titin phosphorylation pattern. These data underline that central signaling pathways, such as PKCα, may similarly be regulated by both contraction modes.

An interesting and central finding of our study is that acute exercise induces divergent titin posttranslational modification patterns in cardiac and skeletal muscle tissues. While acute exercise increases titin PEVK phosphorylation at Ser11878 in

cardiac muscle, the same intervention results in decreased titin PEVK Ser11878 phosphorylation in skeletal muscle. Opposite effects in cardiac and skeletal muscle could also be detected for titin PEVK Ser12022 phosphorylation. This result could indicate that cardiac and skeletal muscles sense exercise-induced mechanical stress by means of intrasarcomeric proteins, e.g., titin, in a different manner. Our data provide the first direct comparison between cardiac and skeletal muscle titin phosphorylation after a single exercise stimulation. Nonetheless these finding has to be proven by further studies to get a clear picture about titin's regulation in different striated muscle tissues.

We conclude from these observations that acute exercise results in stiffer cardiomyocytes accompanied by increased titin PEVK phosphorylation. For skeletal muscle we postulate that the lowered PEVK phosphorylation leads to a decrease in titin based stiffness. According to this hypothesis, acute exercise induces divergent effects on titin posttranslational modifications and thus myocytes mechanical properties. Considering that the titin spring is a central regulator of the A-band position in the contracting sarcomere, the observed differences in titin stiffness between cardiac and skeletal muscles could be important to maintain their structural integrity, especially of the acutely exercised skeletal muscles For cardiac muscle, our data lead to the assumption that a single exercise bout induces rapid changes in titin-based myofilament stiffness, which may help to improve cardiac output by supporting the Frank-Starling mechanism, possibly crucial for cardiac functions during exercising conditions.

ACKNOWLEDGMENTS

The authors thank Sabine Bongardt for her excellent technical assistance. This work was supported by the Deutsche Forschungsgemeinschaft (DFG) (Kr 3409/5-1 to Martina Krüger), and by the research committee of the Medical Faculty of the University of Düsseldorf (grant no. 9772494 to Martina Krüger, and student fellowship to Philipp Lassak).

REFERENCES

Armstrong, R. B., Ogilvie, R. W., and Schwane, J. A. (1983). Eccentric exercise-induced injury to rat skeletal muscle. *J. Appl. Physiol. Respir. Environ. Exerc. Physiol*. 54, 80–93.

Brenner, D. A., Apstein, C. S., and Saupe, K. W. (2001). Exercise training attenuates age-associated diastolic dysfunction in rats. *Circulation* 104, 221–226. doi: 10.1161/01.CIR.104.2.221

Bristow, M. R., Ginsberg, R., Umans, V., Fowler, M., Minobe, W., Rasmussen, R., et al. (1986). β1- and β2-Adrenergic receptor subpopulations in nonfailing and failing human ventricular myocardium: coupling of both receptor subtypes to muscle contraction and selective b1 receptor down-regulation in heart failure. *Circ. Res.* 59, 297–309. doi: 10.1161/01.RES.59.3.297

Carson, L. D., and Korzick, D. H. (2003). Dose-dependent effects of acute exercise on PKC levels in rat heart: is PKC the heart's prophylactic? *Acta Physiol. Scand*. 178, 97–106. doi: 10.1046/j.1365-201X.2003.01131.x

Cazaubon, S., Bornancin, F., and Parker, P. J. (1994). Threonine-497 is a critical site for permissive activation of protein kinase C alpha. *Biochem. J.* 301, 443–448.

Cazorla, O., Freiburg, A., Helmes, M., Centner, T., McNabb, M., Wu, Y., et al. (2000). Differential expression of cardiac titin isoforms and modulation of cellular stiffness. *Circ. Res*. 86, 59–67. doi: 10.1161/01.RES.86.1.59

Chasiotis, D. (1983). The regulation of glycogen phosphorylase and glycogen breakdown in human skeletal muscle. *Acta Physiol. Scand. Suppl.* 518, 1–68.

Ehsani, A. A., Ogawa, T., Miller, T. R., Spina, R. J., and Jilka, S. M. (1991). Exercise training improves left ventricular systolic function in older men. *Circulation* 83, 96–103. doi: 10.1161/01.CIR.83.1.96

Freiburg, A., Trombitas, K., Hell, W., Cazorla, O., Fougerousse, F., Centner, T., et al. (2000). Series of exon-skipping events in the elastic spring region of titin as the structural basis for myofibrillar elastic diversity. *Circ. Res.* 86, 1114–1121. doi: 10.1161/01.RES.86.11.1114

Fridén, J., Kjorell, U., and Thornell, L.-E. (1984). Delayed muscle soreness and cytoskeletal alterations. An immunocytological study in man. *Int. J. Sports Med.* 5, 15–18. doi: 10.1055/s-2008-1025873

Fridén, J., and Lieber, R. L. (1992). The structural and mechanical basis of exercise-induced muscle injury *Med. Sci. Sport Exerc*. 24, 521–530.

Hamann, N., Zaucke, F., Dayakli, M., Brüggemann, G. P., and Niehoff, A. (2013). Growth-related structural, biochemical, and mechanical properties of the functional bone-cartilage unit. *J. Anat.* 222, 248–259. doi: 10.1111/joa.12003

Hamann, N., Zaucke, F., Heilig, J., Oberländer, K. D., Brüggemann, G. P., and Niehoff, A. (2014). Effect of different running modes on the morphological, biochemical, and mechanical properties of articular cartilage. *Scand. J. Med. Sci. Sports* 24, 179–188. doi: 10.1111/j.1600-0838.2012.01513.x

Hamdani, N., Krysiak, J., Kreusser, M. M., Neef, S., Dos Remedios, C. G., Maier, L. S., et al. (2013). Crucial role for Ca2(+)/calmodulindependent protein kinase-II in regulating diastolic stress of normal and failing hearts via titin phosphorylation. *Circ. Res*. 112, 664–674. doi: 10.1161/CIRCRESAHA.111.300105

Hidalgo, C. G., Chung, C. S., Saripalli, C., Methawasin, M., Hutchinson, K. R., Tsaprailis, G., et al. (2013). The multifunctional Ca(2+)/calmodulindependent protein kinase II delta (CaMKIIδ) phosphorylates cardiac titin's spring elements. *J. Mol. Cell. Cardiol*. 54, 90–97. doi: 10.1016/j.yjmcc.2012.11.012

Hidalgo, C., Hudson, B., Bogomolovas, J., Zhu, Y., Anderson, B., Greaser, M., et al. (2009). PKC phosphorylation of titin's PEVK element: a novel and conserved pathway for modulating myocardial stiffness. *Circ. Res*. 105, 631–638. doi: 10.1161/CIRCRESAHA.109.198465

Hidalgo, C., Saripalli, C., and Granzier, H. L. (2014). Effect of exercise training on post-translational and post-transcriptional regulation of titin stiffness in striated muscle of wild type and IG KO mice. *Arch. Biochem. Biophys*. 552, 553, 100–107. doi: 10.1016/j.abb.2014.02.010

Hudson, B., Hidalgo, C., Saripalli, C., and Granzier, H. (2011). Hyperphosphorylation of mouse cardiac titin contributes to transverse aortic constriction-induced diastolic dysfunction. *Circ. Res.* 109, 858–866. doi: 10.1161/CIRCRESAHA.111.246819

Kötter, S., Gout, L., von Frieling-Salewsky, M., Müller, A. E., Helling, S., Marcus, K., et al. (2013). Differential changes in titin domain phosphorylation increase myofilament stiffness in failing human hearts. *Cardiovasc. Res.* 99, 684–656. doi: 10.1093/cvr/cvt144

Krüger, M., Kötter, S., Grützner, A., Lang, P., Andresen, C., Redfield, M. M., et al. (2009). Protein kinase G modulates human myocardial passive stiffness by phosphorylation of the titin springs. *Circ. Res*. 104, 87–94. doi: 10.1161/CIRCRESAHA.108.184408

Krüger, M., and Linke, W. A. (2006). Protein kinase-A phosphorylates titin in human heart muscle and reduces myofibrillar passive tension. *J. Muscle Res. Cell Motil.* 27, 435–444. doi: 10.1007/s10974-006-9090-5

Krüger, M., and Linke, W. A. (2011). The giant protein titin: a regulatory node that integrates myocyte signalling pathways. *J. Biol. Chem.* 286, 9905–9912. doi: 10.1074/jbc.R110.173260

Leosco, D., Parisi, V., Femminella, G. D., Formisano, R., Petraglia, L., Allocca, E., et al. (2013). Effects of exercise training on cardiovascular adrenergic system. *Front. Physiol.* 4:348. doi: 10.3389/fphys.2013.00348

Linke, W. A., and Hamdani, N. (2014). Gigantic business: titin properties and function through thick and thin. *Circ. Res*. 114, 1052–1068. doi: 10.1161/CIRCRESAHA.114.301286

Malfatto, G., Branzi, G., Osculati, G., Valli, P., Cuoccio, P., Ciambellotti, F., et al. (2009). Improvement in left ventricular diastolic stiffness induced by physical training in patients with dilated cardiomyopathy. *J. Card. Fail.* 15, 327–333. doi: 10.1016/j.cardfail.2008.10.032

Methawasin, M., Hutchinson, K. R., Lee, E. J., Smith, J. E. 3rd., Saripalli, C., Hidalgo, C. G., et al. (2014). Experimentally increasing titin compliance in a novel mouse model attenuates the frank-starling mechanism but has a beneficial effect on diastole. *Circulation* 129, 1924–1936. doi: 10.1161/CIRCULATIONAHA.113.005610

Ochi, E., Nakazato, K., and Ishii, N. (2007). Effects of eccentric exercise on joint stiffness and muscle connectin (titin) isoform in the rat hindlimb. *J. Physiol. Sci*. 57, 1–6. doi: 10.2170/physiolsci.RP008806

Opitz, C. A., Leake, M. C., Makarenko, I., Benes, V., and Linke, W. A. (2004). Developmentally regulated switching of titin size alters myofibrillar stiffness in the perinatal heart. *Circ. Res.* 94, 967–975. doi: 10.1161/01.RES.0000124301.48193.E1

Ottenheijm, C. A., van Hees, H. W., Heunks, L. M., and Granzier, H. (2011). Titin-based mechanosensing and signaling: role in diaphragm atrophy during unloading? *Am. J. Physiol. Lung Cell. Mol. Physiol.* 300, L161–L166. doi: 10.1152/ajplung.00288.2010

Prado, L. G., Makarenko, I., Andresen, C., Krüger, M., Opitz, C. A., and Linke, W. A. (2005). Isoform diversity of giant proteins in relation to passive and active contractile properties of rabbit skeletal muscles. *J. Gen. Physiol.* 126, 461–480. doi: 10.1085/jgp.200509364

Raskin, A., Lange, S., Banares, K., Lyon, R. C., Zieseniss, A., Lee, L. K., et al. (2012). A novel mechanism involving four-and-a-half LIM domain protein-1 and extracellular signal-regulated kinase-2 regulates titin phosphorylation and mechanics. *J. Biol. Chem.* 287, 29273–29284. doi: 10.1074/jbc.M112.372839

Rose, A. J., and Hargreaves, M. (2003). Exercise increases Ca2+–calmodulin-dependent protein kinase II activity in human skeletal muscle. *J. Physiol.* 553, 303–309. doi: 10.1113/jphysiol.2003.054171

Rose, A. J., Michell, B. J., Kemp, B. E., and Hargreaves, M. (2004). Effect of exercise on protein kinase C activity and localization in human skeletal muscle. *J. Physiol.* 561, 861–870 doi: 10.1113/jphysiol.2004.075549

Spina, R. J., Turner,M. J., and Ehsani, A. A. (1998). Beta-adrenergic-mediated improvement in left ventricular function by exercise training in older men. *Am. J. Physiol.* 274, H397–H404.

Warren, C. M., Jordan, M. C., Roos, K. P., Krzesinski, P. R., and Greaser, M. L. (2003). Titin isoform expression in normal and hypertensive myocardium. *Cardiovasc. Res.* 59, 86–94. doi: 10.1016/S0008-6363(03)00328-6

Yamasaki, R., Wu, Y., McNabb, M., Greaser, M., Labeit, S., Granzier, H., et al. (2002). Protein kinase A phosphorylates titin's cardiac-specific N2B domain and reduces passive tension in rat cardiac myocytes. *Circ. Res.* 90, 1181–1188. doi: 10.1161/01.RES.0000021115.24712.99

Conflict of Interest Statement: The authors declare that the research was conducted in the absence of any commercial or financial relationships that could be construed as a potential conflict of interest.

Received: 20 June 2014; paper pending published: 20 July 2014; accepted: 03 November 2014; published online: 20 November 2014.

*Citation: Müller AE, Kreiner M, Kötter S, Lassak P, Bloch W, Suhr F and Krüger M (2014) Acute exercise modifies titin phosphorylation and increases cardiac myofilament stiffness. Front. Physiol. **5**:449. doi: 10.3389/fphys.2014.00449*

This article was submitted to Striated Muscle Physiology, a section of the journal Frontiers in Physiology.

Copyright © 2014 Müller, Kreiner, Kötter, Lassak, Bloch, Suhr and Krüger. This is an open-access article distributed under the terms of the Creative Commons Attribution License (CC BY). The use, distribution or reproduction in other forums is permitted, provided the original author(s) or licensor are credited and that the original publication in this journal is cited, in accordance with accepted academic practice. No use, distribution or reproduction is permitted which does not comply with these terms.

frontiers in PHYSIOLOGY

ORIGINAL RESEARCH ARTICLE
published: 02 December 2014
doi: 10.3389/fphys.2014.00461

Length-dependent changes in contractile dynamics are blunted due to cardiac myosin binding protein-C ablation

Ranganath Mamidi, Kenneth S. Gresham and Julian E. Stelzer*

Department of Physiology and Biophysics, School of Medicine, Case Western Reserve University, Cleveland, OH, USA

Edited by:
Julien Ochala, King's College London, UK

Reviewed by:
Corrado Poggesi, University of Florence, Italy
Brett Colson, University of Minnesota, USA

***Correspondence:**
Julian E. Stelzer, Department of Physiology and Biophysics, School of Medicine, Case Western Reserve University, 2109 Adelbert Rd, Robbins E522, Cleveland, OH 44106, USA
e-mail: julian.stelzer@case.edu

Enhanced cardiac contractile function with increased sarcomere length (SL) is, in part, mediated by a decrease in the radial distance between myosin heads and actin. The radial disposition of myosin heads relative to actin is modulated by cardiac myosin binding protein-C (cMyBP-C), suggesting that cMyBP-C contributes to the length-dependent activation (LDA) in the myocardium. However, the precise roles of cMyBP-C in modulating cardiac LDA are unclear. To determine the impact of cMyBP-C on LDA, we measured isometric force, myofilament Ca^{2+}-sensitivity (pCa_{50}) and length-dependent changes in kinetic parameters of cross-bridge (XB) relaxation (k_{rel}), and recruitment (k_{df}) due to rapid stretch, as well as the rate of force redevelopment (k_{tr}) in response to a large slack-restretch maneuver in skinned ventricular multicellular preparations isolated from the hearts of wild-type (WT) and cMyBP-C knockout (KO) mice, at SL's 1.9 μm or 2.1 μm. Our results show that maximal force was not significantly different between KO and WT preparations but length-dependent increase in pCa_{50} was attenuated in the KO preparations. pCa_{50} was not significantly different between WT and KO preparations at long SL (5.82 ± 0.02 in WT vs. 5.87 ± 0.02 in KO), whereas pCa_{50} was significantly different between WT and KO preparations at short SL (5.71 ± 0.02 in WT vs. 5.80 ± 0.01 in KO; $p < 0.05$). The k_{tr}, measured at half-maximal Ca^{2+}-activation, was significantly accelerated at short SL in WT preparations (8.74 ± 0.56 s^{-1} at 1.9 μm vs. 5.71 ± 0.40 s^{-1} at 2.1 μm, $p < 0.05$). Furthermore, k_{rel} and k_{df} were accelerated by 32% and 50%, respectively at short SL in WT preparations. In contrast, k_{tr} was not altered by changes in SL in KO preparations (8.03 ± 0.54 s^{-1} at 1.9 μm vs. 8.90 ± 0.37 s^{-1} at 2.1 μm). Similarly, KO preparations did not exhibit length-dependent changes in k_{rel} and k_{df}. Collectively, our data implicate cMyBP-C as an important regulator of LDA via its impact on dynamic XB behavior due to changes in SL.

Keywords: cMyBP-C, length-dependent activation, sarcomere length, myofilament function, cross-bridge kinetics

INTRODUCTION

Length-dependent activation (LDA) is the mechanism by which force production in the heart becomes more sensitive to Ca^{2+} as the sarcomere length (SL) is increased (Allen and Kentish, 1985). Although it is well recognized that LDA underlies the Frank-Starling's Law of the heart, the cellular and molecular mechanisms that modulate this process are still poorly understood mainly because LDA involves a dynamic and complex interplay between a multitude of thick- and thin-filament-based mechanisms (De Tombe et al., 2010). The thick-filament-based mechanisms involve augmentation of strong crossbridge (XB) formation followed by enhancement in the myofilament Ca^{2+} sensitivity upon a reduction in the myofilament lattice spacing and the radial distance between the thick and thin filaments at long SL (Fuchs and Smith, 2001). The strongly-bound XBs then cooperatively recruit additional near-neighbor XBs into the force-bearing state (Gordon et al., 2000; Regnier et al., 2004). The thin-filament-based mechanisms involve an increased affinity of troponin C (TnC) to Ca^{2+} when the neighboring TnC sites are bound with Ca^{2+} and the increased affinity of TnC to Ca^{2+} is also a result of a positive feedback effect of the strongly-bound XBs (Hannon et al., 1992; Moss et al., 2004; Li et al., 2014). Furthermore, the cooperative effect between neighboring troponin-tropomyosin (Tn-Tm) complexes also impacts the Ca^{2+} binding properties of the thin-filament (Butters et al., 1997; Farman et al., 2010) and thus influence the LDA in cardiac muscle (for details on LDA refer to reviews by Konhilas et al., 2002; Hanft et al., 2008; De Tombe et al., 2010; Campbell, 2011).

Earlier investigations have proposed that LDA in cardiac muscle is influenced by various sarcomeric proteins such as TnC (Gulati et al., 1991), TnI (Konhilas et al., 2003; Tachampa et al., 2007), TnT (Chandra et al., 2006), myosin heavy chain (Korte and McDonald, 2007), essential light chain (Michael et al., 2013), and titin (Fukuda et al., 2003). In addition to the aforementioned sarcomeric proteins, it is also possible that cardiac myosin binding protein-C (cMyBP-C) may be an important modulator of cardiac LDA because cMyBP-C is uniquely positioned in the sarcomere to interact with both the thick- and thin-filaments (Squire

et al., 2003; Shaffer et al., 2009; Previs et al., 2012; Sadayappan and De Tombe, 2012; Mun et al., 2014), and has been shown to be important in regulating key aspects of dynamic XB behavior (Stelzer et al., 2006a,b; Coulton and Stelzer, 2012), and providing structural rigidity to the myofilament lattice (Palmer et al., 2011).

Importantly, recent evidence from low-angle X-ray diffraction experiments showed that cMyBP-C tethers the myosin XBs closer to the thick-filament backbone and that ablation of cMyBP-C results in the radial displacement of XBs closer to the thin-filament (Colson et al., 2007). The role of cMyBP-C in LDA is also underscored by the observation that length-dependent increase in myofilament Ca^{2+} sensitivity was blunted in cardiac preparations from patients with cMyBP-C mutations (Van Dijk et al., 2012; Sequeira et al., 2013). However, the precise roles of cMyBP-C in modulating length-dependent changes in cardiac contractile dynamics are still unknown. Therefore, to determine the impact of cMyBP-C on length-dependent changes in contractile dynamics, we utilized skinned myocardium from a cMyBP-C knock-out (KO) mouse model (Harris et al., 2002), and measured steady-state contractile parameters and we also used stretch activation experiments to measure the kinetic parameters. We measured Ca^{2+}-activated maximal force, myofilament Ca^{2+} sensitivity (pCa_{50}), rate of force redevelopment (k_{tr}), rate of XB relaxation (k_{rel}), and rate of XB recruitment (k_{df}) at short (1.9 μm) and at long (2.1 μm) SL's. Our results show that the length-dependent increase in pCa_{50} was attenuated in the KO preparations compared to wild-type (WT) preparations. Furthermore, length-dependent changes in dynamic contractile parameters k_{tr}, k_{rel}, and k_{df} were blunted in KO preparations compared to WT preparations, indicating that cMyBP-C plays a critical role in the myofilament-mediated response in cardiac LDA.

MATERIALS AND METHODS

ETHICAL APPROVAL AND ANIMAL TREATMENT PROTOCOLS

This study was performed according to the protocols laid out in the *Guide for the Care and Use of Laboratory Animals* (NIH Publication No. 85–23, Revised 1996), and was conducted according to the guidelines of the Institutional Animal Care and Use Committee at Case Western Reserve University. Mice aged 3–6 months, of both sexes, and belonging to SV/129 strain were used for the experiments. KO mice used in this study were previously generated and well-characterized (Harris et al., 2002). WT mice expressing normal, full-length cMyBP-C in the myocardium were used as controls.

ESTIMATION OF cMyBP-C CONTENT AND PHOSPHORYLATION STATUS OF SARCOMERIC PROTEINS IN WT AND KO HEART SAMPLES

Cardiac myofibrils were isolated from frozen mouse ventricles on the day of the experiment (Gresham et al., 2014). A piece of the frozen tissue was thawed in a fresh relaxing solution, homogenized, and the myofibrils were then skinned for 15 min with 1% Triton X-100 (Cheng et al., 2013). Skinned myofibrils were then resuspended in fresh relaxing solution containing protease and phosphatase inhibitors (PhosSTOP and cOmplete ULTRA Tablets; Roche Applied Science, Indianapolis, IN, USA) and stored on ice. To determine the cMyBP-C content and myofilament protein phosphorylation status, ventricular samples were solubilized by adding Laemmli buffer and were heated to 90°C for 5 min. For Western blot analysis, 10 μg of cardiac myofibrils were electrophoretically separated on 4–20% Tris-glycine gels (Lonza Walkersville Inc., Rockland, ME, USA) at 180 V for 60 min. Proteins were transferred to PVDF membranes and incubated overnight with a primary antibody that detects cMyBP-C (Santa Cruz Biotechnology, Santa Cruz, CA, USA) as described previously (Cheng et al., 2013). For Pro-Q phosphoprotein analysis, 2.5 μg of solubilized cardiac myofibrils were electrophoretically separated at 180 V for 85 min then fixed and stained with Pro-Q diamond phosphoprotein stain (Invitrogen, Carlsbad, CA, USA) to assess the phosphorylation status of sarcomeric proteins. After imaging the Pro-Q stained gels, the gels were counterstained with Coomassie blue to determine if there are any changes in the isoform expression of sarcomeric proteins. Densitometric scanning of the stained gels was done using Image J software (U.S. National Institutes of Health, Bethesda, MD, USA) (Gresham et al., 2014).

PREPARATION OF SKINNED VENTRICULAR MULTICELLULAR PREPARATIONS AND Ca^{2+} SOLUTIONS FOR EXPERIMENTS

Skinned ventricular multicellular preparations were prepared as described previously (Cheng et al., 2013; Gresham et al., 2014). In brief, ventricular tissue was homogenized in a relaxing solution and skinned for 60 min using 1% Triton-X 100. Multicellular preparations with dimensions ∼100 μm in width and 400 μm in length were selected for the experiments. The composition of various Ca^{2+} activation solutions used for the experiments was calculated using a computer program (Fabiato, 1988) and known stability constants (Godt and Lindley, 1982). All solutions contained the following (in mM): 100 N, N-bis (2-hydroxyethyl)-2-aminoethanesulfonic acid (BES), 15 creatine phosphate, 5 dithiothreitol, 1 free Mg^{2+}, and 4 MgATP. The maximal activating solution (pCa 4.5; pCa = -log $[Ca^{2+}]_{free}$) also contained 7 EGTA and 7.01 $CaCl_2$; while the relaxing solution (pCa 9.0) contained 7 EGTA and 0.02 $CaCl_2$; and the pre-activating solution contained 0.07 EGTA. The pH of the Ca^{2+} solutions was set to 7.0 with KOH and the ionic strength was 180 mM. A range of pCa solutions, containing varying amounts of $[Ca^{2+}]_{free}$, were then prepared by mixing appropriate volumes of pCa 9.0 and 4.5 stock solutions and the experiments were performed at 22°C.

EXPERIMENTAL APPARATUS FOR THE ESTIMATION OF ISOMETRIC FORCE AND FORCE-pCA RELATIONSHIPS

Detergent-skinned ventricular preparations were held between a motor arm (312C; Aurora Scientific Inc., Aurora, Ontario, Canada) and a force transducer (403A; Aurora Scientific Inc.) as described previously (Merkulov et al., 2012; Cheng et al., 2013). Changes in the motor position and signals from the force transducer were sampled (16-bit resolution, DAP5216a, Microstar Laboratories; Bellevue, WA) at 2.0 kHz using SL control software (Campbell and Moss, 2003). As previously described (Stelzer et al., 2006a,b,c), the experimental set up was positioned on the stage of an inverted microscope (Olympus; Tokyo, Japan) that was fitted with a 40X objective and a closed-circuit television camera (model WV-BL600; Panasonic, Tokyo, Japan). To illuminate the multicellular preparations, we used the light emanating from

a halogen lamp and the light was passed through a cut-off filter (transmission >620 nm) before reaching the preparation. Bitmap images of the preparations were captured using an AGP 4X/2X graphics card and its associated software (ATI Technologies) to assess the SL of our preparations during the experiment. For all mechanical measurements, SL of the muscle preparations was set to 1.9 or 2.1 μm in a relaxing solution and submaximal force (P) developed at each pCa was normalized to maximal force (P_o, at pCa 4.5) i.e., P/P_o to construct the force-pCa relationships (Desjardins et al., 2012; Cheng et al., 2013). SL of the preparations was initially set using a high definition video camera and large video monitor, and was also assessed at the end of experiments to make sure that SL did not deviate from the initial SL following Ca^{2+}-activation. We chose this specific range of SL for our experiments because this range falls within the well-characterized working range (∼1.8–2.3 μm) of the sarcomeres in the heart muscle (Pollack and Huntsman, 1974; Rodriguez et al., 1992; Granzier and Irving, 1995; Hanft et al., 2008). The apparent cooperativity of force development was estimated from the steepness of a Hill plot transformation of the force-pCa relationships. The force-pCa data were fit using the equation $P/P_o = [Ca^{2+}]^{nH}/(k^{nH} + [Ca^{2+}]^{nH})$, where n_H is the Hill coefficient and k is the pCa required to produce half-maximal activation (i.e., pCa_{50}) (Gresham et al., 2014).

MEASUREMENT OF THE RATE OF FORCE REDEVELOPMENT (K_{tr})

k_{tr} was measured at 50% of maximal activation in WT and KO muscle preparations to assess the rate of XB transitions from weak- to strong-binding states (Brenner and Eisenberg, 1986; Campbell, 1997). Measurement of k_{tr} in Ca^{2+}-activated muscle preparations was performed according to a mechanical slack-restretch protocol described previously (Stelzer et al., 2006b; Chen et al., 2010; Cheng et al., 2013). Skinned muscle preparations were transferred from relaxing (pCa 9.0) to an activating Ca^{2+} solution (pCa ranging from 6.2 to 4.5), and once the muscle preparations attained steady-state isometric force, they were rapidly slackened by 20% of their original muscle length and were held for 10 ms using a high-speed length control device (Aurora Scientific Inc.). The slackening was followed by the brief period of unloaded shortening which resulted in a rapid decline in force due to detachment of the strongly-bound XBs. The muscle preparation was then rapidly restretched back to its original length and the time course of force redevelopment was measured. k_{tr} for each slack-restretch maneuver was estimated by linear transformation of the half-time of force redevelopment, i.e., $k_{tr} = 0.693/t_{1/2}$, as described previously (Chen et al., 2010; Cheng et al., 2013; Gresham et al., 2014).

STRETCH ACTIVATION EXPERIMENTS TO MEASURE DYNAMIC CONTRACTILE PARAMETERS

Stretch activation experiments were carried out as previously described (Cheng et al., 2013; Gresham et al., 2014), except that in this study a 2% stretch of initial muscle length perturbation was utilized. Muscle preparations were placed in pCa solutions that produced submaximal force (∼50% of maximal force), and were allowed to develop a steady-state force. Muscle preparations were then rapidly stretched by 2% of their initial muscle length and were held at the increased length for 5 s before being returned back to their initial muscle length. The characteristic features of the stretch activation response in cardiac muscle have been described previously (Stelzer et al., 2006d; Ford et al., 2010), and the stretch activation parameters measured are presented in **Figure 1**. In brief, a sudden 2% stretch of muscle length elicits an instantaneous rise in force (P1) in the muscle preparation, which is due to the strain of elastic elements within the strongly-bound XBs (Phase 1). The force then rapidly declines because the strained XBs rapidly detach (Phase 2) and equilibrate into a non-force producing state, with a characteristic rate constant k_{rel}. Following this phase of rapid decline, force development occurs gradually (Phase 3), with a characteristic rate constant k_{df}, which is a result of length-induced recruitment of new XBs into the force-bearing state (Stelzer et al., 2006d; Gresham et al., 2014). Stretch activation amplitudes were normalized to prestretch Ca^{2+}-activated force and were measured as described previously (Desjardins et al., 2012; Gresham et al., 2014). k_{rel} and k_{df} were estimated using a linear transformation of the half time of force decay and force redevelopment.

DATA ANALYSIS

Data were analyzed using Two-Way analysis of variance (ANOVA). One factor in this analysis was cMyBP-C variant (WT or KO), and the second was SL (1.9 or 2.1 μm). Therefore, we used Two-Way ANOVA to test the hypothesis that the effect of the SL on a given contractile parameter depended on the cMyBP-C

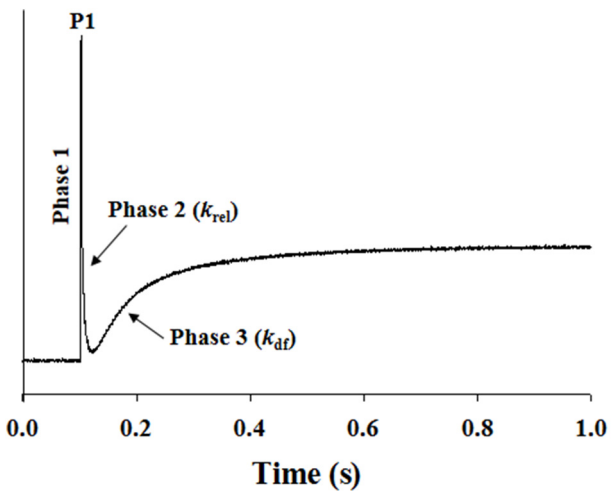

FIGURE 1 | Representative stretch activation response in a WT cardiac muscle preparation. Shown is a typical force response evoked by a sudden 2% stretch in muscle length (ML) in an isometrically-contracting WT muscle preparation set to a SL of 2.1 μm. Highlighted are the important phases of the force response and various stretch activation parameters that are derived from the response. Phase 1 represents the immediate increase in force in response to the sudden stretch in ML. P1 is the magnitude of the immediate force response and is measured from the pre-stretch isometric steady-state force to the peak of phase 1. Phase 2 represents the rapid decline in the force with a dynamic rate constant k_{rel}, an index of the XB detachment rate. Phase 3 represents the delayed force development with a dynamic rate constant k_{df}, an index of the XB recruitment rate (please see methods for additional details).

variant (interaction effect). When the interaction effect was significant, it showed that the effects of SL on various contractile parameters were different in the presence or absence of cMyBP-C. When the interaction effect was not significant, we interpreted the main effect due to cMyBP-C variant or SL. Planned multiple pairwise comparisons were made using Fisher's LSD method (Mamidi and Chandra, 2013; Mamidi et al., 2013a,b) to test the effects of cMyBP-C variant or SL on various contractile parameters. Values are reported as mean ± s.e.m. The criterion for statistical significance was set at $P < 0.05$. Asterisks in figures and tables represent statistical significance using *post-hoc* (Fisher's LSD) comparisons.

RESULTS

EFFECT OF ABLATION OF cMyBP-C ON THE EXPRESSION AND PHOSPHORYLATION LEVELS OF SARCOMERIC PROTEINS

Western blot analysis of WT and KO ventricular samples was done using a primary antibody that detects cMyBP-C protein (Cheng et al., 2013). As predicted, cMyBP-C is present in the WT sample but is completely absent in the KO sample (**Figure 2A**). SDS gels loaded with ventricular samples from WT and KO hearts were stained with Coomassie blue or Pro-Q Diamond stain to assess the effects of cMyBP-C KO on sarcomeric protein isoform expression and phosphorylation levels (**Figures 2B,C**, respectively). As reported in our recent studies (Desjardins et al., 2012; Merkulov et al., 2012) the KO hearts exhibited a slight increase (16 ± 3%) in the level of β-myosin heavy chain (MHC) expression (data not shown). Consistent with our previous studies (Desjardins et al., 2012; Merkulov et al., 2012), the expression and phosphorylation levels of other regulatory contractile sarcomeric proteins such as cardiac TnT, cardiac TnI, and regulatory light chain were not different between WT and KO skinned myocardium (**Figures 2B,C**).

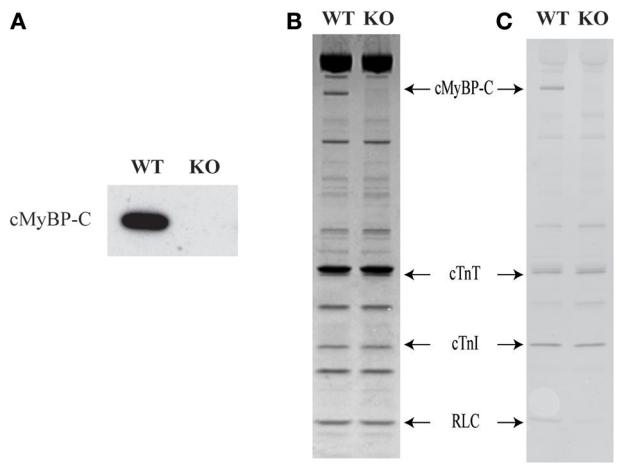

FIGURE 2 | Western blot, SDS-PAGE and Pro-Q analysis to assess the sarcomeric protein expression and phosphorylation levels in WT and KO hearts. Ventricular myofibrils from WT and KO hearts were run on a 4–20% tris-glycine gel. **(A)** Western blot showing the presence of cMyBP-C in WT but not in the KO heart sample. **(B)** Coomassie blue-stained SDS gel showing the complete absence of cMyBP-C in the KO hearts. **(C)** Pro-Q Diamond-stained SDS gel showing that there are no changes in the phosphorylation status of sarcomeric proteins between WT and KO samples. As expected, a Pro-Q band corresponding to cMyBP-C was absent in the lane containing KO sample. WT, wild-type; KO, knock-out; cMyBP-C, cardiac myosin binding protein-C; cTnT, cardiac troponin T; cTnI, cardiac troponin I; RLC, regulatory light chain.

EFFECT OF cMyBP-C ON LENGTH-DEPENDENT CHANGES IN Ca^{2+}-ACTIVATED MAXIMAL FORCE PRODUCTION

To assess the effect of cMyBP-C on length-dependent changes in thin-filament activation, Ca^{2+}-activated maximal force production (at pCa 4.5) was measured at SL's 1.9 and 2.1 μm in WT and KO muscle preparations (values are shown in **Table 1**). Two-Way ANOVA (see Data analysis under Methods section for details) revealed no significant interaction effect, but revealed a significant main effect ($P < 0.005$) of SL on Ca^{2+}-activated maximal force production. To probe the determining factor for the significant main effect, subsequent *post-hoc* tests were carried out. These *post-hoc* tests using multiple planned pairwise comparisons showed that maximal force production was not significantly different between WT and KO groups at either SL (**Table 1**). However, maximal force (F_{max}) was significantly decreased by ∼34% and ∼38% at short SL vs. long SL in WT and KO groups, respectively (**Table 1**). Similar trends were observed regarding the Ca^{2+}-independent forces measured at pCa 9.0 (F_{min}) in WT and KO groups (**Table 1**). Collectively, our results demonstrate that cMyBP-C does not impact the length-dependent changes in Ca^{2+}-activated maximal force and Ca^{2+}-independent force production.

EFFECT OF cMyBP-C ON LENGTH-DEPENDENT CHANGES IN MYOFILAMENT Ca^{2+} SENSITIVITY (pCa_{50}) AND COOPERATIVITY OF FORCE DEVELOPMENT (n_H)

The effect of cMyBP-C on length-dependent changes in pCa_{50} was assessed by plotting normalized force values against a range of pCa and constructing force-pCa relationships at SL's 1.9 and 2.1 μm in WT and KO groups. pCa_{50}, the pCa required to generate half-maximal force, was estimated by fitting the Hill equation to the force-pCa relationships (**Figures 3A,B**, **Table 1**). Two-Way

Table 1 | Steady-state mechanical properties of WT and KO ventricular multicellular preparations.

Group	F_{min} (mN/mm^2)	F_{max} (mN/mm^2)	n_H	pCa_{50}
SL 1.9 μm				
WT	0.82 ± 0.12*	17.29 ± 1.98*	3.41 ± 0.32*	5.71 ± 0.02*
KO	0.90 ± 0.13*	14.93 ± 1.56*	2.30 ± 0.08†	5.80 ± 0.01*†
SL 2.1 μm				
WT	2.14 ± 0.28	26.32 ± 2.93	2.47 ± 0.22	5.82 ± 0.02
KO	1.97 ± 0.25	23.98 ± 2.58	2.49 ± 0.23	5.87 ± 0.02

F_{min}: Ca^{2+}-independent force measured at pCa 9.0; F_{max}: maximal Ca^{2+}-activated force measured at pCa 4.5; n_H: Hill coefficient of the force-pCa relationship; pCa_{50}: pCa value required for the generation of half-maximal force. Values are expressed as mean ± s.e.m., from 7 to 17 multicellular preparations and 3 to 5 hearts per each group.

**Significantly different from the corresponding group at SL 2.1 μm; $P < 0.05$.*

† Significantly different from the corresponding WT group at SL 1.9 μm, $P < 0.05$.

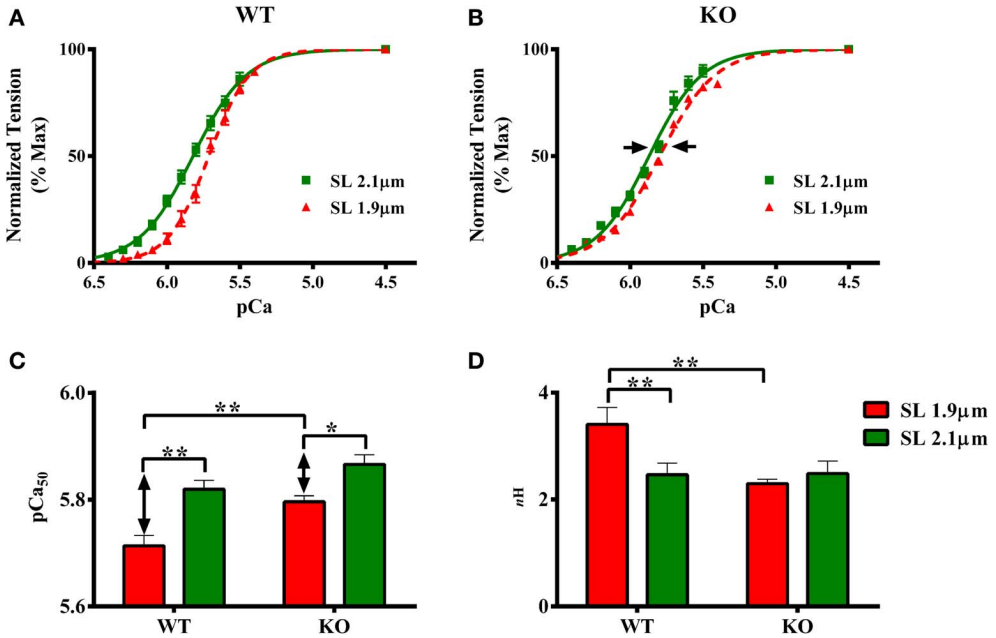

FIGURE 3 | Effect of cMyBP-C on length-dependent changes in myofilament Ca^{2+} sensitivity (pCa_{50}) and cooperativity of force production (n_H). Force-pCa relationships were constructed by plotting normalized forces generated at a range of pCa. The Hill equation was then fitted to force-pCa relationships to estimate pCa_{50} and n_H values in WT and KO groups at SL's 1.9 and 2.1 μm. **(A)** Effect of cMyBP-C on the force-pCa relationships in WT group at SL's 1.9 and 2.1 μm. **(B)** Effect of cMyBP-C on the force-pCa relationships in KO group at SL's 1.9 and 2.1 μm. **(C)** Effect of cMyBP-C on pCa_{50} in WT and KO groups at SL's 1.9 and 2.1 μm. **(D)** Effect of cMyBP-C on n_H in WT and KO groups at SL's 1.9 and 2.1 μm. Two-Way ANOVA revealed no significant interaction effect, but revealed significant main effects of SL ($P < 0.005$) and cMyBP-C ($P < 0.005$) on pCa_{50}. Subsequent *post-hoc* tests revealed that pCa_{50} was significantly higher at 2.1 μm as indicated by a leftward shift in the force-pCa relationships in both WT and KO groups. Also, the SL-dependent increase in pCa_{50}(ΔpCa_{50}) was attenuated in KO group (indicated by arrows in **B, C**). Two-Way ANOVA revealed a significant interaction effect ($P < 0.05$) on n_H suggesting that cMyBP-C influences the effect of SL on n_H. Subsequent *post-hoc* tests revealed that n_H significantly increased at SL 1.9 μm in WT but not in KO group. Determinations were made from 7 to 10 multicellular preparations and 3 to 4 hearts per each group. Values are reported as mean ± s.e.m. $^*P < 0.05$; $^{**}P < 0.005$.

ANOVA revealed no significant interaction effect, but revealed significant main effects of SL ($P < 0.005$) and cMyBP-C ($P < 0.005$) on pCa_{50}. Subsequent *post-hoc* tests revealed that the main effect of SL was because of the following: pCa_{50} significantly increased upon increasing the SL from 1.9 to 2.1 μm as indicated by a leftward shift in the force-pCa relationships in both WT and KO groups (**Figures 3A,B**). The SL-dependent increase in pCa_{50} (ΔpCa_{50}) was attenuated in KO group when compared to ΔpCa_{50} of WT group (**Figure 3B**). In WT group ΔpCa_{50} was 0.11 pCa units whereas in the KO group ΔpCa_{50} was 0.07 pCa units. This attenuation of pCa_{50} can be attributed to the fact that KO group exhibited a significantly higher pCa_{50} at SL 1.9 μm compared to WT group (**Figure 3C**; **Table 1**), indicating that cardiac thin-filaments are more sensitive to Ca^{2+} activation at short SL in the KO group. Collectively, our results demonstrate that cMyBP-C impacts mechanisms that underlie length-dependent increases in myofilament Ca^{2+} sensitivity.

The effect of cMyBP-C on length-dependent changes in n_H was assessed by fitting Hill's equation to the force-pCa relationships constructed at SL's 1.9 and 2.1 μm in WT and KO groups (**Figure 3D**; **Table 1**). Two-Way ANOVA revealed a significant interaction effect ($P < 0.05$) on n_H suggesting that cMyBP-C influenced the effect of SL on n_H. Subsequent *post-hoc* tests revealed that n_H significantly increased by ∼38% at SL 1.9 μm in WT group, a result that agrees with earlier studies (Ford et al., 2012; Gollapudi et al., 2012). However, such an increase in n_H at SL 1.9 μm was not observed in KO group (**Figure 3D**)—suggesting that the absence of cMyBP-C impairs length-dependent changes in cooperative mechanisms in the sarcomere.

EFFECT OF cMyBP-C ON LENGTH-DEPENDENT CHANGES IN THE RATE OF FORCE REDEVELOPMENT (K_{tr})

k_{tr} is a measure of XB transition rate from a weakly- to a strongly-bound XB state (Brenner and Eisenberg, 1986; Campbell, 1997). We have previously shown that ablation of cMyBP-C accelerates submaximal k_{tr} at long SL (Stelzer et al., 2006b)—indicating that KO group exhibited an accelerated rate of XB turnover from weak- to strong-bindings states. We now sought to determine whether such effects are also observed at short SL in the KO group. Therefore, we measured k_{tr} at 1.9 and 2.1 μm to gain insights into the effect of cMyBP-C on length-dependent changes in k_{tr}. Two-Way ANOVA revealed a significant interaction effect ($P < 0.005$) on k_{tr} suggesting that cMyBP-C influenced the effect of SL on k_{tr}. The cause of the interaction effects was assessed by *post-hoc* multiple pairwise comparisons which showed that submaximal k_{tr} was accelerated in KO compared to WT group at long SL (**Figure 4**; **Table 2**) as reported earlier (Stelzer et al., 2006b). Furthermore,

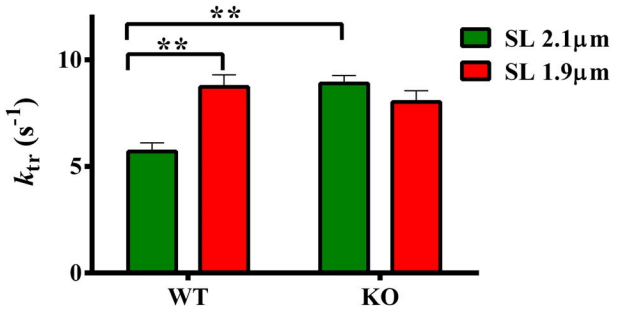

FIGURE 4 | Effect of cMyBP-C on length-dependent changes in the rate of force redevelopment (k_{tr}). k_{tr} was measured at 50% level of activation in WT and KO groups at SL's 2.1 and 1.9 μm using a mechanical slack-restretch protocol (Gresham et al., 2014). Two-Way ANOVA revealed a significant interaction effect ($P < 0.005$) on k_{tr} and *post-hoc* tests showed that k_{tr} significantly accelerated by ∼53% at short SL vs. long SL in WT group. However, such a trend was absent in the KO group. Furthermore, k_{tr} significantly accelerated by ∼56% in KO vs. WT group at long SL. Determinations were made from 6 to 13 multicellular preparations and 3 to 4 hearts per each group. Values are reported as mean ± s.e.m.
$^{**}P < 0.005$.

Table 2 | Dynamic contractile parameters of WT and KO ventricular multicellular preparations.

Group	k_{tr}(s^{-1})	k_{rel}(s^{-1})	k_{df}(s^{-1})	P1
SL 1.9 μm				
WT	8.74 ± 0.56*	45.01 ± 4.06*	12.26 ± 1.53*	0.535 ± 0.022*
KO	8.03 ± 0.54	36.96 ± 2.94	9.64 ± 0.39	0.543 ± 0.048
SL 2.1 μm				
WT	5.71 ± 0.40	34.21 ± 2.12	8.17 ± 0.52	0.604 ± 0.016
KO	8.90 ± 0.37†	45.76 ± 4.01†	11.27 ± 0.67†	0.528 ± 0.026†

k_{tr}: rate force redevelopment; k_{rel}: rate of force decay; k_{df}: rate of force development; P_1: the magnitude of peak force attained following a rapid stretch of muscle length in an isometrically-activated muscle preparation. k_{rel} and k_{df} were estimated using a linear transformation of the half time of force decay and force redevelopment. Values are expressed as mean ± s.e.m., from 6 to 13 multicellular preparations and 3 to 4 hearts per each group.

**Significantly different from the corresponding WT group at SL 2.1 μm; $P < 0.05$.*

†Significantly different from the corresponding WT group at SL 2.1 μm, $P < 0.05$.

k_{tr} was significantly accelerated by ∼53% at short SL compared to long SL in WT group (**Figure 4**; **Table 2**). However, an acceleration of k_{tr} at short SL was absent in KO group (**Figure 4**) such that differences in k_{tr} between WT and KO groups observed at long SL were no longer apparent at short SL. These results indicate that cMyBP-C mediates the length-dependent changes in XB turnover rate.

EFFECTS OF cMyBP-C ON LENGTH-DEPENDENT CHANGES IN THE RATES OF STRETCH-INDUCED XB RELAXATION (K_{rel}) AND XB RECRUITMENT (K_{df})

Our data shows that cMyBP-C affects the length-dependent changes in the XB turnoverrate, k_{tr} (**Figure 4**). Because k_{tr} is proportional to the sum of f (rate of XB attachment) + g (rate of XB detachment) according to a two-state XB model (Brenner, 1988), we sought to determine if the effect of cMyBP-C on length-dependent changes in k_{tr} were due to changes in either the rate of XB detachment or the rate of XB attachment kinetics, or both. We used stretch activation experiments (described in the methods section) to measure k_{rel} and k_{df} which are measures of the rates of XB detachment and XB recruitment, respectively (Cheng et al., 2013; Gresham et al., 2014).

Two-Way ANOVA revealed a significant interaction effect ($P < 0.05$) on k_{rel} suggesting that cMyBP-C influenced the effect of SL on the rate of XB detachment kinetics. The cause of the interaction effect was evident from the *post-hoc* multiple pairwise comparisons which revealed that k_{rel} was significantly accelerated by ∼32% at short SL in WT group but such an acceleration of k_{rel} at short SL was absent in KO group (**Figure 5A**; **Table 2**). Furthermore, in agreement with recent studies (Stelzer et al., 2006a; Merkulov et al., 2012), our data shows that k_{rel} was significantly accelerated by ∼34% in KO group compared to WT group at long SL (**Figure 5A**; **Table 2**).

Two-Way ANOVA revealed a significant interaction effect ($P < 0.005$) on k_{df} suggesting that cMyBP-C influenced the effect of SL on the rate of XB recruitment into the force-bearing state. The cause of the interaction effect was assessed using *post-hoc* tests which revealed that k_{df} was significantly accelerated by ∼50% at short SL in WT but such an acceleration of k_{df} at short SL was absent in KO (**Figure 5B**; **Table 2**). Furthermore, in agreement with a previous study (Stelzer et al., 2006a), our data shows that k_{df} was significantly accelerated by ∼38% in KO compared to WT at long SL. Thus, our stretch activation data shows that both k_{rel} and k_{df} were accelerated at short SL in WT but such trends were absent in the KO (**Figures 5A,B**). These findings suggest that the absence of acceleration of k_{tr} at short SL in the KO group (**Figure 4**) is due to a combined effect of the absence in the accelerations of k_{rel} and k_{df} at short SL in KO group (**Figure 5**). Collectively, our results suggest that cMyBP-C modulates length-dependent changes in the kinetics of XB detachment and attachment in cardiac muscle.

EFFECT OF cMyBP-C ON LENGTH-DEPENDENT CHANGES IN THE MAGNITUDE OF STRETCH-INDUCED INCREASE IN MUSCLE FIBER STIFFNESS (P1)

Our data shows that the XB detachment rate (k_{rel}) was accelerated at short SL compared to long SL in WT group (**Figure 5A**). Also, k_{rel} was accelerated at long SL in KO compared to WT group (**Figure 5A**). We sought to determine whether such accelerations in k_{rel} could have arisen from a decrease in the muscle fiber stiffness because changes in k_{rel} can be correlated with changes in stiffness of XBs (Stelzer et al., 2006c). We imposed a sudden 2% stretch in muscle length in an isometrically-contracting muscle preparation and measured the magnitude of the elicited instantaneous increase in force (P1 in **Figure 1**). P1 is a result of a rapid distortion of the elastic regions of the strongly-bound XBs (Stelzer and Moss, 2006; Ford et al., 2010; Cheng et al., 2013) and is an index of the muscle fiber stiffness because both P1 and muscle fiber stiffness are well correlated to the number of parallel and force-producing XBs that are bound to actin prior to the imposed stretch in muscle length (Campbell et al., 2004; Ford et al., 2010; Cheng et al., 2013).

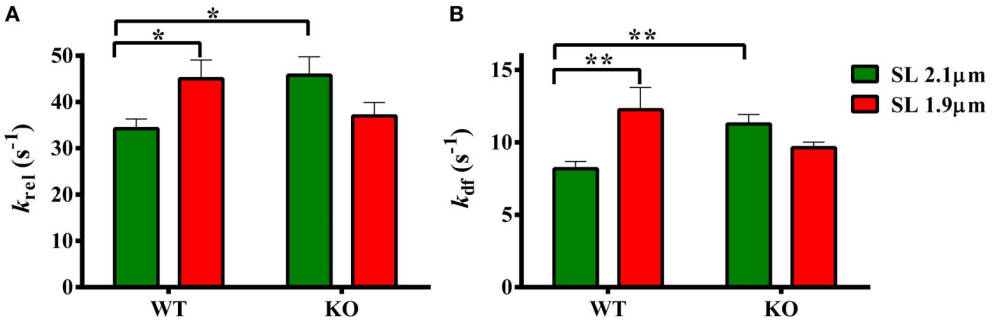

FIGURE 5 | Effect of cMyBP-C on length-dependent changes in the rates of XB detachment (k_{rel}) and XB recruitment (k_{df}). Isometrically-activated ventricular preparations were subjected to a sudden 2% stretch in their muscle length and the elicited force responses were used to estimate **(A)** k_{rel} and **(B)** k_{df} in WT and KO groups at SL's 2.1 and 1.9 μm as described in the methods section (Cheng et al., 2013; Gresham et al., 2014). Two-Way ANOVA revealed a significant interaction effect ($P < 0.05$) on k_{rel} and *post-hoc* tests showed that k_{rel} significantly accelerated by ∼32% at short SL vs. long SL in WT group but such a trend was absent in KO group. k_{rel} significantly accelerated by ∼34% in KO vs. WT group at long SL **(A)**. Two-Way ANOVA revealed a significant interaction effect ($P < 0.005$) on k_{df} and *post-hoc* tests showed that k_{df} significantly accelerated by ∼50% at short SL vs. long SL in WT group but such a trend was absent in KO group. In addition, k_{df} significantly accelerated by ∼39% in KO vs. WT group at long SL **(B)**. Determinations were made from 6 to 13 multicellular preparations and 3 to 4 hearts per each group. Values are reported as mean ± s.e.m. $^{*}P < 0.05$; $^{**}P < 0.005$.

Two-Way ANOVA revealed no significant interaction effect and main effects on P1. *Post-hoc* tests showed that P1 significantly decreased ($P = 0.036$) at short SL compared to long SL in WT group (**Figure 6**; **Table 2**). However, such a decrease in P1 at short SL was absent in KO group. Furthermore, P1 was significantly decreased ($P = 0.032$) at long SL in KO compared to WT (**Figure 6**; **Table 2**). These results suggest that a decrease in the muscle fiber stiffness contributed, at least in part, to the acceleration of k_{rel} observed at short SL compared to long SL in WT, and also at long SL in KO compared to long SL in WT (**Figure 5A**). Decreased XB stiffness could enhance strain-induced rates of XB detachment by increasing XB compliance such that XB's detach rapidly (Stelzer et al., 2006c; Cheng et al., 2013)—indicating that changes in P1 can be correlated with changes in k_{rel}. Thus, it is likely that the absence of differences in P1 at long and short SL's in KO group (**Figure 6**) may have contributed to the lack of differences we observed in k_{rel} at long and short SL's in KO group (**Figure 5A**). Collectively, our data suggests that cMyBP-C modulates length-dependent changes in the rate of XB detachment via its impact on the muscle fiber stiffness.

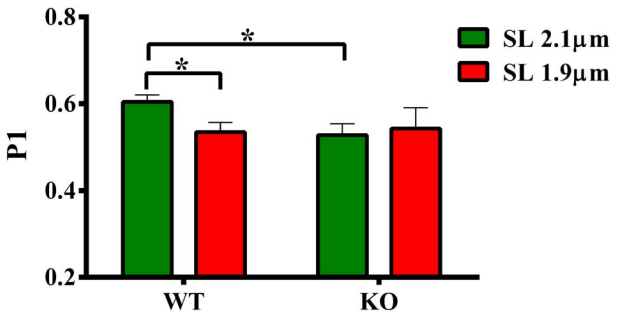

FIGURE 6 | Effect of cMyBP-C on length-dependent changes in the magnitude of sudden-stretch induced increase in muscle fiber stiffness (P1). P1 was calculated from the force responses elicited upon a sudden 2% stretch in muscle length imposed on isometrically-contracting ventricular preparations (Stelzer et al., 2006c). Two-Way ANOVA revealed no significant interaction effect and main effects on P1. *Post-hoc* tests showed that P1 significantly decreased at short SL vs. long SL in WT group but such a trend was absent in KO group. Also, P1 significantly decreased at long SL in KO vs. WT group. Determinations were made from 6 to 13 multicellular preparations and 3 to 4 hearts per each group. Values are reported as mean ± s.e.m. $^{*}P < 0.05$.

DISCUSSION

Given the lack of our understanding regarding cMyBP-C's role in cardiac LDA, we performed a detailed investigation of different aspects of cardiac contractile function both in the presence and absence of cMyBP-C and at SL's 1.9 and 2.1 μm. Results from our studies demonstrate that length-dependent changes in contractile dynamics are significantly impacted in the absence of cMyBP-C in the cardiac sarcomere. Novel findings from our experiments show an attenuated length-dependent response with respect to steady-state myofilament Ca^{2+} sensitivity of force generation, and profoundly blunted length-dependent XB cycling dynamics in ventricular preparations isolated from hearts lacking cMyBP-C—suggesting that cMyBP-C is a key modulator of cardiac LDA.

ABLATION OF cMyBP-C ATTENUATES THE LENGTH-DEPENDENT CHANGES IN MYOFILAMENT Ca^{2+} SENSITIVITY

An increase in myofilament Ca^{2+} sensitivity (pCa_{50}) upon an increase in SL is a hallmark of LDA (Kentish et al., 1986; Dobesh et al., 2002). The effect of cMyBP-C on LDA is important to study because it is known that LDA is depressed in human hearts expressing cMyBP-C mutations (Van Dijk et al., 2012; Sequeira et al., 2013). Our results show that although the absence of cMyBP-C did not affect maximal force production (**Table 1**), it did attenuate the SL-mediated increase in Ca^{2+} sensitivity (ΔpCa_{50}) (**Figures 3A–C**), a result that agrees with an earlier report (Cazorla et al., 2006). Cazorla et al reported an attenuated ΔpCa_{50} in the KO when compared to the WT myocardium

(ΔpCa_{50} of 0.16 pCa units in KO vs. a ΔpCa_{50} of 0.23 pCa units in WT). In this study we found a similar trend, although here the ΔpCa_{50} was 0.11pCa units in WT skinned myocardium whereas it was 0.07 pCa units in KO skinned myocardium (**Figure 3**). In our study, the attenuation of ΔpCa_{50} was due to higher submaximal force production, as suggested by a higher pCa_{50}, at short SL in KO vs. WT group (**Figure 3C**). These results indicate that the SL-based mechanisms governing myofilament Ca^{2+} sensitivity are altered in the KO group, and more so at short SL.

In view of the observation that the absence of cMyBP-C shifts the juxtaposition of the myosin heads toward the thin filament (Colson et al., 2007) thereby enhancing the probability of XB interaction, it is likely that the increased force at submaximal [Ca^{2+}] at short SL in KO group could have arisen from an increased number of XBs interacting with the thin-filament. It is generally accepted that when SL is shortened, the distance between the thick- and thin-filaments increases (Rome, 1968; McDonald and Moss, 1995). It is possible that because cMyBP-C ablation inherently reduces the relative distance between actin and myosin XB's (Colson et al., 2007), the length-dependent increase in acto-myosin distance with decreased SL is diminished in the KO group, thereby, resulting in greater XB interaction and increased force production. It is also possible that the observed increase in Ca^{2+} sensitivity at short SL in the KO group may be due to an increase in the apparent Ca^{2+} binding affinity of TnC mediated by strongly-bound XBs (Pan and Solaro, 1987; Hannon et al., 1992; Moss et al., 2004). In this context, a recent *in situ* time-resolved FRET study showed that the effects of strongly-bound XBs are transmitted allosterically to the N-terminus of TnC (N-TnC) via changes in the interaction between tropomyosin (Tm) and TnI (Li et al., 2014). The net result of the feedback effect of strongly-bound XBs is to shift the Tm to the open state and also to stabilize the open conformation of the N-TnC, thereby enhancing the affinity of TnC for Ca^{2+} to cause increased force production (Li et al., 2014). Thus, enhanced XB interaction at short SL in the absence of cMyBP-C may indirectly increase the Ca^{2+} sensitivity in the KO group via a thin filament mediated mechanism.

ABLATION OF cMyBP-C BLUNTS THE LENGTH-DEPENDENT CHANGES IN XB CYCLING KINETICS

As demonstrated previously (Stelzer et al., 2006b), our present data show that k_{tr} was accelerated in KO compared to WT group at long SL (**Figure 4**). Because changes in k_{tr} indicate a shift in the equilibrium in the transitions between the closed to open states (McKillop and Geeves, 1993) of the thin-filament (Campbell, 1997), our data suggests that in the absence of cMyBP-C the thin-filaments are shifted more toward the open state. To understand the impact of cMyBP-C on length-dependent changes in XB transitions/cycling from weak- to strong-binding states, we measured k_{tr} at short and long SL's. Our data show that k_{tr} was accelerated at short SL compared to long SL in WT group (**Figure 4**) indicating the XB cycling is accelerated at short SL. In support of this observation, an earlier study showed that loaded shortening velocity and k_{tr} were significantly accelerated at short SL compared to long SL in skinned rat cardiac myocytes (Korte and McDonald, 2007). The mechanism for such an increase in k_{tr} at short SL may arise from the acceleration of XB cycling kinetics such that there are more XBs working against a constant load because of increased XB flexibility which allows XBs to radially extend toward the thin-filament at short SL (Korte and McDonald, 2007). Increased flexibility of XBs at short SL may also arise due to decreased stiffness of titin (Granzier and Irving, 1995), a consequence of which is a decreased force exerted by titin on cMyBP-C which can in turn lead to decreased constraint imposed by cMyBP-C on the myosin XBs (Korte and McDonald, 2007). Such increases in k_{tr} at short SL were also reported by Adhikari et al who attributed the increases in k_{tr} to an increased XB detachment rate at short SL (Adhikari et al., 2004).

Because k_{tr} encompasses both the rates of XB attachment (f) and detachment (g) (Brenner and Eisenberg, 1986), we determined if increased k_{tr} observed at short SL in WT was due to increase in either f or g, or both. Using length perturbation experiments (Gresham et al., 2014), we measured the rates of force development (k_{df}) and force decay (k_{rel}), parameters that are analogous to f and g. Our data shows that acceleration of k_{tr} at short SL in WT group was indeed due to a combination of increases in both k_{df} and k_{rel} (**Figure 5**). Our data also shows that both k_{df} and k_{rel} did not increase at short SL in KO skinned myocardium such that the values were not significantly different from those at long SL (**Figure 5**). A recent study (Tanner et al., 2014) showed that XB detachment rates were accelerated in papillary muscle isolated from KO hearts compared to WT hearts but only under a β-MHC background at very long SL (2.2–3.3 μm). Under an α-MHC background, XB detachment rates displayed a slight non-statistically significant increase in KO papillary muscles compared to WT papillary muscles, in contrast to the larger accelerations in XB detachment we observed in KO multicellular preparations at shorter SL (i.e., 2.1 μm), isolated from hearts expressing predominantly α-MHC. Taken together, our data shows that an absence of acceleration in k_{tr} at short SL in KO group was due to the absence of accelerations in both k_{df} and k_{rel} at short SL (**Figure 5**). Thus, our study suggests that the mechanisms influencing length-dependent changes in XB transitions between weak- to strong-binding states are blunted in the absence of cMyBP-C.

ABLATION OF cMyBP-C BLUNTS LENGTH-DEPENDENT CHANGES IN MUSCLE FIBER STIFFNESS AND COOPERATIVE MECHANISMS

To test whether changes in XB detachment (as assessed by k_{rel}, **Figure 5**) due to cMyBP-C ablation or changes in SL were related to altered XB compliance and muscle fiber stiffness, we estimated the magnitude of the instantaneous increase in force P1, a parameter that represents the stretch-induced strain of the strongly-bound XBs and an indicator of XB stiffness (Ford et al., 2010; Cheng et al., 2013). Our measurements showed that P1 values were decreased in WT at short SL compared to long SL, and also in KO at long SL when compared to WT at long SL (**Figure 6**; **Table 2**). Because P1 can be correlated to k_{rel} (Stelzer et al., 2006c; Cheng et al., 2013), our results are consistent with the idea that decreased muscle fiber stiffness contributed to the observed acceleration in the XB detachment. Significantly, our results demonstrate that muscle fiber stiffness decreased at short SL compared to long SL in WT but not in KO group (**Figure 6**),

suggesting that the lack of length-dependent changes in k_{rel} seen in KO group (**Figure 5**) may have been related to the lack of length-dependent changes in the muscle fiber stiffness (**Figure 6**), because muscle fiber stiffness in KO group is already significantly lower than WT group at long SL.

To test whether changes in XB recruitment, (as assessed by k_{df}, **Figure 5**) due to cMyBP-C ablation or changes in SL were related to changes in cooperative mechanisms, we estimated the Hill coefficient, n_H from the pCa-tension relationships. Our estimates showed that n_H values were increased in WT at short SL compared to long SL (**Figure 3D**), a result that is consistent with previous studies (Ford et al., 2012; Gollapudi et al., 2012). This suggests that enhanced cooperative mechanisms may have accelerated the XB recruitment rate at short SL in WT group. This increase in n_H may be a result of enhanced Ca^{2+} binding to Tn, near-neighbor interactions among Tn-Tn, XB-Tn, and XB-XB (Razumova et al., 2000; Campbell et al., 2001). Notably, such an increase in n_H at short SL was absent in KO (**Figure 3D**) which may have likely contributed to the absence of length-dependent changes in k_{df} in the KO group (**Figure 5B**). In the context of the KO model, it is likely that depressed cooperative XB-XB (Razumova et al., 2000; Moss et al., 2004), XB-Tn (Razumova et al., 2000; Chandra et al., 2007) and XB-Ca^{2+}/TnC (Li et al., 2014) interactions at short SL may have contributed to the blunting of the increase in n_H with decrease in SL. Therefore, our data shows that length-dependent changes in cooperative mechanisms are depressed when cMyBP-C is absent in the sarcomere.

CONCLUSIONS

Our study provides evidence to show that cMyBP-C plays a key role in fine-tuning length-dependent cardiac contractile function via its impact on myofilament responsiveness to Ca^{2+}, XB cycling kinetics, and muscle fiber stiffness. Taken together, our findings suggest that impaired LDA may contribute to depressed myocardial contractile function in human patients harboring mutations in cMyBP-C that ultimately cause a significant decrease in the amount of cMyBP-C expression in the sarcomere.

AUTHOR CONTRIBUTIONS

Ranganath Mamidi and Julian E. Stelzer contributed to the conception and design of the experiments. Ranganath Mamidi, Kenneth S. Gresham, and Julian E. Stelzer participated in performing the experiments, data acquisition, data analysis, data interpretation, drafting, and revising the manuscript. All authors approved the final version of the manuscript.

ACKNOWLEDGMENTS

This work was supported by the National Heart, Lung, and Blood Institute Grant (HL-114770-01). We would like to thank Heather Butler, Department of Ophthalmology/Endocrinology at Case Western Reserve University for help with maintaining our mouse colonies.

REFERENCES

Adhikari, B. B., Regnier, M., Rivera, A. J., Kreutziger, K. L., and Martyn, D. A. (2004). Cardiac length dependence of force and force redevelopment kinetics with altered cross-bridge cycling. *Biophys. J.* 87, 1784–1794. doi: 10.1529/biophysj.103.039131

Allen, D. G., and Kentish, J. C. (1985). The cellular basis of the length-tension relation in cardiac muscle. *J. Mol. Cell. Cardiol.* 17, 821–840. doi: 10.1016/S0022-2828(85)80097-3

Brenner, B. (1988). Effect of Ca2+ on cross-bridge turnover kinetics in skinned single rabbit psoas fibers: implications for regulation of muscle contraction. *Proc. Natl. Acad. Sci. U.S.A.* 85, 3265–3269. doi: 10.1073/pnas.85.9.3265

Brenner, B., and Eisenberg, E. (1986). Rate of force generation in muscle: correlation with actomyosin ATPase activity in solution. *Proc. Natl. Acad. Sci. U.S.A.* 83, 3542–3546. doi: 10.1073/pnas.83.10.3542

Butters, C. A., Tobacman, J. B., and Tobacman, L. S. (1997). Cooperative effect of calcium binding to adjacent troponin molecules on the thin filament-myosin subfragment 1 MgATPase rate. *J. Biol. Chem.* 272, 13196–13202. doi: 10.1074/jbc.272.20.13196

Campbell, K. (1997). Rate constant of muscle force redevelopment reflects cooperative activation as well as cross-bridge kinetics. *Biophys. J.* 72, 254–262. doi: 10.1016/S0006-3495(97)78664-8

Campbell, K. B., Chandra, M., Kirkpatrick, R. D., Slinker, B. K., and Hunter, W. C. (2004). Interpreting cardiac muscle force-length dynamics using a novel functional model. *Am. J. Physiol. Heart Circ. Physiol.* 286, H1535–H1545. doi: 10.1152/ajpheart.01029.2003

Campbell, K. B., Razumova, M. V., Kirkpatrick, R. D., and Slinker, B. K. (2001). Nonlinear myofilament regulatory processes affect frequency-dependent muscle fiber stiffness. *Biophys. J.* 81, 2278–2296. doi: 10.1016/S0006-3495(01)75875-4

Campbell, K. S. (2011). Impact of myocyte strain on cardiac myofilament activation. *Pflugers Arch.* 462, 3–14. doi: 10.1007/s00424-011-0952-3

Campbell, K. S., and Moss, R. L. (2003). SLControl: PC-based data acquisition and analysis for muscle mechanics. *Am. J. Physiol. Heart Circ. Physiol.* 285, H2857–H2864. doi: 10.1152/ajpheart.00295.2003

Cazorla, O., Szilagyi, S., Vignier, N., Salazar, G., Kramer, E., Vassort, G., et al. (2006). Length and protein kinase a modulations of myocytes in cardiac myosin binding protein C-deficient mice. *Cardiovasc. Res.* 69, 370–380. doi: 10.1016/j.cardiores.2005.11.009

Chandra, M., Tschirgi, M. L., Ford, S. J., Slinker, B. K., and Campbell, K. B. (2007). Interaction between myosin heavy chain and troponin isoforms modulate cardiac myofiber contractile dynamics. *Am. J. Physiol. Regul. Integr. Comp. Physiol.* 293, R1595–R1607. doi: 10.1152/ajpregu.00157.2007

Chandra, M., Tschirgi, M. L., Rajapakse, I., and Campbell, K. B. (2006). Troponin T modulates sarcomere length-dependent recruitment of cross-bridges in cardiac muscle. *Biophys. J.* 90, 2867–2876. doi: 10.1529/biophysj.105.076950

Chen, P. P., Patel, J. R., Rybakova, I. N., Walker, J. W., and Moss, R. L. (2010). Protein kinase A-induced myofilament desensitization to Ca(2+) as a result of phosphorylation of cardiac myosin-binding protein C. *J. Gen. Physiol.* 136, 615–627. doi: 10.1085/jgp.201010448

Cheng, Y., Wan, X., McElfresh, T. A., Chen, X., Gresham, K. S., Rosenbaum, D. S., et al. (2013). Impaired contractile function due to decreased cardiac myosin binding protein C content in the sarcomere. *Am. J. Physiol. Heart Circ. Physiol.* 305, H52–H65. doi: 10.1152/ajpheart.00929.2012

Colson, B. A., Bekyarova, T., Fitzsimons, D. P., Irving, T. C., and Moss, R. L. (2007). Radial displacement of myosin cross-bridges in mouse myocardium due to ablation of myosin binding protein-C. *J. Mol. Biol.* 367, 36–41. doi: 10.1016/j.jmb.2006.12.063

Coulton, A. T., and Stelzer, J. E. (2012). Cardiac myosin binding protein C and its phosphorylation regulate multiple steps in the cross-bridge cycle of muscle contraction. *Biochemistry* 51, 3292–3301. doi: 10.1021/bi300085x

Desjardins, C. L., Chen, Y., Coulton, A. T., Hoit, B. D., Yu, X., and Stelzer, J. E. (2012). Cardiac myosin binding protein C insufficiency leads to early onset of mechanical dysfunction. *Circ. Cardiovasc. Imaging* 5, 127–136. doi: 10.1161/CIRCIMAGING.111.965772

De Tombe, P. P., Mateja, R. D., Tachampa, K., Ait Mou, Y., Farman, G. P., and Irving, T. C. (2010). Myofilament length dependent activation. *J. Mol. Cell. Cardiol.* 48, 851–858. doi: 10.1016/j.yjmcc.2009.12.017

Dobesh, D. P., Konhilas, J. P., and De Tombe, P. P. (2002). Cooperative activation in cardiac muscle: impact of sarcomere length. *Am. J. Physiol. Heart Circ. Physiol.* 282, H1055–H1062. doi: 10.1152/ajpheart.00667.2001

Fabiato, A. (1988). Computer programs for calculating total from specified free or free from specified total ionic concentrations in aqueous solutions containing multiple metals and ligands. *Meth. Enzymol.* 157, 378–417. doi: 10.1016/0076-6879(88)57093-3

Farman, G. P., Allen, E. J., Schoenfelt, K. Q., Backx, P. H., and De Tombe, P. P. (2010). The role of thin filament cooperativity in cardiac length-dependent calcium activation. *Biophys. J.* 99, 2978–2986. doi: 10.1016/j.bpj.2010.09.003

Ford, S. J., Chandra, M., Mamidi, R., Dong, W., and Campbell, K. B. (2010). Model representation of the nonlinear step response in cardiac muscle. *J. Gen. Physiol.* 136, 159–177. doi: 10.1085/jgp.201010467

Ford, S. J., Mamidi, R., Jimenez, J., Tardiff, J. C., and Chandra, M. (2012). Effects of R92 mutations in mouse cardiac troponin T are influenced by changes in myosin heavy chain isoform. *J. Mol. Cell. Cardiol.* 53, 542–551. doi: 10.1016/j.yjmcc.2012.07.018

Fuchs, F., and Smith, S. H. (2001). Calcium, cross-bridges, and the Frank-Starling relationship. *News Physiol. Sci.* 16, 5–10.

Fukuda, N., Wu, Y., Farman, G., Irving, T. C., and Granzier, H. (2003). Titin isoform variance and length dependence of activation in skinned bovine cardiac muscle. *J. Physiol.* 553, 147–154. doi: 10.1113/jphysiol.2003.049759

Godt, R. E., and Lindley, B. D. (1982). Influence of temperature upon contractile activation and isometric force production in mechanically skinned muscle fibers of the frog. *J. Gen. Physiol.* 80, 279–297. doi: 10.1085/jgp.80.2.279

Gollapudi, S. K., Mamidi, R., Mallampalli, S. L., and Chandra, M. (2012). The N-terminal extension of cardiac troponin T stabilizes the blocked state of cardiac thin filament. *Biophys. J.* 103, 940–948. doi: 10.1016/j.bpj.2012.07.035

Gordon, A. M., Homsher, E., and Regnier, M. (2000). Regulation of contraction in striated muscle. *Physiol. Rev.* 80, 853–924.

Granzier, H. L., and Irving, T. C. (1995). Passive tension in cardiac muscle: contribution of collagen, titin, microtubules, and intermediate filaments. *Biophys. J.* 68, 1027–1044. doi: 10.1016/S0006-3495(95)80278-X

Gresham, K. S., Mamidi, R., and Stelzer, J. E. (2014). The contribution of cardiac myosin binding protein-c Ser282 phosphorylation to the rate of force generation and *in vivo* cardiac contractility. *J. Physiol.* 592, 3747–3765. doi: 10.1113/jphysiol.2014.276022

Gulati, J., Sonnenblick, E., and Babu, A. (1991). The role of troponin C in the length dependence of Ca(2+)-sensitive force of mammalian skeletal and cardiac muscles. *J. Physiol.* 441, 305–324.

Hanft, L. M., Korte, F. S., and McDonald, K. S. (2008). Cardiac function and modulation of sarcomeric function by length. *Cardiovasc. Res.* 77, 627–636. doi: 10.1093/cvr/cvm099

Hannon, J. D., Martyn, D. A., and Gordon, A. M. (1992). Effects of cycling and rigor crossbridges on the conformation of cardiac troponin C. *Circ. Res.* 71, 984–991. doi: 10.1161/01.RES.71.4.984

Harris, S. P., Bartley, C. R., Hacker, T. A., McDonald, K. S., Douglas, P. S., Greaser, M. L., et al. (2002). Hypertrophic cardiomyopathy in cardiac myosin binding protein-C knockout mice. *Circ. Res.* 90, 594–601. doi: 10.1161/01.RES.0000012222.70819.64

Kentish, J. C., Ter Keurs, H. E., Ricciardi, L., Bucx, J. J., and Noble, M. I. (1986). Comparison between the sarcomere length-force relations of intact and skinned trabeculae from rat right ventricle. Influence of calcium concentrations on these relations. *Circ. Res.* 58, 755–768. doi: 10.1161/01.RES.58.6.755

Konhilas, J. P., Irving, T. C., and De Tombe, P. P. (2002). Frank-Starling law of the heart and the cellular mechanisms of length-dependent activation. *Pflugers Arch.* 445, 305–310. doi: 10.1007/s00424-002-0902-1

Konhilas, J. P., Irving, T. C., Wolska, B. M., Jweied, E. E., Martin, A. F., Solaro, R. J., et al. (2003). Troponin I in the murine myocardium: influence on length-dependent activation and interfilament spacing. *J. Physiol.* 547, 951–961. doi: 10.1113/jphysiol.2002.038117

Korte, F. S., and McDonald, K. S. (2007). Sarcomere length dependence of rat skinned cardiac myocyte mechanical properties: dependence on myosin heavy chain. *J. Physiol.* 581, 725–739. doi: 10.1113/jphysiol.2007.128199

Li, K. L., Rieck, D., Solaro, R. J., and Dong, W. (2014). *In situ* time-resolved FRET reveals effects of sarcomere length on cardiac thin-filament activation. *Biophys. J.* 107, 682–693. doi: 10.1016/j.bpj.2014.05.044

Mamidi, R., and Chandra, M. (2013). Divergent effects of alpha- and beta-myosin heavy chain isoforms on the N terminus of rat cardiac troponin T. *J. Gen. Physiol.* 142, 413–423. doi: 10.1085/jgp.201310971

Mamidi, R., Mallampalli, S. L., Wieczorek, D. F., and Chandra, M. (2013a). Identification of two new regions in the N-terminus of cardiac troponin T that have divergent effects on cardiac contractile function. *J. Physiol.* 591, 1217–1234. doi: 10.1113/jphysiol.2012.243394

Mamidi, R., Muthuchamy, M., and Chandra, M. (2013b). Instability in the central region of tropomyosin modulates the function of its overlapping ends. *Biophys. J.* 105, 2104–2113. doi: 10.1016/j.bpj.2013.09.026

McDonald, K. S., and Moss, R. L. (1995). Osmotic compression of single cardiac myocytes eliminates the reduction in Ca2+ sensitivity of tension at short sarcomere length. *Circ. Res.* 77, 199–205. doi: 10.1161/01.RES.77.1.199

McKillop, D. F., and Geeves, M. A. (1993). Regulation of the interaction between actin and myosin subfragment 1: evidence for three states of the thin filament. *Biophys. J.* 65, 693–701. doi: 10.1016/S0006-3495(93)81110-X

Merkulov, S., Chen, X., Chandler, M. P., and Stelzer, J. E. (2012). *In vivo* cardiac myosin binding protein C gene transfer rescues myofilament contractile dysfunction in cardiac myosin binding protein C null mice. *Circ. Heart Fail.* 5, 635–644. doi: 10.1161/CIRCHEARTFAILURE.112.968941

Michael, J. J., Gollapudi, S. K., Ford, S. J., Kazmierczak, K., Szczesna-Cordary, D., and Chandra, M. (2013). Deletion of 1-43 amino acids in cardiac myosin essential light chain blunts length dependency of Ca(2+) sensitivity and cross-bridge detachment kinetics. *Am. J. Physiol. Heart Circ. Physiol.* 304, H253–H259. doi: 10.1152/ajpheart.00572.2012

Moss, R. L., Razumova, M., and Fitzsimons, D. P. (2004). Myosin cross-bridge activation of cardiac thin filaments: implications for myocardial function in health and disease. *Circ. Res.* 94, 1290–1300. doi: 10.1161/01.RES.0000127125.61647.4F

Mun, J. Y., Previs, M. J., Yu, H. Y., Gulick, J., Tobacman, L. S., Beck Previs, S., et al. (2014). Myosin-binding protein C displaces tropomyosin to activate cardiac thin filaments and governs their speed by an independent mechanism. *Proc. Natl. Acad. Sci. U.S.A.* 111, 2170–2175. doi: 10.1073/pnas.1316001111

Palmer, B. M., Sadayappan, S., Wang, Y., Weith, A. E., Previs, M. J., Bekyarova, T., et al. (2011). Roles for cardiac MyBP-C in maintaining myofilament lattice rigidity and prolonging myosin cross-bridge lifetime. *Biophys. J.* 101, 1661–1669. doi: 10.1016/j.bpj.2011.08.047

Pan, B. S., and Solaro, R. J. (1987). Calcium-binding properties of troponin C in detergent-skinned heart muscle fibers. *J. Biol. Chem.* 262, 7839–7849.

Pollack, G. H., and Huntsman, L. L. (1974). Sarcomere length-active force relations in living mammalian cardiac muscle. *Am. J. Physiol.* 227, 383–389.

Previs, M. J., Beck Previs, S., Gulick, J., Robbins, J., and Warshaw, D. M. (2012). Molecular mechanics of cardiac myosin-binding protein C in native thick filaments. *Science* 337, 1215–1218. doi: 10.1126/science.1223602

Razumova, M. V., Bukatina, A. E., and Campbell, K. B. (2000). Different myofilament nearest-neighbor interactions have distinctive effects on contractile behavior. *Biophys. J.* 78, 3120–3137. doi: 10.1016/S0006-3495(00)76849-4

Regnier, M., Martin, H., Barsotti, R. J., Rivera, A. J., Martyn, D. A., and Clemmens, E. (2004). Cross-bridge versus thin filament contributions to the level and rate of force development in cardiac muscle. *Biophys. J.* 87, 1815–1824. doi: 10.1529/biophysj.103.039123

Rodriguez, E. K., Hunter, W. C., Royce, M. J., Leppo, M. K., Douglas, A. S., and Weisman, H. F. (1992). A method to reconstruct myocardial sarcomere lengths and orientations at transmural sites in beating canine hearts. *Am. J. Physiol.* 263, H293–H306.

Rome, E. (1968). X-ray diffraction studies of the filament lattice of striated muscle in various bathing media. *J. Mol. Biol.* 37, 331–344. doi: 10.1016/0022-2836(68)90272-6

Sadayappan, S., and De Tombe, P. P. (2012). Cardiac myosin binding protein-C: redefining its structure and function. *Biophys. Rev.* 4, 93–106. doi: 10.1007/s12551-012-0067-x

Sequeira, V., Wijnker, P. J., Nijenkamp, L. L., Kuster, D. W., Najafi, A., Witjas-Paalberends, E. R., et al. (2013). Perturbed length-dependent activation in human hypertrophic cardiomyopathy with missense sarcomeric gene mutations. *Circ. Res.* 112, 1491–1505. doi: 10.1161/CIRCRESAHA.111.300436

Shaffer, J. F., Kensler, R. W., and Harris, S. P. (2009). The myosin-binding protein C motif binds to F-actin in a phosphorylation-sensitive manner. *J. Biol. Chem.* 284, 12318–12327. doi: 10.1074/jbc.M808850200

Squire, J. M., Luther, P. K., and Knupp, C. (2003). Structural evidence for the interaction of C-protein (MyBP-C) with actin and sequence identification of a possible actin-binding domain. *J. Mol. Biol.* 331, 713–724. doi: 10.1016/S0022-2836(03)00781-2

Stelzer, J. E., Dunning, S. B., and Moss, R. L. (2006a). Ablation of cardiac myosin-binding protein-C accelerates stretch activation in murine skinned myocardium. *Circ. Res.* 98, 1212–1218. doi: 10.1161/01.RES.0000219863.94390.ce

Stelzer, J. E., Fitzsimons, D. P., and Moss, R. L. (2006b). Ablation of myosin-binding protein-C accelerates force development in mouse myocardium. *Biophys. J.* 90, 4119–4127. doi: 10.1529/biophysj.105.078147

Stelzer, J. E., Larsson, L., Fitzsimons, D. P., and Moss, R. L. (2006c). Activation dependence of stretch activation in mouse skinned myocardium: implications for ventricular function. *J. Gen. Physiol.* 127, 95–107. doi: 10.1085/jgp.200509432

Stelzer, J. E., and Moss, R. L. (2006). Contributions of stretch activation to length-dependent contraction in murine myocardium. *J. Gen. Physiol.* 128, 461–471. doi: 10.1085/jgp.200609634

Stelzer, J. E., Patel, J. R., and Moss, R. L. (2006d). Acceleration of stretch activation in murine myocardium due to phosphorylation of myosin regulatory light chain. *J. Gen. Physiol.* 128, 261–272. doi: 10.1085/jgp.200609547

Tachampa, K., Wang, H., Farman, G. P., and De Tombe, P. P. (2007). Cardiac troponin I threonine 144: role in myofilament length dependent activation. *Circ. Res.* 101, 1081–1083. doi: 10.1161/CIRCRESAHA.107.165258

Tanner, B. C., Wang, Y., Robbins, J., and Palmer, B. M. (2014). Kinetics of cardiac myosin isoforms in mouse myocardium are affected differently by presence of myosin binding protein-C. *J. Muscle Res. Cell Motil.* doi: 10.1007/s10974-014-9390-0. [Epub ahead of print].

Van Dijk, S. J., Paalberends, E. R., Najafi, A., Michels, M., Sadayappan, S., Carrier, L., et al. (2012). Contractile dysfunction irrespective of the mutant protein in human hypertrophic cardiomyopathy with normal systolic function. *Circ. Heart Fail.* 5, 36–46. doi: 10.1161/CIRCHEARTFAILURE.111.963702

Conflict of Interest Statement: The authors declare that the research was conducted in the absence of any commercial or financial relationships that could be construed as a potential conflict of interest.

Received: 20 October 2014; accepted: 10 November 2014; published online: 02 December 2014.

*Citation: Mamidi R, Gresham KS and Stelzer JE (2014) Length-dependent changes in contractile dynamics are blunted due to cardiac myosin binding protein-C ablation. Front. Physiol. **5**:461. doi: 10.3389/fphys.2014.00461*

This article was submitted to Striated Muscle Physiology, a section of the journal Frontiers in Physiology.

Copyright © 2014 Mamidi, Gresham and Stelzer. This is an open-access article distributed under the terms of the Creative Commons Attribution License (CC BY). The use, distribution or reproduction in other forums is permitted, provided the original author(s) or licensor are credited and that the original publication in this journal is cited, in accordance with accepted academic practice. No use, distribution or reproduction is permitted which does not comply with these terms.

frontiers in
PHYSIOLOGY

REVIEW ARTICLE
published: 15 January 2015
doi: 10.3389/fphys.2014.00531

Peripartum cardiomyopathy and dilated cardiomyopathy: different at heart

Ilse A. E. Bollen, Elza D. Van Deel, Diederik W. D. Kuster and Jolanda Van Der Velden*

Department of Physiology, Institute for Cardiovascular Research (ICaR-VU), VU University Medical Center, Amsterdam, Netherlands

Edited by:
Julien Ochala, KIng's College London, UK

Reviewed by:
Martina Krüger, Heinrich Heine University Düsseldorf, Germany
Ranganath Mamidi, Case Western Reserve University, USA

***Correspondence:**
Jolanda Van Der Velden, Department of Physiology, Institute for Cardiovascular Research, VU University Medical Center, Van der Boechorststraat 7, 1081 BT Amsterdam, Netherlands
e-mail: j.vandervelden@vumc.nl

Peripartum cardiomyopathy (PPCM) is a severe cardiac disease occurring in the last month of pregnancy or in the first 5 months after delivery and shows many similar clinical characteristics as dilated cardiomyopathy (DCM) such as ventricle dilation and systolic dysfunction. While PPCM was believed to be DCM triggered by pregnancy, more and more studies show important differences between these diseases. While it is likely they share part of their pathogenesis such as increased oxidative stress and an impaired microvasculature, discrepancies seen in disease progression and outcome indicate there must be differences in pathogenesis as well. In this review, we compared studies in DCM and PPCM to search for overlapping and deviating disease etiology, pathogenesis and outcome in order to understand why these cardiomyopathies share similar clinical features but have different underlying pathologies.

Keywords: dilated cardiomyopathy, peripartum cardiomyopathy, oxidative stress, prolactin, microvasculature, heart failure, titin

INTRODUCTION

Peripartum cardiomyopathy (PPCM) is a cardiac disease that can have many different clinical presentations but shares similar clinical symptoms with dilated cardiomyopathy (DCM) such as ventricle dilation, impaired systolic function and arrhythmias (Pearson et al., 2000; Elliott et al., 2008). Therefore, PPCM is often seen as DCM initiated during pregnancy. However, there are some important differences between the two cardiomyopathies which argue for separation of the two disease states. This review aims to compare studies performed in PPCM and DCM patients and animal models in order to better understand why these cardiomyopathies share similar clinical features but have different underlying pathomechanisms.

CLINICAL PRESENTATIONS

Dilated cardiomyopathy has a variety of causes such as: genetic factors, viral infections, alcohol abuse and myocardial infarction. Current classification of DCM excludes cases in which coronary artery disease, loading conditions, hypertension, valvular diseases and congenital heart diseases could have caused the observed phenotype (Elliott et al., 2008). The exact prevalence of idiopathic DCM varies between studies, from 1:2700 in the original epidemiological study (Codd et al., 1989) to 1:250 in a recent study (Hershberger et al., 2013). PPCM, as the name implies, develops during the last month of pregnancy, during delivery or within the first 5 months after delivery (Pearson et al., 2000). The prevalence of PPCM has been established to be 1:4000 to 1:1000 live births in the Western world (Elkayam, 2011; Kolte et al., 2014), although there is regional variation, e.g. the prevalence of PPCM in Haiti is 1:300 live births (Fett et al., 2005). In contrast to DCM, which typically presents later in life (Hershberger et al., 2013), PPCM often develops in young, previously healthy women and is a disease which progresses quickly to cardiac dysfunction and failure as is evident in the high mortality and transplantation rate (Van Hoeven et al., 1993; Hilfiker-Kleiner et al., 2007; Sliwa et al., 2010; Elkayam, 2011; Fett, 2014). As symptoms of PPCM such as dyspnea, fatigue and exercise incapacity are similar to normal pregnancy symptoms, the disease is often diagnosed late. If diagnosed and treated early, women suffering from PPCM may be stabilized upon treatment with β-blockers, ACE inhibitors and bromocriptine (BR) and reversal of the phenotype resulting in favorable outcome and recovery is not uncommon (Van Hoeven et al., 1993; Felker et al., 2000; Hilfiker-Kleiner et al., 2007; Sliwa et al., 2010; Elkayam, 2011; Ballo et al., 2012; Haghikia et al., 2013; Fett, 2014). This is contrary to what is often observed in DCM which is characterized by a late onset and slow disease progression that might be stabilized but unlikely to be reversed upon treatment (Van Hoeven et al., 1993; Fish, 2012; Hershberger et al., 2013).

PHYSIOLOGICAL ADAPTATIONS DURING PREGNANCY

The pathogenesis of PPCM is tightly bound to the cardiac changes that accompany normal pregnancies. It is therefore important to understand the physiological changes that occur during pregnancy. The increased hemodynamic load caused by the increased blood volume results in physiological hypertrophy, in which chamber dimensions increase, concomitant with a proportional increase in wall thickness to cope with the increased

Abbreviations: ADMA, Asymmetric dimethylarginine; BR, Bromocriptine; CD, Cathepsin D; DCM, Dilated cardiomyopathy; EF, Ejection Fraction; HF, Heart Failure; KO, Knock out; *LMNA*, Gene encoding the protein lamin-A/C; LV, Left ventricle; MnSOD, Manganese superoxide dismutase; NOS, Nitric oxide synthase; NOX, NADPH oxidase; PGC-1α, PPARγ coactivator-1α; PPCM, Peripartum cardiomyopathy; PRL, Prolactin; ROS, Reactive oxygen species; sFLT1, fms-like tyrosine kinase 1; STAT3, Signal transducer and activator of transcription 3; *TTN*, Gene encoding the protein titin; UPS, Ubiquitin proteasome system; VEGF, Vascular endothelial growth factor.

hemodynamic load and to facilitate increased cardiac output (Clapp and Capeless, 1997; Umar et al., 2012). This physiological hypertrophy is different from the pathological (eccentric) hypertrophy seen in both PPCM and DCM in which chamber dimensions increase while wall thickness does not increase proportionally in response to increased hemodynamic load (Gaasch and Zile, 2011). According to the law of Laplace this will lead to increased wall stress. Physiological pregnancy-related hypertrophy is reversible post-partum, usually within 1 year after delivery (Clapp and Capeless, 1997). Other differences between pathological and physiological hypertrophy are the absence of fibrosis and the absence of induction of the fetal gene program in physiological hypertrophy (McMullen and Jennings, 2007; Umar et al., 2012). In addition, angiogenic factors such as vascular endothelial growth factor A (VEGF A) are secreted during pregnancy which facilitates myocardial angiogenesis in order to increase capillary density proportionally to cardiomyocyte size. Both capillary density as well as VEGF levels return to pre-pregnancy levels post-partum (Umar et al., 2012; Chung and Leinwand, 2014). Pregnancy is often seen as a cardiac stress model upon which underlying cardiac dysfunction may reveal itself due to the increased hemodynamic load on the heart and hormonal changes during pregnancy (Chung and Leinwand, 2014). However, the increase in hemodynamic load starts early in pregnancy (Clapp and Capeless, 1997) while PPCM develops in the last month of pregnancy or even post-partum. It is therefore unlikely that the increased hemodynamic load is the sole cause of PPCM.

GENETIC PREDISPOSITION AND TITIN ISOFORM SWITCHING

As stated before, DCM can have a genetic cause, leading to a familial form of DCM. Many mutations have been linked to DCM. However, many of these genes are also implicated in hypertrophic and restrictive cardiomyopathies (Hershberger et al., 2013). A common gene which is mutated in 6% of DCM patients is the gene encoding for the protein lamin-A/C (*LMNA*) (Parks et al., 2008). *LMNA* mutations show a relatively high penetrance compared with mutations in other genes and patients carrying *LMNA* mutations often have conduction abnormalities (Parks et al., 2008; Hershberger et al., 2013). In addition, Herman et al. showed a high incidence of truncated variants in the gene encoding for the protein titin (*TTN*) in DCM patients (Herman et al., 2012). In PPCM, little is known about causative pathogenic mutations. However, the fact that multiple PPCM cases within one family have been reported (Van Spaendonck-Zwarts et al., 2014) suggests that gene mutations could play an important role. Furthermore, reports about DCM and PPCM cases within families and the identification of mutations (Morales et al., 2010; Van Spaendonck-Zwarts et al., 2010, 2014) strengthen the suggestion of a genetic cause and overlap in etiology of PPCM and DCM. A recent study showed a high incidence of *TTN* variants in PPCM patients, and this cohort was marked by slow recovery (Van Spaendonck-Zwarts et al., 2014). However, it has been proposed that *TTN* mutations are not always disease causing, but might act as disease modifiers as truncated *TTN* variants are present in 3% of the general population (Herman et al., 2012). Knowledge about pathogenic effects of gene mutations would enable the identification of persons at risk for the development of DCM and PPCM and thereby facilitate early diagnosis and treatment.

The protein titin acts as a multifunctional spring that can exist as two distinct isoforms in the adult human heart; a compliant N2BA isoform and a stiff N2B isoform. A shift to more N2BA titin isoform and subsequent reduced passive stiffness was shown in DCM patients previously (Makarenko et al., 2004; Nagueh et al., 2004). Apart from isoform shift, alterations in titin post-translational modifications such as phosphorylation are able to alter passive force development (Granzier and Labeit, 2002). Titin isoform has also been suggested to play a role in the ability of the heart to adapt contractility in response to stretch, known as the Frank-Starling mechanism (Fukuda et al., 2003). Unfortunately, limited data is available about the role of titin in PPCM, although increased compliant titin isoform and lowered passive tension has been reported in one PPCM patient with a *TTN* mutation (Van Spaendonck-Zwarts et al., 2014). Titin can also be modified under oxidizing conditions in which disulfide bridges can be formed in titin's N2B unique sequence possibly resulting in increased passive stiffness (Grützner et al., 2009). In addition, S-glutathionylation of cysteine residues in the Ig regions of titin under the influence of redox signaling has been suggested to lower passive stiffness (Alegre-Cebollada et al., 2014). As oxidative stress is present in both PPCM and DCM, as described later in this review, it is possible that this will also affect titin function although this has not been established *in vivo* yet.

OXIDATIVE STRESS AND PROLACTIN: A DEADLY COMBINATION

In both DCM and PPCM, oxidative stress is a key player in disease pathogenesis. However the exact consequences of reactive oxygen species (ROS) production differ notably between the two disease states as will be discussed below. In normal pregnancy, ROS production increases during the course of pregnancy and decreases post-partum to normal levels (Toescu et al., 2002). In an attempt to counterbalance the detrimental ROS production, total anti-oxidant capacity also increases during pregnancy and remains elevated post-partum (Toescu et al., 2002). In both PPCM animal models and human PPCM patients, oxidative stress levels are increased compared to healthy controls (Hilfiker-Kleiner et al., 2007). An explanation for the increased oxidative stress in PPCM can be found in the PPCM mouse model with cardiomyocyte restricted deletion of Signal transducer and activator of transcription 3 (STAT3) (Hilfiker-Kleiner et al., 2007). This transcription factor regulates the expression of the superoxide scavenger Manganese superoxide dismutase (MnSOD) (Negoro et al., 2001). Accordingly, in the cardiac STAT3 KO mice PPCM is accompanied by a reduced expression of MnSOD and concomitant oxidative stress (Hilfiker-Kleiner et al., 2007). A crucial pathway in PPCM that is instigated by elevated oxidative stress is the cleavage of the hormone prolactin (PRL) by ROS-activated Cathepsin D (CD) (Hilfiker-Kleiner et al., 2007). Upon ROS activation CD cleaves full-length prolactin (PRL) of 23 kDa into a smaller 16 kDa form which has detrimental effects on cardiomyocyte metabolism and the microvasculature (Hilfiker-Kleiner et al., 2007, 2012; Hilfiker-Kleiner and Sliwa, 2014). The

idea that PRL plays a crucial role in PPCM is further strengthened by the fact that PRL levels rise at the end of pregnancy and remain high post-partum during breast feeding which coincides with the onset of PPCM (Grattan et al., 2008). Accordingly, injection of adenoviral vectors expressing 16 kDa PRL in non-pregnant mice led to the development of cardiac dysfunction, dilation of the left ventricle (LV) and decreased myocardial capillary density (Hilfiker-Kleiner et al., 2007). As decreased levels of STAT3, high levels of oxidative stress, high CD activity and 16 kDa PRL have also been observed in human PPCM patients (Hilfiker-Kleiner et al., 2007; Haghikia et al., 2013), it strengthens the suggestion that insufficient defense against oxidative stress and subsequent formation of 16 kDa PRL plays an important role in PPCM pathogenesis. The compound BR is able to inhibit PRL release from the pituitary gland. Blockade of PRL by BR treatment in PPCM patients has been shown to improve cardiac function and increase survival, although only a limited number of studies containing small patient cohorts have been performed so far (Hilfiker-Kleiner et al., 2007; Sliwa et al., 2010; Ballo et al., 2012; Haghikia et al., 2013). Together these results indicate that cleavage of PRL under oxidative stress is key in the disease development in both human PPCM as well as the cardiac STAT-3 KO PPCM mouse-model (Hilfiker-Kleiner et al., 2007). However, not all patients treated with BR recover (Sliwa et al., 2010; Haghikia et al., 2013). Therefore, even though the PRL-mediated pathway is probably a major determinant in this disease, other pathways are likely to play a role. Since STAT3 signaling has many different functions, it is unlikely that the repressed MnSOD expression alone explains all observations in the STAT3 KO mouse model. Additionally, in heterozygous MnSOD$^{+/-}$ mice a reduction of MnSOD levels of 50% causes cardiac alterations under basal conditions (Remmen et al., 2001) and induces cardiac remodeling after pregnancy (Hilfiker-Kleiner et al., 2007), but it does not lead to the dilated PPCM phenotype often seen in PPCM patients and the cardiac STAT3 KO mouse model. This implies that besides MnSOD additional factors are essential for the development of PPCM.

STATs are activated upon phosphorylation by Janus kinases (JAK) and are multifunctional transcription factors. In cardiomyocytes STAT3 is involved in survival, sarcomere integrity, cell growth and ROS production (Haghikia et al., 2014). In the vasculature STAT3 promotes vascularization through stimulation of VEGF signaling (Osugi et al., 2002). Clearly STAT3 affects multiple cardiac processes besides generation of the 16 kDa PRL (Haghikia et al., 2014). In the cardiac STAT3 KO model, low STAT3 levels have been associated with the up-regulation of miR-199 (Haghikia et al., 2011). MiR-199 down-regulates specific ubiquitin conjugating enzymes thereby affecting the ubiquitin proteasome system (UPS). In an *in vitro* model, this disturbance of the UPS resulted in decreased protein levels of myosin heavy chain and troponin T, thereby causing disruption of sarcomere structure (Haghikia et al., 2011). Also in DCM patients, low STAT3 levels, increased miR-199 levels and decreased levels of ubiquitin conjugating enzymes have been observed (Haghikia et al., 2011). Low STAT3 levels have been observed in both PPCM (Hilfiker-Kleiner et al., 2007) and DCM patients (Podewski, 2003), indicating STAT3 may be part of the common pathway of both diseases. However, it should be noted that MnSOD protein levels and activity have been reported to be unchanged in DCM patients compared to non-failing controls in the myocardium (Dieterich et al., 2000) and a higher MnSOD activity was observed in serum (Wojciechowska et al., 2014). This indicates decreased STAT3 levels might have different downstream effects in DCM and PPCM and loss of MnSOD might form an etiology-specific (additional) source of oxidative stress in PPCM.

Oxidative stress is observed in many forms of heart failure (HF), including PPCM and DCM, and disturbs various pathways. However, the high levels of PRL during the final stages of pregnancy combined with high oxidative stress, likely make PPCM develop at such a high pace. As PRL levels are many fold lower in non-pregnant and non-nursing individuals (Grattan et al., 2008), it is unlikely that PRL also plays a role in DCM patients. Although oxidative stress has many detrimental effects in the failing heart it should be noted that ROS also fulfill a beneficial role in physiological circumstances. For example, NADPH oxidase (NOXs) produce ROS in a tightly regulated manner and play an important role in stretch-induced contraction by sensitization of the ryanodine receptor (RyR2) through oxidation (Prosser et al., 2011). However, in DCM NOX activity is up-regulated leading to increased ROS production (Maack et al., 2003). Amongst others oxidative stress inactivates important ion channels such as the L-type-calcium channel (LTCC) and the sarcoendoplasmic reticulum calcium transport ATPase (SERCA2a) and, in combination with disturbed RyR2 sensitization, may lead to Ca^{2+} depletion from the sarcoplasmic reticulum (Sag et al., 2013). Another general feature of HF is elevated cytosolic Na^{+} levels (Despa, 2002) that result in decreased Ca^{2+} uptake and consequently reduced NADPH generation in mitochondria [28]. This disturbed balance of ions within cardiomyocytes causes cardiac dysfunction due to disturbed excitation-contraction coupling (Sag et al., 2013). In turn reduced mitochondrial NADPH availability leads to reduced generation of mitochondrial antioxidants and increased levels of ROS (Kohlhaas et al., 2010). In addition, ROS causes NADPH oxidation, thereby further reducing NADPH bioavailability for the production of ROS scavenger enzymes. In addition, ROS can reduce the bioavailability of tetrahydrobiopterin (BH_4) and thereby induce the uncoupling of nitric oxide synthase (NOS). As a result NOS no longer produces beneficial nitric oxide (NO) molecules, but itself becomes a producer of superoxide (Verhaar, 2004). In this way ROS production can be self-sustaining and cause additional ROS production (Seddon et al., 2007) thereby locking the heart in a vicious circle of oxidative stress (Kohlhaas et al., 2010). Similarly the NOS inhibitor asymmetric dimethylarginine (ADMA), a factor shown to be up-regulated in both DCM and PPCM and described later in this review, has been suggested to stimulate NOS-uncoupling mediated ROS production (Wilcox, 2012). However, it should be noted that ADMA levels at expected pathological concentrations only had modest effect on ROS production in this study (Druhan et al., 2008). The vicious circle of ROS production amplification and Na^{+}/Ca^{2+} imbalance can be visualized in **Figure 1**. Apart from affecting cardiomyocyte ion balance, ROS has many other detrimental effects on cardiomyocytes such as nitration of creatine kinase, SERCA2a, voltage gated K^{+} channels, desmin, myosin heavy

chain and α-actinin, induction of DNA damage, cell death and fibrosis (Pacher et al., 2007; Seddon et al., 2007). As fibrosis can increase myocardial stiffness and does not contribute to active force development, increased fibrosis can influence both systolic and diastolic function. Increased fibrosis is common in DCM patients (Assomull et al., 2006; Herpel et al., 2006) and the cardiac STAT3 KO mouse model of PPCM (Ricke-Hoch et al., 2014), however, there are limited and contradictory reports about fibrosis in PPCM patients (Kawano et al., 2008; Mouquet et al., 2008; Leurent et al., 2009; Ntusi and Chin, 2009).

Together, alterations induced by ROS can lead to cardiomyocyte dysfunction through impaired Na^+ and Ca^{2+} handling, impaired sarcomere integrity, cardiomyocyte death and fibrosis formation. Although 16 kDa PRL is an important contributor to the pathophysiology of PPCM, it is likely that oxidative stress-induced cardiac pathology in PPCM also involve other ROS induced pathways.

DISTURBED SARCOMERE INTEGRITY AND ANGIOGENIC IMBALANCE

The previously described disturbance in the ubiquitin proteasome system (UPS) system also leads to increased levels of ADMA (Haghikia et al., 2011), a factor involved in reducing NO availability by competing with the NOS substrate L-arginine, and increasing ROS production by endothelial cells thereby contributing to the amplification of ROS production and cardiac dysfunction shown in **Figure 1** (Druhan et al., 2008). Also in human PPCM (Haghikia et al., 2013) and DCM patients increased levels of ADMA have been found and in DCM decreased L-arginine/ADMA ratio was shown to be a predictor of mortality (Anderssohn et al., 2012). The male mice of the cardiac STAT3 KO model showed age-related loss of capillary density and a DCM-like phenotype upon aging including fibrosis and impaired sarcomere organization (Hilfiker-Kleiner et al., 2004). Several studies indicate that damaged microvasculature or disturbance in

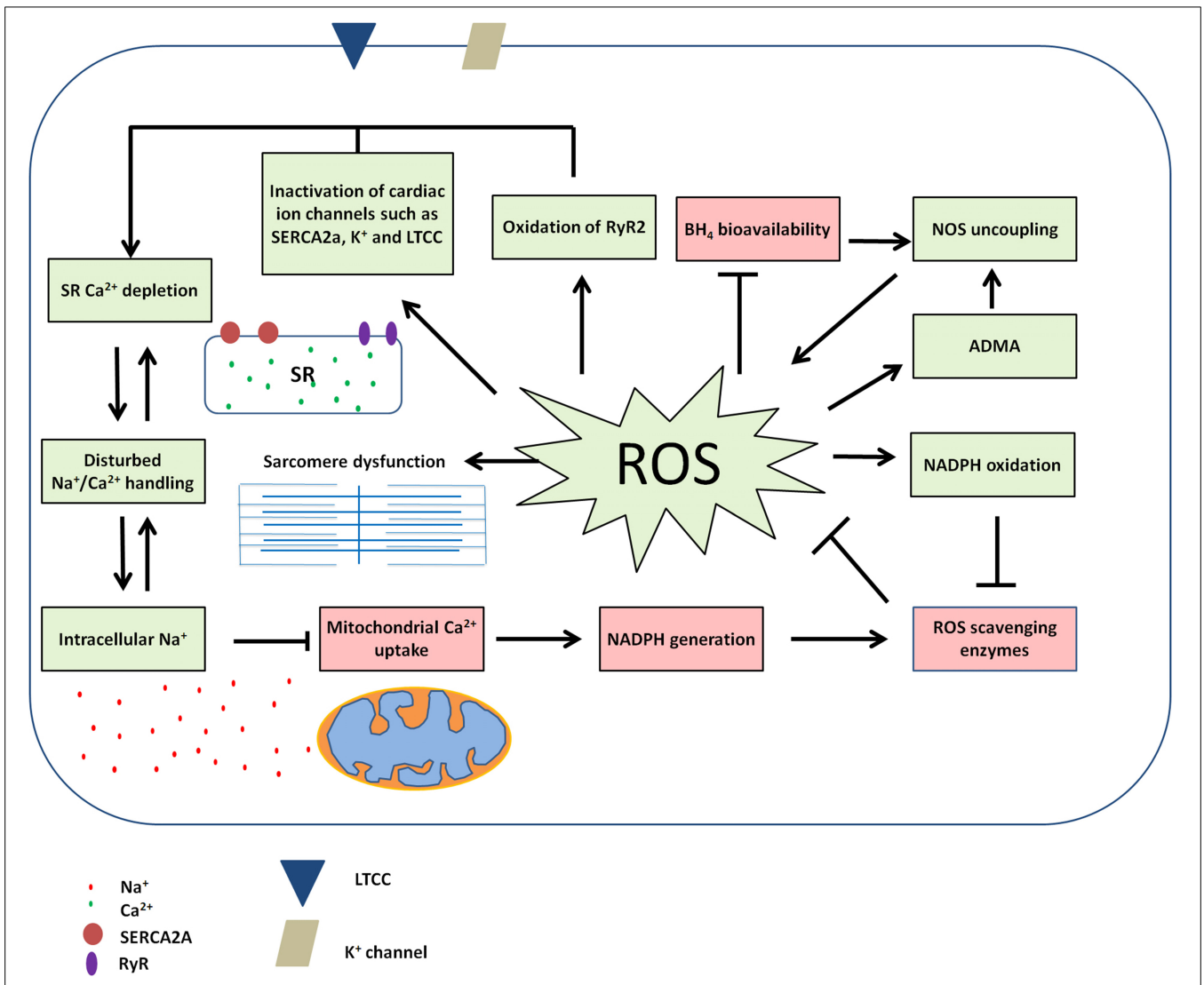

FIGURE 1 | Disturbed Na^+/Ca^{2+} signaling and ROS production can be locked in a vicious circle in heart failure. Red boxes indicate down-regulated or disturbed factors; green boxes indicate up-regulated factors in disease.

pro- and anti-angiogenic factors play a significant role in PPCM pathogenesis. A study by Patten et al. showed a high prevalence (33%) of (pre)eclampsia in their PPCM cohort (Patten et al., 2012), which is believed to be a risk factor for PPCM. It has been shown that PPCM leads to capillary dissociation and endothelial cell apoptosis (Hilfiker-Kleiner et al., 2007). Patten et al. suggested that the anti-angiogenic state might worsen the severity of the disease (Patten et al., 2012). In late pregnancy, anti-angiogenic factors, such as soluble, fms-like tyrosine kinase 1 (sFLT1), are secreted and thereby inhibit the increased VEGF signaling during pregnancy (Chung and Leinwand, 2014). The increase in anti-angiogenic factors is significantly higher in patients with (pre)eclampsia which results in decreased VEGF levels (Levine et al., 2004) and also unusually high levels of sFLT1 have been observed in PPCM patients (Patten et al., 2012). This indicates the anti-angiogenic state is important in both (pre)eclampsia and PPCM pathogenesis and might explain the high prevalence of (pre)eclampsia among PPCM patients. A common finding in PPCM studies is a reduced capillary density in the postpartum phase (Hilfiker-Kleiner et al., 2007; Patten et al., 2012). Disturbed VEGF signaling and decreased capillary density have also been observed in DCM (Abraham et al., 2000; Karch et al., 2005; Lionetti et al., 2014). Another KO mouse model which lacks the cardiac PPARγ coactivator-1α (PGC-1α), also results in the development of PPCM (Patten et al., 2012). PGC-1α promotes angiogenesis by stimulating VEGF signaling (Arany et al., 2008; Patten et al., 2012), (cardiac) mitochondrial biogenesis and metabolism in a tissue specific manner (Lehman et al., 2000; Arany et al., 2005). However, also in this model PPCM development occurs through the MnSOD, ROS and 16 kDa PRL pathway as the phenotype could only be partly rescued by pro-angiogenic therapy in the form of VEGF A and treatment with both VEGF A and BR was needed to obtain full recovery of LV function. Indeed, in PGC-1α KO mice MnSOD was reduced and ROS increased, which is not surprising as PGC-1α is an inducer of MnSOD (Patten et al., 2012). Repressed levels of PGC-1α have also been observed in PPCM patients (Patten et al., 2012). PGC-1α could also be implied in DCM as PGC-1α KO mice showed inability to increase heart rate in response to dobutamine, had markedly depressed levels of ATP in cardiac muscle and showed ventricle dilation and reduced fractional shortening upon aging (7–8 months), indicating PGC-1α deficiency can induce a DCM-like phenotype (Arany et al., 2005). However, depressed levels of PGC-1α-regulated genes, but not expression levels of PGC-1α itself, have been reported in DCM (Sihag et al., 2009). The extend of depression of PGC-1α regulated genes has been shown to be correlated to LV systolic function, which indicate mitochondrial function as regulated by PGC-1α is impaired in HF (Sihag et al., 2009). The 16 kDa PRL increases NFκB activity induced by miR-146 and thereby causes endothelial cell apoptosis (Tabruyn et al., 2003; Halkein et al., 2013). In addition, 16 kDa PRL up-regulates exosome loading with miR-146 of endothelial cells. Uptake of these exosomes by cardiomyocytes causes miR-146 induced impaired metabolic activity (Halkein et al., 2013). An interesting notion is that miR-146 has been shown to be up-regulated in PPCM but not in DCM patients (Haghikia et al., 2013; Halkein et al., 2013). This indicates that although both patient groups suffer from dysfunctional microvasculature, the exact underlying pathogenesis might not be the same. Impaired microvasculature may result in insufficient oxygen and nutrient delivery to cardiomyocytes resulting in increased susceptibility to apoptosis and impaired cardiac function. It is clear that PPCM and DCM can result in similar clinical presentation even without the presence of PRL. The cleaved form of PRL is likely to cause an additional hit in PPCM quickly worsening disease progression and outcome. An overview of the changes in PPCM and DCM compared to healthy controls, grouped by downstream effect, can be seen in **Table 1**.

PREGNANCY IN DCM PATIENTS AND SUBSEQUENT PREGNANCIES IN PPCM PATIENTS

Given the similarities between PPCM and DCM, DCM patients presenting with the wish to conceive are a complicated patient group to counsel. Only a few studies have explored the disease alterations in DCM patients who become pregnant. The effects of pregnancy on cardiac function in DCM patients are contradictory as limited adverse events and recovery toward pre-pregnancy cardiac function (Bernstein and Magriples, 2001; Blatt et al., 2010), but also significant decreased cardiac event-free survival compared to non-pregnant DCM patients has been reported (Grewal et al., 2009). Adverse outcome in pregnant DCM patients was related to high NTproBNP levels, a known indicator for cardiac dysfunction, Blatt et al. (2010) and New York Heart Association functional classification class III or IV (Grewal et al., 2009). Most cardiac adverse events occurred at the beginning of the third trimester, which coincided with an increase in hemodynamic load on the heart (Grewal et al., 2009)

Table 1 | Altered parameters in PPCM and DCM compared to healthy controls.

	Parameter	PPCM	DCM
Structure	Chamber dilation	↑	↑
	Sarcomere mutations	Possible	Possible
	Sarcomere integrity	↓	↓
	Fibrosis	↑ in animals, unknown in human	↑
	Fetal gene program	Unknown	↑
	Titin N2BA/N2B ratio	Unknown	↑
Oxidative stress	Oxidative stress	↑	↑
	MnSOD	↓	=
	16 kDa PRL	↑	Unlikely
	PGC-1α	↓	↓ target gene expression
	STAT3	↓	↓
Vasculature	Capillary density	↓	↓
	VEGF	↓	↓
	miR-146	↑	=
	miR-199	↑	↑
	ADMA	↑	↑

References for the shown parameters are indicated in the text.

while PRL levels are still relatively low. Another case report that showed adverse events during pregnancy in a DCM patient also showed adverse events earlier in pregnancy than is observed in PPCM (Gevaert et al., 2014). Therefore, most adverse events seen in pregnant DCM patients are most likely due to the cardiac stress during pregnancy that is being placed on an already troubled heart. However, most adverse events were successfully treated and recovery to pre-pregnancy cardiac function was often established. A retrospective study by Bernstein et al. showed pregnancy is well-tolerated in stable DCM patients, while maternal outcome was significantly worse in PPCM patients (Bernstein and Magriples, 2001). Therefore, Bernstein et al. suggest the prognosis of PPCM patients should not be used when a stable DCM patient presents herself with the wish to conceive (Bernstein and Magriples, 2001). This strengthens the suggestion that although PPCM and DCM may share similar genetic predispositions and some common disease pathways, PPCM should not be considered as DCM occurring during or soon after pregnancy. However, it is also possible that pregnant DCM patients are protected from the fast deterioration of cardiac function seen in PPCM due to the fact that DCM patients are already treated for heart failure prior to and during pregnancy and are closely monitored. A small study by Hilfiker-Kleiner et al. showed BR treatment of PPCM patients in their subsequent pregnancy was able to improve survival and prevent relapse compared to PPCM patients without BR treatment (Hilfiker-Kleiner et al., 2007). Studies exploring subsequent pregnancies of PPCM patients revealed a HF relapse in 20–30% and the ability to recover was related to cardiac function after PPCM index pregnancy and prior to the subsequent pregnancy (Elkayam et al., 2005; Fett et al., 2010). From these studies it can be concluded that stable DCM patients are unlikely to develop the fast PPCM disease progression and that the outcome of the DCM patient group is often more favorable than that of PPCM patients. The potential uneventful previous and subsequent pregnancies in PPCM patients indicate we do not know all triggers of PPCM since any predisposing mutation and PRL would also have been present in previous and subsequent event-free pregnancies. As PRL is present in both pregnant DCM patients and PPCM patients, we cannot simply state that PPCM is triggered by the presence of PRL in combination with a weakened heart.

FUTURE PERSPECTIVES

LARGE COHORT STUDIES PPCM

At the moment there is still a lack of prospective studies exploring PPCM in larger cohorts. Most studies to date are case studies or small (often retrospective) cohort studies. A large, multicenter, randomized controlled clinical trial to evaluate BR treatment in 60 PPCM patients is ongoing, and the results should shed light on the effectiveness of BR treatment and outcome (US National Library of Medicine, 2012). In addition, the EURObservational Registry on PPCM has started to enroll patients that will be followed in a 1-year prospective study which will help to evaluate PPCM clinical presentations, risk factors, management and the effects on offspring worldwide (Sliwa et al., 2014).

GENETIC PREDISPOSITIONS

Information about disease initiation and predispositions such as pathogenic mutations is still limited in PPCM and DCM. Therefore, more knowledge is needed on which mutations predispose people to DCM and PPCM and how these mutations exert their pathogenic effect in disease initiation and progression. Identification of these mutations would greatly enhance the ability to identify persons at risk to develop PPCM and DCM and by monitoring these patients early diagnosis and treatment could be facilitated thereby enhancing survival.

CARDIAC REMODELING

As cardiac deterioration, heart transplantations and death often occur within a few months after diagnosis in PPCM, it is possible that the cardiac remodeling to cope with the new cardiac state and demands in PPCM is different than in a more slow progressive disease as DCM. For example, in heart failure it has been shown that the fetal gene program is initiated resulting in cardiac remodeling in order to compensate for decreased cardiac function, although it contributes to cardiac dysfunction at a later stage (Thum et al., 2007). The limited time for adaptation of the heart might be detrimental in PPCM patients, as the lack of time to mount a compensatory response causes the need for cardiac transplantation, or lead to death soon after diagnosis. On the other hand, full recovery of PPCM patients may be explained by lack of permanent cardiac remodeling. However, not enough is known about remodeling of the PPCM heart and the recommendation to not use gadolinium in pregnant women has limited the use of magnetic resonance imaging (MRI) to assess fibrosis in PPCM patients. Therefore, other techniques to assess cardiac remodeling such as immunohistochemical staining of biopsies or explanted heart tissue should be explored in order to shed light on cardiac remodeling in PPCM.

OXIDATIVE STRESS

Based on observations in the STAT3 mouse model, mitigation of the intracellular defense mechanism against oxidative stress in human PPCM so far mainly focused on the reduction of MnSOD levels. Indeed reduction of MnSOD levels is an important contributor to elevated ROS levels in PPCM patients. However, to further unravel the patho-mechanism of oxidative stress in PPCM, future studies should involve the potential contribution of other enzymatic and non-enzymatic ROS scavengers as well as that of potential sources of ROS. Reduced MnSOD expression and PRL cleavage as a result of concomitant oxidative stress have been identified as important regulators of PPCM. Still the complete etiology of PPCM is far from completely understood.

SUMMARY AND CONCLUSION

PPCM and DCM likely share part of their pathogenesis such as predisposing mutations, increased oxidative stress, an impaired microvasculature and damaged sarcomere integrity. However, the exact underlying pathways might be differently altered in PPCM and DCM. While 16 kDa PRL is likely to be a key player in PPCM it is unlikely to play a significant role in DCM. It is this 16 kDa PRL that might explain the faster deterioration of cardiac function in PPCM by inducing an additional cascade of cardiovascular impairment. However, given the observation that pregnant DCM patients do better than PPCM patients, this difference in PRL levels between PPCM patients and non-pregnant DCM patients cannot explain all differences observed.

The reports about uneventful subsequent pregnancies in PPCM patients indicate additional causative factors, such as insufficient defense mechanisms against oxidative stress or a vulnerable microvasculature. Therefore, despite their overlap in disease etiology and clinical presentation, differences in underlying pathways, disease progression and outcome argue for separation of the two disease states.

ACKNOWLEDGMENTS

We acknowledge support by the Netherlands organization for scientific research (NWO; VIDI grant 91711344) and the Rembrandt Institute.

REFERENCES

Abraham, D., Hofbauer, R., Schafer, R., Blumer, R., Paulus, P., Miksovsky, A., et al. (2000). Selective downregulation of VEGF-A165, VEGF-R1, and decreased capillary density in patients with dilative but not ischemic cardiomyopathy. *Circ. Res.* 87, 644–647. doi: 10.1161/01.RES.87.8.644

Alegre-Cebollada, J., Kosuri, P., Giganti, D., Eckels, E., Rivas-Pardo, J. A., Hamdani, N., et al. (2014). S-glutathionylation of cryptic cysteines enhances titin elasticity by blocking protein folding. *Cell* 156, 1235–1246. doi: 10.1016/j.cell.2014.01.056

Anderssohn, M., Rosenberg, M., Schwedhelm, E., Zugck, C., Lutz, M., Lüneburg, N., et al. (2012). The L-Arginine-asymmetric dimethylarginine ratio is an independent predictor of mortality in dilated cardiomyopathy. *J. Card. Fail.* 18, 904–911. doi: 10.1016/j.cardfail.2012.10.011

Arany, Z., Foo, S.-Y., Ma, Y., Ruas, J. L., Bommi-Reddy, A., Girnun, G., et al. (2008). HIF-independent regulation of VEGF and angiogenesis by the transcriptional coactivator PGC-1alpha. *Nature* 451, 1008–1012. doi: 10.1038/nature06613

Arany, Z., He, H., Lin, J., Hoyer, K., Handschin, C., Toka, O., et al. (2005). Transcriptional coactivator PGC-1 alpha controls the energy state and contractile function of cardiac muscle. *Cell Metab.* 1, 259–271. doi: 10.1016/j.cmet.2005.03.002

Assomull, R. G., Prasad, S. K., Lyne, J., Smith, G., Burman, E. D., Khan, M., et al. (2006). Cardiovascular magnetic resonance, fibrosis, and prognosis in dilated cardiomyopathy. *J. Am. Coll. Cardiol.* 48, 1977–1985. doi: 10.1016/j.jacc.2006.07.049

Ballo, P., Betti, I., Mangialavori, G., Chiodi, L., Rapisardi, G., and Zuppiroli, A. (2012). Peripartum cardiomyopathy presenting with predominant left ventricular diastolic dysfunction: efficacy of bromocriptine. *Case Rep. Med.* 2012:476903. doi: 10.1155/2012/476903

Bernstein, P. S., and Magriples, U. (2001). Cardiomyopathy in pregnancy: a retrospective study. *Am. J. Perinatol.* 18, 163–168. doi: 10.1055/s-2001-14525

Blatt, A., Svirski, R., Morawsky, G., Uriel, N., Neeman, O., Sherman, D., et al. (2010). Short and long-term outcome of pregnant women with preexisting dilated cardiomypathy: an NTproBNP and echocardiography-guided study. *Isr. Med. Assoc. J.* 12, 613–616.

Chung, E., and Leinwand, L. A. (2014). Pregnancy as a cardiac stress model. *Cardiovasc. Res.* 101, 561–570. doi: 10.1093/cvr/cvu013

Clapp, J. F. I., and Capeless, E. (1997). Cardiovascular function before, during, and after the first and subsequent pregnancies. *Am. J. Cardiol.* 9149, 1469–1473. doi: 10.1016/S0002-9149(97)00738-8

Codd, M. B., Sugrue, D. D., Gersh, B. J., and Melton, L. J. (1989). Epidemiology of idiopathic dilated and hypertrophic cardiomyopathy. A population-based study in Olmsted County, Minnesota. *Circulation* 80, 564–572. doi: 10.1161/01.CIR.80.3.564

Despa, S. (2002). Intracellular Na+ concentration is elevated in heart failure but na/k pump function is unchanged. *Circulation* 105, 2543–2548. doi: 10.1161/01.CIR.0000016701.85760.97

Dieterich, S., Bieligk, U., Beulich, K., Hasenfuss, G., and Prestle, J. (2000). Gene expression of antioxidative enzymes in increased expression of catalase in the end-stage failing heart. *Circulation* 101, 33–39. doi: 10.1161/01.CIR.101.1.33

Druhan, L. J., Forbes, S. P., Pope, A. J., Chen, C., Zweier, J. L., and Cardounel, A. J. (2008). Regulation of eNOS-derived superoxide by endogenous methylarginines †. 47, 7256–7263. doi: 10.1021/bi702377a

Elkayam, U. (2011). Clinical characteristics of peripartum cardiomyopathy in the United States: diagnosis, prognosis, and management. *J. Am. Coll. Cardiol.* 58, 659–670. doi: 10.1016/j.jacc.2011.03.047

Elkayam, U., Akhter, M. W., Singh, H., Khan, S., Bitar, F., Hameed, A., et al. (2005). Pregnancy-associated cardiomyopathy: clinical characteristics and a comparison between early and late presentation. *Circulation* 111, 2050–2055. doi: 10.1161/01.CIR.0000162478.36652.7E

Elliott, P., Andersson, B., Arbustini, E., Bilinska, Z., Cecchi, F., Charron, P., et al. (2008). Classification of the cardiomyopathies: a position statement from the European Society Of Cardiology Working Group on Myocardial and Pericardial Diseases. *Eur. Heart J.* 29, 270–276. doi: 10.1093/eurheartj/ehm342

Felker, G. M., Thompson, R. E., Hare, J. M., Hruban, R. H., Clemetson, D. E., Howard, D., et al. (2000). Underlying causes and long-term survival in patients with initially unexplained cardiomyopathy. *N.Engl. J. Med.* 342, 1077–1084. doi: 10.1056/NEJM200004133421502

Fett, J. D. (2014). Peripartum cardiomyopathy: a puzzle closer to solution. *World J. Cardiol.* 6, 87–99. doi: 10.4330/wjc.v6.i3.87

Fett, J. D., Christie, L. G., Carraway, R. D., and Murphy J. G. (2005). Five-year prospective study of the incidence and prognosis of peripartum cardiomyopathy at a single institution. *Mayo Clin. Proc.* 80, 1602–1606. doi: 10.4065/80.12.1602

Fett, J. D., Fristoe, K. L., and Welsh, S. N. (2010). Risk of heart failure relapse in subsequent pregnancy among peripartum cardiomyopathy mothers. *Int. J. Gynaecol. Obstet.* 109, 34–36. doi: 10.1016/j.ijgo.2009.10.011

Fish, W. (2012). Inherited cardiomyopathies. *Br. J. Anaesth.* 109, 643. author reply: 643–644. doi: 10.1093/bja/aes327

Fukuda, N., Wu, Y., Farman, G., Irving, T. C., and Granzier, H. (2003). Titin isoform variance and length dependence of activation in skinned bovine cardiac muscle. *J. Physiol.* 553, 147–154. doi: 10.1113/jphysiol.2003.049759

Gaasch, W. H., and Zile, M. R. (2011). Left ventricular structural remodeling in health and disease: with special emphasis on volume, mass, and geometry. *J. Am. Coll. Cardiol.* 58, 1733–1740. doi: 10.1016/j.jacc.2011.07.022

Gevaert, S., De Pauw, M., Tromp, F., Ascoop, A.-K., Roelens, K., and De Backer, J. (2014). Treatment of pre-existing cardiomyopathy during pregnancy. *Acta Cardiol.* 69, 193–196. doi: 10.2143/AC.69.2.3017302

Granzier, H., and Labeit, S. (2002). Cardiac titin: an adjustable multi-functional spring. *J. Physiol.* 541, 335–342. doi: 10.1113/jphysiol.2001.014381

Grattan, D. R., Steyn, F. J., Kokay, I. C., Anderson, G. M., and Bunn, S. J. (2008). Pregnancy-induced adaptation in the neuroendocrine control of prolactin secretion. *J. Neuroendocrinol.* 20, 497–507. doi: 10.1111/j.1365-2826.2008.01661.x

Grewal, J., Siu, S. C., Ross, H. J., Mason, J., Balint, O. H., Sermer, M., et al. (2009). Pregnancy outcomes in women with dilated cardiomyopathy. *J. Am. Coll. Cardiol.* 55, 45–52. doi: 10.1016/j.jacc.2009.08.036

Grützner, A., Garcia-Manyes, S., Kötter, S., Badilla, C. L., Fernandez, J. M., and Linke, W. A. (2009). Modulation of titin-based stiffness by disulfide bonding in the cardiac titin N2-B unique sequence. *Biophys. J.* 97, 825–834. doi: 10.1016/j.bpj.2009.05.037

Haghikia, A., Missol-Kolka, E., Tsikas, D., Venturini, L., Brundiers, S., Castoldi, M., et al. (2011). Signal transducer and activator of transcription 3-mediated regulation of miR-199a-5p links cardiomyocyte and endothelial cell function in the heart: a key role for ubiquitin-conjugating enzymes. *Eur. Heart J.* 32, 1287–1297. doi: 10.1093/eurheartj/ehq369

Haghikia, A., Podewski, E., Libhaber, E., Labidi, S., Fischer, D., Roentgen, P., et al. (2013). Phenotyping and outcome on contemporary management in a German cohort of patients with peripartum cardiomyopathy. *Basic Res. Cardiol.* 108, 366. doi: 10.1007/s00395-013-0366-9

Haghikia, A., Ricke-Hoch, M., Stapel, B., Gorst, I., and Hilfiker-Kleiner, D. (2014). STAT3, a key regulator of cell-to-cell communication in the heart. *Cardiovasc. Res.* 102, 281–289. doi: 10.1093/cvr/cvu034

Halkein, J., Tabruyn, S. P., Ricke-hoch, M., Haghikia, A., Nguyen, N., Scherr, M., et al. (2013). MicroRNA-146a is a therapeutic target and biomarker for peripartum cardiomyopathy. *J. Clin. Invest.* 123, 2143–2154. doi: 10.1172/JCI64365

Herman, D. S., Lam, L., Taylor, M. R. G., Wang, L., Teekakirikul, P., Christodoulou, D., et al. (2012). Truncations of titin causing dilated cardiomyopathy. *N. Engl. J. Med.* 366, 619–628. doi: 10.1056/NEJMoa1110186

Herpel, E., Pritsch, M., Koch, A., Dengler, T. J., Schirmacher, P., and Schnabel, P. A. (2006). Interstitial fibrosis in the heart: differences in extracellular matrix proteins and matrix metalloproteinases in end-stage dilated, ischaemic and

valvular cardiomyopathy. *Histopathology* 48, 736–747. doi: 10.1111/j.1365-2559.2006.02398.x

Hershberger, R. E., Hedges, D. J., and Morales, A. (2013). Dilated cardiomyopathy: the complexity of a diverse genetic architecture. *Nat. Rev. Cardiol.* 10, 531–547. doi: 10.1038/nrcardio.2013.105

Hilfiker-Kleiner, D., Hilfiker, A., Fuchs, M., Kaminski, K., Schaefer, A., Schieffer, B., et al. (2004). Signal transducer and activator of transcription 3 is required for myocardial capillary growth, control of interstitial matrix deposition, and heart protection from ischemic injury. *Circ. Res.* 95, 187–195. doi: 10.1161/01.RES.0000134921.50377.61

Hilfiker-Kleiner, D., Kaminski, K., Podewski, E., Bonda, T., Schaefer, A., Sliwa, K., et al. (2007). A cathepsin D-cleaved 16 kDa form of prolactin mediates postpartum cardiomyopathy. *Cell* 128, 589–600. doi: 10.1016/j.cell.2006.12.036

Hilfiker-Kleiner, D., and Sliwa, K. (2014). Pathophysiology and epidemiology of peripartum cardiomyopathy. *Nat. Rev. Cardiol.* 11, 364–370. doi: 10.1038/nrcardio.2014.37

Hilfiker-Kleiner, D., Struman, I., Hoch, M., Podewski, E., and Sliwa, K. (2012). 16-kDa prolactin and bromocriptine in postpartum cardiomyopathy. *Curr. Heart Fail. Rep.* 9, 174–182. doi: 10.1007/s11897-012-0095-7

Karch, R., Neumann, F., Ullrich, R., Neumüller, J., Podesser, B. K., Neumann, M., et al. (2005). The spatial pattern of coronary capillaries in patients with dilated, ischemic, or inflammatory cardiomyopathy. *Cardiovasc. Pathol.* 14, 135–144. doi: 10.1016/j.carpath.2005.03.003

Kawano, H., Tsuneto, A., Koide, Y., Tasaki, H., Sueyoshi, E., Sakamoto, I., et al. (2008). Magnetic resonance imaging in a patient with peripartum cardiomyopathy. *Intern. Med.* 47, 97–102. doi: 10.2169/internalmedicine.47.0316

Kohlhaas, M., Liu, T., Knopp, A., Zeller, T., Ong, M. F., Böhm, M., et al. (2010). Elevated cytosolic Na+ increases mitochondrial formation of reactive oxygen species in failing cardiac myocytes. *Circulation* 121, 1606–1613. doi: 10.1161/CIRCULATIONAHA.109.914911

Kolte, D., Khera, S., Aronow, W. S., Palaniswamy, C., Mujib, M., Ahn, C., et al. (2014). Temporal trends in incidence and outcomes of peripartum cardiomyopathy in the United States: a nationwide population-based study. *J. Am. Heart Assoc.* 3:e001056. doi: 10.1161/JAHA.114.001056

Lehman, J. J., Barger, P. M., Kovacs, A., Saffitz, J. E., Medeiros, D. M., and Kelly, D. P. (2000). Peroxisome proliferator-activated receptor gamma coactivator-1 promotes cardiac mitochondrial biogenesis. *J. Clin. Invest.* 106, 847–856. doi: 10.1172/JCI10268

Leurent, G., Baruteau, A. E., Larralde, A., Ollivier, R., Schleich, J. M., Boulmier, D., et al. (2009). Contribution of cardiac MRI in the comprehension of peripartum cardiomyopathy pathogenesis. *Int. J. Cardiol.* 132, e91–e93. doi: 10.1016/j.ijcard.2007.12.012

Levine, R. J., Maynard, S. E., Qian, C., Lim, K.-H., England, L. J., Yu, K. F., et al. (2004). Circulating angiogenic factors and the risk of preeclampsia. *N. Engl. J. Med.* 350, 672–683. doi: 10.1056/NEJMoa031884

Lionetti, V., Matteucci, M., Ribezzo, M., Di Silvestre, D., Brambilla, F., Agostini, S., et al. (2014). Regional mapping of myocardial hibernation phenotype in idiopathic end-stage dilated cardiomyopathy. *J. Cell. Mol. Med.* 18, 396–414. doi: 10.1111/jcmm.12198

Maack, C., Kartes, T., Kilter, H., Schäfers, H.-J., Nickenig, G., Böhm, M., et al. (2003). Oxygen free radical release in human failing myocardium is associated with increased activity of rac1-GTPase and represents a target for statin treatment. *Circulation* 108, 1567–1574. doi: 10.1161/01.CIR.0000091084.46500.BB

Makarenko, I., Opitz, C. A., Leake, M. C., Neagoe, C., Kulke, M., Gwathmey, J. K., et al. (2004). Passive stiffness changes caused by upregulation of compliant titin isoforms in human dilated cardiomyopathy hearts. *Circ. Res.* 95, 708–716. doi: 10.1161/01.RES.0000143901.37063.2f

McMullen, J. R., and Jennings, G. L. (2007). Differences between pathological and physiological cardiac hypertrophy: novel therapeutic strategies to treat heart failure. *Clin. Exp. Pharmacol. Physiol.* 34, 255–262. doi: 10.1111/j.1440-1681.2007.04585.x

Morales, A., Painter, T., Li, R., Siegfried, J. D., Li, D., Norton, N., et al. (2010). Rare variant mutations in pregnancy-associated or peripartum cardiomyopathy. *Circulation* 121, 2176–2182. doi: 10.1161/CIRCULATIONAHA.109.931220

Mouquet, F., Lions, C., de Groote, P., Bouabdallaoui, N., Willoteaux, S., Dagorn, J., et al. (2008). Characterisation of peripartum cardiomyopathy by cardiac magnetic resonance imaging. *Eur. Radiol.* 18, 2765–2769. doi: 10.1007/s00330-008-1067-x

Nagueh, S. F., Shah, G., Wu, Y., Torre-Amione, G., King, N. M. P., Lahmers, S., et al. (2004). Altered titin expression, myocardial stiffness, and left ventricular function in patients with dilated cardiomyopathy. *Circulation* 110, 155–162. doi: 10.1161/01.CIR.0000135591.37759.AF

Negoro, S., Kunisada, K., Fujio, Y., Funamoto, M., Darville, M. I., Eizirik, D. L., et al. (2001). Activation of signal transducer and activator of transcription 3 protects cardiomyocytes from hypoxia/reoxygenation-induced oxidative stress through the upregulation of manganese superoxide dismutase. *Circulation* 104, 979–981. doi: 10.1161/hc3401.095947

Ntusi, N. B., and Chin, A. (2009). Characterisation of peripartum cardiomyopathy by cardiac magnetic resonance imaging. *Eur. Radiol.* 19, 1324–1325. author reply: 1326–1327. doi: 10.1007/s00330-008-1244-y

Osugi, T., Oshima, Y., Fujio, Y., Funamoto, M., Yamashita, A., Negoro, S., et al. (2002). Cardiac-specific activation of signal transducer and activator of transcription 3 promotes vascular formation in the heart. *J. Biol. Chem.* 277, 6676–6681. doi: 10.1074/jbc.M108246200

Pacher, P., Beckman, J. S., and Liaudet, L. (2007). Nitric oxide and peroxynitrite in health and disease. *Physiol. Rev.* 87, 315–424. doi: 10.1152/physrev.00029.2006

Parks, S. B., Kushner, J. D., Nauman, D., Burgess, D., Ludwigsen, S., Peterson, A., et al. (2008). Lamin A/C mutation analysis in a cohort of 324 unrelated patients with idiopathic or familial dilated cardiomyopathy. *Am. Heart J.* 156, 161–169. doi: 10.1016/j.ahj.2008.01.026

Patten, I. S., Rana, S., Shahul, S., Rowe, G. C., Jang, C., Liu, L., et al. (2012). Cardiac angiogenic imbalance leads to peripartum cardiomyopathy. *Nature* 485, 333–338. doi: 10.1038/nature11040

Pearson, G. D., Veille, J.-C., Rahimtoola, S., Hsia, J., Oakley, C. M., Hosenpud, J. D., et al. (2000). Peripartum cardiomyopathy:national heart, lung and blood institute and office of rare diseases (national institutes of health) workshop recommendations and review. *JAMA* 283, 1183–1188. doi: 10.1001/jama.283.9.1183

Podewski, E. K. (2003). Alterations in Janus Kinase (JAK)-signal transducers and activators of transcription (STAT) signaling in patients with end-stage dilated cardiomyopathy. *Circulation* 107, 798–802. doi: 10.1161/01.CIR.0000057545.82749.FF

Prosser, B. L., Ward, C. W., and Lederer, W. J. (2011). X-ROS signaling: rapid mechano-chemo transduction in heart. *Science* 333, 1440–1445. doi: 10.1126/science.1202768

Remmen, H. V., Williams, M. D., Guo, Z., Estlack, L., Yang, H., Carlson, E. J., et al. (2001). Knockout mice heterozygous for Sod2 show alterations in cardiac mitochondrial function and apoptosis. *Am. J. Physiol. Heart Circ. Physiol.* 281, H1422–H1432.

Ricke-Hoch, M., Bultmann, I., Stapel, B., Condorelli, G., Rinas, U., Sliwa, K., et al. (2014). Opposing roles of Akt and STAT3 in the protection of the maternal heart from peripartum stress. *Cardiovasc. Res.* 101, 587–596. doi: 10.1093/cvr/cvu010

Sag, C. M., Wagner, S., and Maier, L. S. (2013). Role of oxidants on calcium and sodium movement in healthy and diseased cardiac myocytes. *Free Radic. Biol. Med.* 63, 338–349. doi: 10.1016/j.freeradbiomed.2013.05.035

Seddon, M., Looi, Y. H., and Shah, A. M. (2007). Oxidative stress and redox signalling in cardiac hypertrophy and heart failure. *Heart* 93, 903–907. doi: 10.1136/hrt.2005.068270

Sihag, S., Cresci, S., Li, A. Y., Sucharov, C. C., and Lehman, J. J. (2009). PGC-1alpha and ERRalpha target gene downregulation is a signature of the failing human heart. *J. Mol. Cell. Cardiol.* 46, 201–212. doi: 10.1016/j.yjmcc.2008.10.025

Sliwa, K., Blauwet, L., Tibazarwa, K., Libhaber, E., Smedema, J.-P., Becker, A., et al. (2010). Evaluation of bromocriptine in the treatment of acute severe peripartum cardiomyopathy: a proof-of-concept pilot study. *Circulation* 121, 1465–1473. doi: 10.1161/CIRCULATIONAHA.109.901496

Sliwa, K., Hilfiker-Kleiner, D., Mebazaa, A., Petrie, M. C., Maggioni, A. P., Regitz-Zagrosek, V., et al. (2014). EURObservational research programme: a worldwide registry on peripartum cardiomyopathy (PPCM) in conjunction with the Heart Failure Association of the European Society of Cardiology Working Group on PPCM. *Eur. J. Heart Fail.* 16, 583–591. doi: 10.1002/ejhf.68

Tabruyn, S. P., Sorlet, C. M., Rentier-Delrue, F., Bours, V., Weiner, R. I., Martial, J., et al. (2003). The antiangiogenic factor 16K human prolactin induces caspase-dependent apoptosis by a mechanism that requires activation of nuclear factor-kappaB. *Mol. Endocrinol.* 17, 1815–1823. doi: 10.1210/me.2003-0132

Thum, T., Galuppo, P., Wolf, C., Fiedler, J., Kneitz, S., van Laake, L. W., et al. (2007). MicroRNAs in the human heart: a clue to fetal gene reprogramming in heart failure. *Circulation* 116, 258–267. doi: 10.1161/CIRCULATIONAHA.107.687947

Toescu, V., Nuttall, S. L., Martin, U., Kendall, M. J., and Dunne, F. (2002). Oxidative stress and normal pregnancy. *Clin. Endocrinol. (Oxf.)* 57, 609–613. doi: 10.1046/j.1365-2265.2002.01638.x

Umar, S., Nadadur, R., Iorga, A., Amjedi, M., Matori, H., and Eghbali, M. (2012). Cardiac structural and hemodynamic changes associated with physiological heart hypertrophy of pregnancy are reversed postpartum. *J. Appl. Physiol.* 113, 1253–1259. doi: 10.1152/japplphysiol.00549.2012

US National Library of Medicine. (2012). *ClinicalTrials.Gov*. Available online at: http://clinicaltrials.gov/ct2/show/NCT00998556

Van Hoeven, K. H., Kitsis, R. N., Katz, S. D., and Factor, S. M. (1993). Peripartum versus idiopathic dilated cardiomyopathy in young women-a comparison of clinical, pathologic and prognostic features. *Int. J. Cardiol.* 40, 57–65. doi: 10.1016/0167-5273(93)90231-5

Van Spaendonck-Zwarts, K. Y., Posafalvi, A., van den Berg, M. P., Hilfiker-Kleiner, D., Bollen, I. A. E., Sliwa, K., et al. (2014). Titin gene mutations are common in families with both peripartum cardiomyopathy and dilated cardiomyopathy. *Eur. Heart J.* 35, 2165–2173. doi: 10.1093/eurheartj/ehu050

Van Spaendonck-Zwarts, K. Y., van Tintelen, J. P., van Veldhuisen, D. J., van der Werf, R., Jongbloed, J. D. H., Paulus, W. J., et al. (2010). Peripartum cardiomyopathy as a part of familial dilated cardiomyopathy. *Circulation* 121, 2169–2175. doi: 10.1161/CIRCULATIONAHA.109.929646

Verhaar, M. C. (2004). Free radical production by dysfunctional eNOS. *Heart* 90, 494–495. doi: 10.1136/hrt.2003.029405

Wilcox, C. S. (2012). Asymmetric dimethylarginine and reactive oxygen species: unwelcome twin visitors to the cardiovascular and kidney disease tables. *Hypertension* 59, 375–381. doi: 10.1161/HYPERTENSIONAHA.111.187310

Wojciechowska, C., Romuk, E., Tomasik, A., Nowalany-kozielska, E., Birkner, E., and Jache, W. (2014). Oxidative stress markers and C-reactive protein are related to severity of heart failure in patients with dilated *Cardiomyopathy.* 2014:147040 doi: 10.1155/2014/147040

Conflict of Interest Statement: The authors declare that the research was conducted in the absence of any commercial or financial relationships that could be construed as a potential conflict of interest.

Received: 05 December 2014; accepted: 29 December 2014; published online: 15 January 2015.

Citation: Bollen IAE, Van Deel ED, Kuster DWD and Van Der Velden J (2015) Peripartum cardiomyopathy and dilated cardiomyopathy: different at heart. Front. Physiol. ***5****:531. doi: 10.3389/fphys.2014.00531*

This article was submitted to Striated Muscle Physiology, a section of the journal Frontiers in Physiology.

Copyright © 2015 Bollen, Van Deel, Kuster and Van Der Velden. This is an open-access article distributed under the terms of the Creative Commons Attribution License (CC BY). The use, distribution or reproduction in other forums is permitted, provided the original author(s) or licensor are credited and that the original publication in this journal is cited, in accordance with accepted academic practice. No use, distribution or reproduction is permitted which does not comply with these terms.

frontiers in PHYSIOLOGY

HYPOTHESIS AND THEORY ARTICLE
published: 10 October 2014
doi: 10.3389/fphys.2014.00392

Familial hypertrophic cardiomyopathy: functional variance among individual cardiomyocytes as a trigger of FHC-phenotype development

Bernhard Brenner*, Benjamin Seebohm, Snigdha Tripathi, Judith Montag and Theresia Kraft

Institute of Molecular and Cell Physiology, Hannover Medical School, Hannover, Germany

Edited by:
Julien Ochala, KIng's College London, UK

Reviewed by:
Nazareno Paolocci, Johns Hopkins University, USA
Martina Krüger, Heinrich Heine University Düsseldorf, Germany

****Correspondence:***
Bernhard Brenner, Institute of Molecular and Cell Physiology, Hannover Medical School, Carl-Neuberg-Str. 1, 30625 Hannover, Germany
e-mail: brenner.bernhard@mh-hannover.de

Familial hypertrophic cardiomyopathy (FHC) is the most frequent inherited cardiac disease. It has been related to numerous mutations in many sarcomeric and even some non-sarcomeric proteins. So far, however, no common mechanism has been identified by which the many different mutations in different sarcomeric and non-sarcomeric proteins trigger development of the FHC phenotype. Here we show for different *MYH7* mutations variance in force pCa-relations from normal to highly abnormal as a feature common to all mutations we studied, while direct functional effects of the different FHC-mutations, e.g., on force generation, ATPase or calcium sensitivity of the contractile system, can be quite different. The functional variation among individual *M. soleus* fibers of FHC-patients is accompanied by large variation in mutant vs. wildtype β-MyHC-mRNA. Preliminary results show a similar variation in mutant vs. wildtype β-MyHC-mRNA among individual cardiomyocytes. We discuss our previously proposed concept as to how different mutations in the β-MyHC and possibly other sarcomeric and non-sarcomeric proteins may initiate an FHC-phenotype by functional variation among individual cardiomyocytes that results in structural distortions within the myocardium, leading to cellular and myofibrillar disarray. In addition, distortions can activate stretch-sensitive signaling in cardiomyocytes and non-myocyte cells which is known to induce cardiac remodeling with interstitial fibrosis and hypertrophy. Such a mechanism will have major implications for therapeutic strategies to prevent FHC-development, e.g., by reducing functional imbalances among individual cardiomyocytes or by inhibition of their triggering of signaling paths initiating remodeling. Targeting increased or decreased contractile function would require selective targeting of mutant or wildtype protein to reduce functional imbalances.

Keywords: *MYH7*-mutations, allelic imbalance, myocyte disarray, interstitial fibrosis, converter domain of myosin head, myosin head stiffness, calcium sensitivity of muscle fibers, calcium sensitivity of cardiomyocytes

INTRODUCTION

Familial hypertrophic cardiomyopathy (FHC) is the most frequent inherited cardiac disease and the most common cause of sudden cardiac death in otherwise healthy young individuals and athletes (Maron et al., 2003). FHC is characterized by asymmetric hypertrophy of the left ventricle, pronounced myocyte and myofibrillar disarray, and interstitial fibrosis. These structural features together with arrhythmias, unexplained syncopes and sudden cardiac death are hallmarks of the FHC. The clinical phenotype of FHC is heterogeneous ranging from almost asymptomatic to highly malignant with sudden cardiac death or development of end-stage heart failure (Spirito et al., 1987; Maron et al., 2003). More than 300 FHC-related mutations were identified within the in the β-myosin heavy chain (β-MyHC; Moore et al., 2012) revealing allelic genetic heterogeneity. FHC-related mutations, however, were also found in a large number of other sarcomeric proteins (non-allelic genetic heterogeneity in FHC), few even in non-sarcomeric proteins. Mutations in the β-MyHC, cardiac myosin-binding protein C (cMyBPC), cardiac troponin-T (cTnT), and cardiac troponin-I (cTnI) account for nearly 90% of all FHC-cases. About 40% of all genotyped FHC-patients carry missense mutations in *MYH7*, about 30–40% in the cMyBPC gene (Richard et al., 2003; Fokstuen et al., 2008; Ho et al., 2010). So far, however, it is still unclear how altogether several hundred different mutations in a large number of different sarcomeric and some non-sarcomeric proteins result in the characteristic features of FHC.

Since FHC is a monogenic disease, the phenotype is thought to result from the triggering of phenotype development by the respective mutation (Ashrafian et al., 2011). This raised the question about the trigger common to all the different mutations in the different proteins. *In vitro* motility and ATPase-assays on isolated sarcomeric proteins together with the analysis of mouse models led to the hypothesis that enhanced calcium-sensitivity, increased maximal force generation, and higher ATPase activity are the common features of FHC-related mutations (Robinson et al., 2002, 2007; Debold et al., 2007), resulting in impaired energy metabolism (Spindler et al., 1998; Blair et al., 2001) and altered calcium-handling in cardiomyocytes (Baudenbacher et al.,

2008; Guinto et al., 2009). Several data reported about functional effects of FHC-mutations are in conflict with this hypothesis. For example, force generation of cardiomyocytes from tissue samples of affected patients was reduced compared to control for β-MyHC mutations, mutations in the cMyBPC, and for FHC-patients with unidentified mutations (Hoskins et al., 2010; van Dijk et al., 2012; Kraft et al., 2013). For several β-MyHC mutations calcium sensitivity was found reduced, or unchanged but with residual active forces under relaxing conditions (Kirschner et al., 2005; Kraft et al., 2013). For only two out of four β-MyHC mutations ATPase was enhanced but unchanged for the others (Seebohm et al., 2009; Witjas-Paalberends et al., 2014) while two out of three β-MyHC mutations showed higher force generation than controls while force generation was unchanged for the third when force generation was studied in *M. soleus* fibers of affected patients (Seebohm et al., 2009). Thus, the effects of quite many FHC-mutations do not fall into the previously proposed common mechanism for FHC-development of increased contractile functions. This could, in part, be due to secondary effects like myofibrillar disarray affecting some of these parameters, e.g., maximum force generation (Kraft et al., 2013). Thus, altogether no common trigger for FHC-development has been identified so far. Knowing the trigger and subsequent steps in the pathogenesis of FHC holds the potential to identify novel targets for novel therapeutic strategies, e.g., in the prevention cardiac remodeling in FHC-patients harboring different FHC-related mutations.

Here we summarize our work on the functional characterization of FHC-related mutations in the β-MyHC both in skeletal and myocardial tissue samples of affected patients. Our goal was to identify features that might be common to many if not all FHC-related mutations and thus may be a trigger for development of the typical FHC-phenotype by different mutations in different sarcomeric and even non-sarcomeric proteins. We will finally discuss a possibly common feature and how it might initiate myocyte disarray, interstitial fibrosis and hypertrophy, the hallmarks of FHC-related cardiac remodeling.

EFFECTS OF FHC-RELATED MUTATIONS IN THE β-MyHC ON FORCE GENERATION AND FIBER STIFFNESS

MEASUREMENTS ON ISOLATED FIBERS OF *M. SOLEUS* TISSUE SAMPLES OF FHC-PATIENTS

We had focussed our earlier work on the functional effects of missense mutations in the converter domain of the β-MyHC, mutations R719W, R723G, and I736T (cf. **Figure 1**, Rayment et al., 1993). Our goal was to identify direct functional effects of these mutations on muscle function that may be common to all three mutations and common to other FHC-related mutations, including mutations in other proteins.

Tissue samples of *M. soleus* were obtained by open biopsy. The samples were immediately separated in small bundles and fiber membranes were dissolved by incubation in skinning solution, an ATP-containing solution mimicking the intracellular ionic milieu to which 0.5% Triton X100 was added. Fiber bundles were then equilibrated with solutions containing increasing concentrations of sucrose (maximum 2 M) as a cryoprotectant. Fiber bundles were then rapidly frozen in liquid propane and stored in liquid nitrogen until use. For details see Kraft et al. (1995). For experiments fiber bundles were thawed, individual fibers were isolated and mounted between a strain gage force transducer and a motor to control muscle length or load. As a direct measure of length and length changes of the muscle fibers we measured sarcomere length by laser light diffraction. For further details see Seebohm et al. (2009). The mounted individual fibers were bathed in different experimental solutions that mimicked the ionic composition of the intracellular medium. Different free Ca^{++}-ion concentrations were obtained by adding the calcium chelator EGTA and CaEGTA in appropriate proportions. Free Ca^{++}-ion concentrations were calculated according to Föhr et al. (1993). For measurements under rigor conditions, fibers were incubated in solutions without MgATP that contained 3 mM EDTA to quickly remove free Mg^{++}-ions.

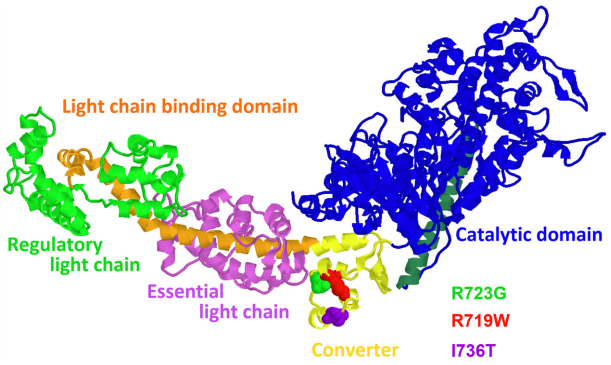

FIGURE 1 | Structural model of the myosin head domain (Rayment et al., 1993) illustrating the locations of the converter mutations R719W, R723G, and I736T. Note location of mutations R719W and R723G more in the core of the converter in a helix close to the long α-helix of the light chain binding domain that is anchored in the converter. Mutation I736T is near the surface of the converter (figure prepared with RasMol).

We first measured stiffness of single *M. soleus* muscle fibers in rigor (**Figures 2A,B**) and during active contraction (**Figures 2C,D**, Seebohm et al., 2009). Stiffness was measured by applying small ramp-shaped length changes, stretches (**Figure 2A**) or releases (**Figure 2C**) for stiffness in rigor or during active contraction, respectively. During these length changes force and change in sarcomere length were recorded. Fiber stiffness was measured as the slope when force was plotted vs. change in sarcomere length (cf. **Figures 2A,C**). For stiffness during active contraction the slope over the initial 2–3 nm of length change was determined (red line in **Figure 2C**) for further details of stiffness measurements see Brenner (1998). Under rigor conditions and during active contraction we observed an increased fiber stiffness for mutations R723G and R719W, while stiffness of fibers with mutation I736T was unchanged (**Figures 2B,C**). The increased stiffness in rigor, i.e., when all myosin heads are attached to actin, immediately suggested that mutations R723G and R719W both increase the stiffness of the myosin head domain.

QUANTITATIVE ESTIMATE OF THE CHANGE IN MYOSIN HEAD STIFFNESS BY MUTATIONS R719W AND R723G

For a quantitative estimate of the increase in stiffness per myosin head we had to determine the elastic distortion of the myosin

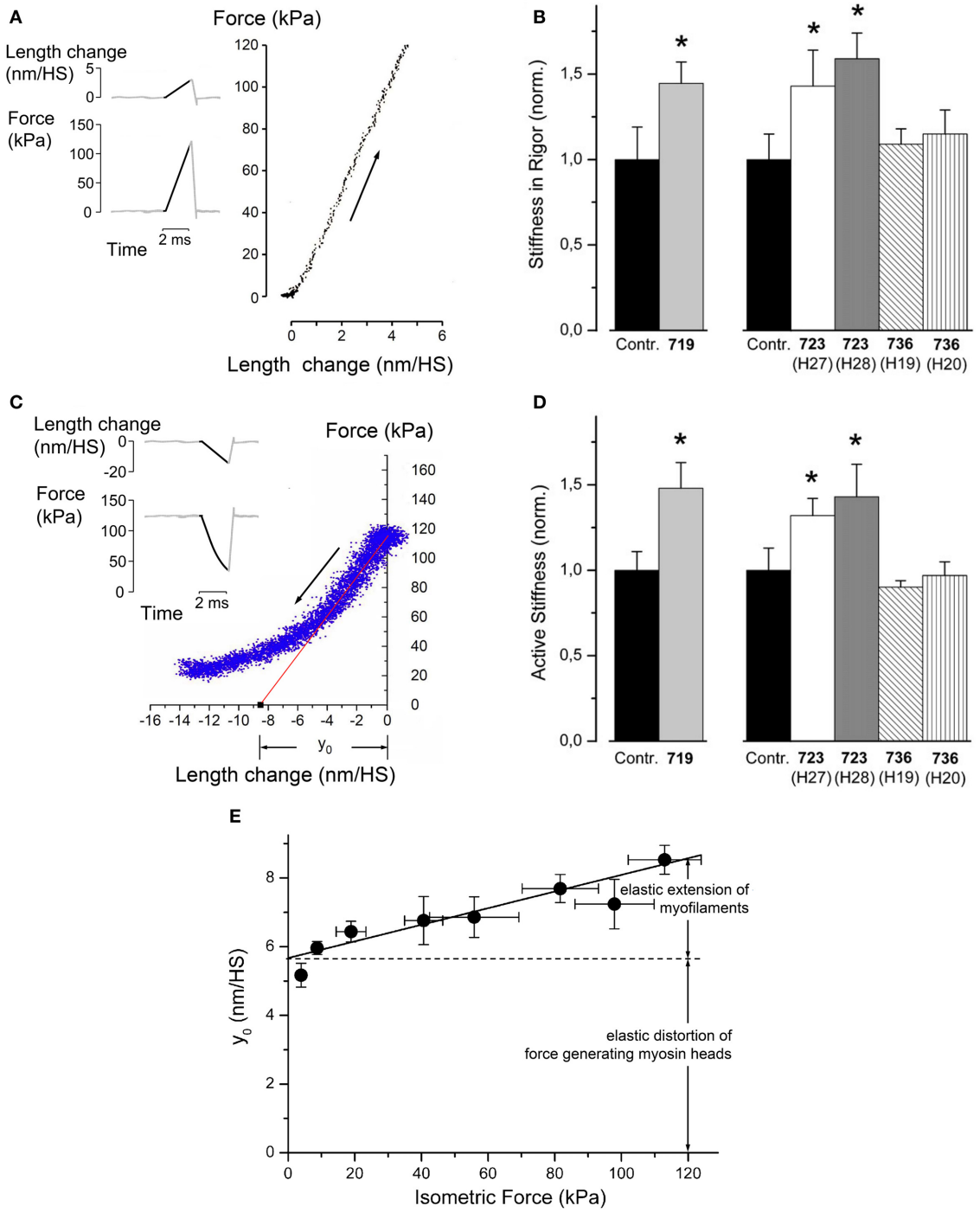

FIGURE 2 | Effects of mutations R719W, R723G, and I736T on stiffness of soleus muscle fibers in rigor (absence of nucleotide) and during active contraction. (A) Principle of stiffness measurement in rigor. In rigor fibers generate no force when put in rigor by rapid removal of free Mg^{2+}-ions together with removal of ATP (Brenner et al., 1986). Thus, stiffness was measured by applying a ramp-shaped stretch (see inset for a schematic illustration). Stiffness is the slope when force change is plotted vs. applied change in sarcomere length, measured in nm/half sarcomere (nm/HS). Note that only the dark part of the traces in the inset are included in the force vs. length change plot. Noise of this plot was reduced by signal-averaging responses of several such maneuvers. **(B)** Fiber stiffness in rigor for the mutations and control fibers. Speed of stretch ~3–5 × 10^3 (nm/half sarcomere)s^{-1}; $T = 5°C$; $n = 5$–10 fibers. Mean values ± *SE*, normalized control fibers, respectively. *Difference to controls statistically significant, $p \leq 0.05$. **(C)** Principle of stiffness measurements during isometric steady state contraction. When fibers have reached constant isometric force a ramp shaped release is imposed on the fiber length. This results in a drop of isometric force (cf. inset for schematic illustration of length change and force response). Over the initial 2–3 nm of length change the plot of force vs. sarcomere length change is linear. Deviation from the linear response later in the release is due to rapid re-equilibration of myosin heads in their different

(Continued)

FIGURE 2 | Continued
force-generating states. The slope of the initial linear part is determined by linear regression (red line) and taken as active fiber stiffness. The intercept of this line with the abscissa is the y_0-value. This is interpreted as the elastic extension of the actin and myosin filaments plus elastic distortion of the force generating myosin heads (Linari et al., 2007). The plot of force vs. length change is noisier than in **(B)**. This is due to the fact that fewer measurements were signal-averaged than under rigor conditions shown in **(A)**. **(D)** Fiber stiffness determined during isometric steady state contraction [speed of release ∼2–4 × 10^3 (nm/half-sarcomere)s^{-1}]; $T = 10$°C to ensure structural integrity of fibers and stability of striation pattern throughout experiments; $n = 6$–14 fibers. Mean values ± *SE*, normalized control fibers, respectively. *Difference to controls statistically significant, $p \leq 0.05$. **(E)** Plot of y_0, vs. isometric force at different levels of calcium-activation. The y_0-values were measured from T-plots (cf. **C**) at pCa values from 4.5 to 6.6; $T = 10$°C. Speed of length release 4–5 × 10^3 (nm/half-sarcomere)s^{-1}. Continuous line obtained by linear regression. Y-axis intercept of solid line is 5.67 nm/HS (HS = half sarcomere) equals elastic extension of force generating heads (cf. double headed arrow). Slope of solid line is filament compliance per half-sarcomere, about 0.025 nm/kPa. Elastic extension of myofilaments at an isometric force of 120 kPa is illustrated by double arrow. Panels **(B, D** and **E)** reprinted with modifications from Seebohm et al. (2009) with permission from Elsevier.

head vs. elastic extension of myofilaments while active force was generated or while fibers were in rigor. This was possible from measurements of active force and active stiffness at different degrees of Ca^{++}-activation (cf. Linari et al., 2007). **Figure 2E** shows these data and illustrates the separation between elastic head distortion and elastic filament extension at different levels of active force. The slope of the solid line in **Figure 2E** is the compliance of the myofilaments. The intercept of this line with the ordinate at about 5.5 nm/HS represents the elastic extension of the force-generating cross bridges. This is assumed to be the same for all levels of Ca^{++}-activation. The y_0-value is the amplitude of fiber release per half-sarcomere that is necessary to drop active force to zero if no fast redistribution of cross-bridges among their different states had occurred (intercept of red solid line in **Figure 2C** with abscissa at about 8.6 nm/HS). In this concept the y_0 equals the elastic extension/distortion of the force generating cross-bridges, about 5.6 nm, plus the elastic extension of the myofilaments that increases with the forces (isometric force) that act on the myofilaments (cf. Linari et al., 2007).

For a quantitative estimate of the changes in stiffness and in the contribution to force generation by the individual myosin head, caused by the converter mutations, we also had to know how many myosin molecules actually carry the FHC-mutation. From the autosomal dominant inheritance one may have assumed that 50% of the myosin molecules carry the mutation while the other 50% have the wildtype sequence. Analysis by mass spectrometry, however, revealed that the abundance of mutant protein is not equal to 50% but instead is characteristic for each particular mutation (allelic imbalance; **Figure 3**, black bars). The same allelic imbalance is found for different members of the same family (cf. I734T, R723G) and for different generations (cf. R723G), but also in unrelated families with the same mutation (cf. V606M, R723G). In addition, the same abundance is found in *M. soleus* fibers and in left ventricular myocardium (cf. R723G). Analysis of expression of the mutant allele at the mRNA-level revealed very similar fractions of mutant mRNA (allelic imbalance) as was found for the mutant protein (**Figure 3**, gray bars vs. black bars).

The known fraction of mutant myosin in our samples allowed us to estimate the change in head stiffness (change in resistance to elastic distortion) from the observed increase in fiber stiffness, i.e., of the mixture of mutant and wildtype myosin molecules, and the known compliance of the myofilaments (**Figure 2C**, Seebohm et al., 2009). This estimate yielded an about 2.6-fold increase in head stiffness for mutation R719W and about 2.9-fold increase for mutation R723G while mutation I736T had no such effect (Seebohm et al., 2009).

Based on the fundamental mechanism of force generation, i.e., that active forces result from elastic distortion of actin attached myosin heads caused by structural changes in the myosin head during its working stroke (Huxley, 1957), an increased head stiffness that corresponds to an increased resistance to elastic distortion is expected to result in increased generation of active force. In fact the estimated increase in stiffness of the individual head domain indicated by our stiffness measurements predicted an increase in force generation that was very close to that observed experimentally, about 2-fold for the head domains with mutation R723G or R719W (Seebohm et al., 2009).

The increased head stiffness by converter mutations R719W and R723G implies that the converter domain itself is a major determinant of head stiffness since a point mutation in a particular domain can result in an increase in head stiffness only if the affected domain is a compliant part of the molecule. Stiffening of an already rigid component would not affect overall "stiffness" of a molecule since overall stiffness is limited by the most compliant element(s) of the molecule. But why should increased head stiffness and increased contribution to force generation by an individual myosin head cause disease?

Since mutations R719W and R723G increased myosin head stiffness while mutation I736T did not, we wondered whether the first two mutations were located at particular points in the converter sequence. We therefore compared the amino acid sequence of the β-cardiac myosin heavy chain (which is also the heavy chain of slow skeletal muscle) with the sequences of fast skeletal myosin heavy chains. This revealed that the FHC-mutations R719W and R723G are located at positions where the β-cardiac/slow MHC differs from fast MyHC isoforms in the otherwise highly conserved converter region (cf. **Table 1**). This raised the question, whether fast and slow skeletal myosins may actually differ in the head stiffness and thus the force generated by a cross-bridge in a force-generating state. We tested this by both stiffness measurements on skinned fibers of human soleus (β-cardiac/slow skeletal MyHC) vs. rabbit psoas (fast skeletal MyHC-2D) and by optical trapping on β-cardiac/slow skeletal myosin subfragment 1 prepared from human and rabbit slow skeletal muscle fibers vs. fast myosin subfragment 1 from the rabbit psoas (Seebohm et al., 2009; Brenner et al., 2012). This revealed that the fast MyHC has ≥3-fold higher head stiffness than the slow/β-cardiac

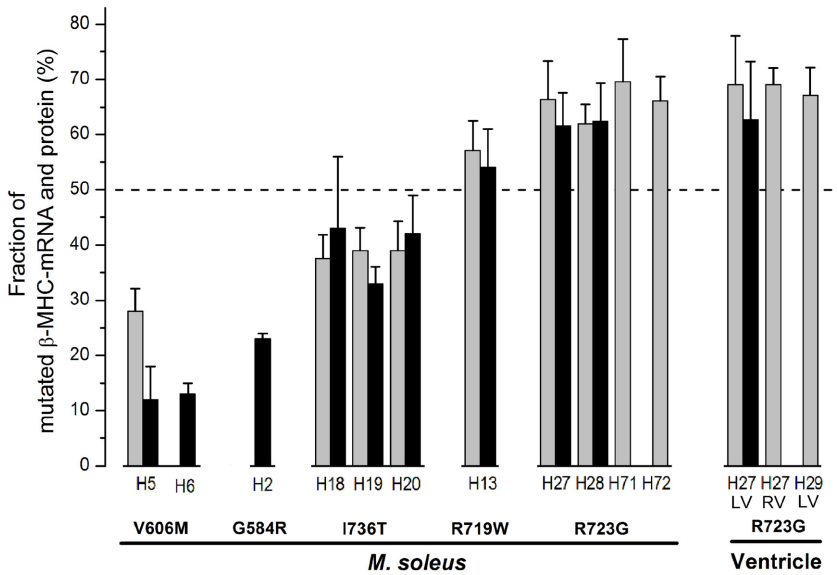

FIGURE 3 | Fractions of mutated β-cardiac/slow skeletal MyHC-mRNA and of β-cardiac/slow skeletal MyHC protein for different FHC-mutations. Gray bars, fractions of mutated mRNA; black bars, fractions of mutated protein. Data for *M. soleus* samples of mutations V606M, G584R, I736T, R719W, and R723G. For mutation R723G data from ventricular myocardium are also included (LV, left ventricle; RV, right ventricle). Note that all mutations significantly deviate from equal abundance of wild-type and mutated transcript (allelic imbalance) with very similar deviations also at the protein level. Allelic imbalance for mutated mRNA and protein were very similar in *M. soleus* and myocardium (mutation R723G). Also note the essentially identical expression of mRNA and protein both within families (I736T, R723G) and among unrelated families (V606M, R723G). Reprinted from Tripathi et al. (2011).

Table 1 | Converter sequences and stiffness per myosin head for β-cardiac/slow skeletal and fast skeletal myosin heavy chain isoforms.

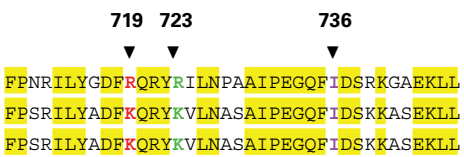

β-cardiac/slow skeletal MyHC I
skeletal MyHC IIA
skeletal MyHC IIX/IID

MyHC isoform (source)	Stiffness/Head	References
FIBER STUDIES		
β-cardiac/slow skeletal MyHC I (human soleus)	0.3–0.5 pN/nm	Seebohm et al., 2009
Fast skeletal MyHC IID (rabbit psoas)	1.7 pN/nm	Linari et al., 2007; Brenner et al., 2012
TRAPPING STUDIES		
Slow skeletal MyHC I (rabbit, rat)	0.3–0.4 pN/nm	Capitanio et al., 2006; Brenner et al., 2012
Fast skeletal MyHC IIA, D (rabbit back muscle, M. psoas)	2–3 pN/nm	Lewalle et al., 2008; Brenner et al., 2012

Yellow, fully conserved residues, unmarked, residues where β-cardiac/slow skeletal myosin heavy chain sequence differs from the fast isoforms. Note that mutations R719W and R723G are located at positions where fast and slow isoforms differ. Mutation I736T is located at a position where fast and slow isoforms are identical. Stiffness per myosin head domain of fast and slow MyHC derived from stiffness measurements in muscle fibers and by optical trapping on myosin head domains (myosin subfragment 1) isolated from muscle tissue.

MyHC (cf. **Table 1**). This was supported by data in the literature (cf. **Table 1**; Capitanio et al., 2006; Lewalle et al., 2008). So increased head stiffness with increased contribution to force generation appears to be physiological in fast skeletal muscle fibers. This made it even more puzzling as to why converter mutations R719W and R723G cause disease. In addition, increased head stiffness with increased contribution to force generation cannot act as a common trigger for FHC-development, not even for myosin mutations since mutation I736T showed no such effect.

POSSIBLE EFFECTS ON CROSS-BRIDGE CYCLING KINETICS

To test whether (additional) effects on cross-bridge cycling kinetics are common to all three converter mutations and may be the common trigger of phenotype development, we measured the rate constant of force redevelopment (k_{redev}) and fiber ATPase (Seebohm et al., 2009).

Figure 4A shows original records of measurements of the rate constant of force redevelopment (top panel) together with the data obtained for the three converter domain mutations (bottom panel). No statistically significant effects were detectable for

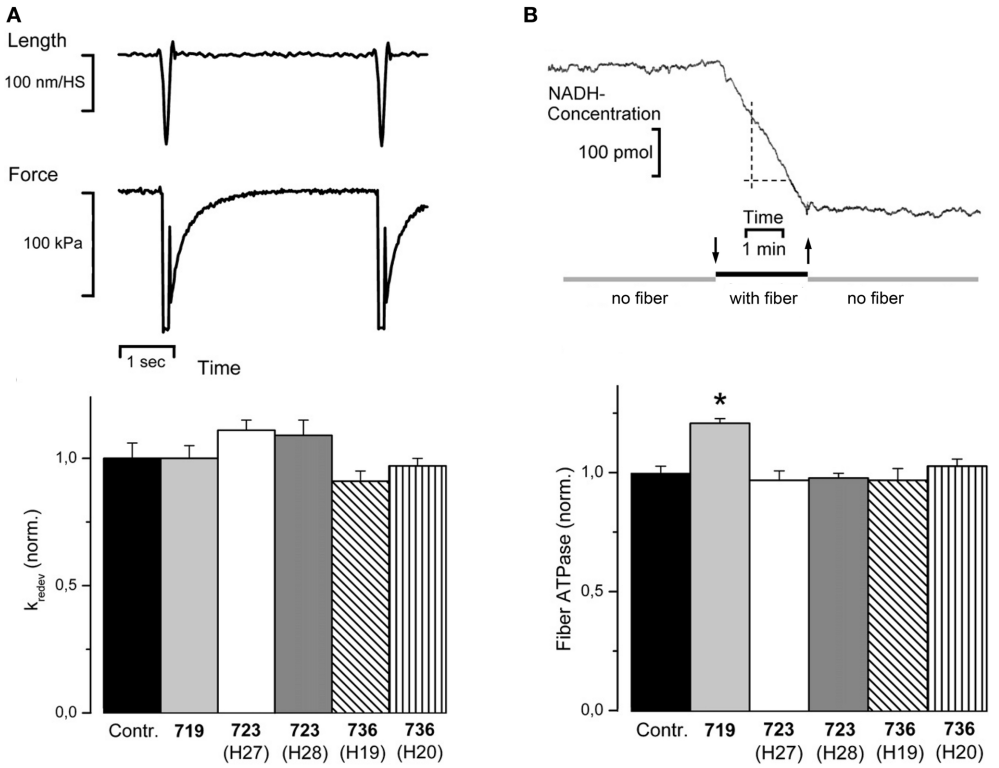

FIGURE 4 | (A) Rate constant of force redevelopment (k_{redev}). Top panel, original traces, fiber length, and isometric force vs. time; control fiber, $T = 20°C$. Release/restretch protocol to initiate force redevelopment (Brenner and Eisenberg, 1986). k_{redev} is the rate constant for the time course of force redevelopment to the isometric steady state, assuming a single exponential function. Isometric force is difference between force in isometric steady state and force level during the period of unloaded shortening where force has dropped to zero. Bottom panel, k_{redev} observed for mutations R719W, R723G, and I736T, normalized to k_{redev} of controls; $n = 7–45$ fibers. Mean values ± *SE*. No statistically significant effects could be observed. **(B)** Top panel, fiber ATPase, pen recorder trace of change in NADH-concentration while a single *M. soleus* fiber was incubated in the ATPase chamber. At downwards pointing arrow fiber was moved from trough with preactivating solution into ATPase chamber, at upwards pointing arrow fiber was moved back to preactivating solution. Maximum calcium activation, $T = 20°C$. ATPase is determined by the NADH-coupled enzyme assay in which rephosphorylation of ADP by phosphoenol pyruvate is coupled to reduction of pyruvate to lactate by NADH. Change in NADH concentration is followed by absorbance at 360 nm, calibrated with NADH test solutions. Bottom panel, effects of mutations R719W, R723G, and I736T, on fiber ATPase during isometric contraction ($n = 6–21$ fibers). $T = 20°C$. Mean values ± *SE* normalized to ATPase of control fibers. ATPase activity is significantly affected only by mutation R719W, indicated by $*p < 0.001$ (reprinted from Seebohm et al., 2009 with permission from Elsevier).

all three mutations. **Figure 4B** shows an original record of fiber ATPase measurements (top panel). These measurements revealed a statistically significant increase in ATPase for mutation R719W by about 20%. These ATPase measurements together with the unchanged rate constant of force redevelopment suggested some changes in cross-bridge cycling kinetics for the R719W mutation. A quantitative estimate, however, showed that the changes in cross-bridge cycling kinetics alone could at most account for about 1/3 of the increased active force by the resulting higher occupancy of force generating cross-bridge states during isometric steady state contraction and required the increased head stiffness to account for the overall increase in active force seen with mutation R719W. The increased stiffness in rigor, however, could not at all be accounted for by these changes in cross-bridge turnover kinetics (Seebohm et al., 2009).

To identify possible effects of the three converter mutations on cross-bridge kinetics under isotonic conditions we determined unloaded shortening velocity and force velocity relations on fibers from *M. soleus* samples of affected patients. Unloaded shortening velocity was determined by the slack-test experiment (**Figure 5**, top panel; cf. Edman, 1979). As we had previously shown, the time to shorten a preset distance (imposed fiber slack) vs. slack amplitude is not a linear relation as expected for a constant shortening velocity. Instead shortening velocity slows down with distance of shortening (Brenner, 1986). When the natural logarithm of velocity, however, was plotted vs. sarcomere length a linear relation was observed from which the shortening velocity at the very beginning of unloaded shortening could be determined (cf. Brenner, 1986). Data of unloaded shortening velocity determined from fibers of affected patients are shown in **Figure 5** (bottom panel). Only fibers from one patient showed an increase in unloaded shortening velocity just above the significance cut-off of $p < 0.05$. All other data were not different from controls.

To test whether our FHC-mutations also significantly reduce maximum power under loaded shortening, as previously found for other FHC-mutations (Lankford et al., 1995), we determined isotonic shortening velocity under different loads for controls and

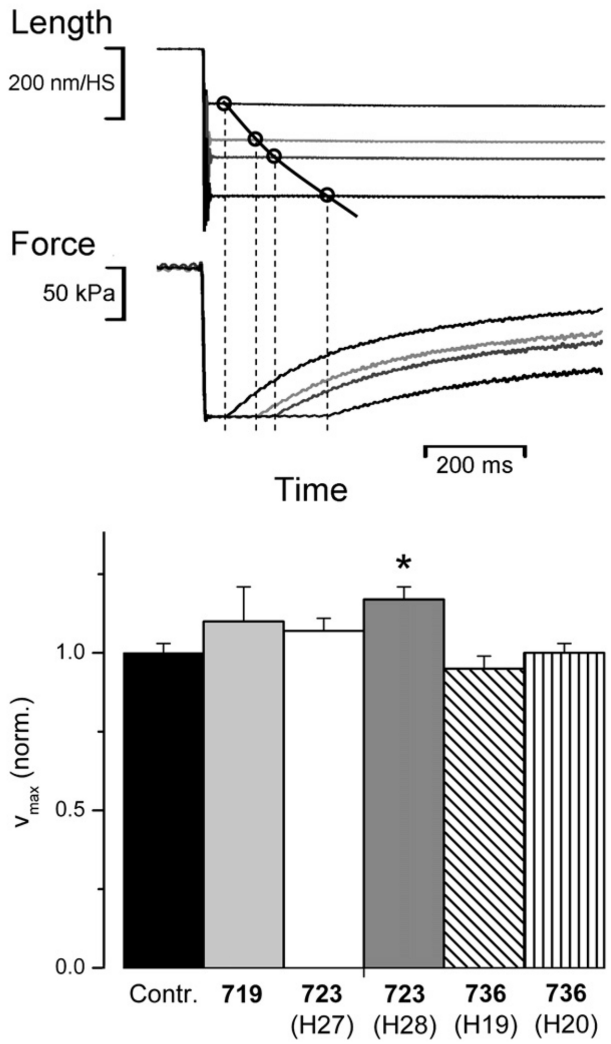

FIGURE 5 | Effect of converter mutations on maximum unloaded shortening velocity (v_{max}). Top panel: sample traces of slack test experiment, length vs. time and force vs. time (cf. Edman, 1979). This illustrates the reconstruction of 4 points of unloaded shortening vs. time from the time required for unloaded shortening to take up the imposed slack, i.e., until force starts to redevelop; v_{max} defined as initial slope of the shortening curve is determined by curve fitting according to Brenner (1986). Control fiber at 20°C. **Bottom panel**, v_{max} for mutations R719W, R723G, and I736T normalized to control fibers; $n = 6$–11 fibers. $T = 20$°C; mean values ± *SE*. *indicates statistically significant difference to controls ($p \leq 0.05$). Reprinted from Seebohm et al. (2009) with permission from Elsevier.

mutations R723G and I736T. For this test, quick releases from isometric steady state contraction to shortening under load conditions were applied (**Figure 6A**). Initial shortening velocity at the different loads was determined by curve fitting according to Brenner (1986) just as done for unloaded shortening velocity. The velocity data were plotted vs. applied load (**Figure 6B**) and the Hill equation was fitted to the data points (**Figure 6B** solid line) to obtain the force-velocity relations. From the Hill equation we determined the power at different loads (**Figure 6C**) to determine whether the converter mutations affect the maximum power under isotonic conditions. As shown in **Figure 6D**, converter mutations R723G and I736T had no significant effect on maximum power under isotonic conditions. For mutation R719W force velocity relations could not be determined because of insufficient size of the biopsy to perform all different experiments. Nevertheless, neither unloaded shortening velocity nor the maximum power output could serve as parameters in which all three converter mutations consistently differ from controls.

FORCE GENERATION AT DIFFERENT DEGREES OF Ca^{++}-ACTIVATION; Ca^{++}-SENSITIVITY

It was previously reported that FHC-related mutations cause an increased Ca^{++}-sensitivity of the contractile apparatus (Robinson et al., 2002; Ashrafian et al., 2011; Marston, 2011). We therefore measured active force-generation at different degrees of Ca^{++}-activation and constructed the force-pCa relations. To exclude effects of different phosphorylation levels of the regulatory light chain of myosin (LC2S or MLC-2 fast; Sweeney et al., 1993) all fibers were dephosphorylated with protein phosphatase 1α (Kirschner et al., 2005). The recorded force-pCa relations are shown in **Figure 7**. Somewhat surprisingly we found for converter mutations R719W and R723G a reduced Ca^{++}-sensitivity. For mutation I736T Ca^{++}-sensitivity was essentially unchanged but we found residual active force generation even under relaxing conditions (Kirschner et al., 2005).

IMPLICATIONS OF THE FUNCTIONAL EFFECTS OBSERVED WITH THE THREE CONVERTER MUTATIONS

Converter mutations R719W and R723G, both located in the core of the converter at positions where slow and fast myosins differ in amino acid sequence, increase head stiffness. This implies that the converter is a main determinant of head stiffness and thus of the contribution of a myosin head to force generation. Mutation I736T, located at the surface of the converter has no such effect. The other surprising effect is that both R719W and R723G, opposite to the expectation for FHC-related mutations (Marston, 2011) reduce Ca^{++}-sensitivity while mutation I736T has no effect on Ca^{++}-sensitivity but causes an incomplete relaxation. In addition, mutation R719W showed some changes in cross-bridge cycling kinetics. Altogether, up to this point, the three converter mutations did not show a common direct functional effect. Thus, whilst increased head stiffness is a direct functional effect of the FHC-mutations R723G and R719W, the FHC-phenotype cannot simply be the result of increased head stiffness. Interestingly, higher head stiffness is in fact normal for fast skeletal muscle myosin when compared with the slow skeletal isoform (**Table 1**). So how does increased head stiffness in the β-myosin heavy chain (β-MyHC) cause disease in myocardium?

HOW MAY MUTATIONS IN THE MYOSIN HEAD DOMAIN TRIGGER DEVELOPMENT OF AN FHC-PHENOTYPE?

A possible insight into the puzzle of how FHC-related mutations in the myosin head domain with different direct functional effects may cause development of an FHC-phenotype was revealed when we compared force-Ca^{++}-relationships of individual *M. soleus* fibers of FHC patients. To our surprise, in

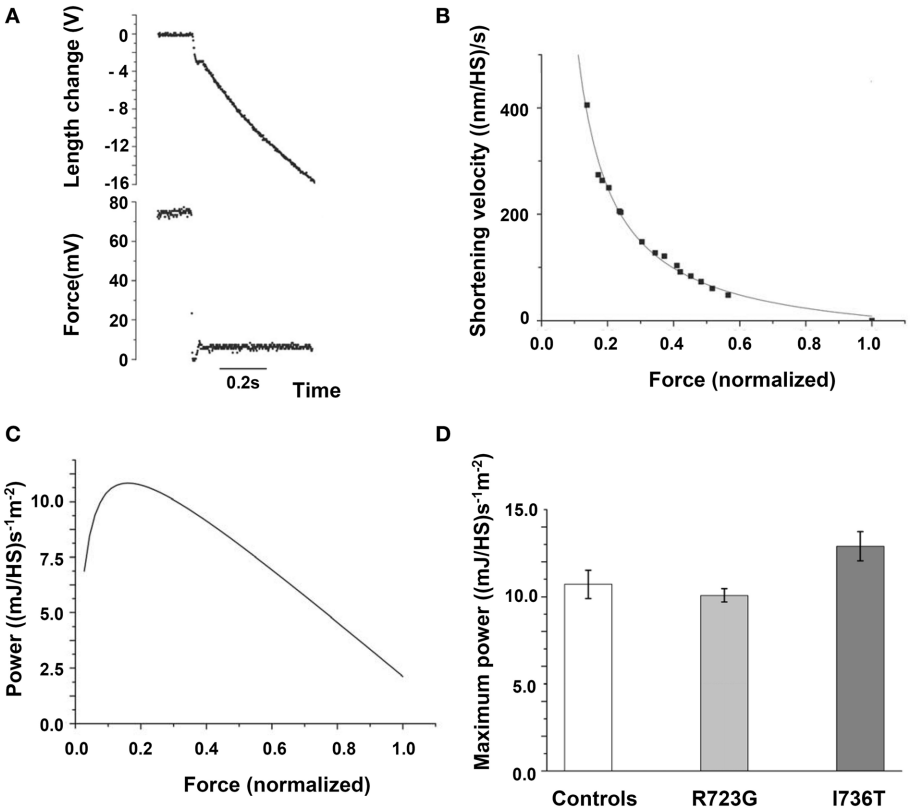

FIGURE 6 | Force-velocity relation and maximum power output. **(A)** Original length and force traces of a quick release experiment in which the fiber was switched from isometric steady state to isotonic shortening. Load during isotonic shortening about 10% of isometric force. Note the curved time course of fiber length similar to the time course of unloaded shortening by the slack test experiment (**Figure 5**, top panel). Initial shortening velocity determined according to Brenner (1986). **(B)** Force-velocity relation constructed by plotting initial shortening velocity vs. applied load, i.e., force exerted by fiber during shortening. Solid line is fit of Hill equation (Hill, 1938) to data points. **(C)** Power at different loads, solid line derived from Hill equation fitted to data points, i.e., solid line in **(B)**. **(D)** Effect of mutations R723G and I736T on maximum power; mean ± *SE*, $n = 12 - 14$ fibers. Differences not statistically significant ($p > 0.05$). $T = 20°C$.

some fibers the force-pCa relations were just like those in unaffected controls while other fibers showed substantially different force-pCa relations (cf. **Figure 8**, Kirschner et al., 2005).

For mutation R719W force-pCa relations of some fibers were shifted substantially further to the right than expected from the "average" fiber (**Figure 8** vs. **Figure 7A**). Similarly, some fibers with mutation R723G were also shifted much further to lower Ca^{++}-sensitivity than the average fiber (**Figure 8** vs. **Figure 7B**). Some fibers with mutation I736T showed substantially increased forces at partial activation and had still substantial active forces even at relaxing Ca^{++}-concentrations, i.e., showed incomplete relaxation while other fibers of the same tissue sample had force-pCa relations indistinguishable from control fibers. The common feature of all three FHC-mutations, however, is the spectrum of force-pCa relations ranging from normal (control) to substantially shifted to "abnormal" Ca^{++}-sensitivity or enhanced partial activation with incomplete relaxation.

The relevance of such spectrum of different Ca^{++}-sensitivities for fibers of the same tissue sample of an individual patient becomes most obvious when considering force generation at partial activation. At Ca^{++}-concentrations resulting in control fibers in about 60% of full activation, e.g., pCa 6.1, the observed active force generated by individual control fibers varies between about 50% and 70% of full activation. Thus, in control fibers the highest observed force levels observed at pCa 6.1 (70% of full activation; **Figure 8**) are about 1.5 times higher than the lowest (50% of full activation). At the same pCa value, about 6.1, for mutations R719W and R723G the highest forces of individual fibers in **Figure 8** are at least 4- to 5-fold larger than the lowest. For mutation I736T the difference between fibers with highest forces vs. fibers with lowest forces at pCa 6.1 are again in this range (**Figure 8**). In addition, for mutation I736T some fibers still generated substantial forces at relaxing Ca^{++}-concentrations where control fibers were fully relaxed (pCa 8.0).

Thus, the common feature for all three FHC-related mutations in the converter is the much larger spectrum of forces generated by individual fibers of one and the same patient at partial activation levels. In skeletal muscle such different force generation among individual fibers at partial activation means that individual fibers contribute differently to the force generated by a whole

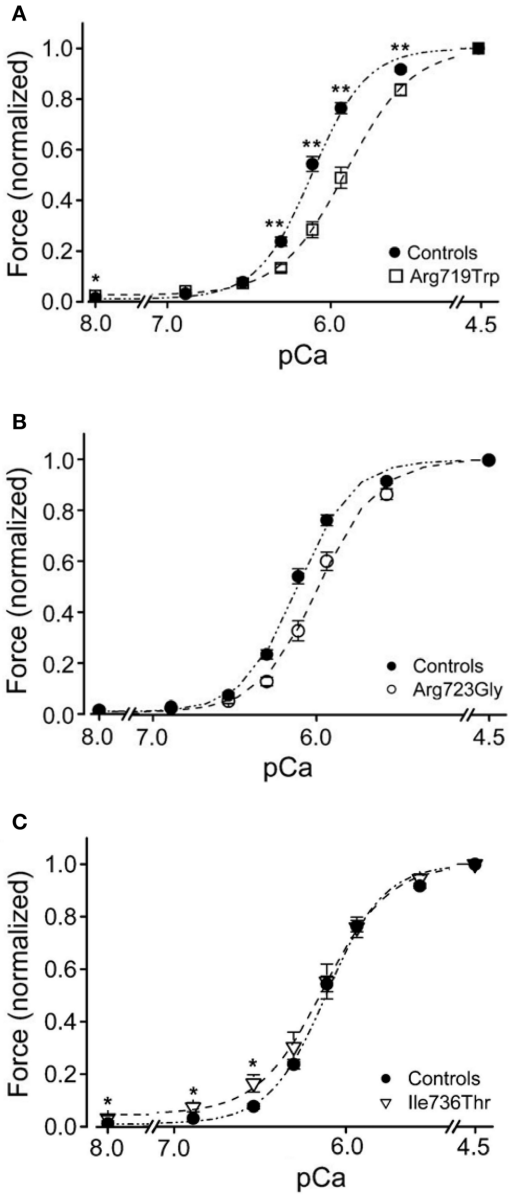

FIGURE 7 | Force-pCa relations of converter mutations vs. controls. $N = 19$ control fibers. pCa_{50} of controls, 6.12 ± 0.02. **(A)** Mutation R719W; $n = 16$ fibers; ** mark data at which difference in active forces are highly significant ($p < 0.001$); pCa_{50} of fibers with mutation R719W, 5.90 ± 0.03, significantly different from control ($p < 0.001$) **(B)** Mutation R723G, $n = 13$ fibers; pCa_{50} 5.98 ± 0.03, significantly different from control ($p < 0.001$). **(C)** Mutation I736T; $n = 10$ fibers; * mark data for which difference in force generation is significant ($p < 0.01$); pCa_{50} of fibers with mutation I736T, 6.15 ± 0.04, not significantly different from control ($p > 0.05$). Note, however, the incomplete relaxation even at pCa 8. All data recorded after treatment of fibers with PP1α; modified from Kirschner et al. (2005). With permission of The American Physiological Society.

muscle. Yet, "stronger" or "weaker" fibers are not expected to interfere with each others function. This is because skeletal muscle fibers do not form cellular networks but contribute to total force of a muscle independently.

WHAT MAY BE THE REASON FOR THE VARIANCE FROM NORMAL TO MUCH ALTERED Ca^{++}-SENSITIVITY AMONG INDIVIDUAL FIBERS OF THE SAME FHC-PATIENT?

We had previously observed that in soleus muscle samples of FHC-patients mutant and wildtype β-cardiac/slow skeletal MyHC were not expressed equally, different to what one may have expected for heterozygous patients with an autosomal dominant disease. Instead each mutation has a characteristic fraction of mutant β-cardiac/slow skeletal MyHC both at the mRNA and protein level (**Figure 3**, Tripathi et al., 2011). We therefore wondered whether the fraction of β-cardiac/slow skeletal MyHC may also vary from fiber to fiber. Because of the very small amount of material obtainable from individual soleus fiber segments we could only determine the fraction of mutant β-cardiac/slow skeletal MyHC at the mRNA level. Individual *M. soleus* fibers of a patient with mutation R723G showed quite different fractions of mutant mRNA, ranging from about 10% to essentially 100% (**Figure 9**). The high number of fibers with almost 100% mutant mRNA is consistent with the observation that in soleus samples (tissue level) the average fraction of mutated mRNA is $\geq$2/3 of total β-cardiac/slow skeletal MyHC-mRNA (cf. **Figure 3**).

In tissue samples of FHC-patients we always found a close correlation between fraction of mutant mRNA and fraction of mutant protein, regardless of the FHC-mutation we studied (**Figure 3**, Tripathi et al., 2011). Thus, the observed large variation in the fraction of mutant mRNA among individual fibers of soleus muscle of affected patients very likely correlates with a similar variation in the fraction of mutant protein. The large variation in mutant mRNA and thus in mutant protein among individual soleus fibers of affected patients could well account for the large functional variation among individual fibers, as judged by the force-pCa relations and the large variation in active force at partial activation (cf. **Figure 8**, Kirschner et al., 2005).

Assuming that the fibers with the largest shift in force-pCa relations have the highest abundance of mutant β-cardiac/slow skeletal MyHC, e.g., 100% as the maximum, forces generated by these fibers would at most be 2-fold larger than force of control fibers. This is because force generation per head with mutations R719W or R723G was estimated to be about 2-fold higher than force generation by wildtype myosin heads; see above (Kirschner et al., 2005). As a consequence, the forces at partial activation ($pCa \geq 6.3$), as low as 1/5 of control fibers in the normalized plots (**Figure 8**), would still be less than half of control in absolute terms. At pCa around 5.8–5.9 fibers with mutant myosin are expected to generate about the same amount of absolute force as controls, at higher activation levels fibers with mutations R719W or R723G would generate higher forces than controls, reaching up to 2-fold higher forces at maximum activation for fibers with 100% mutant myosin. Most importantly, however, even if absolute forces of individual fibers are considered, the large variation in Ca^{++}-sensitivity among individual fibers remains unaffected.

IN MYOCARDIUM DIRECT FUNCTIONAL EFFECTS CAN BE MASKED OR EVEN REVERSED BY SECONDARY EFFECTS

Characterization of functional effects of FHC-related mutations in myocardium for comparison with the effects seen in *M. soleus* fibers became possible by samples from explanted hearts of

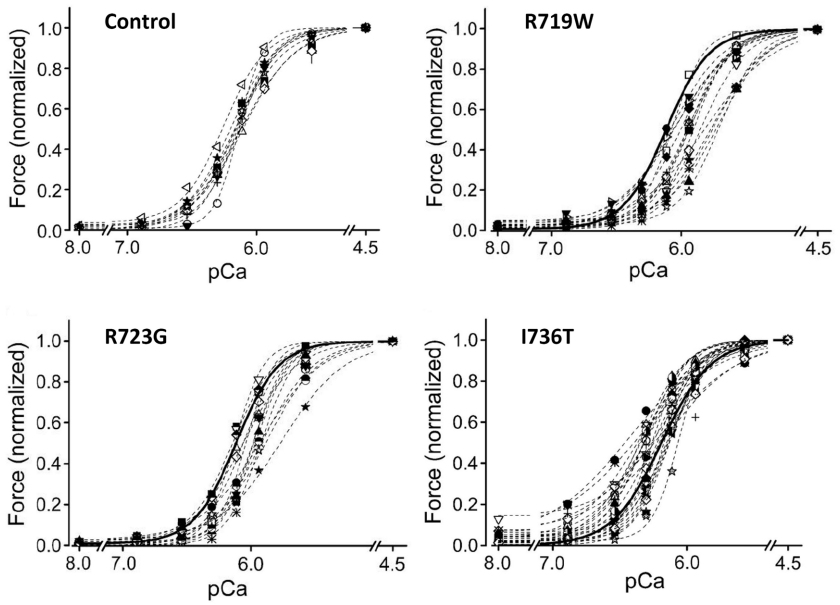

FIGURE 8 | Force-pCa relations of individual *M. soleus* fibers. Controls, 10 fibers of a control individual; R719W, 16 fibers (cf. **Figure 7A**); R723G, 13 fibers (cf. **Figure 7B**); I736T, 25 individual fibers. Heavy solid lines in plots of fibers with mutations represent the average force-pCa relation of the control fibers. Note that for all three mutations the individual force-pCa relations represent a continuum from relations like control fibers to force-pCa relations substantially shifted beyond the average position of the corresponding mutation shown in **Figure 7**, i.e., to the right for mutations R719W and R723G, and upwards to incomplete relaxation for mutation I736T. Modified from Kirschner et al. (2005). With permission of The American Physiological Society.

patients with the myosin missense mutations, R723G, one of the mutations that we had studied on soleus muscle samples.

Cardiomyocytes were mechanically isolated from the flash-frozen tissue samples (van der Velden et al., 2003; Kraft et al., 2013). After chemical permeabilization the isolated cardiomyocytes were attached to a force transducer and motor such that active and passive forces and kinetics of cross-bridge cycling (k_{redev}) could be measured at different concentrations of free Ca^{++}-ions. To our surprise, force-pCa relations of cardiomyocytes isolated from the flash-frozen samples of explanted myocardium of two patients with mutation R723G showed (i) no difference in Ca^{++}-sensitivity and (ii) reduced maximum active force compared to myocytes from donor hearts (**Figure 10A**). This was in total contrast to the reduced Ca^{++}-sensitivity and increased maximum force seen in soleus samples with the same mutation.

Analysis of phosphorylation of contractile proteins revealed substantially lower phosphorylation of troponin I in these myocardial samples with mutations compared to the controls. When the phosphorylation pattern was matched with controls by treatment with protein kinase A (PKA) or by a combination of dephosphorylation by protein phosphatase-1α (PP-1α) followed by phosphorylation with PKA, the mutant samples showed a similarly reduced Ca^{++}-sensitivity as the soleus fibers of patients with the R723G-mutation (**Figure 10A** vs. **Figure 10B**).

Maximum force, however, was still substantially reduced after matching phosphorylation of patient samples with controls (**Figure 10B**, left panel). An explanation for the reduced force generation in myocardium in contrast to the increased force generation in soleus fibers with the same mutation was revealed by electron microscopy of tissue samples of affected patients. In myocardium of affected patients prominent intracellular myofibrillar disarray and reduced packing of myofibrils within cardiomyocytes was observed with non-myofibrillar and non-mitochondrial material taking up substantial intracellular volume (Kraft et al., 2013). Quantitatively, myofibrillar density of cardiomyocytes of affected patients with mutation R723G was reduced by about 26%. Without such reduced myofibrillar density within cardiomyocytes, force generation per cross-sectional area had been essentially the same as in control samples (Kraft et al., 2013). The additional myofibrillar disarray with myofibrils deviating from the longitudinal axis of a cardiomyocyte will add to reduced force generation in axial direction (Friedrich et al., 2010) such that increased force generation is not observed even when accounting for reduced myofibrillar density.

Altogether, the opportunity to compare effects of the R723G missense mutation in both soleus fibers and myocardium of affected patients revealed that at least at stages of disease development when myectomies were taken or when transplantation was necessary, direct functional effects of FHC-related mutations can be masked or even reversed by effects most likely subsequent to the direct functional effects. This suggests that e.g., FHC-typical cardiomyocyte and myofibrillar disarray are not direct results of FHC-related mutations but develop subsequently as a result of functional alterations. Functional effects of different mutations apparently converge to a common path of changes resulting in the FHC-phenotype. Cardiomyocyte and myofibrillar disarray may represent the start of this common path leading to e.g., interstitial fibrosis and hypertrophy.

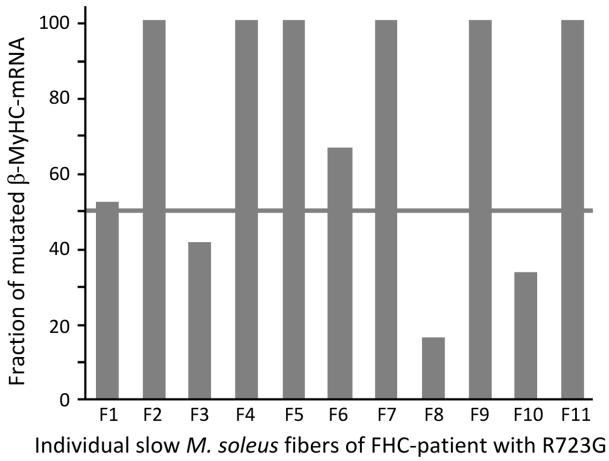

FIGURE 9 | Fraction of mutated β-cardiac/slow skeletal MyHC-mRNA in 11 individual fibers of *M. soleus* of a patient with mutation R723G. A fiber bundle of *M. soleus*, flash-frozen without prior skinning, was freeze dried for isolation of individual fibers (Stienen et al., 1983) without cross-contamination of mRNA from fiber to fiber. For quantification of the fraction of mutated β-cardiac/slow skeletal MyHC-mRNA, isolated segments (2–3 mm) of individual fibers were processed as previously described for *M. soleus* fiber bundles (Tripathi et al., 2011). Note the large variation in the fraction of mutated β-cardiac/slow skeletal MyHC-mRNA among individual fibers.

So what may be a feature common to different FHC-related mutations that could trigger cardiomyocyte and myofibrillar disarray as the start on a common path to an FHC-phenotype?

HYPOTHESIS FOR DEVELOPMENT OF AN FHC-PHENOTYPE IN MYOCARDIUM

In our previous work on FHC-related missense mutations in the β-cardiac/slow skeletal MyHC we made three key observations. (i) A large variation in calcium sensitivity among individual *M. soleus* fibers of FHC-patients with mutations R723G, R719W, and I736T. This variation ranged from essentially normal calcium sensitivity to highly different, e.g., reduced calcium sensitivity for mutations R719w and R723G. (ii) The ratio of mutated vs. wild-type β-cardiac/slow skeletal MyHC is not 1:1 but characteristic for each mutation. In addition this ratio is very similar at both the mRNA and protein level. (iii) Among individual fibers of *M. soleus* samples with the R723G mutation, the ratio of mutant vs. wildtype mRNA varies from almost pure mutant to almost pure wildtype. A substantial variation in the ratio of mutant vs. wild-type protein from fiber to fiber was previously also found for the R403Q mutation in the β-cardiac/slow skeletal MyHC (Malinchik et al., 1997).

Based on these three observations, we proposed the following hypothesis for a common trigger of the FHC-phenotype development (**Figure 11**, Kirschner et al., 2005; Tripathi et al., 2011):

(i) Variation of the fraction of the mutated protein among individual cardiomyocytes (different gray levels of schematic cardiomyocytes in **Figure 11**), just as seen among individual *M. soleus* fibers, results in functional imbalances, e.g., unequal force generation particularly at low activation levels (cf. **Figure 8**) among the individual cardiomyocytes.

(ii) Since cardiomyocytes, different from skeletal muscle fibers, are branched and form a cellular network (**Figure 12A**), such variance in force generation among individual cells will result in uneven contraction, i.e., over-contraction vs. over-stretch of cardiomyocytes during each twitch. Such functional imbalance will not only occur during force generation (pressure development in the ventricles) but also during shortening under load (ejection period). This is because for cells generating higher forces the relative load during ejection period will be lower compared to cells generating lower forces, even if v_{max} is unaffected by a mutation. As a result, over-contraction of some cells while others are overstretched will distort the myocyte network at the cellular and myofibrillar level (Scheme in **Figure 12B** vs. **Figure 12C**, and left panel in **Figure 12D** vs. right panel).

(iii) The structural disorganization, even if initially only a transient feature during each twitch, however, will result in progression of persisting structural disorganization over months and years because of the triggering of secondary changes. Structural distortion could, for example, trigger stretch sensitive signaling, e.g., Tgf-β signaling by cardiomyocytes and non-myocyte-cells (right panel in **Figure 12D**) that was shown to be critical for pathologic remodeling of the myocardium in FHC (Teekakirikul et al., 2010). Stretch induced increase in Tgf-β was found in cell cultures both for cardiomyocytes and non-myocyte-cells (Ruwhof et al., 2000; van Wamel et al., 2001, 2002). In our hypothesis, structural disorganization of the cellular network of the myocardium because of functional imbalance among individual cardiomyocytes initiates, via stretch-sensitive signaling paths, cardiac remodeling (**Figure 12E**) with interstitial fibrosis, cellular disarray and hypertrophy, i.e., hallmarks of the FHC-phenotype (Ho et al., 2010). Increased collagen synthesis in a profibrotic myocardial state (Ho et al., 2010), supports our concept.

Based on this concept, for prevention of FHC-phenotype development therapeutic interventions are required that affect myocardial function differentially, e.g., specifically the altered function of the mutant protein, otherwise the functional imbalance will not be reduced and cardiac remodeling will not be prevented. Alternatively, inhibition of subsequent, e.g., stretch-induced signaling that initiates interstitial fibrosis could be a therapeutic target to prevent fibrosis and cardiac remodeling. This target was recently addressed by Teekakirikul et al. (2010).

Since skeletal muscle fibers are only very rarely branched, a similar extensive disarray is not expected and not observed in *M. soleus* fibers. Central core disease, found in soleus fibers of some FHC-patients are localized changes inside the soleus fibers with absence of mitochondria, smaller myofibrils, some over-contracted sarcomeres and irregular Z-discs (Fananapazir et al., 1993). This, however, is different from the extensive disarray seen in myocardium and may suggest unequal abundance of mutated protein along skeletal muscle fibers. Overcontracted sarcomeres

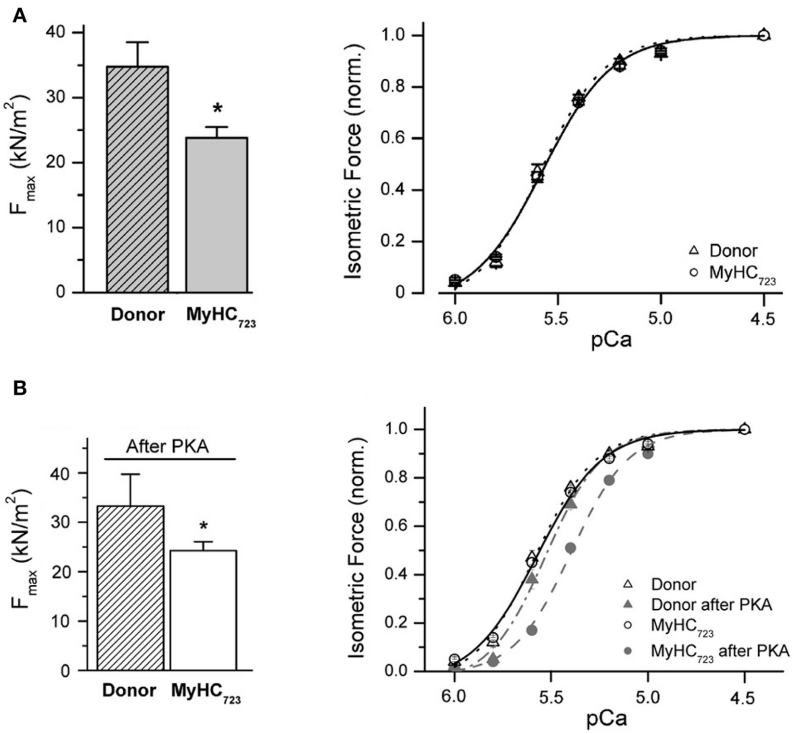

FIGURE 10 | Effect of mutation R723G in myocardium. (A) Isolated cardiomyocytes, native state of phosphorylation. Left panel, maximum active force per cross sectional area at saturating calcium-concentration (F_{max}). F_{max} of MyHC723-cardiomyocytes (light gray bar) is 35% lower than F_{max} of donor cells (hatched bar; $*p < 0.05$). Right panel, force-pCa relation normalized to maximum force at saturating Ca^{++}-ion concentration (pCa 4.5). Solid and dotted lines, fits of a modified Hill equation yielding pCa_{50}. Note that opposite to *M. soleus* fibers, cardiomyocytes isolated from a tissue sample of an explanted heart show a decrease in maximum active force with no shift in the force-pCa relation. **(B)** Isolated cardiomyocytes after incubation with protein kinase A (PKA) to match phosphorylation of contractile proteins, particularly of cTnI. Left panel, F_{max} after treatment with PKA $*p < 0.05$. Note that PKA-treatment does not change the difference in F_{max} between R723G-cardiomyocytes and controls. Right panel, force-pCa relations of MyHC723-cardiomyocytes (gray filled circles, dashed line) vs. donor cardiomyocytes (gray filled triangles, dashed-dotted line). Note the shift of the force-pCa relation of MyHC723-cardiomyocytes vs. donor after PKA treatment. For comparison force-pCa relations obtained before PKA treatment are also plotted in the same graph (open circles and solid line, MyHC723-cardiomyocytes; open triangles and dotted line, controls). Lines are fits of modified Hill equation to data points. Note that after PKA-treatment to match phosphorylation of e.g., cTnI, a similar reduced Ca^{++}-sensitivity becomes detectable for MyHC723-cardiomyocytes just like that seen in the soleus fibers. Modified from Kraft et al. (2013). With permission of the Journal of Molecular and Cellular Cardiology.

and irregular Z-discs may not be unexpected since skeletal muscle fibers have multiple nuclei. Thus, variation in the expression of mutant vs. wildtype mRNA and protein among different nuclei may exist within skeletal muscle fibers and thus cause functional imbalances along these fibers.

In our hypothesis, any functional imbalance among individual cardiomyocytes, resulting from e.g., variable abundance of a mutant protein, has the potential to induce an FHC-phenotype. This could include not only missense mutations that affect force output of cardiomyocytes (poison peptide principle), but also the expression and degradation of truncated proteins, resulting in variable amounts of normal protein (principle of haploinsufficiency). In principle, non-sarcomeric proteins that affect contractile function could also trigger FHC-phenotype development if unequal effects are generated among individual cardiomyocytes, e.g., by variation in expression of the mutant protein. In homozygous patients, found only very rarely, functional imbalance is not expected and the disease is dominated by direct functional effects of the mutations. These are always present and lead to the functional imbalance in the heterozygous patients when mutant protein varies from cell to cell.

TESTING THE HYPOTHESIS

Our hypothesis is based on the assumption that among individual cardiomyocytes a similar variation in the expression of mutant vs. wildtype mRNA exists as shown in **Figure 9** for *M. soleus* fibers, and that this results in functional variation, i.e., imbalances in force generation and shortening among neighboring cardiomyocytes. Thus, quantification of mutant vs. wildtype mRNA in individual cardiomyocytes is a critical test for our hypothesis. First trials of such quantification of mutant vs. wildtype mRNA in individual cardiomyocytes indicate that indeed the expression of mutant mRNA varies among individual cardiomyocytes from near zero to almost pure mutant mRNA (Montag et al., 2014).

IN SUMMARY

Our functional studies on tissue samples of FHC-patients showed that missense mutations in the myosin head domain do not

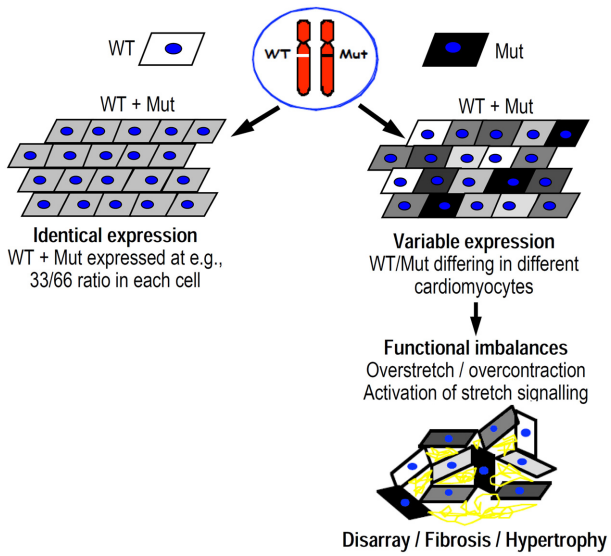

FIGURE 11 | Scheme illustrating the difference between equal abundance of mutant protein in all cardiomyocytes (top left) vs. variation in abundance among individual cardiomyocytes (top right). Gray level illustrates abundance of mutant protein. Unequal abundance of mutant protein in individual cardiomyocytes results in functional imbalance that distorts the cellular network of the myocardium (bottom right). Overstretch vs. overcontraction results in highly variable activation of e.g., stress/strain signaling with development of disarray, hypertrophy, and interstitial fibrosis in the long run.

result in a direct functional effect common to all mutations like increased force generation, increased Ca^{++}-sensitivity, or increased ATPase. One feature common to all mutations we have studied is a large variation in the force-pCa-relation among individual *M. soleus* fibers from normal to highly different. As a consequence, particularly at partial activation large differences in the generated active forces exist among individual fibers. Quantification of mutant mRNA suggests that this functional variation is due to variation in the fraction of mutant β-cardiac/slow skeletal MyHC present in individual fibers. If such functional imbalance among individual cells exists in a cellular network like the myocardium, the functional imbalance will result in distortions of cells within this network. We hypothesize that such structural distortions result in myocyte and myofibrillar disarray and activate stretch-induced signaling, e.g., Tgf-β-signaling, that initiates cardiac remodeling with interstitial fibrosis and hypertrophy, the structural hallmarks of FHC. On this basis, any mutation in a sarcomeric or non-sarcomeric protein that results in similar functional imbalance among individual cardiomyocytes has the potential to trigger development of an FHC-phenotype. Such a mechanism as the trigger of FHC-development would have fundamental implications for therapeutic strategies. For such a pathomechanism either mutation-selective interventions are needed to ameliorate functional imbalances among individual cardiomyocytes to prevent FHC-phenotype development. Alternatively, inhibition of stretch-induced signaling, e.g., Tgf-β-signaling could be another target to prevent cardiac remodeling in FHC.

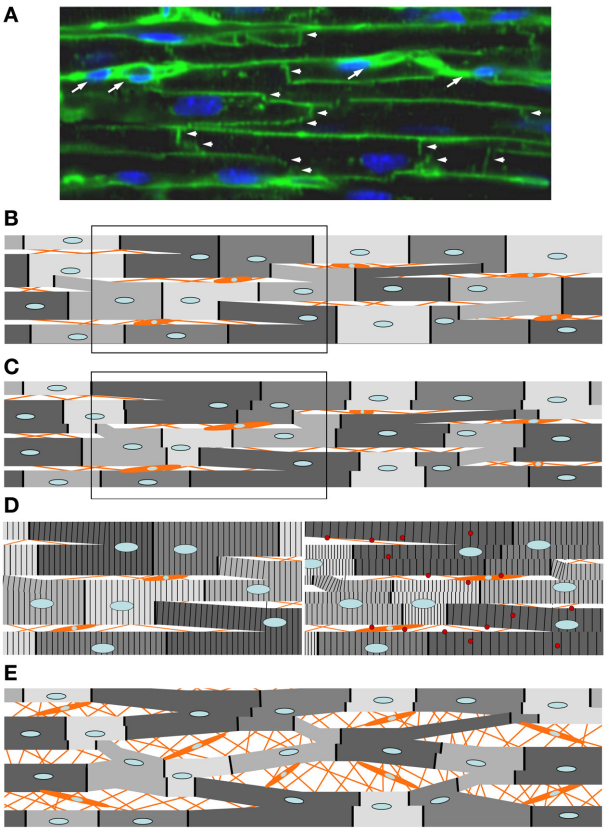

FIGURE 12 | Expected response of the cellular network of myocardium to imbalances in force generation among individual cardiomyocytes, e.g., by mutations R719W or R723G. Orange lines and orange cells represent extracellular connective tissue and non-myocyte cells within the myocardium. **(A)** Confocal image of a longitudinal section through myocardium (adult mouse). Intercalated discs (vertical lines and "staircases" labeled with arrow heads) labeled with a mouse monoclonal antibody to pan Cadherin and an Alexa 488-linked goat-anti-mouse antibody. Horizontal lines are plasma membranes visualized by staining glycoproteins containing β-N-acetyl-D-glucosamine with FITC-conjugated wheat germ agglutinin (for details see Schipke et al., in press). TO-PRO®-3 Iodide used for staining nuclei (blue). By this approach, individual cardiomyocytes are delineated. Note that individual cardiomyocytes are not arranged in independent columns. Instead, cardiomyocytes make contact via intercalated discs with cardiomyocytes of adjacent columns resulting in a cellular network. Presumed non-myocyte cells are labeled with white arrows. **(B)** Schematic representation of the cellular arrangement in myocardium with branched cardiomyocytes while relaxed. The darker the gray-level the higher the abundance of the mutant myosin. The mutation is assumed to result in substantially lower forces at partial activation levels despite higher force at maximum activation, as was seen for mutations R719W and R723G (cf. **Figure 8**) **(C)** Same cellular network during contraction (partial activation like in a twitch). For cardiomyocytes with mutations R723G or R719W higher abundance of the mutant myosin (darker gray levels) results in lower forces at partial activation. Thus, during a twitch these cardiomyocytes become overstretched by those with low abundance of the mutant protein (lighter gray levels). Due to the branching, different parts even of individual cells will experience different forces by the different connections with neighboring cells and will therefore shorten or be stretched to different extent (see steps in intercalated discs, represented by dark solid vertical lines separating adjacent cells). Due to relative movement of cells in parallel strands, branches between the strands will be distorted as will be the non-myocyte cells in between the strands of cardiomyocytes.

(Continued)

FIGURE 12 | Continued
(D) Left panel, boxed part of **(B)** magnified to illustrate striation pattern; right panel, boxed part of **(C)**. Note the developing differences in sarcomere lengths of myofibrils during contraction even within an individual cell. This is due to the branching of the cells and the different forces acting on the branches due to the unequal force generating capability of adjacent cells by the different abundance of mutant protein (functional imbalance). Thus, functional imbalance among individual cardiomyocytes together with the cellular network of the cardiomyocytes are expected to trigger cellular and myofibrillar disarray whenever, by variation in expression, a mutation causes unequal force generation among individual cardiomyocytes during a twitch. This state would represent the profibrotic state of the myocardium (Ho et al., 2010) in which stretch triggers increased expression of e.g., Tgf-β (red spheres) by cardiomyocytes and non-myocyte cells activating development of interstitial fibrosis. Such distortion will take place during force generation (pressure development) and will be enhanced during shortening under load (ejection period). This will occur even if maximum shortening velocity is unaffected by the mutation because the relative load will be lower for "strong" cells (low abundance of mutant protein) vs. "weak" cells (high abundance of mutant protein). Note, that if the mutant protein were expressed equally in all cells, force generation at any time during a twitch would be affected equally and no or only minimal changes in the arrangement of cardiomyocytes would take place during a twitch, i.e., no or only much smaller changes from the arrangement in **(B)** would be seen. Panel **(E)** illustrates a later stage of phenotype development when e.g., stretch-sensitive signaling has triggered development of interstitial fibrosis with increased cellular disarray. The increase in cell size by signaling paths that trigger hypertrophy is not shown.

ACKNOWLEDGMENTS

The authors thank William J. McKenna (The Heart Hospital, London, UK), Antonio Francino and Francesc Navarro-Lopez (Hospital Clinic/IDIBAPS, University of Barcelona, Barcelona, Spain), as well as Andreas Perrot (ECRC at MDC, Cardiovascular Genetics, Charité Berlin, Germany), Cemil Özcelik, (Cardiology, Helios-Clinic Northeim, Germany), Karl-Josef Osterziel,(Cardiopraxis, Amberg, Germany) for tissue samples of FHC-patients. We also like to thank Cristobal G. dos Remedios (Muscle Research Unit, Institute for Biomedical Research, University of Sydney, Sydney, NSW, Australia) for providing us with donor samples of human myocardium. The authors also thank Julia Schipke (Functional and Applied Anatomy, Hannover Medical School) for providing the confocal image shown in **Figure 12A**. We also like to acknowledge the excellent technical support by Birgit Piep, Alexander Lingk, and Torsten Beier (Molecular and Cell Physiology, Hannover Medical School, Germany). This work was supported by grants (KR 1187/5-3/4 and KR 1187/19-1) of the Deutsche Forschungsgemeinschaft to Theresia Kraft.

REFERENCES

Ashrafian, H., McKenna, W. J., and Watkins, H. (2011). Disease pathways and novel therapeutic targets in hypertrophic cardiomyopathy. *Circ. Res.* 109, 86–96. doi: 10.1161/CIRCRESAHA.1111.242974

Baudenbacher, F., Schober, T., Pinto, J. R., Sidorov, V. Y., Hilliard, F., Solaro, R. J., et al. (2008). Myofilament Ca2+ sensitization causes susceptibility to cardiac arrhythmia in mice. *J. Clin. Invest.* 118, 3893–3903. doi: 10.1172/JCI36642

Blair, E., Redwood, C., Ashrafian, H., Oliveira, M., Broxholme, J., Kerr, B., et al. (2001). Mutations in the gamma(2) subunit of AMP-activated protein kinase cause familial hypertrophic cardiomyopathy: evidence for the central role of energy compromise in disease pathogenesis. *Hum. Mol. Genet.* 10, 1215–1220. doi: 10.1093/hmg/10.11.1215

Brenner, B. (1986). The necessity of using two parameters to describe isotonic shortening velocity of muscle tissues: the effect of various interventions upon initial shortening velocity (vi) and curvature (b). *Basic Res. Cardiol.* 81, 54–69. doi: 10.1007/BF01907427

Brenner, B. (1998). "Muscle mechanics II: skinned muscle fibres," in *Current Methods in Muscle Physiology: Advantages, Problems and Limitations*, ed H. Sugi (Oxford: Oxford University Press), 33–69. doi: 10.1093/acprof:oso/9780198523970.003.0002

Brenner, B., Chalovich, J. M., Greene, L. E., Eisenberg, E., and Schoenberg, M. (1986). Stiffness of skinned rabbit psoas fibers in MgATP and $MgPP_i$ solution. *Biophys. J.* 50, 685–691. doi: 10.1016/S0006-3495(86)83509-3

Brenner, B., and Eisenberg, E. (1986). Rate of force generation in muscle: correlation with actomyosin ATPase activity in solution. *Proc. Natl. Acad. Sci. U.S.A.* 83, 3542–3546. doi: 10.1073/pnas.83.10.3542

Brenner, B., Hahn, N., Hanke, E., Matinmehr, F., Scholz, T., Steffen, W., et al. (2012). Mechanical and kinetic properties of beta-cardiac/slow skeletal muscle myosin. *J. Muscle Res. Cell Motil.* 33, 403–417. doi: 10.1007/s10974-012-9315-8

Capitanio, M., Canepari, M., Cacciafesta, P., Lombardi, V., Cicchi, R., Maffei, M., et al. (2006). Two independent mechanical events in the interaction cycle of skeletal muscle myosin with actin. *Proc. Natl. Acad. Sci. U.S.A.* 103, 87–92. doi: 10.1073/pnas.0506830102

Debold, E. P., Schmitt, J. P., Patlak, J. B., Beck, S. E., Moore, J. R., Seidman, J. G., et al. (2007). Hypertrophic and dilated cardiomyopathy mutations differentially affect the molecular force generation of mouse alpha-cardiac myosin in the laser trap assay. *Am. J. Physiol. Heart Circ. Physiol.* 293, H284–H291. doi: 10.1152/ajpheart.00128.2007

Edman, K. A. (1979). The velocity of unloaded shortening and its relation to sarcomere length and isometric force in vertebrate muscle fibres. *J. Physiol.* 291, 143–159.

Fananapazir, L., Dalakas, M. C., Cyran, F., Cohn, G., and Epstein, N. D. (1993). Missense mutations in the beta-myosin heavy-chain gene cause central core disease in hypertrophic cardiomyopathy. *Proc. Natl. Acad. Sci. U.S.A.* 90, 3993–3997. doi: 10.1073/pnas.90.9.3993

Föhr, K. J., Warchol, W., and Gratzl, M. (1993). Calculation and control of free divalent cations in solutions used for membrane fusion studies. *Methods Enzymol.* 221, 149–157. doi: 10.1016/0076-6879(93)21014-Y

Fokstuen, S., Lyle, R., Munoz, A., Gehrig, C., Lerch, R., Perrot, A., et al. (2008). A DNA resequencing array for pathogenic mutation detection in hypertrophic cardiomyopathy. *Hum. Mutat.* 29, 879–885. doi: 10.1002/humu.20749

Friedrich, O., Both, M., Weber, C., Schurmann, S., Teichmann, M. D., von Wegner, F., et al. (2010). Microarchitecture is severely compromised but motor protein function is preserved in dystrophic mdx skeletal muscle. *Biophys. J.* 98, 606–616. doi: 10.1016/j.bpj.2009.1011.1005

Guinto, P. J., Haim, T. E., Dowell-Martino, C. C., Sibinga, N., and Tardiff, J. C. (2009). Temporal and mutation-specific alterations in Ca2+ homeostasis differentially determine the progression of cTnT-related cardiomyopathies in murine models. *Am. J. Physiol. Heart Circ. Physiol.* 297, H614–H626. doi: 10.1152/ajpheart.01143.02008

Hill, A. V. (1938). The heat of shortening and the dynamic constants of muscle. *Proc. R. Soc. Lond. B* 126, 136–195. doi: 10.1098/rspb.1938.0050

Ho, C. Y., Lopez, B., Coelho-Filho, O. R., Lakdawala, N. K., Cirino, A. L., Jarolim, P., et al. (2010). Myocardial fibrosis as an early manifestation of hypertrophic cardiomyopathy. *N. Engl. J. Med.* 363, 552–563. doi: 10.1056/NEJMoa1002659

Hoskins, A. C., Jacques, A., Bardswell, S. C., McKenna, W. J., Tsang, V., dos Remedios, C. G., et al. (2010). Normal passive viscoelasticity but abnormal myofibrillar force generation in human hypertrophic cardiomyopathy. *J. Mol. Cell Cardiol.* 49, 737–745. doi: 10.1016/j.yjmcc.2010.1006.1006

Huxley, H. E. (1957). The double array of filaments in cross striated muscle. *J. Biophys. Biochem. Cytol.* 3, 631–647. doi: 10.1083/jcb.3.5.631

Kirschner, S. E., Becker, E., Antognozzi, M., Kubis, H. P., Francino, A., Navarro-Lopez, F., et al. (2005). Hypertrophic cardiomyopathy-related beta-myosin mutations cause highly variable calcium sensitivity with functional imbalances among individual muscle cells. *Am. J. Physiol. Heart Circ. Physiol.* 288, H1242–H1251. doi: 10.1152/ajpheart.00686.2004

Kraft, T., Messerli, M., Rothen-Rutishauser, B., Perriard, J. C., Wallimann, T., and Brenner, B. (1995). Equilibration and exchange of fluorescently labeled molecules in skinned skeletal muscle fibers visualized by confocal microscopy. *Biophys. J.* 69, 1246–1258. doi: 10.1016/S0006-3495(95)80018-4

Kraft, T., Witjas-Paalberends, E. R., Boontje, N. M., Tripathi, S., Brandis, A., Montag, J., et al. (2013). Familial hypertrophic cardiomyopathy: functional effects of myosin mutation R723G in cardiomyocytes. *J. Mol. Cell Cardiol.* 57, 13–22. doi: 10.1016/j.yjmcc.2013.01.001

Lankford, E. B., Epstein, N. D., Fananapazir, L., and Sweeney, H. L. (1995). Abnormal contractile properties of muscle fibers expressing beta-myosin heavy chain gene mutations in patients with hypertrophic cardiomyopathy. *J. Clin. Invest.* 95, 1409–1414. doi: 10.1172/JCI117795

Lewalle, A., Steffen, W., Stevenson, O., Ouyang, Z., and Sleep, J. (2008). Single-molecule measurement of the stiffness of the rigor myosin head. *Biophys. J.* 94, 2160–2169. doi: 10.1529/biophysj.107.119396

Linari, M., Caremani, M., Piperio, C., Brandt, P., and Lombardi, V. (2007). Stiffness and fraction of Myosin motors responsible for active force in permeabilized muscle fibers from rabbit psoas. *Biophys. J.* 92, 2476–2490. doi: 10.1529/biophysj.106.099549

Malinchik, S., Cuda, G., Podolsky, R. J., and Horowits, R. (1997). Isometric tension and mutant myosin heavy chain content in single skeletal myofibers from hypertrophic cardiomyopathy patients. *J. Mol. Cell Cardiol.* 29, 667–676. doi: 10.1006/jmcc.1996.0309

Maron, B. J., McKenna, W. J., Danielson, G. K., Kappenberger, L. J., Kuhn, H. J., Seidman, C. E., et al. (2003). American college of cardiology/european society of cardiology clinical expert consensus document on hypertrophic cardiomyopathy. a report of the american college of cardiology foundation task force on clinical expert consensus documents and the european society of cardiology committee for practice guidelines. *Eur. Heart J.* 24, 1965–1991. doi: 10.1016/S0195-668X(03)00479-2

Marston, S. B. (2011). How do mutations in contractile proteins cause the primary familial cardiomyopathies? *J. Cardiovasc. Trans. Res.* 4, 245–255. doi: 10.1007/s12265-12011-19266-12262

Montag, J., Tripathi, S., Köhler, J., Dunda, E. S., Seebohm, B., List, D., et al. (2014). Familial hypertrophic cardiomyopathy: unequal expression of mutant and wildtype myosin in individual myocytes as trigger for functional impairment of the heart? *Biophys. J.* 106, p644a–p645a. doi: 10.1016/j.bpj.2013.11.3568

Moore, J. R., Leinwand, L., and Warshaw, D. M. (2012). Understanding cardiomyopathy phenotypes based on the functional impact of mutations in the myosin motor. *Circ. Res.* 111, 375–385. doi: 10.1161/CIRCRESAHA.1110.223842

Rayment, I., Rypniewski, W. R., Schmidt-Base, K., Smith, R., Tomchick, D. R., and Benning, M. M., et al (1993). Three-dimensional structure of myosin subfragment-1: a molecular motor. *Science* 261, 50–58. doi: 10.1126/science.8316857

Richard, P., Charron, P., Carrier, L., Ledeuil, C., Cheav, T., Pichereau, C., et al. (2003). Hypertrophic cardiomyopathy: distribution of disease genes, spectrum of mutations, and implications for a molecular diagnosis strategy. *Circulation* 107, 2227–2232. doi: 10.1161/01.CIR.0000066323.15244.54

Robinson, P., Griffiths, P. J., Watkins, H., and Redwood, C. S. (2007). Dilated and hypertrophic cardiomyopathy mutations in troponin and alpha-tropomyosin have opposing effects on the calcium affinity of cardiac thin filaments. *Circ. Res.* 101, 1266–1273. doi: 10.1161/CIRCRESAHA.107.156380

Robinson, P., Mirza, M., Knott, A., Abdulrazzak, H., Willott, R., Marston, S., et al. (2002). Alterations in thin filament regulation induced by a human cardiac troponin T mutant that causes dilated cardiomyopathy are distinct from those induced by troponin T mutants that cause hypertrophic cardiomyopathy. *J. Biol. Chem.* 277, 40710–40716. doi: 10.1074/jbc.M203446200

Ruwhof, C., van Wamel, A. E., Egas, J. M., and van der Laarse, A. (2000). Cyclic stretch induces the release of growth promoting factors from cultured neonatal cardiomyocytes and cardiac fibroblasts. *Mol. Cell Biochem.* 208, 89–98. doi: 10.1023/A:1007046105745

Schipke, J., Banmann, E., Nikam, S., Voswinckel, R., Kohlstedt, K., Loot, A. E., et al. (in press). The number of cardiac myocytes in the hypertrophic and hypotrophic left ventricle of the obese and calorie-restricted mouse heart. *J. Anat.* doi: 10.1111/joa.12236

Seebohm, B., Matinmehr, F., Kohler, J., Francino, A., Navarro-Lopez, F., Perrot, A., et al. (2009). Cardiomyopathy mutations reveal variable region of myosin converter as major element of cross-bridge compliance. *Biophys. J.* 97, 806–824. doi: 10.1016/j.bpj.2009.05.023

Spindler, M., Saupe, K. W., Christe, M. E., Sweeney, H. L., Seidman, C. E., Seidman, J. G., et al. (1998). Diastolic dysfunction and altered energetics in the alphaMHC403/+ mouse model of familial hypertrophic cardiomyopathy. *J. Clin. Invest.* 101, 1775–1783. doi: 10.1172/JCI1940

Spirito, P., Maron, B. J., Bonow, R. O., and Epstein, S. E. (1987). Occurrence and significance of progressive left ventricular wall thinning and relative cavity dilatation in hypertrophic cardiomyopathy. *Am. J. Cardiol.* 60, 123–129. doi: 10.1016/0002-9149(87)90998-2

Stienen, G. J., Guth, K., and Ruegg, J. C. (1983). Force and force transients in skeletal muscle fibres of the frog skinned by freeze-drying. *Pflugers Arch.* 397, 272–276. doi: 10.1007/BF00580260

Sweeney, H. L., Bowman, B. F., and Stull, J. T. (1993). Myosin light chain phosphorylation in vertebrate striated muscle: regulation and function. *Am. J. Physiol.* 264, C1085–C1095.

Teekakirikul, P., Eminaga, S., Toka, O., Alcalai, R., Wang, L., Wakimoto, H., et al. (2010). Cardiac fibrosis in mice with hypertrophic cardiomyopathy is mediated by non-myocyte proliferation and requires Tgf-beta. *J. Clin. Invest.* 120, 3520–3529. doi: 10.1172/JCI42028

Tripathi, S., Schultz, I., Becker, E., Montag, J., Borchert, B., Francino, A., et al. (2011). Unequal allelic expression of wild-type and mutated beta-myosin in familial hypertrophic cardiomyopathy. *Basic Res. Cardiol.* 106, 1041–1055. doi: 10.1007/s00395-011-0205-9

van der Velden, J., Papp, Z., Boontje, N. M., Zaremba, R., de Jong, J. W., Janssen, P. M., et al. (2003). The effect of myosin light chain 2 dephosphorylation on Ca2+ -sensitivity of force is enhanced in failing human hearts. *Cardiovasc. Res.* 57, 505–514. doi: 10.1016/S0008-6363(02)00662-4

van Dijk, S. J., Paalberends, E. R., Najafi, A., Michels, M., Sadayappan, S., Carrier, L., et al. (2012). Contractile dysfunction irrespective of the mutant protein in human hypertrophic cardiomyopathy with normal systolic function. *Circ. Heart Fail.* 5, 36–46. doi: 10.1161/CIRCHEARTFAILURE.1111.963702

van Wamel, A. J., Ruwhof, C., van der Valk-Kokshoom, L. E., Schrier, P. I., and van der Laarse, A. (2001). The role of angiotensin II, endothelin-1 and transforming growth factor-beta as autocrine/paracrine mediators of stretch-induced cardiomyocyte hypertrophy. *Mol. Cell Biochem.* 218, 113–124. doi: 10.1023/A:1007279700705

van Wamel, A. J., Ruwhof, C., van der Valk-Kokshoorn, L. J., Schrier, P. I., and van der Laarse, A. (2002). Stretch-induced paracrine hypertrophic stimuli increase TGF-beta1 expression in cardiomyocytes. *Mol. Cell Biochem.* 236, 147–153. doi: 10.1023/A:1016138813353

Witjas-Paalberends, E. R., Ferrara, C., Scellini, B., Piroddi, N., Montag, J., Tesi, C., et al. (2014). Faster cross-bridge detachment and increased tension cost in human hypertrophic cardiomyopathy with the R403Q *MYH7* mutation. *J. Physiol.* 592, 3257–3272. doi: 10.1113/jphysiol.2014.274571

Conflict of Interest Statement: The authors declare that the research was conducted in the absence of any commercial or financial relationships that could be construed as a potential conflict of interest.

Received: 21 July 2014; accepted: 22 September 2014; published online: 10 October 2014.

Citation: Brenner B, Seebohm B, Tripathi S, Montag J and Kraft T (2014) Familial hypertrophic cardiomyopathy: functional variance among individual cardiomyocytes as a trigger of FHC-phenotype development. Front. Physiol. ***5****:392. doi: 10.3389/fphys.2014.00392*

This article was submitted to Striated Muscle Physiology, a section of the journal Frontiers in Physiology.

Copyright © 2014 Brenner, Seebohm, Tripathi, Montag and Kraft. This is an open-access article distributed under the terms of the Creative Commons Attribution License (CC BY). The use, distribution or reproduction in other forums is permitted, provided the original author(s) or licensor are credited and that the original publication in this journal is cited, in accordance with accepted academic practice. No use, distribution or reproduction is permitted which does not comply with these terms.

frontiers in PHYSIOLOGY

ORIGINAL RESEARCH ARTICLE
published: 16 December 2014
doi: 10.3389/fphys.2014.00484

Proteasome inhibition slightly improves cardiac function in mice with hypertrophic cardiomyopathy

Saskia Schlossarek[1,2], Sonia R. Singh[1,2], Birgit Geertz[1,2], Herbert Schulz[3,4†], Silke Reischmann[1,2], Norbert Hübner[3,4] and Lucie Carrier[1,2*]

[1] Department of Experimental Pharmacology and Toxicology, Cardiovascular Research Center, University Medical Center Hamburg-Eppendorf, Hamburg, Germany
[2] German Centre for Cardiovascular Research (DZHK), Hamburg/Kiel/Lübeck, Germany
[3] Max-Delbrück-Center for Molecular Medicine (MDC), Berlin, Germany
[4] German Centre for Cardiovascular Research (DZHK), Berlin, Germany

Edited by:
Julien Ochala, King's College London, UK

Reviewed by:
Charles Redwood, University of Oxford, UK
Aldrin V. Gomes, University of California, Davis, USA

***Correspondence:**
Lucie Carrier, Department of Experimental Pharmacology and Toxicology, University Medical Center Hamburg Eppendorf, Martinistraße 52, 20246 Hamburg, Germany
e-mail: l.carrier@uke.de

† Present address:
Herbert Schulz, Cologne Center for Genomics, University of Cologne, Cologne, Germany

A growing line of evidence indicates a dysfunctional ubiquitin-proteasome system (UPS) in cardiac diseases. Anti-hypertrophic effects and improved cardiac function have been reported after treatment with proteasome inhibitors in experimental models of cardiac hypertrophy. Here we tested whether proteasome inhibition could also reverse the disease phenotype in a genetically-modified mouse model of hypertrophic cardiomyopathy (HCM), which carries a mutation in *Mybpc3*, encoding the myofilament protein cardiac myosin-binding protein C. At 7 weeks of age, homozygous mutant mice (KI) have 39% higher left ventricular mass-to-body-weight ratio and 29% lower fractional area shortening (FAS) than wild-type (WT) mice. Both groups were treated with epoxomicin (0.5 mg/kg/day) or vehicle for 1 week via osmotic minipumps. Epoxomicin inhibited the chymotrypsin-like activity by ∼50% in both groups. All parameters of cardiac hypertrophy (including the fetal gene program) were not affected by epoxomicin treatment in both groups. In contrast, FAS was 12% and 35% higher in epoxomicin-treated than vehicle-treated WT and KI mice, respectively. To identify which genes or pathways could be involved in this positive effect, we performed a transcriptome analysis in KI and WT neonatal cardiac myocytes, treated or not with the proteasome inhibitor MG132 (1 μM, 24 h). This revealed 103 genes (four-fold difference; 5% FDR) which are commonly regulated in both KI and WT cardiac myocytes. Thus, even in genetically-modified mice with manifest HCM, proteasome inhibition showed beneficial effects, at least with regard to cardiac function. Targeting the UPS in cardiac diseases remains therefore a therapeutic option.

Keywords: cardiomyopathy, hypertrophic, *Mybpc3*, transgenic mice, ubiquitin-proteasome system, proteasome inhibitors

INTRODUCTION

Along with the autophagy-lysosome pathway, the ubiquitin-proteasome system (UPS) represents the major proteolytic system of eukaryotic cells and degrades highly selectively intracellular cytosolic, nuclear and myofibrillar proteins. A main function of the UPS is to prevent accumulation of damaged, misfolded and mutant proteins, but it is also involved in a variety of biological processes such as cell proliferation, adaptation to stress and cell death (Zolk et al., 2006). The ATP-dependent proteolytic process involves polyubiquitination of the target protein through a series of enzymatic reactions and the subsequent degradation of the polyubiquitinated protein by the 26S proteasome (Mearini et al., 2008). The eukaryotic 26S proteasome itself is composed of the 19S regulatory particle, which recognizes, deubiquitinates and unfolds the target protein, and the 20S core, which degrades the target protein through three distinct proteolytic activities (chymotrypsin-like, trypsin-like, and caspase-like). These proteolytic activities can be inhibited either reversibly by peptide aldehydes and peptide boronates (e.g., bortezomib) or irreversibly by β-lactones (e.g., PS-519) and epoxyketones (e.g., epoxomicin; Kisselev et al., 2012).

Alterations of the UPS have been reported in several human and experimental cardiac diseases. Specifically, accumulation of polyubiquitinated proteins was a common feature of cardiac disorders (Kostin et al., 2003; Weekes et al., 2003; Birks et al., 2008), whereas activities of the proteasome decreased or increased depending on the status of the cardiac disease (Depre et al., 2006; Tsukamoto et al., 2006; Birks et al., 2008; Predmore et al., 2010; Schlossarek et al., 2012a). In the case of an activated UPS, partial and short-term proteasome inhibition has shown beneficial effects in different animal models. Treatment of mice with the irreversible proteasome inhibitor epoxomicin prevented both left ventricular hypertrophy (LVH) and the associated higher proteasome activity induced by short-term transverse aortic constriction (TAC; Depre et al., 2006). Similarly, low doses of the reversible proteasome inhibitor bortezomib suppressed cardiac hypertrophy in Dahl salt-sensitive rats (Meiners et al., 2008). In addition to its hypertrophy-preventing effect, proteasome inhibition has been shown to be even capable to

reverse preexisting hypertrophy. Administration of epoxomicin at a stage of pronounced cardiac hypertrophy led to a stabilization of contractile parameters and a regression of preexisting hypertrophy in mice (Hedhli et al., 2008). Likewise, the irreversible proteasome inhibitor PS-519 attenuated isoprenaline-induced hypertrophy in mice (Stansfield et al., 2008). In the present study, we therefore aimed at evaluating whether epoxomicin may reduce cardiac hypertrophy and improve cardiac function in a genetically-engineered mouse model of hypertrophic cardiomyopathy (HCM), which carries a mutation in *Mybpc3*, encoding the myofilament protein cardiac myosin-binding protein C. The corresponding human c.772G>A *MYBPC3* mutation is one of the most frequent HCM mutations (found in 13% unrelated HCM patients; Olivotto et al., 2008) and associated with a bad prognosis (Richard et al., 2003). Homozygous KI mice develop systolic dysfunction after postnatal day 1 and LVH at postnatal day 3 (Gedicke-Hornung et al., 2013; Mearini et al., 2013). The present study was performed at the age of 7 weeks, an age at which KI mice have been shown to exhibit higher activities of the proteasome than WT littermates (Schlossarek et al., 2012a).

MATERIALS AND METHODS

ANIMALS

Mice were housed in a controlled animal facility with free access to water and standard animal chow. The experimental procedures were in accordance with the German Law for the Protection of Animals and have been approved by the Authority for Health and Consumer Protection of the City State of Hamburg, Germany (Nr. 07/13). Development and initial characterization of the KI mice was previously reported (Vignier et al., 2009). Both KI and WT mice were maintained on a Black Swiss background.

ADMINISTRATION OF EPOXOMICIN

Administration of epoxomicin (Enzo Life Sciences) was delivered to mice by subcutaneously implanted osmotic minipumps (Alzet, model 1007D) with a dose of 0.5 mg/kg/day for 1 week. Epoxomicin was diluted in NaCl (with 10% DMSO), control pumps delivered vehicle alone. After filling, the pumps were incubated in saline at 37°C overnight to achieve the full pumping rate from the beginning. Animals were anesthetized with isoflurane (1.5%, Abbott Inc.) for minipump implantation. No decrease in body weight, no complications and/or side effects related to treatment with epoxomicin were observed.

ECHOCARDIOGRAPHY

Transthoracic echocardiography was performed before minipump implantation and after 1-week treatment using the Vevo 2100 System (VisualSonics, Toronto, Canada). Animals were anesthetized with isoflurane (1–2%, Abbott Inc.) and fixed to a warming platform in a supine position. Anesthetic depth was monitored by electrocardiogram and respiration rate. B-mode images were obtained using a MS 400 transducer with a frame rate of 230–400 frames/s. Two-dimensional short axis views were recorded at the mid-papillary muscle level. The dimensions of the left ventricle were measured in a short axis view in diastole and systole. All images were recorded digitally and off-line analysis was performed using the Vevo 2100 software.

DETERMINATION OF THE CHYMOTRYPSIN-LIKE ACTIVITY

The chymotrypsin-like activity of the proteasome was assessed in ventricular cytosolic lysates as described previously (Schlossarek et al., 2012a). For determination of the activity, 30 μg of protein were diluted in incubation buffer (20 mM HEPES, 0.5 mM EDTA, 5 mM DTT, 0.1 mg/ml ovalbumin) to a final volume of 50 μl. Samples were pre-incubated in this buffer for 2 h at 4°C. Following pre-incubation, the synthetic fluorogenic substrate Suc-LLVY-AMC (Merck Biosciences) was added to the samples at a final concentration of 60 μM. After incubation in the dark for 1 h at 37°C, the fluorescence of the released AMC reporter was measured using the TECAN Safire^2 microplate reader at an excitation wavelength of 380 nm and an emission wavelength of 460 nm. Each sample was measured in triplicate. The mean of the blank (incubation buffer only) was subtracted from the mean of each sample triplicate.

WESTERN BLOT

Western blot was performed in ventricular cytosolic lysates as described previously (Schlossarek et al., 2012b). Primary antibody was directed against the β5-subunit of the proteasome (kindly given by X.J. Wang, University of South Dakota, 1:5000). Secondary antibody was anti-rabbit (Sigma, 1:6000, peroxidase-conjugated). Signals were revealed with SuperSignal® West Dura extended duration substrate (Pierce) and acquired with the Chemie Genius^2 Bio Imaging System.

ANALYSIS OF VENTRICULAR mRNAs

Total RNA was extracted from mouse ventricles using the SV Total RNA Isolation Kit (Promega) according to the manufacturer's instructions. RT-qPCR was performed as described previously (Schlossarek et al., 2012b). The primers used to amplify the β5-subunit of the proteasome (*Psmb5)*, atrial natriuretic peptide (*Nppa)*, α-skeletal actin (*Acta1)*, and guanine nucleotide binding protein, alpha stimulating *(Gnas)* are listed in **Table 1**. *Gnas* was used as an endogenous control to normalize the quantification of the target mRNAs for difference in the amount of total RNA added to each reaction.

Table 1 | PCR primer names and sequences.

Gene name	Target name	Sequence
Psmb5 F	Proteasome subunit, β5	5′-GAGCTTCGCAATAAGGAACG-3′
Psmb5 R	Proteasome subunit, β5	5′-CTGTTCCCCTCGCTGTCTAC-3′
Nppa F	Atrial natriuretic peptide	5′-ATCTGCCCTCTTGAAAAGCA-3′
Nppa R	Atrial natriuretic peptide	5′-ACACACCACAAGGGCTTAGG-3′
Acta1 F	α-skeletal actin	5′-CCCCTGAGGAGCACCCGACT-3′
Acta1 R	α-skeletal actin	5′-CGTTGTGGGTGACACCGTCCC-3′
Gnas F	Guanine nucleotide binding protein, alpha stimulating	5′-CAAGGCTCTGTGGGAGGAT-3′
Gnas R	Guanine nucleotide binding protein, alpha stimulating	5′-CGAAGCAGGTCCTGGTCACT-3′

Abbreviations used are: F, forward primer; R, reverse primer.

TRANSCRIPTOME ANALYSIS

Neonatal mouse cardiac myocytes were isolated from 0 to 4 day-old KI and WT pups and cultured as described previously (Vignier et al., 2009). After 3 days of plating cardiac myocytes were either kept untreated or treated with 1 μM MG132 (Calbiochem) for 24 h. Total RNA was then extracted from cultured cardiac myocytes using RNAzol® (WAK-Chemie), according to the manufacturers' instructions. RNA concentration, purity and quality were analyzed using the NanoDrop® ND-1000 spectrophotometer (Thermo Scientific). Transcriptome analysis of all samples was performed in triplicate using Illumina Beadchips (Mouse WG-6 v2.0). The wet lab methods included amplification and fragmentation of the samples, sample hybridization to the beadchip, and washing, staining and scanning of the beadchip. For analysis, the Illumina Mouse WG-6 v2.0 array data were quantile normalized on probe level (45,281 probes) without background correction using Illumina GenomeStudio V2011.1. Data of the 12 samples (four conditions, three biological replicates) have been $\log_2$-transformed after an offset addition (16). Probes fail to underrun a detection p-value of 0.05 in any sample have been discarded before test statistic (25,080 probes left). Probes and samples were analyzed on significant expression differences according to the genotype (KI or WT) and treatment (MG132-treated or untreated) using Two-Way ANOVA statistic followed by FDR multiple testing corrections (Benjamini and Hochberg, 1995). To avoid batch effects, the Illumina slide was used as a cofactor in the test statistic. Probes which undergo 5% FDR were selected as differentially expressed. Probes, significant and more than four-fold regulated between any of the four conditions, were clustered and heatmap visualized. We performed hierarchical Euclidean average linkage clustering for initial expression profile visualization (**Figure 5**) using the pheatmap R package. Protein interaction of genes regulated by MG132-treatment have been further investigated by using the String platform (Snel et al., 2000) and a high confidence score (0.7).

STATISTICAL ANALYSIS

Data were expressed as mean ± s.e.m. Statistical analyses were performed by Two-Way ANOVA followed by Bonferroni's post-test, or by paired or unpaired Student's t-test as indicated in the figure legends. All analyses were realized using the commercial software GraphPad Prism5 (Software Inc.). A value of $P < 0.05$ was considered statistically significant. For transcriptomic analysis, statistics are explained in the corresponding paragraph above.

RESULTS

REDUCTION OF CHYMOTRYPSIN-LIKE ACTIVITY BY 50% WITH EPOXOMICIN

Seven week-old KI mice presented a 39% higher left ventricular mass-to-body-weight (LVM/BW) ratio and a 29% lower fractional area shortening (FAS) than age-matched WT mice (**Figure 1**). We previously reported higher proteasome activities in 7-week-old KI than WT mice (Schlossarek et al., 2012a). Sex-matched KI and WT mice were treated for 1 week with epoxomicin (0.5 mg/kg/day) or vehicle (NaCl in 10% DMSO) according to Hedhli et al. (2008). Epoxomicin is a specific irreversible inhibitor of the β5-subunit of the proteasome and responsible for the chymotrypsin-like activity (Hedhli and Depre, 2010). The chymotrypsin-like activity in cytosolic protein lysates was ∼50% lower in KI and WT mice treated with epoxomicin than in NaCl-treated mice (**Figure 2A**). Inhibition of the β5-subunit did not come along with changes in the *Psmb5* transcript level (**Figure 2B**), but with the appearance of two β5-subunit bands in Western blot (**Figure 2C**). This was already previously observed (Vignier et al., 2009) and likely represents the free (lower band) and the epoxomicin-bound (upper band) β5-subunit.

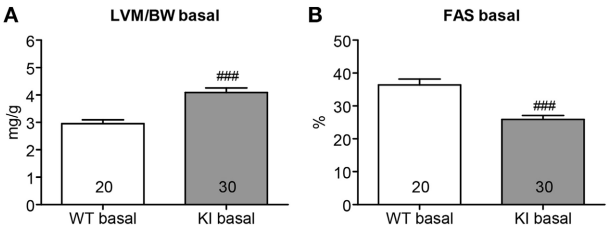

FIGURE 1 | Echocardiographic analysis in KI vs. WT mice under basal conditions. Echocardiographic analyses were performed in KI (gray) and WT (white) mice under basal conditions, i.e., before minipump implantation. **(A)** Left ventricular mass-to-body-weight ratio (LVM/BW). **(B)** Fractional area shortening (FAS). Data are expressed as mean ± s.e.m. with $^{###}P < 0.001$ vs. WT, unpaired Student's t-test. The number of animals is indicated in the bars.

NO REGRESSION OF LEFT VENTRICULAR HYPERTROPHY BY PROTEASOME INHIBITION

To determine whether proteasome inhibition had an effect on LVH, echocardiography was performed after 1 week of treatment. As expected, administration of NaCl did not alter the LVM/BW ratio in both WT and KI mice (**Figure 3A**, left panel). Likewise, the LVM/BW ratio did not differ before and after epoxomicin treatment in both groups (**Figure 3A**, middle panel). Finally, no difference in LVM/BW ratio was observed when comparing the data only after treatment in both WT and KI mice (**Figure 3A**, right panel). The heart-weight-to-body-weight (HW/BW) and heart-weight-to-tibia-length (HW/TL) ratios were 41% and 28% higher in NaCl-treated KI than WT mice, respectively. Epoxomicin treatment did not affect both ratios in both genotypes (**Figure 3B**). Finally, the transcript level of two classical hypertrophy markers *Nppa* and *Acta1* were higher in NaCl-treated KI than WT mice and were not affected by epoxomicin treatment (**Figure 3C**).

SLIGHT IMPROVEMENT OF CARDIAC FUNCTION BY PROTEASOME INHIBITION

Cardiac function was examined by echocardiography after 1 week of treatment. FAS was not affected in WT mice, whereas it was reduced by 19% in KI mice by NaCl treatment (**Figure 4A**). Conversely, FAS was increased by 15% in WT, but not affected in KI mice by epoxomicin treatment (**Figure 4B**). However, when we compared the data after treatment, FAS was 35% higher after epoxomicin than after NaCl administration in KI mice (**Figure 4C**). Although the FAS did not reach the level found in

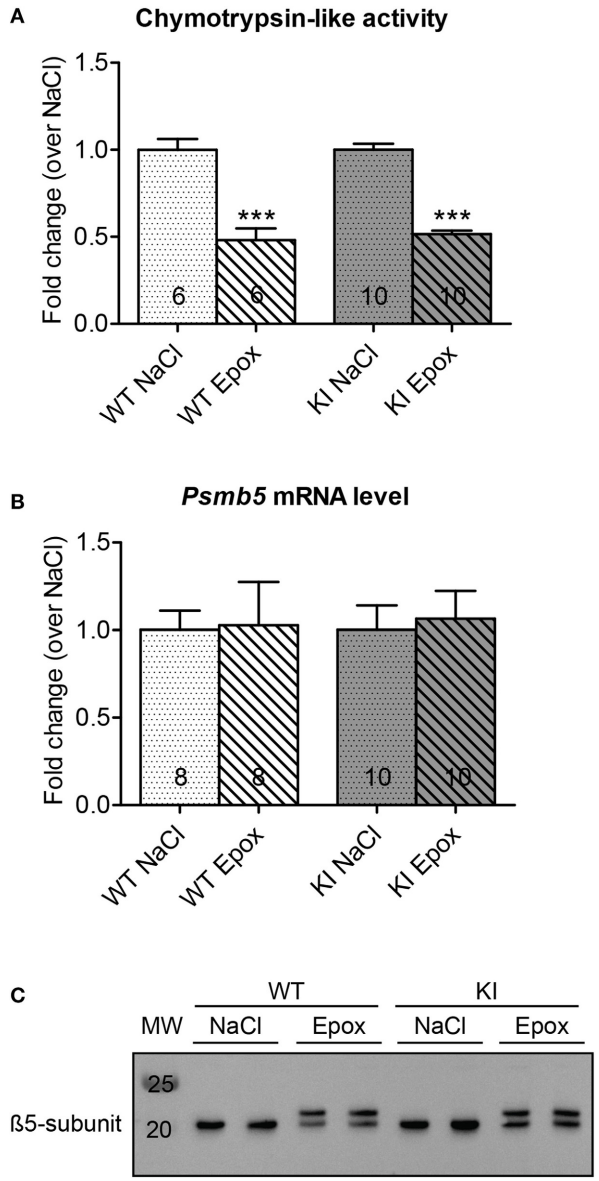

FIGURE 2 | Evaluation of chymotrypsin-like activity and β5-subunit after proteasome inhibition in KI vs. WT mice. Analyses were performed in KI (gray) and WT (white) mice treated for 1 week with epoxomicin (Epox; stripes) or sodium chloride (NaCl; dots) via osmotic minipumps. **(A)** Chymotrypsin-like activity in ventricular cytosolic protein extracts. **(B)** β5-subunit mRNA level determined by RT-qPCR with SYBR Green and normalized to *Gnas*. **(C)** Representative Western blot stained with an anti-β5-subunit antibody. Data are expressed as mean ± s.e.m. with *** $P < 0.001$ vs. corresponding NaCl-treated group, unpaired Student's *t*-test. The number of animals is indicated in the bars.

WT mice, these data suggest that epoxomicin partially rescued the cardiac function in KI mice.

MARKED AND SIGNIFICANT DIFFERENTIAL GENE EXPRESSION IN CARDIAC MYOCYTES AFTER PROTEASOME INHIBITION

To assess whether specific genes or biological pathways could be involved in the improved cardiac function, we performed a transcriptome analysis in WT and KI neonatal cardiac myocytes, treated or not with 1 μM of the reversible proteasome inhibitor MG132 for 24 h. Gene expression profiles were then evaluated by the Illumina Beadchips. ANOVA analysis over 25,080 expressed of 45,281 total probes led to a set of 4639 differential expressed probes (5% FDR) in strain (KI vs. WT; $N = 37$) or treatment (untreated vs. MG132-treated; $N = 4633$). No significant strain × treatment interaction was found. According to the pronounced treatment effects we further focused on markedly regulated probes (5% FDR in strain or treatment and a four-fold regulation between any pair of conditions). Hierarchical clustering of the resulting set of 404 probes (representing 339 genes) confirmed the dominance of MG132 treatment effects (**Figure 5A**). A total of 197 genes (141 down and 56 up) and 161 genes (113 down and 48 up) were regulated by MG132 treatment (four-fold, 5% FDR) in WT and KI cardiac myocytes, respectively. Out of them, 103 genes were commonly regulated in both groups (68 down and 35 up). **Figures 5B,C** show the string network of interaction of most of the genes commonly ≥four-fold down- or up-regulated in both KI and WT. Markedly down-regulated genes encode for example proteins involved in the UPS [such as ankyrin repeat and SOCS box containing 2 (ASB2) or tripartite motif-containing 72 (TRIM72)], myofilament function [such as α-myosin-heavy chain (MYH6) or cardiac troponin I (TNNI3)], or calcium handling (such as phospholamban, PLN). Markedly up-regulated genes encode for example transcription factors [such as paired box 2 (PAX2) or DNA-damage-inducible transcript 3 (DD1T3)], or molecular chaperones [such as heat shock protein 90 kDa alpha (HSP90AA1), heat shock 70 kDa protein 1a (HSPA1A) or F-box protein 2 (FBXO2) involved in protein refolding]. Details for the 404 markedly and significantly regulated probes are in the **Supplemental Table 1**.

DISCUSSION

In the present study we evaluated the cardiac phenotype after 1 week of proteasome inhibition in adolescent homozygous *Mybpc3*-targeted KI and corresponding WT mice. At the investigated age of 7 weeks, KI mice exhibited a manifest LVH and cardiac dysfunction. Based on previous publications (Hedhli et al., 2008; Stansfield et al., 2008), we hypothesized that inhibition of the UPS may be able to reduce preexisting LVH and improve cardiac function in KI mice. The major findings of the present study are: (1) no regression of preexisting hypertrophy in KI mice, (2) slight improvement of cardiac function in WT mice, and (3) a partial, but significant improvement of cardiac function in KI mice by epoxomicin treatment. Finally, MG132 treatment of cardiac myocytes revealed 103 genes which are commonly regulated in KI and WT.

Elevated or impaired UPS function has been regularly reported in experimental models of HCM and heart failure (Depre et al., 2006; Tsukamoto et al., 2006; Schlossarek et al., 2012a), suggesting that the regulation of the UPS belongs to important adaptations in cardiac disease. In this context, proteasome inhibitors have been suggested to be associated with anti-hypertrophic effects and improved cardiac function. However, the *in vivo* effect of proteasome inhibition was so far only investigated in animal models with cardiac hypertrophy induced by isoprenaline, high salt diet

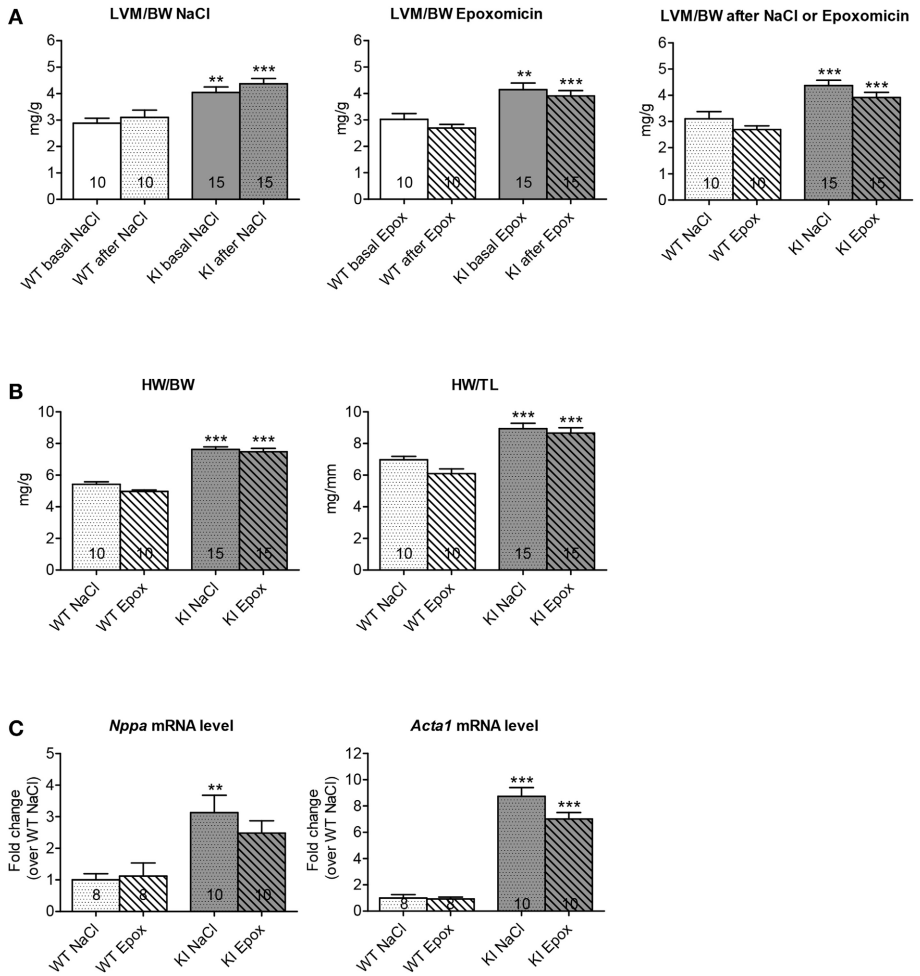

FIGURE 3 | Evaluation of cardiac hypertrophy after proteasome inhibition in KI vs. WT mice. Analyses were performed in KI (gray) and WT (white) mice under basal conditions (basal; plain) or after 1 week of treatment with epoxomicin (Epox; stripes) or sodium chloride (NaCl; dots) via osmotic minipumps. **(A)** Left ventricular mass-to-body-weight ratio (LVM/BW) determined by echocardiography. **(B)** Heart-weight-to-body-weight ratio (HW/BW) and heart-weight-to-tibia-length ratio (HW/TL). **(C)** mRNA levels of hypertrophy markers determined by RT-qPCR with SYBR Green and normalized to *Gnas*. Data are expressed as mean ± s.e.m. with $^{**}P < 0.01$ and $^{***}P < 0.001$ vs. WT in the same condition, Two-Way ANOVA plus Bonferroni's post-test. The number of animals is indicated in the bars. Abbreviations: *Acta1*, α-skeletal actin; *Nppa*, atrial natriuretic peptide.

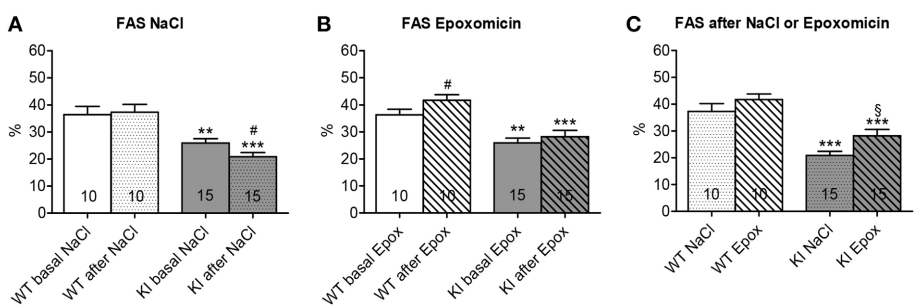

FIGURE 4 | Evaluation of cardiac function after proteasome inhibition in KI vs. WT mice. Fractional area shortening (FAS) was determined by echocardiography in KI (gray) and WT (white) mice under basal conditions (basal; plain; **A, B**) or after 1 week of treatment with epoxomicin (Epox; stripes; **B, C**) or sodium chloride (NaCl; dots; **A, C**) via osmotic minipumps. Data are expressed as mean ± s.e.m. with $^{**}P < 0.01$ and $^{***}P < 0.001$ vs. WT in the same condition, Two-Way ANOVA plus Bonferroni's post-test, $^{\#}P < 0.05$ vs. corresponding basal, paired Student's *t*-test, and $^{\S}P < 0.05$ vs. KI NaCl, unpaired Student's *t*-test. The number of animals is indicated in the bars.

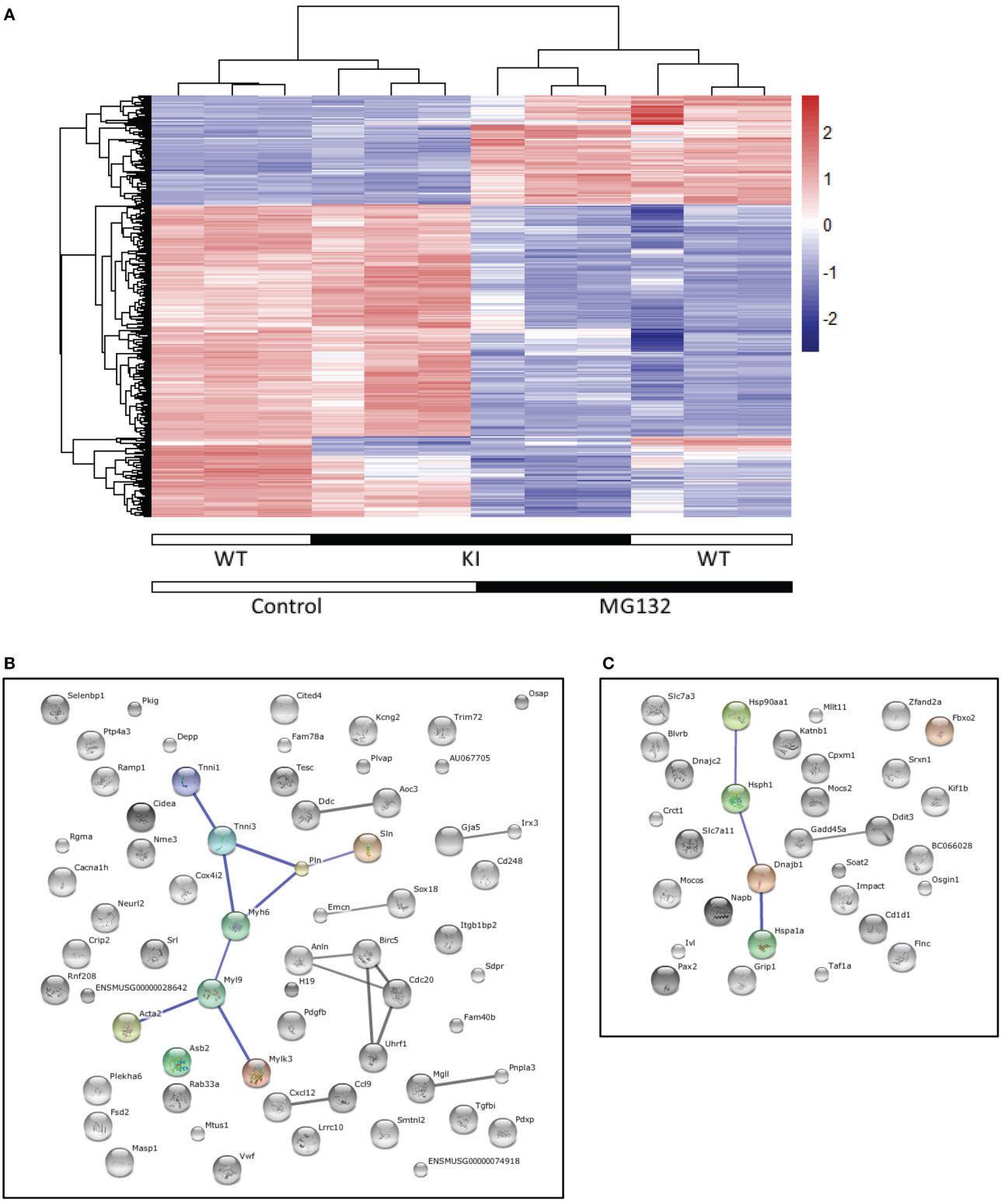

FIGURE 5 | Transcriptome analysis. Cardiac myocytes were isolated from neonatal KI and WT mice and treated with the proteasome inhibitor MG132 (1 μM) or left untreated for 24 h. RNAs were subjected to transcriptome analysis using the Illumina Beadchips. **(A)** Clustering of the four-fold and significantly (5% FDR) regulated expressed probes ($N = 404$). The heatmap and the dendrograms representing the results of the hierarchical clustering of standardized log2 signal values. **(B), (C)** String networks of four-fold and significant differentially expressed (5% FDR) genes commonly regulated in KI and WT cardiac myocytes [$N = 103$, 68 down **(B)** and 35 up **(C)**]. Known and predicted protein interactions including direct (physical) and indirect (functional) associations are visualized in a network. The size of the connecting lines represents the impact of the connection. Only high confidence String interactions are shown.

or TAC, but not in genetically-modified HCM mouse models as it is the case in the present study. In contrast to the previous studies, we did not observe a regression of preexisting cardiac hypertrophy after proteasome inhibition in KI mice. Neither LVM/BW nor HW/BW or HW/TL changed after 1 week of treatment with epoxomicin. Furthermore, mRNA levels of hypertrophy markers did not decrease after treatment. The discrepancy between previous and present findings may be explained by the manifestation of cardiac hypertrophy in the investigated models. In the previous studies cardiac hypertrophy was achieved in mice by 2-week of either TAC (Hedhli et al., 2008) or isoprenaline infusion (Stansfield et al., 2008). In contrast, the KI mice already develop LVH at postnatal day 3 (Gedicke-Hornung et al., 2013) and proteasome inhibition was performed at the age of 7 weeks. Therefore, cardiac hypertrophy was present for a longer time period than in previous studies and could be associated with more remodeling of the cardiac tissue.

Analysis of the cardiac function, on the other hand, displayed already challenging findings after 1 week of treatment. First, and unexpectedly, KI, but not WT mice exhibited a slight, but significant decrease in cardiac function after 1 week of NaCl administration (**Figure 4A**). The reason is not certain but it could be related to the combination of stress due to minipump implantation plus mutation in KI mice. This is in agreement with our previous data obtained in heterozygous KI mice (Schlossarek et al., 2012b). The stress induced by minipump implantation does not affect the WT mice, likely because they do not have a disease phenotype. Second, epoxomicin treatment improved cardiac function in WT, but not at first glance in KI mice (**Figure 4B**). Since the WT mice are able to cope with the stress, we directly see the effect of epoxomicin. On the contrary, since the KI mice are not able to cope with the stress (negative effect on FAS), the positive effect of epoxomicin cannot be seen directly (=no change in FAS). However, directly comparing the effects of epoxomicin and NaCl after 1 week of treatment suggests that epoxomicin indeed had a positive effect also in KI mice (**Figure 4C**).

To identify which genes or pathways could be involved in this positive effect, transcriptome analysis was performed in KI and WT neonatal cardiac myocytes, treated or not with the proteasome inhibitor MG132. This revealed marked and significant differentially expressed genes. Focus on the commonly regulated genes in MG132-treated KI and WT cardiac myocytes revealed up-regulation of genes encoding transcription factors or proteins involved in protein re-folding, as well as down-regulation of genes encoding proteins involved in the UPS or calcium handling. The latter for example includes PLN, which is an inhibitor of the sarcoplasmic reticulum calcium-ATPase, and therefore its down-regulation could contribute to the better cardiac function observed upon epoxomicin treatment *in vivo*.

Since the UPS plays a role in many fundamental biological processes, targeting this system for therapy is complex and particularly some conflicting data exist that argue against the anti-hypertrophic and function-stabilizing effects of proteasome inhibitors in chronic application (Herrmann et al., 2013). In addition, while bortezomib (reversible proteasome inhibitor) is generally well tolerated by patients with multiple myeloma, it has been shown to increase the occurrence of cardiac complications ranging from arrhythmia to congestive heart failure in elderly patients or patients with preexisting cardiac problems (Enrico et al., 2007; Hacihanefioglu et al., 2008; Bockorny et al., 2012).

In conclusion, whereas chronic proteasome inhibition may give additional stress to the heart and promote transition to heart failure, our data revealed that partial and short-term proteasome inhibition does not suppress LVH but slightly improved cardiac function in a mouse model of HCM. Targeting the UPS acutely therefore remains a therapeutic option for cardiac diseases with reduced cardiac function.

AUTHOR CONTRIBUTIONS

Saskia Schlossarek, conception and design of research, management of the mouse cohorts, execution of experiments, analysis and interpretation of data, figure preparation, drafting of the manuscript. Sonia R. Singh, isolation and treatment of cardiac myocytes, execution of experiments. Birgit Geertz, recording and analysis of the echocardiographic data. Herbert Schulz, transcriptome analysis. Silke Reischmann, execution of experiments. Norbert Hübner, transcriptome analysis. Lucie Carrier, conception and design of research, analysis and interpretation of data, drafting of the manuscript. All authors critically discussed the results, and reviewed and approved the manuscript before submission.

ACKNOWLEDGMENTS

This work was supported by the German Centre for Cardiovascular Research (DZHK) and the German Ministry of Research Education (BMBF), as well as by the Leducq Foundation (Research Grant Nr. 11, CVD 04).

SUPPLEMENTARY MATERIAL

The Supplementary Material for this article can be found online at: http://www.frontiersin.org/journal/10.3389/fphys.2014.00484/abstract

Supplemental Table 1 | Results of the descriptive and test statistic of 404 significant expressed probes are documented.

REFERENCES

Benjamini, Y., and Hochberg, Y. (1995). Controlling the false discovery rate: a practical and powerful approach to multiple testing. *J. R. Stat. Soc. B Stat. Methodol.* 57, 289–300.

Birks, E. J., Latif, N., Enesa, K., Folkvang, T., Luong Le, A., Sarathchandra, P., et al. (2008). Elevated p53 expression is associated with dysregulation of the ubiquitin-proteasome system in dilated cardiomyopathy. *Cardiovasc. Res.* 79, 472–480. doi: 10.1093/cvr/cvn083

Bockorny, M., Chakravarty, S., Schulman, P., Bockorny, B., and Bona, R. (2012). Severe heart failure after bortezomib treatment in a patient with multiple myeloma: a case report and review of the literature. *Acta Haematol.* 128, 244–247. doi: 10.1159/000340050

Depre, C., Wang, Q., Yan, L., Hedhli, N., Peter, P., Chen, L., et al. (2006). Activation of the cardiac proteasome during pressure overload promotes ventricular hypertrophy. *Circulation* 114, 1821–1828. doi: 10.1161/CIRCULATIONAHA.106.637827

Enrico, O., Gabriele, B., Nadia, C., Sara, G., Daniele, V., Giulia, C., et al. (2007). Unexpected cardiotoxicity in haematological bortezomib treated patients. *Br. J. Haematol.* 138, 396–397. doi: 10.1111/j.1365-2141.2007.06659.x

Gedicke-Hornung, C., Behrens-Gawlik, V., Reischmann, S., Geertz, B., Stimpel, D., Weinberger, F., et al. (2013). Rescue of cardiomyopathy through U7snRNA-mediated exon skipping in Mybpc3-targeted knock-in mice. *EMBO Mol. Med.* 5, 1128–1145. doi: 10.1002/emmm.201202168

Hacihanefioglu, A., Tarkun, P., and Gonullu, E. (2008). Acute severe cardiac failure in a myeloma patient due to proteasome inhibitor bortezomib. *Int. J. Hematol.* 88, 219–222. doi: 10.1007/s12185-008-0139-7

Hedhli, N., and Depre, C. (2010). Proteasome inhibitors and cardiac cell growth. *Cardiovasc. Res.* 85, 321–329. doi: 10.1093/cvr/cvp226

Hedhli, N., Lizano, P., Hong, C., Fritzky, L. F., Dhar, S. K., Liu, H., et al. (2008). Proteasome inhibition decreases cardiac remodeling after initiation of pressure overload. *Am. J. Physiol. Heart Circ. Physiol.* 295, H1385–H1393. doi: 10.1152/ajpheart.00532.2008

Herrmann, J., Wohlert, C., Saguner, A. M., Flores, A., Nesbitt, L. L., Chade, A., et al. (2013). Primary proteasome inhibition results in cardiac dysfunction. *Eur. J. Heart Fail.* 15, 614–623. doi: 10.1093/eurjhf/hft034

Kisselev, A. F., Van Der Linden, W. A., and Overkleeft, H. S. (2012). Proteasome inhibitors: an expanding army attacking a unique target. *Chem. Biol.* 19, 99–115. doi: 10.1016/j.chembiol.2012.01.003

Kostin, S., Pool, L., Elsasser, A., Hein, S., Drexler, H. C., Arnon, E., et al. (2003). Myocytes die by multiple mechanisms in failing human hearts. *Circ. Res.* 92, 715–724. doi: 10.1161/01.RES.0000067471.95890.5C

Mearini, G., Schlossarek, S., Willis, M. S., and Carrier, L. (2008). The ubiquitin-proteasome system in cardiac dysfunction. *Biochim. Biophys. Acta* 1782, 749–763. doi: 10.1016/j.bbadis.2008.06.009

Mearini, G., Stimpel, D., Kramer, E., Geertz, B., Braren, I., Gedicke-Hornung, C., et al. (2013). Repair of Mybpc3 mRNA by 5′-trans-splicing in a mouse model of hypertrophic cardiomyopathy. *Mol. Ther. Nucleic Acids* 2, e102. doi: 10.1038/mtna.2013.31

Meiners, S., Dreger, H., Fechner, M., Bieler, S., Rother, W., Gunther, C., et al. (2008). Suppression of cardiomyocyte hypertrophy by inhibition of the ubiquitin-proteasome system. *Hypertension* 51, 302–308. doi: 10.1161/HYPERTENSIONAHA.107.097816

Olivotto, I., Girolami, F., Ackerman, M. J., Nistri, S., Bos, J. M., Zachara, E., et al. (2008). Myofilament protein gene mutation screening and outcome of patients with hypertrophic cardiomyopathy. *Mayo Clin. Proc.* 83, 630–638. doi: 10.1016/S0025-6196(11)60890-2

Predmore, J. M., Wang, P., Davis, F., Bartolone, S., Westfall, M. V., Dyke, D. B., et al. (2010). Ubiquitin proteasome dysfunction in human hypertrophic and dilated cardiomyopathies. *Circulation* 121, 997–1004. doi: 10.1161/CIRCULATIONAHA.109.904557

Richard, P., Charron, P., Carrier, L., Ledeuil, C., Cheav, T., Pichereau, C., et al. (2003). Hypertrophic cardiomyopathy: distribution of disease genes, spectrum of mutations and implications for molecular diagnosis strategy. *Circulation* 107, 2227–2232. doi: 10.1161/01.CIR.0000066323.15244.54

Schlossarek, S., Englmann, D. R., Sultan, K. R., Sauer, M., Eschenhagen, T., and Carrier, L. (2012a). Defective proteolytic systems in Mybpc3-targeted mice with cardiac hypertrophy. *Basic. Res. Cardiol.* 107, 1–13. doi: 10.1007/s00395-011-0235-3

Schlossarek, S., Schuermann, F., Geertz, B., Mearini, G., Eschenhagen, T., and Carrier, L. (2012b). Adrenergic stress reveals septal hypertrophy and proteasome impairment in heterozygous Mybpc3-targeted knock-in mice. *J. Muscle Res. Cell Motil.* 33, 5–15. doi: 10.1007/s10974-011-9273-6

Snel, B., Lehmann, G., Bork, P., and Huynen, M. A. (2000). STRING: a web-server to retrieve and display the repeatedly occurring neighbourhood of a gene. *Nucleic Acids Res.* 28, 3442–3444. doi: 10.1093/nar/28.18.3442

Stansfield, W. E., Tang, R. H., Moss, N. C., Baldwin, A. S., Willis, M. S., and Selzman, C. H. (2008). Proteasome inhibition promotes regression of left ventricular hypertrophy. *Am. J. Physiol. Heart. Circ. Physiol.* 294, H645–H650. doi: 10.1152/ajpheart.00196.2007

Tsukamoto, O., Minamino, T., Okada, K., Shintani, Y., Takashima, S., Kato, H., et al. (2006). Depression of proteasome activities during the progression of cardiac dysfunction in pressure-overloaded heart of mice. *Biochem. Biophys. Res. Commun.* 340, 1125–1133. doi: 10.1016/j.bbrc.2005.12.120

Vignier, N., Schlossarek, S., Fraysse, B., Mearini, G., Kramer, E., Pointu, H., et al. (2009). Nonsense-mediated mRNA decay and ubiquitin-proteasome system regulate cardiac myosin-binding protein C mutant levels in cardiomyopathic mice. *Circ. Res.* 105, 239–248. doi: 10.1161/CIRCRESAHA.109.201251

Weekes, J., Morrison, K., Mullen, A., Wait, R., Barton, P., and Dunn, M. J. (2003). Hyperubiquitination of proteins in dilated cardiomyopathy. *Proteomics* 3, 208–216. doi: 10.1002/(SICI)1522-2683(19990101)20:4/5<898::AID-ELPS898>3.0.CO;2-B

Zolk, O., Schenke, C., and Sarikas, A. (2006). The ubiquitin-proteasome system: focus on the heart. *Cardiovasc. Res.* 70, 410–421. doi: 10.1016/j.cardiores.2005.12.021

Conflict of Interest Statement: The authors declare that the research was conducted in the absence of any commercial or financial relationships that could be construed as a potential conflict of interest.

Received: 02 October 2014; accepted: 25 November 2014; published online: 16 December 2014.

Citation: Schlossarek S, Singh SR, Geertz B, Schulz H, Reischmann S, Hübner N and Carrier L (2014) Proteasome inhibition slightly improves cardiac function in mice with hypertrophic cardiomyopathy. Front. Physiol. ***5****:484. doi: 10.3389/fphys.2014.00484*

This article was submitted to Striated Muscle Physiology, a section of the journal Frontiers in Physiology.

Copyright © 2014 Schlossarek, Singh, Geertz, Schulz, Reischmann, Hübner, and Carrier. This is an open-access article distributed under the terms of the Creative Commons Attribution License (CC BY). The use, distribution or reproduction in other forums is permitted, provided the original author(s) or licensor are credited and that the original publication in this journal is cited, in accordance with accepted academic practice. No use, distribution or reproduction is permitted which does not comply with these terms.

frontiers in PHYSIOLOGY

ORIGINAL RESEARCH ARTICLE
published: 22 September 2014
doi: 10.3389/fphys.2014.00353

Remodeling of the heart in hypertrophy in animal models with myosin essential light chain mutations

Katarzyna Kazmierczak*, Chen-Ching Yuan, Jingsheng Liang, Wenrui Huang, Ana I. Rojas and Danuta Szczesna-Cordary*

Department of Molecular and Cellular Pharmacology, University of Miami Miller School of Medicine, Miami, FL, USA

Edited by:
Julien Ochala, King's College London, UK

Reviewed by:
Ingo Morano, Max-Delbrüxk-Center for Molecular Medicine, Germany
Yin-Biao Sun, King's College London, UK

****Correspondence:***
Katarzyna Kazmierczak and Danuta Szczesna-Cordary, University of Miami Miller School of Medicine, 1600 NW 10th Ave, Miami, FL 33136, USA
e-mail: kkazmierczak@med.miami.edu; dszczesna@med.miami.edu

Cardiac hypertrophy represents one of the most important cardiovascular problems yet the mechanisms responsible for hypertrophic remodeling of the heart are poorly understood. In this report we aimed to explore the molecular pathways leading to two different phenotypes of cardiac hypertrophy in transgenic mice carrying mutations in the human ventricular myosin essential light chain (ELC). Mutation-induced alterations in the heart structure and function were studied in two transgenic (Tg) mouse models carrying the A57G (alanine to glycine) substitution or lacking the N-terminal 43 amino acid residues (Δ43) from the ELC sequence. The first model represents an HCM disease as the A57G mutation was shown to cause malignant HCM outcomes in humans. The second mouse model is lacking the region of the ELC that was shown to be important for a direct interaction between the ELC and actin during muscle contraction. Our earlier studies demonstrated that >7 month old Tg-Δ43 mice developed substantial cardiac hypertrophy with no signs of histopathology or fibrosis. Tg mice did not show abnormal cardiac function compared to Tg-WT expressing the full length human ventricular ELC. Previously reported pathological morphology in Tg-A57G mice included extensive disorganization of myocytes and interstitial fibrosis with no abnormal increase in heart mass observed in >6 month-old animals. In this report we show that strenuous exercise can trigger hypertrophy and pathologic cardiac remodeling in Tg-A57G mice as early as 3 months of age. In contrast, no exercise-induced changes were noted for Tg-Δ43 hearts and the mice maintained a non-pathological cardiac phenotype. Based on our results, we suggest that exercise-elicited heart remodeling in Tg-A57G mice follows the pathological pathway leading to HCM, while it induces no abnormal response in Tg-Δ43 mice.

Keywords: hypertrophic cardiomyopathy (HCM), transgenic mice, myosin essential light chain, mutation, cardiac remodeling, histopathology

INTRODUCTION

In response to various types of stimuli (genetic, mechanical, hemodynamic, hormonal, physiological, environmental factors or their combination), the heart has the ability to adapt to increased workloads through the hypertrophy of muscle cells (Hunter and Chien, 1999; Lorell and Carabello, 2000). The hypertrophic response is considered physiological if the heart fully adapts to the new loading condition, reaching a new steady state. This type of hypertrophy is characterized by a normal organization of cardiac structure (normal cardiac morphology), normal or enhanced cardiac function and a relatively normal pattern of gene expression (Bernardo et al., 2010). Hypertrophy can also be developed as a response to physiological stimuli such as chronic exercise. On the other hand, pathological hypertrophy is associated with an altered pattern of gene expression, presence of myofibrillar disarray, fibrosis, and contractile dysfunction and thus can lead to heart failure and sudden cardiac death (SCD) (Ho, 2010; Ho et al., 2010; Abel and Doenst, 2011). Most commonly hypertrophic cardiomyopathy (HCM) occurs in response to genetic mutations in all major sarcomeric proteins, including the myosin essential light chain (ELC) encoded by the *MYL3* gene (Alcalai et al., 2008).

There are number of studies demonstrating that physiological and pathological cardiac hypertrophy may be associated with distinct structural and functional as well as metabolic features (Abel and Doenst, 2011; Weeks and McMullen, 2011). It has also been shown that both physiologic and pathologic cardiac hypertrophy may display distinct biochemical and molecular signaling pathways (Iemitsu et al., 2001; Heineke and Molkentin, 2006; Bernardo et al., 2010). Pathological cardiac hypertrophy is manifested by alterations in cardiac contractile proteins [α-skeletal actin and the α- to β- myosin heavy chain (MHC) switch], increased expression of fetal genes such as atrial natriuretic peptide (ANP), B-type natriuretic peptide (BNP). The down- or up-regulation of calcium handling proteins such as the cardiac sarcoplasmic reticulum Ca^{2+}-ATPase pump, SERCA2a can also be observed. Physiological cardiac hypertrophy may be associated with increased levels of peptide growth factors such as insulin-like growth factor-IGF 1 and epidermal growth factor and is often coupled to phosphatidylinositol 3-kinase (PI3K)/Akt

pathway. It is known that many mutations in sarcomeric proteins cause cardiomyopathy and may ultimately initiate the hypertrophic gene remodeling program. Studies utilizing transgenic mouse models of hypertrophy are great tools for understanding the molecular pathways responsible for different forms of cardiac remodeling *in vivo*. Presented in this article study focuses on one particular sarcomeric protein, the essential light chain of myosin that is located in the neck region of the myosin cross-bridge (Rayment et al., 1993), and was shown to be important for myosin contractile function in health and in heart disease (Sawicki et al., 2005; Kazmierczak et al., 2009, 2013; Muthu et al., 2011; Cadete et al., 2012). Cardiac ventricular muscle exclusively expresses the long ELC isoform, containing the N-terminal extension, which was found to be important for the myosin-actin interaction during contraction and is expected to regulate heart performance (Winstanley et al., 1977; Sutoh, 1982; Henry et al., 1985; Trayer et al., 1987; Milligan et al., 1990; Morano et al., 1995; Timson et al., 1998; Morano, 1999; Timson, 2003). The structural modeling study by Morano (Aydt et al., 2007) depicts the N-terminus of the long myosin ELC as a rod-like 91 Å-long extension that can function as a bridge between the ELC core of the myosin head and the binding site of the ELC on the actin filament.

In this report we have studied cardiac remodeling in two forms of cardiac hypertrophy (pathological and non-pathological) related to the ventricular myosin ELC using transgenic mouse models carrying mutations in the human ventricular myosin ELC, Tg-A57G, and Tg-Δ43. The A57G (Alanine replaced by Glycine) variant of ELC was found in two unrelated Korean families and one Japanese patient diagnosed with HCM (review in Hernandez et al., 2007). The phenotype associated with this mutation was manifested as a classic asymmetric septal hypertrophy and SCD (Lee et al., 2001). In the Tg-Δ43 mouse model, the endogenous mouse ventricular ELC is partially replaced with the 43-amino-acid N-terminal truncated human ventricular ELC protein. We previously reported that Tg-Δ43 mice hypertrophied with age (>7 month-old), but the ventricles did not show any pathologic morphology. In support of the non-pathologic hypertrophy phenotype, an MRI (magnetic resonance imaging) assessment of Tg-Δ43 hearts demonstrated normal cardiac function compared to age matched controls (Kazmierczak et al., 2009).

Despite intensive research in many laboratories, questions about critical molecular mechanisms responsible for the transition from hypertrophy to heart failure still remain unanswered. Presented here transgenic mouse models carrying either the A57G mutation or the Δ43 truncation in ELC protein, generated in our laboratory (Kazmierczak et al., 2009, 2013; Muthu et al., 2011) represent different types of hypertrophy and therefore are valuable tools in understanding the pathological vs. non-pathological remodeling of the heart. We have examined the effects of both A57G and Δ43 mutations on heart remodeling before and after strenuous exercise and characterized the functional effects of these mutations in mice subjected to strenuous exercise by swimming. The observed effects were compared to those seen in Tg-WT (wild-type) mice expressing the full length non-mutated human ventricular ELC. We show that remodeling of the heart in Tg-A57G mice follows the pathological pathway leading to HCM, while cardiac phenotype observed in Tg-Δ43 mice is of non-pathological nature.

MATERIAL AND METHODS

TRANSGENIC MICE

All animal studies were conducted in accordance with institutional guidelines and the protocol was reviewed and approved by the Animal Care and Use Committee at the University of Miami Miller School of Medicine (UMMSM). UMMSM has an Animal Welfare Assurance (A-3224-01, effective July 11, 2007) on file with the Office of Laboratory Animal Welfare (OLAW), National Institutes of Health. The generation and characterization of transgenic (Tg) mice used in this study and Tg protein expression profiles have been described earlier (Kazmierczak et al., 2009, 2013; Muthu et al., 2011). Previously produced Tg-WT lines, L1, L3, and L4 expressing 88, 30, and 77% of WT-ELC (UniProtKB: P08590) and Tg-A57G lines, L1, L2, and L5 expressing 80, 55, and 75% of A57G-mutant, respectively were used in this study. As for Tg-Δ43, two lines were used for this study, one previously generated expressing 40% of Δ43 protein (L9), and the second line expressing 55% transgene which was generated by cross breeding of existing mice (L8 × L8) in order to increase transgenic protein expression (Kazmierczak et al., 2009). The percent of protein expression indicates the amount of replacement of the endogenous mouse cardiac ELC by human ventricular WT (UniProtKB: P08590) or its two mutants. In all experiments Tg-A57G and Tg-Δ43 mice were gender and age matched with Tg-WT controls (Kazmierczak et al., 2009; Muthu et al., 2011; Kazmierczak et al., 2013).

Chronic 4 week-long training by swimming of Tg-WT, Tg-A57G, and Tg-Δ43 mice was performed in water at 30–32°C (to avoid thermal stress). Initial swim time was set as 10 min, thereafter gradually increasing until 90 min sessions were reached. The 90-min training schedule was continued twice a day (separated by 4–5 h), 7 days a week, for 4 weeks. This protocol was demonstrated to be highly effective in promoting physiological hypertrophy in mice (Evangelista et al., 2003; Galindo et al., 2009).

HISTOLOGICAL EVALUATION OF THE HEARTS FROM TRANSGENIC ELC MICE

After euthanasia, the hearts from 3 to 5-month-old Tg-Δ43, Tg-A57G, and Tg-WT mice were excised, weighed and immersed in 10% buffered formalin. Slides of whole mouse hearts were prepared at the Histology Laboratory (University of Miami Miller School of Medicine, Miami FL). The paraffin-embedded longitudinal sections of left ventricles (LV) of H&E (hematoxylin and eosin) and Masson's trichrome stained hearts were examined for overall morphology and fibrosis using a Dialux 20 microscope, 40×/0.65 NA (numerical aperture) Leitz Wetzlar objective and an AxioCam HRc (Zeiss) as described previously (Kazmierczak et al., 2009, 2013; Muthu et al., 2011).

SKINNED PAPILLARY MUSCLE STRIPS FROM TRANSGENIC MICE

The papillary muscles of the left ventricles from 3 to 5 months old Tg-A57G L1 mice, Tg-Δ43 (L9 and inbred cross of L8) and Tg-WT (L1, L3, and L4) mice were isolated, dissected into small

muscle bundles and chemically skinned in 50% glycerol and 50% pCa 8 solution (10^{-8} M [Ca^{2+}], 1 mM free [Mg^{2+}] (total MgPr (propionate) = 3.88 mM), 7 mM EGTA, 2.5 mM [Mg-ATP^{2-}], 20 mM Mops, pH 7.0, 15 mM creatine phosphate and 15 units/ml of phosphocreatine kinase, ionic strength = 150 mM adjusted with KPr) containing 1% Triton X-100 for 24 h at 4°C. Then the bundles were transferred to the same solution without Triton X-100 and stored at −20°C for 4–6 days (Kazmierczak et al., 2012).

STEADY-STATE FORCE MEASUREMENTS

Small muscle strips ∼1.4 mm in length and 100 μm in diameter were isolated from a batch of glycerinated skinned mouse papillary muscle bundles and attached by tweezer clips to the force transducer of the Guth Muscle Research System (Heidelberg, Germany). They were placed in a 1 ml cuvette and skinned in 1% Triton X-100 dissolved in pCa 8 buffer for 30 min, as described in Kazmierczak et al. (2012). Then they were rinsed in pCa 8 and their length adjusted to remove the slack. This procedure results in sarcomere length (SL) ∼2.1 μm as judged by the first order optical diffraction pattern as described in Muthu et al. (2011); Wang et al. (2013a,b); Huang et al. (2014). Muscle strips were then tested for steady state force development in pCa 4 solution (composition is the same as pCa 8 buffer except the [Ca^{2+}] = 10^{-4} M). All experiments were carried out at 21°C. Maximal steady state tension measured in pCa 4 solution was expressed in Newtons per cross section of the muscle strip (kN/m^2). The measurement of diameter was taken at ∼3 points along the muscle strip length with an SZ6045 Olympus microscope (zoom ratio of 6.3:1, up to 189x maximum magnification) and averaged (Muthu et al., 2012).

THE Ca^{2+} DEPENDENCE OF FORCE DEVELOPMENT

After the initial steady state force was determined, muscle strips were relaxed in pCa 8 buffer and then exposed to solutions of increasing Ca^{2+} concentrations from pCa 8 to 4 (Dweck et al., 2005). Steady-state force was measured in each "pCa" solution followed by relaxation in pCa 8 solution. Data were analyzed using the Hill equation (Hill et al., 1980) where "$[Ca^{2+}]_{50}$ or pCa_{50}" is the free Ca^{2+} concentration which produces 50% maximum force, and "n_H" is the Hill coefficient.

ASSESSMENT OF MYOSIN CONTENT IN SEDENTARY AND EXERCISED ANIMALS

Mouse cardiac myofibrils were prepared according to the method described previously (Kazmierczak et al., 2013). Briefly, after euthanasia, the hearts from 3 to 5 months old transgenic mice were isolated and frozen in liquid nitrogen and stored at −80°C until processed. For the preparation of myofibrils the tissue was thawed in the CMF (cardiac myofibril) buffer consisting 5 mM NaH_2PO_4, 5 mM Na_2HPO_4(pH 7.0), 0.1 mM NaCl, 5 mM $MgCl_2$, 0.5 mM EGTA, 5 mM ATP, 5 nM microcystin, 0.1% Triton X-100, 20 mM NaF (phosphatase inhibitor), 5 mM DTT and 1 μl/ml protease inhibitor cocktail (Sigma-Aldrich Corp., St. Louis, MO, USA). The tissue was then homogenized in a Mixer-Mill MM301 (Retsch) until homogenous. The homogenate was centrifuged for 4 min at 8000 g and the supernatant was discarded. After centrifugation, the pellets were left on ice for 4 min. This step was repeated three times until the pellet turned white. The pellets were then resuspended in the CMF buffer and the myofibrils were subsequently dissolved in Laemmli sample buffer and loaded on 15% SDS-PAGE. The thick and thin filament proteins were detected by Coomassie brilliant blue staining. Band intensities were measured using Image J software and ratios of total myosin regulatory light chain (RLC_{tot}) to tropomyosin ($RLC_{tot.}$/Tm) and $RLC_{tot.}$/TnI (troponin I) were determined.

MYOFILAMENT PROTEIN PHOSPHORYLATION IN SEDENTARY AND EXERCISED MICE

Mouse cardiac myofibrils were used to determine sarcomeric protein phosphorylation. After separation of the samples on 15% SDS-PAGE Pro-Q Diamond phosphoprotein gel stain reagent (Invitrogen) was used (as described in the manufacturer's manual) to assess phosphorylation of troponin (TnT, TnI) and myosin RLC. The total protein was further detected in the same gel using the Coomassie brilliant blue staining. Myofilament protein phosphorylation ratio (ProQ) was calculated relative to the corresponding Coomassie brilliant blue staining (ProQ/Coomassie) using Image J software.

ASSESSMENT OF GENE EXPRESSION CHANGES IN THE HEARTS OF Tg-A57G AND Tg-Δ43 MICE

Total RNA was isolated from ventricles of sedentary and exercised Tg-WT, Tg-A57G, and Tg-Δ43 mice and converted to double stranded cDNAs using Random Primers and a High-Capacity cDNA Reverse Transcription Kit (Applied Biosystems) as described earlier (Kazmierczak et al., 2009). Quantitative PCR was conducted using SYBR Green I chemistry with gene-specific Quantitect Primer Sets (Qiagen) for murine: ANP (atrial natriuretic factor: NM_008725), BNP: NM_008726), Myh6 (α-myosin heavy chain, cardiac: NM_010856), Myh7 (β-MHC: NM_080728), ColVIIIa (collagen type 8a, NM_007739), and ATP2a2 (NM_001110140.3) which encodes two Ca^{2+}-transporting ATPase isoforms, SERCA2a (cardiac) and SERCA2b (non-muscle). SERCA2a is the predominant Ca^{2+} pump in the myocardium (Vangheluwe et al., 2003). All reactions were performed in triplicate and run using BIO-RAD iQ5 Multicolor Real-Time PCR Detection System with the following cycle parameters: cycle of 50°C (2 min) followed by 95°C (10 min), 40 cycles of 95°C (15 s) followed by 60°C (1 min). Raw data were analyzed using the BIO-RAD CFX Manager Software, and fold change in expression of each gene was calculated using the relative quantification (RQ) ΔΔCt method with the levels of GAPDH (glyceraldehyde-3-phosphate dehydrogenase: NM_008084) as the normalizer gene (Kazmierczak et al., 2009).

STATISTICAL ANALYSIS

All data were expressed as mean ± s.e.m. Statistical comparisons were performed using ANOVA or independent *t*-test (Sigma Plot 11; Systat Software, San Jose, CA). *P*-values <0.05 indicated statistically significant differences.

RESULTS

HISTOLOGICAL EVALUATION OF THE HEARTS FROM Tg-A57G AND Tg-Δ43 MICE

The evaluation performed for sedentary animals shows normal gross morphology for all tested 3–5 month-old male mice (Tg-WT, Tg-Δ43, and Tg-A57G) (**Figure 1A**). In our earlier study on sedentary Tg-Δ43 mice, we observed cardiac hypertrophy in mice ∼7 months of age while the hearts of ∼2 month-old Tg-Δ43 animals were indistinguishable from control Tg-WT mice (Kazmierczak et al., 2009). As we confirmed later, the hypertrophy in Tg-Δ43 mice appeared to be age dependent and profound hypertrophy was observed in ∼12 month-old Tg-Δ43 mice compared with age matched Tg-WT hearts (Muthu et al., 2011). Thus, the lack of abnormal heart growth observed in 3–5 month-old sedentary Tg-Δ43 mice (**Figure 1A**), is not surprising and suggests that Tg-Δ43 mice have to be at least 7 months of age to develop cardiac hypertrophy. Regarding sedentary Tg-A57G mice, similar to what we reported earlier (Muthu et al., 2011), no cardiac growth could be observed in 3–5 month-old mice (**Figure 1A**) or the mice as old as ∼12 months of age (Muthu et al., 2011). However, exercised 3–5 month-old Tg-A57G animals do show cardiac hypertrophy while the hearts of Tg-Δ43 mice were comparable in size to Tg-WT controls (**Figure 1B**).

Histology examination of animals subjected to strenuous exercise is presented in **Figure 2**. H&E and Masson's trichrome stained left ventricular (LV) sections from Tg-Δ43 hearts revealed that the hearts of exercised 3–5 month-old mice demonstrated no tissue abnormalities, myofilament disarray or fibrosis compared to Tg-WT controls. In contrast, the evaluation of LV heart sections from Tg-A57G mice showed occurrences of fibrosis, especially in the interventricular septum compartment (**Figure 2**). This is in accord to previously reported pathological morphology in sedentary Tg-A57G mice, which included extensive disorganization of myocytes and interstitial fibrosis (Muthu et al., 2011; Kazmierczak et al., 2013).

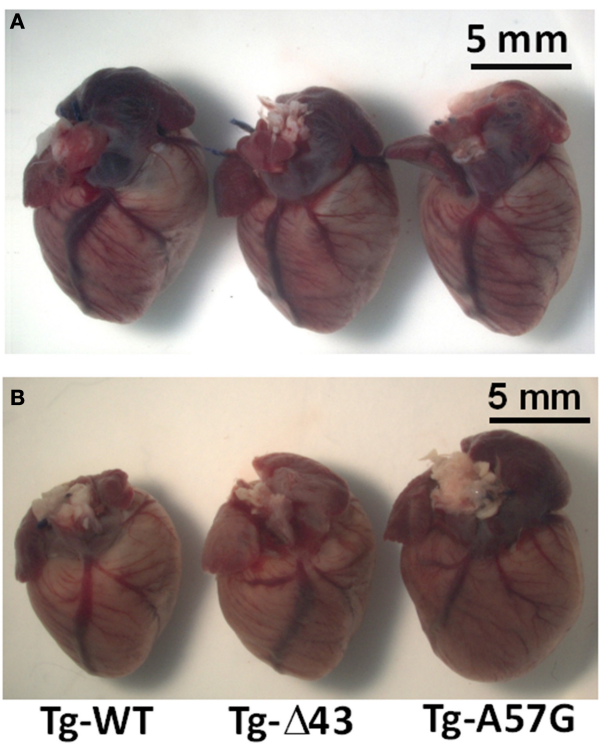

FIGURE 1 | Gross morphology of representative hearts from ∼5 month-old sedentary (A) and ∼3 month-old exercised (B) Tg-WT, Tg-Δ43 and Tg-A57G male mice.

SIGNALING PATHWAYS AND CHANGES IN THE GENE EXPRESSION PROFILE IN THE HEARTS OF TWO DIFFERENT MODELS OF HYPERTROPHY

Hypertrophic remodeling in Tg-Δ43 and Tg-A57G animal models was studied by looking at mutation-induced alterations in cardiac contractile proteins (α- to β-MHC switch), expression of the fetal genes such as ANP and BNP. We also examined whether cardiac remodeling in these mice involved changes in the calcium handling proteins such as SERCA2a. Studies of gene expression using real-time PCR in mouse myocardium were performed for sedentary and exercised Tg animals and the results are presented in **Figures 3**, **4**, respectively. For sedentary Tg-A57G mice, the expression of sarcoplasmic ATP2a2 was higher compared with sedentary Tg-WT (∼1.6 fold). The upregulation of mRNA SERCA2a in Tg-A57G mice (**Figure 3**) may translate to a faster relaxation of the A57G myosin cross-bridges and potentially lower contractile force generation in Tg-A57G mice, what is actually observed (**Figure 5A**). For sedentary Tg-Δ43 mice the expression levels of ANP and BNP were higher compared with sedentary Tg-WT (2- and 2.4 fold, respectively) (**Figure 3**).

This upregulation of both natriuretic peptides in Tg-Δ43 mice most likely manifests their protective role against excessive cardiac remodeling and preventing uncontrolled myocardial growth of Tg-Δ43 hearts (Tsuruda et al., 2002; Gardner, 2003).

To evaluate a combined effect of strenuous exercise and ELC mutation on heart remodeling we have also studied the molecular mechanisms and signaling pathways that change due to exercise. **Figure 4** presents the gene expression analysis using real-time PCR in mouse myocardium performed for exercised Tg ELC animals. In Tg-A57G mice the exercise training reactivated the fetal gene program and upregulation in the β-MHC, ANP and BNP was observed. Expression of ANP and BNP was respectively 1.9- and 2.1 fold higher compared with exercised Tg-WT (both differences statistically significant $P < 0.05$). Additionally, upregulation of collagen VIIIa (1.9 fold change, significant $P < 0.05$) and β-MHC (not significant) and downregulation of α-MHC was observed for exercised Tg-A57G compared with exercised Tg-WT mice (**Figure 4**). On the other hand, exercised Tg-Δ43 mice showed a 0.6-fold lower expression level of ANP ($P < 0.05$) and no change in BNP marker compared to exercised Tg-WT controls (**Figure 4**). Changes in gene expression observed in Tg-A57G mice in response to strenuous exercise represent a pathologic type of remodeling occurring in the disease mouse model. In contrast, lack of changes in expression levels of BNP, β-MHC and collagen VIIIa in exercised Tg-Δ43 mice represents an adaptive response to exercise and non-pathological remodeling in Tg-Δ43 animals.

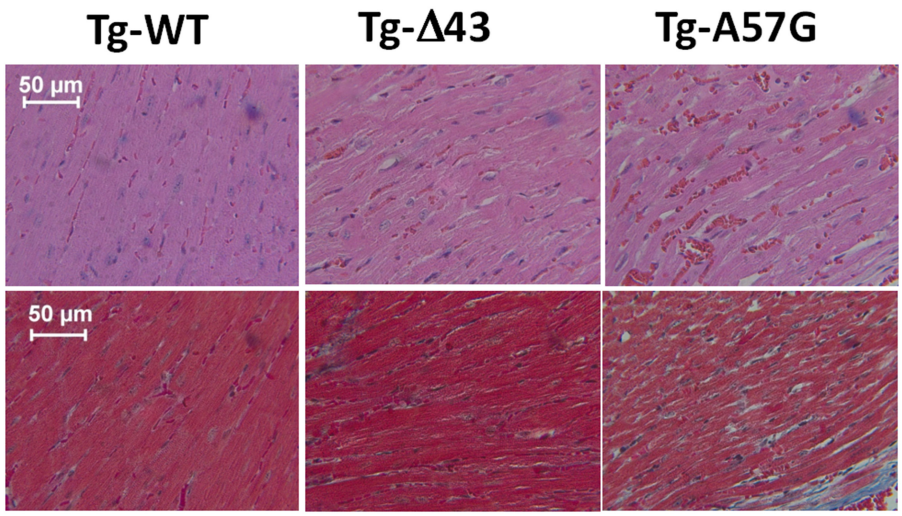

FIGURE 2 | H&E (upper panel) and Masson's trichrome (bottom panel) stained LV sections from exercised ∼3 month-old Tg-WT, Tg-Δ43, and Tg-A57G male mice.

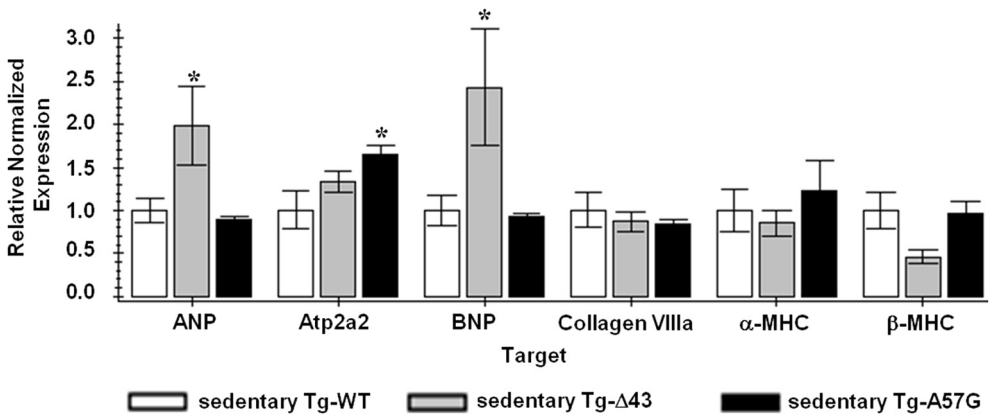

FIGURE 3 | QPCR data for sedentary ELC animals. Sedentary Tg-WT was used as a control sample (FC = 1); *indicates $P < 0.05$ compared to sedentary Tg-WT.

STEADY-STATE FORCE MEASUREMENTS AND Ca^{2+} DEPENDENCE OF FORCE DEVELOPMENT

The data from functional measurements assessed in skinned mouse papillary muscle strips from Tg-Δ43 and Tg-A57G animals are presented in **Figure 5**, and the values of maximal force and pCa_{50} are summarrized in **Table 1**. Different pattern of contractile force generation and the Ca^{2+} sensitivity of force was observed betweenTg-A57G and Tg-Δ43 mice. Similar to our earlier study (Kazmierczak et al., 2013), sedentary Tg-A57G mice showed the lowest maximal force (∼20% lower vs. sedentary Tg-WT) and a slightly increased Ca^{2+} sensitivity of force (ΔpCa_{50} ≅0.04 vs. sedentary Tg-WT), both changes statistically significant. As we demonstrated earlier and in this study, sedentary Tg-A57G animals showed reduced maximal (pCa 4) force and increased Ca^{2+} sensitivity following the pattern of pathological hypertrophy (Muthu et al., 2011; Kazmierczak et al., 2013) (**Figures 5**, **6**). Contrary, maximal force for sedentary Tg-Δ43 mice was similar to that of Tg-WT and the Ca^{2+} sensitivity was not changed (ΔpCa_{50} ≅0.02; not statistically significant) compared to Tg-WT controls. The previously reported reduction in steady-state force in ∼2 month-old and ∼7 month-old Tg-Δ43 mice (Kazmierczak et al., 2009) was likely associated with a decrease in the myosin content observed in these animals vs. the lack of changes in myosin expression seen in the current investigation (**Figure 7**).

In response to exercise, all transgenic animals showed a higher level of maximal force per cross-section of muscle strip vs. their sedentary controls (**Table 1**). Similarly to the direction of changes observed for sedentary animals, in response to swimming, the maximal force for Tg-Δ43 was similar while that for Tg-A57G was significantly reduced (∼20% lower, $P < 0.005$) compared to exercised Tg-WT. Additionally, for exercised Tg-A57G, the

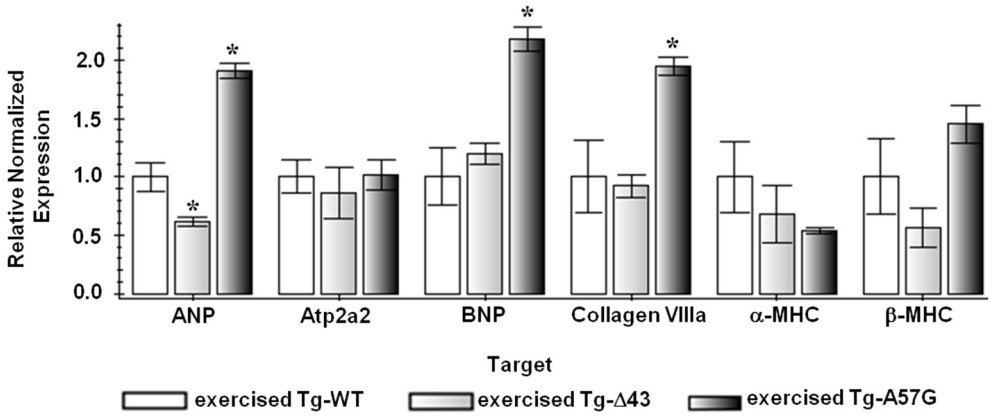

FIGURE 4 | QPCR data for exercised ELC animals. Exercised Tg-WT is used as a control sample (FC = 1); *indicates $P < 0.05$ compared to exercised Tg-WT mice.

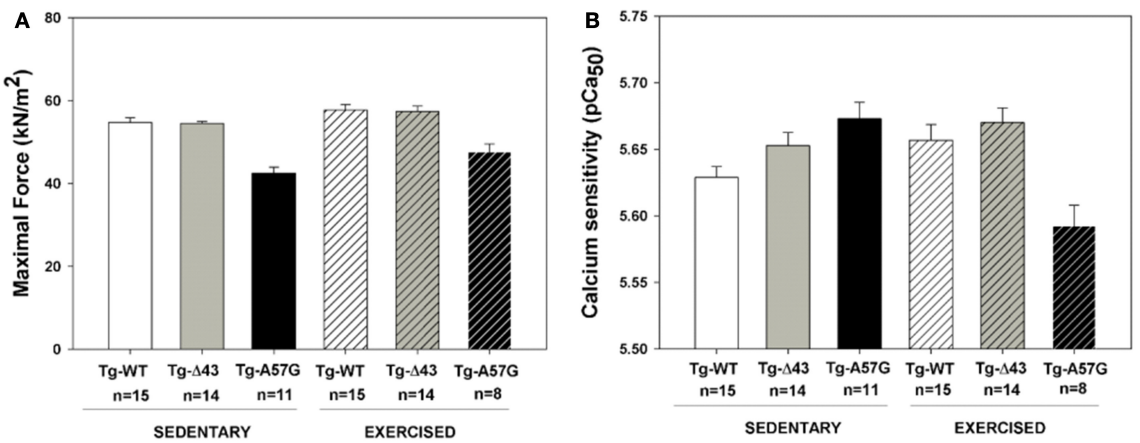

FIGURE 5 | Measurements of steady-state force in skinned papillary muscle strips from sedentary and exercised transgenic ELC male mice. (A) Maximal force assessment at pCa4. **(B)** Calcium sensitivity of force.

Ca^{2+} sensitivity of force was significantly lower compared to sedentary Tg-A57G mice ($\Delta pCa_{50} \cong 0.08$) (**Figures 5B**, **6** and **Table 1**). Tendency toward desensitization of myofilaments to Ca^{2+} observed in Tg-A57G mice (**Table 1**) may represent a key step in the signaling pathway for the pathological hypertrophic remodeling in this animal model of HCM. As expected, there were no significant changes in the Ca^{2+} sensitivity of force between exercised and sedentary Tg-WT mice. Likewise, no significant changes in the Ca^{2+} sensitivity were present between the exercised and sedentary Tg-Δ43 mice (**Table 1**). No changes in the cooperativity (Hill coefficient) values for all groups of mice ($n_H = 2.6 \pm 0.3$) were noted (**Figure 6**).

Table 1 | Maximal pCa 4 force and calcium sensitivity of force in transgenic ELC skinned mouse papillary muscle strips.

System	pCa_{50}	F_{max} (kN/m^2)
Sedentary Tg-WT	5.629 ± 0.008	54.804 ± 1.133
Sedentary Tg-Δ43	5.653 ± 0.010	54.581 ± 0.399
Sedentary Tg-A57G	5.673 ± 0.012	42.482 ± 1.458
Exercised Tg-WT	5.657 ± 0.012	57.731 ± 1.273
Exercised Tg-Δ43	5.670 ± 0.011	57.421 ± 1.279
Exercised Tg-A57G	5.592 ± 0.016	47.615 ± 1.967

Data are mean ± SEM of n = 8–15 individual strips for each group of mice.

ASSESSMENT OF MYOSIN CONTENT IN SEDENTARY AND EXERCISED ANIMALS

As mentioned above, the reduced level of maximal contractile force measured in our previous study for sedentary Tg-Δ43 mice was most likely associated with deficiency in myosin content detected in the myocardium of Tg-Δ43 vs. Tg-WT mice (Kazmierczak et al., 2009). Therefore, myosin content in sedentary and exercised animals was assessed in this study and correlated with the ability of the myocardium to develop contractile force. **Figure 7** presents the ratios of $RLC_{tot.}$/Tm and $RLC_{tot.}$/TnI determined in cardiac myofibrillar preparations from sedentary and exercised Tg-WT, Tg-A57G, and Tg-Δ43 mice. Compared

to respective Tg-WT myofibrils (100%), the ratios of $RLC_{tot.}$/Tm and $RLC_{tot.}$/TnI obtained for sedentary and exercised Tg-A57G mice were similar to Tg-WT indicating no change in myosin expression in all tested animals (**Figure 7**). Therefore, the lower maximal force observed for the A57G mutation in this study is not due to the lower myosin content but due to defective function of the A57G-myocardium. The values of $RLC_{tot.}$/Tm and $RLC_{tot.}$/TnI ratios obtained for sedentary and exercised Tg-Δ43 mice were also very similar to Tg-WT (∼110%), indicating no previously observed deficiency of myosin in the hearts of Tg-Δ43 animals (Kazmierczak et al., 2009).

MYOFILAMENT PROTEIN PHOSPHORYLATION IN SEDENTARY AND EXERCISED MICE

The force-generating capacity of sarcomeres has been known to be tightly regulated by sarcomeric proteins phosphorylation (Sweeney et al., 1993; Sadayappan et al., 2009; Nixon et al., 2012). To test whether the ELC mutation (Δ43 or A57G) and/or exercise had any effect on phosphorylation of sarcomeric proteins, we have examined phosphorylation of myosin binding protein C (MyBP-C), Tm, troponin (TnT and TnI) and myosin RLC in mouse cardiac myofibrils using the Pro-Q Diamond staining. As shown in **Figure 8**, no significant changes in endogenous MyBP-C, Tm, TnT, TnI, or RLC phosphorylation were found in sedentary or exercised Tg-Δ43 or Tg-A57G animals compared to Tg-WT mice. The lack of the effect of exercise on protein phosphorylation is somewhat surprising but has been observed by other laboratories. No effect of exercise on phosphorylation of myosin RLC in the ventricles or atria of mice was found by Fewell et al. (1997). Likewise, no changes in phosphorylation of titin and TnI in mice upon exercise training were recently reported by the Granzier group (Hidalgo et al., 2014). These results suggest no immediate molecular contacts between the ELC protein and the phosphorylation domains of MyBP-C, Tm, TnT, TnI, or RLC.

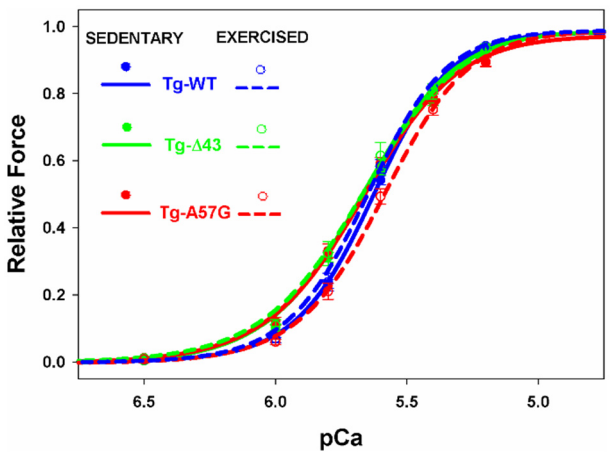

FIGURE 6 | The force- pCa relationship in transgenic skinned mouse papillary muscle strips from Tg-WT, Tg-Δ43, and Tg-A57G male mice.

DISCUSSION

Hypertrophic remodeling is a highly important phenomenon; however, the molecular mechanisms and signaling pathways underlying these processes have not yet been fully understood. In particular, molecular pathways that play a causal role in the development of pathological vs. physiological hypertrophy need to be recognized due to the known association between cardiac hypertrophy and nearly all forms of heart failure (Levy et al., 1990). Recognition of functional, structural, metabolic, and molecular differences between pathological and non-pathological hypertrophy may help to develop potential therapeutic approaches to benefit patients with HCM and heart failure.

REMODELING IN SEDENTARY MICE

Since the ELC is a highly essential element of the myosin molecule, its structure and the interaction with the MHC and actin play important roles in the sarcomeric assembly and force production (Hernandez et al., 2007). This investigation was designed to look at two different cardiac phenotypes induced by structural alterations in the myosin ELC in mouse models of pathologic (Tg-A57G) and physiologic (Tg-Δ43) HCM. The effects of both ELC mutations on heart function and cardiac remodeling are summarized in **Figure 9**. Data obtained for

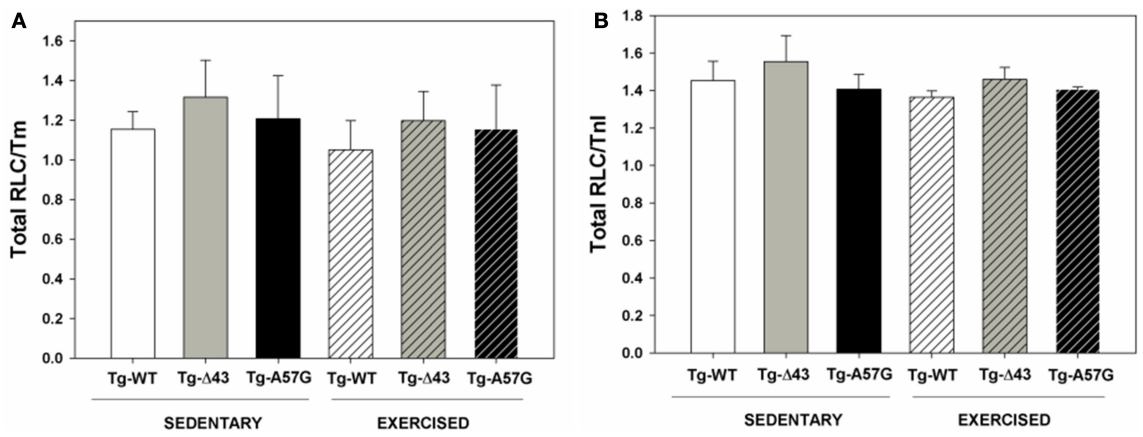

FIGURE 7 | Thick and thin filament protein content in sedentary and exercised Tg-Δ43 and Tg-A57G mice compared to control Tg-WT.

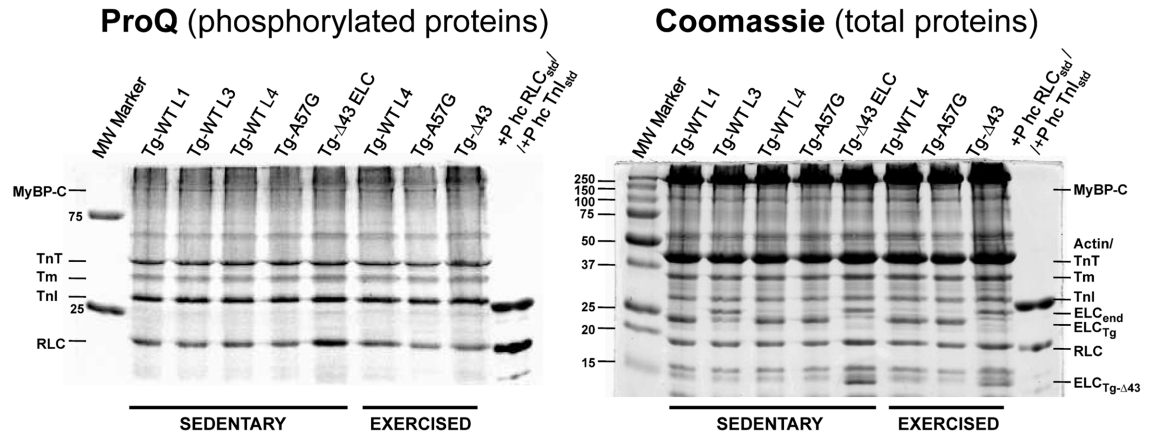

FIGURE 8 | Assessment of protein phosphorylation in sedentary and exercised Tg-WT, Tg-Δ43, and Tg-A57G mouse myofibrils. MyBP-C, myosin binding protein C; TnT, troponin T; Tm, tropomyosin; TnI, troponin I; RLC, myosin regulatory light chain; ELC_{end}, myosin ELC (all mouse isoforms); ELC_{Tg}, transgenic human ELC; +P hc std, phosphorylated human cardiac protein standard.

sedentary and exercised Tg-A57G and Tg-Δ43 animals show clear differences between these two phenotypes. Consistent with our earlier reports, we monitored significantly compromised contractile function (lower maximal force and higher Ca^{2+} sensitivity) in sedentary Tg-A57G mice, which coincided with upregulation of the calcium handling protein SERCA2a compared to sedentary Tg-WT animals. It has been reported that in animal models, severe compensated hypertrophy in response to pressure overload is accompanied by a large decrease in the mRNA and protein content of SERCA2a (Buttrick et al., 1994; Rockman et al., 1994). However, in rats with moderate cardiac hypertrophy, the level of SERCA2a mRNA or protein was unaltered or even upregulated (Rockman et al., 1994; Arai et al., 1996). SERCA2a is a key protein responsible for maintaining a balanced concentration of Ca^{2+} during the cardiac cycle and it controls the transport of Ca^{2+} to the SR during relaxation. The upregulation of mRNA SERCA2a in Tg-A57G mice (**Figure 3**) may translate to an increased protein activity, which would lead to faster relaxation of the A57G myosin cross-bridges and potentially lower contractile force generation in Tg-A57G myocardium (**Figure 5A**).

These adverse effects were not present in sedentary Tg-Δ43 mice, the model of non-pathological cardiac phenotype. The maximal force and Ca^{2+} sensitivity values were similar to those determined for sedentary Tg-WT mice, indicating a normal heart function in Tg-Δ43 animals. As we reported earlier (Kazmierczak et al., 2009, 2013; Muthu et al., 2011) both mouse models demonstrated cardiac hypertrophic growth, but the pathological features were only observed in sedentary A57G animals (Kazmierczak et al., 2009; Muthu et al., 2011; Kazmierczak et al., 2013). Discrepancies exist regarding the lack of reduction in maximal force observed in Tg-Δ43 mice in the current study (**Table 1**) and the previously reported decrease in steady-state force in Tg-Δ43 mice (Kazmierczak et al., 2009). The reason for a lower force reported in Kazmierczak et al. (2009) was an approximately 30% deficit in myosin cross-bridge content in the myocardium of Tg-Δ43 mice (Kazmierczak et al., 2009). This deficit in myosin content was not observed in the current work (**Figure 7**), indicating a compensatory response in transgenic Tg-Δ43 mice over time. Consequently, the lack of abnormalities in myosin expression was most likely responsible for no changes in force per cross-section of muscle seen in Tg-Δ43 mice in the current investigation (**Table 1**). Additionaly, recently published data utilizing the same Tg-Δ43 mouse model, showed only a slight (and not significant) decrease in maximal tension between Tg-WT and Tg-Δ43 (Michael et al., 2013; Wang et al., 2013a).

Sedentary Tg-Δ43 mice also showed an upregulation of ANP and BNP (**Figure 3**). Upregulation of these transcripts is considered a highly conserved feature of ventricular hypertrophy (Lee et al., 1988; Dagnino et al., 1992; Buttrick et al., 1994; Nakagawa et al., 1995), but there are contradictory reports in the literature on the correlation of upregulation of natriuretic peptides with physiological hypertrophy that can be induced by various training programs in animals. Some publications report an upregulation (Buttrick et al., 1994; Allen et al., 2001), while some report no change (Azizi et al., 1995; Jin et al., 2000) or downregulation (Diffee et al., 2003) of ANP and/or BNP expression in these animal models. Both natriuretic peptides were shown to function as modulators of cardiac hypertrophy preventing uncontrolled myocardial growth and regulating ventricular remodeling secondary to compensatory hypertrophy (Tsuruda et al., 2002; Gardner, 2003). It is therefore possible that in the case of sedentary Tg-Δ43 mice, mild upregulation of ANP and BNP manifests their protective role against excessive cardiac remodeling and controlling the extent of cardiac hypertrophy.

There are some discrepancies between our earlier study and current investigation on the hypertrophic growth in sedentary Tg-Δ43 mice. In Kazmierczak et al. (2009), we presented the gross morphology images of young (∼2 mo-old) and adult (∼7 mo-old) Tg-Δ43 animals. The hypertrophy was only noted for the older animals. The hearts of young Tg-Δ43 mice were indistinguishable from age matched control Tg-WT mice. In the current study, the hearts of 3–5 month-old sedentary Tg-Δ43 mice were not much different than those of age matched Tg-WT controls (**Figure 1A**). These data suggest that hypertrophy in Tg-Δ43 mice

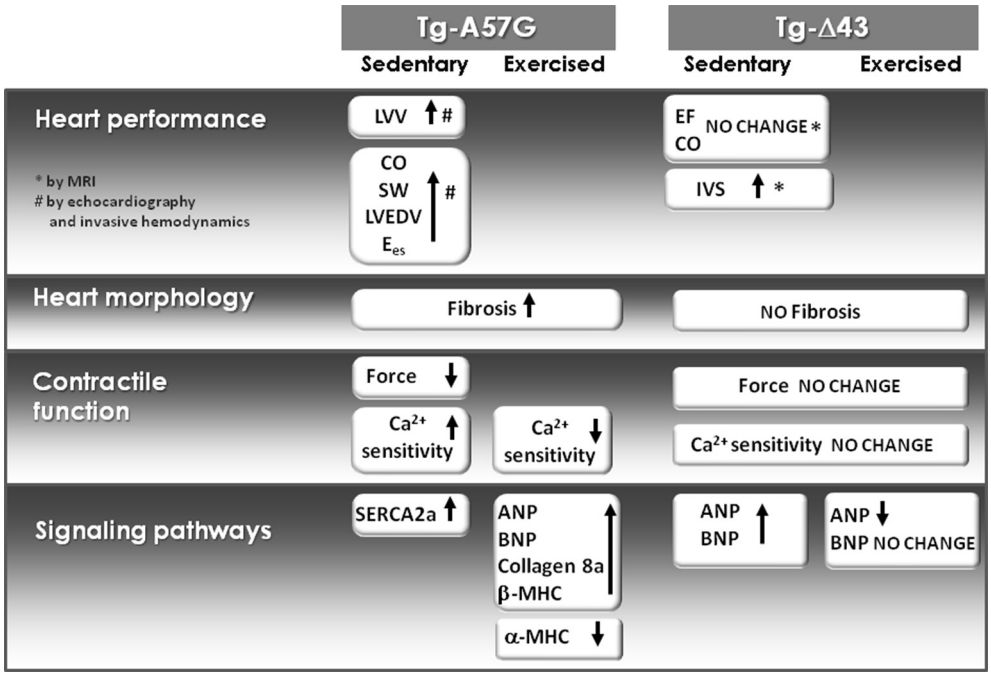

FIGURE 9 | Molecular effects of A57G and Δ43 mutations in the myosin ELC on heart morphology and function and expression of hypertrophic markers in sedentary and exercised Tg ELC mice. All data are compared with either sedentary or exercised Tg-WT ELC. The *in vivo* data were published previously. LVV, LV-volume; CO, cardiac output; SW, stroke work; LVEDV, LV-end diastolic volume; E_{es}, measure of myocardial contractility defined by the slope of the end-systolic pressure-volume relationship.

is an age dependent process and the fact that it was not present in <5 month-old Tg-Δ43 animals (**Figure 1A**), i.e., ∼2 months before the apparent threshold when the animals reach ∼7 months of age (Kazmierczak et al., 2009) is not surprising. In line with this, a profound hypertrophy in ∼12 month-old Tg-Δ43 mice was recently reported by our group (Muthu et al., 2011).

REMODELING IN EXERCISED MICE

Swimming exercise is known for its efficiency in inducing cardiac hypertrophy and significant increases in LV end-diastolic volumes in rats (Geenen et al., 1988). We hypothesized that strenuous exercise applied to Tg-Δ43 and Tg-A57G mice would lead to differential cardiac remodeling in these animal models displaying two distinct phenotypes of a "healthy" (Δ43) vs. "diseased" (A57G) heart. Our data on exercised animals confirmed our hypothesis. For Tg-A57G animals, we observed a significant upregulation of hypertrophic markers that were activated upon exercise initiating pathological hypertrophic remodeling in Tg-A57G mice (**Figure 9**). Upregulation of ANP and BNP transcripts observed in exercised Tg-A57G mice (**Figure 4**) manifests their sensitivity in monitoring ventricular hypertrophy (Lee et al., 1988; Dagnino et al., 1992; Nakagawa et al., 1995). ANP and BNP are released by the heart usually in response to heart failure (cardiac injury). The BNP levels in plasma have been shown to be useful in monitoring therapy for heart failure and typically a good response to effective treatment correlates with decreased concentrations of BNP (Lee et al., 2002; Yoshimura et al., 2002). Upregulation of ANP, BNP, and Collagen VIIIa was paralleled by a visible increase in heart size in Tg-A57G mice (**Figure 1B**), manifesting pathological hypertrophic remodeling in Tg-A57G mice (**Figure 9**).

Force generation and the Ca^{2+} sensitivity of force in Tg-A57G mice were significantly reduced after strenuous excise (**Tables 1**, **2**) manifesting pathological hypertrophic remodeling. Although maximal force in these animals was slightly improved compared to sedentary mice it was still significantly lower than that monitored for other exercised mice. It is possible that strenuous exercise caused activation of the β-adrenergic pathway in Tg-A57G hearts that could lead to compromised heart performance. Decreased Ca^{2+} sensitivity in these animals compared to sedentary Tg-A57G mice might be indicative of progressing toward heart failure as observed in animal models of HF (Cazorla et al., 2005; Belin et al., 2007) and in humans (Van Dijk et al., 2009; Hoskins et al., 2010; Sequeira et al., 2013; Witjas-Paalberends et al., 2013). The presence of collagen deposits in the myocardium of Tg-A57G mice (**Figure 2**) indicates the propensity of the heart to increase its LV stiffness that ultimately may result in diastolic dysfunction in Tg-A57G mice (Wu et al., 2007).

A different response on the strenuous exercise was observed for the second Tg-Δ43 animal model. Function of the heart remained normal and both maximal force and the Ca^{2+} sensitivity were similar to exercised Tg-WT mice. Additionally, exercised Tg-Δ43 animals showed similar pattern of gene expression to that observed in exercised Tg-WT mice, indicating that hypertrophic remodeling of the heart was no longer present in this animal model. The lack of changes in expression levels of BNP, β-MHC,

Table 2 | Statistics for measurements of steady-state force in skinned papillary muscle strips from sedentary and exercised transgenic ELC animals.

	Statistics (*P*-value)		
	Tg-WT ELC	**Tg-Δ43**	**Tg-A57G**
pCa_{50}			
Sedentary WT vs. mutant	N/A	0.0676	0.0049
Exercised WT vs. mutant	N/A	0.4212	0.0037
Sedentary vs. exercised	0.0601	0.2488	0.0008
F max			
Sedentary WT vs. mutant	N/A	0.8580	<0.0001
Exercised WT vs. mutant	N/A	0.8648	0.0002
Sedentary vs. exercised	0.0970	0.0437	0.0466

and collagen VIIIa in exercised Tg-Δ43 mice represents an adaptive response to exercise and non-pathological remodeling in Tg-Δ43 animals compared to detrimental heart remodeling observed in exercised Tg-A57G mice.

CONCLUSIVE REMARKS

Our previous X-ray studies on sedentary Tg-A57G and Tg-Δ43 mice demonstrated a mutation-induced decrease in the filament lattice spacing in skinned papillary muscles of Tg-A57G compared to Tg-WT controls (Muthu et al., 2011). These structural changes may initiate hypertrophic remodeling of the heart triggered by mutation-induced conformational changes within the sarcomere that lead to abnormal interaction of two major contractile proteins, myosin and actin causing abnormalities in contractile force production and heart performance. Pathological ventricular remodeling and anatomical changes observed in Tg-A57G hearts mostly develop in older animals and, as we anticipated, they were augmented in response to strenuous exercise. In contrast, X-ray diffraction studies on Tg-Δ43 mice demonstrated a shift of cross-bridge mass from the thick filament backbone toward the thin filaments and no changes in the interfilament spacing compared with Tg-WT controls (Muthu et al., 2011). These data indicate that the lack of the N-terminal ELC extension in Tg-Δ43 animals may lead to changes in myosin head orientation positioning it closer (at smaller angle) to the actin filaments (Muthu et al., 2011). The important function of the N-terminal extension of the ELC protein was also demonstrated in other study showing that the length-dependent activation in Tg-Δ43 strips was blunted in Tg-Δ43 animals (Michael et al., 2013). This could eventually lead to hypertrophy in Tg-Δ43 animals but of the non-pathological nature.

Combined knowledge of the genetic basis of HCM with biophysical and transcriptional analyses may help to better understand the pathophysiology of heart remodeling and make predictive correlations between the specific mutations with disease prognosis. The heart may tolerate various types of stimuli, but compensatory/adaptive responses that aim to maintain function may fail in case of patients with pre-existing HCM (hearts with disease-causing mutations), resulting in a wide range of functional deficits and/or cardiomyopathy. The strenuous exercise of competitive athletes has been known to make symptoms of HCM more apparent and because of the risk of SCD during exercise, HCM patients are excluded from most competitive sports (Michels et al., 2009). Our data confirm that it is reasonable to caution people with diagnosed genetic HCM against intensive exercise programs. Our previous and current studies suggest that the A57G mutation can initiate pathologic cardiac remodeling and drive the heart toward cardiomyopathy disease and/or heart failure while the Δ43–dependent pathway displays a tendency toward a non-pathological cardiac phenotype.

AUTHOR CONTRIBUTIONS

Katarzyna Kazmierczak, Conception and design of research, execution of experiments, analysis and interpretation of data, figure preparation, drafting of the manuscript. Chen-ching Yuan, Execution of experiments, analysis of data. Jingsheng Liang, Execution of experiments, analysis of data. Wenrui Huang, Execution of experiments, analysis of data, figure preparation. Ana I. Rojas, Breeding mouse colonies and *in vivo* data collection. Danuta Szczesna-Cordary, Conception and design of research, analysis and interpretation of data, figure preparation, drafting of the manuscript.

FUNDING

This work was supported by the National Institutes of Health Grants R01 HL-108343 and HL-071778 (to DSC).

REFERENCES

Abel, E. D., and Doenst, T. (2011). Mitochondrial adaptations to physiological vs. pathological cardiac hypertrophy. *Cardiovasc. Res.* 90, 234–242. doi: 10.1093/cvr/cvr015

Alcalai, R., Seidman, J. G., and Seidman, C. E. (2008). Genetic basis of hypertrophic cardiomyopathy: from bench to the clinics. *J. Cardiovasc. Electrophysiol.* 19, 104–110. doi: 10.1097/HCO.0b013e3283375698

Allen, D. L., Harrison, B. C., Maass, A., Bell, M. L., Byrnes, W. C., and Leinwand, L. A. (2001). Cardiac and skeletal muscle adaptations to voluntary wheel running in the mouse. *J. Appl. Physiol. (1985)* 90, 1900–1908.

Arai, M., Suzuki, T., and Nagai, R. (1996). Sarcoplasmic reticulum genes are upregulated in mild cardiac hypertrophy but downregulated in severe cardiac hypertrophy induced by pressure overload. *J. Mol. Cell. Cardiol.* 28, 1583–1590. doi: 10.1006/jmcc.1996.0149

Aydt, E. M., Wolff, G., and Morano, I. (2007). Molecular modeling of the myosin-S1(A1) isoform. *J. Struct. Biol.* 159, 158–163. doi: 10.1016/j.jsb.2007.04.002

Azizi, C., Bouissou, P., Galen, F. X., Lattion, A. L., Lartigue, M., and Carayon, A. (1995). Alterations in atrial natriuretic peptide gene expression during endurance training in rats. *Eur. J. Endocrinol.* 133, 361–365. doi: 10.1530/eje.0.1330361

Belin, R. J., Sumandea, M. P., Allen, E. J., Schoenfelt, K., Wang, H., Solaro, R. J., et al. (2007). Augmented protein kinase C-alpha-induced myofilament protein phosphorylation contributes to myofilament dysfunction in experimental congestive heart failure. *Circ. Res.* 101, 195–204. doi: 10.1161/CIRCRESAHA.107.148288

Bernardo, B. C., Weeks, K. L., Pretorius, L., and McMullen, J. R. (2010). Molecular distinction between physiological and pathological cardiac hypertrophy: experimental findings and therapeutic strategies. *Pharmacol. Ther.* 128, 191–227. doi: 10.1016/j.pharmthera.2010.04.005

Buttrick, P. M., Kaplan, M., Leinwand, L. A., and Scheuer, J. (1994). Alterations in gene expression in the rat heart after chronic pathological and physiological loads. *J. Mol. Cell. Cardiol.* 26, 61–67. doi: 10.1006/jmcc.1994.1008

Cadete, V. J., Sawicka, J., Jaswal, J. S., Lopaschuk, G. D., Schulz, R., Szczesna-Cordary, D., et al. (2012). Ischemia/reperfusion-induced myosin light chain 1 phosphorylation increases its degradation by matrix metalloproteinase 2. *FEBS J.* 279, 2444–2454. doi: 10.1111/j.1742-4658.2012.08622.x

Cazorla, O., Szilagyi, S., Le Guennec, J. Y., Vassort, G., and Lacampagne, A. (2005). Transmural stretch-dependent regulation of contractile properties in rat heart and its alteration after myocardial infarction. *FASEB J.* 19, 88–90. doi: 10.1096/fj.04-2066fje

Dagnino, L., Lavigne, J. P., and Nemer, M. (1992). Increased transcripts for B-type natriuretic peptide in spontaneously hypertensive rats. Quantitative polymerase chain reaction for atrial and brain natriuretic peptide transcripts. *Hypertension* 20, 690–700. doi: 10.1161/01.HYP.20.5.690

Diffee, G. M., Seversen, E. A., Stein, T. D., and Johnson, J. A. (2003). Microarray expression analysis of effects of exercise training: increase in atrial MLC-1 in rat ventricles. *Am. J. Physiol. Heart Circ. Physiol.* 284, H830–H837. doi: 10.1152/ajpheart.00761.2002

Dweck, D., Reyes-Alfonso, A. Jr., and Potter, J. D. (2005). Expanding the range of free calcium regulation in biological solutions. *Anal. Biochem.* 347, 303–315. doi: 10.1016/j.ab.2005.09.025

Evangelista, F. S., Brum, P. C., and Krieger, J. E. (2003). Duration-controlled swimming exercise training induces cardiac hypertrophy in mice. *Braz. J. Med. Biol. Res.* 36, 1751–1759. doi: 10.1590/S0100-879X2003001200018

Fewell, J. G., Osinska, H., Klevitsky, R., Ng, W., Sfyris, G., Bahrehmand, F., et al. (1997). A treadmill exercise regimen for identifying cardiovascular phenotypes in transgenic mice. *Am. J. Physiol.* 273, H1595–H1605.

Galindo, C. L., Skinner, M. A., Errami, M., Olson, L. D., Watson, D. A., Li, J., et al. (2009). Transcriptional profile of isoproterenol-induced cardiomyopathy and comparison to exercise-induced cardiac hypertrophy and human cardiac failure. *BMC Physiol.* 9:23. doi: 10.1186/1472-6793-9-23

Gardner, D. G. (2003). Natriuretic peptides: markers or modulators of cardiac hypertrophy? *Trends Endocrinol. Metab.* 14, 411–416. doi: 10.1016/S1043-2760(03)00113-9

Geenen, D., Buttrick, P., and Scheuer, J. (1988). Cardiovascular and hormonal responses to swimming and running in the rat. *J. Appl. Physiol. (1985)* 65, 116–123.

Heineke, J., and Molkentin, J. D. (2006). Regulation of cardiac hypertrophy by intracellular signalling pathways. *Nat. Rev. Mol. Cell Biol.* 7, 589–600. doi: 10.1038/nrm1983

Henry, G. D., Winstanley, M. A., Dalgarno, D. C., Scott, G. M., Levine, B. A., and Trayer, I. P. (1985). Characterization of the actin-binding site on the alkali light chain of myosin. *Biochim. Biophys. Acta* 830, 233–243. doi: 10.1016/0167-4838(85)90279-1

Hernandez, O. M., Jones, M., Guzman, G., and Szczesna-Cordary, D. (2007). Myosin essential light chain in health and disease. *Am. J. Physiol. Heart Circ. Physiol.* 292, H1643–H1654. doi: 10.1152/ajpheart.00931.2006

Hidalgo, C., Saripalli, C., and Granzier, H. L. (2014). Effect of exercise training on post-translational and post-transcriptional regulation of titin stiffness in striated muscle of wild type and IG KO mice. *Arch. Biochem. Biophys.* 552–553, 100–107. doi: 10.1016/j.abb.2014.02.010

Hill, T. L., Einsenberg,. E., and Greene, L. E. (1980). Theoretical model for the cooperative equilibrium binding of myosin subfragment-1 to the actin-troponin-tropomyosin complex. *Proc. Natl. Acad. Sci. U.S.A.* 77, 3186–3190. doi: 10.1073/pnas.77.6.3186

Ho, C. Y. (2010). Hypertrophic cardiomyopathy. *Heart Fail. Clin.* 6, 141–159. doi: 10.1016/j.hfc.2009.12.001

Ho, C. Y., Lopez, B., Coelho-Filho, O. R., Lakdawala, N. K., Cirino, A. L., Jarolim, P., et al. (2010). Myocardial fibrosis as an early manifestation of hypertrophic cardiomyopathy. *N. Engl. J. Med.* 363, 552–563. doi: 10.1056/NEJMoa1002659

Hoskins, A. C., Jacques, A., Bardswell, S. C., McKenna, W. J., Tsang, V., Dos Remedios, C. G., et al. (2010). Normal passive viscoelasticity but abnormal myofibrillar force generation in human hypertrophic cardiomyopathy. *J. Mol. Cell. Cardiol.* 49, 737–745. doi: 10.1016/j.yjmcc.2010.06.006

Huang, W., Liang, J., Kazmierczak, K., Muthu, P., Duggal, D., Farman, G. P., et al. (2014). Hypertrophic cardiomyopathy associated lys104glu mutation in the myosin regulatory light chain causes diastolic disturbance in mice. *J. Mol. Cell. Cardiol.* 74, 318–329. doi: 10.1016/j.yjmcc.2014.06.0111

Hunter, J. J., and Chien, K. R. (1999). Signaling pathways for cardiac hypertrophy and failure. *N. Engl. J. Med.* 341, 1276–1283. doi: 10.1056/NEJM199910213411706

Iemitsu, M., Miyauchi, T., Maeda, S., Sakai, S., Kobayashi, T., Fujii, N., et al. (2001). Physiological and pathological cardiac hypertrophy induce different molecular phenotypes in the rat. *Am. J. Physiol. Regul. Integr. Comp. Physiol.* 281, R2029–R2036.

Jin, H., Yang, R., Li, W., Lu, H., Ryan, A. M., Ogasawara, A. K., et al. (2000). Effects of exercise training on cardiac function, gene expression, and apoptosis in rats. *Am. J. Physiol. Heart Circ. Physiol.* 279, H2994–H3002.

Kazmierczak, K., Muthu, P., Huang, W., Jones, M., Wang, Y., and Szczesna-Cordary, D. (2012). Myosin regulatory light chain mutation found in hypertrophic cardiomyopathy patients increases isometric force production in transgenic mice. *Biochem. J.* 442, 95–103. doi: 10.1042/BJ20111145

Kazmierczak, K., Paulino, E. C., Huang, W., Muthu, P., Liang, J., Yuan, C. C., et al. (2013). Discrete effects of A57G-myosin essential light chain mutation associated with familial hypertrophic cardiomyopathy. *Am. J. Physiol. Heart Circ. Physiol.* 305, H575–H589. doi: ajpheart.00107.2013

Kazmierczak, K., Xu, Y., Jones, M., Guzman, G., Hernandez, O. M., Kerrick, W. G. L., et al. (2009). The role of the N-terminus of the myosin essential light chain in cardiac muscle contraction. *J. Mol. Biol.* 387, 706–725. doi: 10.1016/j.jmb.2009.02.006

Lee, R. T., Bloch, K. D., Pfeffer, J. M., Pfeffer, M. A., Neer, E. J., and Seidman, C. E. (1988). Atrial natriuretic factor gene expression in ventricles of rats with spontaneous biventricular hypertrophy. *J. Clin. Invest.* 81, 431–434. doi: 10.1172/JCI113337

Lee, S. C., Stevens, T. L., Sandberg, S. M., Heublein, D. M., Nelson, S. M., Jougasaki, M., et al. (2002). The potential of brain natriuretic peptide as a biomarker for New York Heart Association class during the outpatient treatment of heart failure. *J. Card. Fail.* 8, 149–154. doi: 10.1054/jcaf.2002.125368

Lee, W., Hwang, T. H., Kimura, A., Park, S. W., Satoh, M., Nishi, H., et al. (2001). Different expressivity of a ventricular essential myosin light chain gene Ala57Gly mutation in familial hypertrophic cardiomyopathy. *Am. Heart J.* 141, 184–189. doi: 10.1067/mhj.2001.112487

Levy, D., Garrison, R. J., Savage, D. D., Kannel, W. B., and Castelli, W. P. (1990). Prognostic implications of echocardiographically determined left ventricular mass in the framingham heart study. *N. Engl. J. Med.* 322, 1561–1566. doi: 10.1056/NEJM199005313222203

Lorell, B. H., and Carabello, B. A. (2000). Left ventricular hypertrophy: pathogenesis, detection, and prognosis. *Circulation* 102, 470–479. doi: 10.1161/01.CIR.102.4.470

Michael, J. J., Gollapudi, S. K., Ford, S. J., Kazmierczak, K., Szczesna-Cordary, D., and Chandra, M. (2013). Deletion of 1-43 amino acids in cardiac myosin essential light chain blunts length dependency of Ca(2+) sensitivity and cross-bridge detachment kinetics. *Am. J. Physiol. Heart Circ. Physiol.* 304, H253–H259. doi: 10.1152/ajpheart.00572.2012

Michels, M., Soliman, O. I., Phefferkorn, J., Hoedemaekers, Y. M., Kofflard, M. J., Dooijes, D., et al. (2009). Disease penetrance and risk stratification for sudden cardiac death in asymptomatic hypertrophic cardiomyopathy mutation carriers. *Eur. Heart J.* 30, 2593–2598. doi: 10.1093/eurheartj/ehp306

Milligan, R. A., Whittaker, M., and Safer, D. (1990). Molecular structure of F-actin and location of surface binding sites. *Nature* 348, 217–221. doi: 10.1038/348217a0

Morano, I. (1999). Tuning the human heart molecular motors by myosin light chains. *J. Mol. Med.* 77, 544–555. doi: 10.1007/s001099900031

Morano, I., Ritter, O., Bonz, A., Timek, T., Vahl, C. F., and Michel, G. (1995). Myosin light chain-actin interaction regulates cardiac contractility. *Circ. Res.* 76, 720–725. doi: 10.1161/01.RES.76.5.720

Muthu, P., Kazmierczak, K., Jones, M., and Szczesna-Cordary, D. (2012). The effect of myosin RLC phosphorylation in normal and cardiomyopathic mouse hearts. *J. Cell. Mol. Med.* 16, 911–919. doi: 10.1111/j.1582-4934.2011.01371.x

Muthu, P., Wang, L., Yuan, C. C., Kazmierczak, K., Huang, W., Hernandez, O. M., et al. (2011). Structural and functional aspects of the myosin essential light chain in cardiac muscle contraction. *FASEB J.* 25, 4394–4405. doi: 10.1096/fj.11-191973

Nakagawa, O., Ogawa, Y., Itoh, H., Suga, S., Komatsu, Y., Kishimoto, I., et al. (1995). Rapid transcriptional activation and early mRNA turnover of brain natriuretic peptide in cardiocyte hypertrophy. Evidence for brain natriuretic peptide as an "emergency" cardiac hormone against ventricular overload. *J. Clin. Invest.* 96, 1280–1287. doi: 10.1172/JCI118162

Nixon, B. R., Thawornkaiwong, A., Jin, J., Brundage, E. A., Little, S. C., Davis, J. P., et al. (2012). AMP-activated protein kinase phosphorylates cardiac troponin I at Ser-150 to increase myofilament calcium sensitivity and blunt PKA-dependent function. *J. Biol. Chem.* 287, 19136–19147. doi: 10.1074/jbc.M111.323048

Rayment, I., Rypniewski, W. R., Schmidt-Base, K., Smith, R., Tomchick, D. R., Benning, M. M., et al. (1993). Three-dimensional structure of myosin

subfragment-1: a molecular motor. *Science* 261, 50–58. doi: 10.1126/science.8316857

Rockman, H. A., Ono, S., Ross, R. S., Jones, L. R., Karimi, M., Bhargava, V., et al. (1994). Molecular and physiological alterations in murine ventricular dysfunction. *Proc. Natl. Acad. Sci. U.S.A.* 91, 2694–2698. doi: 10.1073/pnas.91.7.2694

Sadayappan, S., Gulick, J., Klevitsky, R., Lorenz, J. N., Sargent, M., Molkentin, J. D., et al. (2009). Cardiac myosin binding protein-C phosphorylation in a {beta}-myosin heavy chain background. *Circulation* 119, 1253–1262. doi: 10.1161/CIRCULATIONAHA.108.798983

Sawicki, G., Leon, H., Sawicka, J., Sariahmetoglu, M., Schulze, C. J., Scott, P. G., et al. (2005). Degradation of myosin light chain in isolated rat hearts subjected to ischemia-reperfusion injury: a new intracellular target for matrix metalloproteinase-2. *Circulation* 112, 544–552. doi: 10.1161/CIRCULATIONAHA.104.531616

Sequeira, V., Wijnker, P. J., Nijenkamp, L. L., Kuster, D. W., Najafi, A., Witjas-Paalberends, E. R., et al. (2013). Perturbed length-dependent activation in human hypertrophic cardiomyopathy with missense sarcomeric gene mutations. *Circ. Res.* 112, 1491–1505. doi: 10.1161/CIRCRESAHA.111.300436

Sutoh, K. (1982). An actin-binding site on the 20K fragment of myosin subfragment 1. *Biochemistry* 21, 4800–4804. doi: 10.1021/bi00262a043

Sweeney, H. L., Bowman, B. F., and Stull, J. T. (1993). Myosin light chain phosphorylation in vertebrate striated muscle: regulation and function. *Am. J. Physiol.* 264, C1085–C1095.

Timson, D. J. (2003). Fine tuning the myosin motor: the role of the essential light chain in striated muscle myosin. *Biochimie* 85, 639–645. doi: 10.1016/S0300-9084(03)00131-7

Timson, D. J., Trayer, H. R., and Trayer, I. P. (1998). The N-terminus of A1-type myosin essential light chains binds actin and modulates myosin motor function. *Eur. J. Biochem.* 255, 654–662. doi: 10.1046/j.1432-1327.1998.2550654.x

Trayer, I. P., Trayer, H. R., and Levine, B. A. (1987). Evidence that the N-terminal region of A1-light chain of myosin interacts directly with the C-terminal region of actin. A proton magnetic resonance study. *Eur. J. Biochem.* 164, 259–266. doi: 10.1111/j.1432-1033.1987.tb11019.x

Tsuruda, T., Boerrigter, G., Huntley, B. K., Noser, J. A., Cataliotti, A., Costello-Boerrigter, L. C., et al. (2002). Brain natriuretic Peptide is produced in cardiac fibroblasts and induces matrix metalloproteinases. *Circ. Res.* 91, 1127–1134. doi: 10.1161/01.RES.0000046234.73401.70

Van Dijk, S. J., Dooijes, D., Dos Remedios, C., Michels, M., Lamers, J. M., Winegrad, S., et al. (2009). Cardiac myosin-binding protein C mutations and hypertrophic cardiomyopathy: haploinsufficiency, deranged phosphorylation, and cardiomyocyte dysfunction. *Circulation* 119, 1473–1483. doi: 10.1161/CIRCULATIONAHA.108.838672

Vangheluwe, P., Louch, W. E., Ver Heyen, M., Sipido, K., Raeymaekers, L., and Wuytack, F. (2003). Ca2+ transport ATPase isoforms SERCA2a and SERCA2b are targeted to the same sites in the murine heart. *Cell Calcium* 34, 457–464. doi: 10.1016/S0143-4160(03)00126-X

Wang, L., Muthu, P., Szczesna-Cordary, D., and Kawai, M. (2013a). Characterizations of myosin essential light chain's N-terminal truncation mutant Delta43 in transgenic mouse papillary muscles by using tension transients in response to sinusoidal length alterations. *J. Muscle Res. Cell Motil.* 34, 93–105. doi: 10.1007/s10974-013-9337-x

Wang, L., Muthu, P., Szczesna-Cordary, D., and Kawai, M. (2013b). Diversity and similarity of motor function and cross-bridge kinetics in papillary muscles of transgenic mice carrying myosin regulatory light chain mutations D166V and R58Q. *J. Mol. Cell. Cardiol.* 62, 153–163. doi: 10.1016/j.yjmcc.2013.05.012

Weeks, K. L., and McMullen, J. R. (2011). The athlete's heart vs. the failing heart: can signaling explain the two distinct outcomes? *Physiology (Bethesda)* 26, 97–105. doi: 10.1152/physiol.00043.2010

Winstanley, M. A., Trayer, H. R., and Trayer, I. P. (1977). Role of the myosin light chains in binding to actin. *FEBS Lett.* 77, 239–242. doi: 10.1016/0014-5793(77)80242-1

Witjas-Paalberends, E. R., Piroddi, N., Stam, K., Van Dijk, S. J., Oliviera, V. S., Ferrara, C., et al. (2013). Mutations in MYH7 reduce the force generating capacity of sarcomeres in human familial hypertrophic cardiomyopathy. *Cardiovasc. Res.* 99, 432–441. doi: 10.1093/cvr/cvt119

Wu, Y., Peng, J., Campbell, K. B., Labeit, S., and Granzier, H. (2007). Hypothyroidism leads to increased collagen-based stiffness and re-expression of large cardiac titin isoforms with high compliance. *J. Mol. Cell. Cardiol.* 42, 186–195. doi: 10.1016/j.yjmcc.2006.09.017

Yoshimura, M., Mizuno, Y., Nakayama, M., Sakamoto, T., Sugiyama, S., Kawano, H., et al. (2002). B-type natriuretic peptide as a marker of the effects of enalapril in patients with heart failure. *Am. J. Med.* 112, 716–720. doi: 10.1016/S0002-9343(02)01121-X

Conflict of Interest Statement: The authors declare that the research was conducted in the absence of any commercial or financial relationships that could be construed as a potential conflict of interest.

Received: 19 June 2014; accepted: 29 August 2014; published online: 22 September 2014.

Citation: Kazmierczak K, Yuan C-C, Liang J, Huang W, Rojas AI and Szczesna-Cordary D (2014) Remodeling of the heart in hypertrophy in animal models with myosin essential light chain mutations. Front. Physiol. ***5****:353. doi: 10.3389/fphys.2014.00353*

This article was submitted to Striated Muscle Physiology, a section of the journal Frontiers in Physiology.

Copyright © 2014 Kazmierczak, Yuan, Liang, Huang, Rojas and Szczesna-Cordary. This is an open-access article distributed under the terms of the Creative Commons Attribution License (CC BY). The use, distribution or reproduction in other forums is permitted, provided the original author(s) or licensor are credited and that the original publication in this journal is cited, in accordance with accepted academic practice. No use, distribution or reproduction is permitted which does not comply with these terms.

frontiers in
PHYSIOLOGY

REVIEW ARTICLE
published: 25 August 2014
doi: 10.3389/fphys.2014.00315

Investigating the role of uncoupling of troponin I phosphorylation from changes in myofibrillar Ca^{2+}-sensitivity in the pathogenesis of cardiomyopathy

Andrew E. Messer* and Steven B. Marston

National Heart & Lung Institute, Imperial College London, London, UK

Edited by:
Julien Ochala, KIng's College London, UK

Reviewed by:
Jose Renato Pinto, Florida State University, USA
Ranganath Mamidi, Case Western Reserve University, USA

****Correspondence:***
Andrew E. Messer, Imperial Centre for Translational and Experimental Medicine, Hammersmith Campus, Du Cane Road, London, UK
e-mail: a.messer@imperial.ac.uk

Contraction in the mammalian heart is controlled by the intracellular Ca^{2+} concentration as it is in all striated muscle, but the heart has an additional signaling system that comes into play to increase heart rate and cardiac output during exercise or stress. β-adrenergic stimulation of heart muscle cells leads to release of cyclic-AMP and the activation of protein kinase A which phosphorylates key proteins in the sarcolemma, sarcoplasmic reticulum and contractile apparatus. Troponin I (TnI) and Myosin Binding Protein C (MyBP-C) are the prime targets in the myofilaments. TnI phosphorylation lowers myofibrillar Ca^{2+}-sensitivity and increases the speed of Ca^{2+}-dissociation and relaxation (lusitropic effect). Recent studies have shown that this relationship between Ca^{2+}-sensitivity and TnI phosphorylation may be unstable. In familial cardiomyopathies, both dilated and hypertrophic (DCM and HCM), a mutation in one of the proteins of the thin filament often results in the loss of the relationship (uncoupling) and blunting of the lusitropic response. For familial dilated cardiomyopathy in thin filament proteins it has been proposed that this uncoupling is causative of the phenotype. Uncoupling has also been found in human heart tissue from patients with hypertrophic obstructive cardiomyopathy as a secondary effect. Recently, it has been found that Ca^{2+}-sensitizing drugs can promote uncoupling, whilst one Ca^{2+}-desensitizing drug Epigallocatechin 3-Gallate (EGCG) can reverse uncoupling. We will discuss recent findings about the role of uncoupling in the development of cardiomyopathies and the molecular mechanism of the process.

Keywords: troponin I, phosphorylation, cardiomyopathies, Ca sensitivity, heart muscle, myofilament

INTRODUCTION

The heart has a unique system for rapidly and precisely adjusting cardiac output to meet the demands put upon it. The rhythmic contraction and relaxation of heart muscle is due to the rise and fall of sarcoplasmic calcium ion (Ca^{2+}) concentration under neural control. Contraction is initiated by Ca^{2+} release from the sarcoplasmic reticulum via the Ryanodine receptor and is terminated by Ca^{2+}-uptake by the ATP-powered sarcoplasmic Ca^{2+} pump (SERCA). Ca^{2+} binds to troponin C (TnC), the Ca^{2+} receptor of the contractile apparatus to switch on contractile interactions between actin and the myosin motor protein in the thick filaments (Gordon et al., 2000; Macleod et al., 2010).

Independently of this Ca^{2+}-switch, the speed and force of contraction is modulated in a graded way by changing the inotropic state of muscle. The inotropic state is largely controlled by the sympathetic system that releases β-adrenergic agonists at nerve endings and into the circulation from the adrenal glands. These bind to and activate β1 receptors on the cardiomyocyte surface and initiate a cascade leading to increased intracellular cyclic AMP concentrations which in turn activate the cyclic AMP dependent protein kinase (PKA) (Macleod et al., 2010). PKA phosphorylates several proteins in the sarcolemma, sarcoplasmic reticulum and the contractile apparatus, thus regulating their activity. The combined result of the action of PKA is a co-ordinated increase in cardiac output due to increased heart rate (chronotropy) increased force of contraction (inotropy) and increased rate of relaxation (lusitropy) (Layland et al., 2005).

PKA phosphorylates Myosin Binding Protein-C (MyBP-C) and troponin I (TnI) within the cardiac myofibril. TnI is the inhibitory component of the trimeric troponin molecule that makes up the Ca^{2+}-switch of the contractile apparatus. TnI binds to TnC when Ca^{2+} is bound to TnC, whilst in the absence of Ca^{2+}, the C-terminus of TnI is released and is able to interact with actin and tropomyosin to inhibit the thin filament's interaction with the motor protein, myosin. Thus, the interactions of TnC with TnI and Ca^{2+} are crucial for the Ca^{2+} control of muscle. Early studies showed that β-adrenergic stimulation of contraction was associated with enhanced phosphorylation of TnI (England, 1976; Solaro et al., 1976), that TnI was bis-phosphorylated at serines 22 and 23 in the cardiac-specific N-terminal extension by PKA (Mittmann et al., 1990; Al-Hillawi et al., 1995; Ayaz-Guner et al., 2009) and that the primary effect of phosphorylation of TnI *in vitro* was reduced Ca^{2+}-sensitivity and faster dissociation of Ca^{2+} from TnC (Solaro et al., 1976; Robertson et al., 1982; Zhang et al., 1995; Dong et al., 2007). This can cause an increase in the rate of relaxation (lusitropic response) which is essential when

heart rate is increased (Kentish et al., 2001; Layland et al., 2005). Transgenic mouse studies have demonstrated the physiological importance of TnI phosphorylation since mice with unphosphorylatable TnI have a blunted response to β-adrenergic stimulation and this leads to an enhanced susceptibility to the development of heart failure under stress (Fentzke et al., 1999; Pi et al., 2002; Yasuda et al., 2007).

Over the last 10 years it has become evident that the modulation of myofilament Ca^{2+}-sensitivity by TnI phosphorylation is quite a labile system and that mutations associated with cardiomyopathies in particular, can lead to disruption of the system. This was first noted with mutations in TnI that caused hypertrophic cardiomyopathy (HCM) (Deng et al., 2001, 2003) but its physiological significance was uncovered by studies on dilated cardiomyopathy (DCM) (Dyer et al., 2007, 2009; Memo et al., 2013). DCM is a major cause of heart failure in humans and a substantial proportion of cases of DCM are inherited. Mutations in the thin filament proteins [actin, tropomyosin, troponin T (TnT), TnI, and TnC] that are associated with familial DCM have been studied particularly closely (reviewed in Chang and Potter, 2005; Morimoto, 2008; Marston, 2011). By studying isolated thin filaments with the quantitative *in vitro* motility assay (IVMA) it was found that in all of these DCM-causing mutations the myofilament Ca^{2+}-sensitivity is independent of the level of TnI phosphorylation. Therefore, by analogy with the S22/23A transgenic mice, it was proposed that this uncoupling was necessary and sufficient to cause the DCM phenotype (Memo et al., 2013).

In this review we show that "uncoupling" of TnI phosphorylation from changes in Ca^{2+}-sensitivity is a widespread phenomenon with significant implications for the understanding of heart disease and its treatment.

METHODOLOGY

PHOSPHORYLATION MEASUREMENT

As there is a link between troponin (Tn) phosphorylation and Ca^{2+}-sensitivity in cardiac muscle, measurement of troponin I (TnI) phosphorylation levels *in situ* is very important. Quantitative methods such as Top-down mass spectrometry and phosphate affinity SDS-PAGE has clearly established that serines 22 and 23 are the main amino acids phosphorylated in native heart tissue in rats, mice or humans (Zabrouskov et al., 2008; Ayaz-Guner et al., 2009; Marston and Walker, 2009; Messer et al., 2009; Sancho Solis et al., 2009; Wang et al., 2012) (these are often numbered 23 and 24 according to the coding sequence, however the N terminal methionine is missing in all mature TnI in heart tissue). The first quantitative studies used non-equilibrium pH gradient electrophoresis in 1 or 2D (Ardelt et al., 1998; Kobayashi et al., 2005). Measurement of phosphorylation became much easier with the introduction of specific methods to detect phosphoproteins using the phosphoprotein gel stain, Pro-Q Diamond (Steinberg et al., 2003) or antibodies to phosphorylated Tn (Al-Hillawi et al., 1998; Haworth et al., 2004). This methodology has been widely adopted, but has its limitations, since to be quantitative it requires the use of an external standard, which may introduce systematic errors (**Figure 1A**) (Messer et al., 2007; Zaremba et al., 2007).

Thus, to overcome this, we developed the use of phosphate affinity SDS-PAGE which was first developed by the Kinoshita group (Kinoshita et al., 2006). Phos-Tags are Mn^{2+}-dependent specific chelators of phosphoproteins, when added to standard SDS-PAGE, phosphoproteins are retarded in proportion to the number of phosphates per mole of protein (Messer et al., 2009). Thus, unphosphorylated, monophosphorylated and bisphosphorylated species of phosphoproteins can be separated (**Figure 1B**). We have used Phos-Tags in conjunction with a specific cardiac TnI antibody to accurately measure phosphorylation levels in myofibrillar extracts from human heart tissue. The advantage of phosphate affinity SDS-PAGE is that it permits rapid identification and direct quantification of the mono and bisphosphorylated TnI.

All the methods for measuring Ser22/23 phosphorylation in intact tissue give similar results: flash-frozen mouse or rat heart yield a phosphorylation level of 1–1.5 mol Pi/ mol TnI with up to 40% of TnI being the bis-phosphorylated species, whilst human donor heart samples have 1.5–2 mols Pi/mol TnI with up to 60% of bis-phosphorylated species. These types of samples have been widely used in the study of the role of TnI phosphorylation in modulating muscle regulation, however there is still controversy as to whether these samples are actually representative of the "normal" heart (Jweied et al., 2007; Marston and Detombe, 2008).

In contrast, pathological samples from hearts transplanted for idiopathic dilated cardiomyopathy or septal myectomies from patients with hypertrophic obstructive cardiomyopathy (HOCM) generally have a low level of phosphorylation (0.1–0.4 mols Pi/mol TnI) (Van Der Velden et al., 2003; Messer et al., 2007, 2009; Zaremba et al., 2007; Ayaz-Guner et al., 2009; Hamdani et al., 2009; Jacques et al., 2009; Bayliss et al., 2012b).

MANIPULATION OF TnI PHOSPHORYLATION LEVELS

To investigate the relationship between TnI phosphorylation and myofilament Ca^{2+}-sensitivity, the Ca^{2+}-sensitivity needs to be compared with phosphorylated and unphosphorylated Tn, thus the phosphorylation levels need to be manipulated. Initial *in vitro* work used Tn reconstituted from recombinant subunits expressed in E.coli; TnI could then be readily phosphorylated with PKA catalytic subunit. For transgenic mouse studies, unphosphorylatable TnI could be overexpressed (either slow skeletal TnI in place of cardiac or mutant TnI with Ser 22/23 mutated to alanine Fentzke et al., 1999; Pi et al., 2002; Yasuda et al., 2007). Phosphorylated TnI could be simulated with Ser 22/23 mutated to aspartic acid (Dohet et al., 1995; Mamidi et al., 2012). The first studies of native human heart Tn in IVMA or skinned myocyte contractility compared donor and failing human heart muscle samples, since they had high and low levels of phosphorylation respectively (Van Der Velden et al., 2003; Messer et al., 2007). However, it was not certain whether differences in Ca^{2+}-sensitivity observed (**Figure 2A**) were due to the different phosphorylation levels or other disease-related factors.

Ideally, one should be able to study the same sample at different phosphorylation levels. This can be done by dephosphorylation or phosphorylation. The phosphorylation level of Tn isolated from heart tissue may be reduced by treatment with a

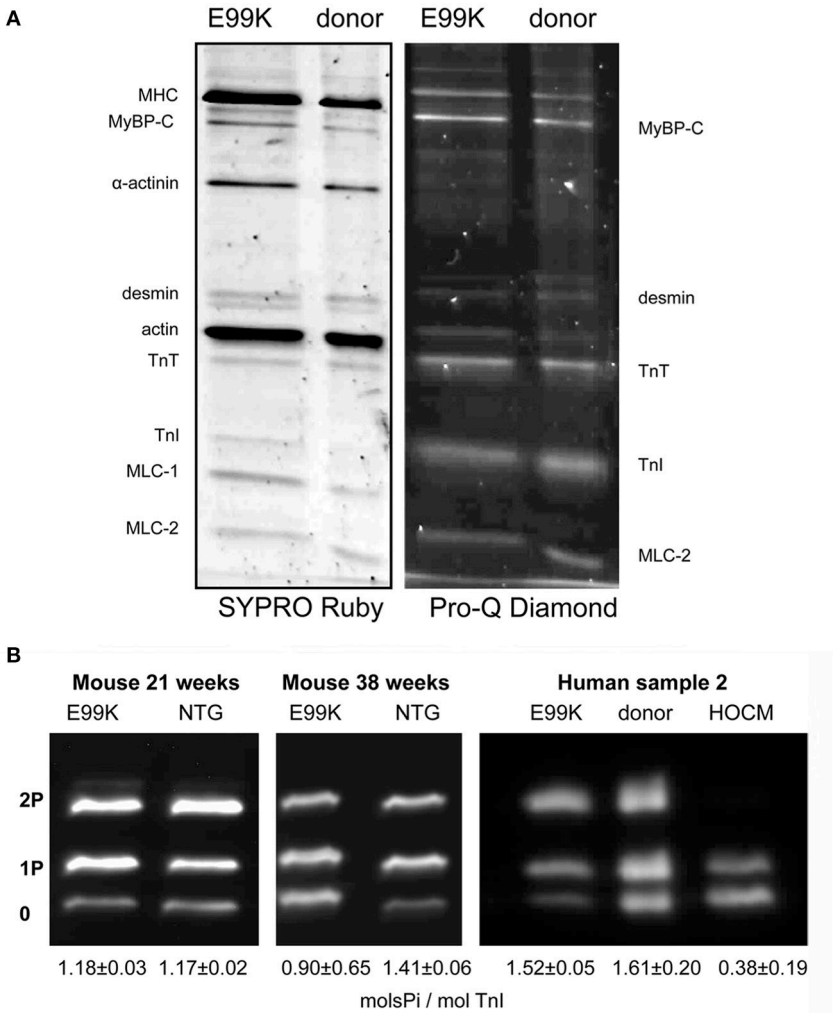

FIGURE 1 | SDS-PAGE analysis of myofibrillar proteins and phosphoproteins. (A) Myofibril fraction of heart muscle separated by SDS-PAGE and stained successively with Pro-Q Diamond phosphoprotein stain and SYPRO Ruby total protein stain. Left, NTG and ACTC E99K mouse heart myofibrils (38 weeks male). Right, donor and ACTC E99K heart sample 2 myofibrils (Song et al., 2011). The TnI band is strongly stained together with MyBP-C, TnT and MLC-2. **(B)** Phosphate affinity SDS-PAGE analysis of TnI phospho-species. Left, comparison of TnI phosphorylation in 21-week-old female ACTC E99K and NTG mouse myofibrils. Right, comparison of TnI phosphorylation in myofibrils from ACTC E99K sample 2, donor heart and a typical interventricular septum sample from a patient with hypertrophic obstructive cardiomyopathy (HOCM) (Song et al., 2011). All samples show a high level of phosphorylation, except for the failing heart sample.

phosphatase (shrimp alkaline phosphatase has proved to be the most reliable enzyme) or increased by PKA treatment (Bayliss et al., 2012b). PKA treatment has been used successfully for many years to increase the level of phosphorylation of isolated myocytes or skinned muscle strips (Hamdani et al., 2009; Kooij et al., 2010) but dephosphorylation is not usually successful, either there is inadequate reduction in phosphorylation level or the enzyme preparations cause degradation of the muscle. To dephosphorylate heart muscle in laboratory animals a different method may be used. For instance, mice can be treated with Propranolol (8 mg/kg) to block β1-adrenoreceptors and deactivate PKA to reduce phosphorylation levels of PKA substrates including Tn and MyBP-C (Bailin, 1979; Wang et al., 2011; Vikhorev et al., 2013).

NORMAL RELATIONSHIP BETWEEN TnI PHOSPHORYLATION AND Ca^{2+}-REGULATION

It was established, soon after the discovery of troponin I (TnI) phosphorylation, that phosphorylation of troponin (Tn) modulates Ca^{2+}-regulation by Tn by reducing the Ca^{2+}-sensitivity and increasing the force or crossbridge turnover rate at maximally activating Ca^{2+} concentrations (Ray and England, 1976; Bailin, 1979; Mope et al., 1980). The magnitude of the Ca^{2+}-sensitivity shift has been consistently been measured in the 2–3-fold range. It has been demonstrated that the reduced Ca^{2+}-sensitivity is due to an increase in the rate of Ca^{2+}-dissociation from Tn in the thin filaments (Robertson et al., 1982; Zhang et al., 1995; Dong et al., 2007), thereby providing a mechanism for the lusitropic (faster relaxation) response to β-adrenergic stimulation. Two

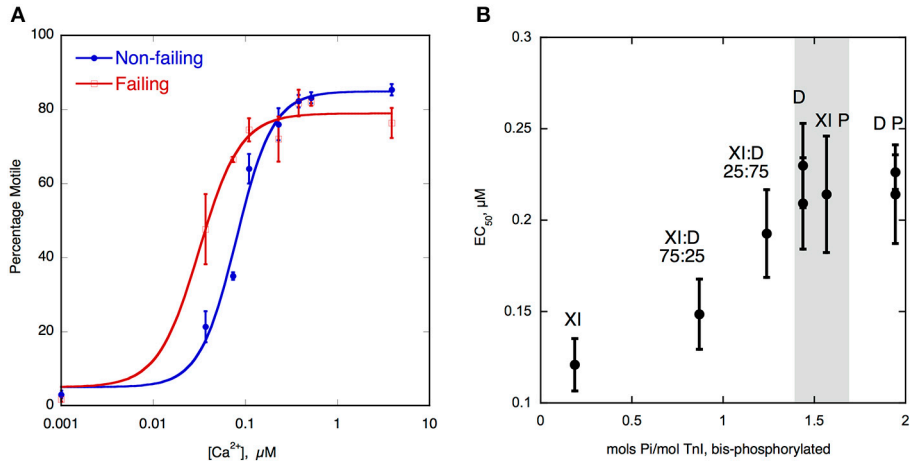

FIGURE 2 | (A) Ca^{2+}-regulation of thin filament motility by non-failing (donor) and failing heart troponin. Thin filament motility was measured by motility assay over a range of $[Ca^{2+}]$ in paired cells. The percentage of filaments motile is plotted as a function of $[Ca^{2+}]$ for a representative experiment. In blue lines and points, non-failing thin filaments, red lines and open points, failing thin filaments. TnI phosphorylation levels are shown in **Figure 1B**. The points ± s.e.m. are the mean of four determinations of percentage motile measured in one motility cell. The curves are fits of the data to the Hill equation (Messer et al., 2014). **(B)** Relationship between EC_{50} for Ca^{2+}-activation of thin filaments and TnI bisphosphorylation. EC_{50} for thin filaments containing human heart Tn was plotted against the level of TnI bis-phosphorylation. EC_{50} was measured by IVMA and bis-phosphorylation of TnI (approximates to phosphorylation at Ser22 and 23) was measured by phosphate affinity SDS-PAGE. D, donor heart Tn, XI donor Tn with TnI exchanged, XI:D mixed donor and cTnI-exchanged donor, XI P PKA-treated cTnI-exchanged donor, D P PKA treated donor heart Tn. The gray band corresponds to the phosphorylation level range of human donor and wild-type mouse Tn, see **Figure 1B** (Memo et al., 2013).

recent studies have directly shown the relationship between phosphorylation and Ca^{2+}-sensitivity. A study by Messer et al. used the *in vitro* motility assay (IVMA) with isolated human cardiac Tn in reconstituted thin filaments. By manipulating the level of Tn phosphorylation and then measuring the level using phosphate affinity SDS-PAGE (Phos-Tags) (Messer et al., 2009), a consistent relationship between phosphorylation level and Ca^{2+}-sensitivity was found (Memo et al., 2013) (**Figure 2B**). A similar study by Kooij et al. measured the force in individual cardiomyocytes and found a similar relationship between TnI phosphorylation at Ser22/23 and Ca^{2+}-sensitivity (Kooij et al., 2010). A reduced level of cTnI phosphorylation has been observed in end-stage failing hearts and this correlates with the increased Ca^{2+}-sensitivity seen when failing hearts were compared to donor hearts (**Figure 2A**) (Wolff et al., 1995; Bodor et al., 1997; Van Der Velden et al., 2003; Messer et al., 2007).

THE DISCOVERY OF UNCOUPLING IN FAMILIAL CARDIOMYOPATHIES

Initial investigations into the functional consequences of cardiomyopathy mutations did not consider the role of TnI phosphorylation, but when this was investigated, uncoupling was immediately apparent. Uncoupling was first reported in a series of studies from Kornelia Jaquet's laboratory. Deng et al. studied the cTnI HCM mutation R145G and compared phosphorylated and unphosphorylated recombinant R145G mutant Tn in reconstituted thin filaments regulating actomyosin ATPase. The authors found that the shift in pCa_{50} due to bisphosphorylation, observed with wild-type Tn, was not statistically significant (Deng et al., 2001). Later, two other HCM-causing mutations in cTnI, G203S, and K206Q, were also shown to uncouple, although the effect with G203S was only partial (Deng et al., 2003). A study on the cTnI HCM mutation R21C found that the Ca^{2+}-sensitivity decrease due to PKA phosphorylation was smaller when compared to wild-type (Gomes et al., 2005). A similar study on the cTnC HCM mutation L29Q also found that the Ca^{2+}-sensitivity (measured by both actomyosin ATPase activity and IVMA) was not affected by PKA phosphorylation of cTnI (Schmidtmann et al., 2005). In fact, this study was the first to suggest that the mutation hindered the transduction of the phosphorylation signal from TnI to TnC. Dong et al. have investigated the effects of cTnI phosphorylation on the kinetics of Ca^{2+} regulation of Tn both in wild-type and mutant Tn (Dong et al., 2007). The authors not only looked at the HCM-causing L29Q mutation in TnC but also the DCM-causing mutation TnC G159D and found that both mutations inhibited the ability of PKA phosphorylation of cTnI to reduce Ca^{2+}-sensitivity and speed up Ca^{2+} dissociation (Dong et al., 2008).

The DCM-causing TnC G159D mutation is one of the best characterized clinically (Mogensen et al., 2004; Kaski et al., 2007) and the uncoupling phenomenon was also investigated in two further studies. Biesiadecki et al. reported that the cTnC G159D mutation, exchanged into skinned mouse cardiac fibers, had no direct effect on the myofilament response to Ca^{2+} but it blunted the phosphorylation-dependent change in Ca^{2+} sensitive tension development without altering cross-bridge cycling rate (Biesiadecki et al., 2007). Dyer et al., investigated Tn containing the TnC G159D mutation in mutant Tn isolated from an explanted heart muscle sample in comparison with donor heart Tn using IVMA and similarly found that, unlike donor heart, Ca^{2+}-sensitivity and maximum sliding speed of thin filaments containing G159D Tn were not sensitive

to changes in TnI phosphorylation levels (Dyer et al., 2007, 2009).

These seminal studies on uncoupling investigated mutations in the regions of TnI and TnC that could be directly involved in the phosphorylation-dependent interaction that modulates Ca^{2+}-sensitivity. However, subsequent studies showed that mutations in any protein of the thin filament can induce uncoupling, including actin (ACTC E361G and E99K mutations) tropomyosin (E40K, E54K, and D230N mutations) and troponin T (TnT) (4 mutations recorded to date) in addition to 5 mutations in cTnC and 5 mutations in TnI. The currently known mutations causing uncoupling are summarized in **Table 1**. Thus, uncoupling may be induced by indirect allosteric effects of mutations anywhere within the thin filament and uncoupling seems to be correlated with mutations identified as causing cardiomyopathies.

UNCOUPLING AS A PRIMARY CAUSE OF FAMILIAL DILATED CARDIOMYOPATHY

The recent study by Memo et al. (2013) investigated the uncoupling phenomenon in thin filaments containing a wide range of mutations associated with familial DCM, using the IVMA to measure myofilament Ca^{2+}-sensitivity. It was found that when TnI was fully phosphorylated, the mutations had different effects on Ca^{2+}-sensitivity of thin filaments compared to non-failing; some increased Ca^{2+}-sensitivity (cTnT R141W and ΔK210, cTnI3 K36Q and α-Tropomyosin E40K), some decreased it (α-Tropomyosin D230N, cTnC G159D) whereas for α-actin E361G and α-Tropomyosin E54K there was no change in Ca^{2+}-sensitivity. This confirmed that the simple hypothesis that Ca^{2+}-sensitivity is always reduced by DCM-causing mutations, that we and others had proposed, is no longer tenable (Chang and Potter, 2005; Mirza et al., 2005; Morimoto, 2008). In contrast, when the Ca^{2+}-sensitivity of thin filaments containing phosphorylated and unphosphorylated TnI were compared, it was found that incorporation of any of these mutations caused uncoupling (Memo et al., 2013) (**Figure 3**).

Another study found uncoupling in rare TnC variants identified in DCM: cTnC Y5H, M103I, and I148V either decreased or abolished the effects of PKA phosphorylation on Ca^{2+}-sensitivity (Pinto et al., 2011). Since all the known DCM-causing mutations in thin filament proteins have now been shown to cause uncoupling, whilst having a very variable effect on absolute Ca^{2+}-sensitivity and no DCM mutation has been demonstrated to have normal coupling, there is a strong case for uncoupling to be causative of DCM due to mutations of thin filament components. Thus, a blunting of the heart's response to β-adrenergic stimulation seems to be necessary and sufficient to generate the DCM phenotype. Mechanisms and physiological consequences of uncoupling are discussed in detail later in this review.

UNCOUPLING IS A COMMON FEATURE OF CARDIOMYOPATHIES

Uncoupling is widespread, not only is it observed with mutations that cause familial DCM, it is also observed with mutations that cause hypertrophic cardiomyopathy (HCM). The HCM phenotype has been generally thought to be due to mutations

Table 1 | Mutations that have been reported to cause uncoupling.

Mutation	Effect of mutation on Ca^{2+}-sensitivity	Measurement method	Publication
DCM			
ACTC E361G	No difference	IVMA	Song et al., 2010; Memo et al., 2013
TPM1 E54K	No difference	IVMA	Memo et al., 2013
TPM1 E40K	Decrease	IVMA	Memo et al., 2013
TPM1 D230N	Increase	IVMA	Memo et al., 2013
TNNC1 G159D	Increase	IVMA/Ca binding	Biesiadecki et al., 2007; Dong et al., 2008; Dyer et al., 2009; Memo et al., 2013
TNNC1 Y5H	Decrease	Skinned fiber	Pinto et al., 2011
TNNC1 M103I	Decrease	Skinned fiber	Pinto et al., 2011
TNNC1 I148V	Decrease	Skinned fiber	Pinto et al., 2011
TNNT2 ΔK210	Decrease	IVMA/Skinned fiber	Du et al., 2007; Inoue et al., 2013; Memo et al., 2013
TNNT2 R141W	Decrease	IVMA	Memo et al., 2013
TNNI3 K36Q	Decrease	IVMA/ATPase	Carballo et al., 2009; Memo et al., 2013
HCM			
ACTC E99K	Increase	IVMA	Song et al., 2011
TPM1 E180G	Increase	Skinned fiber	Alves et al., 2014
TNNC1 L29Q	Increase	Ca binding/ATPase	Schmidtmann et al., 2005; Dong et al., 2008; Li et al., 2013
TNNT2 K280N	Increase	IVMA	Bayliss et al., 2012a
TNNI3 R145G	Increase	IVMA/ATPase	Deng et al., 2001
TNNI3 R21C	Increase	Skinned fiber	Gomes et al., 2005; Wang et al., 2011
TNNI3 G203S	Increase	ATPase/IVMA	Deng et al., 2003
TNNI3 K206Q	Increase	ATPase/IVMA	Deng et al., 2003
TNNT2 R92W	Increase	Cardiac myocytes	Guinto et al., 2009

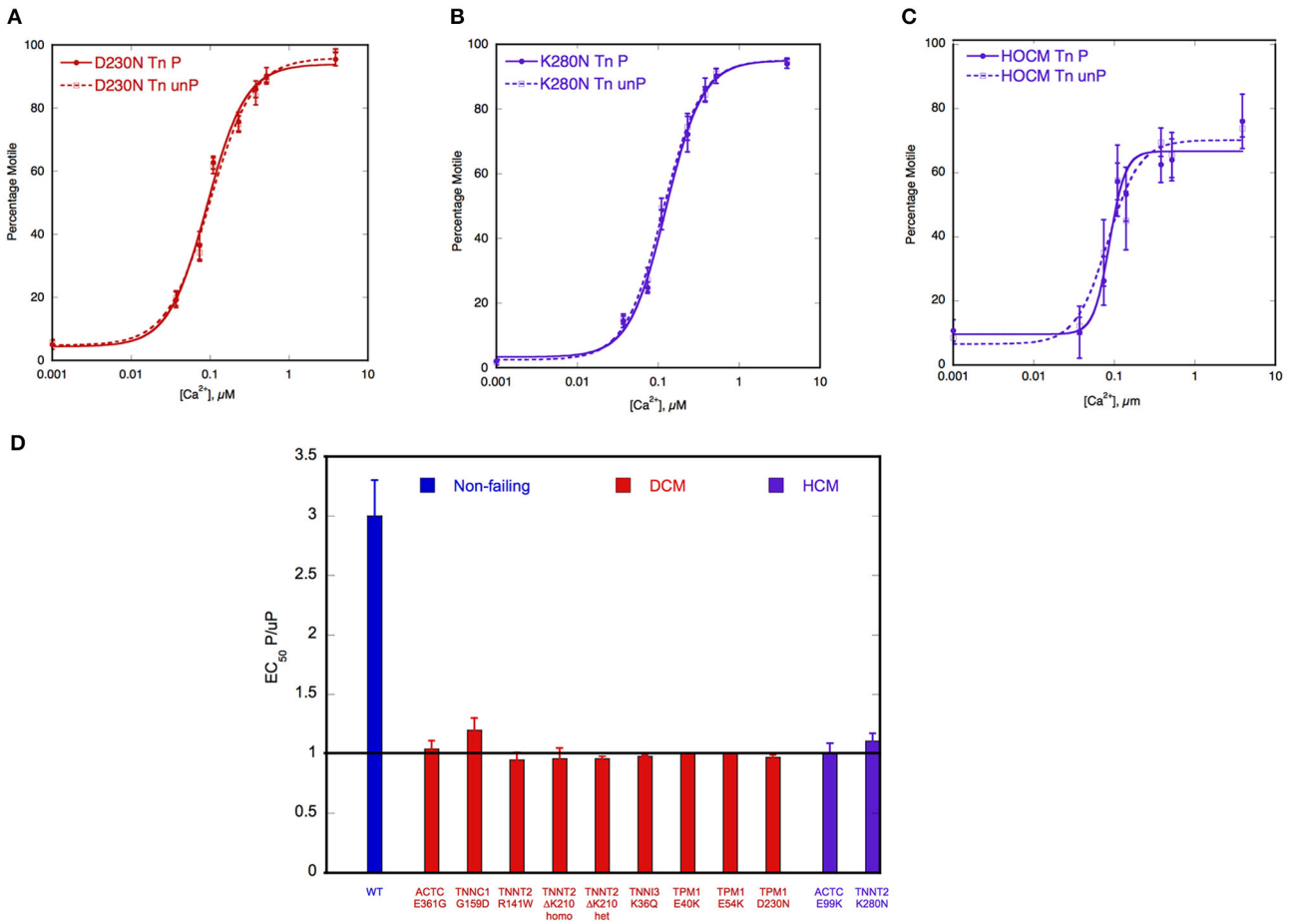

FIGURE 3 | Demonstration of uncoupling due to DCM and HCM mutations and secondary to HOCM. Thin filament motility was measured by motility assay over a range of $[Ca^{2+}]$ in paired cells. The percentage of filaments motile is plotted as a function of $[Ca^{2+}]$ for a representative experiment. Solid lines and points, phosphorylated thin filaments, dotted line and open points, unphosphorylated thin filaments (obtained by phosphatase treatment). The points ± s.e.m. are the mean of four determinations of percentage motile measured in one motility cell. The curves are fits of the data to the Hill equation. **(A)** Natively phosphorylated and unphosphorylated human donor heart Tn with DCM related α- tropomyosin D230N (100%) and rabbit skeletal muscle α-actin (Memo et al., 2013). **(B)** Natively phosphorylated and unphosphorylated human donor heart Tn with exchanged recombinant HCM related TnT K280N, human heart tropomyosin and rabbit skeletal muscle α-actin (Messer et al., 2014). **(C)** Thin filaments containing Tn from a HOCM heart (0.1 mol Pi/mol TnI) or protein kinase A-treated HOCM heart Tn (1.6 mol Pi/mol TnI) (Bayliss et al., 2012b). **(D)** EC_{50} of phosphorylated Tn relative to EC_{50} of unphosphorylated Tn is plotted for wild-type thin filaments and thin filaments containing DCM and HCM-causing mutations. Error bars show s.e.m. of up to 7 replicate comparative measurements (Memo et al., 2013; Messer et al., 2014).

increasing myofilament Ca^{2+}-sensitivity, but it is possible that uncoupling is also characteristic of HCM (Marston, 2011). In addition to the early reports of HCM-causing TnI mutations, described above, uncoupling has also been demonstrated in cTnT R92W (Guinto et al., 2009), cTnT K280N (Messer et al., 2012), α-Tropomyosin E180G (Alves et al., 2014), cardiac actin E99K (Song et al., 2011) and cTnI R21C (Wang et al., 2011) (see **Table 1**). The situation is less clear-cut in studies using human heart samples; Sequeira et al. (2013) reported that some HCM mutations were uncoupled, but others showed a partial decrease in Ca^{2+}-sensitivity when phosphorylated indicating that uncoupling is not necessarily an all-or-nothing effect in human heart but may be graded. Relevant to these observations is the report that in human heart samples the effect of phosphorylation on EC_{50} was dependent upon background phosphorylation levels of other myofilament proteins (Kooij et al., 2010).

Uncoupling has been demonstrated to occur as a secondary effect unrelated to any mutation. In the obstructive variant of HCM (HOCM) the hypertrophied interventricular septum causes LVOTO (left ventricular outflow tract obstruction) and pressure overload. Several abnormalities in the contractile proteins in septal tissue from HOCM patients have been observed including; low phosphorylation levels of TnI and MyBP-C (Messer et al., 2009; Copeland et al., 2010b), differences in actin isoform expression (Copeland et al., 2010a) and loss of function in myosin (Jacques et al., 2008). Most of these abnormalities are shared with end-stage failing heart, but the Ca^{2+}-sensitivity of Tn from HOCM samples, studied by IVMA, was not as expected from its low TnI phosphorylation level and

this was found to be due to uncoupling of the relationship between Ca^{2+}-sensitivity and TnI phosphorylation (Gallon et al., 2007; Jacques et al., 2008; Bayliss et al., 2012b). Uncoupling was demonstrated directly by comparing HOCM Tn with PKA-treated HOCM Tn to bring phosphorylation up to the same level as donor heart Tn. There was no change in Ca^{2+}-sensitivity (**Figures 3C,D**). This uncoupling was independent of the mutation causing HCM and was even observed when no mutation was identified. Exchange experiments were carried out to identify which component of the Tn complex was responsible for the uncoupling and the abnormality was shown to be in TnT, although no covalent modifications were found (Bayliss et al., 2012b). This uncoupling in HOCM may be related to the severe pressure overload that patients having myectomy operations exhibit and therefore it is possible that the uncoupling is caused by the pressure overload itself. It would, for instance, be interesting to look at aortic stenosis samples where the patients have pressure overload but not HCM (Marston et al., 2012).

The occurrence of uncoupling in other types of cardiomyopathy has not been tested; it is clear that in most cases of idiopathic DCM, Ca^{2+}-sensitivity is fully coupled to the level of TnI phosphorylation (Messer et al., 2007). On the other hand, it is possible that mutations in sarcomeric proteins that are not part of the contractile apparatus, such as titin or Z-line proteins, also undergo uncoupling, since these can show a blunted response to β-adrenergic stimulation *in vitro* that is characteristic of uncoupling. Recent studies have shown a blunted β-adrenergic response in MLP W4R and TCAP KO mice (Knoell et al., 2010, 2011) and uncoupling could be inferred from experiments on a mouse model with a titin mutation (Gramlich et al., 2009).

UNCOUPLING CAN BE INDUCED BY SMALL MOLECULES AND PHOSPHORYLATION

The key to the modulation of Ca^{2+}-sensitivity by cTnI phosphorylation is the interaction of the N-terminal peptide 1–29 of cTnI with TnC, therefore it may be possible to induce uncoupling with small molecules that bind to TnC and change the Ca^{2+}-sensitivity (Ca^{2+} sensitizers or desensitizers). Of particular interest are the Ca^{2+}-sensitizing drugs EMD57033 and Bepridil (Li et al., 2008). When tested in the IVMA, with thin filaments containing native human Tn, both these drugs increased Ca^{2+}-sensitivity by 2–3-fold and at the same time uncoupled Ca^{2+}-sensitivity from TnI phosphorylation (see **Figure 4A**). The effect of these drugs is therefore quite analogous to the effect of many HCM-causing mutations (**Table 1**, **Figures 3**, **4**).

In contrast EGCG [(−)-Epigallocatechin 3-Gallate], is a Ca^{2+}-desensitizer that binds at a site formed by the TnI-TnC complex and it has been found to enhance the binding of the N terminal helix1 of TnI to TnC (Robertson et al., 2009; Tadano et al., 2010; Botten et al., 2013). When tested in the IVMA, with thin filaments containing native human Tn, EGCG decreased Ca^{2+}-sensitivity both in wild-type and in DCM-mutant thin filaments and in both phosphorylated and unphosphorylated filaments, thus preserving coupling (**Figure 4B**). Most strikingly it is also capable of restoring coupling to thin filaments containing mutations that induce uncoupling (Messer et al., 2014).

Another perturbation that can induce uncoupling is phosphorylation of troponin subunits. A study by Nixon et al. found that phosphorylation of cTnI at Ser 150 by AMP-activated protein kinase (AMPK) increased Ca^{2+}-sensitivity of isolated cardiac myofibrils. It also blunted the PKA-dependent calcium desensitization induced by phosphorylation at Ser 22/23 and uncoupled

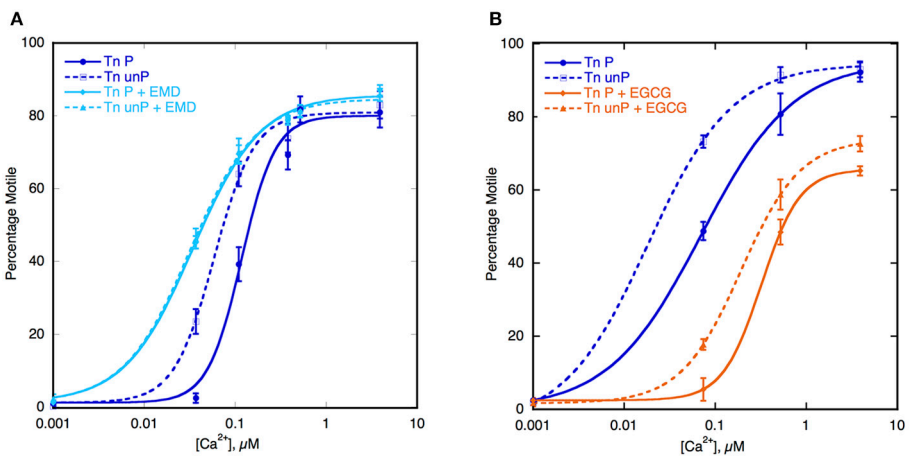

FIGURE 4 | Effect of Ca^{2+}-sensitizers and desensitizers on coupling in thin filaments. Thin filament motility was measured by motility assay over a range of $[Ca^{2+}]$ in paired cells. The percentage of filaments motile is plotted as a function of $[Ca^{2+}]$ for representative experiments. Solid lines and points, phosphorylated thin filaments, dotted line and open points, unphosphorylated thin filaments (obtained by phosphatase treatment). The points ± s.e.m. are the mean of four determinations of percentage motile measured in one motility cell. The curves are fits of the data to the Hill equation. **(A)** The effect of the Ca^{2+}-sensitizer EMD57033 (EMD). In dark blue, thin filaments in the absence of EMD and in light blue are thin filaments in the presence of 30 μM EMD (Messer et al., 2014). **(B)** The effect of the Ca^{2+}-desensitizer EGCG. In dark blue, thin filaments in the absence of EGCG and in orange, thin filaments in the presence of 100 μM EGCG (Messer et al., 2014).

the effects of phosphorylation from β-adrenergic stimulation (Nixon et al., 2012).

MOLECULAR MECHANISM OF UNCOUPLING

The phosphorylation dependence of cardiac Tn Ca^{2+} regulation is due to the interaction of a 30 amino acid N-terminal extension of TnI, containing the PKA-specific phosphorylation sites at Ser 22 and 23, with cTnC (Solaro et al., 2008).

The N-terminal segment of cTnI interacts with the regulatory Ca^{2+}-binding loop in the N-terminal lobe of TnC in the unphosphorylated state. This affects the cTnC interaction with both the regulatory Ca^{2+} and the TnI switch peptide (144–160) (Li et al., 2008). When TnI is unphosphorylated there is a weak ionic bond between the N terminal and the regulatory Ca^{2+}-binding EF hand of TnC (Howarth et al., 2007). When Ser 22 and 23 are phosphorylated the binding is further weakened (Keane et al., 1990; Ferrieres et al., 2000; Ward et al., 2004a,b; Baryshnikova et al., 2008). Therefore, the unphosphorylated state of TnI is a special state, which is destabilized by phosphorylation, resulting in a lower Ca^{2+}-sensitivity and higher rate of Ca^{2+} dissociation. Since the initial interaction is quite weak, the loss of the interaction produces only a 2–3-fold change in Ca^{2+}-sensitivity and the rate of Ca^{2+} dissociation. This appears to be sufficient to generate the lusitropic effect since heart rate also increases by a maximum of 2–3-fold.

We propose that the unphosphorylated state can also be disrupted by mutations or other alterations in any component of the thin filament resulting in the same destabilized state for both phosphorylated and unphosphorylated Tn; in this way uncoupling could be considered as a default state in cardiomyopathies (Liu et al., 2012; Memo et al., 2013).

Recent studies have begun to determine the structure of TnI in complex with TnC in the phosphorylated and unphosphorylated states that forms the basis of the coupling mechanism. X-ray crystallography has defined the core structure of Tn but mobile segments, including the N-terminus of TnI, were not present in the crystal structure (Takeda et al., 2003). NMR studies have defined the structure of the missing peptides based on their binary complexes. A best guess structure of the N-terminal peptide conformation in the phosphorylated and unphosphorylated states was proposed by building these structures onto the Tn core structure (Howarth et al., 2007). Molecular dynamics simulations of the entire Tn molecule have further refined these structures.

The molecular dynamics simulations indicate a possible structure of TnI N-terminus interacting with TnC (Gould et al., 2014) (**Figure 5**). The most striking feature is that in the presence of Ca^{2+}, the unphosphorylated N terminus of TnI settles in a position looping over the N-terminus of TnC within 50 ns of the start of simulation. The peptide is mostly very mobile and unstructured except for ^{20}RRSS^{24} that was consistently close to TnC for up to 1 μs of simulation. These four amino acids also exhibited a lower root mean square fluctuation (RMSF) than surrounding residues. When the Ser 22 and 23 were phosphorylated *in silico*, the two serines become more mobile relative to arginines 20 and 21 suggesting a weakening of their interaction with TnC. In addition, Ca^{2+} becomes more exposed to solvent and the interaction of the "switch peptide" with TnC is altered. Thus,

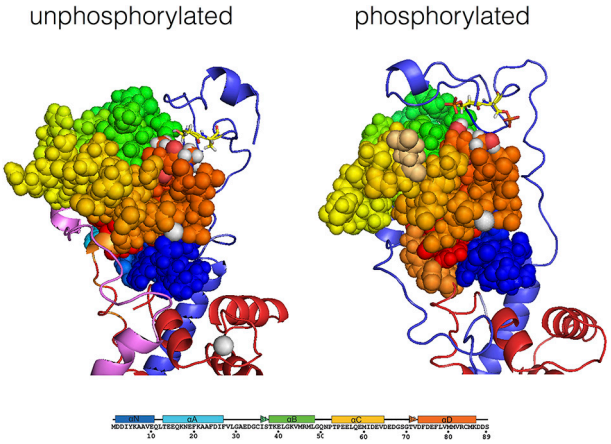

FIGURE 5 | Modulation of the interaction of TnI Ser 22 and 23 with the N terminal lobe of TnC by phosphorylation, determined by molecular dynamics simulations. Average structure after 700 ns simulation for unphosphorylated Tn, left. The Tn was phosphorylated *in silico* after 550 ns of simulation and the average structure after a further 200 ns is shown, right. The N-terminal lobe of cTnC is shown as spheres with color coding along the peptide chain as indicated by the sequence below; Ser 69 and Thr 71 are colored according to their atoms (oxygen red, hydrogen white). The backbone of cTnI N-terminus is shown in blue; Ser 22 and 23 are shown in yellow in stick representation. Molecular dynamics suggests that with unphosphorylated Tn there is a close interaction of Ser 22 and 23 with cTnC Ser 69 and Thr 71 which is much less prominent when phosphorylated (Gould et al., 2014).

coupling can be accounted for by the formation of a weak ionic complex between TnC and TnI Ser 22 and 23 that is destabilized by phosphorylation.

It is interesting to note that when the DCM-causing mutation K36Q in cTnI was introduced in the presence of Ca^{2+}, the simulation showed that Ser 22 and 23 no longer interacted closely with cTnC, in accord with our hypothesis that the Ca^{2+}-cTnC-cTnI N terminus interaction is unique and is destabilized directly by phosphorylation and also allosterically by mutations and other perturbations. Molecular dynamics simulations also show that phosphorylation is associated with long-range conformational changes in Tn and associated proteins that provides a mechanism for mutations in TnT, tropomyosin and actin to induce uncoupling (Manning et al., 2011). It should be noted that this mechanism for uncoupling is the opposite to one proposed by Biesiadecki et al. (2007) where the DCM mutation TnC G159D was proposed to *stabilize* the interaction of Ser 22 and 23 with cTnC when *phosphorylated*.

PHYSIOLOGICAL RELEVANCE OF UNCOUPLING

How is uncoupling of the relationship between TnI phosphorylation and myofilament Ca^{2+}-sensitivity related to the DCM phenotype associated with such mutations? We think it is likely that uncoupling would compromise the heart's response to β1-adrenergic stimulation leading to a reduced cardiac reserve.

The effects of cardiomyopathy-causing mutations on the heart's response to β-adrenergic agonists have not been routinely measured. However, the studies of Song et al. on the ACTC

mutations E361G and E99K investigated this question and clearly showed that the response to dobutamine stimulation was blunted (Song et al., 2010, 2011; Marston et al., 2013) (**Figure 6**). The effect of adrenergic agonists was tested in several other models of HCM and DCM (see **Table 2**) and they all showed blunting of the response in at least one parameter. It is particularly interesting to note the blunting effect of the muscle LIM protein (MLP) W4R mutation associated with DCM (Knoell et al., 2010), since this protein is a component of the Z-line and is not known to have any function in regulating the contractile apparatus: in this case the putative uncoupling might be a secondary effect similar to that seen in myectomy samples. Nguyen et al. found that young, pre-hypertrophic *TNNI3* G203S HCM transgenic mice lacked the normal physiological response to chronic intense swimming exercise, compatible with a blunted response to adrenergic stimulation independent of disease phenotype (Nguyen et al., 2007).

This loss of cardiac reserve is likely to predispose the heart to failure when under stress. It is notable that most mouse models of DCM-causing mutations show little or no phenotype at rest (ACTC E361G, TNNT2 ΔK210, MYBPC3 knock-in (KI) (see **Table 2**) and TTN KI Gramlich et al., 2009), especially when heterozygous like the patients with these mutations. This is compatible with the primary defect being in the response to β-adrenergic stimulation that is absent at rest. Several experiments have addressed this question by exposing transgenic mice with HCM or DCM-causing mutations to chronic stress by pressure overload (TAC) or by chronic stimulation with isoprenaline or angiotensin II. In general, they demonstrate that the mutant-containing mice show earlier and more severe symptoms of

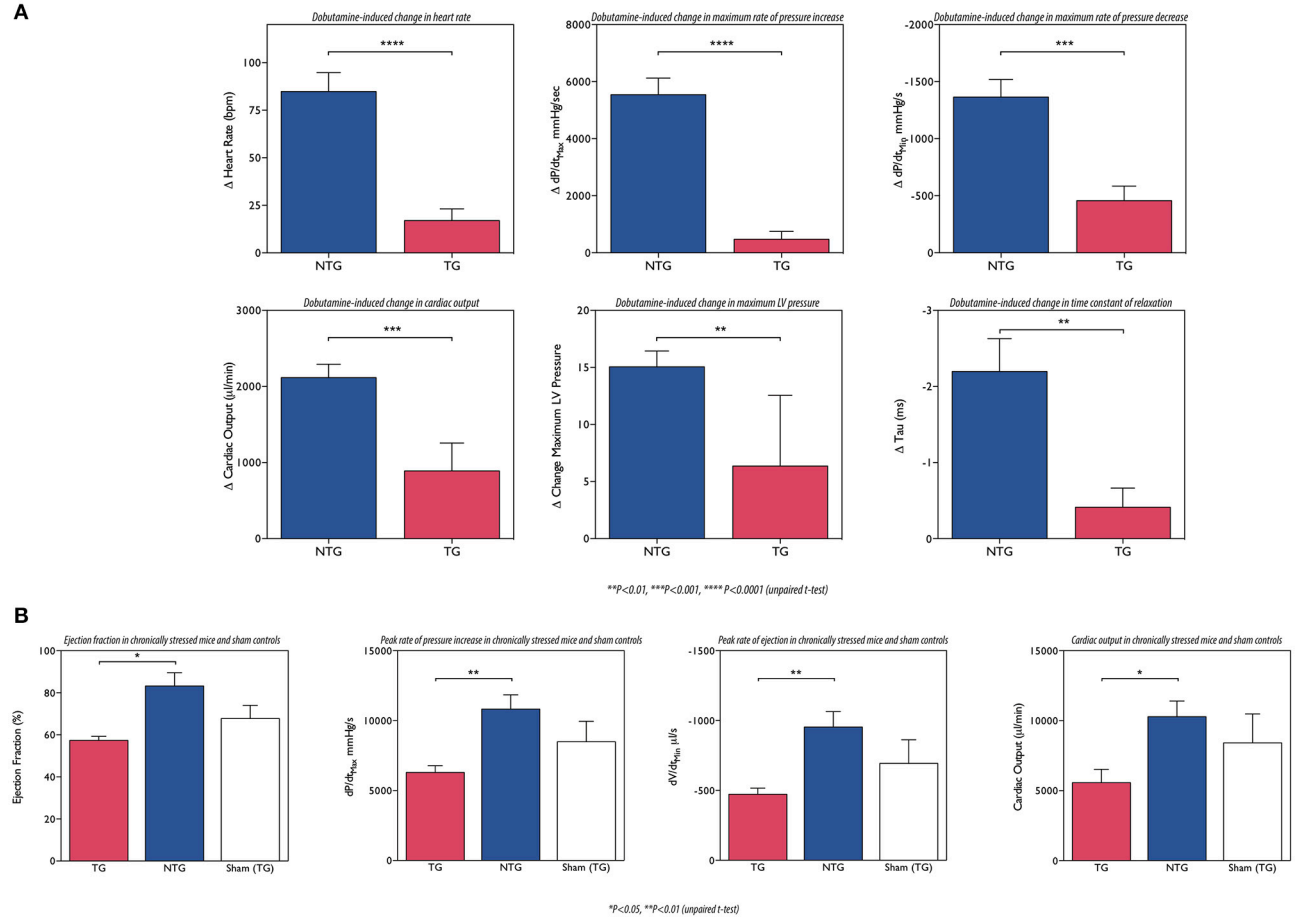

FIGURE 6 | (A) The ACTC E361G mutation blunts the lusitropic, inotropic and chronotropic response to dobutamine *in vivo*: mice were examined using a pressure volume catheter. The dobutamine-induced acceleration of relaxation (peak rate of relaxation and time constant of relaxation) was significantly lower in ACTC E361G mice indicating a blunted lusitropic response. The inotropic response to dobutamine was also blunted in ACTC E361G mice as indicated by a blunted increase in maximum pressure and the peak rate of pressure increase. Furthermore, dobutamine-induced increase in heart rate (chronotropic effect) was also blunted. Taken together with the attenuated increase in cardiac output these data suggest a significantly diminished cardiac reserve in ACTC E361G mice *in vivo* (Wilkinson, 2014). **(B)** The ACTC E361G mutation predisposes TG mice to systolic heart failure under chronic stress: chronic stress was achieved using subcutaneously implanted Alzet osmotic mini pumps to deliver a 4-week infusion of angiotensin II (2 mg/kgBW/day, in saline). Sham controls received mini pumps carrying saline only. At the end of the 4-week infusion period the mice were examined using a pressure volume catheter. The chronic stress treatment evoked symptoms of systolic heart failure in ACTC E361G mice, characterized by decreased ejection fraction, cardiac output and maximum rates of contraction and ejection compared to NTG mice (Wilkinson, 2014).

Table 2 | Mutations reported to blunt response to β-agonists.

Mutation	Measurement method, agonist and (parameters blunted)	Publication
ACTC E361G	Echocardiography and cine MRI Dobutamine stimulation (mri: EF, HR,COEcho: wall thickening and CO)	Song et al., 2010
ACTC E99K	Echocardiography Dobutamine stimulation (heart rate, wall thickening, and fractional shortening)	Song et al., 2011
TPM1 E54K	Echocardiography Isoprenaline stimulation (+dP/dt, −dP/dt)	Rajan et al., 2007
TNNT2 ΔK210	PV catheter Isoprenaline stimulation (LVESP)	Du et al., 2007
TNNT2 R173W	iPSC myocyte cluster contraction, noradrenaline stimulation (beating rate)	Sun et al., 2012
TNNT2 ΔE160	Isolated heart isovolumic pressure recording, Dobutamine stimulation (−dP/dt)	Moore et al., 2013
TNNT2 R92Q	Isolated heart isovolumic pressure recording, Dobutamine stimulation (SP, +dP/dt, −dP/dt, DevP)	Javadpour et al., 2003
TNNT2 I79N	Echocardiography, Isoprenaline stimulation (FS)	Knollmann et al., 2001
MYBPC3 KI	Engineered heart tissue Isoprenaline stimulation (ΔForce)	Stöhr et al., 2013
MYBPC3 KO	PV catheter Dobutamine stimulation (dP/dt_{max})	Carrier et al., 2004
MLP W4R	Echocardiography and PV catheter Adrenaline stimulation (ESV,EDV and LV contractility)	Knoell et al., 2010

dilation and heart failure than wild-type. For instance: Wilkinson applied chronic stress by angiotensin II infusion (2 mg/KgBV/da by osmotic minipumps). After 4 weeks *ACTC* E361G DCM mice had significantly lower dP/dtmax, cardiac output and ejection fraction, compared to NTG (Wilkinson, 2014) (**Figure 6**). Similarly Gramlich et al. studied a titin mutation that causes DCM (TTN 2-bp insertion mutation (c.43628insAT)) (Gramlich et al., 2009). The authors induced cardiac hypertrophy by a 2-week infusion with angiotensin II. Both wild-type and KI mice developed cardiac hypertrophy after 1 week. After 2 weeks, hypertrophy in wild-type animals was further increased, whereas their heterozygous littermates showed left ventricular dilatation with impaired systolic function and increased myocardial fibrosis.

Whilst it is recognized that the uncoupling phenomenon provides a satisfactory molecular mechanism for thin-filament based mutations that cause DCM, the role of uncoupling in HCM is not as clear. Since Ca^{2+}-sensitivity has been observed to be increased 2–3-fold in virtually every HCM mutation investigated (Marston, 2011), it is likely that this is the primary trigger for the HCM phenotype and that it dominates over the uncoupling phenomenon. It is possible that increased Ca^{2+}-sensitivity and uncoupling are linked properties of thin filaments since the Ca^{2+}-sensitizers EMD57033 and bepridil are also uncouplers and the coupling constant is generally greatest when Ca^{2+}-sensitivity is lowest. It will be very interesting to investigate whether any HCM mutations (or Ca^{2+}-sensitizers) can be found that increase Ca^{2+}-sensitivity but do not uncouple.

CLINICAL RELEVANCE OF UNCOUPLING

Uncoupling inevitably leads to blunting of the response to β-adrenergic agonists but the lack of response to dobutamine is of course not only due to uncoupling. Heart failure is associated also with desensitization of β-receptors, such that the activation of PKA is attenuated, or the activity of phosphatase increased whilst coupling is intact (Houser and Margulies, 2003; Champion, 2005; El-Armouche et al., 2007; Messer et al., 2007).

Patient studies from the 80 and 90 s using echocardiography showed that IDCM and HCM patients could be classified into dobutamine responders and non-responders and that the non-responders have a poor prognosis whilst the responders can respond to treatment (Borow et al., 1988; Dubois-Randé et al., 1992; Naqvi et al., 1999) These studies predate the discovery of mutations in contractile proteins that cause familial DCM as well as the discovery of uncoupling, but given our current understanding of FDCM we would predict that the dobutamine non-responders correspond to those patients with FDCM mutations causing uncoupling and hence presumably the dobutamine response would be of clinical interest as a potential diagnostic to distinguish familial DCM from acquired IDCM.

This dichotomy would suggest that different treatments would be optimum for the two cases. Drugs are available that impact on β-receptors but so far no drugs act positively on the TnI-phosphorylation-Ca^{2+}-sensitivity coupling mechanism. Our recent finding that EGCG is capable of recoupling *in vitro*, although it has different effects *in vivo* (Feng et al., 2012), suggests that specific modulation of the coupling process may be a viable target for future therapy.

ACKNOWLEDGMENT

This work was supported by grants from The British Heart Foundation (RG/11/20/29266 and FS/12/29568).

REFERENCES

Al-Hillawi, E., Bhandari, D. G., Trayer, H. R., and Trayer, I. P. (1995). The effects of phosphorylation of cardiac troponin-I on its interactions with actin and troponin-C. *Eur. J. Biochem.* 228, 962–970. doi: 10.1111/j.1432-1033.1995.tb20347.x

Al-Hillawi, E., Chilton, D., Trayer, I. P., and Cummins, P. (1998). Phosphorylation-specific antibodies for human cardiac troponin-I. *Eur. J. Biochem.* 256, 535–540. doi: 10.1046/j.1432-1327.1998.2560535.x

Alves, M. L., Dias, F. A. L., Gaffin, R. D., Simon, J. N., Montminy, E. M., and Wolska, B. M. (2014). Desensitization of myofilaments to Ca2+ as a therapeutic target for hypertrophic cardiomyopathy with mutations in thin filament proteins. *Circ. Cardiovasc. Gen.* 7, 132–143. doi: 10.1161/CIRCGENETICS.113.000324

Ardelt, P., Dorka, P., Jaquet, K., Heilmeyer, L. M. G., Kortke, H., Korfer, R., et al. (1998). Microanalysis and distribution of cardiac troponin I phosphospecies in heart areas. *Biol. Chem.* 379, 341–347. doi: 10.1515/bchm.1998.379.3.341

Ayaz-Guner, S., Zhang, J., Li, L., Walker, J. W., and Ge, Y. (2009). *In vivo* phosphorylation site mapping in mouse cardiac troponin i by high resolution top-down electron capture dissociation mass spectrometry: Ser22/23 are the only sites basally phosphorylated. *Biochemistry* 48, 8161–8170. doi: 10.1021/bi900739f

Bailin, G. (1979). Phosphorylation of a bovine cardiac actin complex. *Am. J. Physiol.* 236, C41–C46.

Baryshnikova, O. K., Li, M. X., and Sykes, B. D. (2008). Modulation of cardiac troponin C function by the cardiac-specific N-terminus of troponin I: influence of PKA phosphorylation and involvement in cardiomyopathies. *J. Mol. Biol.* 375, 735–751. doi: 10.1016/j.jmb.2007.10.062

Bayliss, C., Messer, A., Leung, M.-C., Ward, D., Van Der Velden, J., Poggesi, C., et al. (2012a). *Functional investigation of troponin with the homozygous HCM mutation, TNNT2 K280M, obtained from an explanted heart. *Cardiovasc. Res.* 93, S107. doi: 10.1093/cvr/cvr336

Bayliss, C. R., Jacques, A. M., Leung, M.-C., Ward, D. G., Redwood, C. S., Gallon, C. E., et al. (2012b). Myofibrillar Ca2+-sensitivity is uncoupled from troponin i phosphorylation in hypertrophic obstructive cardiomyopathy due to abnormal troponin T. *Cardiovasc. Res.* 97, 500–508. doi: 10.1093/cvr/cvs322

Biesiadecki, B. J., Kobayashi, T., Walker, J. S., John Solaro, R., and De Tombe, P. P. (2007). The troponin C G159D mutation blunts myofilament desensitization induced by troponin I Ser23/24 phosphorylation. *Circ. Res.* 100, 1486–1493. doi: 10.1161/01.RES.0000267744.92677.7f

Bodor, G. S., Oakeley, A. E., Allen, P. D., Crimmins, D. L., Ladenson, J. H., and Anderson, P. A.W. (1997). Troponin I phosphorylation in the normal and failing adult human heart. *Circulation* 96, 1495–1500. doi: 10.1161/01.CIR.96.5.1495

Borow, K. M., Lang, R. M., Neumann, A., Carroll, J. D., and Rajfer, S. I. (1988). Physiologic mechanisms governing hemodynamic responses to positive inotropic therapy in patients with dilated cardiomyopathy. *Circulation* 77, 625–637. doi: 10.1161/01.CIR.77.3.625

Botten, D., Fugallo, G., Fraternali, F., and Molteni, C. (2013). A computational exploration of the interactions of the green tea polyphenol (-)-epigallocatechin 3-gallate with cardiac muscle troponin C. *PLoS ONE* 8:e70556. doi: 10.1371/journal.pone.0070556

Carballo, S., Robinson, P., Otway, R., Fatkin, D., Jongbloed, J. D., De Jonge, N., et al. (2009). Identification and functional characterization of cardiac troponin I as a novel disease gene in autosomal dominant dilated cardiomyopathy. *Circ. Res.* 105, 375–382. doi: 10.1161/CIRCRESAHA.109.196055

Carrier, L., Knoll, R., Vignier, N., Keller, D. I., Bausero, P., Prudhon, B., et al. (2004). Asymmetric septal hypertrophy in heterozygous cMyBP-C null mice. *Cardiovasc. Res.* 63, 293–304. doi: 10.1016/j.cardiores.2004.04.009

Champion, H. C. (2005). Targeting protein phosphatase 1 in heart failure. *Circ. Res.* 96, 708–710. doi: 10.1161/01.RES.0000164359.95588.25

Chang, A. N., and Potter, J. D. (2005). Sarcomeric protein mutations in dilated cardiomyopathy. *Heart Fail. Rev.* 10, 225–235. doi: 10.1007/s10741-005-5252-6

Copeland, O., Nowak, K., Laing, N., Ravenscroft, G., Messer, A. E., Bayliss, C. R., et al. (2010a). Investigation of changes in skeletal muscle alpha-actin expression in normal and pathological human and mouse hearts. *J. Mus. Res. Cell. Motil.* 31, 207–214. doi: 10.1007/s10974-010-9224-7

Copeland, O., Sadayappan, S., Messer, A. E., Stienen, G. J., Velden, J., and Marston, S. B. (2010b). Analysis of cardiac myosin binding protein-C phosphorylation in human heart muscle. *J. Mol. Cell. Cardiol.* 49, 1003–1011. doi: 10.1016/j.yjmcc.2010.09.007

Deng, Y., Schmidtmann, A., Kruse, S., Filatov, V., Heilmeyer, L. M. Jr., Jaquet, K., et al. (2003). Phosphorylation of human cardiac troponin I G203S and K206Q linked to familial hypertrophic cardiomyopathy affects actomyosin interaction in different ways. *J. Mol. Cell. Cardiol.* 35, 1365–1374. doi: 10.1016/j.yjmcc.2003.08.003

Deng, Y., Schmidtmann, A., Redlich, A., Westerdorf, B., Jaquet, K., and Thieleczek, R. (2001). Effects of phosphorylation and mutation R145G on human cardiac troponin I function. *Biochemistry* 40, 14593–14602. doi: 10.1021/bi0115232

Dohet, C., Al-Hillawi, E., Trayer, I. P., and Ruegg, J. C. (1995). Reconstitution of skinned cardiac fibres with human recombinant cardiac troponin-I mutants and troponin-C. *FEBS Lett.* 377, 131–134. doi: 10.1016/0014-5793(95)01319-9

Dong, W. J., Jayasundar, J. J., An, J., Xing, J., and Cheung, H. C. (2007). Effects of PKA phosphorylation of cardiac troponin I and strong crossbridge on conformational transitions of the N-domain of cardiac troponin C in regulated thin filaments. *Biochemistry* 46, 9752–9761. doi: 10.1021/bi700574n

Dong, W., Xing, J., Ouyang, Y., An, J., and Cheung, H. C. (2008). Structural kinetics of Cardiac troponin C mutants linked to familial hypertrophic and dilated cardiomyopathy in troponin complexes. *J. Biol. Chem.* 283, 3424–3432. doi: 10.1074/jbc.M703822200

Du, C. K., Morimoto, S., Nishii, K., Minakami, R., Ohta, M., Tadano, N., et al. (2007). Knock-in mouse model of dilated cardiomyopathy caused by troponin mutation. *Circ. Res.* 101, 185–194. doi: 10.1161/CIRCRESAHA.106.146670

Dubois-Randé, J. L., Merlet, P., Roudot, F., Benvenuti, C., Adnot, S., Hittinger, L., et al. (1992). Beta-adrenergic contractile reserve as a predictor of clinical outcome in patients with idiopathic dilated cardiomyopathy. *Am. Heart J.* 124, 679–685. doi: 10.1016/0002-8703(92)90278-4

Dyer, E., Jacques, A., Hoskins, A., Ward, D., Gallon, C., Messer, A., et al. (2009). Functional analysis of a unique troponin C mutation, Gly159Asp that causes familial dilated cardiomyopathy, studied in explanted heart muscle. *Circ. Heart Fail.*2, 456–464. doi: 10.1161/CIRCHEARTFAILURE.108.818237

Dyer, E., Wells, D., Redwood, C., and Marston, S. B. (2007). **In vitro* motility studies of HCM and DCM mutations in cardiac muscle actin. *Biophys. J.* 92, 481A.

El-Armouche, A., Pohlmann, L., Schlossarek, S., Starbatty, J., Yeh, Y. H., Nattel, S., et al. (2007). Decreased phosphorylation levels of cardiac myosin-binding protein-C in human and experimental heart failure. *J. Mol. Cell. Cardiol.* 43, 223–229. doi: 10.1016/j.yjmcc.2007.05.003

England, P. J. (1976). Studies on the phosphorylation of the inhibitory subunit of troponin during modification of contraction in perfused rat heart. *Biochem. J.* 160, 295–304.

Feng, W., Hwang, H. S., Kryshtal, D. O., Yang, T., Padilla, I. T., Tiwary, A. K., et al. (2012). Coordinated regulation of murine cardiomyocyte contractility by nanomolar (-)-epigallocatechin-3-gallate, the major green tea catechin. *Mol. Pharmacol.* 82, 993–1000. doi: 10.1124/mol.112.079707

Fentzke, R. C., Buck, S. H., Patel, J. R., Lin, H., Wolska, B. M., Stojanovic, M. O., et al. (1999). Impaired cardiomyocyte relaxation and diastolic function in transgenic mice expressing slow skeletal troponin I in the heart. *J. Physiol.* 517, 143–157. doi: 10.1111/j.1469-7793.1999.0143z.x

Ferrieres, G., Pugniere, M., Mani, J. C., Villard, S., Laprade, M., Doutre, P., et al. (2000). Systematic mapping of regions of human cardiac troponin I involved in binding to cardiac troponin C: N- and C-terminal low affinity contributing regions. *FEBS Lett.* 479, 99–105. doi: 10.1016/S0014-5793(00)01881-0

Gallon, C., Jacques, A., Messer, A., Tsang, V., McKenna, W., and Marston, S. (2007). *Altered functions and post-translational modification of contractile proteins in myectomy samples from HOCM patients. *J. Mol. Cell. Cardiol.* 42, S167. doi: 10.1016/j.yjmcc.2007.03.437

Gomes, A. V., Harada, K., and Potter, J. D. (2005). A mutation in the N-terminus of troponin I that is associated with hypertrophic cardiomyopathy affects the Ca(2+)-sensitivity, phosphorylation kinetics and proteolytic susceptibility of troponin. *J. Mol. Cell. Cardiol.* 39, 754–765. doi: 10.1016/j.yjmcc.2005.05.013

Gordon, A. M., Homsher, E., and Regnier, M. (2000). Regulation of contraction in striated muscle. *Physiol. Rev.* 80, 853–924.

Gould, I., Messer, A. E., Papadaki, M., and Marston, S. B. (2014). *Modulation of the interaction between troponin I N-terminal peptide and troponin C by phosphorylation studied by molecular dynamics. *Biophys. J.* 106, 349a.

Gramlich, M., Michely, B., Krohne, C., Heuser, A., Erdmann, B., Klaassen, S., et al. (2009). Stress-induced dilated cardiomyopathy in a knock-in mouse model mimicking human titin-based disease. *J. Mol. Cell. Cardiol.* 47, 352–358. doi: 10.1016/j.yjmcc.2009.04.014

Guinto, P. J., Haim, T. E., Dowell-Martino, C. C., Sibinga, N., and Tardiff, J. C. (2009). Temporal and mutation-specific alterations in Ca2+ homeostasis differentially determine the progression of cTnT-related cardiomyopathies in murine models. *Am. J. Physiol. Heart Circ. Physiol.* 297, H614–H626. doi: 10.1152/ajpheart.01143.2008

Hamdani, N., De Waard, M., Messer, A. E., Boontje, N. M., Kooij, V., Van Dijk, S., et al. (2009). Myofilament dysfunction in cardiac disease from mice to men. *J. Musc. Res. Cell. Motil* 29, 189–201. doi: 10.1007/s10974-008-9160-y

Haworth, R. S., Cuello, F., Herron, T. J., Franzen, G., Kentish, J. C., Gautel, M., et al. (2004). Protein kinase D is a novel mediator of cardiac troponin I phosphorylation and regulates myofilament function. *Circ. Res.* 95, 1091–1099. doi: 10.1161/01.RES.0000149299.34793.3c

Houser, S. R., and Margulies, K. B. (2003). Is depressed myocyte contractility centrally involved in heart failure? *Circ. Res.* 92, 350–358. doi: 10.1161/01.RES.0000060027.40275.A6

Howarth, J. W., Meller, J., Solaro, R. J., Trewhella, J., and Rosevear, P. R. (2007). Phosphorylation-dependent conformational transition of the cardiac specific N-extension of troponin I in cardiac troponin. *J. Mol. Biol.* 373, 706–722. doi: 10.1016/j.jmb.2007.08.035

Inoue, T., Kobirumaki-Shimozawa, F., Kagemoto, T., Fujii, T., Terui, T., Kusakari, Y., et al. (2013). Depressed Frank-Starling mechanism in the left ventricular muscle of the knock-in mouse model of dilated cardiomyopathy with troponin T deletion mutation ΔK210. *J. Mol. Cell. Cardiol.* 63, 69–78. doi: 10.1016/j.yjmcc.2013.07.001

Jacques, A., Briceno, N., Messer, A., Gallon, C., Jalizadeh, S., Garcia, E., et al. (2008). The molecular phenotype of human cardiac myosin associated with hypertrophic obstructive cardiomyopathy. *Cardiovasc. Res.* 79, 481–491. doi: 10.1093/cvr/cvn094

Jacques, A., Hoskins, A., Kentish, J., and Marston, S. B. (2009). From genotype to phenotype: a longitudinal study of a patient with hypertrophic cardiomyopathy due to a mutation in the MYBPC3 gene. *J. Musc. Res. Cell. Motil.* 29, 239–246. doi: 10.1007/s10974-009-9174-0

Javadpour, M. M., Tardiff, J. C., Pinz, I., and Ingwall, J., S. (2003). Decreased energetics in murine hearts bearing the R92Q mutation in cardiac troponin T. *J. Clin. Invest.* 112, 768–775. doi: 10.1172/JCI15967

Jweied, E., Detombe, P., and Buttrick, P. M. (2007). The use of human cardiac tissue in biophysical research: the risks of translation. *J. Mol. Cell. Cardiol.* 42, 722–726. doi: 10.1016/j.yjmcc.2007.02.002

Kaski, J. P., Burch, M., and Elliott, P. M. (2007). Mutations in the cardiac Troponin C gene are a cause of idiopathic dilated cardiomyopathy in childhood. *Cardiol. Young* 17, 675–677. doi: 10.1017/S1047951107001291

Keane, A. M., Trayer, I. P., Levine, B. A., Zeugner, C., and Ruegg, C. J. (1990). Peptide mimetics of an actin-binding site on myosin span two functional domains on actin. *Nature* 344, 265–268. doi: 10.1038/344265a0

Kentish, J. C., McCloskey, D. T., Layland, J., Palmer, S., Leiden, J. M., Martin, A. F., et al. (2001). Phosphorylation of troponin I by protein kinase A accelerates relaxation and crossbridge cycle kinetics in mouse ventricular muscle. *Circ. Res.* 88, 1059–1065. doi: 10.1161/hh1001.091640

Kinoshita, E., Kinoshita-Kikuta, E., Takiyama, K., and Koike, T. (2006). Phosphate-binding tag, a new tool to visualize phosphorylated proteins. *Mol. Cell. Proteomics* 5, 749–757. doi: 10.1074/mcp.T500024-MCP200

Knoell, R., Kostin, S., Klede, S., Savvatis, K., Klinge, L., Stehle, I., et al. (2010). A common MLP (muscle LIM protein) variant is associated with cardiomyopathy. *Circ. Res.* 106, 695–704. doi: 10.1161/CIRCRESAHA.109.206243

Knoell, R., Linke, W. A., Zou, P., Miocic, S., Kostin, S., Buyandelger, B., et al. (2011). Telethonin deficiency is associated with maladaptation to biomechanical stress in the mammalian heart. *Circ. Res.* 109, 758–769. doi: 10.1161/CIRCRESAHA.111.245787

Knollmann, B. C., Blatt, S. A., Horton, K., De Freitas, F., Miller, T., Bell, M., et al. (2001). Inotropic stimulation induces cardiac dysfunction in transgenic mice expressing a troponin T (I79N) mutation linked to familial hypertrophic cardiomyopathy. *J. Biol. Chem.* 276, 10039–10048. doi: 10.1074/jbc.M006745200

Kobayashi, T., Yang, X., Walker, L. A., Van Breemen, R. B., and Solaro, R. J. (2005). A non-equilibrium isoelectric focusing method to determine states of phosphorylation of cardiac troponin I: identification of Ser-23 and Ser-24 as significant sites of phosphorylation by protein kinase C. *J. Mol. Cell. Cardiol.* 38, 213–218. doi: 10.1016/j.yjmcc.2004.10.014

Kooij, V., Saes, M., Jaquet, K., Zaremba, R., Foster, D. B., Murphy, A., et al. (2010). Effect of troponin I Ser23/24 phosphorylation on Ca2+-sensitivity in human myocardium depends on the phosphorylation background. *J. Mol. Cell. Cardiol.* 48, 954–963. doi: 10.1016/j.yjmcc.2010.01.002

Layland, J., Solaro, R. J., and Shah, A. M. (2005). Regulation of cardiac contractile function by troponin I phosphorylation. *Cardiovasc. Res.* 66, 12–21. doi: 10.1016/j.cardiores.2004.12.022

Li, A. Y., Stevens, C. M., Liang, B., Rayani, K., Little, S., Davis, J., et al. (2013). Familial hypertrophic cardiomyopathy related cardiac troponin C L29Q mutation alters length-dependent activation and functional effects of phosphomimetic troponin I*. *PLoS ONE* 8:e79363. doi: 10.1371/journal.pone.0079363

Li, M. X., Robertson, I. M., and Sykes, B. D. (2008). Interaction of cardiac troponin with cardiotonic drugs: a structural perspective. *Biochem. Biophys. Res. Commun.* 369, 88–99. doi: 10.1016/j.bbrc.2007.12.108

Liu, B., Tikunova, S. B., Kline, K. P., Siddiqui, J. K., and Davis, J. P. (2012). Disease-related cardiac troponins alter thin filament Ca2+ association and dissociation rates. *PLoS ONE* 7:e38259. doi: 10.1371/journal.pone.0038259

Macleod, K. T., Marston, S. B., Poole-Wilson, P. A., Severs, N. J., and Sugden, P. H. (2010). "Cardiac myocytes and the cardiac action potential," in *Oxford Textbook of Medicine*, 5th Edn. eds D. A. Warrel, T. M. Cox, and J. D. Firth (Oxford, UK: Oxford University Press), 2603–2617.

Mamidi, R., Gollapudi, S. K., Mallampalli, S. L., and Chandra, M. (2012). Alanine or aspartic acid substitutions at serine23/24 of cardiac troponin I decrease thin filament activation, with no effect on crossbridge detachment kinetics. *Arch. Biochem. Biophys.* 525, 1–8. doi: 10.1016/j.abb.2012.05.024

Manning, E. P., Tardiff, J. C., and Schwartz, S. D. (2011). A model of calcium activation of the cardiac thin filament. *Biochemistry* 50, 7405–7413. doi: 10.1021/bi200506k

Marston, S. B. (2011). How do mutations in contractile proteins cause the primary familial cardiomyopathies? *J. Cardiovasc. Transl. Res.* 4, 245–255. doi: 10.1007/s12265-011-9266-2

Marston, S. B., Copeland, O. A. N., and Messer, A. (2012). *Pressure overload is associated with low levels of troponin I and myosin binding protein C phosphorylation in the hearts of patients with aortic stenosis. *Circulation* 126, A14155.

Marston, S. B., Song, W., Wilkinson, R., and Vikhorev, P. G. (2013). DCM-causing mutation ACTC E361G blunts responses to adrener- gic agonists, reduces cardiac reserve and predispose to heart failure under chronic stress in a transgenic mouse model. *J. Mol. Cell. Cardiol.* 65, s108. doi: 10.1016/j.vjmcc.2013.10.011

Marston, S. B., and Walker, J. W. (2009). Back to the future: new techniques show that forgotten phosphorylation sites are present in contractile proteins of the heart whilst intensively studied sites appear to be absent. *J. Mus. Res. Cell. Motil.* 30, 93–95. doi: 10.1007/s10974-009-9184-y

Marston, S., and Detombe, P. (2008). Point/Counterpoint. Troponin phosphorylation and myofilament Ca2+-sensitivity in heart failure: increased or decreased? *J. Mol. Cell. Cardiol.* 45, 603–607. doi: 10.1016/j.yjmcc.2008.07.004

Memo, M., Leung, M.-C., Ward, D. G., Dos Remedios, C., Morimoto, S., Zhang, L., et al. (2013). Mutations in thin filament proteins that cause familial dilated cardiomyopathy uncouple troponin I phosphorylation from changes in myofibrillar Ca2+-sensitivity. *Cardiovasc. Res.* 99, 65–73. doi: 10.1093/cvr/cvt071

Messer, A. E., Jacques, A. M., and Marston, S. B. (2007). Troponin phosphorylation and regulatory function in human heart muscle: dephosphorylation of Ser23/24 on troponin I could account for the contractile defect in end-stage heart failure. *J. Mol. Cell. Cardiol.* 42, 247–259. doi: 10.1016/j.yjmcc.2006.08.017

Messer, A. E., Memo, M., Bayliss, C. R., Leung, M.-C., and Marston, S. B. (2012). *Does uncoupling of troponin I phosphorylation from changes in myofibrillar Ca2+-sensitivity play a role in the pathogenesis of cardiomyopathy? *Biophys. J.* 102, 556a. doi: 10.1016/j.bpj.2011.11.3033

Messer, A. E., Papadaki, M., and Marston, S. B. (2014). *Effects of EMD57033 and EGCG on Modulation of Ca2+-Sensitivity by Pka Phosphorylation. *Biophys. J.* 106, 726a–727a. doi: 10.1016/j.bpj.2013.11.4010

Messer, A., Gallon, C., McKenna, W., Elliott, P., Dos Remedios, C., and Marston, S. (2009). The use of phosphate-affinity SDS-PAGE to measure the troponin I phosphorylation site distribution in human heart muscle. *Proteomics Clin. Appl.* 3, 1371–1382. doi: 10.1002/prca.200900071

Mirza, M., Marston, S., Willott, R., Ashley, C., Mogensen, J., McKenna, W., et al. (2005). Dilated cardiomyopathy mutations in three thin filament regulatory proteins result in a common functional phenotype. *J. Biol. Chem.* 280, 28498–28506. doi: 10.1074/jbc.M412281200

Mittmann, K., Jaquet, K., and Heilmeyer, L. M. Jr. (1990). A common motif of two adjacent phosphoserines in bovine, rabbit and human cardiac troponin I. *FEBS Lett.* 273, 41–45. doi: 10.1016/0014-5793(90)81046-Q

Mogensen, J., Murphy, R. T., Shaw, T., Bahl, A., Redwood, C., Watkins, H., et al. (2004). Severe disease expression of cardiac troponin C and T mutations in patients with idiopathic dilated cardiomyopathy. *J. Am. Coll. Cardiol.* 44, 2033–2040. doi: 10.1016/j.jacc.2004.08.027

Moore, R. K., Grinspan, L. T., Jimenez, J., Guinto, P. J., Ertz-Berger, B., and Tardiff, J. C. (2013). HCM-linked Δ160E cardiac troponin T mutation causes unique progressive structural and molecular ventricular remodeling in transgenic mice. *J. Mol. Cell. Cardiol.* 58, 188–198. doi: 10.1016/j.yjmcc.2013.02.004

Mope, L., McClellan, G. B., and Winegrad, S. (1980). Calcium sensitivity of the contractile system and phosphorylation of troponin in hyperpermeable cardiac cells. *J. Gen. Physiol.* 75, 271–282. doi: 10.1085/jgp.75.3.271

Morimoto, S. (2008). Sarcomeric proteins and inherited cardiomyopathies. *Cardiovasc. Res.* 77, 659–666. doi: 10.1093/cvr/cvm084

Naqvi, T. Z., Goel, R. K., Forrester, J. S., and Siegel, R. J. (1999). Myocardial contractile reserve on dobutamine echocardiography predicts late spontaneous

improvement in cardiac function in patients with recent onset idiopathic dilated cardiomyopathy. *J. Am. Coll. Cardiol.* 34, 1537–1544. doi: 10.1016/S0735-1097(99)00371-X

Nguyen, L., Chung, J., Lam, L., Tsoutsman, T., and Semsarian, C. (2007). Abnormal cardiac response to exercise in a murine model of familial hypertrophic cardiomyopathy. *Int. J. Cardiol.* 119, 245–248. doi: 10.1016/j.ijcard.2006.09.001

Nixon, B. R., Thawornkaiwong, A., Jin, J., Brundage, E. A., Little, S. C., Davis, J. P., et al. (2012). AMP-activated protein kinase phosphorylates cardiac troponin I at Ser-150 to increase myofilament calcium sensitivity and blunt PKA-dependent function. *J. Biol. Chem.* 287, 19136–19147. doi: 10.1074/jbc.M111.323048

Pi, Y.-Q., Kemnitz, K. R., Zhang, D., Kranias, E. G., and Walker, J. W. (2002). Phosphorylation of troponin I controls cardiac twitch dynamics. Evidence from phosphorylation site mutants expressed on a troponin I-null background in mice. *Circ. Res.* 90, 649–656. doi: 10.1161/01.RES.0000014080.82861.5F

Pinto, J. R., Siegfried, J. D., Parvatiyar, M. S., Li, D., Norton, N., Jones, M. A., et al. (2011). Functional characterization of TNNC1 rare variants identified in dilated cardiomyopathy. *J. Biol. Chem.* 286, 34404–34412. doi: 10.1074/jbc.M111.267211

Rajan, S., Ahmed, R. P., Jagatheesan, G., Petrashevskaya, N., Boivin, G. P., Urboniene, D., et al. (2007). Dilated cardiomyopathy mutant tropomyosin mice develop cardiac dysfunction with significantly decreased fractional shortening and myofilament calcium sensitivity. *Circ. Res.* 101, 205–214. doi: 10.1161/CIRCRESAHA.107.148379

Ray, K. P., and England, P. J. (1976). Phosphorylation of the inhibitory subunit of troponin and its effect on the calcium dependence of cardiac myofibril adenosine triphosphatase. *FEBS Lett.* 70, 11–16. doi: 10.1016/0014-5793(76)80716-8

Robertson, I. M., Li, M. X., and Sykes, B. D. (2009). Solution structure of human cardiac troponin C in complex with the green tea polyphenol, (-)-epigallocatechin 3-gallate. *J. Biol. Chem.* 284, 23012–23023. doi: 10.1074/jbc.M109.021352

Robertson, S. P., Johnson, J. D., Holroyde, M. J., Kranias, E. G., Potter, J. D., and Solaro, R. J. (1982). The effect of troponin I phosphorylation on the Ca2+-binding properties of the Ca2+-regulatory site of bovine cardiac troponin. *J. Biol. Chem.* 257, 260–263.

Sancho Solis, R., Ge, Y., and Walker, J. W. (2009). Single amino acid sequence polymorphisms in rat cardiac troponin revealed by top-down tandem mass spectrometry. *J. Mus. Res. Cell. Motil.* 29, 203–212. doi: 10.1007/s10974-009-9168-y

Schmidtmann, A., Lindow, C., Villard, S., Heuser, A., Mügge, A., Gessner, R., et al. (2005). Cardiac troponin C-L29Q, related to hypertrophic cardiomyopathy, hinders the transduction of the protein kinase A dependent phosphorylation signal from cardiac troponin I to C. *FEBS J.* 272, 6087–6097. doi: 10.1111/j.1742-4658.2005.05001.x

Sequeira, V., Wijnker, P. J., Nijenkamp, L. L., Kuster, D. W., Najafi, A., Witjas-Paalberends, E. R., et al. (2013). Perturbed length-dependent activation in human hypertrophic cardiomyopathy with missense sarcomeric gene mutations. *Circ. Res.* 112, 1491–1505. doi: 10.1161/CIRCRESAHA.111.300436

Solaro, R. J., Moir, A. G. J., and Perry, S. V. (1976). Phosphorylation of troponin I and the inotropic effect of adrenaline in the perfused rabbit heart. *Nature* 262, 615–616. doi: 10.1038/262615a0

Solaro, R. J., Rosevear, P., and Kobayashi, T. (2008). The unique functions of cardiac troponin I in the control of cardiac muscle contraction and relaxation. *Biochem. Biophys. Res. Commun.* 369, 82–87. doi: 10.1016/j.bbrc.2007.12.114

Song, W., Dyer, E., Stuckey, D., Copeland, O., Leung, M., Bayliss, C., et al. (2011). Molecular mechanism of the Glu99lys mutation in cardiac actin (ACTC gene) that causes apical hypertrophy in man and mouse. *J. Biol. Chem.* 286, 27582–27593. doi: 10.1074/jbc.M111.252320

Song, W., Dyer, E., Stuckey, D., Leung, M.-C., Memo, M., Mansfield, C., et al. (2010). Investigation of a transgenic mouse model of familial dilated cardiomyopathy. *J. Mol. Cell. Cardiol.* 49, 380–389. doi: 10.1016/j.yjmcc.2010.05.009

Steinberg, T. H., Agnew, B. J., Gee, K. R., Leung, W. Y., Goodman, T., Schulenberg, B., et al. (2003). Global quantitative phosphoprotein analysis using multiplexed proteomics technology. *Proteomics* 3, 1128–1144. doi: 10.1002/pmic.200300434

Stöhr, A., Friedrich, F. W., Flenner, F., Geertz, B., Eder, A., Schaaf, S., et al. (2013). Contractile abnormalities and altered drug response in engineered heart tissue from Mybpc3-targeted knock-in mice. *J. Mol. Cell. Cardiol.* 63, 189–198. doi: 10.1016/j.yjmcc.2013.07.011

Sun, N., Yazawa, M., Liu, J., Han, L., Sanchez-Freire, V., Abilez, O. J., et al. (2012). Patient-specific induced pluripotent stem cells as a model for familial dilated cardiomyopathy. *Sci. Transl. Med.* 4:130ra147. doi: 10.1126/scitranslmed.3003552

Tadano, N., Du, C., Yumoto, F., Morimoto, S., Ohta, M., Xie, M., et al. (2010). Biological actions of green tea catechins on cardiac troponin C. *Br. J. Pharmacol.* 161, 1034–1043. doi: 10.1111/j.1476-5381.2010.00942.x

Takeda, N., Yamashita, A., Maeda, K., and Maeda, Y. (2003). Structure of the core domain of human cardiac troponin in the Ca2+-saturated form. *Nature* 424, 35–41. doi: 10.1038/nature01780

Van Der Velden, J., Papp, Z., Zaremba, R., Boontje, N. M., De Jong, J. W., Owen, V. J., et al. (2003). Increased Ca2+-sensitivity of the contractile apparatus in end-stage human heart failure results from altered phosphorylation of contractile proteins. *Cardiovasc. Res.* 57, 37–47. doi: 10.1016/S0008-6363(02)00606-5

Vikhorev, S. W., Wilkinson, R., Copeland, O. A. N., Messer, A. E., Ferenczi, M. A., and Marston, S. B. (2013). Modulation of cardiac myofibril Ca2+-sensitivity by phosphorylation, sarcomere length and a DCM-causing mutation. *Biophys. J. Rev.* 104, 312a. doi: 10.1016/j.bpj.2012.11.1730

Wang, Y., Pinto, J. R., Solis, R. S., Dweck, D., Liang, J., Diaz-Perez, Z., et al. (2012). Generation and functional characterization of knock-in mice harboring the cardiac troponin I-R21C mutation associated with hypertrophic cardiomyopathy. *J. Biol. Chem.* 287, 2156–2167. doi: 10.1074/jbc.M111.294306

Wang, Y., Pinto, J., Sancho Solis, R., Dweck, D., Liang, J., Diaz-Perez, Z., et al. (2011). The generation and functional characterization of knock in mice harboring the cardiac Troponin I-R21C mutation associated with hypertrophic cardiomyopathy. *J. Biol. Chem.* 287, 2156–2167. doi: 10.1074/jbc.M111.294306

Ward, D. G., Brewer, S. M., Calvert, M. J., Gallon, C. E., Gao, Y., and Trayer, I. P. (2004a). Characterization of the interaction between the N-terminal extension of human cardiac troponin I and troponin C. *Biochemistry* 43, 4020–4027. doi: 10.1021/bi036128l

Ward, D. G., Brewer, S. M., Gallon, C. E., Gao, Y., Levine, B. A., and Trayer, I. P. (2004b). NMR and mutagenesis studies on the phosphorylation region of human cardiac troponin I. *Biochemistry* 43, 5772–5781. doi: 10.1021/bi036310m

Wilkinson, R. (2014). *An Investigation Into the Disease Causing Mechanism in Familial Dilated Cardiomyopathy*. Ph.D., Imperial College, London.

Wolff, M. R., Whitesell, L. F., and Moss, R. L. (1995). Calcium sensitivity of isometric tension is increased in canine experimental heart failure. *Circ. Res.* 76, 781–789. doi: 10.1161/01.RES.76.5.781

Yasuda, S., Coutu, P., Sadayappan, S., Robbins, J., and Metzger, J. M. (2007). Cardiac transgenic and gene transfer strategies converge to support an important role for troponin I in regulating relaxation in cardiac myocytes. *Circ. Res.* 101, 377–386. doi: 10.1161/CIRCRESAHA.106.145557

Zabrouskov, V., Ge, Y., Schwartz, J., and Walker, J. W. (2008). Unraveling molecular complexity of phosphorylated human cardiac troponin I by top down electron capture dissociation/electron transfer dissociation mass spectrometry. *Mol. Cell. Proteomics* 7, 1838–1849. doi: 10.1074/mcp.M700524-MCP200

Zaremba, R., Merkus, D., Hamdani, N., Lamers, J., Paulus, W., Dos Remedios, C., et al. (2007). Quantitative analysis of myofilament protein phosphorylation in small cardiac biopsies. *Proteomics Clin. Appl.* 1, 1285–1290. doi: 10.1002/prca.200600891

Zhang, R., Zhao, J., Mandveno, A., and Potter, J. D. (1995). Cardiac troponin I phosphorylation increases the rate of cardiac muscle relaxation. *Biophys. J.* 76, 1028–1035.

Conflict of Interest Statement: The authors declare that the research was conducted in the absence of any commercial or financial relationships that could be construed as a potential conflict of interest.

Received: 20 June 2014; accepted: 02 August 2014; published online: 25 August 2014.
Citation: Messer AE and Marston SB (2014) Investigating the role of uncoupling of troponin I phosphorylation from changes in myofibrillar Ca^{2+}-sensitivity in the pathogenesis of cardiomyopathy. Front. Physiol. ***5****:315. doi: 10.3389/fphys.2014.00315*
This article was submitted to Striated Muscle Physiology, a section of the journal Frontiers in Physiology.
Copyright © 2014 Messer and Marston. This is an open-access article distributed under the terms of the Creative Commons Attribution License (CC BY). The use, distribution or reproduction in other forums is permitted, provided the original author(s) or licensor are credited and that the original publication in this journal is cited, in accordance with accepted academic practice. No use, distribution or reproduction is permitted which does not comply with these terms.

frontiers in PHYSIOLOGY

ORIGINAL RESEARCH ARTICLE
published: 29 September 2014
doi: 10.3389/fphys.2014.00375

Alterations in thin filament length during postnatal skeletal muscle development and aging in mice

David S. Gokhin[1]*, Emily A. Dubuc[1], Kendra Q. Lian[1], Luanne L. Peters[2] and Velia M. Fowler[1]

[1] Department of Cell and Molecular Biology, The Scripps Research Institute, La Jolla, CA, USA
[2] The Jackson Laboratory, Bar Harbor, ME, USA

Edited by:
Julien Ochala, King's College London, UK

Reviewed by:
Bruno Bastide, University of Lille, France
Ranganath Mamidi, Case Western Reserve University, USA

***Correspondence:**
David S. Gokhin, Department of Cell and Molecular Biology, The Scripps Research Institute, 10550 N Torrey Pines Rd., CB163, La Jolla, CA 92037, USA
e-mail: dgokhin@scripps.edu

The lengths of the sarcomeric thin filaments vary in a skeletal muscle-specific manner and help specify the physiological properties of skeletal muscle. Since the extent of overlap between the thin and thick filaments determines the amount of contractile force that a sarcomere can actively produce, thin filament lengths are accurate predictors of muscle-specific sarcomere length-tension relationships and sarcomere operating length ranges. However, the striking uniformity of thin filament lengths within sarcomeres, specified during myofibril assembly, has led to the widely held assumption that thin filament lengths remain constant throughout an organism's lifespan. Here, we rigorously tested this assumption by using computational super-resolution image analysis of confocal fluorescence images to explore the effects of postnatal development and aging on thin filament length in mice. We found that thin filaments shorten in postnatal tibialis anterior (TA) and gastrocnemius muscles between postnatal days 7 and 21, consistent with the developmental program of myosin heavy chain (MHC) gene expression in this interval. By contrast, thin filament lengths in TA and extensor digitorum longus (EDL) muscles remained constant between 2 mo and 2 yr of age, while thin filament lengths in soleus muscle became shorter, suggestive of a slow-muscle-specific mechanism of thin filament destabilization associated with aging. Collectively, these data are the first to show that thin filament lengths change as part of normal skeletal muscle development and aging, motivating future investigations into the cellular and molecular mechanisms underlying thin filament adaptation across the lifespan.

Keywords: tropomodulin, actin, sarcomere, mouse, myofibril, myofilament

INTRODUCTION

In skeletal muscle fibers, contractile force is generated via cross-bridge interactions between the myosin (thick) filaments and actin (thin) filaments in the sarcomeres arranged in series along contractile myofibrils. The capacity for a sarcomere to generate force is best described by the sliding filament theory of muscle contraction, which states that the extent of overlap between the thick and thin filaments determines the number of crossbridge interactions and, hence, the extent of active force production. The sliding filament theory can be quantified by the sarcomere length-tension relationship, which depicts a sarcomere's force output as a function of sarcomere length, and whose shape can be accurately modeled from thick and thin filament lengths (Huxley and Hanson, 1954; Edman, 1966; Gordon et al., 1966; Walker and Schrodt, 1974; Granzier et al., 1991). While thick filament lengths are constant (~1.65 μm) in all muscle types and species examined, thin filament lengths vary widely (from 0.95 to 1.40 μm) across muscle types and species, resulting in correspondingly wide variations in sarcomere length-tension relationships (reviewed in Gokhin and Fowler, 2013). The best correlate of thin filament lengths that has been identified to date is a muscle's fiber type distribution, as determined by myosin heavy chain (MHC) isoform expression, with slow-twitch muscles expressing predominantly type-I MHC (such as the soleus) having longer thin filaments, and fast-twitch muscles expressing predominantly type-II MHCs [such as the tibialis anterior (TA)] having shorter thin filament lengths in all mammalian species studied (Castillo et al., 2009; Gokhin et al., 2010, 2012). However, MHC isoform effects on thin filament length are correlative and not causative; by contrast, perturbations in thin filament pointed-end capping by tropomodulin (Tmod) can directly induce alterations in filament lengths by inhibiting actin subunit dynamics in both slow- and fast-twitch skeletal muscles (Gokhin et al., 2014).

Thin filament lengths are not fixed after their initial specification during myofibril assembly, but, rather, can exhibit remarkable plasticity in response to experimental perturbations. For example, in cardiac myocytes and *Drosophila* indirect flight muscle, thin filaments can be shortened or lengthened by increasing or decreasing, respectively, the extent of pointed-end capping by Tmod (Gregorio et al., 1995; Sussman et al., 1998; Littlefield et al., 2001; Mardahl-Dumesnil and Fowler, 2001; Tsukada et al., 2010; Bliss et al., 2014). This inverse relationship between Tmod activity and thin filament lengths appears to extend to mammalian skeletal muscle as well, as it was recently shown that proteolysis of Tmod by m-calpain can result in longer thin filaments in mouse models of Duchenne muscular dystrophy

(Gokhin et al., 2014). However, it remains unclear whether changes in thin filament lengths might also be characteristic of normal muscle adaptation during an organism's lifespan (i.e., during postnatal development and aging). To address this question, we used a super-resolution computational image analysis technique (termed Distributed Deconvolution; Littlefield and Fowler, 2002) to measure thin filament lengths in skeletal muscles from mice at various stages of postnatal development, as well as from aged mice. We found that, in postnatal TA and gastrocnemius (GAS) muscles, thin filaments become shorter from postnatal days 7 to 21 (P7 to P21). This is consistent with the known developmental shift away from embryonic and neonatal MHC expression toward a fast-twitch phenotype associated with predominantly type-II MHC isoform expression (Allen and Leinwand, 2001; Agbulut et al., 2003; Gokhin et al., 2008). By contrast, in aged (2-yr-old) mice, thin filament lengths in TA and extensor digitorum longus (EDL) muscles remained constant with respect to 2-mo-old mice, while thin filament lengths in soleus muscle became shorter, suggesting muscle-specific mechanisms of length modulation. Collectively, these data identify changes in thin filament lengths as a novel feature of skeletal muscle development and aging.

MATERIALS AND METHODS

EXPERIMENTAL ANIMALS AND TISSUES

Mice ($n = 3$–4 mice per time-point) were sacrificed at P7, P14, P21, 2 months after birth, or 2 years after birth. Mice sacrificed at P7, P14, and P21 were C57Bl/6J mice, while mice sacrificed at 2 months or 2 years after birth were BALB/cBy mice. Two different mouse strains were used to test whether thin filament lengths in adult skeletal muscle vary with mouse strain (i.e., C57Bl/6J at P21 vs. BALB/cBy at 2 months). Mice were sacrificed by isoflurane inhalation followed by cervical dislocation, in accordance with ethics guidelines set forth by the Institutional Animal Care and Use Committee at The Scripps Research Institute.

In experiments with P7–P21 mice, TA and GAS muscles were examined because their larger size facilitated tissue dissection and handling, and because EDL and soleus muscles are not readily distinguishable from the surrounding musculature at P7. For experiments with 2-mo- and 2-yr-old tissues, TA, EDL, and soleus muscles were examined because these muscles reflect a diversity of muscle fiber types and architectures in adult mice (Burkholder et al., 1994; Agbulut et al., 2003). GAS muscle was not analyzed in 2-mo- and 2-yr-old mice, due to its fiber type similarity with the TA and EDL (Burkholder et al., 1994).

IMMUNOSTAINING AND CONFOCAL IMAGING

Leg muscles were stretched *in situ* via ankle joint manipulation, pinned to cork, relaxed overnight in EGTA-containing relaxing buffer, fixed overnight in 4% paraformaldehyde in relaxing buffer, dissected, embedded in Optimum Cutting Temperature compound, cryosectioned, and immunostained as previously described (Gokhin et al., 2010). Primary antibodies were as follows: mouse anti-α-actinin (EA53, 1:100; Sigma-Aldrich, St. Louis, MO) to label Z-lines; affinity-purified rabbit polyclonal anti-human Tmod1 (R1749, 3.1 μg/ml) (Gokhin et al., 2010) or rabbit polyclonal antiserum to chicken Tmod4 preadsorbed by passage through a Tmod1 Sepharose column (R3577, 1:25) (Gokhin et al., 2010) to label thin filament pointed ends; rabbit anti-nebulin M1M2M3 (NEB-1, 1:100; Myomedix, Mannheim, Germany) to label the nebulin N-terminus at the proximal/distal segment boundary of the thin filament (Gokhin and Fowler, 2013). Secondary antibodies were Alexa-488-conjugated goat anti-rabbit IgG (1:200; Life Technologies, Carlsbad, CA) and Alexa-647-conjugated goat anti-mouse IgG (1:200; Life Technologies). F-actin was stained with rhodamine-phalloidin (1:100; Life Technologies). Single optical sections were collected on a Bio-Rad Radiance 2100 laser-scanning confocal microscope mounted on a Nikon TE2000-U microscope using a 100× Plan-Apochromat oil-objective lens. Images were processed in Adobe Photoshop CS5.1, and figures were constructed in Adobe Illustrator CS5.1.

THIN FILAMENT LENGTH MEASUREMENTS

Distributed Deconvolution analysis was used to measure distances of fluorescently labeled peaks of Tmod and nebulin M1M2M3 from the Z-line as well as half the breadth of the F-actin (phalloidin) signal across the Z-lines of adjacent half-sarcomeres (I-Z-I arrays), as previously described (Littlefield and Fowler, 2002; Gokhin and Fowler, 2013). Both Tmod1- and Tmod4-stained images were used for determining Tmod distances, as Tmod1 and Tmod4 are equally faithful markers of the thin filament pointed ends in all mammalian species examined (Gokhin et al., 2010, 2012). We used a distributed deconvolution plugin for ImageJ that generates the best-fit of a model intensity distribution function for a given thin filament component (Tmod, nebulin M1M2M3, or F-actin), to a background-corrected 1D myofibril fluorescence intensity profile (line-scan) of 3–5 thin filament arrays obtained for each fluorescent probe (anti-Tmod, anti-nebulin M1M2M3, or rhodamine-phalloidin). The distributed deconvolution plugin and supporting documentation are available for public download at http://www.scripps.edu/fowler/.

STATISTICS

Differences between two groups were determined using Student's *t*-test. Differences between three groups were determined using One-Way ANOVA with *post-hoc* Fisher's PLSD tests. Statistical analysis was performed in Microsoft Excel. Significance was defined as $p < 0.05$.

RESULTS

To examine changes in thin filament length during postnatal skeletal muscle development, we used confocal fluorescence microscopy and a super-resolution computational image analysis approach (Distributed Deconvolution; Littlefield and Fowler, 2002) to measure thin filament lengths in mouse skeletal muscles from P7 to P21. Organized myofibrils with well-regulated thin filament lengths were evident in all muscles examined at all postnatal time-points, as evidenced by striated Tmod1, Tmod4, nebulin M1M2M3, F-actin, and α-actinin staining patterns (sample images from P14 muscle shown **Figure 1**). In the postnatal GAS, thin filament lengths determined by Tmod1 localization steadily decreased from 1.26 to 1.09 μm from P7 to P21 (**Figure 2**; **Table 1**). In the postnatal TA, thin filament lengths stayed constant at ∼1.17 μm from P7 to P14, but decreased to 1.10 μm

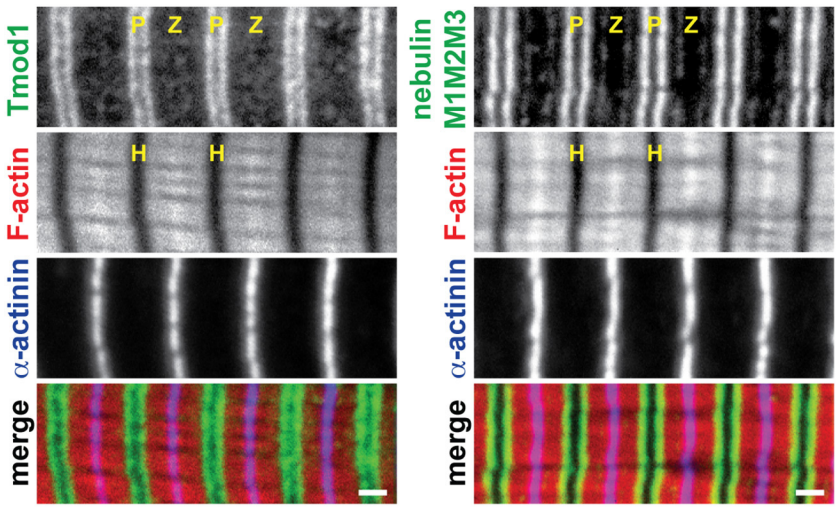

FIGURE 1 | Sample immunofluorescence images of P14 mouse muscles. Longitudinal TA cryosections were phalloidin-stained for F-actin and immunostained for α-actinin, along with either Tmod1 or nebulin M1M2M3, and imaged by confocal microscopy. P, thin filament pointed ends; Z, Z-line; H, H-zone. Bars, 1 μm.

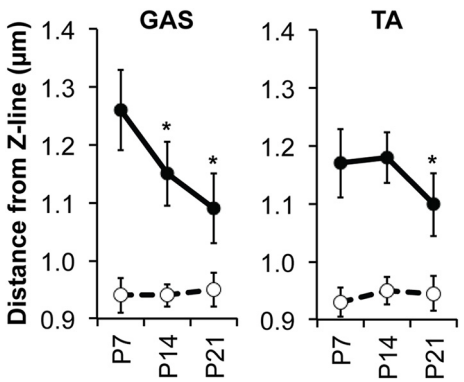

FIGURE 2 | Thin filament lengths during postnatal muscle development in mice. Graphs depict distances of Tmod (solid circles) and nebulin M1M2M3 (open circles) from the Z-line in GAS and TA muscles from P7 to P21 mice. Tmod distance reflects the variable position of the thin filament pointed end with respect to the Z-line, while nebulin M1M2M3 distance reflects the relatively constant position of the proximal/distal segment boundary of the thin filament with respect to the Z-line (Gokhin and Fowler, 2013). Tmod distances reflect pooled Tmod1 and Tmod4 distances. Error bars reflect mean ± *SD* for $n \geq 100$ myofibrils/time-point for Tmod, $n \geq 50$ myofibrils/time-point for nebulin M1M2M3. *$p < 0.01$ with respect to the previous time-point.

Table 1 | Thin filament lengths determined by Distributed Deconvolution analysis of fluorescence images.

		Tmod	Phalloidin	Nebulin M1M2M3
GAS	P7	1.26 ± 0.07	1.16 ± 0.03	0.94 ± 0.03
	P14	1.15 ± 0.06*	1.06 ± 0.02*	0.94 ± 0.02
	P21	1.09 ± 0.06*	0.98 ± 0.02*	0.95 ± 0.03
TA	P7	1.17 ± 0.06	1.10 ± 0.02	0.93 ± 0.02
	P14	1.18 ± 0.04	1.09 ± 0.02	0.95 ± 0.02
	P21	1.10 ± 0.07*	1.01 ± 0.04*	0.95 ± 0.03
	2 mo	1.11 ± 0.06	1.03 ± 0.04	0.93 ± 0.03
	2 yr	1.08 ± 0.07	1.00 ± 0.04	0.94 ± 0.03
EDL	2 mo	1.07 ± 0.07	1.00 ± 0.06	0.94 ± 0.02
	2 yr	1.09 ± 0.06	1.03 ± 0.05	0.94 ± 0.02
Soleus	2 mo	1.19 ± 0.05	1.14 ± 0.11	0.96 ± 0.03
	2 yr	1.11 ± 0.02*	1.06 ± 0.05*	0.95 ± 0.03

*Length values (all in μm) correspond to the breadth of phalloidin staining and the distances of Tmod and nebulin M1M2M3 from the Z-line. Data are shown mean ± SD for $n \geq 100$ myofibrils/time-point for Tmod and phalloidin, $n \geq 50$ myofibrils/time-point for nebulin M1M2M3. *$p < 0.01$ with respect to the previous time-point.*

by P21 (**Figure 2**; **Table 1**). Thin filament lengths determined by F-actin breadth from the Z-line to the H-zone paralleled those determined by Tmod1 localization in both neonatal GAS and TA muscles at all time-points (**Table 1**). Nebulin M1M2M3 distances from the Z-line remained constant at ∼0.94 μm in both neonatal GAS and TA (**Figure 2**; **Table 1**), consistent with the nebulin-coated proximal segment of the thin filament having a fixed length, regardless of the length of the nebulin-free distal segment (Gokhin and Fowler, 2013).

Next, to examine changes in thin filament length during skeletal muscle aging, we further used confocal fluorescence microscopy and Distributed Deconvolution analysis to compare thin filament lengths in 2-mo-old vs. 2-yr-old mice. Aged muscles showed no evidence of gross myofibril disorganization or deterioration, as evidenced by striated Tmod1, nebulin M1M2M3, F-actin, and α-actinin staining (data not shown). In the TA and EDL, no statistically significant differences in thin filament lengths were observed between 2-mo-old vs. 2-yr-old muscles (∼1.11 μm in both muscles at both time points) (**Figure 3**;

Table 1). However, in the soleus, thin filament length decreased from ∼1.20 μm in 2-mo-old muscles to ∼1.11 μm in 2-yr-old muscles (**Figure 3**; **Table 1**). As observed with our measurements of thin filament lengths in neonatal muscles, thin filament lengths determined by F-actin breadth from the Z-line to the H-zone paralleled those determined by Tmod1 localization (**Table 1**), and nebulin M1M2M3 distances from the Z-line remained constant at ∼0.95 μm (**Figure 3**; **Table 1**). Moreover, thin filament lengths in the TA muscles of 2-mo-old BALB/cBy mice were identical to thin filament lengths in the TA muscles of P21 C57Bl/6J mice (**Table 1**; also compare **Figure 2** and **Figure 3**), indicating that thin filament lengths do not change between P21 and 2 months of age, and that lengths are not mouse strain-dependent. Thin filament lengths in adult mice in these strains also agree with lengths previously reported in adult mixed-background FVB/N:129/SvJ:C57Bl/6 mice (Gokhin et al., 2010).

DISCUSSION

This study provides the first evidence that skeletal muscle thin filaments undergo adaptive remodeling to alter their lengths during the mouse lifespan, implying age-dependent alterations in sarcomere length-tension relationships and optimum sarcomere length ranges. What molecular mechanisms might drive these changes in thin filament lengths? When examining neonatal muscles, we observed thin filament shortening between P7 and P21 in both the TA and GAS (**Figure 2**). These changes are mostly associated with developmental transitions away from expression of embryonic and neonatal MHC isoforms and toward expression of adult type-II MHC isoforms (Allen and Leinwand, 2001; Agbulut et al., 2003; Gokhin et al., 2008). The presence of type-II MHC isoforms is, in turn, associated with shorter thin filament lengths (Castillo et al., 2009; Gokhin et al., 2010, 2012). This suggests a model in which immature mouse muscles, expressing predominantly embryonic and neonatal MHCs, are all initially specified with "generic" thin filament lengths during the terminal stages of myofibril assembly, despite these muscles' functional differences in adult mice (Allen and Leinwand, 2001; Agbulut et al., 2003; Gokhin et al., 2008). Then, as the various muscles adopt their characteristic use profiles and MHC isoform distributions during postnatal acquisition of adult movement patterns, thin filament lengths may gradually diversify, ultimately leading to the multitude of muscle-specific thin filament lengths observed in adult mice (i.e., longer thin filaments characteristic of slower fiber types and shorter filaments characteristic of faster fiber types) (Gokhin et al., 2010, 2014). Simultaneously, postnatal changes in tropomyosin and troponin isoform expression (Amphlett et al., 1976; Briggs et al., 1990) may also be involved in regulating thin filament lengths during postnatal skeletal muscle development. Evidence supporting this possibility is the fact that a nemaline myopathy-causing tropomyosin mutation can cause markedly shorter thin filaments *in vivo* (Ochala et al., 2012), and that both tropomyosin and troponin have been shown to enhance actin filament pointed-end stability *in vitro* (Broschat et al., 1989; Broschat, 1990; Weigt et al., 1990).

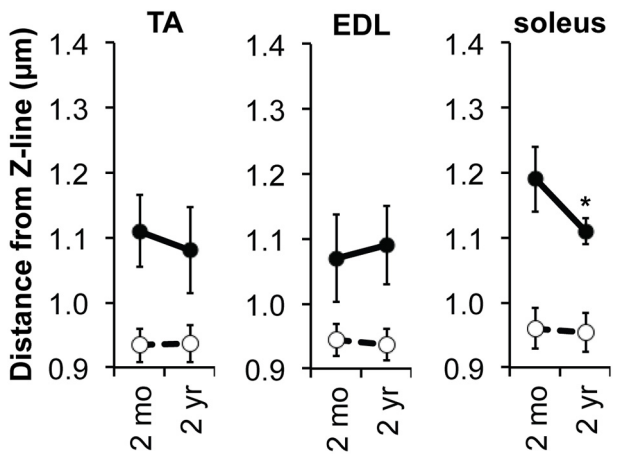

FIGURE 3 | Thin filament lengths in aged mouse muscles. Graphs depict distances of Tmod (solid circles) and nebulin M1M2M3 (open circles) from the Z-line in TA, EDL, and soleus muscles from 2-mo-old to 2-yr-old mice. Tmod distance reflects the variable position of the thin filament pointed end with respect to the Z-line, indicative of variations in length, while nebulin M1M2M3 distance reflects the relatively constant position of the proximal/distal segment boundary of the thin filament with respect to the Z-line (Gokhin and Fowler, 2013). Tmod distances reflect pooled Tmod1 and Tmod4 distances. Error bars reflect mean ± *SD* for $n \geq 100$ myofibrils/time-point for Tmod, $n \geq 50$ myofibrils/time-point for nebulin M1M2M3. *$p < 0.01$ with respect to the previous time-point.

When comparing 2-mo-old and 2-yr-old muscles, we observed no statistically significant changes in thin filament length in the TA or EDL, but a marked decrease in thin filament length was observed in the 2-yr-old soleus (**Figure 3**). The fact that thin filament shortening during aging is restricted to the soleus muscle implies a mechanism specific to heavily recruited, slow-twitch muscles. Such a mechanism most likely does not involve shifts toward expression of type-II MHC isoforms during aging, unlike the MHC isoform shifts described above for postnatal muscle development, because studies of rat soleus have shown continued enrichment of type-I MHC with decreases in type-II MHC during aging (Butler-Browne and Whalen, 1984; Larsson et al., 1995). Indeed, an increase in type-I MHC with concomitant thin filament shortening is not consistent with a causative effect of MHC isoforms in regulating thin filament lengths. Other molecules whose alterations might directly induce slow-muscle-specific thin filament shortening in aging are tropomyosin (an actin side-binding and stabilizing protein), whose α isoforms are decreased in aged muscle (Gelfi et al., 2006; O'Connell et al., 2007), as well as ADF/cofilin (an actin-severing protein) and profilin (an actin monomer-sequestering protein), whose levels are increased in degenerating muscle (Nagaoka et al., 1996). Moreover, slow-muscle-specific changes in thin filament protein phosphorylation, glycosylation, or other posttranslational modifications might also contribute to slow-muscle-specific thin filament shortening in aging. Understanding the contributions and interplay of these molecules and pathways to thin filament shortening in aging requires further studies.

An alternative mechanism for slow-muscle-specific thin filament shortening in aging involves preferential induction of proteolytic pathways in slow-twitch muscles (Sultan et al., 2001), leading to breakdown of thin filament-associated proteins and

reduced F-actin stability. Such proteolytic pathways might be specifically induced in old muscle, or might be ongoing in heavily recruited muscles and begin in mid-life. A number of proteolytic pathways have been implicated in skeletal muscle aging and aging-related sarcopenia, including activation of intracellular proteases (calpains and caspases), the ubiquitin-proteasome system, the autophagy-lysosome system, and reactive oxygen species (for reviews, see Fulle et al., 2004; Dargelos et al., 2008; Ryall et al., 2008; Combaret et al., 2009). Activation of m-calpain can lead to Tmod proteolysis that is more widespread in slow muscle in mouse models of Duchenne muscular dystrophy, but this mechanism results in actin subunit addition onto pointed ends and resultant thin filament elongation, and not thin filament shortening (Gokhin et al., 2014). More likely targets whose proteolysis could lead to shorter thin filaments are actin filament side-binding proteins such as nebulin and tropomyosin, which stabilize thin filaments to prevent aberrant thin filament shortening (Bang et al., 2006; Ottenheijm et al., 2009; Pappas et al., 2010; Ochala et al., 2012). Ongoing work seeks to understand the regulatory framework governing the interplay between aging and pathology of skeletal muscle, alterations in thin filament proteins, and regulation of thin filament lengths.

ACKNOWLEDGMENTS

This work was supported by stipends from the Summer Undergraduate Research Fellowship program at The Scripps Research Institute (to Emily A. Dubuc and Kendra Q. Lian), a development grant from the Muscular Dystrophy Association (to David S. Gokhin), an NIH/NIAMS Pathway to Independence award (K99-AR066534 to David S. Gokhin), a grant from NIH/NIA to the Nathan Shock Center of Excellence in the Basic Biology of Aging at The Jackson Laboratory (P30-AG038070 to Luanne L. Peters), and a grant from NIH/NIAMS to the Imaging Core of the San Diego Skeletal Muscle Research Center (P30-AR061303 to Velia M. Fowler).

REFERENCES

Agbulut, O., Noirez, P., Beaumont, F., and Butler-Browne, G. (2003). Myosin heavy chain isoforms in postnatal muscle development of mice. *Biol. Cell* 95, 399–406. doi: 10.1016/S0248-4900(03)00087-X

Allen, D. L., and Leinwand, L. A. (2001). Postnatal myosin heavy chain isoform expression in normal mice and mice null for IIb or IId myosin heavy chains. *Dev. Biol.* 229, 383–395. doi: 10.1006/dbio.2000.9974

Amphlett, G. W., Syska, H., and Perry, S. V. (1976). The polymorphic forms of tropomyosin and troponin I in developing rabbit skeletal muscle. *FEBS Lett.* 63, 22–26. doi: 10.1016/0014-5793(76)80186-X

Bang, M. L., Li, X., Littlefield, R., Bremner, S., Thor, A., Knowlton, K. U., et al. (2006). Nebulin-deficient mice exhibit shorter thin filament lengths and reduced contractile function in skeletal muscle. *J. Cell Biol.* 173, 905–916. doi: 10.1083/jcb.200603119

Bliss, K. T., Tsukada, T., Novak, S. M., Dorovkov, M. V., Shah, S. P., Nworu, C., et al. (2014). Phosphorylation of tropomodulin1 contributes to the regulation of actin filament architecture in cardiac muscle. *FASEB J.* doi: 10.1096/fj.13-246009. [Epub ahead of print].

Briggs, M. M., McGinnis, H. D., and Schachat, F. (1990). Transitions from fetal to fast troponin T isoforms are coordinated with changes in tropomyosin and alpha-actinin isoforms in developing rabbit skeletal muscle. *Dev. Biol.* 140, 253–260. doi: 10.1016/0012-1606(90)90075-T

Broschat, K. O. (1990). Tropomyosin prevents depolymerization of actin filaments from the pointed end. *J. Biol. Chem.* 265, 21323–21329.

Broschat, K. O., Weber, A., and Burgess, D. R. (1989). Tropomyosin stabilizes the pointed end of actin filaments by slowing depolymerization. *Biochemistry* 28, 8501–8506. doi: 10.1021/bi00447a035

Burkholder, T. J., Fingado, B., Baron, S., and Lieber, R. L. (1994). Relationship between muscle fiber types and sizes and muscle architectural properties in the mouse hindlimb. *J. Morphol.* 221, 177–190. doi: 10.1002/jmor.1052210207

Butler-Browne, G. S., and Whalen, R. G. (1984). Myosin isozyme transitions occurring during the postnatal development of the rat soleus muscle. *Dev. Biol.* 102, 324–334. doi: 10.1016/0012-1606(84)90197-0

Castillo, A., Nowak, R., Littlefield, K. P., Fowler, V. M., and Littlefield, R. S. (2009). A nebulin ruler does not dictate thin filament lengths. *Biophys. J.* 96, 1856–1865. doi: 10.1016/j.bpj.2008.10.053

Combaret, L., Dardevet, D., Bechet, D., Taillandier, D., Mosoni, L., and Attaix, D. (2009). Skeletal muscle proteolysis in aging. *Curr. Opin. Clin. Nutr. Metab. Care* 12, 37–41. doi: 10.1097/MCO.0b013e32831b9c31

Dargelos, E., Poussard, S., Brule, C., Daury, L., and Cottin, P. (2008). Calcium-dependent proteolytic system and muscle dysfunctions: a possible role of calpains in sarcopenia. *Biochimie* 90, 359–368. doi: 10.1016/j.biochi.2007.07.018

Edman, K. A. (1966). The relation between sarcomere length and active tension in isolated semitendinosus fibres of the frog. *J. Physiol.* 183, 407–417.

Fulle, S., Protasi, F., Di Tano, G., Pietrangelo, T., Beltramin, A., Boncompagni, S., et al. (2004). The contribution of reactive oxygen species to sarcopenia and muscle ageing. *Exp. Gerontol.* 39, 17–24. doi: 10.1016/j.exger.2003.09.012

Gelfi, C., Vigano, A., Ripamonti, M., Pontoglio, A., Begum, S., Pellegrino, M. A., et al. (2006). The human muscle proteome in aging. *J. Proteome Res.* 5, 1344–1353. doi: 10.1021/pr050414x

Gokhin, D. S., and Fowler, V. M. (2013). A two-segment model for thin filament architecture in skeletal muscle. *Nat. Rev. Mol. Cell Biol.* 14, 113–119. doi: 10.1038/nrm3510

Gokhin, D. S., Kim, N. E., Lewis, S. A., Hoenecke, H. R., D'Lima, D. D., and Fowler, V. M. (2012). Thin-filament length correlates with fiber type in human skeletal muscle. *Am. J. Physiol. Cell Physiol.* 302, C555–C565. doi: 10.1152/ajpcell.00299.2011

Gokhin, D. S., Lewis, R. A., McKeown, C. R., Nowak, R. B., Kim, N. E., Littlefield, R. S., et al. (2010). Tropomodulin isoforms regulate thin filament pointed-end capping and skeletal muscle physiology. *J. Cell Biol.* 189, 95–109. doi: 10.1083/jcb.201001125

Gokhin, D. S., Tierney, M. T., Sui, Z., Sacco, A., and Fowler, V. M. (2014). Calpain-mediated proteolysis of tropomodulin isoforms leads to thin filament elongation in dystrophic skeletal muscle. *Mol. Biol. Cell* 25, 852–865. doi: 10.1091/mbc.E13-10-0608

Gokhin, D. S., Ward, S. R., Bremner, S. N., and Lieber, R. L. (2008). Quantitative analysis of neonatal skeletal muscle functional improvement in the mouse. *J. Exp. Biol.* 211, 837–843. doi: 10.1242/jeb.014340

Gordon, A. M., Huxley, A. F., and Julian, F. J. (1966). The variation in isometric tension with sarcomere length in vertebrate muscle fibres. *J. Physiol.* 184, 170–192.

Granzier, H. L., Akster, H. A., and Ter Keurs, H. E. (1991). Effect of thin filament length on the force-sarcomere length relation of skeletal muscle. *Am. J. Physiol.* 260, C1060–C1070.

Gregorio, C. C., Weber, A., Bondad, M., Pennise, C. R., and Fowler, V. M. (1995). Requirement of pointed-end capping by tropomodulin to maintain actin filament length in embryonic chick cardiac myocytes. *Nature* 377, 83–86. doi: 10.1038/377083a0

Huxley, H., and Hanson, J. (1954). Changes in the cross-striations of muscle during contraction and stretch and their structural interpretation. *Nature* 173, 973–976. doi: 10.1038/173973a0

Larsson, L., Muller, U., Li, X., and Schiaffino, S. (1995). Thyroid hormone regulation of myosin heavy chain isoform composition in young and old rats, with special reference to IIX myosin. *Acta Physiol. Scand.* 153, 109–116. doi: 10.1111/j.1748-1716.1995.tb09841.x

Littlefield, R., Almenar-Queralt, A., and Fowler, V. M. (2001). Actin dynamics at pointed ends regulates thin filament length in striated muscle. *Nat. Cell Biol.* 3, 544–551. doi: 10.1038/35078517

Littlefield, R., and Fowler, V. M. (2002). Measurement of thin filament lengths by distributed deconvolution analysis of fluorescence images. *Biophys. J.* 82, 2548–2564. doi: 10.1016/S0006-3495(02)75598-7

Mardahl-Dumesnil, M., and Fowler, V. M. (2001). Thin filaments elongate from their pointed ends during myofibril assembly in *Drosophila*

indirect flight muscle. *J. Cell Biol.* 155, 1043–1053. doi: 10.1083/jcb.200108026

Nagaoka, R., Minami, N., Hayakawa, K., Abe, H., and Obinata, T. (1996). Quantitative analysis of low molecular weight G-actin-binding proteins, cofilin, ADF and profilin, expressed in developing and degenerating chicken skeletal muscles. *J. Muscle Res. Cell Motil.* 17, 463–473. doi: 10.1007/BF00123362

Ochala, J., Gokhin, D. S., Penisson-Besnier, I., Quijano-Roy, S., Monnier, N., Lunardi, J., et al. (2012). Congenital myopathy-causing tropomyosin mutations induce thin filament dysfunction via distinct physiological mechanisms. *Hum. Mol. Genet.* 21, 4473–4485. doi: 10.1093/hmg/dds289

O'Connell, K., Gannon, J., Doran, P., and Ohlendieck, K. (2007). Proteomic profiling reveals a severely perturbed protein expression pattern in aged skeletal muscle. *Int. J. Mol. Med.* 20, 145–153. doi: 10.3892/ijmm.20.2.145

Ottenheijm, C. A., Witt, C. C., Stienen, G. J., Labeit, S., Beggs, A. H., and Granzier, H. (2009). Thin filament length dysregulation contributes to muscle weakness in nemaline myopathy patients with nebulin deficiency. *Hum. Mol. Genet.* 18, 2359–2369. doi: 10.1093/hmg/ddp168

Pappas, C. T., Krieg, P. A., and Gregorio, C. C. (2010). Nebulin regulates actin filament lengths by a stabilization mechanism. *J. Cell Biol.* 189, 859–870. doi: 10.1083/jcb.201001043

Ryall, J. G., Schertzer, J. D., and Lynch, G. S. (2008). Cellular and molecular mechanisms underlying age-related skeletal muscle wasting and weakness. *Biogerontology* 9, 213–228. doi: 10.1007/s10522-008-9131-0

Sultan, K. R., Dittrich, B. T., Leisner, E., Paul, N., and Pette, D. (2001). Fiber type-specific expression of major proteolytic systems in fast- to slow-transforming rabbit muscle. *Am. J. Physiol. Cell Physiol.* 280, C239–C247.

Sussman, M. A., Baque, S., Uhm, C. S., Daniels, M. P., Price, R. L., Simpson, D., et al. (1998). Altered expression of tropomodulin in cardiomyocytes disrupts the sarcomeric structure of myofibrils. *Circ. Res.* 82, 94–105. doi: 10.1161/01.RES.82.1.94

Tsukada, T., Pappas, C. T., Moroz, N., Antin, P. B., Kostyukova, A. S., and Gregorio, C. C. (2010). Leiomodin-2 is an antagonist of tropomodulin-1 at the pointed end of the thin filaments in cardiac muscle. *J. Cell Sci.* 123, 3136–3145. doi: 10.1242/jcs.071837

Walker, S. M., and Schrodt, G. R. (1974). I segment lengths and thin filament periods in skeletal muscle fibers of the Rhesus monkey and the human. *Anat. Rec.* 178, 63–81. doi: 10.1002/ar.1091780107

Weigt, C., Schoepper, B., and Wegner, A. (1990). Tropomyosin-troponin complex stabilizes the pointed ends of actin filaments against polymerization and depolymerization. *FEBS Lett.* 260, 266–268. doi: 10.1016/0014-5793(90)80119-4

Conflict of Interest Statement: The authors declare that the research was conducted in the absence of any commercial or financial relationships that could be construed as a potential conflict of interest.

Received: 27 August 2014; accepted: 10 September 2014; published online: 29 September 2014.

*Citation: Gokhin DS, Dubuc EA, Lian KQ, Peters LL and Fowler VM (2014) Alterations in thin filament length during postnatal skeletal muscle development and aging in mice. Front. Physiol. **5**:375. doi: 10.3389/fphys.2014.00375*

This article was submitted to Striated Muscle Physiology, a section of the journal Frontiers in Physiology.

Copyright © 2014 Gokhin, Dubuc, Lian, Peters and Fowler. This is an open-access article distributed under the terms of the Creative Commons Attribution License (CC BY). The use, distribution or reproduction in other forums is permitted, provided the original author(s) or licensor are credited and that the original publication in this journal is cited, in accordance with accepted academic practice. No use, distribution or reproduction is permitted which does not comply with these terms.

frontiers in PHYSIOLOGY

MINI REVIEW ARTICLE
published: 30 October 2014
doi: 10.3389/fphys.2014.00421

O-GlcNAcylation, contractile protein modifications and calcium affinity in skeletal muscle

Caroline Cieniewski-Bernard[1,2], Matthias Lambert[1,2], Erwan Dupont[1,2], Valérie Montel[1,2], Laurence Stevens[1,2] and Bruno Bastide[1,2]*

[1] *Université Lille, Lille, France*
[2] *EA4488, APMS, URePsss, Université de Lille 1, Villeneuve d'Ascq, France*

Edited by:
Julien Ochala, King's College London, UK

Reviewed by:
Christina Karatzaferi, University of Thessaly, Greece
Ranganath Mamidi, Case Western Reserve University, USA

****Correspondence:***
Bruno Bastide, EA4488 Laboratoire Activité Physique, Muscle et Santé, Biology Department, Université de Lille 1, Bât SN4, UFR Biology, 59655 Villeneuve d'Ascq, France
e-mail: bruno.bastide@univ-lille1.fr

O-GlcNAcylation, a generally undermined atypical protein glycosylation process, is involved in a dynamic and highly regulated interplay with phosphorylation. Akin to phosphorylation, O-GlcNAcylation is also involved in the physiopathology of several acquired diseases, such as muscle insulin resistance or muscle atrophy. Recent data underline that the interplay between phosphorylation and O-GlcNAcylation acts as a modulator of skeletal muscle contractile activity. In particular, the O-GlcNAcylation level of the phosphoprotein myosin light chain 2 seems to be crucial in the modulation of the calcium activation properties, and should be responsible for changes in calcium properties observed in functional atrophy. Moreover, since several key structural proteins are O-GlcNAc-modified, and because of the localization of the enzymes involved in the O-GlcNAcylation/de-O-GlcNAcylation process to the nodal Z disk, a role of O-GlcNAcylation in the modulation of the sarcomeric structure should be considered.

Keywords: O-GlcNAcylation, phosphorylation, O-GlcNAcylation/phosphorylation interplay, contractile proteins, MLC2, contractile properties, sarcomeric structure

O-GlcNAcylation, AN ATYPICAL GLYCOSYLATION

Nowadays, it is well admitted that the phosphorylation does not act alone in the fine modulation of numerous cellular processes, but rather, presents a dynamic and highly regulated interplay with an atypical glycosylation, the O-linked N-acetyl-glucosaminylation (termed O-GlcNAcylation), occurring on nuclear, cytoplasmic and mitochondrial proteins (Hart et al., 2007; Cao et al., 2013; Johnsen et al., 2013). This minireview is based on significant references focused on the recent advancements concerning the link between O-GlcNAcylation, contractile proteins and calcium affinity in skeletal muscle (**Figure 1**).

The O-GlcNAcylation of proteins results from the transfer of N-acetyl-β-D-glucosamine from the high energy donor substrate UDP-GlcNAc (synthesized through the hexosamine biosynthesis pathway) onto the hydroxyl group of serine and threonine residues of target proteins by the uridine diphospho-N-acetyl glucosaminyl transferase (O-GlcNAc transferase or OGT). The β-N-acetylglucosaminidase (O-GlcNAcase or OGA) catalyzes the removal of O-GlcNAc residues from proteins (Dong and Hart, 1994; Gao et al., 2001; Wells et al., 2002). Thus, like phosphorylation, the addition/removal of GlcNAc moieties on the proteins results from the concerted action of two antagonist enzymes. Reversible, O-GlcNAcylation is highly dynamic, and responds rapidly to changes in environmental conditions (Hart et al., 2007). Since OGT is coded from only one gene (Kreppel et al., 1997), the regulation of its activity, its localization in cell, or its specificity toward protein targets are ensured by targeting proteins, such as protein phosphatase 1 (PP1), Milton (OIP106), p38MAP kinase, myosin phosphatase 1 (MYPT1) or peroxisome-proliferator-activated receptor-co-activator-1alpha (PGC1α), transiently associated with OGT through tetratricopeptide repeats (TPR domains) at the N-termini of the transferase (Iyer and Hart, 2003; Iyer et al., 2003; Wells et al., 2004; Cheung and Hart, 2008; Cheung et al., 2008; Housley et al., 2009). In the same way, the OGA could also be associated with other proteins like calcineurin or heat shock proteins among others (Wells et al., 2001). Moreover, an unusual association of the two opposing OGA/OGT was described, forming a single O-GlcNAczyme complex (Whisenhunt et al., 2006).

The analysis of O-GlcNAc pattern, the quantification of variation of O-GlcNAcylation on proteins and the identification of the glycosylated sites are crucial for the understanding of the role of this atypical glycosylation. Methodological approaches include western blot analyses using antibodies directed against O-GlcNAc moieties or lectins (Zachara et al., 2011), or the labeling of O-GlcNAcylated proteins with galactosyltransferase and coupling of different kind of substrates (Zachara et al., 2011). Moreover, the identification and mapping of O-GlcNAc modification sites have been at the origin of several technical developments during the 10 last years (Ma and Hart, 2014 for review).

O-GlcNAcylation has been shown to be involved in almost all cellular processes, including signal transduction, protein degradation or regulation of gene expression (Hart et al., 2011; Bond and Hanover, 2013). O-GlcNAcylation has been also demonstrated to act as an inducible, cytoprotective stress response. Indeed, increase in O-GlcNAcylation of nucleocytoplasmic proteins

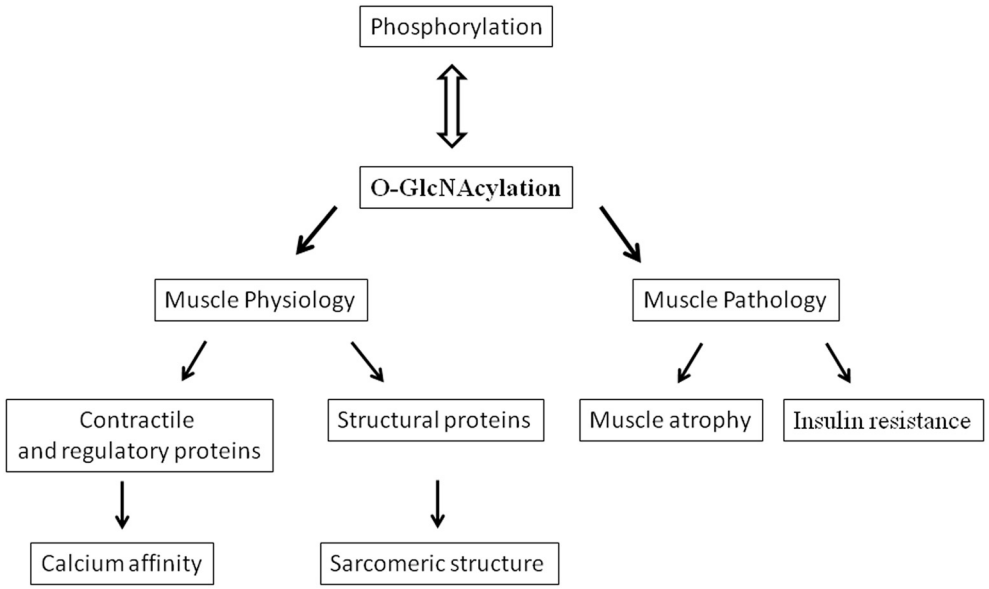

FIGURE 1 | Diagram showing various effects and implications of O-GlcNAcylation in skeletal muscle.

protects cells with an induction of heat shock proteins (Zachara et al., 2004). In cardiomyocytes, O-GlcNAcylation can attenuate oxidative stress through inhibition of calcium overload and ROS generation (Ngoh et al., 2010). Studies performed with OGT and OGA knockout mice have demonstrated that O-GlcNAc is crucial for life since O-GlcNAcylation was essential for embryonic stem cell viability and is implicated in the aging process, elevation of O-GlcNAcylation being altered in different tissues of different ages (Shafi et al., 2000; Yang et al., 2012). Moreover, many reports demonstrate that O-GlcNAcylation might play a role in the physiopathology of several acquired diseases, such as cancer, cardiovascular diseases, neurodegenerative diseases, Alzheimer or type II diabetes (Lefebvre et al., 2010; Slawson et al., 2010; Nakamura et al., 2012; Bond and Hanover, 2013; Ma and Hart, 2013; Ma and Vosseller, 2013; Förster et al., 2014). Indeed, increased O-GlcNAcylation is closely linked to insulin resistance and hyperglycemia-induced glucose toxicity.

O-GlcNAcylation, SKELETAL MUSCLE, AND INSULIN-RESISTANCE

The concept of a role of O-GlcNAcylation in skeletal muscle has emerged from studies considering muscle as one of the crucial insulin-sensitive tissue; indeed, skeletal muscle is responsible for more than 80% of insulin-stimulated glucose uptake in humans. In the past decades, studies in rodents (Hawkins et al., 1997a,b) suggested a correlation between the development of insulin resistance and increased UDP-GlcNAc concentrations in muscle. Thus, raising O-GlcNAc level in skeletal muscle has been demonstrated to induce insulin resistance (Arias and Cartee, 2005, **Figure 1**), while coinfusion of insulin and glucosamine, increasing UDP-GlcNAc, enhances the O-GlcNAc modification on numerous unidentified skeletal muscle proteins (Yki-Jarvinen et al., 1998). Moreover, transgenic mice overexpressing GLUT1 in skeletal muscle was insulin resistant and exhibit chronically increased glucose flow and increased UDP-GlcNAc concentrations in muscle (Buse et al., 1996); indeed, 2–5% of the glucose entering into the cell is directed to the hexosamine biosynthesis pathway, leading to the synthesis of UDP-GlcNAc, the donor for O-GlcNAcylation. More recently, it has been suggested that mitochondrial and contractile dysfunctions, observed in the development of Type 2 diabetes, were linked to the increase in O-GlcNAcylation level (Johnsen et al., 2013). Thus, in rats artificially selected for Low Running Capacity (LCR rats), predisposed to becoming obese, and developing insulin resistance and cardiovascular dysfunction, the increase in O-GlcNAcylation on mitochondrial proteins and SERCA was associated with mitochondrial dysfunction and changes in contractile properties (Koch et al., 2012). In the LCR heart myocytes, the cardiovascular dysfunction could be attributed to the decline in the contractility, correlated to the impaired intracellular Ca^{2+} handling and signaling (Koch et al., 2012). Hu et al. (2005) demonstrated also the correlation between O-GlcNAcylation and diabetes since they demonstrated that adenoviral transfer of OGA into the myocardium of streptozotocin induced diabetic mice, reversed the excessive O-GlcNAc modifications associated with diabetes, particularly in the contractile dysfunctions and Ca^{2+} handling capacities (Hu et al., 2005). The decline in contractibility could be related to the decrease in calcium affinity and sensitivity reported in skinned cardiac fibers in presence of GlcNAc (Ramirez-Correa et al., 2008) but rather involved changes in expression of SERCA (Hu et al., 2005; Johnsen et al., 2013). This role of O-GlcNAcylation should be considered also in skeletal muscle since dysfunction of contractibility as well as the Ca^{2+} handling were also measured in skeletal muscle of rat models of diabetes (Eshima et al., 2013), via impaired SERCA and Glut 4 (Safwat et al., 2013).

O-GlcNAcylation/PHOSPHORYLATION INTERPLAY AND SKELETAL MUSCLE CONTRACTILE ACTIVITY

Phosphorylation was well-admitted for a long time to regulate many key processes in muscle physiology. Among them, phosphorylation is a key regulator of the intracellular signaling pathways involved in muscle mass and phenotype adaptation to physiological demands. Moreover, phosphorylation is involved in myofibrillar physiology, such as muscular contraction or cellular structuration through the modulation of protein-protein interactions. Indeed, phosphorylation has been demonstrated to play a crucial role in the regulation of the contractile properties in striated muscle, but recent reports suggested that O-GlcNAcylation might play a role as important as phosphorylation in muscle physiology. Thus, many proteins of muscle proteome have been identified to be O-GlcNAc modified (Cieniewski-Bernard et al., 2004, 2012; Hedou et al., 2007; Ramirez-Correa et al., 2008). Among them, several key contractile proteins of striated muscle are concerned, i.e., myosin heavy chains (slow MHCI as well as the fast isoforms MHCIIA and MHCIIB), myosin light chains (essential MLC or MLC1 and regulatory MLC or MLC2), actin, both α and β isoforms of tropomyosin as well as isoforms of TnI and TnT. It is noteworthy that it is not known whether TnC, the calcium-sensor, bears an O-GlcNAc moiety or not.

While contraction is triggered by calcium release, it is regulated by several myofilament proteins such as the regulatory myosin light chain (termed MLC2). MLC2 phosphorylation is not essential for skeletal muscle contraction but is an important regulatory mechanism since it can produce changes in thick filament structure and enhance crossbridge attachment (Szczesna et al., 2002). For instance, phosphorylation of MLC2, catalyzed by a Ca^{2+}/calmodulin-dependant MLC kinase, increases the force development at submaximal calcium concentration, conferring a higher calcium sensitivity to the fibers (Persechini et al., 1985; Stephenson and Stephenson, 1993; Sweeney et al., 1993; Szczesna et al., 2002).

Our recent data highlight the key role of O-GlcNAcylation as a modulator of skeletal muscle contractile activity, in particular on the calcium activation properties (Hedou et al., 2007; Cieniewski-Bernard et al., 2012). Indeed, muscle skinned fibers, when exposed to N-acetyl-D-glucosamine, present a reversible decrease in calcium sensitivity and affinity, whereas the cooperativity within the thin filament was not changed (Hedou et al., 2007). This modulation probably involved disruption of protein-protein interactions through O-GlcNAc moieties. Interestingly, a similar effect was observed in rats as well as in human skinned fibers (Cieniewski-Bernard et al., 2009) and also measured in cardiac trabeculae (Ramirez-Correa et al., 2008).

Further experiments performed after the pharmacological increase of O-GlcNAcylation level of contractile protein glycosylation, using PUGNAc or Thiamet G, two inhibitors of OGA (Gloster and Vocadlo, 2010), leads to an increase of calcium affinity on slow soleus skinned fibers (Cieniewski-Bernard et al., 2012). Several regulatory contractile proteins, predominantly fast isoforms, presented a drastic increase in their O-GlcNAc level. Since the only slow isoform of contractile protein (and so the more representative isoforms in the slow skeletal muscle) presenting an increase of O-GlcNAc level was the myosin regulatory light chains MLC2, the effect of enhanced O-GlcNAcylation pattern on calcium activation parameters of slow soleus fibers was attributed to the increase of the O-GlcNAcylation of sMLC2 (Cieniewski-Bernard et al., 2012).

All these data closely linked O-GlcNAcylation to the modulation of contractile activity of skeletal muscle, a decrease in O-GlcNAcylation being associated to a decrease in calcium affinity and reciprocally (**Figure 1**). Moreover, analysis of the proteins presenting changes in their O-GlcNAc level states suggests that MLC2 could play an important role in this modulation. Since MLC2 was identified to be O-GlcNAcylated (Hedou et al., 2007), and because of the potential antagonism between phosphorylation and O-GlcNAcylation, i.e., the potential O-GlcNAcylated site corresponds to the only site of phosphorylation in MLC2 located in Ser 14 for the rat slow MLC2 isoform (Blumenthal and Stull, 1980; Ramirez-Correa et al., 2008), the O-GlcNAcylation should be considered as a potential new mechanism that could modulate the contractile properties of skeletal muscle as well as the phosphorylated states of MLC2.

O-GlcNAcylation/PHOSPHORYLATION INTERPLAY, AND SKELETAL MUSCLE CONTRACTILE DYSFUNCTION IN ATROPHIED MUSCLE

Muscle atrophy characterized skeletal muscle adaptation to a large variety of disuse conditions (immobilization, microgravity, bed rest, or nerve injury). This atrophy results from a reduction in fiber diameter, protein content and is associated with slow to fast phenotype transitions accompanied by functional changes such as loss in force and increased fatigability (Baldwin et al., 1996; Fitts et al., 2000; Fluck and Hoppeler, 2003; Mounier et al., 2009). Moreover a role of O-GlcNAcylation in the development of muscle atrophy has been suggested (Cieniewski-Bernard et al., 2006; **Figure 1**). Indeed, a correlation between variations in O-GlcNAcylation levels and the development of atrophy after hindlimb unloading was shown, suggesting that O-GlcNAc variations could control the muscle protein homeostasis (Cieniewski-Bernard et al., 2006). In particular, it was suggested that O-GlcNAcylation should be implicated in the regulation of muscular atrophy as a protective mechanism against proteasomal degradation (Cieniewski-Bernard et al., 2006). It was also recently described that muscle-specific overexpression of NCOATGK, a splice variant of O-GlcNAcase, induces skeletal muscle atrophy (Huang et al., 2011).

We have demonstrated that the slow-to-fast transition (at MHC and MLC2 level) concomittantly to soleus muscle atrophy was correlated with an increase of the global level of MLC2 phosphorylation in rat hindlimb unloading model (Bozzo et al., 2005) as well as in human patients who were subjected to 2-months Bed Rest (Stevens et al., 2013). However, similar variations in MLC2 phosphorylation have been observed when clenbuterol was administrated to rats; in such case, muscle hypertrophy was associated to slow-to-fast transition in rats (Bozzo et al., 2003).

Thus, the slow-to-fast MLC2 transition was associated to an increase of phosphorylation level of the two isoforms regardless of whether hypertrophy or atrophy develops. Moreover, although numerous data argue that MLC2 phosphorylation lead to higher calcium sensitivity in skeletal muscle, an increase in MLC2

phosphorylation was measured after muscle atrophy whereas the calcium sensitivity decreases (Bozzo et al., 2003). Similar data were obtained from phosphoproteome analysis in human aged muscle (Gannon et al., 2008). These data could indicate that the decrease in calcium sensitivity occurring during hindlimb unloading could involve another type of regulation than classical phosphorylation. Since we demonstrated that a decrease in calcium affinity was measured when O-GlcNAcylation is reduced, and since a decrease in O-GlcNAcylation is observed in atrophied muscle, one hypothesis is that O-GlcNAcylation might be involved in this alteration.

To support this hypothesis, the variation of O-GlcNAcylation level on MLC2, as well as its interplay with phosphorylation, was investigated in atrophied soleus muscle (Cieniewski-Bernard et al., in press). Interestingly, an antagonism between phosphorylation and O-GlcNAcylation was demonstrated on the slow MLC2 in a rat model of hindlimb unloading, largely used to induce functional atrophy of antigravitary muscles such as soleus (Cieniewski-Bernard et al., in press), since a decrease in MLC2 O-GlcNAcylation was measured in atrophied soleus associated to the increase in phosphorylation states as previously described. More importantly, the use of Phos-Tag acrylamide gels allowed the authors to analyze the O-GlcNAcylation state on each phosphorylated form of MLC2 (Cieniewski-Bernard et al., in press). It was demonstrated that the two post-translational modifications were mutually exclusive, and that this interplay was closely associated to load because of the reversibility of these processes occurring during reloading. Interestingly, it was demonstrated that the enzymes involved in the phosphorylation/dephosphorylation and O-GlcNAcylation/de-O-GlcNAcylation processes were associated within a multi-enzymatic complex, and were localized to the nodal Z disk region of the sarcomere. All these results are in favor of an interplay between phosphorylation and O-GlcNAcylation on MLC2, probably through the same site.

This interplay between phosphorylation and O-GlcNAcylation in the fine modulation of MLC2 activity was also observed in humans (Stevens et al., 2013). Indeed, the post-translational modifications of MLC2 were investigated in soleus biopsies obtained from 60-days Bed-Rest female subjects. In this cohort, several groups were formed: 60-days Bed Rest (BR), BR + Exercice (combined aerobic and resistive exercises), and BR + Nutritional protocol (leucine and valine diet). The slow-fast phenotype transition of MLC2 was associated to an increase of the phosphorylation states of slow and fast isoforms MLC2 while the global MLC2 glycosylation level was decreased. Interestingly, aerobic and resistive exercises, which preserved muscles from BR changes (and so slow-to-fast transition), also prevented this antagonism.

Taken together, all these data clearly corroborated the interplay between phosphorylation and O-GlcNAcylation on MLC2, in animal and in human models of functional atrophy. Indeed, the decrease in calcium sensitivity as well as calcium affinity measured in skinned fibers of atrophied muscle soleus cannot be obviously explained by the increase in MLC2 phosphorylation state, as it was previously described (Bozzo et al., 2003). Since previous experiments have demonstrated that decrease in O-GlcNAcylation was associated to a decrease in calcium sensitivity and affinity, whereas its phosphorylated state increased in atrophied muscle, MLC2 O-GlcNAcylation state could be predominantly involved in the alteration of contractile parameters observed in atrophied soleus. In contrast, the MLC2 phosphorylation might be rather associated to phenotype transition than to changes in contractile parameters in atrophied muscle. Interestingly, some data support for a structural role of MLC2 phosphorylation: MLC2 phosphorylation induces stress fiber assembly in nonmuscle cells (Katoh et al., 2001) and mediates sarcomere organization during hypertrophic growth in cardiac muscle (Aoki et al., 2000).

However, further functional experiments need to be performed to demonstrate unambiguously that the phosphorylation/O-GlcNAcylation balance of MLC2 might be directly involved in the decrease in calcium sensitivity and affinity observed in atrophied muscles. While recent reports focused on MLC2, other regulatory contractile proteins have been demonstrated to be O-GlcNAcylated such as Tropomyosin, TnT and TnI (Cieniewski-Bernard et al., 2012). We cannot totally exclude that the glycosylation state of these proteins nor that unidentified O-GlcNAc proteins (more particularly, TnC is one of them) might play a role in the modulation of contractile activity.

MYOFIBRILLAR PROTEINS O-GlcNAcylation AND PERSPECTIVES

From the data described above, it seems very likely that O-GlcNAcylation plays a major role in modulating the contractile activity in skeletal muscle. However, the role of the O-GlcNAcylation might also concern other mechanisms involved in the sarcomeric structure. The preferential localization of OGT and OGA in the sarcomere, more particularly at the Z disk region (Cieniewski-Bernard et al., in press), argue for an important role of O-GlcNAcylation in this nodal region that could influence mechanisms other than the modulation of the contractile activity. Indeed, it was demonstrated that myosin, actin but also key proteins involved in the sarcomeric structure (desmin, actinin, αB-crystallin, and ZASP) were modified by O-GlcNAc moieties (Cieniewski-Bernard et al., 2012; Leung et al., 2013). Interestingly, we demonstrated that the O-GlcNAc sites on myosin were localized in a region involved in polymerization and interaction of myosin with proteins partner such as myomesin, M-protein or titin (Hedou et al., 2009) supporting a role for O-GlcNAcylation in the organization of the sarcomere (**Figure 1**). This hypothesis is underlined by the fact that numerous structural proteins are modified by O-GlcNAc: beta3 integrin (Ahmad et al., 2006), vinculin (Laczy et al., 2010), spectrin (Zhang and Bennett, 1996), alphaB-crystallin (Roquemore et al., 1996), laminin (Kwak et al., 2010), or cytokeratin (Ku and Omary, 1995), and variation of O-GlcNAcylation of the intermediate filaments has been demonstrated to lead to defective phosphorylated states and so to polymerization (Farah and Galileo, 2008; Slawson et al., 2008). Moreover, O-GlcNAcylation modulates organization and solubilization of cytokeratin (Rotty et al., 2010; Srikanth et al., 2010). Interestingly, It has been demonstrated that the intermediate filament proteins, vimentin and desmin, possess lectin-like properties toward O-GlcNAc moieties, supporting

physiological interaction between GlcNAc-bearing ligands (and so O-GlcNAc proteins) and lectinic proteins (Ise et al., 2010). The assembly and regular arrangement of the sarcomere results from highly regulated interactions between myofibrillar proteins and structural proteins which are at the origin of a sarcomeric cytoskeleton. It's becoming evident from recent data that a role of O-GlcNAcylation in the organization of the sarcomere should be considered. Since phosphorylation has been demonstrated to be involved in protein-protein interactions, a balance between phosphorylation and O-GlcNAcylation might modulate the dynamics of the sarcomere structural organization. Future investigations will be conducted with aim to determine the role of O-GlcNAcylation in the organization and dynamic of the sarcomere. This work may provide new insights in the understanding of molecular mechanisms of diseases characterized by a disintegration of myofibrils and marked disorganization of the Z band region such as myofibrillar and congenital myopathies.

ACKNOWLEDGMENTS

This work was supported by grants from the Région Nord-Pas-de-Calais 2011 (Emergent Research Project n°12003808) and the CNES (French Spatial Agency, n°4800000716).

REFERENCES

Ahmad, I., Hoessli, D. C., Walker-Nasir, E., Choudhary, M. I., Rafik, S. M., Shakoori, A. R., et al. (2006). Phosphorylation and glycosylation interplay: protein modifications at hydroxy amino acids and prediction of signaling functions of the human beta3 integrin family. *J. Cell. Biochem.* 99, 706–718. doi: 10.1002/jcb.20814

Aoki, H., Sadoshima, J., and Izumo, S. (2000). Myosin light chain kinase mediates sarcomere organization during cardiac hypertrophy *in vitro*. *Nat. Med.* 6, 183–188. doi: 10.1038/72287

Arias, E. B., and Cartee, G. D. (2005). Relationship between protein O-linked glycosylation and insulin-stimulated glucose transport in rat skeletal muscle following calorie restriction or exposure to O-(2-acetamido-2-deoxy-d-glucopyranosylidene)amino-N-phenylcarbamate. *Acta Physiol. Scand.* 183, 281–289. doi: 10.1111/j.1365-201X.2004.01403.x

Baldwin, K. M., White, T. P., Arnaud, S. B., Edgerton, V. R., Kraemer, W. J., Kram, R., et al. (1996). Musculoskeletal adaptations to weightlessness and development of effective countermeasures. *Med. Sci. Sports Exerc.* 28, 1247–1253. doi: 10.1097/00005768-199610000-00007

Blumenthal, D. K., and Stull, J. T. (1980). Activation of skeletal muscle myosin light chain kinase by calcium$^{(2+)}$ and calmodulin. *Biochemistry* 19, 5608–5614. doi: 10.1021/bi00565a023

Bond, M. R., and Hanover, J. A. (2013). O-GlcNAc cycling: a link between metabolism and chronic disease. *Annu. Rev. Nutr.* 33, 205–229. doi: 10.1146/annurev-nutr-071812-161240

Bozzo, C., Spolaore, B., Toniolo, L., Stevens, L., Bastide, B., Cieniewski-Bernard, C., et al. (2005). Nerve influence on myosin light chain phosphorylation in slow and fast skeletal muscles. *FEBS J.* 272, 5771–5785. doi: 10.1111/j.1742-4658.2005.04965.x

Bozzo, C., Stevens, L., Toniolo, L., Mounier, Y., and Reggiani, C. (2003). Increased phosphorylation of myosin light chain associated with slow-to-fast transition in rat soleus. *Am. J. Physiol. Cell Physiol.* 285, C575–C583. doi: 10.1152/ajpcell.00441.2002

Buse, M. G., Robinson, K. A., Marshall, B. A., and Mueckler, M. (1996). Differential effects of GLUT1 and GLUT4 overexpression on hexosamine biosynthesis by muscles of transgenic mice. *J. Biol. Chem.* 271, 23197–23202. doi: 10.1074/jbc.271.38.23197

Cao, W., Cao, J., Huang, J., Yao, J., Yan, G., Xu, H., et al. (2013). Discovery and confirmation of O-GlcNAcylated proteins in rat liver mitochondria by combination of mass spectrometry and immunological methods. *PLoS ONE* 8:e76399. doi: 10.1371/journal.pone.0076399

Cheung, W. D., and Hart, G. W. (2008). AMP-activated protein kinase and p38 MAPK activate O-GlcNAcylation of neuronal proteins during glucose deprivation. *J. Biol. Chem.* 283, 13009–13020. doi: 10.1074/jbc.M801222200

Cheung, W. D., Sakabe, K., Housley, M. P., Dias, W. B., and Hart, G. W. (2008). O-linked beta-N-acetylglucosaminyltransferase substrate specificity is regulated by myosin phosphatase targeting and other interacting proteins. *J. Biol. Chem.* 283, 33935–33941. doi: 10.1074/jbc.M806199200

Cieniewski-Bernard, C., Bastide, B., Lefebvre, T., Lemoine, J., Mounier, Y., and Michalski, J. C. (2004). Identification of O-linked N-acetylglucosamine proteins in rat skeletal muscle using two-dimensional gel electrophoresis and mass spectrometry. *Mol. Cell. Proteomics* 3, 577–585. doi: 10.1074/mcp.M400024-MCP200

Cieniewski-Bernard, C., Dupont, E., Richard, E., and Bastide, B. (in press). Phospho-GlcNAc modulation of slow MLC2 during soleus atrophy through a multienzymatic and sarcomeric complex. *Pflugers Arch.* doi: 10.1007/s00424-014-1453-y

Cieniewski-Bernard, C., Montel, V., and Bastide, B. (2012). Increasing O-GlcNAcylation level on organ culture of soleus modulates the calcium activation parameters of muscle fibers. *PLoS ONE* 7:e48218. doi: 10.1371/journal.pone.0048218

Cieniewski-Bernard, C., Montel, V., Stevens, L., and Bastide, B. (2009). O-GlcNAcylation, an original modulator of contractile activity in striated muscle. *J. Muscle Res. Cell Motil.* 30, 281–287. doi: 10.1007/s10974-010-9201-1

Cieniewski-Bernard, C., Mounier, Y., Michalski, J. C., and Bastide, B. (2006). O-GlcNAc level variations are associated with the development of skeletal muscle atrophy. *J. Appl. Physiol.* 100, 1499–1505. doi: 10.1152/japplphysiol.00865.2005

Dong, D. L., and Hart, G. W. (1994). Purification and characterization of an O-GlcNAc selective N-acetyl-beta-D-glucosaminidase from rat spleen cytosol. *J. Biol. Chem.* 269, 19321–19330.

Eshima, H., Tanaka, Y., Sonobe, T., Inagaki, T., Nakajima, T., Poole, D. C., et al. (2013). *In vivo* imaging of intracellular Ca^{2+} after muscle contractions and direct Ca^{2+} injection in rat skeletal muscle in diabetes. *Am. J. Physiol.* 305, R610–R618. doi: 10.1152/ajpregu.00023.2013

Farah, A. M., and Galileo, D. S. (2008). O-GlcNAc modification of radial glial vimentin filaments in the developing chick brain. *Brain Cell Biol.* 36, 191–202. doi: 10.1007/s11068-008-9036-5

Fitts, R. H., Riley, D. R., and Widrick, J. J. (2000). Physiology of a microgravity environment invited review: microgravity and skeletal muscle. *J. Appl. Physiol.* 89, 823–839.

Fluck, M., and Hoppeler, H. (2003). Molecular basis of skeletal muscle plasticity–from gene to form and function. *Rev. Physiol. Biochem. Pharmacol.* 146, 159–216. doi: 10.1007/s10254-002-0004-7

Förster, S., Welleford, A. S., Triplett, J. C., Sultana, R., Schmitz, B., and Butterfield, D. A. (2014). Increased O-GlcNAc levels correlate with decreased O-GlcNAcase levels in Alzheimer disease brain. *Biochim. Biophys. Acta.* 1842, 1333–1339. doi: 10.1016/j.bbadis.2014.05.014

Gannon, J., Staunton, L., O'Connell, K., Doran, P., and Ohlendieck, K. (2008). Drastic increase of myosin light chain MLC-2 in senescent skeletal muscle indicates fast-to-slow fibre transition in sarcopenia of old age. *Int. J. Mol. Med.* 22, 33–42. doi: 10.1016/j.ejcb.2009.06.004

Gao, Y., Wells, L., Comer, F. I., Parker, G. J., and Hart, G. W. (2001). Dynamic O-glycosylation of nuclear and cytosolic proteins: cloning and characterization of a neutral, cytosolic beta-N-acetylglucosaminidase from human brain. *J. Biol. Chem.* 276, 9838–9845. doi: 10.1074/jbc.M010420200

Gloster, T. M., and Vocadlo, D. J. (2010). Mechanism, structure, and inhibition of O-GlcNAc processing enzymes. *Curr. Signal Transduct. Ther.* 5, 74–91. doi: 10.2174/157436210790226537

Hart, G. W., Housley, M. P., and Slawson, C. (2007). Cycling of O-linked beta-Nacetylglucosamine on nucleocytoplasmic proteins. *Nature* 446, 1017–1022. doi: 10.1038/nature05815

Hart, G. W., Slawson, C., Ramirez-Correa, G., and Lagerlof, O. (2011). Cross talk between O-GlcNAcylation and phosphorylation: roles in signaling, transcription, and chronic disease. *Annu. Rev. Biochem.* 80, 825–858. doi: 10.1146/annurev-biochem-060608-102511

Hawkins, M., Angelov, I., Liu, R., Barzilai, N., and Rossetti, L. (1997a). The tissue concentration of UDP-N-acetylglucosamine modu lates the stimulatory effect of insulin on skeletal muscle glucose uptake. *J. Biol. Chem.* 272, 4889–4895. doi: 10.1074/jbc.272.8.4889

Hawkins, M., Barzilai, N., Liu, R., Hu, M., Chen, W., and Rosetti, L. (1997b). Role of the glucosamine pathway in fat-induced insulin resistance. *J. Clin. Invest.* 99, 2173–2182. doi: 10.1172/JCI119390

Hedou, J., Bastide, B., Page, A., Michalski, J. C., and Morelle, W. (2009). Mapping of O-linked beta-N-acetylglucosamine modification sites in key contractile proteins of rat skeletal muscle. *Proteomics* 9, 2139–2148. doi: 10.1002/pmic.200800617

Hedou, J., Cieniewski-Bernard, C., Leroy, Y., Michalski, J. C., Mounier, Y., and Bastide, B. (2007). O-linked N-acetylglucosaminylation is involved in the Ca^{2+} activation properties of rat skeletal muscle. *J. Biol. Chem.* 282, 10360–10369. doi: 10.1074/jbc.M606787200

Housley, M. P., Udeshi, N. D., Rodgers, J. T., Shabanowitz, J., Puigserver, P., Hunt, D. F., et al. (2009). A PGC-1alpha-O-GlcNAc transferase complex regulates FoxO transcription factor activity in response to glucose. *J. Biol. Chem.* 284, 5148–5157. doi: 10.1074/jbc.M808890200

Hu, Y., Belke, D., Suarez, J., Swanson, E., Clark, R., Hoshijima, M., et al. (2005). Adenovirus-mediated overexpression of O-GlcNAcase improves contractile function in the diabetic heart. *Circ. Res.* 96, 1006–1013. doi: 10.1161/01.RES.0000165478.06813.58

Huang, P., Ho, S. R., Wang, K., Roessler, B. C., Zhang, F., Hu, Y., et al. (2011). Muscle-specific overexpression of NCOATGK, splice variant of O-GlcNAcase, induces skeletal muscle atrophy. *Am. J. Physiol. Cell Physiol.* 300, C456–C465. doi: 10.1152/ajpcell.00124.2010

Ise, H., Kobayashi, S., Goto, M., Sato, T., Kawakubo, M., Takahashi, M., et al. (2010). Vimentin and desmin possess GlcNAc-binding lectin-like properties on cell surfaces. *Glycobiology* 20, 843–864. doi: 10.1093/glycob/cwq039

Iyer, S. P., Akimoto, Y., and Hart, G. W. (2003). Identification and cloning of a novel family of coiled-coil domain proteins that interact with O-GlcNAc transferase. *J. Biol. Chem.* 278, 5399–5409. doi: 10.1074/jbc.M209384200

Iyer, S. P., and Hart, G. W. (2003). Roles of the tetratricopeptide repeat domain in O-GlcNAc transferase targeting and protein substrate specificity. *J. Biol. Chem.* 278, 24608–24616. doi: 10.1074/jbc.M300036200

Johnsen, V. L., Belke, D. D., Hughey, C. C., Hittel, D. S., Hepple, R. T., Koch, L. G., et al. (2013). Enhanced cardiac protein glycosylation (O-GlcNAc) of selected mitochondrial proteins in rats artificially selected for low running capacity. *Physiol. Genomics*. 45, 17–25. doi: 10.1152/physiolgenomics.00111.2012

Katoh, K., Kano, Y., Amano, M., Kaibuchi, K., and Fujiwara, K. (2001). Stress fiber organization regulated by MLCK and Rho-kinase in cultured human fibroblasts. *Am. J. Physiol. Cell Physiol.* 280, C1669–C1679.

Koch, L. G., Britton, S. L., and Wisløff, U. (2012). A rat model system to study complex disease risks, fitness, aging, and longevity. *Trends Cardiovasc. Med.* 22, 29–34. doi: 10.1016/j.tcm.2012.06.007

Kreppel, L. K., Blomberg, M. A., and Hart, G. W. (1997). Dynamic glycosylation of nuclear and cytosolic proteins. Cloning and characterization of a unique O-GlcNAc transferase with multiple tetratricopeptide repeats. *J. Biol. Chem.* 272, 9308–9315. doi: 10.1074/jbc.272.14.9308

Ku, N. O., and Omary, M. B. (1995). Identification and mutational analysis of the glycosylation sites of human keratin 18. *J. Biol. Chem.* 270, 11820–11827. doi: 10.1074/jbc.270.20.11820

Kwak, T. K., Kim, H., Jung, O., Lee, S. A., Kang, M., Kim, H. J., et al. (2010). Glucosamine treatment-mediated O-GlcNAc modification of paxillin depends on adhesion state of rat insulinoma INS- 1 cells. *J. Biol. Chem.* 285, 36021–36031. doi: 10.1074/jbc.M110.129601

Laczy, B., Marsh, S. A., Brocks, C. A., Wittmann, I., and Chatham, J. C. (2010). Inhibition of O-GlcNAcase in perfused rat hearts by NAG-thiazolines at the time of reperfusion is cardioprotective in an O-GlcNAc-dependent manner. *Am. J. Physiol. Heart Circ. Physiol.* 299, H1715–H1727. doi: 10.1152/ajpheart.00337.2010

Lefebvre, T., Dehennaut, V., Guinez, C., Olivier, S., Drougat, L., Mir, A. M., et al. (2010). Dysregulation of the nutrient/stress sensor O-GlcNAcylation is involved in the etiology of cardiovascular disorders, type-2 diabetes and Alzheimer's disease. *Biochim. Biophys. Acta* 1800, 67–79. doi: 10.1016/j.bbagen.2009.08.008

Leung, M. C., Hitchen, P. G., Ward, D. G., Messer, A. E., and Marston, S. B. (2013). Z-band alternatively spliced PDZ motif protein (ZASP) is the major O-linked β-N-acetylglucosamine-substituted protein in human heart myofibrils. *J. Biol. Chem.* 288, 4891–4898. doi: 10.1074/jbc.M112.410316

Ma, J., and Hart, G. W. (2013). Protein O-GlcNAcylation in diabetes and diabetic complications. *Expert Rev. Proteomics.* 10, 365–380. doi: 10.1586/14789450.2013.820536

Ma, J., and Hart, G. W. (2014). O-GlcNAc profiling: from proteins to proteomes. *Clin. Proteomics.* 11:8. doi: 10.1186/1559-0275-11-8

Ma, Z., and Vosseller, K. (2013). O-GlcNAc in cancer biology. *Amino. Acids* 45, 719–733. doi: 10.1007/s00726-013-1543-8

Mounier, Y., Tiffreau, V., Montel, V., Bastide, B., and Stevens, L. (2009). Phenotypical transitions and Ca2_ activation properties in human muscle fibers: effects of a 60-day bed rest and countermeasures. *J. Appl. Physiol.* 106, 1086–1099. doi: 10.1152/japplphysiol.90695.2008

Nakamura, S., Nakano, S., Nishii, M., Kaneko, S., and Kusaka, H. (2012). Localization of O-GlcNAc-modified proteins in neuromuscular diseases. *Med. Mol. Morphol.* 45, 86–90. doi: 10.1007/s00795-011-0542-7

Ngoh, G. A., Watson, L. J., Facundo, H. T., and Jones, S. P. (2010). Augmented O-GlcNAc signaling attenuates oxidative stress and calcium overload in cardiomyocytes. *Amino Acids.* 40, 895–911. doi: 10.1007/s00726-010-0728-7

Persechini, A., Stull, J. T., and Cooke, R. (1985). The effect of myosin phosphorylation on the contractile properties of skinned rabbit skeletal muscle fibers. *J. Biol. Chem.* 260, 7951–7954.

Ramirez-Correa, G. A., Jin, W., Wang, Z., Zhong, X., Gao, W. D., Dias, W. B., et al. (2008). O-linked GlcNAc modification of cardiac myofilament proteins: a novel regulator of myocardial contractile function. *Circ. Res.* 103, 1354–1358. doi: 10.1161/CIRCRESAHA.108.184978

Roquemore, E. P., Chevrier, M. R., Cotter, R. J., and Hart, G. W. (1996). Dynamic O-GlcNAcylation of the small heat shock protein alpha B-crystallin. *Biochemistry* 35, 3578–3586. doi: 10.1021/bi951918j

Rotty, J. D., Hart, G. W., and Coulombe, P. A. (2010). Stressing the role of O-GlcNAc: linking cell survival to keratin modification. *Nat. Cell Biol.* 12, 847–849. doi: 10.1038/ncb0910-847

Safwat, Y., Yassin, N., Gamal, E. D., and Kassem, L. (2013). Modulation of skeletal muscle performance and SERCA by exercice and adiponectin gene therapy in insulin-resistant rat. *DNA Cell Biol.* 32, 378–385. doi: 10.1089/dna.2012.1919

Shafi, R., Iyer, S. P., Ellies, L. G., O'Donnell, N., Marek, K. W., Chui, D., et al. (2000). The O-GlcNAc transferase gene resides on the X chromosome and is essential for embryonic stem cell viability and mouse ontogeny. *Proc. Natl. Acad. Sci. U.S.A.* 97, 5735–5739. doi: 10.1073/pnas.100471497

Slawson, C., Copeland, R. J., and Hart, G. W. (2010). O-GlcNAc signaling: a metabolic link between diabetes and cancer? *Trends Biochem. Sci.* 35, 547–555. doi: 10.1016/j.tibs.2010.04.005

Slawson, C., Lakshmanan, T., Knapp, S., and Hart, G. W. (2008). A mitotic GlcNAcylation/phosphorylation signaling complex alters the posttranslational state of the cytoskeletal protein vimentin. *Mol. Biol. Cell* 19, 4130–4140. doi: 10.1091/mbc.E07-11-1146

Srikanth, B., Vaidya, M. M., and Kalraiya, R. D. (2010). O-GlcNAcylation determines the solubility, filament organization, and stability of keratins 8 and 18. *J. Biol. Chem.* 285, 34062–34071. doi: 10.1074/jbc.M109.098996

Stephenson, G. M., and Stephenson, D. G. (1993). Endogenous MLC2 phosphorylation and $Ca^{(2+)}$-activated force in mechanically skinned skeletal muscle fibres of the rat. *Pflugers Arch.* 424, 30–38. doi: 10.1007/BF00375099

Stevens, L., Bastide, B., Hedou, J., Cieniewski-Bernard, C., Montel, V., Cochon, L., et al. (2013). Potential regulation of human muscle plasticity by MLC2 post-translational modifications during bed rest and countermeasures. *Arch. Biochem. Biophys.* 540, 125–132. doi: 10.1016/j.abb.2013.10.016

Sweeney, H. L., Bowman, B. F., and Stull, J. T. (1993). Myosin light chain phosphorylation in vertebrate striated muscle: regulation and function. *Am. J. Physiol.* 264, C1085–C1095.

Szczesna, D., Zhao, J., Jones, M., Zhi, G., Stull, J., and Potter, J. D. (2002). Phosphorylation of the regulatory light chains of myosin affects Ca^{2+} sensitivity of skeletal muscle contraction. *J. Appl. Physiol.* 92, 1661–1670.

Wells, L., Gao, Y., Mahoney, J. A., Vosseller, K., Chen, C., Rosen, A., et al. (2002). Dynamic O-glycosylation of nuclear and cytosolic proteins: further characterization of the nucleocytoplasmic beta-N-acetylglucosaminidase, O-GlcNAcase. *J. Biol. Chem.* 277, 1755–1761. doi: 10.1074/jbc.M109656200

Wells, L., Kreppel, L. K., Comer, F. I., Wadzinski, B. E., and Hart, G. W. (2004). O-GlcNAc transferase is in a functional complex with protein phosphatase 1 catalytic subunits. *J. Biol. Chem.* 279, 38466–38470. doi: 10.1074/jbc.M406481200

Wells, L., Vosseller, K., and Hart, G. W. (2001). Glycosylation of nucleocytoplasmic proteins: signal transduction and O-GlcNAc. *Science* 23, 2376–2378. doi: 10.1126/science.1058714

Whisenhunt, T. R., Yang, X., Bowe, D. B., Paterson, A. J., Van Tine, B. A., and Kudlow, J. E. (2006). Disrupting the enzyme complex regulating

O-GlcNAcylation blocks signaling and development. *Glycobiology* 16, 551–563. doi: 10.1093/glycob/cwj096

Yang, Y. R., Song, M., Lee, H., Jeon, Y., Choi, E. J., Jang, H. J., et al. (2012). O-GlcNAcase is essential for embryonic development and maintenance of genomic stability. *Aging Cell*. 11, 439–448. doi: 10.1111/j.1474-9726.2012.00801.x

Yki-Jarvinen, H., Virkama ki, A., Daniels, M. C., McClain, D., and Gottschalk, W. K. (1998). Insulin and glucosamine infusions increase O-linked N-acetylglucosamine in skeletal muscle proteins *in vivo*. *Metab. Clin. Exp.* 47, 449–455. doi: 10.1016/S0026-0495(98)90058-0

Zachara, N. E., O'Donnell, N., Cheung, W. D., Mercer, J. J., Marth, J. D., and Hart, G. W. (2004). Dynamic O-GlcNAc modification of nucleocytoplasmic proteins in response to stress. A survival response of mammalian cells. *J. Biol. Chem*. 16, 30133–30142. doi: 10.1074/jbc.M403773200

Zachara, N. E., Vosseller, K., and Hart, G. W. (2011). Detection and analysis of proteins modified by O-linked N-acetylglucosamine. *Curr. Protoc. Protein Sci.* Chapter 12:Unit12.8. doi: 10.1002/0471140864.ps1208s66

Zhang, X., and Bennett, V. (1996). Identification of O-linked N-acetylglucosamine modification of ankyrinG isoforms targeted to nodes of Ranvier. *J. Biol. Chem*. 271, 31391–31398. doi: 10.1074/jbc.271.49.31391

Conflict of Interest Statement: The authors declare that the research was conducted in the absence of any commercial or financial relationships that could be construed as a potential conflict of interest.

Received: 08 September 2014; accepted: 11 October 2014; published online: 30 October 2014.

Citation: Cieniewski-Bernard C, Lambert M, Dupont E, Montel V, Stevens L and Bastide B (2014) O-GlcNAcylation, contractile protein modifications and calcium affinity in skeletal muscle. Front. Physiol. ***5****:421. doi: 10.3389/fphys.2014.00421*

This article was submitted to Striated Muscle Physiology, a section of the journal Frontiers in Physiology.

Copyright © 2014 Cieniewski-Bernard, Lambert, Dupont, Montel, Stevens and Bastide. This is an open-access article distributed under the terms of the Creative Commons Attribution License (CC BY). The use, distribution or reproduction in other forums is permitted, provided the original author(s) or licensor are credited and that the original publication in this journal is cited, in accordance with accepted academic practice. No use, distribution or reproduction is permitted which does not comply with these terms.

frontiers in Physiology

ORIGINAL RESEARCH
published: 28 April 2015
doi: 10.3389/fphys.2015.00116

Pseudo-acetylation of K326 and K328 of actin disrupts *Drosophila melanogaster* indirect flight muscle structure and performance

*Meera C. Viswanathan, Anna C. Blice-Baum, William Schmidt, D. Brian Foster and Anthony Cammarato **

Division of Cardiology, Department of Medicine, Johns Hopkins University School of Medicine, Baltimore, MD, USA

In striated muscle tropomyosin (Tm) extends along the length of F-actin-containing thin filaments. Its location governs access of myosin binding sites on actin and, hence, force production. Intermolecular electrostatic associations are believed to mediate critical interactions between the proteins. For example, actin residues K326, K328, and R147 were predicted to establish contacts with E181 of Tm. Moreover, K328 also potentially forms direct interactions with E286 of myosin when the motor is strongly bound. Recently, LC-MS/MS analysis of the cardiac acetyl-lysine proteome revealed K326 and K328 of actin were acetylated, a post-translational modification (PTM) that masks the residues' inherent positive charges. Here, we tested the hypothesis that by removing the vital actin charges at residues 326 and 328, the PTM would perturb Tm positioning and/or strong myosin binding as manifested by altered skeletal muscle function and structure in the *Drosophila melanogaster* model system. Transgenic flies were created that permit tissue-specific expression of K326Q, K328Q, or K326Q/K328Q acetyl-mimetic actin and of wild-type actin via the UAS-GAL4 bipartite expression system. Compared to wild-type actin, muscle-restricted expression of mutant actin had a dose-dependent effect on flight ability. Moreover, excessive K328Q and K326Q/K328Q actin overexpression induced indirect flight muscle degeneration, a phenotype consistent with hypercontraction observed in other *Drosophila* myofibrillar mutants. Based on F-actin-Tm and F-actin-Tm-myosin models and on our physiological data, we conclude that acetylating K326 and K328 of actin alters electrostatic associations with Tm and/or myosin and thereby augments contractile properties. Our findings highlight the utility of *Drosophila* as a model that permits efficient targeted design and assessment of molecular and tissue-specific responses to muscle protein modifications, *in vivo*.

Keywords: tropomyosin, myosin, acetylation, muscle contraction, post-translational modification

OPEN ACCESS

Edited by:
Julien Ochala, King's College London, UK

Reviewed by:
Frieder Schoeck, McGill University, Canada
Richard Cripps, University of New Mexico, USA

****Correspondence:***
Anthony Cammarato, Division of Cardiology, Department of Medicine, Johns Hopkins University School of Medicine, 720 Rutland Avenue, Ross 1050, Baltimore, MD 21205, USA
acammar3@jhmi.edu

Specialty section:
This article was submitted to Striated Muscle Physiology, a section of the journal Frontiers in Physiology

Received: *07 November 2014*
Accepted: *26 March 2015*
Published: *28 April 2015*

Citation:
Viswanathan MC, Blice-Baum AC, Schmidt W, Foster DB and Cammarato A (2015) Pseudo-acetylation of K326 and K328 of actin disrupts Drosophila melanogaster indirect flight muscle structure and performance. Front. Physiol. 6:116. doi: 10.3389/fphys.2015.00116

Introduction

Striated muscle contraction results from transient interactions between myosin-containing thick filaments and actin-containing thin filaments. Contractile regulation is achieved by Ca^{2+}-dependent modulation of myosin S1 cross-bridge binding to actin by the thin filament-associated

troponin-tropomyosin complex (reviewed in Tobacman, 1996; Gordon et al., 2000; Brown and Cohen, 2005; Lehman and Craig, 2008). The location of continuous troponin-tropomyosin complexes along the surface of F-actin governs the access of myosin binding sites and, hence, force production (Haselgrove, 1973; Huxley, 1973; Parry and Squire, 1973; McKillop and Geeves, 1993; Lehman et al., 1994; Vibert et al., 1997). Under conditions of low Ca^{2+}, the troponin complex constrains tropomyosin (Tm) in a position that occludes myosin target sites on actin. Consequently, Tm sterically blocks and limits myosin binding, and relaxation results. During muscle activation, Ca^{2+} binds to troponin and triggers movement of Tm away from myosin binding sites. This relocation partially relieves the structural blocking imposed by Tm. Initial myosin binding on thin filaments further displaces Tm and exposes myosin binding sites along F-actin, thereby contributing to the cooperative activation of contraction.

Although the specific residues that constitute the binding interface of actin and Tm are not completely known, it is well accepted that the association of Tm with actin is largely electrostatic (Lorenz et al., 1995; Brown and Cohen, 2005; Barua et al., 2011, 2013; Li et al., 2011). Recently, models of the conserved binding interface between actin and Tm in various states have been proposed based on molecular evolutionary and mutational analysis, computational chemistry, and electron microscopy reconstructions (Barua et al., 2011, 2013; Li et al., 2011; Behrmann et al., 2012; Von Der Ecken et al., 2015). Structural studies of F-actin-Tm and F-actin-Tm-myosin revealed that several amino acids on actin can potentially form distinct contacts with Tm in the absence and presence of myosin S1 (Li et al., 2011; Behrmann et al., 2012; Von Der Ecken et al., 2015). For example, in the absence of S1, a cluster of basic actin residues comprised of K326, K328, and R147 appeared poised to clasp onto E181 of Tm to establish highly favorable associations (**Figure 1**) (Li et al., 2011). Interestingly, K328 also interacts electrostatically with E286 of S1 to help define a strong contact point between actin and rigor-bound myosin (Behrmann et al., 2012).

Alterations to thin filament proteins affect the properties of muscle. Missense mutations, for instance, can disrupt conserved interfaces among cardiac thin filament subunits and initiate diverse cardiomyopathies (Tardiff, 2011). Similar to disease-causing mutations, post translational modifications (PTMs) also alter the chemical nature of thin filament subunits. Although less-well appreciated, these modifications are widely employed *in vivo*, occur through enzymatic and non-enzymatic mechanisms, and direct both physiological and pathological processes (Terman and Kashina, 2013). PTMs add or remove a functional group to or from specific amino acid residues, which can induce changes in protein structure, activity, or binding partners (van Eyk, 2011). To date, more than 400 different PTMs have been described, although far fewer have been documented in higher organisms (Agnetti et al., 2011). In the cardiac subproteome, phosphorylation is by far the best-described PTM (Sumandea et al., 2004; Agnetti et al., 2011; Solaro and Kobayashi, 2011; van Eyk, 2011). It has been observed for 80% of the myofilamentous proteins (Agnetti et al., 2011). However, the effects of the majority of the potential PTMs have not been fully

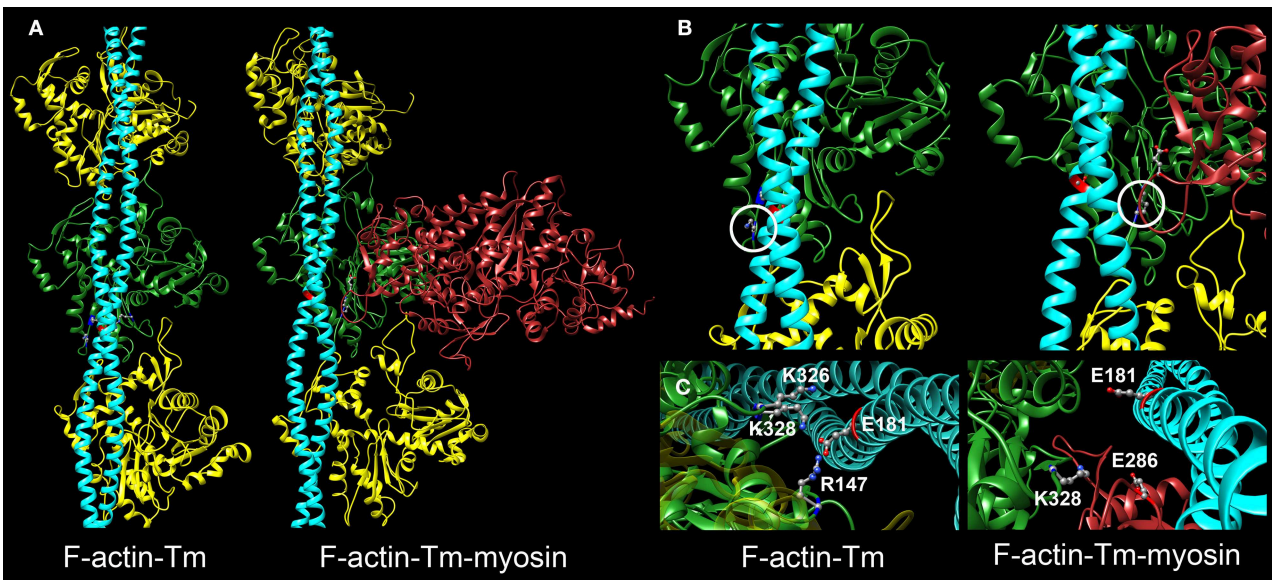

FIGURE 1 | Critical electrostatic F-actin-Tm and F-actin-Tm-myosin interactions. (A) Molecular models showing the location of tropomyosin (Tm) (blue) on actin (yellow and green) in the absence and presence of the myosin head (S1) (red) bound in rigor. The F-actin-Tm and rigor F-actin-Tm-myosin structures are based on those generated by Li et al. (2011) and Behrmann et al. (2012) respectively. **(B)** Enlarged views illustrate critical electrostatic associations between actin and Tm in the absence or presence of S1. K328 on actin (circled) interacts with E181 of Tm in the absence of myosin (left) and with E286 of myosin when S1 is bound in rigor (right). Note the azimuthal movement of Tm across F-actin. **(C)** Projected and enlarged views highlight vital electrostatic interactions of actin residues R147, K326, and K328 with E181 of Tm, in the absence of myosin, and of K328 of actin and E286 of S1 when myosin is bound in rigor. These associations are likely critical for thin filament and muscle function.

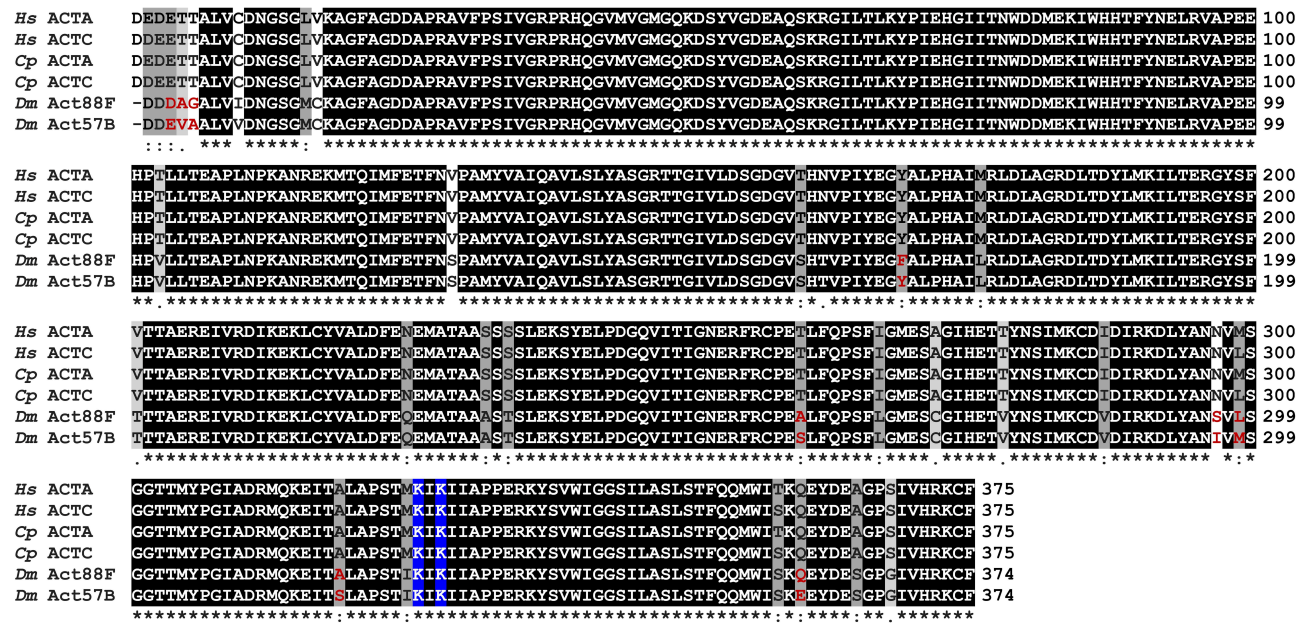

FIGURE 2 | Multiple sequence alignment of actin isoforms. Multiple sequence alignment of skeletal and cardiac actin from *Homo sapiens* (*Hs*), *Cavia porcellus* (*Cp*), and *Drosophila melanogaster* (*Dm*) reveals highly conserved proteins. ACTA, skeletal muscle actin; ACTC, cardiac muscle actin; Act88F, *Drosophila* indirect flight muscle actin; Act57B, *Drosophila* cardiac actin. Residues are shaded based on degree of conservation. An (*) indicates positions that have identical residues, a (:) indicates substitution with high structural similarity, and a (.) indicates substitution low structural similarity.

investigated, in part because of a lack of technologies needed to target and reliably identify them. Moreover, compared to inherited mutations, the influence of relatively few PTMs on contractile performance have been examined in the physiological context of muscle.

Actin is an abundant and highly conserved protein (**Figure 2**). It participates in more protein-protein interactions than any known protein and is subject to a number of PTMs (Herman, 1993; Dominguez and Holmes, 2011; Terman and Kashina, 2013). Characterizing these modifications constitutes a rapidly expanding area within actin studies and muscle biology (Terman and Kashina, 2013). Phosphorylation, methylation, ADP-ribosylation, oxidation, arginylation, O-GlcNAcylation, ubiquitylation, and acetylation are examples of major actin modifications, many of which have now been confirmed in sarcomeric actin. For example, K326 and K328 of actin isolated from various cell lines were shown to be acetylated (Choudhary et al., 2009) and, as recently described by Foster et al. (2013) these residues were also shown to be acetylated on actin recovered from the myofilament fraction of guinea pig hearts. Acetylation is a reversible PTM that neutralizes the positive charge of K326 and K328 on actin. Unlike the N-terminal acetylation, acetylation of these residues has unknown function. Based on *in vitro* and *in silico* structural predictions, removal of positively charged amino acids that are potentially critical to Tm and myosin electrostatic associations likely alters muscle performance substantially and in diverse ways.

Here, we aimed to investigate the *in vivo* physiological and morphological consequences of acetylating actin residues K326 and K328 on muscle. We chose the indirect flight muscle (IFM) of *D. melanogaster* as our primary experimental vehicle. *Drosophila* IFMs are highly amenable to mechanical and structural analyses, are not required for viability, exhibit a stretch activation response that is similar to that of cardiac muscle, and provide ample material that is easily isolated for biochemical and biophysical experimentation (Bing et al., 1998; Razzaq et al., 1999; Cammarato et al., 2004; Vikhorev et al., 2010; Swank, 2012). The vast array of genetic tools available to manipulate the fly's genome also provides unique opportunities to examine how thin filament modifications affect muscle structure and performance. The GAL4-UAS system simplifies tissue-specific expression of mutant transgenes (Brand and Perrimon, 1993). However, previous studies suggested that IFM myofibril assembly and flight ability are highly sensitive to the stoichiometry of muscle proteins (Beall and Fyrberg, 1991; Bernstein et al., 1993), and therefore, the utility of this bipartite expression system for investigating major contractile components has been questioned. For example, despite normal sarcomere appearance, overexpression of several *UAS-GFP-actin* alleles was shown to exclusively affect IFM function, leading to flightless adults that were otherwise healthy (Röper et al., 2005). The effects of non-GFP fusion constructs on IFM performance were not tested. Therefore, to determine if the IFM can serve as a viable, conditional model system for probing the effects of PTMs on myofibrillar components, we tested the hypotheses that (1) GAL4-UAS-mediated overexpression of a *Drosophila* cardiac actin isoform in the IFM would not perturb gross morphology or flight performance as determined by standard metrics and that (2) expression of K326Q, K328Q, or K326Q/K328Q acetyl-mimetic cardiac actin disrupts vital electrostatic interactions required for Tm positioning and/or

strong myosin binding, *in vivo*, as manifested by perturbed IFM structure and function. Using four muscle-specific GAL4 drivers we found that expressing wild-type *Drosophila* cardiac actin had no effect on flight or gross muscle organization. Relatively high expression levels of K326Q cardiac actin mildly affected flight ability, whereas excessive amounts of K328Q and K326Q/K328Q cardiac actin eliminated flight and triggered IFM destruction. Based on F-actin-Tm and F-actin-Tm-myosin models and on our physiological data, we propose that acetylating K326 and K328 of actin alters crucial electrostatic associations with Tm and/or myosin and thereby promotes actomyosin associations and modulates muscle performance. Our findings highlight the utility of *Drosophila* as a model that permits efficient targeted design and assessment of tissue-specific responses to muscle protein modifications, *in vivo*.

Materials and Methods

Structural Modeling

Models of the F-actin-Tm (Li et al., 2011; Orzechowski et al., 2014) and the rigor F-actin-Tm-myosin (PDB ID: 4A7F) (Behrmann et al., 2012) binding interfaces were generated using the molecular modeling program, Chimera version 1.9 (Pettersen et al., 2004).

Multiple Sequence Alignment

Sequence comparison of skeletal and cardiac actin isoforms from *Homo sapiens*, *Cavia porcellus*, and *D. melanogaster* was performed using the Clustal Omega multiple sequence alignment program. Residues were shaded based on degree of conservation.

Fly Stocks

All flies were raised at 25°C on a standard cornmeal-yeast-sucrose-agar medium. The w^{1118} strain was obtained from Genetic Services Inc. (Sudbury, MA) and the *Mef2-GAL4* driver line (y^1 w^*; *P{GAL4-Mef2.R}3*) from the Bloomington *Drosophila* Stock Center (Bloomington, IN). The *MHC-GAL4* (*MHC-GAL4*^{82}) line described by Marek et al. (2000) was obtained from Dr. Rolf Bodmer (Sanford Burnham Medical Research Institute, La, Jolla, CA). The *UH3-GAL4* (Singh et al., 2014) and the *Act88F-GAL4* (88F2) (Bryantsev et al., 2012) lines were gifts from Dr. Upendra Nongthomba (Indian Institute of Science, Banglore, India) and Dr. Richard M. Cripps (University of New Mexico, Albuquerque, NM) respectively. The Mhc^{10} (w; Mhc^{10}/Mhc^{10}; *TM2/MKRS)* IFM-specific myosin null line was acquired from Dr. Sanford I. Bernstein (San Diego State University, San Diego, CA). *Mef2-GAL4>* *UAS-Act57B*^{WT}; Mhc^{10}/+ and *UAS-Act57B*^{K328Q}; Mhc^{10}/+ *Drosophila* were generated by standard mating procedures.

Construction of *UAS-Actin* Transgenes

The N-terminally-labeled GFP-actin construct (*pUASp.Act57B*$^{GFP.WT}$) was generously provided by Dr. Katja Röper (MRC- Laboratory of Molecular Biology, Cambridge, UK). The *Act57B*$^{GFP.WT}$ and *Act57B*^{WT} cDNA sequences were subsequently inserted into the pUASTattB vector (obtained from Dr. Christopher Potter, Johns Hopkins University) using the KpnI and XbaI and the NotI and XbaI restriction sites respectively. The pUASTattB vector includes the *Drosophila miniwhite* (w^+) gene as a selectable eye color marker. The Act57B actin acetyl-mimetic mutations, K326Q, K328Q, and K326Q/K328Q, were generated by site-directed mutagenesis using specific primer pairs and the QuikChange Site-directed mutagenesis kit (Agilent Technologies).

List of primers for site-directed mutagenesis:

Act57B^{K326Q} (+) primer	5′ CCATCCACCATCCAGA TCAAGATCATT 3′
Act57B^{K326Q} (−) primer	5′ AATGATCTTGATCTGG ATGGTGGATGG 3′
Act57B^{K328Q} (+) primer	5′ ACCATCAAGATCCAGA TCATTGCTCCC 3′
Act57B^{K328Q} (−) primer	5′ GGGAGCAATGATCTGG ATCTTGATGGT 3′
Act57B$^{K326Q/K328Q}$ (+) primer	5′ TCCACCATCCAGATCC AGATCATTGCT 3′
Act57B$^{K326Q/K328Q}$ (−) primer	5′ AGCAATGATCTGGAT CTGGATGGTGGA 3′

Generation of Transgenic *Drosophila*

The pUASTattB constructs were injected into attp40 *Drosophila* embryos for PhiC31 integrase mediated site-specific transgenesis (transgene landing site cytolocation 25C7) by Genetic Services, Inc. Injected adults were crossed to w^{1118} flies and the progeny screened for pigmented eye color, which reflects the presence of the *miniwhite* (w^+) marker and the transgene, an indicator of successful transformation. Each transformant fly was then crossed into the w^{1118} background to generate stable transgenic lines.

Verification of Transgene Expression

Transgenic actin expression was verified by isolating total RNA from bisected thoraces or dissected IFMs of 10 *Mef2-GAL4>* *UAS-Act57B*^{WT}, *UAS-Act57B*^{K326Q}, *UAS-Act57B*^{K328Q}, or *UAS-Act57B*$^{K326Q/K328Q}$ flies using the Quick-RNA microprep kit (Zymo Research Corp). Contaminating DNA was removed with RNase free DNase I (Zymo Research Corp). One step RT-PCR was carried out with the Qiagen QuantiTect Reverse Transcription Kit (Qiagen Inc) and 10 ng RNA per reaction. The cDNA was amplified using an *Act57B* primer pair (5′ CCCTGTACGCCTCCGGTCGTA 3′ and 5′ TTAGAAGCACTTGCGGTGGAC 3′) and the amplified product was sequenced at the Johns Hopkins Synthesis and Sequencing facility.

Transgenic muscle-restricted protein expression was confirmed using the *UAS-Act57B*$^{GFP.WT}$ reporter line in conjunction with either the *MHC-GAL4* or *Mef2-GAL4* drivers. Two-day-old adult progeny were imaged using a Leica M165FC fluorescent stereo microscope and a Leica EC3 digital camera.

Protein Quantification

Virgin *MHC-*, *Mef2-*, *UH3-*, and *Act88F-GAL4* female flies were crossed with male flies harboring the *UAS-Act57B*$^{GFP.WT}$ transgene. To quantitate the amount of Act57B$^{GFP.WT}$ transgenic

actin driven by each muscle-specific driver, two whole thoraces of, or IFMs from three resulting progeny were dissected and homogenized in Laemmli Sample Buffer (Bio-Rad Laboratories). Each biological sample was then incubated briefly at 100°C and increasing amounts of protein from each sample were loaded on a 4–15% SDS-PAGE gel (Bio-Rad Laboratories), electrophoresed, and blotted onto a nitrocellulose membrane using the Trans-Blot® TurboTM Transfer system (Bio-Rad Laboratories). Membranes were blocked with gentle shaking in PBS odyssey blocking buffer (LI-COR Biosciences) for one hour, and incubated with primary rabbit anti-actin (Proteintech), goat anti-GFP (R&D), and goat anti-GAPDH (Genscript) antibodies overnight at 4°C. The membranes were rinsed three–four times, 10–15 min each in 1x TBST (1X TBS with 0.1% tween-20) and then probed with Donkey anti-rabbit and Donkey anti-goat IRDye secondary antibodies (LI-COR Biosciences) for 60–90 min at room temperature. The membranes were rinsed again two–three times, 10–15 min each with 1X TBST followed by a final rinse in 1X TBS. The membranes were subsequently scanned using an Odyssey Infrared Imager (LI-COR Biosciences) ($\lambda = 700$ and 800 nm) and analyzed using Odyssey Application Software (v3.030, LI-COR Biosciences). Thoracic and IFM protein quantification was performed on five or eight independent biological samples respectively, with six or four technical replicates each. Mean values (± SEM) of actin and GFP intensities normalized to respective GAPDH intensities were determined. Significance was assessed via One-Way ANOVA with a Bonferroni's multiple comparison test for thoracic, and via the Mann-Whitney test for IFM samples using GraphPad Prism5.

Flight Testing

Flight tests were performed as described by Drummond et al. (1991). Newly eclosed male and female flies were aged for two days at 25°C. Each fly was released into the center of a plexiglass chamber with a light source positioned at the top at 23°C and assigned a flight index of six for upward flight, four for horizontal, two for downward, or zero for no flight. The average flight index from 100–300 flies was calculated for each genotype. Flight assays for *Act88F-GAL4*-expressing flies were conducted exclusively on females as males consistently displayed severe flight impairment. Values represent mean ± SEM. Significance was assessed using a Kruskal-Wallis One-Way ANOVA.

Climbing Assay

Climbing tests were conducted on two-day-old flies at room temperature. Small groups of ∼20 flies were placed in covered, cylindrical vials (2.5 cm diameter × 20 cm high), which were aligned with one centimeter markings to measure the height each fly climbed in five seconds. The test was repeated 10 times for each set of flies. The average climbing distance for each fly was recorded for 30–160 flies per genotype. Values represent mean ± SEM. Significance was assessed using a Kruskal-Wallis One-Way ANOVA.

Imaging of Indirect Flight Muscles

Polarized light microscopy of hemi-thoraces to examine the gross morphology of two-day-old *Mef2-GAL4> UAS-Act57B^{WT}*, *UAS-Act57B^{K326Q}*, *UAS-Act57B^{K328Q}*, or *UAS-Act57B$^{K326Q/K328Q}$* adult *Drosophila* IFM was performed as described previously (Nongthomba and Ramachandra, 1999). Briefly, flies were anesthetized, and heads and abdomens removed. Thoraces were fixed overnight in 4% formaldehyde at 4°C and rinsed in PBS the following day. The specimens were laid supine on a glass slide and snap frozen in liquid nitrogen for 10 s. Frozen thoraces were immediately bisected down the midsagittal plane using a razor blade and IFMs were visualized using a Leica DM5000B microscope at 10X magnification with polarizing filters. Images were taken with a Hamamatsu digital camera.

Fluorescent microscopy was employed to improve pathohistological characterization of IFMs from young (< four hour old) and two-day-old adult *Act88F-GAL4> UAS-Act57B^{WT}*, *UAS-Act57B^{K326Q}*, *UAS-Act57B^{K328Q}*, and *UAS-Act57B$^{K326Q/K328Q}$ Drosophila*. Thoraces were prepared and bisected as described above, followed by staining with 1:100 Alexa-594 Phalloidin in PBST overnight at 4°C. Samples were rinsed with PBS before imaging with the EVOS® FL Cell Imaging System (Life Technologies) at 4X magnification.

Results

Actin Sequence Analysis

The genomes of human, guinea pig, and fly contain six highly conserved actin genes. As found in vertebrates, *D. melanogaster* expresses specific isoforms of actin in adult skeletal and cardiac muscle. The *Actin88F* (*Act88F*) gene encodes all sarcomeric actin of *Drosophila* IFM (Fyrberg et al., 1983; Hiromi and Hotta, 1985; Nongthomba et al., 2001) while *Actin57B* (*Act57B*) is one of two genes encoding sarcomeric actin in the adult fly heart (Cammarato et al., 2011; Shah et al., 2011). The skeletal and cardiac actin isoforms differ in only a few amino acids within and between species (**Figure 2**).

Generation of Transgenic *Drosophila* and Confirmation of Muscle-Restricted Transgene Expression

To determine the consequences of masking the inherent charge of actin residues K326 and K328 *in vivo*, we generated multiple transgenic acetyl-mimetic lines that permitted muscle targeted gene expression. Use of the PhiC31 integrase system ensured all *UAS-Act57B* transgenes were integrated at an identical, predetermined genomic location (Groth et al., 2004). Thus, our results were directly comparable and any phenotypic differences in control vs. mutant flies could be directly attributed to neutralized lysine charges on the ectopically expressed actin.

To confirm transcription of transgenic actin, flies with constructs consisting of an upstream activating sequence (UAS) followed by a downstream *Act57B^{WT}*, *Act57B^{K326Q}*, *Act57B^{K328Q}*, or *Act57B$^{K326Q/K328Q}$* transgene were crossed with flies carrying the *GAL4* transactivation gene under the control of the *Mef2*-promoter (Ranganayakulu et al., 1996). The progeny inherit both genes and express the *UAS-Act57B* transgenes exclusively in musculature. Total RNA was isolated from the thoraces of

young (< two days old) flies of each genotype. First-strand cDNA was synthesized followed by *Act57B* cDNA amplification. The amplified cDNA contained nucleotide sequences unique to the *Act57B* alleles, confirming transcription of the *WT*, *K326Q*, *K328Q*, or the *K326Q/K328Q Act57B* cardiac actin transgene (**Figure 3**). To rule out the possibility of contaminating endogenous *Act57B* cDNA originating from non-IFM thoracic musculature, amplified cDNA from the dissected IFMs of *Mef2-GAL4> UAS-Act57B*^{WT} flies was also sequenced, which verified the presence and transcription of *Act57B*^{WT} in *Act88F*-exclusive musculature (not shown).

To visualize muscle-restricted expression of *UAS-Act57B* transgenes, *in vivo*, flies carrying the *UAS-Act57B*$^{GFP.WT}$ construct were crossed with flies harboring either the *MHC*- or *Mef2-GAL4* muscle-specific drivers. MHC-GAL4-driven transgenic Act57B$^{GFP.WT}$ was readily observed in the thoracic musculature, which is predominantly comprised of 13 pairs of relatively large IFM fibers (**Figure 4**). Mef2-GAL4-driven Act57B$^{GFP.WT}$, however, was detected far more extensively, in most somatic musculature.

Relative to *MHC-GAL4, Mef2-GAL4* Drives Elevated Expression Levels of Transgenic Actin

The PhiC31 integrase system for transgenic fly production limits transgene expression variability and, when used in conjunction with the GAL4-UAS system, permits the onset and magnitude of expression to be manipulated via distinct drivers (Brand and Perrimon, 1993; Groth et al., 2004; Goentoro et al., 2006). To quantify differences in transgenic protein abundance, dissected thoraces from flies expressing Act57B$^{GFP.WT}$ actin by either MHC- or Mef2-GAL4 drivers, as well as from control "non-driven" flies, were subjected to SDS-PAGE, transferred to nitrocellulose, and probed for actin and for GFP (**Figure 5A**). The resulting signal intensities from GFP and actin were measured and normalized to that from GAPDH (**Figures 5B,C**). As expected very little GFP was distinguished among the various controls. Thoracic muscles from *MHC*- and *Mef2-GAL4> UAS-Act57B*$^{GFP.WT}$ flies, however, exhibited detectable amounts of GFP-actin. Mef2-GAL4 induced significantly higher expression levels of the GFP-tagged actin in the thoracic musculature compared to MHC-GAL4. The resulting normalized signal was greater than two-fold higher than that determined for *MHC-GAL4> UAS-Act57B*$^{GFP.WT}$ flies (1.66 ± 0.41 vs. 0.69 ± 0.07). These findings were corroborated using dissected IFMs, which displayed a normalized Act57B$^{GFP.WT}$ signal that was roughly three-fold higher for *Mef2-GAL4> UAS-Act57B*$^{GFP.WT}$ compared to *MHC-GAL4> UAS-Act57B*$^{GFP.WT}$ fibers (6.04 ± 1.85 vs. 1.73 ± 0.37). The thoracic or IFM actin/GAPDH ratio did not differ significantly among the genotypes tested (**Figure 5C**). Estimation of signal intensities from the protein bands, detected exclusively with the anti-actin antibody, suggested that Mef2-GAL4> Act57B$^{GFP.WT}$ comprises ~10–20% of total thoracic actin (not shown).

GFP-labeled and Acetyl-Mimetic Cardiac Actin Depress *Drosophila* Flight Ability and Climbing Performance

Flight tests were performed on two-day-old *MHC*- and *Mef2-GAL4> UAS-Act57B*$^{GFP.WT}$, *UAS-Act57B*^{WT}, *UAS-Act57B*^{K326Q}, *UAS-Act57B*^{K328Q}, or *UAS-Act57B*$^{K326Q/K328Q}$ transgenic *Drosophila* lines to determine if expression of wildtype or acetyl-mimetic cardiac actin can support IFM function. The driver lines, and the progeny of each driver line crossed to w^{1118} flies, served as additional controls. *MHC*- and *Mef2-GAL4 Drosophila* by themselves, and the offspring of the driver lines crossed to w^{1118}, showed normal flight indices ($FI = 5.69–5.83$) in accord with published values calculated for wildtype flies (**Figure 6A**) (Drummond et al., 1991; Swank et al., 2003; Suggs et al., 2007;

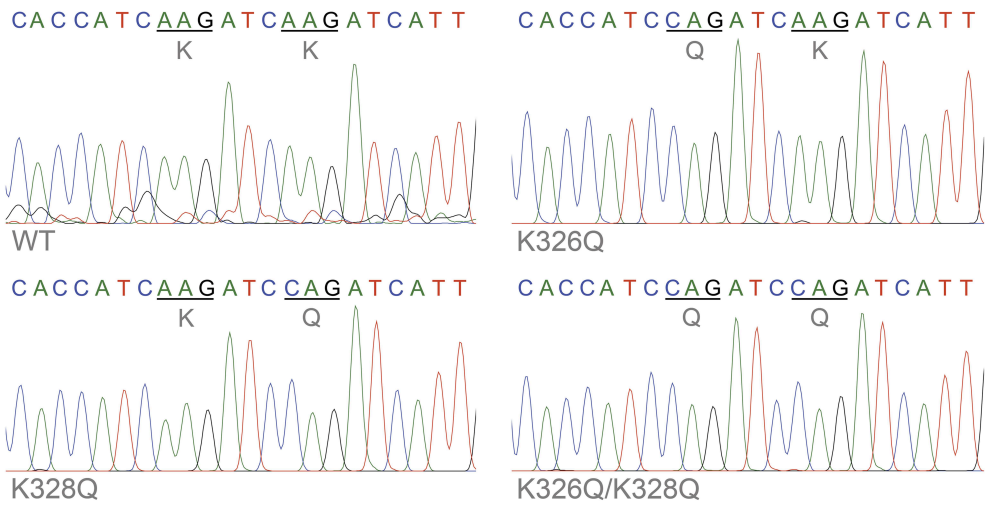

FIGURE 3 | Confirmation of transgenic actin transcription. Sequence chromatograms of an amplified stretch of *Act57B* cDNA revealed transcription of the *UAS-Act57B* transgenes in the thoracic musculature of *Mef2-GAL4> UAS-Act57B* transgenic flies. The chromatograms also confirmed the presence and expression of K326Q, K328Q, or K326Q/K328Q actin mutations (identified by the AAG → CAG nucleotide transversion) in the sequenced *Act57B* cDNA fragments.

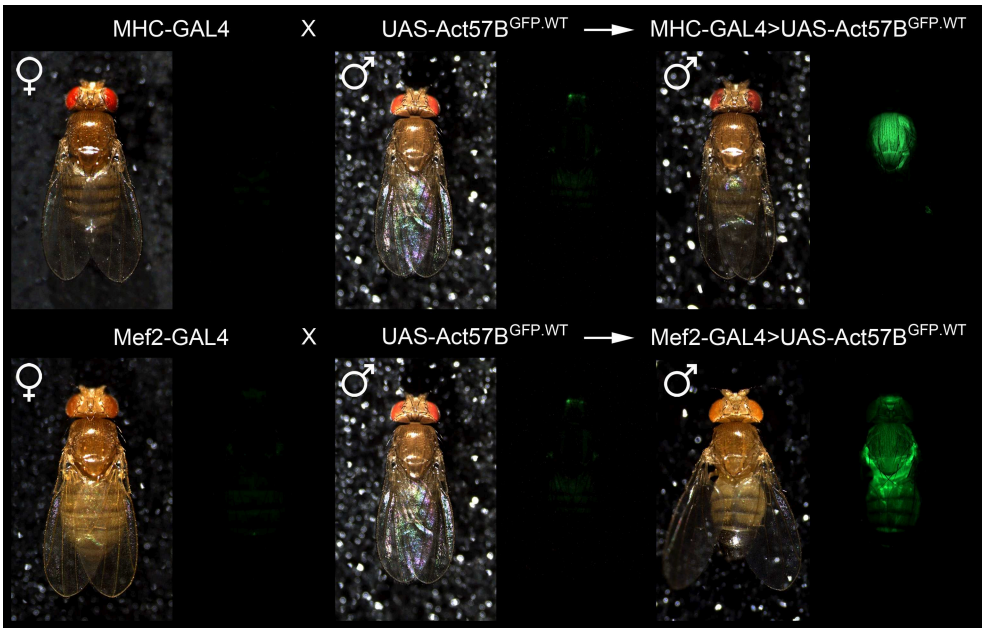

FIGURE 4 | Confirmation of muscle-restricted gene expression. Virgin female flies expressing either the muscle-specific MHC-GAL4 or the Mef2-GAL4 driver were mated with male flies carrying the *UAS-Act57B*$^{GFP.WT}$ construct. Background fluorescence coming from the musculature of the parental lines was minimal. However, fluorescence emitted from the musculature of progeny, which inherit both a GAL4 driver and the UAS-construct, was readily observed in both genotypes, confirming tissue-specific expression of transgenic Act57B actin.

Cammarato et al., 2008; Wang et al., 2012). "Low dose" ectopic expression of all *UAS-Act57B* actin constructs by MHC-GAL4 had no effect on flight ability. All lines performed equally well (*FI* = 5.46–5.78). Thus, MHC-GAL4-driven GFP-tagged, wildtype, or acetyl-mimetic Act57B actin supported flight.

Similar to previous results (Röper et al., 2005), *Mef2-GAL4> Act57B*$^{GFP.WT}$ expression eliminated flight ability (*FI* = 0.03 ± 0.01) (**Figure 6A**). Interestingly, relatively "high dose" expression of *Act57B* cardiac actin that lacked the GFP fusion tag had no observable effect on flight as *Mef2-GAL4> UAS-Act57B*^{WT} *Drosophila* demonstrated wildtype-like flight ability (*FI* = 5.62 ± 0.04). Unlike what was found in combination with MHC-GAL4, expression of *UAS-Act57B*^{K326Q} by Mef2-GAL4 had a slight, but significant effect on the average flight value (*FI* = 4.99 ± 0.09) whereas *UAS-Act57B*^{K328Q} and *UAS -Act57B*$^{K326Q/K328Q}$ expression abolished IFM function (*FI* = 0.11 ± 0.02 and 0.08 ± 0.04, respectively). Notably, Mef2-GAL4-driven *UAS-Act57B*$^{K326Q/K328Q}$ actin expression predominantly resulted in pupal lethality with relatively few adult flies emerging from their puparia. Thus, Mef2-GAL4-driven GFP-tagged or acetyl-mimetic Act57B actin impaired flight and muscle performance.

To assess if expression of acetyl-mimetic cardiac actin affected additional somatic musculature, the climbing ability of w^{1118}, *Mef2-GAL4> UAS-Act57B*^{WT}, *UAS-Act57B*^{K326Q}, *UAS-Act57B*^{K328Q}, and *UAS-Act57B*$^{K326Q/K328Q}$ flies was examined (**Figure 6B**). Expression of *UAS-Act57B*^{WT} actin had no significant effect on climbing distance (8.33 ± 0.54 cm) relative to w^{1118} controls (8.85 ± 0.49 cm). All acetyl-mimetic actin-expressing flies, however, exhibited climbing defects compared to w^{1118} and to *Mef2-GAL4> UAS-Act57B*^{WT} *Drosophila*. Flies expressing *UAS-Act57B*^{K326Q} had a small but significant reduction in climbing ability (6.14 ± 0.50 cm), while flies expressing *UAS-Act57B*^{K328Q} or *UAS-Act57B*$^{K326Q/K328Q}$ had strikingly reduced climbing capabilities (4.22 ± 0.30 cm and 0.93 ± 0.24 cm respectively) compared to controls. Furthermore, flies expressing *UAS-Act57B*$^{K326Q/K328Q}$ actin performed significantly worse than those expressing *UAS-Act57B*^{K328Q} actin.

Mef2-GAL4> UAS-Act57B^{K328Q} and *UAS-Act57B*$^{K326Q/K328Q}$ Lack of Flight is Associated with Loss of IFM Fibers

In addition to inducing a lack of flight, Mef2-GAL4> *Act57B*^{K328Q} and *Act57B*$^{K326Q/K328Q}$ acetyl-mimetic cardiac actin expression also resulted in a "wings up" phenotype. This phenotype is commonly associated with "hypercontracted" and damaged IFM that occurs due to mutations in *Drosophila* muscle proteins (Fyrberg et al., 1990; Beall and Fyrberg, 1991; Kronert et al., 1995; An and Mogami, 1996; Reedy et al., 2000; Nongthomba et al., 2003). Polarized light microscopy was employed to investigate disturbances in gross IFM morphology (**Figure 6C**). *Mef2-GAL4> UAS-Act57B*^{WT} and *UAS-Act57B*^{K326Q} *Drosophila* displayed similar IFM fiber structure. Both perpendicularly-oriented sets of fibers were continuous and straight, spanning the entire thorax in each line. However, *Mef2-GAL4> UAS-Act57B*^{K328Q} and *UAS-Act57B*$^{K326Q/K328Q}$ *Drosophila* were characterized by the absence of continuous IFM fibers. Only occasionally was light observed emerging from birefringent material closely associated with the thoracic cuticle, which we assumed were IFM fiber remnants. Interestingly, *Mef2-GAL4> UAS-Act57B*^{K328Q}; *Mhc*^{10}/+

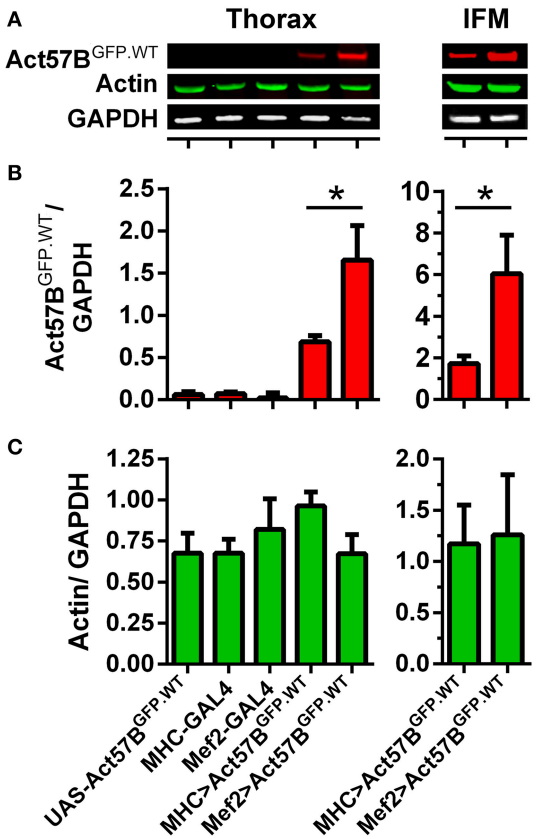

FIGURE 5 | Mef2-GAL4 drives higher expression levels of transgenic actin relative to MHC-GAL4. Quantitative western blot analysis of steady-state Act57B$^{GFP.WT}$ and total actin was performed on thoraces and IFMs of *Mef2-GAL4> UAS-Act57B$^{GFP.WT}$* and *MHC-GAL4> UAS-Act57B$^{GFP.WT}$* flies and of control flies two days after eclosion. **(A)** Representative western blots showing elevated thoracic (left) and IFM (right) levels of Act57B$^{GFP.WT}$ (probed with an anti-GFP primary antibody) when driven by Mef2-GAL4 compared to MHC-GAL4. Actin and GAPDH (probed with anti-actin and anti-GAPDH antibodies) abundance appeared relatively consistent among genotypes. The GFP **(B)** and actin **(C)** intensities were measured, normalized to that of GAPDH for five thoracic samples with six technical replicates each and for eight IFM samples with four technical replicates each, and averaged for each genotype. Mef2-GAL4 drove significantly higher amounts of transgenic actin relative to MHC-GAL4 (*$P < 0.05$).

Drosophila displayed a greater abundance of thoracic material and birefringent musculature consistent with previous studies that demonstrated a reduced number of myosin motors can suppress mutant fiber destruction (Beall and Fyrberg, 1991; Nongthomba et al., 2003). However, the extent of suppression was incomplete as IFMs were still largely absent.

Relative to *UH3-GAL4, Act88F-GAL4* Drives Elevated Expression Levels of IFM-Restricted Transgenic Actin

IFM-specific GAL4 drivers provide an additional resource to further characterize the effects of pseudo-acetylated cardiac actin on flight muscle function and morphology. To quantify differences in transgenic protein abundance exclusively in IFMs, dissected fibers from flies expressing *Act57B$^{GFP.WT}$* driven by either UH3- or Act88F-GAL4, as well as fibers from control "non-driven" flies, were subjected to quantitative western blot analysis (**Figure 7A**). The signal intensities from the GFP and actin bands were measured and normalized to that from GAPDH. As found in whole thoraces, GFP signals in IFMs from all control lines were negligible (not shown), while IFMs from *UH3-* and *Act88F-GAL4> UAS-Act57B$^{GFP.WT}$* flies showed detectable amounts of GFP-actin. Act88F-GAL4 induced significantly higher expression levels of GFP-actin in the IFMs compared to UH3-GAL4 (10.31 ± 2.94 vs. 1.57 ± 0.52). No differences in the relative abundance of non GFP-labeled, endogenous IFM actin were identified (not shown).

IFM-Specific Expression of GFP-labeled or Acetyl-Mimetic Actin Decreases Flight Ability in a Dose-Dependent Manner

Flight tests were performed on two-day-old *UH3-* and *Act88F-GAL4* driver lines and on the progeny of each driver line crossed to w^{1118} control, *UAS-Act57B$^{GFP.WT}$*, *UAS-Act57B^{WT}*, *UAS-Act57B^{K326Q}*, *UAS-Act57B^{K328Q}*, or *UAS-Act57B$^{K326Q/K328Q}$* transgenic *Drosophila* (**Figure 7B**). The *UH3-GAL4* line, and the progeny of *UH3-GAL4* crossed to w^{1118} displayed unperturbed flight ability (FI = 5.88 ± 0.03 and 5.72 ± 0.05, respectively). "Low dose" expression of all *UAS-Act57B* actin constructs using the UH3-GAL4 driver had no effect on flight ability. All lines displayed flight indices similar to controls (FI = 5.42 – 5.61). Therefore, UH3-GAL4-driven GFP-tagged, wildtype, or acetyl-mimetic Act57B permitted flight.

Act88F-GAL4 (88F2) *Drosophila* displayed markedly reduced flight ability (FI = 1.31 ± 0.12) (**Figure 7B**). This was consistent with impaired flight phenotypes observed with publicly available *Act88F-GAL4* lines (*w**; *P{Act88F-GAL4.1.3}3* and *w**; *P{Act88FGAL4.1.3}81B*, *P{Act88F:GFP}2/ SM6b*) (not shown). When crossed to w^{1118} control flies however, female progeny harboring a single *Act88F-GAL4* (88F2) gene exhibited wildtype-like flight performance (FI = 5.52 ± 0.07). In contrast, no progeny from the two publicly available *Act88F-GAL4* lines, when crossed to w^{1118} control flies, regained flight ability (not shown). Therefore, we exclusively tested and compared flight performance of the female offspring of *Act88F-GAL4* (88F2) *Drosophila* crossed to each *UAS-Act57B* actin transgenic line.

"High dose" *Act88F-GAL4> UAS-Act57B$^{GFP.WT}$* expression eradicated flight (FI = 0.04 ± 0.02) (**Figure 7B**). Notably, *Act88F-GAL4> UAS-Act57B^{WT}* flies demonstrated wildtype-like flight ability (FI = 5.25 ± 0.09). As with Mef2-GAL4, expression of *UAS-Act57B^{K326Q}* via Act88F-GAL4 slightly depressed flight ability, which closely approached statistical significance. However, Act88F-GAL4-mediated expression of *UAS-Act57B^{K328Q}* and *UAS-Act57B$^{K326Q/K328Q}$* caused a complete loss of flight (FI = 0.04 ± 0.01 and 0.03 ± 0.01, respectively).

The *Act88F-GAL4> UAS-Act57B^{K328Q}* and *UAS-Act57B$^{K326Q/K328Q}$* Flightless Phenotype is Associated with Hypercontracted IFM

Fluorescent microscopy was employed to inspect the IFM histopathology in the acetyl-mimetic relative to control flies

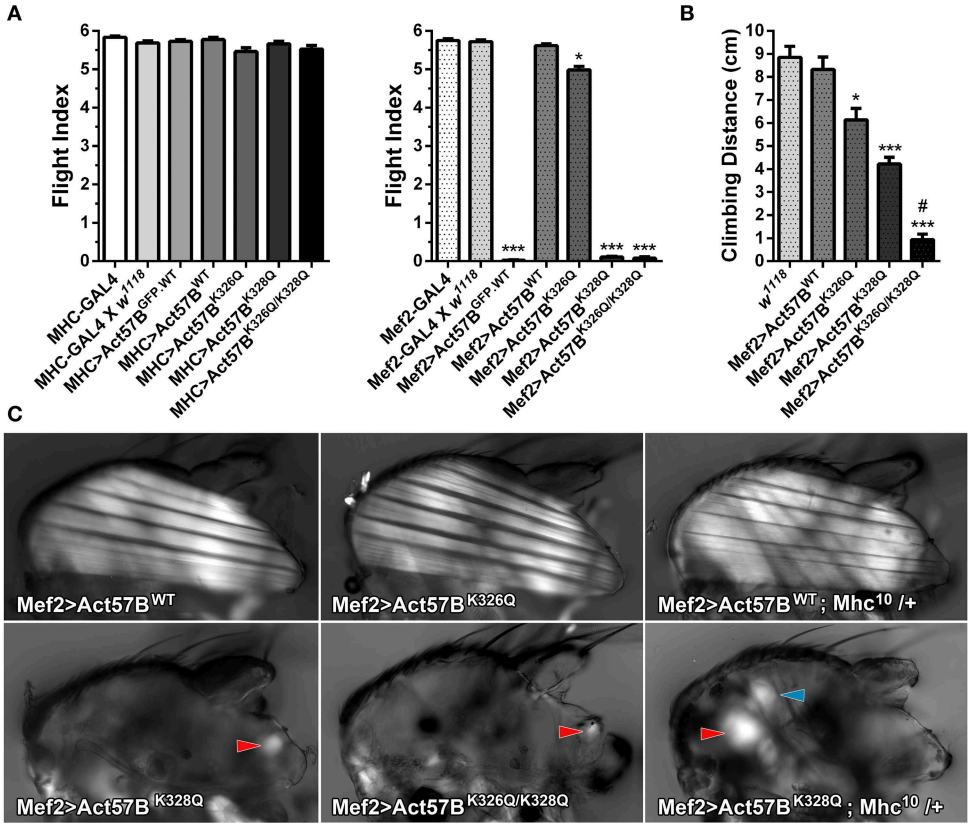

FIGURE 6 | Excessive expression levels of GFP-tagged or acetyl-mimetic actin disrupt muscle function and structure. (A) Flight indices of control and of *MHC-GAL4>* or *Mef2-GAL4> UAS-Act57B*$^{GFP.WT}$, *UAS-Act57B*^{WT}, *UAS-Act57B*^{K326Q}, *UAS-Act57B*^{K328Q}, or *UAS-Act57B*$^{K326Q/K328Q}$ transgenic *Drosophila*. MHC-GAL4 "low-dose"-driven *UAS-Act57B* constructs did not affect flight ability in any transgenic line. "High-dose" expression of *UAS-Act57B*$^{GFP.WT}$ by Mef2-GAL4 abolished flight whereas *UAS-Act57B*^{WT} transgene expression had no effect on flight performance. Mef2-GAL4-driven expression of *UAS-Act57B*^{K326Q} caused a slight but significant reduction in flight ability (*$P < 0.05$ compared to controls), while expression of *UAS-Act57B*^{K328Q} or *UAS-Act57B*$^{K326Q/K328Q}$ completely eliminated flight (***$P < 0.001$ compared to controls). **(B)** Effects of pseudo-acetylation on climbing ability. Pseudo-acetylated K326Q actin showed the least and K326Q/K328Q actin the most damaging effects, which illustrates the PTM can also influence performance of non-fibrillar muscle (*$P < 0.05$, ***$P < 0.001$ compared to controls; #$P < 0.01$ compared to *Mef2-GAL4> UAS-Act57B*^{K328Q}) **(C)** Polarized light micrographs of IFM from *Mef2-GAL4> UAS-Act57B*^{WT}, *UAS-Act57B*^{K326Q}, *UAS-Act57B*^{K328Q}, or *UAS-Act57B*$^{K326Q/K328Q}$ flies. *Mef2-GAL4> UAS-Act57B*^{K326Q} IFM appeared indistinguishable from *Mef2-GAL4> UAS-Act57B*^{WT} control. Mef2-GAL4-mediated expression of *UAS-Act57B*^{K328Q} and *UAS-Act57B*$^{K326Q/K328Q}$, however, resulted in a phenotype consistent with severe hypercontraction. Minor traces of birefringent material, assumed to be IFM remnants (red arrowheads), were occasionally observed. A single copy of *Mhc*^{10}, the IFM-specific myosin null allele, had no influence on gross muscle morphology in *Mef2-GAL4> UAS-Act57B*^{WT}; *Mhc*^{10}/+ thoraces. *Mef2-GAL4> UAS-Act57B*^{K328Q}; *Mhc*^{10}/+ *Drosophila* displayed increased abundance of birefringent thoracic musculature (red arrowhead) relative to *Mef2-GAL4> UAS-Act57B*^{K328Q} flies. The blue arrowhead indicates the tergal depressor of trochanter (jump) muscle. These findings are consistent with previous studies that demonstrated reduced MHC partially suppresses fiber destruction and they suggest that IFM expressing Mef2-GAL4-driven *UAS-Act57B*^{K328Q} requires relatively little myosin to hypercontract.

(**Figure 7C**). Two-day-old *Act88F-GAL4> UAS-Act57B*^{K326Q} *Drosophila* did not show obvious differences in fiber morphology compared to *Act88F-GAL4> UAS-Act57B*^{WT}. Similarly-aged *Act88F-GAL4> UAS-Act57B*^{K328Q} and *UAS-Act57B*$^{K326Q/K328Q}$ *Drosophila,* in contrast, showed prominently hypercontracted IFM fibers, characterized by separation and accumulation of fiber material at one or both attachment sites as previously observed in other *Drosophila* muscle mutants (Fyrberg et al., 1990; Nongthomba et al., 2003). IFMs in very young *UAS-Act57B*^{K328Q} expressing adults (< four hour old) had a substantially less severe phenotype (**Figure 7C**). Most fibers could be distinctly visualized with minimal thinning and separation. The results indicated that the hypercontracted phenotype associated with Act57B^{K328Q}, and potentially with Act57B$^{K326Q/K328Q}$ acetyl-mimetic actin, was progressive and deteriorates with age and/or use.

Discussion

Post-translational modifications represent a means to reversibly or irreversibly alter the physical and chemical nature of proteins. PTMs thereby modulate the molecules' properties and dramatically increase the complexity of biological systems. For example, even a single protein can exist as a diverse mixture of many modified forms (Agnetti et al., 2011). Specific

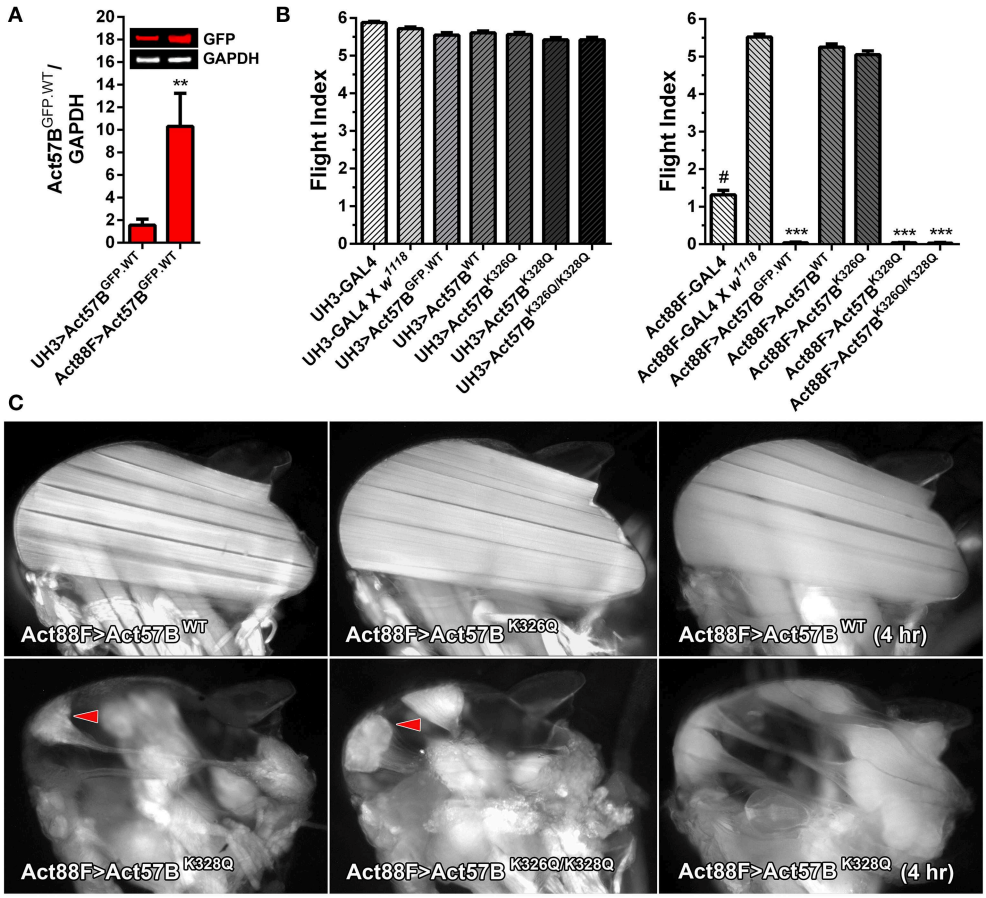

FIGURE 7 | Disproportionately high expression of *UAS-Act57B^{K328Q}* via the Act88F-GAL4 IFM-specific driver induces hypercontraction. **(A)** Quantitative western blot analysis of Act57B$^{GFP.WT}$ abundance driven by UH3-GAL4 vs. Act88F-GAL4. GFP intensities were normalized to that of GAPDH and averaged for eight IFM samples with four technical replicates each. Act88F-GAL4 drove significantly higher amounts of transgenic actin relative to UH3-GAL4 (**$P < 0.01$). **(B)** Flight indices of *UH3-GAL4>* and *Act88F-GAL4> UAS-Act57B$^{GFP.WT}$*, *UAS-Act57B^{WT}*, *UAS-Act57B^{K326Q}*, *UAS-Act57B^{K328Q}*, and *UAS-Act57B$^{K326Q/K328Q}$* transgenic *Drosophila*. UH3-GAL4, and "low dose" expression of all *UAS-Act57B* actin constructs by the driver, had no effect on flight. *Act88F-GAL4 Drosophila* exhibited significantly reduced flight performance relative to female progeny of *Act88F-GAL4* x *w^{1118}* (#$P < 0.001$). The latter demonstrated wild-type-like flight ability. "High-dose" expression of *UAS-Act57B$^{GFP.WT}$* by Act88F-GAL4 eliminated flight whereas *UAS-Act57B^{WT}* transgene expression had no effect on flight performance. "High dose" expression of *UAS-Act57B^{K326Q}* reduced flight ability, an effect which approached statistical significance. *Act88F-GAL4> UAS-Act57B^{K328Q}* and *UAS-Act57B$^{K326Q/K328Q}$ Drosophila* were flightless (***$P < 0.001$). **(C)** Fluorescent images of dorsal longitudinal IFMs from two-day-old *Act88F-GAL4> UAS-Act57B^{WT}*, *UAS-Act57B^{K326Q}*, *UAS-Act57B^{K328Q}*, and *UAS-Act57B$^{K326Q/K328Q}$* flies. *Act88F-GAL4> UAS-Act57B^{K326Q}* IFMs were indistinguishable from *Act88F-GAL4> UAS-Act57B^{WT}* control IFMs. *Act88F-GAL4> UAS-Act57B^{K328Q}* and *UAS-Act57B$^{K326Q/K328Q}$ Drosophila*, however, displayed hypercontracted IFM with separated and bunched fibers (red arrowheads) at attachment sites. IFMs from young (four hour old) *UAS-Act57B^{K328Q}*-expressing flies had a considerably less severe phenotype with minimal thinning and separation of the fibers.

measurements of a number of PTMs have revealed that several residues of a particular protein can be modified. Moreover, different PTMs may compete with each other for access to a single residue on the same protein. Based on an annotated human database, 62% of cardiac proteins have at least one PTM with phosphorylation dominating, whereas 25% have multiple types of modifications (van Eyk, 2011).

The cardiac thin filament is subject to a host of PTMs that markedly influence the properties of the constituent subunits and can directly affect contractile regulation and muscle performance (Metzger and Westfall, 2004; Sumandea et al., 2004; Agnetti et al., 2011; Solaro and Kobayashi, 2011; van Eyk, 2011). However, the modified status of these proteins is infrequently accounted for in *in silico* and *in vitro* experiments. As investigation and discovery of myocardial protein PTMs intensify, determining the *in vivo* consequences of modifying amino acid residues that lie at highly conserved and at potentially critical locations becomes increasingly important. Establishing model systems that limit genetic diversity and benefit from robust and relatively efficient transgenic tools for organism development and high throughput physiological assessment is imperative.

Here we provide novel data pertaining to recently identified PTMs using *Drosophila* that express pseudo-acetylated K326Q, K328Q, or K326Q/K328Q cardiac actin in a muscle-restricted

manner. Transgenic actin expression was confirmed via thoracic and IFM-specific cDNA analysis and by GFP-based reporter imaging. As previously found with similar GFP-tagged constructs (Röper et al., 2005; Perkins and Tanentzapf, 2014), we observed restricted and repetitive incorporation of transgenic GFP-actin along IFM myofibrils, which, as evaluated by phalloidin labeling, were indistinguishable from wild-type myofibrils (not shown). Röper et al. reported that the IFM was the only muscle in which function was affected by overexpression of GFP-labeled actin (Röper et al., 2005). Muscle-restricted expression of muscle or cytoplasmic GFP-actins using the UAS-GAL4 system was shown to yield flightless adults that were otherwise healthy and fertile. Consistent with earlier studies, it was postulated that impaired IFM function, and in some cases the disrupted flight muscle structure, resulted from an imbalance in the relative amounts of actin and myosin (Beall et al., 1989; Bernstein et al., 1993; Röper et al., 2005; Vigoreaux, 2006). Furthermore, Fyrberg et al. (1998) showed that *Drosophila* exclusively expressing chimeric actin, consisting of part of Act57B fused with the remaining portion of Act88F in their IFM, exhibited decreased flight ability. Thus, in addition to actin and myosin stoichiometric discrepancies that potentially influence performance, these findings suggest functional non-equivalence of actin isoforms and that the IFM is also exquisitely sensitive to actin sequence variation. However, we observed that "low dose" expression of GFP-actin using the *MHC-* or *UH3-GAL4* driver did not impair flight and that expression of non-GFP-tagged wildtype Act57B actin via *MHC-*, *Mef2-*, *UH3-*, or *Act88F-GAL4* muscle-specific drivers had no influence on *Drosophila* flight ability. Therefore, despite differences in 9 amino acid residues between Act88F and Act57B actin isoforms (**Figure 2**), incorporation of non-mutant cardiac actin into IFM myofibrils appeared to support flight at expression levels dictated by each GAL4 driver. These results imply that the GFP moiety of excessively overexpressed GFP-fused actins directly impairs flight. This may be due, in part, to perturbed Tm movement or myosin crossbridge binding in the IFM consistent with the N-terminal fluorescent protein tag located proximal to Tm and myosin binding sites on actin. Importantly, our findings illustrate that GAL4-mediated transgene expression *can be employed to investigate the effects of non-GFP tagged cardiac actin* modifications on the readily measurable index of flight.

Compared to *UAS-Act57B^{WT}* cardiac actin expression, expression of mutant acetyl-mimetic cardiac actin had a dose-dependent effect on flight ability. Moreover, robust expression of *UAS-Act57B^{K328Q}* and *UAS-Act57B$^{K326Q/K328Q}$* via Mef2- or Act88F-GAL4 induced a greater reduction in flight performance relative to *UAS-Act57B^{K326Q}*. Mef2- or Act88F-GAL4-driven Act57B^{K326Q} also had no resolvable effect on gross IFM morphology. It is conceivable that, rather than a direct effect of K→Q substitution on contraction, the milder phenotype associated with Act57B^{K326Q} might be attributable to reduced actin monomer incorporation, owing to a decrease in protein stability or increase in protease accessibility caused by the mutation. Though difficult to rule out confounding effects on protein stability, the preponderance of buttressing evidence suggests that Act57B^{K326Q} exerts direct yet modest effects on contractile function. Namely, in addition to slightly depressing flight ability, *Mef2-GAL4> UAS-Act57B^{K326Q}* flies exhibited significantly reduced climbing ability. Moreover, *Mef2-GAL4> UAS-Act57B$^{K326Q/K328Q}$* flies displayed impaired climbing relative to *Mef2-GAL4> UAS-Act57B^{K328Q}* flies. The latter results also highlight an influence of pseudo-acetylated actin on non-fibrillar adult somatic muscles.

The absence of flight in *Act57B^{K328Q}* and *Act57B$^{K326Q/K328Q}$*-expressing flies was associated with a "wings up" phenotype and a loss of IFM fibers. Mutations in *Drosophila* muscle proteins frequently produce a phenotype referred to as hypercontraction (Fyrberg et al., 1990; Beall and Fyrberg, 1991; Kronert et al., 1995; An and Mogami, 1996; Reedy et al., 2000; Nongthomba et al., 2003). This degenerative syndrome is characterized by muscles that begin to develop normally, and then auto-destruct in an apparently myosin-dependent manner. The IFM of the troponin I and T mutants, *hdp^2* and *up^{101}*, respectively, initially develop normally and begin to show signs of degeneration 78 h after puparium formation, concomitant with initial muscle twitching in the developing imago (Naimi et al., 2001; Nongthomba et al., 2003). By the second day of adult life very few sarcomeres remain (Beall and Fyrberg, 1991). The onset of hypercontraction suggests that it is a result of muscle activation, and is not due to abnormal development (Nongthomba et al., 2003).

Both *hdp^2* and *up^{101}* thin filaments exhibit aberrantly positioned Tm in the absence of Ca^{2+}, which results in exposed myosin binding sites at rest (Cammarato et al., 2004; Viswanathan et al., 2014). Consequently, IFM hypercontraction is believed to result from excessive actomyosin interaction and unregulated force production. Models of the F-actin-Tm interface reveal K326 and K328 of actin participate in vital intermolecular electrostatic associations with Tm to establish an energetically favorable conformation (Brown and Cohen, 2005; Li et al., 2011; Barua et al., 2012, 2013; Lehman et al., 2013). Here, Tm is located in an azimuthal location that occludes myosin binding sites on F-actin. Moreover, a recent model of the F-actin-Tm-myosin interface reveals K328 on actin can also directly interact with strongly bound myosin heads (Behrmann et al., 2012). Our data suggest that sufficiently high acetylation of these actin residues can weaken actin-Tm interaction and disrupt the ability of Tm to properly block crossbridge formation and force transmission to the thin filament. Therefore, as with the aforementioned troponin mutations, the acetyl-mimetic actin may similarly trigger hypercontraction. Interestingly, the effect of modifying K328 triggered more severe defects relative to K326, which indicates K328 may be most essential for proper relaxation, *in vivo*. Moreover, since K328Q actin may also impair strong S1 binding, which is predicted to oppose hypercontraction, our data imply the effects of potentially weakening S1-actin association are less harmful than those that influence Tm positioning, as the muscles still hypercontract.

The importance of these actin residues in thin filament regulation, and the effects associated with potential loss of charge, are further underscored by naturally occurring mutations. For example, the K326N nemaline myopathy actin mutation, which differs from the K326Q acetyl-mimetic isoform investigated here by a single methylene bridge, was reported in patients

with stiff muscles and spontaneous contractures, suggesting a hypercontractile phenotype (Jain et al., 2012). Computation of the energy landscape for this mutant revealed reduced actin-Tm interaction energy, which would facilitate a shift of Tm away from myosin binding sites, and would explain the increased Ca^{2+}-sensitivity and hypercontractility of affected muscles (Jain et al., 2012; Orzechowski et al., 2014). Considering the severity of the effects accompanied by high expression of the K328Q mutation observed in the current study, similar charge loss at K328 may not be well-tolerated in higher organisms.

Based on F-actin-Tm, F-actin-Tm-myosin models, and our physiological data, we believe that acetylation of K326 and K328 of actin alters electrostatic associations with Tm and/or myosin, destabilizes Tm's inhibitory position, and thereby enhances actomyosin associations and promotes IFM hypercontraction and muscle destruction. However, our approach does not preclude possible alternative contributors to muscle pathology. For example, the amino acid substitutions may compromise the folding efficiency, thermal stability, and/or polymerization properties of actin filaments as recently observed for particular cardiomyopathy-causing lesions (Mundia et al., 2012; Müller et al., 2012). Thus, increased F-actin and thin filament lability may promote myofilament and sarcomeric degeneration. Additionally, though our data suggest that sufficiently high doses of actyl-mimetic actins are required to elicit dysfunction, we cannot rule out a potential contribution from early transgene activation via the Mef2-GAL4 driver, relative to the others, that disrupts muscle development (Markstein et al., 2008). Thus, the most severe IFM phenotype, which was observed in *Mef2-GAL4> UAS-Act57B*^{K328Q} and *UAS-Act57B*$^{K326Q/K328Q}$ *Drosophila*, may be due to both abundant quantities and premature activation times of transgene expression. If K326 and K328 of actin are required for proper thin filament regulation, excessive myosin binding and force production during early muscle development may alter the core building blocks required for proper IFM formation and irreversibly disrupt myofibrillogenesis. This is not unreasonable since during development actomyosin associations appear compulsory for well-ordered and properly functioning IFM (Cripps et al., 1999). However, we detected a greater abundance of birefringent IFM material in *Mef2-GAL4> UAS-Act57B*^{K328Q} thoraces when myosin was reduced. Moreover, relative to *Mef2-GAL4> UAS-Act57B*^{K328Q}, delayed expression of *UAS-Act57B*^{K328Q} actin via Act88F-GAL4 led to a less severe phenotype characterized by post-eclosion progressive separation and accumulation of fiber material to IFM attachment sites. Thus, we interpret these results as consistent with the previously described myosin-dependent, degenerative hypercontraction syndrome and not with a complete lack of IFM development (Nongthomba et al., 2003).

Here we provide *in vivo* confirmation of a requirement for positively charged lysine residues at amino acid positions 326 and 328 on actin for proper thin filament function. We demonstrate how PTMs that sufficiently mask these vital charges can have dramatic consequences on muscle performance and structure. While LC-MS/MS analysis of myofilament enriched subfractions of guinea pig hearts revealed lysines 326 and 328 were acetylated, stoichiometry was not assessed (Foster et al., 2013). Our current data suggest Mef2-GAL4-driven transgenic actin comprises approximately 10–20% of total actin (not shown), while MHC-GAL4 drives significantly less. Therefore, minor changes in a potentially small acetylated myofilamentous actin pool may have substantial repercussions on muscle properties. Masking the charges at K326 and K328 apparently increases muscle function by potentially lowering actin-Tm interaction energy, altering Tm positioning, and perpetually promoting myosin crossbridge formation and contraction. Disproportionately excessive amounts of K326 and K328 acetylation and hypercontractile activity in vertebrate hearts may be deleterious as observed here. Nonetheless, small populations of acetylated K326 and K328 could have beneficial effects under normal conditions that act to augment the contractile properties of muscle. In disease however, particularly afflictions characterized by nutrient excess such as diabetes, elevated acetyl-CoA levels may lead to increased acetylation of these critical actin residues and possibly exacerbate pathology.

Investigating the effects of myofilament protein modifications on distinct *Drosophila* muscles will facilitate our effort to understand the molecular basis of contractile regulation and, importantly, of potentially tempering myopathic responses. Biochemical, biophysical, and structural studies frequently neglect to account for PTMs of myofilamentous proteins, which can greatly modulate contractile behavior. Thus, to truly comprehend muscle performance in health and disease, consideration needs to be given to these dynamic protein modifications. *Drosophila* facilitates genetic manipulation of thin filament components and evaluation of the consequences of perturbation. Moreover, since abundant quantities of native IFM thin filaments and actin can be isolated for *in vitro* studies (Bing et al., 1998; Razzaq et al., 1999; Cammarato et al., 2004; Vikhorev et al., 2010), the models permit hierarchical investigation of the effects of such PTMs on contractile machinery from the molecular through the tissue level. Overall, our findings emphasize the utility of *Drosophila* as a model system that allows for control of genetic modifiers and environmental factors and that enables efficient targeted design and assessment of molecular and tissue-specific responses to protein modifications in the physiological context of muscle.

Acknowledgments

Fly stocks obtained from the Bloomington *Drosophila* Stock Center (NIH P40OD018537) were used in this study. The authors thank Dr. Sanford I. Bernstein (San Diego State University) for helpful comments and suggestions on the manuscript. ACBB and WS were supported by NIH/NHLBI T-32 HL-07227. Scientist Development Grants from the AHA (12SDG12060056 to DBF and 10SDG4180089 to AC) and NIH/NHLBI R21HL108052 (to DBF) and NIH/NHLBI R56HL124091 (to AC) also supported this study.

References

Agnetti, G., Husberg, C., and van Eyk, J. E. (2011). Divide and conquer the application of organelle proteomics to heart failure. *Circ. Res.* 108, 512–526. doi: 10.1161/CIRCRESAHA.110.226910

An, H. S., and Mogami, K. (1996). Isolation of 88F actin mutants of *Drosophila melanogaster* and possible alterations in the mutant actin structures. *J. Mol. Biol.* 260, 492–505. doi: 10.1006/jmbi.1996.0417

Barua, B., Fagnant, P. M., Winkelmann, D. A., Trybus, K. M., and Hitchcock-Degregori, S. E. (2013). A periodic pattern of evolutionarily conserved basic and acidic residues constitutes the binding interface of actin-tropomyosin. *J. Biol. Chem.* 288, 9602–9609. doi: 10.1074/jbc.M113.451161

Barua, B., Pamula, M. C., and Hitchcock-Degregori, S. E. (2011). Evolutionarily conserved surface residues constitute actin binding sites of tropomyosin. *Proc. Natl. Acad. Sci. U.S.A.* 108, 10150–10155. doi: 10.1073/pnas.1101221108

Barua, B., Winkelmann, D. A., White, H. D., and Hitchcock-Degregori, S. E. (2012). Regulation of actin-myosin interaction by conserved periodic sites of tropomyosin. *Proc. Natl. Acad. Sci. U.S.A.* 109, 18425–18430. doi: 10.1073/pnas.1212754109

Beall, C. J., and Fyrberg, E. (1991). Muscle abnormalities in *Drosophila melanogaster heldup* mutants are caused by missing or aberrant troponin-I isoforms. *J. Cell Biol.* 114, 941–951. doi: 10.1083/jcb.114.5.941

Beall, C. J., Sepanski, M. A., and Fyrberg, E. A. (1989). Genetic dissection of *Drosophila* myofibril formation: effects of actin and myosin heavy chain null alleles. *Genes Dev.* 3, 131–140. doi: 10.1101/gad.3.2.131

Behrmann, E., Müller, M., Penczek, P. A., Mannherz, H. G., Manstein, D. J., and Raunser, S. (2012). Structure of the rigor actin-tropomyosin-myosin complex. *Cell* 150, 327–338. doi: 10.1016/j.cell.2012.05.037

Bernstein, S. I., O'donnell, P. T., and Cripps, R. M. (1993). Molecular genetic analysis of muscle development, structure, and function in *Drosophila*. *Int. Rev. Cytol.* 143, 63–152. doi: 10.1016/S0074-7696(08)61874-4

Bing, W., Razzaq, A., Sparrow, J., and Marston, S. (1998). Tropomyosin and troponin regulation of wild type and E93K mutant actin filaments from *Drosophila* flight muscle. Charge reversal on actin changes actin-tropomyosin from on to off state. *J. Biol. Chem.* 273, 15016–15021. doi: 10.1074/jbc.273.24.15016

Brand, A. H., and Perrimon, N. (1993). Targeted gene expression as a means of altering cell fates and generating dominant phenotypes. *Development* 118, 401–415.

Brown, J. H., and Cohen, C. (2005). Regulation of muscle contraction by tropomyosin and troponin: how structure illuminates function. *Adv. Protein Chem.* 71, 121–159. doi: 10.1016/S0065-3233(04)71004-9

Bryantsev, A. L., Baker, P. W., Lovato, T. L., Jaramillo, M. S., and Cripps, R. M. (2012). Differential requirements for Myocyte Enhancer Factor-2 during adult myogenesis in Drosophila. *Dev. Biol.* 361, 191–207. doi: 10.1016/j.ydbio.2011.09.031

Cammarato, A., Ahrens, C. H., Alayari, N. N., Qeli, E., Rucker, J., Reedy, M. C., et al. (2011). A mighty small heart: the cardiac proteome of adult *Drosophila melanogaster*. *PLoS ONE* 6:e18497. doi: 10.1371/journal.pone.0018497

Cammarato, A., Dambacher, C. M., Knowles, A. F., Kronert, W. A., Bodmer, R., Ocorr, K., et al. (2008). Myosin transducer mutations differentially affect motor function, myofibril structure, and the performance of skeletal and cardiac muscles. *Mol. Biol. Cell* 19, 553–562. doi: 10.1091/mbc.E07-09-0890

Cammarato, A., Hatch, V., Saide, J., Craig, R., Sparrow, J. C., Tobacman, L. S., et al. (2004). *Drosophila* muscle regulation characterized by electron microscopy and three-dimensional reconstruction of thin filament mutants. *Biophys. J.* 86, 1618–1624. doi: 10.1016/S0006-3495(04)74229-0

Choudhary, C., Kumar, C., Gnad, F., Nielsen, M. L., Rehman, M., Walther, T. C., et al. (2009). Lysine acetylation targets protein complexes and co-regulates major cellular functions. *Science* 325, 834–840. doi: 10.1126/science.1175371

Cripps, R. M., Suggs, J. A., and Bernstein, S. I. (1999). Assembly of thick filaments and myofibrils occurs in the absence of the myosin head. *EMBO J.* 18, 1793–1804. doi: 10.1093/emboj/18.7.1793

Dominguez, R., and Holmes, K. C. (2011). Actin structure and function. *Annu. Rev. Biophys.* 40, 169. doi: 10.1146/annurev-biophys-042910-155359

Drummond, D. R., Hennessey, E. S., and Sparrow, J. C. (1991). Characterisation of missense mutations in the *Act88F* gene of *Drosophila melanogaster*. *Mol. Gen. Genet.* 226, 70–80. doi: 10.1007/BF00273589

Foster, D. B., Liu, T., Rucker, J., O'meally, R. N., Devine, L. R., Cole, R. N., et al. (2013). The cardiac acetyl-lysine proteome. *PLoS ONE* 8:e67513. doi: 10.1371/journal.pone.0067513

Fyrberg, E., Fyrberg, C. C., Beall, C., and Saville, D. L. (1990). *Drosophila melanogaster* troponin-T mutations engender three distinct syndromes of myofibrillar abnormalities. *J. Mol. Biol.* 216, 657–675. doi: 10.1016/0022-2836(90)90390-8

Fyrberg, E. A., Fyrberg, C. C., Biggs, J. R., Saville, D., Beall, C. J., and Ketchum, A. (1998). Functional nonequivalence of *Drosophila* actin isoforms. *Biochem. Genet.* 36, 271–287. doi: 10.1023/A:1018785127079

Fyrberg, E. A., Mahaffey, J. W., Bond, B. J., and Davidson, N. (1983). Transcripts of the six *Drosophila* actin genes accumulate in a stage- and tissue-specific manner. *Cell* 33, 115–123. doi: 10.1016/0092-8674(83)90340-9

Goentoro, L. A., Yakoby, N., Goodhouse, J., Schupbach, T., and Shvartsman, S. Y. (2006). Quantitative analysis of the GAL4/UAS system in *Drosophila* oogenesis. *Genesis* 44, 66–74. doi: 10.1002/gene.20184

Gordon, A. M., Homsher, E., and Regnier, M. (2000). Regulation of contraction in striated muscle. *Physiol. Rev.* 80, 853–924.

Groth, A. C., Fish, M., Nusse, R., and Calos, M. P. (2004). Construction of transgenic *Drosophila* by using the site-specific integrase from phage PhiC31. *Genetics* 166, 1775–1782. doi: 10.1534/genetics.166.4.1775

Haselgrove, J. (1973). "X-ray evidence for a conformational change in the actin-containing filaments of vertebrate striated muscle," in *Cold Spring Harbor Symposia on Quantitative Biology* (Cold Spring Harbor, NY: Cold Spring Harbor Laboratory Press), 341–352.

Herman, I. M. (1993). Actin isoforms. *Curr. Opin. Cell Biol.* 5, 48–55. doi: 10.1016/S0955-0674(05)80007-9

Hiromi, Y., and Hotta, Y. (1985). Actin gene mutations in *Drosophila*; heat shock activation in the indirect flight muscles. *EMBO J.* 4, 1681–1687.

Huxley, H. (1973). "Structural changes in the actin-and myosin-containing filaments during contraction," in *Cold Spring Harbor Symposia on Quantitative Biology* (Cold Spring Harbor, NY: Cold Spring Harbor Laboratory Press), 361–376.

Jain, R. K., Jayawant, S., Squier, W., Muntoni, F., Sewry, C. A., Manzur, A., et al. (2012). Nemaline myopathy with stiffness and hypertonia associated with an *ACTA1* mutation. *Neurology* 78, 1100–1103. doi: 10.1212/WNL.0b013e31824e8ebe

Kronert, W. A., O'donnell, P. T., Fieck, A., Lawn, A., Vigoreaux, J. O., Sparrow, J. C., et al. (1995). Defects in the *Drosophila* myosin rod permit sarcomere assembly but cause flight muscle degeneration. *J. Mol. Biol.* 249, 111–125. doi: 10.1006/jmbi.1995.0283

Lehman, W., and Craig, R. (2008). Tropomyosin and the steric mechanism of muscle regulation. *Adv. Exp. Med. Biol.* 644, 95–109. doi: 10.1007/978-0-387-85766-4_8

Lehman, W., Craig, R., and Vibert, P. (1994). Ca(2+)-induced tropomyosin movement in *Limulus* thin filaments revealed by three-dimensional reconstruction. *Nature* 368, 65–67. doi: 10.1038/368065a0

Lehman, W., Orzechowski, M., Li, X. E., Fischer, S., and Raunser, S. (2013). Gestalt-binding of tropomyosin on actin during thin filament activation. *J. Muscle Res. Cell Motil.* 34, 155–163. doi: 10.1007/s10974-013-9342-0

Li, X. E., Tobacman, L. S., Mun, J. Y., Craig, R., Fischer, S., and Lehman, W. (2011). Tropomyosin position on F-actin revealed by EM reconstruction and computational chemistry. *Biophys. J.* 100, 1005–1013. doi: 10.1016/j.bpj.2010.12.3697

Lorenz, M., Poole, K. J., Popp, D., Rosenbaum, G., and Holmes, K. C. (1995). An atomic model of the unregulated thin filament obtained by X-ray fiber diffraction on oriented actin-tropomyosin gels. *J. Mol. Biol.* 246, 108–119. doi: 10.1006/jmbi.1994.0070

Marek, K. W., Ng, N., Fetter, R., Smolik, S., Goodman, C. S., and Davis, G. W. (2000). A genetic analysis of synaptic development: pre- and postsynaptic dCBP control transmitter release at the *Drosophila* NMJ. *Neuron* 25, 537–547. doi: 10.1016/S0896-6273(00)81058-2

Markstein, M., Pitsouli, C., Villalta, C., Celniker, S. E., and Perrimon, N. (2008). Exploiting position effects and the gypsy retrovirus insulator to engineer precisely expressed transgenes. *Nat. Genet.* 40, 476–483. doi: 10.1038/ng.101

McKillop, D. F., and Geeves, M. A. (1993). Regulation of the interaction between actin and myosin subfragment 1: evidence for three states of the thin filament. *Biophys. J.* 65, 693–701. doi: 10.1016/S0006-3495(93)81110-X

Metzger, J. M., and Westfall, M. V. (2004). Covalent and noncovalent modification of thin filament action: the essential role of troponin in cardiac muscle regulation. *Circ. Res.* 94, 146–158. doi: 10.1161/01.RES.0000110083.17024.60

Müller, M., Mazur, A. J., Behrmann, E., Diensthuber, R. P., Radke, M. B., Qu, Z., et al. (2012). Functional characterization of the human alpha-cardiac actin mutations Y166C and M305L involved in hypertrophic cardiomyopathy. *Cell Mol. Life Sci.* 69, 3457–3479. doi: 10.1007/s00018-012-1030-5

Mundia, M. M., Demers, R. W., Chow, M. L., Perieteanu, A. A., and Dawson, J. F. (2012). Subdomain location of mutations in cardiac actin correlate with type of functional change. *PLoS ONE* 7:e36821. doi: 10.1371/journal.pone.0036821

Naimi, B., Harrison, A., Cummins, M., Nongthomba, U., Clark, S., Canal, I., et al. (2001). A tropomyosin-2 mutation suppresses a troponin I myopathy in *Drosophila*. *Mol. Biol. Cell* 12, 1529–1539. doi: 10.1091/mbc.12.5.1529

Nongthomba, U., Cummins, M., Clark, S., Vigoreaux, J. O., and Sparrow, J. C. (2003). Suppression of muscle hypercontraction by mutations in the myosin heavy chain gene of *Drosophila melanogaster*. *Genetics* 164, 209–222.

Nongthomba, U., Pasalodos-Sanchez, S., Clark, S., Clayton, J. D., and Sparrow, J. C. (2001). Expression and function of the *Drosophila* ACT88F actin isoform is not restricted to the indirect flight muscles. *J. Muscle Res. Cell Motil.* 22, 111–119. doi: 10.1023/A:1010308326890

Nongthomba, U., and Ramachandra, N. B. (1999). A direct screen identifies new flight muscle mutants on the *Drosophila* second chromosome. *Genetics* 153, 261–274.

Orzechowski, M., Fischer, S., Moore, J. R., Lehman, W., and Farman, G. P. (2014). Energy landscapes reveal the myopathic effects of tropomyosin mutations. *Arch. Biochem. Biophys.* 564, 89–99. doi: 10.1016/j.abb.2014.09.007

Parry, D. A., and Squire, J. M. (1973). Structural role of tropomyosin in muscle regulation: analysis of the x-ray diffraction patterns from relaxed and contracting muscles. *J. Mol. Biol.* 75, 33–55. doi: 10.1016/0022-2836(73)90527-5

Perkins, A. D., and Tanentzapf, G. (2014). An ongoing role for structural sarcomeric components in maintaining *Drosophila melanogaster* muscle function and structure. *PLoS ONE* 9:e99362. doi: 10.1371/journal.pone.0099362

Pettersen, E. F., Goddard, T. D., Huang, C. C., Couch, G. S., Greenblatt, D. M., Meng, E. C., et al. (2004). UCSF Chimera–a visualization system for exploratory research and analysis. *J. Comput. Chem.* 25, 1605–1612. doi: 10.1002/jcc.20084

Ranganayakulu, G., Schulz, R. A., and Olson, E. N. (1996). Wingless signaling induces *nautilus* expression in the ventral mesoderm of the *Drosophila* embryo. *Dev. Biol.* 176, 143–148. doi: 10.1006/dbio.1996.9987

Razzaq, A., Schmitz, S., Veigel, C., Molloy, J. E., Geeves, M. A., and Sparrow, J. C. (1999). Actin residue glu(93) is identified as an amino acid affecting myosin binding. *J. Biol. Chem.* 274, 28321–28328. doi: 10.1074/jbc.274.40.28321

Reedy, M. C., Bullard, B., and Vigoreaux, J. O. (2000). Flightin is essential for thick filament assembly and sarcomere stability in *Drosophila* flight muscles. *J. Cell Biol.* 151, 1483–1500. doi: 10.1083/jcb.151.7.1483

Röper, K., Mao, Y., and Brown, N. H. (2005). Contribution of sequence variation in *Drosophila* actins to their incorporation into actin-based structures *in vivo*. *J. Cell Sci.* 118, 3937–3948. doi: 10.1242/jcs.02517

Shah, A. P., Nongthomba, U., Kelly Tanaka, K. K., Denton, M. L., Meadows, S. M., Bancroft, N., et al. (2011). Cardiac remodeling in *Drosophila* arises from changes in actin gene expression and from a contribution of lymph gland-like cells to the heart musculature. *Mech. Dev.* 128, 222–233. doi: 10.1016/j.mod.2011.01.001

Singh, S. H., Kumar, P., Ramachandra, N. B., and Nongthomba, U. (2014). Roles of the troponin isoforms during indirect flight muscle development in *Drosophila*. *J. Genet.* 93, 379–388. doi: 10.1007/s12041-014-0386-8

Solaro, R. J., and Kobayashi, T. (2011). Protein phosphorylation and signal transduction in cardiac thin filaments. *J. Biol. Chem.* 286, 9935–9940. doi: 10.1074/jbc.R110.197731

Suggs, J. A., Cammarato, A., Kronert, W. A., Nikkhoy, M., Dambacher, C. M., Megighian, A., et al. (2007). Alternative S2 hinge regions of the myosin rod differentially affect muscle function, myofibril dimensions and myosin tail length. *J. Mol. Biol.* 367, 1312–1329. doi: 10.1016/j.jmb.2007.01.045

Sumandea, M. P., Burkart, E. M., Kobayashi, T., De Tombe, P. P., and Solaro, R. J. (2004). Molecular and integrated biology of thin filament protein phosphorylation in heart muscle. *Ann. N.Y. Acad. Sci.* 1015, 39–52. doi: 10.1196/annals.1302.004

Swank, D. M., Knowles, A. F., Kronert, W. A., Suggs, J. A., Morrill, G. E., Nikkhoy, M., et al. (2003). Variable N-terminal regions of muscle myosin heavy chain modulate ATPase rate and actin sliding velocity. *J. Biol. Chem.* 278, 17475–17482. doi: 10.1074/jbc.M212727200

Swank, D. M. (2012). Mechanical analysis of *Drosophila* indirect flight and jump muscles. *Methods* 56, 69–77. doi: 10.1016/j.ymeth.2011.10.015

Tardiff, J. C. (2011). Thin filament mutations: developing an integrative approach to a complex disorder. *Circ. Res.* 108, 765–782. doi: 10.1161/CIRCRESAHA.110.224170

Terman, J. R., and Kashina, A. (2013). Post-translational modification and regulation of actin. *Curr. Opin. Cell Biol.* 25, 30–38. doi: 10.1016/j.ceb.2012.10.009

Tobacman, L. S. (1996). Thin filament-mediated regulation of cardiac contraction. *Annu. Rev. Physiol.* 58, 447–481. doi: 10.1146/annurev.ph.58.030196.002311

van Eyk, J. E. (2011). Overview The maturing of proteomics in cardiovascular research. *Circ. Res.* 108, 490–498. doi: 10.1161/CIRCRESAHA.110.226894

Vibert, P., Craig, R., and Lehman, W. (1997). Steric-model for activation of muscle thin filaments. *J. Mol. Biol.* 266, 8–14. doi: 10.1006/jmbi.1996.0800

Vigoreaux, J. O. (2006). Nature's Versatile *Engine: Insect Flight Muscle Inside and Out*. New York, NY: Landes Bioscience/Eurekah. com.

Vikhorev, P. G., Vikhoreva, N. N., Cammarato, A., and Sparrow, J. C. (2010). *In vitro* motility of native thin filaments from *Drosophila* indirect flight muscles reveals that the *held-up*^{2} TnI mutation affects calcium activation. *J. Muscle Res. Cell Motil.* 31, 171–179. doi: 10.1007/s10974-010-9221-x

Viswanathan, M. C., Kaushik, G., Engler, A. J., Lehman, W., and Cammarato, A. (2014). A *Drosophila melanogaster* model of diastolic dysfunction and cardiomyopathy based on impaired troponin-T function. *Circ. Res.* 114, e6–e17. doi: 10.1161/CIRCRESAHA.114.302028

Von Der Ecken, J., Muller, M., Lehman, W., Manstein, D. J., Penczek, P. A., and Raunser, S. (2015). Structure of the F-actin-tropomyosin complex. *Nature* 519, 114–117. doi: 10.1038/nature14033

Wang, Y., Melkani, G. C., Suggs, J. A., Melkani, A., Kronert, W. A., Cammarato, A., et al. (2012). Expression of the inclusion body myopathy 3 mutation in *Drosophila* depresses myosin function and stability and recapitulates muscle inclusions and weakness. *Mol. Biol. Cell* 23, 2057–2065. doi: 10.1091/mbc.E12-02-0120

Conflict of Interest Statement: The authors declare that the research was conducted in the absence of any commercial or financial relationships that could be construed as a potential conflict of interest.

Copyright © 2015 Viswanathan, Blice-Baum, Schmidt, Foster and Cammarato. This is an open-access article distributed under the terms of the Creative Commons Attribution License (CC BY). The use, distribution or reproduction in other forums is permitted, provided the original author(s) or licensor are credited and that the original publication in this journal is cited, in accordance with accepted academic practice. No use, distribution or reproduction is permitted which does not comply with these terms.

frontiers in
PHYSIOLOGY

REVIEW ARTICLE
published: 26 September 2014
doi: 10.3389/fphys.2014.00369

Skeletal muscle myofilament adaptations to aging, disease, and disuse and their effects on whole muscle performance in older adult humans

Mark S. Miller[1], Damien M. Callahan[2] and Michael J. Toth[2,3]*

[1] *Department of Kinesiology, School of Public Health and Health Sciences, University of Massachusetts, Amherst, MA, USA*
[2] *Department of Molecular Physiology and Biophysics, College of Medicine, University of Vermont, Burlington, VT, USA*
[3] *Department of Medicine, College of Medicine, University of Vermont, Burlington, VT, USA*

Edited by:
Julien Ochala, King's College London, UK

Reviewed by:
Ranganath Mamidi, Case Western Reserve University, USA
Lars G. Hvid, University of Southern Denmark, Denmark

***Correspondence:**
Michael J. Toth, Health Science Research Facility 126B, University of Vermont, 149 Beaumont Ave., Burlington, VT 05405, USA
e-mail: michael.toth@uvm.edu

Skeletal muscle contractile function declines with aging, disease, and disuse. *In vivo* muscle contractile function depends on a variety of factors, but force, contractile velocity and power generating capacity ultimately derive from the summed contribution of single muscle fibers. The contractile performance of these fibers are, in turn, dependent upon the isoform and function of myofilament proteins they express, with myosin protein expression and its mechanical and kinetic characteristics playing a predominant role. Alterations in myofilament protein biology, therefore, may contribute to the development of functional limitations and disability in these conditions. Recent studies suggest that these conditions are associated with altered single fiber performance due to decreased expression of myofilament proteins and/or changes in myosin-actin cross-bridge interactions. Furthermore, cellular and myofilament-level adaptations are related to diminished whole muscle and whole body performance. Notably, the effect of these various conditions on myofilament and single fiber function tends to be larger in older women compared to older men, which may partially contribute to their higher rates of disability. To maintain functionality and provide the most appropriate and effective countermeasures to aging, disease, and disuse in both sexes, a more thorough understanding is needed of the contribution of myofilament adaptations to functional disability in older men and women and their contribution to tissue level function and mobility impairment.

Keywords: myosin, actin, cross-bridge kinetics, single fiber, isometric tension, contractile velocity, sex differences, physical activity

INTRODUCTION

Aging, disease, and disuse decrease whole skeletal muscle contractile performance, which reduces an individual's ability to accomplish tasks associated with daily living, eventually leading to physical disability (Guralnik et al., 1995; Janssen et al., 2002; Kortebein et al., 2008). Knowledge of the mechanisms underlying the loss of skeletal muscle performance will aid in the development of suitable exercise and pharmacological countermeasures to forestall or counteract these detrimental changes.

Whole muscle contractile performance has been identified as an important determinant of functional limitations in older adults (Reid and Fielding, 2012). As whole muscle performance is dependent upon the functional character of single muscle fibers (Harridge et al., 1996; D'Antona et al., 2006), which are, in turn, largely determined by the type of myofilament proteins they express and their function (Bottinelli, 2001), alterations in myofilament protein biology may contribute to the development of disability in these conditions. Unfortunately, myofilament properties cannot be discerned from measurements performed at the whole muscle level due to methodological limitations (e.g., estimation of muscle size, muscle architecture), subjective factors (e.g., volitional effort) and the interceding effects of other physiological systems that regulate whole muscle function (e.g., neural, excitation-contraction coupling, connective tissue properties). That is, because myofilaments are the end effectors of muscle contraction, the interceding effects of higher order regulatory factors (i.e., at the cellular, tissue or organ/tissue systems level) can mask variation in myofilament function. Thus, to reliably assess the effects of aging, disease, and disuse on skeletal muscle myofilament biology, a reductionist approach is required, where measurements are obtained at the cellular and molecular levels.

This review will focus on human studies that have examined skeletal muscle myofilament structure and function at the cellular and/or molecular levels. As aging, disease, and disuse may alter muscle structure or function by changing muscle quantity [i.e., cross-sectional area (CSA) and/or amount of mass per unit muscle size] or quality (i.e., performance per unit muscle size), we will specifically address these variables in each condition. The review is organized based upon a continuum of whole muscle performance we have observed in our laboratories, which indicates that aging reduces whole muscle performance, both isometric and

isokinetic, with progressively larger reductions associated with decreasing activity level, the presence of acute or chronic disease and finally profound, protracted muscle disuse (**Figure 1**). The reader is referred to several recent reviews of other important aspects of the neuromuscular system that undoubtedly conspire with myofilament adaptations to contribute to functional impairments with aging, disease, and disuse (Raj et al., 2010; Rehn et al., 2012; Reid and Fielding, 2012; Russ et al., 2012; Calvani et al., 2013).

MYOSIN-ACTIN CROSS-BRIDGE (XB) INTERACTIONS

The formation of the myosin-actin XB is the end effector of muscle contraction. This interaction of two myofilament proteins, myosin and actin, dictate single fiber force and contractile velocity, which can be summarized into simple equations by making several assumptions about the myosin-actin interaction: (1) myosin is either strongly bound to actin producing force or detached from actin producing no force and (2) the XB behaves as a Hookian spring, as detailed (Palmer et al., 2007). In brief, the amount of force that can be produced by a half-sarcomere during isometric contraction can be represented as the number of strongly-bound XBs multiplied by the force generated per XB (F_{uni}) (Huxley, 1957; Brenner, 1988). The number of strongly-bound XBs at any point in time is a function of the total number of functional myosin heads (N) multiplied by the fraction of time a strongly-bound XB is formed (t_{on}) as a function of total myosin cycle time ($t_{on} + t_{off}$), where t_{on} is the amount of time myosin is strongly bound to actin and t_{off} is the amount of time myosin is detached from actin. Accordingly, the amount of force that can be produced by the half-sarcomere during isometric tension can be written as: N ($t_{on}/(t_{on} + t_{off})$) F_{uni}. Notably, $t_{on}/(t_{on} + t_{off})$ is commonly called the myosin duty ratio and, although difficult to measure, may be altered under various circumstances, with this effect perhaps best exemplified by differences between the myosin isoforms found in human skeletal muscle (Linari et al., 2004). The force generated per XB may also be altered and can be represented as the elastic stiffness of the XB (k_{stiff}) multiplied by the unitary displacement of the myosin power stroke (d_{uni}). Contractile velocity is represented most simply as d_{uni} divided by t_{on}, in agreement with single fiber findings showing faster velocities with shorter t_{on} (i.e., higher myosin detachment rate) (Piazzesi et al., 2007). Although controversial, recent experimental and modeling work indicates that velocity is also faster with shorter t_{off} (i.e., higher myosin attachment rate) (Hooft et al., 2007; Walcott et al., 2012), potentially via mechanisms that ultimately shorten t_{on} (Walcott et al., 2012). Considered in this context, aging, disease, and/or disuse could alter skeletal muscle force production or velocity by altering the interaction of myosin and actin, which would ultimately affect whole muscle performance and functional capabilities.

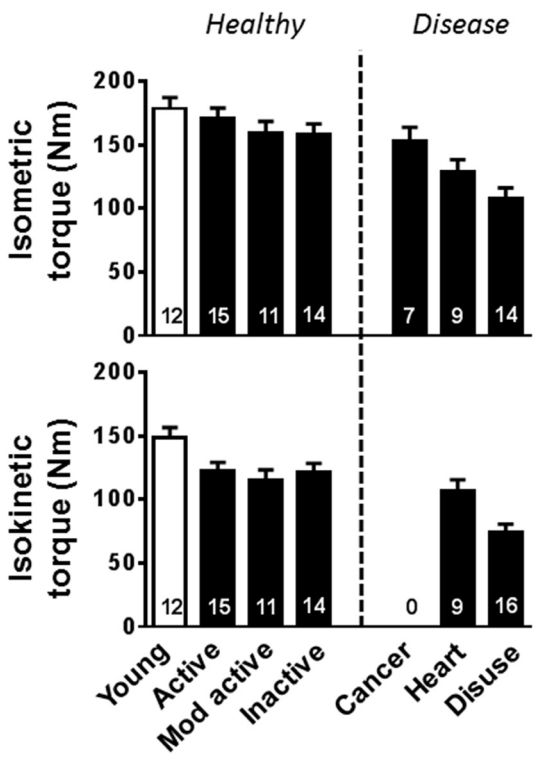

FIGURE 1 | Whole leg muscle contractile performance changes with aging, disease, and disuse. Young (open bars) and older (closed bars) are arranged such that whole muscle performance progressively decreases to the right along the x-axis. Volunteers identified as "Young" and "Mod active" are from Miller et al. (2013), "Active" and "Disuse" are from Callahan et al. (2014b), "Inactive" and "Heart" are from Toth et al. (2012), and "Cancer" are from Toth et al. (2013). Isokinetic torque measurements were collected at 60°/s. Mod, moderately; Heart, Heart failure.

What is the relative importance of XB kinetics (e.g., t_{on} and t_{off}) vs. XB mechanical properties (e.g., F_{uni} and d_{uni}) in determining single fiber function? Single myosin molecule studies comparing myosin heavy chain (MHC) isoforms between [smooth from turkey vs. skeletal from chicken (Guilford et al., 1997)] and within [α vs. β cardiac in rabbit (Palmiter et al., 1999) and rat (Sugiura et al., 1998)] species have shown no differences in F_{uni} or d_{uni}, indicating that isoform differences in force and velocity are due primarily to alterations in XB kinetics. In support of XB kinetics being the primary determinants of fiber function, frog single fiber experiments within a single isoform show that F_{uni} and d_{uni} remain consistent over a range of velocities (Piazzesi et al., 2007). In contrast, when looking across fiber types, human single fiber experiments indicate that both XB kinetics and F_{uni} are responsible for the higher forces generated by faster contracting MHC isoforms (Linari et al., 2004). Similarly, single fiber (Brenner et al., 2012) and single molecule (Capitanio et al., 2006) measurements comparing slow isoforms from one species to fast isoforms from another species indicate faster MHC isoforms have higher XB stiffness (k_{stiff}), most likely resulting in a higher F_{uni}. However, these isoform differences may potentially be due to normal sequence variations as isolated myosin from animal species varying in body size contract at distinctly different velocities (Pellegrino et al., 2003). Overall, these results indicate that XB kinetics play an important role in setting both force and velocity in single muscle fibers, while the role of XB mechanical properties is not clearly defined. Thus, the evaluation of XB kinetics and mechanics as mediators of cellular and tissue level contractile function remains an important area of future study, especially in humans.

Alterations in single fiber force and velocity can also occur via changes in muscle quantity and/or structure. Human skeletal muscle fibers contains three different isoforms (I, IIA, or IIX), with individual fibers expressing either one or multiple isoforms leading to six different fiber types (I, I/IIA, IIA, IIA/IIX, IIX, I/IIA/IIX), with pure MHC I and IIA being the two most prevalent. Parenthetically, an additional embryonic isoform of myosin may be expressed in some physiological/pathophysiological conditions (D'Antona et al., 2003, 2006). A simple shift in the type of MHC isoform expressed in the fiber will produce different tissue level velocity and tension (force per CSA) characteristics, as faster contracting MHCs (I < IIA < IIX) produce more tension (D'Antona et al., 2003, 2006; Pansarasa et al., 2009; Krivickas et al., 2011). Thus, this myofilament variation can alter whole muscle performance (Thorstensson et al., 1977; Ryushi and Fukunaga, 1986; Harridge et al., 1996). In addition to changes in MHC isoform, reducing the amount of myofilament proteins by having smaller fiber CSA, reduced myofibrillar fractional area (e.g., less myofibril area due to an increase in inter-myofibrillar space or other non-contractile elements), or the removal of thick (myosin containing) or thin (actin containing) filaments would decrease single fiber force production. Myofilament ultrastructure plays an important role in setting contractile performance by providing the framework for XB interactions. For instance, at the fiber level, the amount of isometric force produced is equal to the total number of heads interacting in each half-sarcomere (each half-sarcomere must produce identical forces or the sarcomere will change its length). Thus, removal of myosin heads, either from the ends of the thick filament or randomly throughout the thick filament, or a reduction in the number of thin filaments would reduce the number of heads able to interact in a half-sarcomere and result in lower force production. Although fiber CSA is commonly measured in healthy adults as well as during aging, disuse, and disease, changes in myofilament protein content and ultrastructure have not been routinely examined, especially in combination with contractile measurements.

AGING

Aging reduces whole muscle contractile performance, in part due to a loss of skeletal muscle mass, but also due to reduced muscle quality (Jubrias et al., 1997; Lindle et al., 1997; Lynch et al., 1999; Morse et al., 2005; Delmonico et al., 2009). This age-related diminution in muscle contraction tends to affect dynamic more than isometric function (Lanza et al., 2003; Callahan and Kent-Braun, 2011; Miller et al., 2013), which suggests skeletal muscle properties are altered in a manner that maintains higher forces at slower speeds of movement. Identification of interventions to halt or reverse age-related alterations in skeletal muscle quantity and quality, therefore, can help to maintain physical function and independent living in older adults.

MUSCLE QUALITY

Multiple human studies have examined whether aging alters contractile performance at the single fiber and myofilament levels with differing results. Findings are generally concordant across fiber types within an individual study, but age-related adaptations in MHC I and IIA fiber contractile performance (isometric tension and velocity) vary widely across studies, with some showing decreases (Larsson et al., 1997; Frontera et al., 2000, 2008; Krivickas et al., 2001; D'Antona et al., 2003; Ochala et al., 2007; Yu et al., 2007) and others showing that function remains unchanged or even increases (Frontera et al., 2003; Trappe et al., 2003; Korhonen et al., 2006; Reid et al., 2012, 2014; Miller et al., 2013). Notably, longitudinal studies show that single fiber tension and velocity either increase or remain constant (Frontera et al., 2008; Reid et al., 2014), suggesting that older adults do not show continued loss of contractile performance and may, in fact, experience improved myofilament function as a compensatory mechanism to offset whole muscle functional decline.

Although single fiber performance results vary widely, myosin protein function appears to decrease from early (e.g., 20–35 year age range) to the older adult (e.g., 60 years and older). In single fibers, and especially in MHC IIA fibers, aging lowers ATPase (Larsson et al., 1997), slows the time response to changes in fiber length (Ochala et al., 2006, 2007), as well as lengthening t_{on} and potentially t_{off} (Miller et al., 2013), indicating slowing of XB kinetics with age. Using isolated myosin, *in vitro* motility studies show that MHC I actin sliding velocity is decreased (Hook et al., 2001; D'Antona et al., 2003) or unchanged (Canepari et al., 2005) with age, while these same studies agree that MHC IIA actin sliding velocity is unchanged (Hook et al., 2001; D'Antona et al., 2003; Canepari et al., 2005). Thus, in contrast to single fibers, results from studies of isolated myosin suggest that MHC I has the larger aging response of slowing XB kinetics (as slower velocity is indicative of a longer t_{on} and/or t_{off}), while MHC IIA is unaffected. These divergent results between these two assays may be related to their experimental conditions as single fiber experiments are performed with their native regulatory protein content and three-dimensional structure using solutions similar to physiologic conditions, while, in order to specifically determine myosin's role in contractile performance, isolated myosin studies remove the myosin from its fiber structure and are typically performed with unregulated actin (Hook et al., 2001; D'Antona et al., 2003; Canepari et al., 2005). Our laboratory (Okada et al., 2008; Miller et al., 2010) and others (Thedinga et al., 1999; D'Antona et al., 2003) have similarly found divergent results when examining myofilament function in isolated myofilaments preparations vs. chemically-skinned single fiber preparations, including when examining genetically-altered animal models (Palmiter et al., 1999; Wang et al., 2013). Based on this evidence, caution must be exercised when interpreting results from these different experimental preparations. Nonetheless, with this caveat in mind, these results collectively suggest that aging generally decreases XB kinetics.

How would slower XB kinetics alter single fiber contractile performance? We would predict that the slowing of XB kinetics, especially longer t_{on} (Miller et al., 2013), should lead to a decrease in contractile velocity. This conclusion is supported by findings of an age-related reduction in contractile velocity that occurs in concert with indications of slower XB kinetics [reduced ATPase activity (Larsson et al., 1997) and longer time response to changes in fiber length (Ochala et al., 2006, 2007)]. At the same time that decreases in XB kinetics reduce velocity, it could have the reciprocal effect of increasing tension, as slower XB kinetics appear

to drive an increase in myofilament stiffness, or improved force transmission, that leads to higher isometric tension (Miller et al., 2013). Similarly, slower XB kinetics in older adults occur with an increase in single fiber stiffness, although their overall isometric tension was reduced (Ochala et al., 2006, 2007), which could be explained by reductions in the overall number of XBs secondary to decreased myosin protein expression (D'Antona et al., 2003). Collectively, these studies indicate that the slowing of XB kinetics with age most likely decreases contractile velocity, but may have the paradoxical effect of improving myofilament stiffness and isometric tension.

When findings indicate almost any alteration with age is possible, most noticeable in single fiber contractile performance, this pattern of differences suggests that factors related to the populations studied or the methods employed may explain variation among studies. As the methodology used and experimental conditions are generally standard across studies, variation in the populations studied likely explains the divergent results across studies. One potential reason behind these varying results is differences in physical activity among the populations studied (**Figure 1**), a factor that is difficult to control for and has commonly not been addressed. Physical activity in older adults is well-known to alter single fiber contractile properties (Trappe et al., 2000, 2001; D'Antona et al., 2003, 2007; Frontera et al., 2003; Parente et al., 2008; Harber et al., 2009; Toth et al., 2012), with higher levels of daily activity or specific exercise training regimens tending to reduce or eliminate age-related differences. Such adaptations are not, however, simply linear throughout the activity spectrum, as immobilization in older individuals has been found to increase velocity (D'Antona et al., 2003, 2007), suggesting that complete loss of weight-bearing activity is characterized by very different adaptations, in keeping with findings from animal studies (Reiser et al., 1987) and muscle unloading due to short duration spaceflight in humans (Widrick et al., 1999). Nonetheless, a modulatory role for physical activity with age would suggest that exercise training may mitigate disability, in part, through a reduction of the deleterious age-related changes in myofilaments.

Another potential confounding factor is differences between men and women in their response to aging. Older women have been found to generate higher isometric tensions in MHC I and IIA fibers (Yu et al., 2007; Miller et al., 2013) and have slower contractile velocities in MHC I (Krivickas et al., 2001; Yu et al., 2007) and IIA (Krivickas et al., 2001) fibers. These results are consistent with the finding of slower XB kinetics being more prominent in both of these fiber types in older women (Miller et al., 2013), as we predict slower kinetics would increase tension and decrease velocity. Sex has also been found to have an effect on force production based upon fiber size, as MHC I and IIA fibers with large CSAs produce less force in women compared to men and MHC I fibers with small CSAs produce more force in women (Frontera et al., 2000). However, other studies have found no statistical differences in the single fiber contractile properties of isometric tension and velocity between older men and women (Trappe et al., 2003; Krivickas et al., 2006), with individual laboratories sometimes showing differing results from study to study (Krivickas et al., 2001, 2006). Such variation among studies may reflect differences in other subject characteristics (e.g., physical activity), the number of fibers being examined [i.e., only 7 MHC IIA fibers in older women (Trappe et al., 2003)], or sample sizes as studies not observing sex differences were smaller ($n = 16$–24) than those observing differences ($n = 24$–38). Notably, a large cross-sectional study ($n = 71$) indicates older mobility-limited females produce higher isometric tension in MHC IIA fibers compared to males (Reid et al., 2012), although a three-year longitudinal study ($n = 16$) from the same laboratory found no sex effects on single fiber performance between healthy and mobility-limited older adults (Reid et al., 2014). Regardless of the reason for variation among studies, these findings raise the possibility that sex differences in myofilament function may contribute to the discrepancies in age-related changes in single fiber performance among studies.

MUSCLE QUANTITY/STRUCTURE

In general, studies using individual skinned fibers find no change in MHC I and IIA CSA with age (Frontera et al., 2000, 2003, 2008; Ochala et al., 2007; Hvid et al., 2010; Reid et al., 2012, 2014), although some have found decreases in MHC I (D'Antona et al., 2003), IIA (Larsson et al., 1997), or both (Korhonen et al., 2006). CSA also decreases with inactivity in both fiber types (D'Antona et al., 2003). Moreover, CSA has either no (Frontera et al., 2000; Reid et al., 2012, 2014) or varied response to aging in men vs. women, with older men having larger CSAs than young in MHC I fibers (Miller et al., 2013) and older men (Yu et al., 2007) or women (Trappe et al., 2003; Miller et al., 2013) having smaller CSAs than their young counterparts. An advantage of CSA measurements in single skinned fibers is that they are typically performed at the experimental sarcomere length (usually ∼2.50–2.75 μm), providing a consistent standard across fiber types and age groups. However, one caveat to the skinned fiber preparation is that it undergoes swelling, which may complicate age comparisons. When CSA measurements are determined from both skinned fibers used for contractile performance and fresh frozen preparations via histochemistry within the same group of volunteers, the two techniques can produce different results, with histochemistry results finding no change in MHC I fibers with age and decreasing in MHC IIA with age (Korhonen et al., 2006; Miller et al., 2013; Callahan et al., 2014a). However, recent studies suggest that age-related differences in skinned human single muscle fibers are comparable to differences observed with fresh frozen preparations (Hvid et al., 2011). Parenthetically, studies in genetic animal models (Blaauw et al., 2009), where muscle fiber protein content is dramatically altered (e.g., 50% hypertrophy in 3 weeks due to activation of Akt signaling) showed disparate CSA results between skinned and fresh frozen preparations, suggesting that variation in the degree of swelling may occur with alterations in fiber protein content, urging caution with this approach. Studies examining whole vastus lateralis muscle indicate that the age-related reduction in muscle size is due to fibers being lost and a decrease in CSA, especially in MHC II fibers (Lexell et al., 1988; Lexell and Downham, 1991; Lexell, 1995). In contrast, a recent metaanalysis, which did not include skinned fiber results, indicates CSA is unchanged with age, but is larger with higher physical activity levels (Gouzi et al., 2013). Thus, the variation in CSA

with age between the various studies may be due to other confounding factors. Overall, these results indicate that CSA with age either remains unchanged or decreases in MHC II fibers, with alterations possibly affected by sex. Despite potential changes in CSA, recent data indicates that the amount of myofilaments as well as their general structure and stoichiometry is unaltered with age or sex (Callahan et al., 2014a). However, studies do indicate age-related changes in post-translational modifications, such as decreased phosphorylation of the fast isoform of the regulatory myosin light chain (Gelfi et al., 2006; Miller et al., 2013), and in gene expression of protein isoforms, such as an increased gene expression of tropomyosin 2 (Roth et al., 2002). These types of alterations have not been commonly examined in human, but may play a role in functional adaptations as they can affect XB performance.

As the MHC isoform distribution and content can alter contractile performance, several studies have examined the age-related changes in these properties. MHC isoform distribution remained unchanged in longitudinal studies (Frontera et al., 2008) and when physical activity was matched between young and older volunteers (D'Antona et al., 2007; Miller et al., 2013). However, activity level is generally thought to modify MHC isoform distribution, with lower activity causing a shift toward a faster phenotype, or an increase in MHC IIX (D'Antona et al., 2003, 2007), and higher activity causing a shift toward a slower phenotype, or an increase in MHC I (Korhonen et al., 2006; D'Antona et al., 2007). MHC content also remained unchanged in studies matching for physical activity levels (Trappe et al., 2003; Miller et al., 2013) and decreases with reductions in physical activity and immobilization (D'Antona et al., 2003). Altogether, these studies indicate that the amount or types of MHC are not altered by age, but can be changed in older adults based upon their habitual level of exercise.

HEART FAILURE

Heart failure represents the final common pathway for most chronic cardiovascular disease, and is characterized by an inability of the heart to pump blood to meet the metabolic demands of the body, or that it can only do so at elevated filling pressures. Accordingly, exercise intolerance is the hallmark symptom of the disorder, leading to high rates of disability (Pinsky et al., 1990). Although reduced cardiac contractile performance undoubtedly contributes to reduced functional capacity, changes in skeletal muscle physiology, including muscle atrophy, weakness and reduced oxidative capacity are well-accepted contributors (Zizola and Schulze, 2013). A more complete understanding of the mechanisms causing muscle dysfunction, therefore, is important for identifying appropriate countermeasures to maintain or improve the whole muscle performance and, in turn, reducing disability in these patients.

MUSCLE QUANTITY/STRUCTURE

Skeletal muscle atrophy in patients with end-stage heart failure has been recognized for decades (Pittman and Cohen, 1964) and studies have identified reductions in single muscle fiber size in patients, especially in MHC IIA fibers (Mancini et al., 1989; Massie et al., 1996; Szentesi et al., 2005), although others have shown that CSA remains unchanged in stable, ambulatory heart failure patients (Sullivan et al., 1990; Schaufelberger et al., 1995, 1997; Miller et al., 2009). Prior results of reduced CSA may be partially explained by muscle disuse-related atrophy, as few studies have controlled for this confounding factor, or because patients were studied shortly following hospitalization. Interestingly, human studies (Toth et al., 2005; Miller et al., 2009), along with animal models (Van Hees et al., 2007), have shown a phenotype of reduced myosin content/functional XB number at the whole tissue and single fiber levels per unit protein or fiber CSA using biochemical (gel electrophoresis) and mechanical (rigor stiffness) measurements, and this loss is observed in patients even when compared to activity-matched controls (Miller et al., 2009). These studies have also suggested that there was no specific reduction in actin protein or thin filament content with heart failure (Miller et al., 2009). At the ultrastructural level, myosin loss could present as a decreased number of thick filaments, shortened thick filaments or a combination of both adaptations. However, no change in either thick-to-thin filament stoichiometry or thick filament length has been found (Miller et al., 2009). Based on this evidence, we hypothesized that myosin was lost at random throughout the thick filament, which would agree with studies that indicate remodeling of the thick filaments takes place by removing and replacing myosin molecules at random throughout the length of the filament (Wenderoth and Eisenberg, 1987; Franchi et al., 1990). Further confirmation of this pattern of thick filament adaption in heart failure will be difficult, as the resolution of current microscopic approaches is insufficient to rigorously test this hypothesis. Nonetheless, the loss of myosin from muscle fibers has clear functional relevance (discussed below).

On a more macroscopic level, heart failure has long been associated with a shift in skeletal muscle fiber type toward a more fast-twitch phenotype (Mancini et al., 1989; Vescovo et al., 1996; Sullivan et al., 1997; Toth et al., 2005). A shift in MHC isoform distribution of this nature could contribute to reduced exercise tolerance given the differing oxidative potential of MHC I and II fibers and this has been demonstrated in patients (Vescovo et al., 1998). However, this pattern of isoform distribution is also emblematic of muscle disuse (Narici and De Boer, 2011) and heart failure patients expend about half as many calories in volitional activity as healthy controls (Toth et al., 1997), suggesting that this adaptation might be due to inactivity accompanying the disease, rather than the disease process itself. This appears to be the case, as we have recently found no alteration in muscle MHC protein isoform expression in patients when compared to activity-matched controls (Miller et al., 2009), and others have shown no differences in MHC isoform expression between patients and controls matched for peak aerobic fitness (Mettauer et al., 2001). There is limited information regarding shifts in isoform expression of other myofilament proteins. One study showed a shift in myosin light chain and troponin T, I, and C toward a slow-twitch isoform distribution in diaphragm muscle in heart failure patients commensurate with a shift in MHC expression toward the MHC I isoform (Tikunov et al., 1996). However, unlike peripheral skeletal muscle, the diaphragm muscle undergoes different functional adaptations (i.e., increased

work due to increased pulmonary resistance vs. muscle disuse in peripheral skeletal muscle). In peripheral skeletal muscle, myosin light chain isoform distributions in MHC IIA single fibers were found to show a trend toward greater expression of MLC 1f in heart failure patients (Miller et al., 2010), but this was not associated with differences in single fiber function. Although an indirect measure, an alteration in Ca^{2+} sensitivity was noted in MHC IIA fibers, which could reflect adaptations in actin-associated regulatory proteins, albeit this was not directly measured.

MUSCLE QUALITY

Independent of variation in muscle size, numerous studies have suggested that there are reductions in skeletal muscle contractile function at the whole muscle [i.e., tissue level (Harrington et al., 1997; Toth et al., 2010)], suggesting decreased intrinsic function of muscle that may be due to myofilament deficiencies, impaired excitation-contraction coupling (Reiken et al., 2003) or a combination of the two. Studies in humans and animal models over the past 5–10 years have shed light on the possible involvement of myofilaments in these contractile deficits.

The most prominent quantitative/structural change that would be predicted to contribute to strength losses per unit muscle size is a loss of MHC, which should decrease the total number of functional myosin heads, causing a reduction in single fiber isometric tension. Indeed, recent studies have found reduced tension in both in MHC I and IIA fibers from heart failure patients (Szentesi et al., 2005) and in experimental models (Van Hees et al., 2007). However, studies from our laboratory, in which heart failure patients were matched for both age and physical activity level, unlike prior studies (Szentesi et al., 2005), found no diminution in single fiber tension (Miller et al., 2010), arguing that prior results of reduced tension with heart failure were explained more by muscle disuse and/or aging than by heart failure *per se*. The question then becomes: how is tension maintained in the face of a reduction in the overall amount of myosin/functional XBs? We found that XB kinetics were slowed, manifested most prominently as a longer t_{on}, in MHC I and IIA fibers, in patients compared to controls (Miller et al., 2010), a result that has also been observed in animal models of heart failure (Van Hees et al., 2007). This reduction in XB kinetics, if not compensated for by an increase in t_{off}, would lead to an increase in residence time of myosin in the strongly-bound state and, in turn, more myosin heads bound to actin as a function of total myosin cycle time. This is indeed the case, as we found no evidence for a reduction in strongly-bound myosin-actin XBs during maximal Ca^{2+} activation in heart failure patients using different techniques (Miller et al., 2009, 2010). Thus, adaptations in myosin kinetic properties compensate for the loss of myosin protein content to preserve isometric contractile strength. In fact, building off of our findings from myofilament ultrastructural measures that suggested a random loss of myosin heads along the length of the thick filament detailed above (Miller et al., 2009), we recently reported the results of modeling studies which suggest that this pattern of myosin loss is associated with an increase in myosin attachment time (Tanner et al., 2014). Thus, we hypothesize that a random removal of myosin from the thick filament alters the load imparted to a strongly-bound XB causing a lengthening of t_{on}, leading to a higher duty ratio and higher tension generation.

Although single muscle fiber tension is maintained, reductions in myosin kinetics in heart failure patients may not be without functional consequences. We would predict that reduced XB kinetics, and increased t_{on} specifically, would reduce contractile velocity (Miller and Toth, 2013). Indeed, recent studies from our laboratory show that this is the case in MHC IIA fibers, where lower XB kinetics were associated with decreased single fiber shortening velocity and, in turn, power output (Callahan et al., 2014b). Thus, while we found no evidence for decrements in single fiber tension that would scale to the tissue level to explain reduced isometric force production (Harrington et al., 1997; Toth et al., 2010), reduced myosin-actin XB kinetics may explain reduced muscle power output during dynamic contractile conditions (Toth et al., 2010). This is noteworthy, as reductions in lower-extremity power output are a primary determinant of physical disability (Reid and Fielding, 2012). Thus, alterations in myofilament properties to yield a reduction in the overall capacity for muscle power output during dynamic activities would mean that any activity would be performed at greater percentage of the muscle's physiological capacity and, in turn, may be more fatiguing. In this context, myofilament adaptations may partially contribute to the subjective sensation of exercise intolerance present in heart failure patients, the primary symptom of the disease.

CANCER

Cancer has well-known effects on skeletal muscle that have been the subject of intense investigation for decades. The most notable effects of cancer are to reduce overall muscle mass secondary to the profound wasting that occurs with the disease [i.e., cancer cachexia (Fearon et al., 2012)], which has, by far, been studied most extensively. However, atrophy is usually confined to certain cancers (e.g., lung, pancreatic, head, and neck) or the later stages of the disease. In contrast, estimates suggest that up to 90% of patients experience subjective functional deficits, manifested most notably as cancer-related fatigue (Cella et al., 2001). Subjective fatigue is a complex psycho-physiological construct, but likely has some roots in reductions in physiological capacity and a recent study suggests that this may relate, in part, to alterations in myofilament biology (Toth et al., 2013).

MUSCLE QUANTITY/STRUCTURE

Cancer is primarily thought to influence skeletal muscle through its ability to promote muscle atrophy, and has recently been reviewed in detail (Fearon et al., 2012). Despite the well-known atrophic effects of cancer, there are surprisingly few studies that have examined its effects on single muscle fiber size in humans (Weber et al., 2009), although recent work confirms that the atrophy observed at the tissue level extends to the cellular level (Toth et al., 2013). Although profound reductions in the overall amount of contractile tissue occur, recent ultrastructural studies suggest that atrophy is characterized by stoichiometric reductions in the myofilament content relative to fiber CSA (Toth et al., 2013). In contrast to these anatomic measurements, studies

that have evaluated myofilament protein content using biochemical approaches in both pre-clinical models (Acharyya et al., 2004) and patients (Eley et al., 2008) have suggested that atrophy in cancer is associated with a selective loss of the contractile protein myosin, with relative preservation of other contractile proteins. If present, one would predict that such an adaptation would diminish muscle contractile force production (Geiger et al., 2000) by decreasing the number of available myosin heads to form strongly-bound XBs. However, more recent studies in the same animal models, as well as patients with cancer, have found no reduction in myosin protein content (Cosper and Leinwand, 2012; Toth et al., 2013). In fact, one study showed that prior findings of a select loss of myosin were likely a methodological artifact (Cosper and Leinwand, 2012). Notably, MHC isoform distribution also remains unchanged with cancer (Toth et al., 2013). Thus, from a quantitative perspective, cancer reduces overall muscle function primarily through its effect to decrease the overall mass of myofilament protein in muscle via simple atrophy, seemingly without selective loss of the major myofilament proteins myosin and actin. This gross loss of contractile tissue manifests functionally as muscle weakness, which undoubtedly contributes to physical disability in cancer patients.

MUSCLE QUALITY

Because of the prevalence of muscle atrophy in the cancer population, it is difficult to discern whether impaired muscle performance is related to a fundamental defect in contractility, or relates instead to the loss of the contractile components (i.e., myofilaments). In humans, to our knowledge, only three studies have simultaneously evaluated skeletal muscle contractile function and muscle size, with one study showing that muscle weakness was completely explained by atrophy (Weber et al., 2009), whereas the others suggested that there was a reduction in intrinsic contractility, or force production per unit muscle size (Stephens et al., 2012; Toth et al., 2013). Further reinforcing the notion of intrinsic contractile dysfunction, one recent study (Gallagher et al., 2012) reported that surgical removal of the tumor in colorectal cancer patients increased knee extensor isometric torque (∼20%; personal communication with the authors) after a mean follow-up of 8 months despite reductions in body weight (and presumably muscle mass). Thus, from whole muscle measurements, the balance of evidence suggests that cancer is associated with some degree of intrinsic skeletal muscle contractile dysfunction.

Evidence to support intrinsic contractile dysfunction in cancer patients comes from studies at the single fiber level (Toth et al., 2013). We recently found evidence for contractile dysfunction in both MHC I and IIA fibers. In MHC IIA fibers, a reduction (∼15%) in isometric tension was observed in cancer patients compared to fibers from healthy controls, which has been corroborated by a recent study from another laboratory (Taskin et al., 2014). These results provide strong evidence for intrinsic contractile dysfunction in cancer. Molecular level functional assessments suggested a potential mechanism for decreased isometric tension; namely, that the number of strongly-attached myosin-actin XBs was reduced in cancer patients, as single fiber force production is proportional to the number of strongly-bound XBs during Ca^{2+} activation. In addition to reduced tension in MHC IIA fibers, myosin-actin cross-bride kinetics were reduced in MHC I fibers (Toth et al., 2013). Specifically, myosin attachment time was increased in MHC I fibers from cancer patients compared to controls. From a functional standpoint, we would predict that this reduction in XB kinetics could decrease single fiber power output, as an increase in myosin attachment time would decrease single fiber contractile velocity (Piazzesi et al., 2007). Thus, this molecular level alteration may have functional significance to cellular and tissue level function. In support of this notion, we found that slower myosin rate of force production, another marker of reduced myosin-actin XB kinetics, were related to reduced knee extensor torque (Toth et al., 2013).

The mechanisms underlying intrinsic skeletal muscle contractile dysfunction with cancer are unclear. Data from whole muscle studies, in which knee extensor strength was measured before and after surgical removal of tumors indicates that alterations in function occur independent of changes in overall muscle size [i.e., improved function occurred in the setting of continued weight, and presumably muscle, loss (Stephens et al., 2012)]. In other words, intrinsic contractile dysfunction is not dependent upon or related to the atrophy process. One potential mediator that could explain contractile dysfunction is oxidative stress, as cancer is associated with increased oxidative stress in skeletal muscle (Barreiro et al., 2005; Ramamoorthy et al., 2009; Marin-Corral et al., 2010). Increased oxidant activity could promote contractile dysfunction via post-translational modification of myofilament proteins (Reid and Moylan, 2011). Indeed, pre-clinical studies that have treated skinned muscle fibers with oxidants have shown that oxidative modification of myofilament proteins reduces tension, velocity, myosin ATPase/XB kinetics and strongly-bound XBs (Wilson et al., 1991; Galler et al., 1997; Perkins et al., 1997; Callahan et al., 2001; Heunks et al., 2001; Coirault et al., 2007), effects that resemble the myofilament functional phenotype we observe in cancer patients (Toth et al., 2013). In support of this mechanism, we recently found that treatment of human single MHC I muscle fibers with *N*-ethylmaleimide (NEM) slowed XB kinetics, as evidenced by increased myosin attachment time. In fact, by down-titrating the NEM, which modifies protein thiol groups, a common target of cellular oxidants, we showed that we could reduce myosin kinetics with no change in single fiber tension (Callahan et al., 2014b), a phenotype that bears remarkable resemblance to the adaptations we observed in cancer patients. Additionally, cancer patients exhibited profound mitochondrial rarefaction and remodeling, with the former being associated with reduced XB kinetics in MHC I fibers and tending to be related to reduced strongly-bound XBs in MHC IIA fibers (Toth et al., 2013). Taken together, these results suggest disruption in mitochondrial biology, and possibly increased oxidant activity, in the skeletal muscle of cancer patients may contribute to myofilament dysfunction in both fiber types. As oxidative stress has also been forwarded as a potential mediator of muscle atrophy in cancer patients (Buck and Chojkier, 1996; Di Marco et al., 2005), our results suggest increased oxidant activity as a potential common mediator of the complex muscle phenotype of muscle atrophy and contractile dysfunction in cancer.

CHRONIC OBSTRUCTIVE PULMONARY DISEASE (COPD)

COPD is a lung disorder characterized by progressive airflow obstruction from inflammation and remodeling of the airways, which often results from emphysema secondary to cigarette smoking. Like heart failure, exercise intolerance is the cardinal symptom, which, along with the obvious contribution of the primary lung pathology, is thought to be due, in part, to a combination of atrophy and reduced oxidative capacity of skeletal muscles (Maltais et al., 2014). In fact, some authors have suggested similar pathoetiology of peripheral skeletal muscle adaptations in the two conditions (Gosker et al., 2000). The majority of research on peripheral skeletal muscle adaptations in COPD patients has focused on oxidative adaptations and atrophy and, to our knowledge, no study has specifically characterized myofilament function. In contrast, a considerable amount of work has been done examining diaphragm muscle myofilament protein expression and function, including two excellent studies evaluating single fiber function (Ottenheijm et al., 2005; Stubbings et al., 2008). This focus is logical considering the importance of respiratory muscle function in COPD. However, respiratory and peripheral skeletal muscle undergo very different adaptations in response to COPD (Levine et al., 2013), owing to the different pathophysiological demands—increased airway resistance necessitating increased muscle work in respiratory muscles and decreased muscle use owing to reduced physical activity in peripheral skeletal muscles (Watz et al., in press). For the purposes of the current review, we have focused primarily on studies that have evaluated myofilament adaptations in peripheral skeletal muscles.

MUSCLE QUANTITY AND STRUCTURE

Muscle atrophy in patients with COPD has largely been inferred from cross-sectional studies comparing whole muscle size in patients to non-diseased controls, with findings of reduced muscle size in COPD patients that is exacerbated with more severe disease (Remels et al., 2013; Maltais et al., 2014). These results are corroborated at the cellular level, with several studies showing decreased single muscle fiber size in COPD patients (Whittom et al., 1998; Gosker et al., 2002; Fermoselle et al., 2012). Interestingly, a recent study showed a similar rate of decline in lean tissue mass (a proxy of muscle mass) in individuals with COPD vs. non-diseased controls (Van Den Borst et al., 2011), suggesting that some differences in muscle fiber size may relate to early adaptations to cigarette smoking and/or could be a manifestation of the population that goes on to develop COPD. Regardless of the etiology, a loss of muscle fiber size would have clear relevance to decreased functional capacity and contribute to disability.

Numerous studies have suggested that that there is a skeletal muscle fiber type shift in COPD toward a more fast-twitch phenotype, manifested as a reduced relative expression of MHC I vs. MHC II fiber types (Gosker et al., 2007), with accompanying shifts in myosin light chain isoforms (Satta et al., 1997). Some studies have failed to find such a fiber type shift in deltoid muscle (Gea et al., 2001), arguing that fiber type adaptations to COPD in the lower extremity musculature may reflect the effects of muscle disuse. Thus, similar to heart failure, as discussed above, this fiber type adaptation may simply be function of chronic disuse in COPD patients, rather than an effect of the disease process *per se*.

MUSCLE QUALITY

As mentioned above, there are few studies that have directly measured muscle fiber function in COPD patients and nearly all of these have evaluated diaphragm muscle (Levine et al., 2003; Ottenheijm et al., 2005; Stubbings et al., 2008). There has been one study that evaluated function of isolated vastus lateralis muscle fiber bundles in COPD patients and controls (Debigare et al., 2003), which found no differences in maximal isometric tetanic contraction or adaptation in the force-frequency response, albeit the latter tended to be shifted to the right in COPD patients. Importantly, this study utilized an excitable muscle preparation, meaning that the contractile response reflects the effects of COPD on both myofilaments and Ca^{2+} release dynamics. Thus, the altered force-frequency response could be explained by alterations in Ca^{2+} release/reuptake, myofilament Ca^{2+} sensitivity or a combination of these changes. Caution is urged in interpreting this study, however, as the viability of an excitable muscle fiber bundle preparation is questionable.

In diaphragm muscle fibers, early studies in two COPD patients showed reduced single fiber tension (Levine et al., 2003). Studies in a larger population ($n = 8$) similarly showed reduced single fiber tension in MHC I and IIA fibers from COPD patients compared to controls and this reduction was attributed primarily to a reduction in myosin protein content (Ottenheijm et al., 2005). Moreover, the rate constant for force redevelopment following a following a rapid length decrease, a proxy measure of cross-bridge kinetics, was slower in COPD patients. A more recent study has further corroborated slowed cross-bridge cycling, as the ATPase rate of MHC I and IIA fibers was lower in COPD patients (Stubbings et al., 2008), although this study did not observe altered single fiber tension. Moreover, Stubbings et al. found reduced maximal power production from MHC IIA fibers in COPD patients. Collectively, these decrements in respiratory muscle function could limit pulmonary function and, in turn, contribute to exercise intolerance, the hallmark symptom of COPD and a clear contributor to disability. How these adaptations in myofilament function in diaphragm fibers reflect peripheral skeletal muscle myofilament adaptations, however, is unclear. Although there are some myofilament adaptations with COPD that generalize to striated skeletal muscle [e.g., myofilament protein oxidation (Caron et al., 2009)] and could reasonably be expected to impact function, as discussed above in regards to cancer-related myofilament dysfunction (Callahan et al., 2014b), studies on skinned single fibers from peripheral muscles of COPD patients are needed to confirm involvement of the myofilaments in reduced peripheral muscle contractile function that is also believed to contribute to disability (Maltais et al., 2014).

DISUSE

The specific adaptations of muscle to acute or chronic disuse are particularly interesting to physiologists and clinicians due to: (1) the profound effects of inactivity on multiple aspects of muscle size, protein composition and function and (2) the relevance

of disuse for skeletal muscle adaptations to numerous clinically-relevant conditions (e.g., acute hospitalization, surgical recovery, chronic disease, etc.). Because chronic physical inactivity is both a risk factor and consequence of aging- and disease-related changes in skeletal muscle, it is difficult to disentangle the relative influence of aging/disease vs. disuse. As the effects of disuse have been studied rather extensively in healthy, younger humans (Adams et al., 2003; Narici and De Boer, 2011), this review will focus on adaptations to muscle disuse in older adult humans, which has received increased attention recently. Before beginning this discussion, we need to define acute and chronic disuse. As there are no widely-accepted definitions for the length of either acute or chronic or any biological hallmark that serves as a temporal cut-point, we have decided to put these into the context of clinically-relevant events that may impose disuse upon older adults. Acute periods of disuse occur with the onset or exacerbation of disease or other clinical events (e.g., surgery) and their subsequent period of convalescence. These can last for a few days, but may persist for several months (e.g., 3–6 months), as in the case of recovery from surgical interventions (e.g., joint replacement, hip fracture, coronary artery bypass graft surgery), with the defining characteristic being that muscle use patterns eventually return to "normal," pre-event levels. In contrast, chronic muscle disuse is marked by a failure to re-establish prior levels of muscle use, with accommodation at a lower absolute level of muscle use. Therefore, by definition, this type of disuse lasts for years and may never be fully remediated.

MUSCLE QUANTITY/STRUCTURE

Muscle disuse is known to cause marked reductions in muscle CSA in healthy young individuals (Adams et al., 2003; Narici and De Boer, 2011) and recent studies suggest that bed rest-induced muscle disuse is similarly associated with lower extremity muscle atrophy (−6%) in older adults (Kortebein et al., 2007). More recent studies that imposed disuse using leg casting in older adult men for a shorter period of time (4 d) have shown more robust atrophy (∼10% reduction in both MHC I and II fiber types) compared to baseline when single muscle fiber CSA was evaluated (Suetta et al., 2012). Interestingly, when casting is maintained for 14 d, the degree of atrophy did not increase dramatically (∼13% reduction) and this differs from younger men, who showed a more marked reduction in single muscle fiber CSA (−20%) (Suetta et al., 2012). Thus, disuse-related atrophy may be attenuated in older adults over time. In general, this atrophy was evenly distributed between MHC I and II fibers in shorter-term studies (4–5 d), but was more pronounced in MHC II fibers over longer periods (14 d) (Suetta et al., 2012; Wall et al., 2014).These data suggest that, like their younger counterparts, older adults appear to have a relatively robust atrophy response to experimentally-induced, acute muscle disuse. Additionally, one study showed that myosin protein content of single muscle fibers was profoundly reduced (−44% in MHC I and −31% in MHC IIA fibers, albeit differences in MHC II fibers did not reach significance) in two older adult men who were studied 3 months following leg immobilization for clinical purposes (D'Antona et al., 2003), but corroboration of these findings or characterization of the anatomical phenotype of myosin loss is lacking. Despite changes in muscle size, short term immobilization did not alter myosin isoform distribution (Hvid et al., 2010), while longer immobilization specifically increased MHC IIX expression (D'Antona et al., 2003).

Few studies have explored the effects of chronic muscle disuse on skeletal muscle size and structure in humans, primarily because experimentally-imposed disuse for extended periods of time on humans of any age would be deemed unethical. However, one could argue that this type of muscle disuse is very relevant to the muscle adaptations that occur in disease states (e.g., heart failure, COPD, etc.), where activity levels are lower than their non-diseased counterparts (Toth et al., 1997; Watz et al., in press). To study chronic disuse, several laboratories have evaluated patients with osteoarthritis, where physical inactivity is chronically depressed due to joint pain. If patients are selected to be free of other confounding pathologies, these patients could be considered a model of the effects of chronic disuse on skeletal muscle. Studies have shown that these patients have lower (∼9%) quadriceps CSA in their limb with osteoarthritis compared to their unaffected limb (Suetta et al., 2007), and a greater degree of atrophy compared to non-diseased controls (Callahan et al., 2014b). Moreover, at the cellular level, there was profound atrophy (−14 to 32% depending on fiber type) in muscle fibers. Here again, the extent of atrophy is greater when examined at the single fiber vs. the tissue level. To date, no study has reported the effects of either acute or chronic muscle disuse on myofilament ultrastructure or other sub-cellular components.

MUSCLE QUALITY

Skeletal muscle performance is impaired with disuse in younger healthy adults, reflected in reduced whole muscle force and power production (Narici and De Boer, 2011), and this is similarly observed in older healthy adults in response to short periods of bed rest (Kortebein et al., 2008). That these changes may be associated with adaptations in myofilament function is suggested by several recent studies showing that chemically-skinned, single muscle fiber contractile function is impaired in older adults with acute muscle disuse. Single fiber tension after 4 and 14 days of leg casting is reduced similarly in young and older men in both MHC I and IIA fibers (Hvid et al., 2011, 2013), although reductions in MHC I fibers did not reach significance in response to 14 d of disuse. There were differential responses in Ca^{2+} sensitivity in young and older adult men that showed fiber type differences, with reductions in older men in MHC I and in young men in MHC IIA fibers, suggesting the possibility for age-related differences in the adaptations in actin-associated regulatory proteins. These findings provide important contributions to our understanding of the effects of acute disuse and encourage further study of how this combination of physiologic responses manifest to change *in vivo* voluntary torque production and mobility in at-risk populations, particularly as it pertains to acute hospitalization.

Building on these results, our recent studies suggest the functional effects of chronic disuse vary by sex (Callahan et al., 2014b). Although we similarly found reductions in single muscle fiber tension in older adults compared to active controls, these

differences were only apparent in MHC IIA fibers and dissipated when fibers were evaluated at temperatures closer to *in vivo* conditions (25°C), suggesting that the effects of more chronic disuse on myofilament force production per unit fiber CSA is limited. In contrast, we found differences in contractile velocity; more specifically, that contractile velocity was reduced in females, but actually increased in males with chronic disuse. Perhaps most importantly, these differences in contractile velocity translated to reduced single fiber power output in women relative to men. Greater contractile velocity (and, in turn, power output) in men was accompanied by faster cross-bridge kinetics, as indicated by a reduced myosin attachment time and greater rate of myosin force production, suggesting that adaptations in molecular contractile function translate to the cellular level.

Do these adaptations in myofilament function at the molecular and cellular level contribute to the whole muscle phenotype of reduced power output in the lower extremity musculature? Extrapolation from the myofilament to the whole muscle level is difficult, as there are changes in numerous other physiological systems with disuse that regulate whole muscle torque (Narici and De Boer, 2011). Recent studies suggest that acute disuse has more prominent effects in older adults on dynamic muscle contractions with higher power output when compared to lower power output and isometric contractions (Hvid et al., 2014), which is in keeping with results in aging studies showing greater impairments in dynamic muscle contractile function and, in particular, higher velocity dynamic contractions (Lanza et al., 2003; Callahan and Kent-Braun, 2011; Miller et al., 2013). This may be explained by more pronounced slowing of cross-bridge kinetics in older adults, an adaptation that is larger in older adult women (Miller et al., 2013). With more chronic disuse, however, there may be compensatory adaptations to maintain myofilament contractile function specifically in men (Callahan et al., 2014b), with women lacking such adaptations. These myofilament adpatations with disuse may serve to diminish whole muscle deteroration, as recent longitudinal studies have shown that reductions in whole muscle function over time are accompanied by improvements in single muscle fiber myofilament force, velocity and power output (Reid et al., 2014). A failure to undergo such myofilament adaptations may predispose women to a more rapid development of disability. Thus, rather than a straight forward relationship of reduced myofilament function to decreased whole muscle function and, in turn, disability, variation in compensatory *increases* in myofilament function with longer-term disuse may explain a greater disposition toward lower extremity muscle function and disability in some individuals. This scenario provides potential cellular and molecular level mechanisms underlying higher disability rates in older women (Jette and Branch, 1981) and suggests that it may be important to consider the sex-specific response to disuse in men and women to completely characterize the functional phenotype. Notably, all studies examining the effect of acute disuse have been conducted in men, which makes it difficult to discern whether sex-specific adaptations are a feature of both acute and chronic disuse. Nonetheless, these findings show that myofilament adaptations may play an important role in the whole muscle and disability phenotypes that accompany muscle disuse.

CELLULAR/MOLECULAR EFFECTS ON WHOLE MUSCLE FUNCTION

The contribution of myofilament adaptations to whole muscle contractile dysfunction and, in turn, physical disability with aging, disease, and disuse is difficult to discern because of the myriad of physiological systems that regulate whole muscle performance. Despite this multitude of confounding, higher level regulatory systems, several studies have shown relationships between myofilament properties and whole muscle performance. In older adults, a positive, but non-linear, relationship was found between single fiber and whole muscle tension (Frontera et al., 2000), indicating that the age-related decrease in single fiber performance may be partially responsible for decrements in whole muscle function. In our recent work examining young and older populations matched for physical activity level, although isokinetic knee torque was reduced with age, we found no differences in whole muscle isometric performance or relationships between isometric performance and single fiber functional parameters. However, slower XB kinetics and increased single fiber isometric tension in MHC IIA fibers predicted lower whole muscle isokinetic power with aging (Miller et al., 2013). Thus, age-related myofilament adaptations were correlated with the primary decrement in whole muscle performance with age. Similarly in cancer patients, reduced whole muscle isometric torque was related to slower XB kinetics (Toth et al., 2013). Both the cancer and aging populations also showed a relationship between slower XB kinetics and mitochondrial fractional area or size (Toth et al., 2013; Callahan et al., 2014a), suggesting the intriguing hypothesis that maladaptations in cellular energy homeostasis may contribute to myofilament dysfunction via post-translational oxidative modifications. Finally, in knee osteoarthritis patients, variation in XB kinetics in MHC IIA fibers scaled to the cellular level to yield sex-specific differences in single fiber power output (Callahan et al., 2014b). These molecular and cellular level differences were reflected in a similar pattern of differences in isokinetic torque at the whole muscle (i.e., lower torque in female knee osteoarthritis patients), albeit these tissue-level differences did not reach statistical significance, possibly due to our small sample size and/or sex-specific effects of pain-induced neural inhibition associated with knee osteoarthritis. Although preliminary, these studies collectively demonstrate that alterations at the molecular and cellular levels generally scale to the tissue level, suggesting that adaptations in myofilament protein expression and function may partially explain reductions in muscle function and lead to greater rates of physical functional disability with aging and disease.

SUMMARY

Aging, disease, and disuse alter single fiber and myofilament structure and function, although the changes vary depending upon the specific disease/physiological condition and sex. Structurally, the most significant changes were the loss of myosin content in heart failure patients and the general loss of CSA in a number of conditions (**Table 1**). Functionally, the parameter that was consistently changed with these conditions was XB kinetics (**Table 2**). Although XB kinetics tend to decrease in most instances, reductions are dependent upon sex and fiber type, with

Table 1 | Summary of structural changes in single fiber and myofilament structure with aging, disease, and disuse.

Structure	Aging	Heart failure	Cancer	Disuse
Ultrastructure	↔	↔	↔	n.a.
MHC content	↔	↓	↔	↔
MHC isoform phenotype	↔	↑ ↔	↔	↑ ↔
Cross-sectional area	↔ ↓	↔ ↓	↔ ↓	↔ ↓

↑, increase/faster; ↔, no change; ↓, decrease/slower; n.a., not available. Ultrastructure includes thick filament length, thick-to-thin filament ratio, and myofibrillar volume fraction; MHC, myosin heavy chain.

Table 2 | Summary of functional changes in single fiber and myofilament structure with aging, disease, and disuse.

Function	Aging	Heart failure	Cancer	Disuse
MOLECULAR LEVEL				
Cross-bridge kinetics	↓ ♀ > ♂	↓	↓ MHC I ↔ MHC IIA	↓ MHC I of ♀ ↑ MHC IIA of ♂
SINGLE FIBER LEVEL				
Isometric tension	↑ ↔ ↓	↔ ↓	↔ ↓	↔ ↓
Contractile velocity	↑ ↔ ↓	↓ *	↓ *	↔ MHC I ↑ MHC IIA of ♂ ↓ MHC IIA of ♀

*↑, increase/faster; ↔ , no change, ↓, decrease/slower, ♂, male, ♀, female, >, greater than; *predicted from XB kinetic differences.*

chronic muscle disuse in MHC IIA fibers in older men being the exception to the rule. Several studies have found relationships between cellular and molecular level myofilament function and whole muscle function (Frontera et al., 2000; Miller et al., 2013; Toth et al., 2013), underscoring their potential importance. However, the effects of each condition on function at the molecular, cellular and whole muscle levels become less clear when examined across multiple studies within each condition. This is most clearly evident in variation in myofilament function with aging, where data suggest that single fiber tension and velocity increase, remain unchanged, and decrease with age. We posit that such variation is due to the modifying effects of confounding factors, such as the habitual activity level and sex distribution of the populations studied, which have not commonly been accounted for in experimental designs or statistical analyses. While integrated myofilament function has been evaluated in the context of single muscle fiber function, sometimes extending to the cross-bridge level, few studies have interrogated the specific changes in myofilament protein, expression and/or post-translational modification might be accounting for these adaptation. Overall, these findings indicate that a more thorough understanding of the myofilament adaptations to aging, disease, and disuse in both sexes would assist with the development of preventative and rehabilitative interventions to improve muscle function and, in turn, decrease functional disability in older men and women.

ACKNOWLEDGMENTS

This study was supported by grants from the National Institutes of Health T32-HL-007647, K01-AG-031303, R01-HL-077418, and R01-AG-033547.

REFERENCES

Acharyya, S., Ladner, K. J., Nelsen, L. L., Damrauer, J., Reiser, P. J., Swoap, S., et al. (2004). Cancer cachexia is regulated by selective targeting of skeletal muscle gene products. *J. Clin. Invest.* 114, 370–378. doi: 10.1172/JCI20174

Adams, G. R., Caiozzo, V. J., and Baldwin, K. M. (2003). Skeletal muscle unweighting: spaceflight and ground-based models. *J. Appl. Physiol. (1985)* 95, 2185–2201. doi: 10.1152/japplphysiol.00346.2003.

Barreiro, E., De La Puente, B., Busquets, S., Lopez-Soriano, F. J., Gea, J., and Argiles, J. M. (2005). Both oxidative and nitrosative stress are associated with muscle wasting in tumour-bearing rats. *FEBS Lett.* 579, 1646–1652. doi: 10.1016/j.febslet.2005.02.017

Blaauw, B., Canato, M., Agatea, L., Toniolo, L., Mammucari, C., Masiero, E., et al. (2009). Inducible activation of Akt increases skeletal muscle mass and force without satellite cell activation. *FASEB J.* 23, 3896–3905. doi: 10.1096/fj.09-131870

Bottinelli, R. (2001). Functional heterogeneity of mammalian single muscle fibres: do myosin isoforms tell the whole story? *Pflugers Arch.* 443, 6–17. doi: 10.1007/s004240100700

Brenner, B. (1988). Effect of Ca^{2+} on cross-bridge turnover kinetics in skinned single rabbit psoas fibers: implications for regulation of muscle contraction. *Proc. Natl. Acad. Sci. U.S.A.* 85, 3265–3269. doi: 10.1073/pnas.85.9.3265

Brenner, B., Hahn, N., Hanke, E., Matinmehr, F., Scholz, T., Steffen, W., et al. (2012). Mechanical and kinetic properties of beta-cardiac/slow skeletal muscle myosin. *J. Muscle Res. Cell Motil.* 33, 403–417. doi: 10.1007/s10974-012-9315-8

Buck, M., and Chojkier, M. (1996). Muscle wasting and dedifferentiation induced by oxidative stress in a murine model of cachexia is prevented by inhibitors of nitric oxide synthesis and antioxidants. *EMBO J.* 15, 1753–1765.

Callahan, D. M., Bedrin, N. G., Subramanian, M., Berking, J., Ades, P. A., Toth, M. J., et al. (2014a). Age-related structural alterations in human skeletal muscle fibers and mitochondria are sex specific: relationship to single-fiber function. *J. Appl. Physiol. (1985)* 116, 1582–1592. doi: 10.1152/japplphysiol.01362.2013

Callahan, D. M., and Kent-Braun, J. A. (2011). Effect of old age on human skeletal muscle force-velocity and fatigue properties. *J. Appl. Physiol. (1985)* 111, 1345–1352. doi: 10.1152/japplphysiol.00367.2011

Callahan, D. M., Miller, M. S., Sweeney, A. P., Tourville, T. W., Slauterbeck, J. R., Savage, P. D., et al. (2014b). Muscle disuse alters skeletal muscle contractile function at the molecular and cellular levels in older adult humans in a sex-specific manner. *J. Physiol.* doi: 10.1113/jphysiol.2014.279034

Callahan, L. A., She, Z. W., and Nosek, T. M. (2001). Superoxide, hydroxyl radical, and hydrogen peroxide effects on single-diaphragm fiber contractile apparatus. *J. Appl. Physiol. (1985)* 90, 45–54.

Calvani, R., Joseph, A. M., Adhihetty, P. J., Miccheli, A., Bossola, M., Leeuwenburgh, C., et al. (2013). Mitochondrial pathways in sarcopenia of aging and disuse muscle atrophy. *Biol. Chem.* 394, 393–414. doi: 10.1515/hsz-2012-0247

Canepari, M., Rossi, R., Pellegrino, M. A., Orrell, R. W., Cobbold, M., Harridge, S., et al. (2005). Effects of resistance training on myosin function studied by the *in vitro* motility assay in young and older men. *J. Appl. Physiol. (1985)* 98, 2390–2395. doi: 10.1152/japplphysiol.01103.2004

Capitanio, M., Canepari, M., Cacciafesta, P., Lombardi, V., Cicchi, R., Maffei, M., et al. (2006). Two independent mechanical events in the interaction cycle of skeletal muscle myosin with actin. *Proc. Natl. Acad. Sci. U.S.A.* 103, 87–92. doi: 10.1073/pnas.0506830102

Caron, M. A., Debigare, R., Dekhuijzen, P. N., and Maltais, F. (2009). Comparative assessment of the quadriceps and the diaphragm in patients with COPD. *J. Appl. Physiol. (1985)* 107, 952–961. doi: 10.1152/japplphysiol.00194.2009

Cella, D., Davis, K., Breitbart, W., Curt, G., and Fatigue, C. (2001). Cancer-related fatigue: prevalence of proposed diagnostic criteria in a United States sample of cancer survivors. *J. Clin. Oncol.* 19, 3385–3391.

Coirault, C., Guellich, A., Barbry, T., Samuel, J. L., Riou, B., and Lecarpentier, Y. (2007). Oxidative stress of myosin contributes to skeletal muscle dysfunction in rats with chronic heart failure. *Am. J. Physiol. Heart Circ. Physiol.* 292, H1009–H1017. doi: 10.1152/ajpheart.00438.2006

Cosper, P. F., and Leinwand, L. A. (2012). Myosin heavy chain is not selectively decreased in murine cancer cachexia. *Int. J. Cancer* 130, 2722–2727. doi: 10.1002/ijc.26298

D'Antona, G., Lanfranconi, F., Pellegrino, M. A., Brocca, L., Adami, R., Rossi, R., et al. (2006). Skeletal muscle hypertrophy and structure and function of skeletal muscle fibres in male body builders. *J. Physiol.* 570, 611–627. doi: 10.1113/jphysiol.2005.101642

D'Antona, G., Pellegrino, M. A., Adami, R., Rossi, R., Carlizzi, C. N., Canepari, M., et al. (2003). The effect of ageing and immobilization on structure and function of human skeletal muscle fibres. *J. Physiol.* 552, 499–511. doi: 10.1113/jphysiol.2003.046276

D'Antona, G., Pellegrino, M. A., Carlizzi, C. N., and Bottinelli, R. (2007). Deterioration of contractile properties of muscle fibres in elderly subjects is modulated by the level of physical activity. *Eur. J. Appl. Physiol.* 100, 603–611. doi: 10.1007/s00421-007-0402-2

Debigare, R., Cote, C. H., Hould, F. S., Leblanc, P., and Maltais, F. (2003). *In vitro* and *in vivo* contractile properties of the vastus lateralis muscle in males with COPD. *Eur. Respir. J.* 21, 273–278. doi: 10.1183/09031936.03.00036503

Delmonico, M. J., Harris, T. B., Visser, M., Park, S. W., Conroy, M. B., Velasquez-Mieyer, P., et al. (2009). Longitudinal study of muscle strength, quality, and adipose tissue infiltration. *Am. J. Clin. Nutr.* 90, 1579–1585. doi: 10.3945/ajcn.2009.28047

Di Marco, S., Mazroui, R., Dallaire, P., Chittur, S., Tenenbaum, S. A., Radzioch, D., et al. (2005). NF-kappa B-mediated MyoD decay during muscle wasting requires nitric oxide synthase mRNA stabilization, HuR protein, and nitric oxide release. *Mol. Cell. Biol.* 25, 6533–6545. doi: 10.1128/MCB.25.15.6533-6545.2005

Eley, H. L., Skipworth, R. J., Deans, D. A., Fearon, K. C., and Tisdale, M. J. (2008). Increased expression of phosphorylated forms of RNA-dependent protein kinase and eukaryotic initiation factor 2alpha may signal skeletal muscle atrophy in weight-losing cancer patients. *Br. J. Cancer* 98, 443–449. doi: 10.1038/sj.bjc.6604150

Fearon, K. C., Glass, D. J., and Guttridge, D. C. (2012). Cancer cachexia: mediators, signaling, and metabolic pathways. *Cell Metab.* 16, 153–166. doi: 10.1016/j.cmet.2012.06.011

Fermoselle, C., Rabinovich, R., Ausin, P., Puig-Vilanova, E., Coronell, C., Sanchez, F., et al. (2012). Does oxidative stress modulate limb muscle atrophy in severe COPD patients? *Eur. Respir. J.* 40, 851–862. doi: 10.1183/09031936.00137211

Franchi, L. L., Murdoch, A., Brown, W. E., Mayne, C. N., Elliott, L., and Salmons, S. (1990). Subcellular localization of newly incorporated myosin in rabbit fast skeletal muscle undergoing stimulation-induced type transformation. *J. Muscle Res. Cell Motil.* 11, 227–239. doi: 10.1007/BF01843576

Frontera, W. R., Hughes, V. A., Krivickas, L. S., Kim, S. K., Foldvari, M., and Roubenoff, R. (2003). Strength training in older women: early and late changes in whole muscle and single cells. *Muscle Nerve* 28, 601–608. doi: 10.1002/mus.10480

Frontera, W. R., Reid, K. F., Phillips, E. M., Krivickas, L. S., Hughes, V. A., Roubenoff, R., et al. (2008). Muscle fiber size and function in elderly humans: a longitudinal study. *J. Appl. Physiol. (1985)* 105, 637–642. doi: 10.1152/japplphysiol.90332.2008

Frontera, W. R., Suh, D., Krivickas, L. S., Hughes, V. A., Goldstein, R., and Roubenoff, R. (2000). Skeletal muscle fiber quality in older men and women. *Am. J. Physiol. Cell Physiol.* 279, C611–C618.

Gallagher, I. J., Stephens, N. A., Macdonald, A. J., Skipworth, R. J., Husi, H., Greig, C. A., et al. (2012). Suppression of skeletal muscle turnover in cancer cachexia: evidence from the transcriptome in sequential human muscle biopsies. *Clin. Cancer Res.* 18, 2817–2827. doi: 10.1158/1078-0432.CCR-11-2133

Galler, S., Hilber, K., and Gobesberger, A. (1997). Effects of nitric oxide on force-generating proteins of skeletal muscle. *Pflugers Arch.* 434, 242–245. doi: 10.1007/s004240050391

Gea, J. G., Pasto, M., Carmona, M. A., Orozco-Levi, M., Palomeque, J., and Broquetas, J. (2001). Metabolic characteristics of the deltoid muscle in patients with chronic obstructive pulmonary disease. *Eur. Respir. J.* 17, 939–945. doi: 10.1183/09031936.01.17509390

Geiger, P. C., Cody, M. J., Macken, R. L., and Sieck, G. C. (2000). Maximum specific force depends on myosin heavy chain content in rat diaphragm muscle fibers. *J. Appl. Physiol. (1985)* 89, 695–703.

Gelfi, C., Vigano, A., Ripamonti, M., Pontoglio, A., Begum, S., Pellegrino, M. A., et al. (2006). The human muscle proteome in aging. *J. Proteome Res.* 5, 1344–1353. doi: 10.1021/pr050414x

Gosker, H. R., Engelen, M. P., Van Mameren, H., Van Dijk, P. J., Van Der Vusse, G. J., Wouters, E. F., et al. (2002). Muscle fiber type IIX atrophy is involved in the loss of fat-free mass in chronic obstructive pulmonary disease. *Am. J. Clin. Nutr.* 76, 113–119.

Gosker, H. R., Wouters, E. F., Van Der Vusse, G. J., and Schols, A. M. (2000). Skeletal muscle dysfunction in chronic obstructive pulmonary disease and chronic heart failure: underlying mechanisms and therapy perspectives. *Am. J. Clin. Nutr.* 71, 1033–1047.

Gosker, H. R., Zeegers, M. P., Wouters, E. F., and Schols, A. M. (2007). Muscle fibre type shifting in the vastus lateralis of patients with COPD is associated with disease severity: a systematic review and meta-analysis. *Thorax* 62, 944–949. doi: 10.1136/thx.2007.078980

Gouzi, F., Maury, J., Molinari, N., Pomies, P., Mercier, J., Prefaut, C., et al. (2013). Reference values for vastus lateralis fiber size and type in healthy subjects over 40 years old: a systematic review and metaanalysis. *J. Appl. Physiol. (1985)* 115, 346–354. doi: 10.1152/japplphysiol.01352.2012

Guilford, W. H., Dupuis, D. E., Kennedy, G., Wu, J., Patlak, J. B., and Warshaw, D. M. (1997). Smooth muscle and skeletal muscle myosins produce similar unitary forces and displacements in the laser trap. *Biophys. J.* 72, 1006–1021. doi: 10.1016/S0006-3495(97)78753-8

Guralnik, J. M., Ferrucci, L., Simonsick, E. M., Salive, M. E., and Wallace, R. B. (1995). Lower-extremity function in persons over the age of 70 years as a predictor of subsequent disability. *N. Engl. J. Med.* 332, 556–561. doi: 10.1056/NEJM199503023320902

Harber, M. P., Konopka, A. R., Douglass, M. D., Minchev, K., Kaminsky, L. A., Trappe, T. A., et al. (2009). Aerobic exercise training improves whole muscle and single myofiber size and function in older women. *Am. J. Physiol. Regul. Integr. Comp. Physiol.* 297, R1452–R1459. doi: 10.1152/ajpregu.00354.2009

Harridge, S. D., Bottinelli, R., Canepari, M., Pellegrino, M. A., Reggiani, C., Esbjornsson, M., et al. (1996). Whole-muscle and single-fibre contractile properties and myosin heavy chain isoforms in humans. *Pflugers Arch.* 432, 913–920. doi: 10.1007/s004240050215

Harrington, D., Anker, S. D., Chua, T. P., Webb-Peploe, K. M., Ponikowski, P. P., Poole-Wilson, P. A., et al. (1997). Skeletal muscle function and its relation to exercise tolerance in chronic heart failure. *J. Am. Coll. Cardiol.* 30, 1758–1764. doi: 10.1016/S0735-1097(97)00381-1

Heunks, L. M., Cody, M. J., Geiger, P. C., Dekhuijzen, P. N., and Sieck, G. C. (2001). Nitric oxide impairs Ca^{2+} activation and slows cross-bridge cycling kinetics in skeletal muscle. *J. Appl. Physiol. (1985)* 91, 2233–2239.

Hooft, A. M., Maki, E. J., Cox, K. K., and Baker, J. E. (2007). An accelerated state of myosin-based actin motility. *Biochemistry* 46, 3513–3520. doi: 10.1021/bi0614840

Hook, P., Sriramoju, V., and Larsson, L. (2001). Effects of aging on actin sliding speed on myosin from single skeletal muscle cells of mice, rats, and humans. *Am. J. Physiol. Cell Physiol.* 280, C782–C788.

Huxley, A. F. (1957). Muscle structure and theories of contraction. *Prog. Biophys. Biophys. Chem.* 7, 255–318.

Hvid, L., Aagaard, P., Justesen, L., Bayer, M. L., Andersen, J. L., Ortenblad, N., et al. (2010). Effects of aging on muscle mechanical function and muscle fiber morphology during short-term immobilization and subsequent retraining. *J. Appl. Physiol. (1985)* 109, 1628–1634. doi: 10.1152/japplphysiol.00637.2010

Hvid, L. G., Ortenblad, N., Aagaard, P., Kjaer, M., and Suetta, C. (2011). Effects of ageing on single muscle fibre contractile function following short-term immobilisation. *J. Physiol.* 589, 4745–4757. doi: 10.1113/jphysiol.2011.215434

Hvid, L. G., Suetta, C., Aagaard, P., Kjaer, M., Frandsen, U., and Ortenblad, N. (2013). Four days of muscle disuse impairs single fiber contractile function in young and old healthy men. *Exp. Gerontol.* 48, 154–161. doi: 10.1016/j.exger.2012.11.005

Hvid, L. G., Suetta, C., Nielsen, J. H., Jensen, M. M., Frandsen, U., Ortenblad, N., et al. (2014). Aging impairs the recovery in mechanical muscle function following 4 days of disuse. *Exp. Gerontol.* 52, 1–8. doi: 10.1016/j.exger.2014.01.012

Janssen, I., Heymsfield, S. B., and Ross, R. (2002). Low relative skeletal muscle mass (sarcopenia) in older persons is associated with functional impairment and physical disability. *J. Am. Geriatr. Soc.* 50, 889–896. doi: 10.1046/j.1532-5415.2002.50216.x

Jette, A. M., and Branch, L. G. (1981). The Framingham disability study: II. Physical disability among the aging. *Am. J. Public Health* 71, 1211–1216. doi: 10.2105/AJPH.71.11.1211

Jubrias, S. A., Odderson, I. R., Esselman, P. C., and Conley, K. E. (1997). Decline in isokinetic force with age: muscle cross-sectional area and specific force. *Pflugers Arch.* 434, 246–253. doi: 10.1007/s004240050392

Korhonen, M. T., Cristea, A., Alen, M., Hakkinen, K., Sipila, S., Mero, A., et al. (2006). Aging, muscle fiber type, and contractile function in sprint-trained athletes. *J. Appl. Physiol. (1985)* 101, 906–917. doi: 10.1152/japplphysiol.00299.2006

Kortebein, P., Ferrando, A., Lombeida, J., Wolfe, R., and Evans, W. J. (2007). Effect of 10 days of bed rest on skeletal muscle in healthy older adults. *JAMA* 297, 1772–1774. doi: 10.1001/jama.297.16.1772-b

Kortebein, P., Symons, T. B., Ferrando, A., Paddon-Jones, D., Ronsen, O., Protas, E., et al. (2008). Functional impact of 10 days of bed rest in healthy older adults. *J. Gerontol. A Biol. Sci. Med. Sci.* 63, 1076–1081. doi: 10.1093/gerona/63.10.1076

Krivickas, L. S., Dorer, D. J., Ochala, J., and Frontera, W. R. (2011). Relationship between force and size in human single muscle fibres. *Exp. Physiol.* 96, 539–547. doi: 10.1113/expphysiol.2010.055269

Krivickas, L. S., Fielding, R. A., Murray, A., Callahan, D., Johansson, A., Dorer, D. J., et al. (2006). Sex differences in single muscle fiber power in older adults. *Med. Sci. Sports Exerc.* 38, 57–63. doi: 10.1249/01.mss.0000180357.58329.b1

Krivickas, L. S., Suh, D., Wilkins, J., Hughes, V. A., Roubenoff, R., and Frontera, W. R. (2001). Age- and gender-related differences in maximum shortening velocity of skeletal muscle fibers. *Am. J. Phys. Med. Rehabil.* 80, 447–455; quiz: 456–447. doi: 10.1097/00002060-200106000-00012

Lanza, I. R., Towse, T. F., Caldwell, G. E., Wigmore, D. M., and Kent-Braun, J. A. (2003). Effects of age on human muscle torque, velocity, and power in two muscle groups. *J. Appl. Physiol. (1985)* 95, 2361–2369. doi: 10.1152/japplphysiol.00724.2002

Larsson, L., Li, X., and Frontera, W. R. (1997). Effects of aging on shortening velocity and myosin isoform composition in single human skeletal muscle cells. *Am. J. Physiol.* 272, C638–C649.

Levine, S., Bashir, M. H., Clanton, T. L., Powers, S. K., and Singhal, S. (2013). COPD elicits remodeling of the diaphragm and vastus lateralis muscles in humans. *J. Appl. Physiol. (1985)* 114, 1235–1245. doi: 10.1152/japplphysiol.01121.2012

Levine, S., Nguyen, T., Kaiser, L. R., Rubinstein, N. A., Maislin, G., Gregory, C., et al. (2003). Human diaphragm remodeling associated with chronic obstructive pulmonary disease: clinical implications. *Am. J. Respir. Crit. Care Med.* 168, 706–713. doi: 10.1164/rccm.200209-1070OC

Lexell, J. (1995). Human aging, muscle mass, and fiber type composition. *J. Gerontol. A Biol. Sci. Med. Sci.* 50 Spec No: 11–16.

Lexell, J., and Downham, D. Y. (1991). The occurrence of fibre-type grouping in healthy human muscle: a quantitative study of cross-sections of whole vastus lateralis from men between 15 and 83 years. *Acta Neuropathol.* 81, 377–381. doi: 10.1007/BF00293457

Lexell, J., Taylor, C. C., and Sjostrom, M. (1988). What is the cause of the ageing atrophy? Total number, size and proportion of different fiber types studied in whole vastus lateralis muscle from 15- to 83-year-old men. *J. Neurol. Sci.* 84, 275–294. doi: 10.1016/0022-510X(88)90132-3

Linari, M., Bottinelli, R., Pellegrino, M. A., Reconditi, M., Reggiani, C., and Lombardi, V. (2004). The mechanism of the force response to stretch in human skinned muscle fibres with different myosin isoforms. *J. Physiol.* 554, 335–352. doi: 10.1113/jphysiol.2003.051748

Lindle, R. S., Metter, E. J., Lynch, N. A., Fleg, J. L., Fozard, J. L., Tobin, J., et al. (1997). Age and gender comparisons of muscle strength in 654 women and men aged 20-93 yr. *J. Appl. Physiol. (1985)* 83, 1581–1587.

Lynch, N. A., Metter, E. J., Lindle, R. S., Fozard, J. L., Tobin, J. D., Roy, T. A., et al. (1999). Muscle quality. I. Age-associated differences between arm and leg muscle groups. *J. Appl. Physiol. (1985)* 86, 188–194.

Maltais, F., Decramer, M., Casaburi, R., Barreiro, E., Burelle, Y., Debigare, R., et al. (2014). An official American Thoracic Society/European Respiratory Society statement: update on limb muscle dysfunction in chronic obstructive pulmonary disease. *Am. J. Respir. Crit. Care Med.* 189, e15–e62. doi: 10.1164/rccm.201402-0373ST

Mancini, D. M., Coyle, E., Coggan, A., Beltz, J., Ferraro, N., Montain, S., et al. (1989). Contribution of intrinsic skeletal muscle changes to 31P NMR skeletal muscle metabolic abnormalities in patients with chronic heart failure. *Circulation* 80, 1338–1346. doi: 10.1161/01.CIR.80.5.1338

Marin-Corral, J., Fontes, C. C., Pascual-Guardia, S., Sanchez, F., Olivan, M., Argiles, J. M., et al. (2010). Redox balance and carbonylated proteins in limb and heart muscles of cachectic rats. *Antioxid. Redox Signal.* 12, 365–380. doi: 10.1089/ars.2009.2818

Massie, B. M., Simonini, A., Sahgal, P., Wells, L., and Dudley, G. A. (1996). Relation of systemic and local muscle exercise capacity to skeletal muscle characteristics in men with congestive heart failure. *J. Am. Coll. Cardiol.* 27, 140–145. doi: 10.1016/0735-1097(95)00416-5

Mettauer, B., Zoll, J., Sanchez, H., Lampert, E., Ribera, F., Veksler, V., et al. (2001). Oxidative capacity of skeletal muscle in heart failure patients versus sedentary or active control subjects. *J. Am. Coll. Cardiol.* 38, 947–954. doi: 10.1016/S0735-1097(01)01460-7

Miller, M. S., Bedrin, N. G., Callahan, D. M., Previs, M. J., Jennings, M. E. 2nd., Ades, P. A., et al. (2013). Age-related slowing of myosin actin cross-bridge kinetics is sex specific and predicts decrements in whole skeletal muscle performance in humans. *J. Appl. Physiol. (1985)* 115, 1004–1014. doi: 10.1152/japplphysiol.00563.2013

Miller, M. S., and Toth, M. J. (2013). Myofilament protein alterations promote physical disability in aging and disease. *Exerc. Sport Sci. Rev.* 41, 93–99. doi: 10.1097/JES.0b013e31828bbcd8

Miller, M. S., Vanburen, P., Lewinter, M. M., Braddock, J. M., Ades, P. A., Maughan, D. W., et al. (2010). Chronic heart failure decreases cross-bridge kinetics in single skeletal muscle fibres from humans. *J. Physiol.* 588, 4039–4053. doi: 10.1113/jphysiol.2010.191957

Miller, M. S., Vanburen, P., Lewinter, M. M., Lecker, S. H., Selby, D. E., Palmer, B. M., et al. (2009). Mechanisms underlying skeletal muscle weakness in human heart failure: alterations in single fiber myosin protein content and function. *Circ. Heart Fail.* 2, 700–706. doi: 10.1161/CIRCHEARTFAILURE.109.876433

Morse, C. I., Thom, J. M., Reeves, N. D., Birch, K. M., and Narici, M. V. (2005). *In vivo* physiological cross-sectional area and specific force are reduced in the gastrocnemius of elderly men. *J. Appl. Physiol. (1985)* 99, 1050–1055. doi: 10.1152/japplphysiol.01186.2004

Narici, M. V., and De Boer, M. D. (2011). Disuse of the musculo-skeletal system in space and on earth. *Eur. J. Appl. Physiol.* 111, 403–420. doi: 10.1007/s00421-010-1556-x

Ochala, J., Dorer, D. J., Frontera, W. R., and Krivickas, L. S. (2006). Single skeletal muscle fiber behavior after a quick stretch in young and older men: a possible explanation of the relative preservation of eccentric force in old age. *Pflugers Arch.* 452, 464–470. doi: 10.1007/s00424-006-0065-6

Ochala, J., Frontera, W. R., Dorer, D. J., Van Hoecke, J., and Krivickas, L. S. (2007). Single skeletal muscle fiber elastic and contractile characteristics in young and older men. *J. Gerontol. A Biol. Sci. Med. Sci.* 62, 375–381. doi: 10.1093/gerona/62.4.375

Okada, Y., Toth, M. J., and Vanburen, P. (2008). Skeletal muscle contractile protein function is preserved in human heart failure. *J. Appl. Physiol. (1985)* 104, 952–957. doi: 10.1152/japplphysiol.01072.2007

Ottenheijm, C. A., Heunks, L. M., Sieck, G. C., Zhan, W. Z., Jansen, S. M., Degens, H., et al. (2005). Diaphragm dysfunction in chronic obstructive pulmonary disease. *Am. J. Respir. Crit. Care Med.* 172, 200–205. doi: 10.1164/rccm.200502-262OC

Palmer, B. M., Suzuki, T., Wang, Y., Barnes, W. D., Miller, M. S., and Maughan, D. W. (2007). Two-state model of acto-myosin attachment-detachment predicts C-process of sinusoidal analysis. *Biophys. J.* 93, 760–769. doi: 10.1529/biophysj.106.101626

Palmiter, K. A., Tyska, M. J., Dupuis, D. E., Alpert, N. R., and Warshaw, D. M. (1999). Kinetic differences at the single molecule level account for the functional diversity of rabbit cardiac myosin isoforms. *J. Physiol.* 519 pt 3, 669–678. doi: 10.1111/j.1469-7793.1999.0669n.x

Pansarasa, O., Rinaldi, C., Parente, V., Miotti, D., Capodaglio, P., and Bottinelli, R. (2009). Resistance training of long duration modulates force and unloaded shortening velocity of single muscle fibres of young women. *J. Electromyogr. Kinesiol.* 19, e290–e300. doi: 10.1016/j.jelekin.2008.07.007

Parente, V., D'Antona, G., Adami, R., Miotti, D., Capodaglio, P., De Vito, G., et al. (2008). Long-term resistance training improves force and unloaded shortening velocity of single muscle fibres of elderly women. *Eur. J. Appl. Physiol.* 104, 885–893. doi: 10.1007/s00421-008-0845-0

Pellegrino, M. A., Canepari, M., Rossi, R., D'Antona, G., Reggiani, C., and Bottinelli, R. (2003). Orthologous myosin isoforms and scaling of shortening velocity with body size in mouse, rat, rabbit and human muscles. *J. Physiol.* 546, 677–689. doi: 10.1113/jphysiol.2002.027375

Perkins, W. J., Han, Y. S., and Sieck, G. C. (1997). Skeletal muscle force and actomyosin ATPase activity reduced by nitric oxide donor. *J. Appl. Physiol. (1985)* 83, 1326–1332.

Piazzesi, G., Reconditi, M., Linari, M., Lucii, L., Bianco, P., Brunello, E., et al. (2007). Skeletal muscle performance determined by modulation of number of myosin motors rather than motor force or stroke size. *Cell* 131, 784–795. doi: 10.1016/j.cell.2007.09.045

Pinsky, J. L., Jette, A. M., Branch, L. G., Kannel, W. B., and Feinleib, M. (1990). The Framingham disability study: relationship of various coronary heart disease manifestations to disability in older persons living in the community. *Am. J. Public Health* 80, 1363–1367. doi: 10.2105/AJPH.80.11.1363

Pittman, J. G., and Cohen, P. (1964). The pathogenesis of cardiac cachexia. *N. Engl. J. Med.* 271, 403–409. doi: 10.1056/NEJM196408202710807

Raj, I. S., Bird, S. R., and Shield, A. J. (2010). Aging and the force-velocity relationship of muscles. *Exp. Gerontol.* 45, 81–90. doi: 10.1016/j.exger.2009.10.013

Ramamoorthy, S., Donohue, M., and Buck, M. (2009). Decreased Jun-D and myogenin expression in muscle wasting of human cachexia. *Am. J. Physiol. Endocrinol. Metab.* 297, E392–E401. doi: 10.1152/ajpendo.90529.2008

Rehn, T. A., Munkvik, M., Lunde, P. K., Sjaastad, I., and Sejersted, O. M. (2012). Intrinsic skeletal muscle alterations in chronic heart failure patients: a disease-specific myopathy or a result of deconditioning? *Heart Fail. Rev.* 17, 421–436. doi: 10.1007/s10741-011-9289-4

Reid, K. F., Doros, G., Clark, D. J., Patten, C., Carabello, R. J., Cloutier, G. J., et al. (2012). Muscle power failure in mobility-limited older adults: preserved single fiber function despite lower whole muscle size, quality and rate of neuromuscular activation. *Eur. J. Appl. Physiol.* 112, 2289–2301. doi: 10.1007/s00421-011-2200-0

Reid, K. F., and Fielding, R. A. (2012). Skeletal muscle power: a critical determinant of physical functioning in older adults. *Exerc. Sport Sci. Rev.* 40, 4–12. doi: 10.1097/JES.0b013e31823b5f13

Reid, K. F., Pasha, E., Doros, G., Clark, D. J., Patten, C., Phillips, E. M., et al. (2014). Longitudinal decline of lower extremity muscle power in healthy and mobility-limited older adults: influence of muscle mass, strength, composition, neuromuscular activation and single fiber contractile properties. *Eur. J. Appl. Physiol.* 114, 29–39. doi: 10.1007/s00421-013-2728-2

Reid, M. B., and Moylan, J. S. (2011). Beyond atrophy: redox mechanisms of muscle dysfunction in chronic inflammatory disease. *J. Physiol.* 589, 2171–2179. doi: 10.1113/jphysiol.2010.203356

Reiken, S., Lacampagne, A., Zhou, H., Kherani, A., Lehnart, S. E., Ward, C., et al. (2003). PKA phosphorylation activates the calcium release channel (ryanodine receptor) in skeletal muscle: defective regulation in heart failure. *J. Cell Biol.* 160, 919–928. doi: 10.1083/jcb.200211012

Reiser, P. J., Kasper, C. E., and Moss, R. L. (1987). Myosin subunits and contractile properties of single fibers from hypokinetic rat muscles. *J. Appl. Physiol. (1985)* 63, 2293–2300.

Remels, A. H., Gosker, H. R., Langen, R. C., and Schols, A. M. (2013). The mechanisms of cachexia underlying muscle dysfunction in COPD. *J. Appl. Physiol. (1985)* 114, 1253–1262. doi: 10.1152/japplphysiol.00790.2012

Roth, S. M., Ferrell, R. E., Peters, D. G., Metter, E. J., Hurley, B. F., and Rogers, M. A. (2002). Influence of age, sex, and strength training on human muscle gene expression determined by microarray. *Physiol. Genomics* 10, 181–190. doi: 10.1152/physiolgenomics.00028.2002

Russ, D. W., Gregg-Cornell, K., Conaway, M. J., and Clark, B. C. (2012). Evolving concepts on the age-related changes in "muscle quality." *J. Cachexia Sarcopenia Muscle* 3, 95–109. doi: 10.1007/s13539-011-0054-2

Ryushi, T., and Fukunaga, T. (1986). Influence of subtypes of fast-twitch fibers on isokinetic strength in untrained men. *Int. J. Sports Med.* 7, 250–253. doi: 10.1055/s-2008-1025769

Satta, A., Migliori, G. B., Spanevello, A., Neri, M., Bottinelli, R., Canepari, M., et al. (1997). Fibre types in skeletal muscles of chronic obstructive pulmonary disease patients related to respiratory function and exercise tolerance. *Eur. Respir. J.* 10, 2853–2860. doi: 10.1183/09031936.97.10122853

Schaufelberger, M., Eriksson, B. O., Grimby, G., Held, P., and Swedberg, K. (1995). Skeletal muscle fiber composition and capillarization in patients with chronic heart failure: relation to exercise capacity and central hemodynamics. *J. Card. Fail.* 1, 267–272. doi: 10.1016/1071-9164(95)90001-2

Schaufelberger, M., Eriksson, B. O., Grimby, G., Held, P., and Swedberg, K. (1997). Skeletal muscle alterations in patients with chronic heart failure. *Eur. Heart J.* 18, 971–980. doi: 10.1093/oxfordjournals.eurheartj.a015386

Stephens, N. A., Gray, C., Macdonald, A. J., Tan, B. H., Gallagher, I. J., Skipworth, R. J., et al. (2012). Sexual dimorphism modulates the impact of cancer cachexia on lower limb muscle mass and function. *Clin. Nutr.* 31, 499–505. doi: 10.1016/j.clnu.2011.12.008

Stubbings, A. K., Moore, A. J., Dusmet, M., Goldstraw, P., West, T. G., Polkey, M. I., et al. (2008). Physiological properties of human diaphragm muscle fibres and the effect of chronic obstructive pulmonary disease. *J. Physiol.* 586, 2637–2650. doi: 10.1113/jphysiol.2007.149799

Suetta, C., Aagaard, P., Magnusson, S. P., Andersen, L. L., Sipila, S., Rosted, A., et al. (2007). Muscle size, neuromuscular activation, and rapid force characteristics in elderly men and women: effects of unilateral long-term disuse due to hip-osteoarthritis. *J. Appl. Physiol. (1985)* 102, 942–948. doi: 10.1152/japplphysiol.00067.2006

Suetta, C., Frandsen, U., Jensen, L., Jensen, M. M., Jespersen, J. G., Hvid, L. G., et al. (2012). Aging affects the transcriptional regulation of human skeletal muscle disuse atrophy. *PLoS ONE* 7:e51238. doi: 10.1371/journal.pone.0051238

Sugiura, S., Kobayakawa, N., Fujita, H., Yamashita, H., Momomura, S., Chaen, S., et al. (1998). Comparison of unitary displacements and forces between 2 cardiac myosin isoforms by the optical trap technique: molecular basis for cardiac adaptation. *Circ. Res.* 82, 1029–1034. doi: 10.1161/01.RES.82.10.1029

Sullivan, M. J., Duscha, B. D., Klitgaard, H., Kraus, W. E., Cobb, F. R., and Saltin, B. (1997). Altered expression of myosin heavy chain in human skeletal muscle in chronic heart failure. *Med. Sci. Sports Exerc.* 29, 860–866. doi: 10.1097/00005768-199707000-00004

Sullivan, M. J., Green, H. J., and Cobb, F. R. (1990). Skeletal muscle biochemistry and histology in ambulatory patients with long-term heart failure. *Circulation* 81, 518–527. doi: 10.1161/01.CIR.81.2.518

Szentesi, P., Bekedam, M. A., Van Beek-Harmsen, B. J., Van Der Laarse, W. J., Zaremba, R., Boonstra, A., et al. (2005). Depression of force production and ATPase activity in different types of human skeletal muscle fibers from patients with chronic heart failure. *J. Appl. Physiol. (1985)* 99, 2189–2195. doi: 10.1152/japplphysiol.00542.2005

Tanner, B. C., McNabb, M., Palmer, B. M., Toth, M. J., and Miller, M. S. (2014). Random myosin loss along thick-filaments increases myosin attachment time and the proportion of bound myosin heads to mitigate force decline in skeletal muscle. *Arch. Biochem. Biophys.* 552–553, 117–127. doi: 10.1016/j.abb.2014.01.015

Taskin, S., Stumpf, V. I., Bachmann, J., Weber, C., Martignoni, M. E., and Friedrich, O. (2014). Motor protein function in skeletal abdominal muscle of cachectic cancer patients. *J. Cell. Mol. Med.* 18, 69–79. doi: 10.1111/jcmm.12165

Thedinga, E., Karim, N., Kraft, T., and Brenner, B. (1999). A single-fiber *in vitro* motility assay. *in vitro* sliding velocity of F-actin vs. unloaded shortening velocity in skinned muscle fibers. *J. Muscle Res. Cell Motil.* 20, 785–796. doi: 10.1023/A:1005658825375

Thorstensson, A., Larsson, L., Tesch, P., and Karlsson, J. (1977). Muscle strength and fiber composition in athletes and sedentary men. *Med. Sci. Sports* 9, 26–30.

Tikunov, B. A., Mancini, D., and Levine, S. (1996). Changes in myofibrillar protein composition of human diaphragm elicited by congestive heart failure. *J. Mol. Cell. Cardiol.* 28, 2537–2541. doi: 10.1006/jmcc.1996.0245

Toth, M. J., Gottlieb, S. S., Goran, M. I., Fisher, M. L., and Poehlman, E. T. (1997). Daily energy expenditure in free-living heart failure patients. *Am. J. Physiol.* 272, E469–E475.

Toth, M. J., Matthews, D. E., Ades, P. A., Tischler, M. D., Vanburen, P., Previs, M., et al. (2005). Skeletal muscle myofibrillar protein metabolism in heart failure: relationship to immune activation and functional capacity. *Am. J. Physiol. Endocrinol. Metab.* 288, E685–E692. doi: 10.1152/ajpendo.00444.2004

Toth, M. J., Miller, M. S., Callahan, D. M., Sweeny, A. P., Nunez, I., Grunberg, S. M., et al. (2013). Molecular mechanisms underlying skeletal muscle weakness in human cancer: reduced myosin-actin cross-bridge formation and kinetics. *J. Appl. Physiol. (1985)* 114, 858–868. doi: 10.1152/japplphysiol.01474.2012

Toth, M. J., Miller, M. S., Vanburen, P., Bedrin, N. G., Lewinter, M. M., Ades, P. A., et al. (2012). Resistance training alters skeletal muscle structure and function in human heart failure: effects at the tissue, cellular and molecular levels. *J. Physiol.* 590, 1243–1259. doi: 10.1113/jphysiol.2011.219659

Toth, M. J., Shaw, A. O., Miller, M. S., Vanburen, P., Lewinter, M. M., Maughan, D. W., et al. (2010). Reduced knee extensor function in heart failure is not explained by inactivity. *Int. J. Cardiol.* 143, 276–282. doi: 10.1016/j.ijcard.2009.02.040

Trappe, S., Gallagher, P., Harber, M., Carrithers, J., Fluckey, J., and Trappe, T. (2003). Single muscle fibre contractile properties in young and old men and women. *J. Physiol.* 552, 47–58. doi: 10.1113/jphysiol.2003.044966

Trappe, S., Godard, M., Gallagher, P., Carroll, C., Rowden, G., and Porter, D. (2001). Resistance training improves single muscle fiber contractile function in older women. *Am. J. Physiol. Cell Physiol.* 281, C398–C406.

Trappe, S., Williamson, D., Godard, M., Porter, D., Rowden, G., and Costill, D. (2000). Effect of resistance training on single muscle fiber contractile function in older men. *J. Appl. Physiol. (1985)* 89, 143–152.

Van Den Borst, B., Koster, A., Yu, B., Gosker, H. R., Meibohm, B., Bauer, D. C., et al. (2011). Is age-related decline in lean mass and physical function accelerated by obstructive lung disease or smoking? *Thorax* 66, 961–969. doi: 10.1136/thoraxjnl-2011-200010

Van Hees, H. W., Van Der Heijden, H. F., Ottenheijm, C. A., Heunks, L. M., Pigmans, C. J., Verheugt, F. W., et al. (2007). Diaphragm single-fiber weakness and loss of myosin in congestive heart failure rats. *Am. J. Physiol. Heart Circ. Physiol.* 293, H819–H828. doi: 10.1152/ajpheart.00085.2007

Vescovo, G., Dalla Libera, L., Serafini, F., Leprotti, C., Facchin, L., Volterrani, M., et al. (1998). Improved exercise tolerance after losartan and enalapril in heart failure: correlation with changes in skeletal muscle myosin heavy chain composition. *Circulation* 98, 1742–1749. doi: 10.1161/01.CIR.98.17.1742

Vescovo, G., Serafini, F., Facchin, L., Tenderini, P., Carraro, U., Dalla Libera, L., et al. (1996). Specific changes in skeletal muscle myosin heavy chain composition in cardiac failure: differences compared with disuse atrophy as assessed on microbiopsies by high resolution electrophoresis. *Heart* 76, 337–343. doi: 10.1136/hrt.76.4.337

Walcott, S., Warshaw, D. M., and Debold, E. P. (2012). Mechanical coupling between myosin molecules causes differences between ensemble and single-molecule measurements. *Biophys. J.* 103, 501–510. doi: 10.1016/j.bpj.2012.06.031

Wall, B. T., Dirks, M. L., Snijders, T., Senden, J. M., Dolmans, J., and Van Loon, L. J. (2014). Substantial skeletal muscle loss occurs during only 5 days of disuse. *Acta Physiol. (Oxf.)* 210, 600–611. doi: 10.1111/apha.12190

Wang, Y., Tanner, B. C., Lombardo, A. T., Tremble, S. M., Maughan, D. W., Vanburen, P., et al. (2013). Cardiac myosin isoforms exhibit differential rates of MgADP release and MgATP binding detected by myocardial viscoelasticity. *J. Mol. Cell. Cardiol.* 54, 1–8. doi: 10.1016/j.yjmcc.2012.10.010

Watz, H., Pitta, F., Rochester, C., Garcia-Aymerich, J., Zuwallack, R., Troosters, T., et al. (in press). An official ERS statement on physical activity in chronic obstructive pulmonary disease. *Eur. Respir. J.*

Weber, M. A., Krakowski-Roosen, H., Schroder, L., Kinscherf, R., Krix, M., Kopp-Schneider, A., et al. (2009). Morphology, metabolism, microcirculation, and strength of skeletal muscles in cancer-related cachexia. *Acta Oncol.* 48, 116–124. doi: 10.1080/02841860802130001

Wenderoth, M. P., and Eisenberg, B. R. (1987). Incorporation of nascent myosin heavy chains into thick filaments of cardiac myocytes in thyroid-treated rabbits. *J. Cell Biol.* 105, 2771–2780. doi: 10.1083/jcb.105.6.2771

Whittom, F., Jobin, J., Simard, P. M., Leblanc, P., Simard, C., Bernard, S., et al. (1998). Histochemical and morphological characteristics of the vastus lateralis muscle in patients with chronic obstructive pulmonary disease. *Med. Sci. Sports Exerc.* 30, 1467–1474. doi: 10.1097/00005768-199810000-00001

Widrick, J. J., Knuth, S. T., Norenberg, K. M., Romatowski, J. G., Bain, J. L., Riley, D. A., et al. (1999). Effect of a 17 day spaceflight on contractile properties of human soleus muscle fibres. *J. Physiol.* 516(pt 3), 915–930. doi: 10.1111/j.1469-7793.1999.0915u.x

Wilson, G. J., Dos Remedios, C. G., Stephenson, D. G., and Williams, D. A. (1991). Effects of sulphydryl modification on skinned rat skeletal muscle fibres using 5,5′-dithiobis(2-nitrobenzoic acid). *J. Physiol.* 437, 409–430.

Yu, F., Hedstrom, M., Cristea, A., Dalen, N., and Larsson, L. (2007). Effects of ageing and gender on contractile properties in human skeletal muscle and single fibres. *Acta Physiol. (Oxf.)* 190, 229–241. doi: 10.1111/j.1748-1716.2007.01699.x

Zizola, C., and Schulze, P. C. (2013). Metabolic and structural impairment of skeletal muscle in heart failure. *Heart Fail. Rev.* 18, 623–630. doi: 10.1007/s10741-012-9353-8

Conflict of Interest Statement: The authors declare that the research was conducted in the absence of any commercial or financial relationships that could be construed as a potential conflict of interest.

Received: 23 July 2014; accepted: 07 September 2014; published online: 26 September 2014.

*Citation: Miller MS, Callahan DM and Toth MJ (2014) Skeletal muscle myofilament adaptations to aging, disease, and disuse and their effects on whole muscle performance in older adult humans. Front. Physiol. **5**:369. doi: 10.3389/fphys.2014.00369*

This article was submitted to Striated Muscle Physiology, a section of the journal Frontiers in Physiology.

Copyright © 2014 Miller, Callahan and Toth. This is an open-access article distributed under the terms of the Creative Commons Attribution License (CC BY). The use, distribution or reproduction in other forums is permitted, provided the original author(s) or licensor are credited and that the original publication in this journal is cited, in accordance with accepted academic practice. No use, distribution or reproduction is permitted which does not comply with these terms.

frontiers in PHYSIOLOGY

REVIEW ARTICLE
published: 14 October 2014
doi: 10.3389/fphys.2014.00393

Altered cross-bridge properties in skeletal muscle dystrophies

Aziz Guellich[1,2†], Elisa Negroni[3,4,5,6†], Valérie Decostre[6], Alexandre Demoule[3,4,5,6,7] and Catherine Coirault[3,4,5,6*]

[1] Service de Cardiologie, Hôpital Henri Mondor, University Paris-Est Créteil, Créteil, France
[2] Equipe 8, Institut National de la Santé et de la Recherche Médicale, Créteil, France
[3] UMRS 974, Institut National de la Santé et de la Recherche Médicale, Paris, France
[4] UM 76, Université Pierre et Marie Curie, Sorbonne Universités, Paris, France
[5] UMR 7215, Centre National de la Recherche Scientifique, Paris, France
[6] Institut de Myologie, Paris, France
[7] Assistance Publique-Hopitaux de Paris, Service de Pneumologie et Reanimation Medicale, Paris, France

Edited by:
Julien Ochala, King's College London, UK

Reviewed by:
Ranganath Mamidi, Case Western Reserve University, USA
Massimo Reconditi, University of Florence, Italy

***Correspondence:**
Catherine Coirault, Institut National de la Santé et de la Recherche Médicale U974, Bâtiment Babinski, 47 Bd de l'Hôpital, 75013 Paris, France
e-mail: catherine.coirault@inserm.fr

† Co-first authors.

Force and motion generated by skeletal muscle ultimately depends on the cyclical interaction of actin with myosin. This mechanical process is regulated by intracellular Ca^{2+} through the thin filament-associated regulatory proteins i.e.; troponins and tropomyosin. Muscular dystrophies are a group of heterogeneous genetic affections characterized by progressive degeneration and weakness of the skeletal muscle as a consequence of loss of muscle tissue which directly reduces the number of potential myosin cross-bridges involved in force production. Mutations in genes responsible for skeletal muscle dystrophies (MDs) have been shown to modify the function of contractile proteins and cross-bridge interactions. Altered gene expression or RNA splicing or post-translational modifications of contractile proteins such as those related to oxidative stress, may affect cross-bridge function by modifying key proteins of the excitation-contraction coupling. Micro-architectural change in myofilament is another mechanism of altered cross-bridge performance. In this review, we provide an overview about changes in cross-bridge performance in skeletal MDs and discuss their ultimate impacts on striated muscle function.

Keywords: myosin, cross-bridge kinetics, skeletal muscle, muscle dystrophy, myopathies

INTRODUCTION

Muscular dystrophies (MDs) are a group of more than 30 clinical and molecular heterogeneous genetic disorders that cause progressive degeneration of the skeletal muscle fibers. They are characterized by severe muscle weakness that generally affects limb, axial, and/or facial muscles to a variable extent. The age of onset, severity and rate of progression greatly vary in the different forms of MD. The primary cause of various forms of MDs is an individual mutation in genes encoding a wide variety of proteins, including extracellular matrix (ECM) proteins, transmembrane, and membrane-associated proteins, cytoplasmic proteases and nuclear proteins. Detailed classification and list of causative genes in MD have been recently reviewed (Cohn and Campbell, 2000; Flanigan, 2012; Kaplan and Hamroun, 2012; Mercuri and Muntoni, 2013). Although still incompletely understood, considerable progress has been now made to reveal the pathophysiological mechanisms in MDs. It has been shown that most MDs share common pathologic features, such as altered Ca^{2+} homeostasis, infiltration of muscle tissue by inflammatory immune cells, accretion of proinflammatory and profibrotic cytokines, activation of proteolytic enzymes, metabolic/mitochondrial alterations, intracellular accumulation of reactive oxygen species (ROS) production, and/or defective autophagy, which can contribute to muscle wasting. At the earliest stages of the disease, reduced myofibrillar protein content can occur in apparent uninjured fibers, secondary to an imbalance between protein synthesis and proteolysis (McKeran et al., 1977; Warnes et al., 1981). Then, successive rounds of degeneration and regeneration lead to fibrosis and fatty replacement of muscle tissue and in turn reduce the number of potential cross-bridges (CBs) generating force (**Figure 1**). In addition, functional changes in the CB properties may contribute to muscle weakness in distinct types of muscle disease. It is well-established that shift in the relative myosin isoform expression is associated with modifications of the kinetics of actomyosin interactions (Bar and Pette, 1988; Schiaffino et al., 1989; Schiaffino and Reggiani, 1996). However, there are also increasing evidences that CB properties can change with no change in myosin isoform content (Coirault et al., 2002; Canepari et al., 2009), suggesting that post-translational modifications of contractile proteins have significant role in muscle

Abbreviations: ADP, adenosine 5′-diphosphate; ATP, adenosine 5′-triphosphate; CB, cross-bridge; DMD, Duchenne muscular dystrophy; ECM, extracellular matrix; FSHD, fascioscapulohumeral muscular dystrophy; MD, muscular dystrophy; MsrA and MrB, methionine sulfoxyde reductase A and B; MyHC, myosin heavy chain; nNOS, neuronal NO synthase; NO, nitric oxide; Pi, inorganic phosphate; ROS, reactive oxygen species; Tm, tropomyosin.

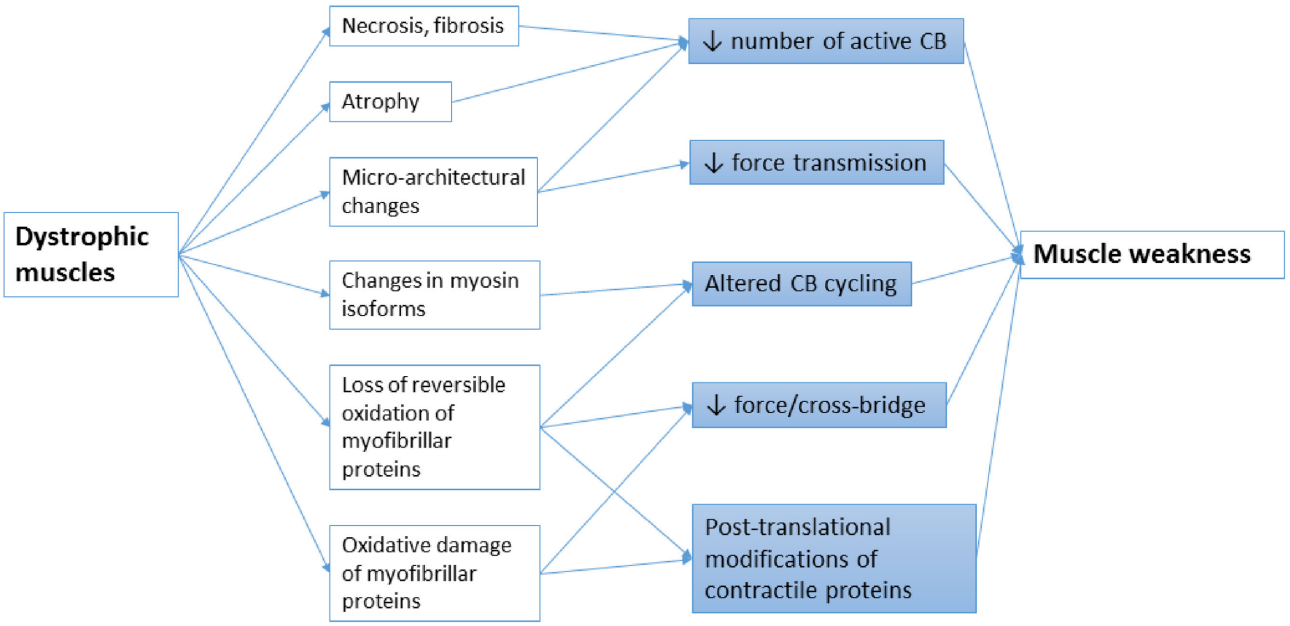

FIGURE 1 | Schematic representation of the main mechanisms leading to muscle weakness in MDs. Altered CB cycle in muscular dystrophy can arise from multiples causes including progressive loss of muscle tissue due to necrosis, fibrosis, atrophy, or oxidative damage, micro-architectural alterations in myofilaments, altered redox regulation or pathological changes in contractile protein isoforms. These abnormalities in turn directly reduce the number, the force, the kinetics of active CBs or the transmission of force produced by the CBs.

weakness (**Figure 1**). The present review focuses on the changes in the function of contractile proteins and in CB performance that may occur in the context of skeletal muscle dystrophies (MDs) and their contribution to the pathophysiological mechanisms of these diseases.

CYCLICAL INTERACTIONS OF ACTIN WITH MYOSIN

Contractile force of striated muscle is produced within the half-sarcomere—the functional contractile unit—by the cyclical interactions of actin filament with myosin molecule, the muscle molecular motor. These cyclical interactions are controlled by membrane-located mechanisms that trigger intracellular raise of $Ca^{2+}$and mechanisms inside the sarcomere itself. In skeletal muscle, sarcomeric mechanisms mainly involve the Ca^{2+}-controlled conformational change of the regulatory proteins troponins and tropomyosin (Tm), the functional properties of myosin, and strong cooperative interaction between neighboring troponin-Tm unit along the actin filament (Gordon et al., 2000).

In resting muscle, intracellular Ca^{2+} concentration ($[Ca^{2+}]_i$) is low and the C-terminal domain of troponin I immobilizes the Tm in a position that prevents the binding of myosin to actin (Galinska-Rakoczy et al., 2008). Upon membrane depolarization, Ca^{2+} is released from the sarcoplasmic reticulum and binds to troponin C, initiating azimuthal movement of Tm around the actin-containing thin filament. This in turn exposes the sites on actin on which the myosin heads can attach (Kress et al., 1986; Geeves et al., 2005). In the conventional view, myosin binding is solely determined by the Ca^{2+} transient causing structural changes in the thin filament. However, numerous studies have reported Ca^{2+}-induced structural change in the myosin-containing thick filaments before myosin binding to the thin filament (Huxley et al., 1982; Lowy and Poulsen, 1990; Yagi, 2003; Reconditi et al., 2011). This has led to the proposal of a modified model of muscle activation in which fast coordinated changes in the structures of both thick and thin filaments follow concomitantly upon the rise in intracellular free Ca^{2+} concentration (Reconditi et al., 2014).

Myosin head binding to actin occurs first in a low binding, pre-force-generating state (**Figure 2**, step a). At this state, the CB has already hydrolyzed the adenosine 5′-triphosphate (ATP), but the products adenosine 5′-diphosphate (ADP) and inorganic phosphate (Pi) are still bound to the myosin head (Lymn and Taylor, 1971; Pate and Cooke, 1989). Then, the CB goes through the power stroke (**Figure 2**, step b), during which the myosin head can generate a force of several piconewtons or an axial displacement of the actin filament toward the center of the sarcomere of 5–10 nm *in vitro* (Molloy et al., 1995; Veigel et al., 1998; Mehta et al., 1999; Reconditi et al., 2011) or 8–13 nm *in situ* (Reconditi et al., 2004). There are evidences that force generation precedes the Pi release (Dantzig et al., 1992; Caremani et al., 2008). Subsequent steps involve the release of ADP (**Figure 2**, step c), and the binding of ATP that rapidly dissociates the actomyosin complex (**Figure 2**, step d). When unbound from actin, myosin hydrolyzes ATP and reverses the power stroke, thus returning to its original position and allowing a new cycle to start (Eisenberg and Greene, 1980; Steffen and Sleep, 2004) (**Figure 2**, step e). Thus, at the molecular level, skeletal myosin is a molecular motor that transduces chemical energy produced by the hydrolysis of one ATP molecule into mechanical work (Huxley, 1957; Huxley and Simmons, 1971; Lymn and Taylor, 1971; Eisenberg et al.,

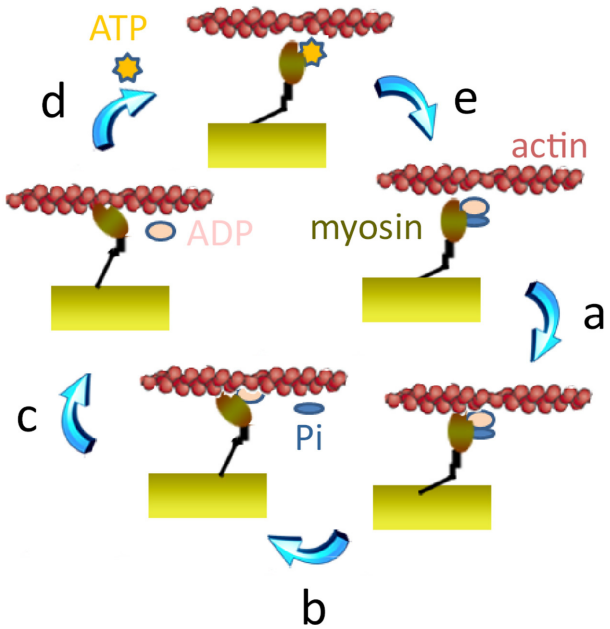

FIGURE 2 | The CB cycle. Step a: attachment of myosin to actin. This step begins with the "weak binding" of actin (in magenta) to the myosin head (in brown). A stereospecific interaction between actin and myosin leads to strong binding of actin to myosin. Step b: power stroke. The loss of inorganic phosphate (Pi) is assumed to trigger the onset of the power stroke and a reversal of the previous conformational bent. Step c: ADP release step. The power stroke induces reopening of the nucleotide binding pocket and ADP release. Step d: ATP binding. ATP can then rapidly bind to myosin which dissociates from actin. Step e: ATP hydrolysis. ATP is then rapidly hydrolyzed to ADP and Pi.

1980; Pate and Cooke, 1989; Gordon et al., 2000). Skeletal MDs may reduce the number of active CBs producing force but may also potentially affect various steps of the cyclical interactions of actin with myosin, thus reducing the unitary force produced by each CB and/or modifying the CB kinetics.

CHANGES IN CB KINETICS RELATED TO MD-INDUCED SHIFT IN MYOSIN ISOFORM

The events in the CB cycle are essentially the same for all muscle myosins, but the kinetics of acto-myosin interaction varies widely among myosin heavy chain (MyHC) isoforms. Although the physiological differences between fast and slow skeletal muscle fibers depend on more than just differences in MyHC isoforms, it is well established that MyHC isoforms are a major determinant of the large variability in contractile and energetic properties of muscle fibers (Pette and Staron, 1990; Bottinelli et al., 1994a,b). The existence of several MyHC isoforms differentially distributed in various fibers makes MyHCs useful to study fiber heterogeneity and plasticity in mammalian muscles. In the adult skeletal muscle, four MyHC isoforms can be expressed, namely the slow MyHC -1 and the fast MyHC -2A, MyHC-2X, and MyHC-2B, coded respectively by the *Myh7*, *Myh2*, *Myh1*, and *Myh4* genes (Bar and Pette, 1988; Schiaffino et al., 1989; Schiaffino and Reggiani, 1996).

Changes in the proportion of fast relative to slow fiber types are frequently observed in muscular dystrophy, and may result either from a reduced muscular activity in affected patients or from a physiopathological consequence of the gene mutation. The pattern of wasted muscle and affected fibers is highly variable among the types of MDs. Preferential involvement in fast type 2 muscle fibers is a common feature in Duchenne Muscular Dystrophy (DMD) (Webster et al., 1988), with early disappearance of muscle fibers expressing MyHC-2X transcripts (Pedemonte et al., 1999). Likewise, slow type 1 muscle fiber predominance has been reported in patients with facioscapulohumeral muscular dystrophy (FSHD) (Celegato et al., 2006), dysferlinopathy (Fanin and Angelini, 2002) and congenital muscular dystrophy type Ullrich (Schessl et al., 2008), suggesting a selective loss of fast-twitch/type 2 muscle fibers (D'Antona et al., 2007) or an active fiber typing conversion process (Schessl et al., 2008; De La Torre et al., 2009). This preferential involvement of the fastest fiber type leads to a fast to slow shift among fast MyHC isoforms in the dystrophic muscles (Stedman et al., 1991; Petrof et al., 1993; Coirault et al., 1999), which may represent an adaptive response that would tend to preserve the economy of force contraction. However, fiber-type composition has been shown to be differently affected in other MDs. Hypertrophy of type 2 fibers without type 1 fiber atrophy have been found in biopsies of patients with laminopathies (Kajino et al., 2014), whereas MyHC-2a fibers are markedly atrophied in affected cricopharyngeal muscle of oculopharyngeal muscular dystrophy patients (Gidaro et al., 2013). How mutations responsible for MDs differently affect myofiber-type specification and/or MyHC deserve further studies. In addition to adult myosin isoform remodeling, dystrophic fiber can express developmental embryonic and neonatal MyHCs, coded by *Myh3* and *Myh8*, respectively (Wieczorek et al., 1985; Sartore et al., 1987). Such developmental or neonatal MyHC-expressing fibers can either be regenerating fibers or fibers that expressed inappropriate and immature MyHC, as has been observed in some congenital myopathies (Sewry, 1998).

Importantly, the different MyHC isoforms display large functional differences regarding the actin-activated ATPase activity of myosin, the rate of ADP release from acto-myosin during the time of attachment, and the velocity with which they can move actin. This results in large variability in contractile, thermodynamic, and kinetic coupling according to the fiber type (Barany, 1967). For instance, fibers containing MyHC-1 have nearly threefold slower ATPase and lower tension cost than fibers with MyHC-2X, while fibers with MyHC-2A are intermediate (Stienen et al., 1996). Therefore, an increased proportion of the slow MyHC isoforms would tend to improve muscle efficiency and may represent an adaptive response at least in some MDs. An opposite response, namely a slow-to-fast shift with preferential atrophy of slow fiber, accelerates the time cycle, reduces muscle efficiency (Coirault et al., 1999) and thus may contribute to the exercise intolerance in DMD patients. MyHC shift may also impact on CB recruitment, given that attachment of fast myosin involves a CB-mediated facilitation mechanism absent in slow MyHC isoforms (Galler et al., 2009). Indeed, fast myosin heads already attached to actin substantially accelerate the further attachment of neighboring myosin heads, thereby enabling a rapid change in the rate of force development at high levels of activation (Galler et al., 2009).

In contrast, slow MyHC isoforms have moderate dependence on level of activation, enabling slow CB recruitment to become faster only gradually at higher levels of activation (Galler et al., 2009). Thus, pathologic changes in myosin isoforms modify specific steps of the CB cycling as well as the overall kinetics of the CB cycle, with functional consequences on muscle performance and energy cost of contraction.

CB ALTERATIONS CAUSED BY MICRO-ARCHITECTURAL CHANGES IN MYOFILAMENTS

Striated muscles are characterized by a highly ordered structure that is critical for normal function and muscle homeostasis. Micro-architectural changes in myofilaments are likely contributors to muscle weakness in MDs, either directly by affecting the function of critical structural proteins, or indirectly, by increasing the activity of Ca^{2+}-dependent proteases.

In striated muscle, the dystrophin glycoprotein complex is preferentially located at the costamere (Ervasti and Campbell, 1991), a protein network connecting the outermost myofibrils to the sarcolemma at each Z-disc (Pardo et al., 1983; Ervasti and Campbell, 1991; Bloch and Gonzalez-Serratos, 2003; Ervasti, 2003; Michele and Campbell, 2003). These lateral linkages are critical in the maintenance of sarcomere stability and in the transmission of forces generated by the CBs (**Figure 3**) (Rybakova et al., 2000; Bloch and Gonzalez-Serratos, 2003; Ervasti, 2003). Indeed, while part of the forces generated in sarcomeres is longitudinally transmitted down myofibrils in muscle to the tendon, costameres are critical to transmit the forces laterally to the ECM and neighboring muscle fibers (Street, 1983; Ervasti, 2003; Bloch et al., 2004; Ramaswamy et al., 2011). Dystrophin deficiency reduces the lateral transfer of forces between activated fibers (Ramaswamy et al., 2011), thus compromising the homogeneity of sarcomere contraction between adjacent fibers and impairing the efficacy of force transmission. As a result, each fiber tends to act as an independent longitudinal force generator, thus increasing the susceptibility of muscle membrane to contraction-induced muscle damage.

Skeletal muscle fiber contains the ubiquitously expressed and well-conserved family of Ca^{2+}-dependent cysteine proteases calpains, μ-calpain, and m-calpain, as well as a muscle-specific calpain i.e., calpain-3 (Goll et al., 2003; Bartoli and Richard, 2005). Elevated calpain amount, primarily due to a significant increase in m-calpain concentration is observed in dystrophic muscles from the mdx mice (Spencer et al., 1995), a mouse model of DMD. Increased activity of calpains has been implicated in the progression of muscle wasting in dystrophic muscles (Spencer et al., 1995; Alderton and Steinhardt, 2000; Tidball and Spencer, 2000; Zhang et al., 2008). The two ubiquitous μ- and m-calpains both cleave the same substrates *in vitro*, including the troponin complex (Troponin C, Troponin I, and Troponin T), Tm, α-actinin, titin, desmin, the Z-disk protein fodrin and the sarcolemmal associated spectrin complex of proteins (Goll et al., 2003). Such substrates are consistent with a role of μ- and m-calpains in sarcomeric organization and/or dismantling. Interestingly, the two sarcomeric tropomodulin isoforms Tmod1 and Tmod4 have been recently identified as proteolytic targets of m-calpain in dystrophic muscle (Gokhin et al., 2014). Tropomodulins are dynamic actin filament pointed-end-capping proteins (Weber et al., 1994), that localize in sarcomere to each side of the M-line (Fowler et al., 1993). Absence of Tmod1 and its replacement by Tmod3 and Tmod4 in turn impair initial Tm movement over actin subunits during thin filament activation, thus reducing both the fraction of actomyosin CBs in the strongly bound state and fiber force-generating capacity (Ochala et al., 2014). Calpain-3 binds to the N2A region of titin (Sorimachi et al., 1995), but has also been identified in the nucleus of muscle cells (Baghdiguian et al., 1999).

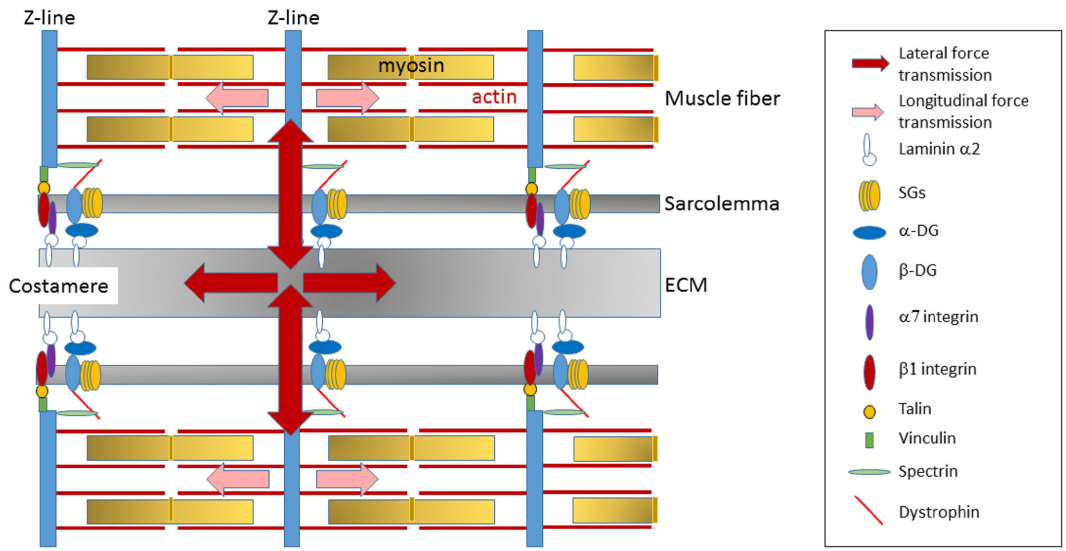

FIGURE 3 | Transmission of the forces generated in sarcomere. The dystrophin-glycoprotein complex is preferentially located at the costamere, a protein network that reside at the sarcolemma membrane in register with the Z-lines of sarcomeres and that is critical in the lateral transmission of forces generated by the CB to the ECM and neighboring muscle fibers. Dystrophin deficiency at the lateral membrane alters costamere assembly and thus may impair the efficacy of lateral force transmission.

Interestingly, it has been shown that calpain-3 binding to the myofibrillar structure *in vitro* is modulated by the presence of CBs locked in rigor (Murphy et al., 2006; Murphy and Lamb, 2009), thus supporting the hypothesis that CB interactions modulate calpain-3 activity. This may explain why *in vivo*, eccentric exercise is the only physiological circumstance shown to result in the activation of calpain-3 (Murphy et al., 2007). A number of myofibrillar proteins have been identified as potential calpain-3 substrates *in vitro*, but none have been confirmed as *in vivo* targets. These include titin (at the PEVK region, adjacent to the N2A region of titin), and myosin light chain (Cohen et al., 2006). Future works are needed to determine the interrelation between calpain-3 and the CB interactions.

MODULATIONS AND DAMAGE OF CB KINETICS BY OXIDATIVE STRESS

DEFINITION AND INTRACELLULAR SOURCES OF OXIDATIVE STRESS IN MDs

Oxidative stress has been reported as *primum movens* in both loss of cell viability and contractile dysfunction in MDs (Ragusa et al., 1997; Rando et al., 1998; Tidball and Wehling-Henricks, 2007; Menazza et al., 2010; Lawler, 2011). By definition, oxidative stress refers to a deregulation of the cellular redox-status due to an imbalance between reactive oxygen species (ROS) production and antioxidant capacities.

There are numerous potential intracellular sources of ROS in muscle tissue including the mitochondria (Murphy, 2009; Brand, 2010), the family of nicotinamide adenine dinucleotide phosphatate oxidases, now collectively known as NOX enzymes family, and a wide range of enzymes, such as xanthine oxidase, nitric oxide synthase, cyclo oxygenases, cytochrome P450 enzymes and lipoxygenases (Cheng et al., 2001). In addition, extracellular sources of ROS can arise from other non-muscle cell types, including activated neutrophils and macrophages (Moylan and Reid, 2007).

Because striated muscle cells have to adapt very rapidly and in a co-ordinated manner to changes in energy supply and oxygen flux, the control of ROS production and redox-status is tightly regulated during contraction. Importantly, the neuronal form of nitric oxide synthase (nNOS) is normally present in the sarcolemma of fast-twitch muscle fibers and associates with dystrophin (Brenman et al., 1995). Although the reaction between nitric oxide (NO) and the superoxide anion is known to form peroxynitrite, NO can also act as a protective molecule against the damaging actions of ROS (Wink et al., 1995). Accordingly, the absence of nNOS and NO in DMD muscle removes this protective action, increasing the susceptibility of DMD muscle to the damaging action of ROS (Brenman et al., 1995; Haycock et al., 1996; Disatnik et al., 1998).

PHYSIOLOGICAL STRESS INDUCES REVERSIBLE MODIFICATIONS OF PROTEINS THAT CONTRIBUTE TO NORMAL MUSCLE PHYSIOLOGY

There is increasing evidence that ROS reversibly modulate important intracellular pathways involved in muscle homeostasis (Droge, 2002; Smith and Reid, 2006; Jackson, 2008; Musaro et al., 2010). Small, compartmentalized, and transient increases in ROS regulate intracellular signals by reversible oxidation of specific protein residues (Meng et al., 2002; Ghezzi, 2005; Janssen-Heininger et al., 2008; Drazic et al., 2013). Hydrogen peroxide modifies protein function by oxidizing the thiol (-SH) groups of redox sensitive cysteine residues to form disulfide bonds with adjacent cysteine residues, glutathione (glutathionylation), or small protein thiols such as thioredoxin. Reduction of the disulfide bond can then be obtained through the action of enzymes such as glutaredoxin or the peroxiredoxins (Rhee, 2006; Hashemy et al., 2007). Accordingly, specific cysteine and methionine residues can function as redox-dependent switches, thereby modulating the function of myofibrillar proteins (Nogueira et al., 2009; Mollica et al., 2012; Gross and Lehman, 2013), phosphatase or transcriptional activities (Xanthoudakis et al., 1992; Ji et al., 2004; Powers et al., 2005, 2011; Jackson, 2008; Ugarte et al., 2010). Indeed, recent findings indicate that myosin, actin, troponin I and Tm from skeletal muscle have cysteines that are critical to the effects from oxidants (Nogueira et al., 2009; Mollica et al., 2012; Gross and Lehman, 2013), and that accessibility depends on the conformation of the CB (Gross and Lehman, 2013). In addition, the function of myosin (Nogueira et al., 2009) and of the ryanodine 1 receptor (Bellinger et al., 2009) can be reversibly modified by S-nitrosylation, a redox-related modification of cysteine thiol by NO. Reversible oxidation of contractile proteins likely regulates muscle force production and actomyosin interactions, thereby contributing to the physiological adaptation of muscle to mechanical challenge (Powers and Jackson, 2008). Disturbance or removal of this redox sensitive modulations may limit the adaptability of the CB kinetics, with deleterious effects on muscle function and homeostasis (Stone and Yang, 2006; Linnane et al., 2007). Apart cysteine, methionine residue can be oxidized to its sulfoxyde, generating a mixture of two diastereoimers, denoted S and R. The S and the R forms are reduced back to methionine by methionine sulfoxyde reductase A (MsrA) and B (MsrB), respectively (Stadtman et al., 2002; Petropoulos and Friguet, 2005; Ugarte et al., 2010). Interestingly, recent studies have highlighted a new role for these Msr enzymes, identifying them as actors controlling the assembly/disassembly of actin filaments (Hung et al., 2013; Lee et al., 2013). A specific oxidation-reduction (redox) enzyme, the Mical protein, selectively modifies two methionines on the conserved pointed-end in actin filaments. Oxidized methionines at these positions simultaneously disassemble and decrease the polymerization of actin filaments (Hung et al., 2013). Recently, Hung et al. and Lee et al. showed in *Drosophila* bristle processes model and in mouse macrophages that MsrB1 stereospecifically reverses the oxidative modification of the methionines introduced by Mical, indicating that Msr system antagonizes the Mical-actin depolymerization dependent process and reversibly control actin polymerization (Hung et al., 2013; Lee et al., 2013). These data indicate new post-translational regulatory mechanisms involving oxidoreductase systems, but also open up new paths of investigation in the field of muscle diseases.

IRREVERSIBLE MODIFICATIONS OF PROTEINS: OXIDIZED PROTEINS ARE DYSFUNCTIONAL AND ARE TARGETED TO REMOVAL

In contrast to reversible modifications caused by low oxidative stress, chronic disruption of the oxidative balance and/or high

levels of free ROS radicals cause potential biological damage, termed oxidative stress. This is a complex process that probably depends on the type of oxidant, on the site and intensity of its production, on the composition and activity of various antioxidants and on the ability of skeletal muscle to repair damaged fibers. Irreversible damage of myofibrillar proteins may affect the CB cycle, as observed after nitrosylation and carbonylation of myosin (Coirault et al., 2007; Guellich et al., 2007), and target them for catabolic proteolysis (Jung et al., 2007). Alternatively, oxidative stress can activate caspases that in turn cleave myofibrillar proteins and impair CB properties (Du et al., 2004).

FUNCTIONAL CONSEQUENCES OF ALTERED CB CYCLING ON MUSCLE CONTRACTION

The functional consequences of altered CB cycle in MD remain to be precisely determined. It has been reported that the reduced muscle strength per cross section in *mdx* diaphragm is associated with an accelerated cycle compared with control diaphragm muscle (Coirault et al., 1999). Assuming that one molecule of ATP is hydrolyzed per CB cycle (Huxley, 1957; Huxley and Simmons, 1971; Eisenberg et al., 1980), these data suggested that the overall cycle of ATP splitting takes place more rapidly in *mdx* than in control mouse diaphragm, thus reducing the efficiency of muscle contraction to sustain force. Overall, these data suggested that absence of the sarcolemmal dystrophin protein leads to damaged or dysfunctional myosin molecules that impair CB kinetics and may account for the contractile deficit in *mdx* diaphragm. However, while mechanical differences are observed between *mdx* and control diaphragms at the intact muscle strip level, these differences are not observed at the single permeabilized cell (Bates et al., 2013). In addition, it was reported that myosin extracted from bulk *mdx* mouse diaphragm muscle moves actin filaments in an "*in vitro* motility assay" at a lower velocity than myosin extracted from controls (Coirault et al., 2002). Consistent reduction in actin sliding velocity has been found in pure MyHC-2 isoform from mdx gastrocnemius muscle, but not in type 1 myosin from wild-type and *mdx* muscle (Canepari et al., 2009). Therefore, observed changes in myosin velocity have been related to a change in the intrinsic properties of the molecule, but was not attributed to a change in the proportion of different myosin isoforms in the sample. In addition, it has been shown that nebulin in skeletal muscle increases thin filament activation via increasing CB cycling kinetics leading to an increased force and efficiency of contraction (Chandra et al., 2009). Results from that study provide novel insights regarding nebulin-based nemaline myopathy. Thus, complex mechanisms other than translational changes in myosin isoform may contribute to CB modifications in muscular disorders. Future studies are needed to precisely determine the contribution of post-translational modifications of contractile proteins to muscle weakness in MDs.

CONCLUSIONS AND FUTURE DIRECTIONS

The mechanisms of muscle weakness have been a fundamental question of the physiopathology of muscle dystrophy for more than 50 years. It is now clear that the molecular causes responsible for the impaired performance in MDs involve both structural and functional modifications of the acto-myosin interactions. The precise mechanisms are complex with probably some specificities related to each individual mutation responsible for the MD, the severity of the translational and post-translational alterations in myofibrillar proteins, and on the ability of skeletal muscle to adapt to these changes. Whereas the functional consequences of translational changes in contractile proteins have been extensively studied, the impact of post-translational changes on the function of various contractile proteins still remains to be precisely assessed in the context of MDs. This is a particularly exciting time to study this question as recent findings strongly suggest that the loss of transient structural modifications of the contractile proteins such as reversible oxidation of specific protein residues impair the ability of CBs to adapt very rapidly to changes in workload and energy supply. Future works will assess the impact of non-permanent structural modifications of actin, myosin, and regulatory proteins on muscle performance and determine their potential contribution to muscle weakness in MDs.

REFERENCES

Alderton, J. M., and Steinhardt, R. A. (2000). Calcium influx through calcium leak channels is responsible for the elevated levels of calcium-dependent proteolysis in dystrophic myotubes. *J. Biol. Chem.* 275, 9452–9460. doi: 10.1074/jbc.275.13.9452

Baghdiguian, S., Martin, M., Richard, I., Pons, F., Astier, C., Bourg, N., et al. (1999). Calpain 3 deficiency is associated with myonuclear apoptosis and profound perturbation of the IkappaB alpha/NF-kappaB pathway in limb-girdle muscular dystrophy type 2A. *Nat. Med.* 5, 503–511. doi: 10.1038/10579

Bar, A., and Pette, D. (1988). Three fast myosin heavy chains in adult rat skeletal muscle. *FEBS Lett.* 235, 153–155. doi: 10.1016/0014-5793(88)81253-5

Barany, M. (1967). ATPase activity of myosin correlated with speed of muscle shortening. *J. Gen. Physiol.* 50(Suppl.), 197–218. doi: 10.1085/jgp.50.6.197

Bartoli, M., and Richard, I. (2005). Calpains in muscle wasting. *Int. J. Biochem. Cell Biol.* 37, 2115–2133. doi: 10.1016/j.biocel.2004.12.012

Bates, G., Sigurdardottir, S., Kachmar, L., Zitouni, N. B., Benedetti, A., Petrof, B. J., et al. (2013). Molecular, cellular, and muscle strip mechanics of the mdx mouse diaphragm. *Am. J. Physiol. Cell Physiol.* 304, C873–C880. doi: 10.1152/ajpcell.00220.2012

Bellinger, A. M., Reiken, S., Carlson, C., Mongillo, M., Liu, X., Rothman, L., et al. (2009). Hypernitrosylated ryanodine receptor calcium release channels are leaky in dystrophic muscle. *Nat. Med.* 15, 325–330. doi: 10.1038/nm.1916

Bloch, R. J., and Gonzalez-Serratos, H. (2003). Lateral force transmission across costameres in skeletal muscle. *Exerc. Sport Sci. Rev.* 31, 73–78. doi: 10.1097/00003677-200304000-00004

Bloch, R. J., Reed, P., O'Neill, A., Strong, J., Williams, M., Porter, N., et al. (2004). Costameres mediate force transduction in healthy skeletal muscle and are altered in muscular dystrophies. *J. Muscle Res. Cell Motil.* 25, 590–592.

Bottinelli, R., Betto, R., Schiaffino, S., and Reggiani, C. (1994a). Maximum shortening velocity and coexistence of myosin heavy chain isoforms in single skinned fast fibres of rat skeletal muscle. *J. Muscle Res. Cell Motil.* 15, 413–419. doi: 10.1007/BF00122115

Bottinelli, R., Canepari, M., Reggiani, C., and Stienen, G. J. (1994b). Myofibrillar ATPase activity during isometric contraction and isomyosin composition in rat single skinned muscle fibres. *J. Physiol.* 481(Pt 3), 663–675.

Brand, M. D. (2010). The sites and topology of mitochondrial superoxide production. *Exp. Gerontol.* 45, 466–472. doi: 10.1016/j.exger.2010.01.003

Brenman, J. E., Chao, D. S., Xia, H., Aldape, K., and Bredt, D. S. (1995). Nitric oxide synthase complexed with dystrophin and absent from skeletal muscle sarcolemma in Duchenne muscular dystrophy. *Cell* 82, 743–752. doi: 10.1016/0092-8674(95)90471-9

Canepari, M., Rossi, R., Pansarasa, O., Maffei, M., and Bottinelli, R. (2009). Actin sliding velocity on pure myosin isoforms from dystrophic mouse muscles. *Muscle Nerve* 40, 249–256. doi: 10.1002/mus.21302

Caremani, M., Dantzig, J., Goldman, Y. E., Lombardi, V., and Linari, M. (2008). Effect of inorganic phosphate on the force and number of myosin cross-bridges

during the isometric contraction of permeabilized muscle fibers from rabbit psoas. *Biophys. J.* 95, 5798–5808. doi: 10.1529/biophysj.108.130435

Celegato, B., Capitanio, D., Pescatori, M., Romualdi, C., Pacchioni, B., Cagnin, S., et al. (2006). Parallel protein and transcript profiles of FSHD patient muscles correlate to the D4Z4 arrangement and reveal a common impairment of slow to fast fibre differentiation and a general deregulation of MyoD-dependent genes. *Proteomics* 6, 5303–5321. doi: 10.1002/pmic.200600056

Chandra, M., Mamidi, R., Ford, S., Hidalgo, C., Witt, C., Ottenheijm, C., et al. (2009). Nebulin alters cross-bridge cycling kinetics and increases thin filament activation: a novel mechanism for increasing tension and reducing tension cost. *J. Biol. Chem.* 284, 30889–30896. doi: 10.1074/jbc.M109.049718

Cheng, G., Cao, Z., Xu, X., Van Meir, E. G., and Lambeth, J. D. (2001). Homologs of gp91phox: cloning and tissue expression of Nox3, Nox4, and Nox5. *Gene* 269, 131–140. doi: 10.1016/S0378-1119(01)00449-8

Cohen, N., Kudryashova, E., Kramerova, I., Anderson, L. V., Beckmann, J. S., Bushby, K., et al. (2006). Identification of putative *in vivo* substrates of calpain 3 by comparative proteomics of overexpressing transgenic and nontransgenic mice. *Proteomics* 6, 6075–6084. doi: 10.1002/pmic.200600199

Cohn, R. D., and Campbell, K. P. (2000). Molecular basis of muscular dystrophies. *Muscle Nerve* 23, 1456–1471. doi: 10.1002/1097-4598(200010)23:10<1456::AID-MUS2>3.0.CO;2-T

Coirault, C., Guellich, A., Barbry, T., Samuel, J. L., Riou, B., and Lecarpentier, Y. (2007). Oxidative stress of myosin contributes to skeletal muscle dysfunction in rats with chronic heart failure. *Am. J. Physiol. Heart Circ. Physiol.* 292, H1009–H1017. doi: 10.1152/ajpheart.00438.2006

Coirault, C., Lambert, F., Marchand-Adam, S., Attal, P., Chemla, D., and Lecarpentier, Y. (1999). Myosin molecular motor dysfunction in dystrophic mouse diaphragm. *Am. J. Physiol.* 277, C1170–C1176.

Coirault, C., Lambert, F., Pourny, J. C., and Lecarpentier, Y. (2002). Velocity of actomyosin sliding *in vitro* is reduced in dystrophic mouse diaphragm. *Am. J. Respir. Crit. Care Med.* 165, 250–253. doi: 10.1164/ajrccm.165.2.2105088

D'Antona, G., Brocca, L., Pansarasa, O., Rinaldi, C., Tupler, R., and Bottinelli, R. (2007). Structural and functional alterations of muscle fibres in the novel mouse model of facioscapulohumeral muscular dystrophy. *J. Physiol.* 584, 997–1009. doi: 10.1113/jphysiol.2007.141481

Dantzig, J. A., Goldman, Y. E., Millar, N. C., Lacktis, J., and Homsher, E. (1992). Reversal of the cross-bridge force-generating transition by photogeneration of phosphate in rabbit psoas muscle fibres. *J. Physiol.* 451, 247–278.

De La Torre, C., Illa, I., Faulkner, G., Soria, L., Robles-Cedeno, R., Dominguez-Perles, R., et al. (2009). Proteomics identification of differentially expressed proteins in the muscle of dysferlin myopathy patients. *Proteomics Clin. Appl.* 3, 486–497. doi: 10.1002/prca.200800087

Disatnik, M. H., Dhawan, J., Yu, Y., Beal, M. F., Whirl, M. M., Franco, A. A., et al. (1998). Evidence of oxidative stress in mdx mouse muscle: studies of the pre-necrotic state. *J. Neurol. Sci.* 161, 77–84. doi: 10.1016/S0022-510X(98)00258-5

Drazic, A., Miura, H., Peschek, J., Le, Y., Bach, N. C., Kriehuber, T., et al. (2013). Methionine oxidation activates a transcription factor in response to oxidative stress. *Proc. Natl. Acad. Sci. U.S.A.* 110, 9493–9498. doi: 10.1073/pnas.1300578110

Droge, W. (2002). Free radicals in the physiological control of cell function. *Physiol. Rev.* 82, 47–95. doi: 10.1152/physrev.00018.2001

Du, J., Wang, X., Miereles, C., Bailey, J. L., Debigare, R., Zheng, B., et al. (2004). Activation of caspase-3 is an initial step triggering accelerated muscle proteolysis in catabolic conditions. *J. Clin. Invest.* 113, 115–123. doi: 10.1172/JCI18330

Eisenberg, E., and Greene, L. E. (1980). The relation of muscle biochemistry to muscle physiology. *Annu. Rev. Physiol.* 42, 293–309. doi: 10.1146/annurev.ph.42.030180.001453

Eisenberg, E., Hill, T. L., and Chen, Y. (1980). Cross-bridge model of muscle contraction. Quantitative analysis. *Biophys. J.* 29, 195–227. doi: 10.1016/S0006-3495(80)85126-5

Ervasti, J. M. (2003). Costameres: the Achilles' heel of Herculean muscle. *J. Biol. Chem.* 278, 13591–13594. doi: 10.1074/jbc.R200021200

Ervasti, J. M., and Campbell, K. P. (1991). Membrane organization of the dystrophin-glycoprotein complex. *Cell* 66, 1121–1131. doi: 10.1016/0092-8674(91)90035-W

Fanin, M., and Angelini, C. (2002). Muscle pathology in dysferlin deficiency. *Neuropathol. Appl. Neurobiol.* 28, 461–470. doi: 10.1046/j.1365-2990.2002.00417.x

Flanigan, K. M. (2012). The muscular dystrophies. *Semin. Neurol.* 32, 255–263. doi: 10.1055/s-0032-1329199

Fowler, V. M., Sussmann, M. A., Miller, P. G., Flucher, B. E., and Daniels, M. P. (1993). Tropomodulin is associated with the free (pointed) ends of the thin filaments in rat skeletal muscle. *J. Cell Biol.* 120, 411–420. doi: 10.1083/jcb.120.2.411

Galinska-Rakoczy, A., Engel, P., Xu, C., Jung, H., Craig, R., Tobacman, L. S., et al. (2008). Structural basis for the regulation of muscle contraction by troponin and tropomyosin. *J. Mol. Biol.* 379, 929–935. doi: 10.1016/j.jmb.2008.04.062

Galler, S., Andruchov, O., Stephenson, G. M., and Stephenson, D. G. (2009). Qualitatively different cross-bridge attachments in fast and slow muscle fiber types. *Biochem. Biophys. Res. Commun.* 385, 44–48. doi: 10.1016/j.bbrc.2009.05.017

Geeves, M. A., Fedorov, R., and Manstein, D. J. (2005). Molecular mechanism of actomyosin-based motility. *Cell. Mol. Life Sci.* 62, 1462–1477. doi: 10.1007/s00018-005-5015-5

Ghezzi, P. (2005). Oxidoreduction of protein thiols in redox regulation. *Biochem. Soc. Trans.* 33, 1378–1381. doi: 10.1042/BST20051378

Gidaro, T., Negroni, E., Perie, S., Mirabella, M., Laine, J., Lacau St Guily, J., et al. (2013). Atrophy, fibrosis, and increased PAX7-positive cells in pharyngeal muscles of oculopharyngeal muscular dystrophy patients. *J. Neuropathol. Exp. Neurol.* 72, 234–243. doi: 10.1097/NEN.0b013e3182854c07

Gokhin, D. S., Tierney, M. T., Sui, Z., Sacco, A., and Fowler, V. M. (2014). Calpain-mediated proteolysis of tropomodulin isoforms leads to thin filament elongation in dystrophic skeletal muscle. *Mol. Biol. Cell* 25, 852–865. doi: 10.1091/mbc.E13-10-0608

Goll, D. E., Thompson, V. F., Li, H., Wei, W., and Cong, J. (2003). The calpain system. *Physiol. Rev.* 83, 731–801. doi: 10.1152/physrev.00029.2002

Gordon, A. M., Homsher, E., and Regnier, M. (2000). Regulation of contraction in striated muscle. *Physiol. Rev.* 80, 853–924.

Gross, S. M., and Lehman, S. L. (2013). Accessibility of myofilament cysteines and effects on ATPase depend on the activation state during exposure to oxidants. *PLoS ONE* 8:e69110. doi: 10.1371/journal.pone.0069110

Guellich, A., Damy, T., Lecarpentier, Y., Conti, M., Claes, V., Samuel, J. L., et al. (2007). Role of oxidative stress in cardiac dysfunction of PPARalpha-/- mice. *Am. J. Physiol. Heart Circ. Physiol.* 293, H93–H102. doi: 10.1152/ajpheart.00037.2007

Hashemy, S. I., Johansson, C., Berndt, C., Lillig, C. H., and Holmgren, A. (2007). Oxidation and S-nitrosylation of cysteines in human cytosolic and mitochondrial glutaredoxins: effects on structure and activity. *J. Biol. Chem.* 282, 14428–14436. doi: 10.1074/jbc.M700927200

Haycock, J. W., Jones, P., Harris, J. B., and Mantle, D. (1996). Differential susceptibility of human skeletal muscle proteins to free radical induced oxidative damage: a histochemical, immunocytochemical and electron microscopical study *in vitro*. *Acta Neuropathol.* 92, 331–340. doi: 10.1007/s004010050527

Hung, R. J., Spaeth, C. S., Yesilyurt, H. G., and Terman, J. R. (2013). SelR reverses Mical-mediated oxidation of actin to regulate F-actin dynamics. *Nat. Cell Biol.* 15, 1445–1454. doi: 10.1038/ncb2871

Huxley, A. F. (1957). Muscle structure and theories of contraction. *Prog. Biophys. Biophys. Chem.* 7, 255–318.

Huxley, A. F., and Simmons, R. M. (1971). Proposed mechanism of force generation in striated muscle. *Nature* 233, 533–538. doi: 10.1038/233533a0

Huxley, H. E., Faruqi, A. R., Kress, M., Bordas, J., and Koch, M. H. (1982). Time-resolved X-ray diffraction studies of the myosin layer-line reflections during muscle contraction. *J. Mol. Biol.* 158, 637–684. doi: 10.1016/0022-2836(82)90253-4

Jackson, M. J. (2008). Redox regulation of skeletal muscle. *IUBMB Life* 60, 497–501. doi: 10.1002/iub.72

Janssen-Heininger, Y. M., Mossman, B. T., Heintz, N. H., Forman, H. J., Kalyanaraman, B., Finkel, T., et al. (2008). Redox-based regulation of signal transduction: principles, pitfalls, and promises. *Free Radic. Biol. Med.* 45, 1–17. doi: 10.1016/j.freeradbiomed.2008.03.011

Ji, L. L., Gomez-Cabrera, M. C., Steinhafel, N., and Vina, J. (2004). Acute exercise activates nuclear factor (NF)-kappaB signaling pathway in rat skeletal muscle. *FASEB J.* 18, 1499–1506. doi: 10.1096/fj.04-1846com

Jung, T., Bader, N., and Grune, T. (2007). Oxidized proteins: intracellular distribution and recognition by the proteasome. *Arch. Biochem. Biophys.* 462, 231–237. doi: 10.1016/j.abb.2007.01.030

Kajino, S., Ishihara, K., Goto, K., Ishigaki, K., Noguchi, S., Nonaka, I., et al. (2014). Congenital fiber type disproportion myopathy caused by LMNA mutations. *J. Neurol. Sci.* 340, 94–98. doi: 10.1016/j.jns.2014.02.036

Kaplan, J. C., and Hamroun, D. (2012). The 2013 version of the gene table of monogenic neuromuscular disorders (nuclear genome). *Neuromuscul. Disord.* 22, 1108–1135. doi: 10.1016/j.nmd.2012.10.021

Kress, M., Huxley, H. E., Faruqi, A. R., and Hendrix, J. (1986). Structural changes during activation of frog muscle studied by time-resolved X-ray diffraction. *J. Mol. Biol.* 188, 325–342. doi: 10.1016/0022-2836(86)90158-0

Lawler, J. M. (2011). Exacerbation of pathology by oxidative stress in respiratory and locomotor muscles with Duchenne muscular dystrophy. *J. Physiol.* 589, 2161–2170. doi: 10.1113/jphysiol.2011.207456

Lee, B. C., Peterfi, Z., Hoffmann, F. W., Moore, R. E., Kaya, A., Avanesov, A., et al. (2013). MsrB1 and MICALs regulate actin assembly and macrophage function via reversible stereoselective methionine oxidation. *Mol. Cell* 51, 397–404. doi: 10.1016/j.molcel.2013.06.019

Linnane, A. W., Kios, M., and Vitetta, L. (2007). The essential requirement for superoxide radical and nitric oxide formation for normal physiological function and healthy aging. *Mitochondrion* 7, 1–5. doi: 10.1016/j.mito.2006.11.009

Lowy, J., and Poulsen, F. R. (1990). Studies of the diffuse x-ray scattering from contracting frog skeletal muscles. *Biophys. J.* 57, 977–985. doi: 10.1016/S0006-3495(90)82617-5

Lymn, R. W., and Taylor, E. W. (1971). Mechanism of adenosine triphosphate hydrolysis by actomyosin. *Biochemistry* 10, 4617–4624. doi: 10.1021/bi00801a004

McKeran, R. O., Halliday, D., and Purkiss, P. (1977). Increased myofibrillar protein catabolism in Duchenne muscular dystrophy measured by 3-methylhistidine excretion in the urine. *J. Neurol. Neurosurg. Psychiatry* 40, 979–981. doi: 10.1136/jnnp.40.10.979

Mehta, A. D., Rief, M., Spudich, J. A., Smith, D. A., and Simmons, R. M. (1999). Single-molecule biomechanics with optical methods. *Science* 283, 1689–1695. doi: 10.1126/science.283.5408.1689

Menazza, S., Blaauw, B., Tiepolo, T., Toniolo, L., Braghetta, P., Spolaore, B., et al. (2010). Oxidative stress by monoamine oxidases is causally involved in myofiber damage in muscular dystrophy. *Hum. Mol. Genet.* 19, 4207–4215. doi: 10.1093/hmg/ddq339

Meng, T. C., Fukada, T., and Tonks, N. K. (2002). Reversible oxidation and inactivation of protein tyrosine phosphatases *in vivo*. *Mol. Cell* 9, 387–399. doi: 10.1016/S1097-2765(02)00445-8

Mercuri, E., and Muntoni, F. (2013). Muscular dystrophies. *Lancet* 381, 845–860. doi: 10.1016/S0140-6736(12)61897-2

Michele, D. E., and Campbell, K. P. (2003). Dystrophin-glycoprotein complex: post-translational processing and dystroglycan function. *J. Biol. Chem.* 278, 15457–15460. doi: 10.1074/jbc.R200031200

Mollica, J. P., Dutka, T. L., Merry, T. L., Lamboley, C. R., McConell, G. K., McKenna, M. J., et al. (2012). S-glutathionylation of troponin I (fast) increases contractile apparatus Ca2+ sensitivity in fast-twitch muscle fibres of rats and humans. *J. Physiol.* 590, 1443–1463. doi: 10.1113/jphysiol.2011.224535

Molloy, J. E., Burns, J. E., Kendrick-Jones, J., Tregear, R. T., and White, D. C. (1995). Movement and force produced by a single myosin head. *Nature* 378, 209–212. doi: 10.1038/378209a0

Moylan, J. S., and Reid, M. B. (2007). Oxidative stress, chronic disease, and muscle wasting. *Muscle Nerve* 35, 411–429. doi: 10.1002/mus.20743

Murphy, M. P. (2009). How mitochondria produce reactive oxygen species. *Biochem. J.* 417, 1–13. doi: 10.1042/BJ20081386

Murphy, R. M., Goodman, C. A., McKenna, M. J., Bennie, J., Leikis, M., and Lamb, G. D. (2007). Calpain-3 is autolyzed and hence activated in human skeletal muscle 24 h following a single bout of eccentric exercise. *J. Appl. Physiol. (1985)* 103, 926–931. doi: 10.1152/japplphysiol.01422.2006

Murphy, R. M., and Lamb, G. D. (2009). Endogenous calpain-3 activation is primarily governed by small increases in resting cytoplasmic [Ca2+] and is not dependent on stretch. *J. Biol. Chem.* 284, 7811–7819. doi: 10.1074/jbc.M808655200

Murphy, R. M., Verburg, E., and Lamb, G. D. (2006). Ca2+ activation of diffusible and bound pools of mu-calpain in rat skeletal muscle. *J. Physiol.* 576, 595–612. doi: 10.1113/jphysiol.2006.114090

Musaro, A., Fulle, S., and Fano, G. (2010). Oxidative stress and muscle homeostasis. *Curr. Opin. Clin. Nutr. Metab. Care* 13, 236–242. doi: 10.1097/MCO.0b013e3283368188

Nogueira, L., Figueiredo-Freitas, C., Casimiro-Lopes, G., Magdesian, M. H., Assreuy, J., and Sorenson, M. M. (2009). Myosin is reversibly inhibited by S-nitrosylation. *Biochem. J.* 424, 221–231. doi: 10.1042/BJ20091144

Ochala, J., Gokhin, D. S., Iwamoto, H., and Fowler, V. M. (2014). Pointed-end capping by tropomodulin modulates actomyosin crossbridge formation in skeletal muscle fibers. *FASEB J.* 28, 408–415. doi: 10.1096/fj.13-239640

Pardo, J. V., Siliciano, J. D., and Craig, S. W. (1983). A vinculin-containing cortical lattice in skeletal muscle: transverse lattice elements ("costameres") mark sites of attachment between myofibrils and sarcolemma. *Proc. Natl. Acad. Sci. U.S.A.* 80, 1008–1012. doi: 10.1073/pnas.80.4.1008

Pate, E., and Cooke, R. (1989). A model of crossbridge action: the effects of ATP, ADP and Pi. *J. Muscle Res. Cell Motil.* 10, 181–196. doi: 10.1007/BF01739809

Pedemonte, M., Sandri, C., Schiaffino, S., and Minetti, C. (1999). Early decrease of IIx myosin heavy chain transcripts in Duchenne muscular dystrophy. *Biochem. Biophys. Res. Commun.* 255, 466–469. doi: 10.1006/bbrc.1999.0213

Petrof, B. J., Stedman, H. H., Shrager, J. B., Eby, J., Sweeney, H. L., and Kelly, A. M. (1993). Adaptations in myosin heavy chain expression and contractile function in dystrophic mouse diaphragm. *Am. J. Physiol.* 265, C834–C841.

Petropoulos, I., and Friguet, B. (2005). Protein maintenance in aging and replicative senescence: a role for the peptide methionine sulfoxide reductases. *Biochim. Biophys. Acta* 1703, 261–266. doi: 10.1016/j.bbapap.2004.08.018

Pette, D., and Staron, R. S. (1990). Cellular and molecular diversities of mammalian skeletal muscle fibers. *Rev. Physiol. Biochem. Pharmacol.* 116, 1–76.

Powers, S. K., and Jackson, M. J. (2008). Exercise-induced oxidative stress: cellular mechanisms and impact on muscle force production. *Physiol. Rev.* 88, 1243–1276. doi: 10.1152/physrev.00031.2007

Powers, S. K., Ji, L. L., Kavazis, A. N., and Jackson, M. J. (2011). Reactive oxygen species: impact on skeletal muscle. *Compr. Physiol.* 1, 941–969. doi: 10.1002/cphy.c100054

Powers, S. K., Kavazis, A. N., and Deruisseau, K. C. (2005). Mechanisms of disuse muscle atrophy: role of oxidative stress. *Am. J. Physiol. Regul. Integr. Comp. Physiol.* 288, R337–R344. doi: 10.1152/ajpregu.00469.2004

Ragusa, R. J., Chow, C. K., and Porter, J. D. (1997). Oxidative stress as a potential pathogenic mechanism in an animal model of Duchenne muscular dystrophy. *Neuromuscul. Disord.* 7, 379–386. doi: 10.1016/S0960-8966(97)00096-5

Ramaswamy, K. S., Palmer, M. L., van der Meulen, J. H., Renoux, A., Kostrominova, T. Y., Michele, D. E., et al. (2011). Lateral transmission of force is impaired in skeletal muscles of dystrophic mice and very old rats. *J. Physiol.* 589, 1195–1208. doi: 10.1113/jphysiol.2010.201921

Rando, T. A., Disatnik, M. H., Yu, Y., and Franco, A. (1998). Muscle cells from mdx mice have an increased susceptibility to oxidative stress. *Neuromuscul. Disord.* 8, 14–21. doi: 10.1016/S0960-8966(97)00124-7

Reconditi, M., Brunello, E., Fusi, L., Linari, M., Martinez, M. F., Lombardi, V., et al. (2014). Sarcomere-length dependence of myosin filament structure in skeletal muscle fibres of the frog. *J. Physiol.* 592, 1119–1137. doi: 10.1113/jphysiol.2013.267849

Reconditi, M., Brunello, E., Linari, M., Bianco, P., Narayanan, T., Panine, P., et al. (2011). Motion of myosin head domains during activation and force development in skeletal muscle. *Proc. Natl. Acad. Sci. U.S.A.* 108, 7236–7240. doi: 10.1073/pnas.1018330108

Reconditi, M., Linari, M., Lucii, L., Stewart, A., Sun, Y. B., Boesecke, P., et al. (2004). The myosin motor in muscle generates a smaller and slower working stroke at higher load. *Nature* 428, 578–581. doi: 10.1038/nature02380

Rhee, S. G. (2006). Cell signaling. H2O2, a necessary evil for cell signaling. *Science* 312, 1882–1883. doi: 10.1126/science.1130481

Rybakova, I. N., Patel, J. R., and Ervasti, J. M. (2000). The dystrophin complex forms a mechanically strong link between the sarcolemma and costameric actin. *J. Cell Biol.* 150, 1209–1214. doi: 10.1083/jcb.150.5.1209

Sartore, S., Mascarello, F., Rowlerson, A., Gorza, L., Ausoni, S., Vianello, M., et al. (1987). Fibre types in extraocular muscles: a new myosin isoform in the fast fibres. *J. Muscle Res. Cell Motil.* 8, 161–172. doi: 10.1007/BF01753992

Schessl, J., Goemans, N. M., Magold, A. I., Zou, Y., Hu, Y., Kirschner, J., et al. (2008). Predominant fiber atrophy and fiber type disproportion in early ullrich disease. *Muscle Nerve* 38, 1184–1191. doi: 10.1002/mus.21088

Schiaffino, S., Gorza, L., Sartore, S., Saggin, L., Ausoni, S., Vianello, M., et al. (1989). Three myosin heavy chain isoforms in type 2 skeletal muscle fibres. *J. Muscle Res. Cell Motil.* 10, 197–205. doi: 10.1007/BF01739810

Schiaffino, S., and Reggiani, C. (1996). Molecular diversity of myofibrillar proteins: gene regulation and functional significance. *Physiol. Rev.* 76, 371–423.

Sewry, C. A. (1998). The role of immunocytochemistry in congenital myopathies. *Neuromuscul. Disord.* 8, 394–400. doi: 10.1016/S0960-8966(98)00053-4

Smith, M. A., and Reid, M. B. (2006). Redox modulation of contractile function in respiratory and limb skeletal muscle. *Respir. Physiol. Neurobiol.* 151, 229–241. doi: 10.1016/j.resp.2005.12.011

Sorimachi, H., Kinbara, K., Kimura, S., Takahashi, M., Ishiura, S., Sasagawa, N., et al. (1995). Muscle-specific calpain, p94, responsible for limb girdle muscular dystrophy type 2A, associates with connectin through IS2, a p94-specific sequence. *J. Biol. Chem.* 270, 31158–31162. doi: 10.1074/jbc.270.52.31158

Spencer, M. J., Croall, D. E., and Tidball, J. G. (1995). Calpains are activated in necrotic fibers from mdx dystrophic mice. *J. Biol. Chem.* 270, 10909–10914. doi: 10.1074/jbc.270.18.10909

Stadtman, E. R., Moskovitz, J., Berlett, B. S., and Levine, R. L. (2002). Cyclic oxidation and reduction of protein methionine residues is an important antioxidant mechanism. *Mol. Cell Biochem.* 234–235, 3–9. doi: 10.1023/A:1015916831583

Stedman, H. H., Sweeney, H. L., Shrager, J. B., Maguire, H. C., Panettieri, R. A., Petrof, B., et al. (1991). The mdx mouse diaphragm reproduces the degenerative changes of Duchenne muscular dystrophy. *Nature* 352, 536–539. doi: 10.1038/352536a0

Steffen, W., and Sleep, J. (2004). Repriming the actomyosin crossbridge cycle. *Proc. Natl. Acad. Sci. U.S.A.* 101, 12904–12909. doi: 10.1073/pnas.0400227101

Stienen, G. J., Kiers, J. L., Bottinelli, R., and Reggiani, C. (1996). Myofibrillar ATPase activity in skinned human skeletal muscle fibres: fibre type and temperature dependence. *J. Physiol.* 493(Pt 2), 299–307.

Stone, J. R., and Yang, S. (2006). Hydrogen peroxide: a signaling messenger. *Antioxid. Redox Signal.* 8, 243–270. doi: 10.1089/ars.2006.8.243

Street, S. F. (1983). Lateral transmission of tension in frog myofibers: a myofibrillar network and transverse cytoskeletal connections are possible transmitters. *J. Cell. Physiol.* 114, 346–364. doi: 10.1002/jcp.1041140314

Tidball, J. G., and Spencer, M. J. (2000). Calpains and muscular dystrophies. *Int. J. Biochem. Cell Biol.* 32, 1–5. doi: 10.1016/S1357-2725(99)00095-3

Tidball, J. G., and Wehling-Henricks, M. (2007). The role of free radicals in the pathophysiology of muscular dystrophy. *J. Appl. Physiol. (1985)* 102, 1677–1686. doi: 10.1152/japplphysiol.01145.2006

Ugarte, N., Petropoulos, I., and Friguet, B. (2010). Oxidized mitochondrial protein degradation and repair in aging and oxidative stress. *Antioxid. Redox Signal.* 13, 539–549. doi: 10.1089/ars.2009.2998

Veigel, C., Bartoo, M. L., White, D. C., Sparrow, J. C., and Molloy, J. E. (1998). The stiffness of rabbit skeletal actomyosin cross-bridges determined with an optical tweezers transducer. *Biophys. J.* 75, 1424–1438. doi: 10.1016/S0006-3495(98)74061-5

Warnes, D. M., Tomas, F. M., and Ballard, F. J. (1981). Increased rates of myofibrillar protein breakdown in muscle-wasting diseases. *Muscle Nerve* 4, 62–66. doi: 10.1002/mus.880040111

Weber, A., Pennise, C. R., Babcock, G. G., and Fowler, V. M. (1994). Tropomodulin caps the pointed ends of actin filaments. *J. Cell Biol.* 127, 1627–1635. doi: 10.1083/jcb.127.6.1627

Webster, C., Silberstein, L., Hays, A. P., and Blau, H. M. (1988). Fast muscle fibers are preferentially affected in Duchenne muscular dystrophy. *Cell* 52, 503–513. doi: 10.1016/0092-8674(88)90463-1

Wieczorek, D. F., Periasamy, M., Butler-Browne, G. S., Whalen, R. G., and Nadal-Ginard, B. (1985). Co-expression of multiple myosin heavy chain genes, in addition to a tissue-specific one, in extraocular musculature. *J. Cell Biol.* 101, 618–629. doi: 10.1083/jcb.101.2.618

Wink, D. A., Cook, J. A., Pacelli, R., Liebmann, J., Krishna, M. C., and Mitchell, J. B. (1995). Nitric oxide (NO) protects against cellular damage by reactive oxygen species. *Toxicol. Lett.* 82–83, 221–226. doi: 10.1016/0378-4274(95)03557-5

Xanthoudakis, S., Miao, G., Wang, F., Pan, Y. C., and Curran, T. (1992). Redox activation of Fos-Jun DNA binding activity is mediated by a DNA repair enzyme. *EMBO J.* 11, 3323–3335.

Yagi, N. (2003). An x-ray diffraction study on early structural changes in skeletal muscle contraction. *Biophys. J.* 84, 1093–1102. doi: 10.1016/S0006-3495(03)74925-X

Zhang, B. T., Yeung, S. S., Allen, D. G., Qin, L., and Yeung, E. W. (2008). Role of the calcium-calpain pathway in cytoskeletal damage after eccentric contractions. *J. Appl. Physiol. (1985)* 105, 352–357. doi: 10.1152/japplphysiol.90320.2008

Conflict of Interest Statement: The authors declare that the research was conducted in the absence of any commercial or financial relationships that could be construed as a potential conflict of interest.

Received: 22 August 2014; accepted: 23 September 2014; published online: 14 October 2014.

Citation: Guellich A, Negroni E, Decostre V, Demoule A and Coirault C (2014) Altered cross-bridge properties in skeletal muscle dystrophies. Front. Physiol. ***5****:393. doi: 10.3389/fphys.2014.00393*

This article was submitted to Striated Muscle Physiology, a section of the journal Frontiers in Physiology.

Copyright © 2014 Guellich, Negroni, Decostre, Demoule and Coirault. This is an open-access article distributed under the terms of the Creative Commons Attribution License (CC BY). The use, distribution or reproduction in other forums is permitted, provided the original author(s) or licensor are credited and that the original publication in this journal is cited, in accordance with accepted academic practice. No use, distribution or reproduction is permitted which does not comply with these terms.

frontiers in PHYSIOLOGY

ORIGINAL RESEARCH ARTICLE
published: 29 October 2014
doi: 10.3389/fphys.2014.00416

X-ray diffraction from flight muscle with a headless myosin mutation: implications for interpreting reflection patterns

Hiroyuki Iwamoto[1]*, Károly Trombitás[2], Naoto Yagi[1], Jennifer A. Suggs[3] and Sanford I. Bernstein[3]

[1] Research and Utilization Division, Japan Synchrotron Radiation Research Institute, SPring-8, Hyogo, Japan
[2] Veterinary and Comparative Anatomy, Pharmacology and Physiology, Washington State University, Pullman, WA, USA
[3] Department of Biology, Molecular Biology Institute, Heart Institute, San Diego State University, San Diego, CA, USA

Edited by:
Julien Ochala, King's College London, UK

Reviewed by:
Han-Zhong Feng, Wayne State University School of Medicine, USA
Thomas Charles Irving, Illinois Institute of Technology, USA

***Correspondence:**
Hiroyuki Iwamoto, Research and Utilization Division, Japan Synchrotron Radiation Research Institute, SPring-8, 1-1-1 Kouto, Sayo-cho, Sayo-gun, Hyogo 679-5198, Japan
e-mail: iwamoto@spring8.or.jp

Fruit fly (*Drosophila melanogaster*) is one of the most useful animal models to study the causes and effects of hereditary diseases because of its rich genetic resources. It is especially suitable for studying myopathies caused by myosin mutations, because specific mutations can be induced to the flight muscle-specific myosin isoform, while leaving other isoforms intact. Here we describe an X-ray-diffraction-based method to evaluate the structural effects of mutations in contractile proteins in *Drosophila* indirect flight muscle. Specifically, we describe the effect of the headless myosin mutation, Mhc^{10}-*Y97*, in which the motor domain of the myosin head is deleted, on the X-ray diffraction pattern. The loss of general integrity of the filament lattice is evident from the pattern. A striking observation, however, is the prominent meridional reflection at $d = 14.5$ nm, a hallmark for the regularity of the myosin-containing thick filament. This reflection has long been considered to arise mainly from the myosin head, but taking the 6th actin layer line reflection as an internal control, the 14.5-nm reflection is even stronger than that of wild-type muscle. We confirmed these results via electron microscopy, wherein image analysis revealed structures with a similar periodicity. These observations have major implications on the interpretation of myosin-based reflections.

Keywords: myosin mutation, insect flight muscle, synchrotron radiation, X-ray diffraction, *Drosophila*, electron microscopy

INTRODUCTION

Despite the long phylogenic distance between humans and insects, striking similarities exist in the structure of their muscles. Both the skeletal or cardiac muscles of vertebrates and somatic muscles of insects are cross-striated, have similar sarcomeric structure and are regulated by the thin-filament-based system involving troponin and tropomyosin. In this respect, *Drosophila melanogaster* is one of the best-suited model animals to study congenital myopathies that occur in humans, owing to its rich genetic resources and ease of breeding. Its indirect flight muscle is the preferred target, because it is the bulkiest of all muscles in the insect, and many of its constituent contractile proteins, including myosin and actin, are expressed as tissue-specific isoforms (Bernstein et al., 1993). Therefore, the mutations or knock-outs of these isoforms are usually viable because non-flight muscle isoforms remain intact.

Here we evaluate the structural consequences of the headless mutant of flight muscle myosin isoform, in which an adult myosin rod transgene (*Y97*) is expressed in Mhc^{10} myosin-null background (Cripps et al., 1999). All of the motor domain and a part of the binding site for the essential light chain are missing from the rod molecule, but the binding site for the regulatory light chain remains intact (Cripps et al., 1999). Electron microscopy of the flight muscle in this mutant has shown that the rod molecules form thick filaments with hollow centers as in wild type, and that these thick filaments are often surrounded by thin filaments and form a hexagonal lattice, but the integrity of the whole myofibrils is inferior to that in wild type (Cripps et al., 1999).

We adopt another approach to evaluate the structure of the mutated flight muscle, i.e., X-ray diffraction. The technique of X-ray diffraction is especially suitable for reporting the regularity of arrangement of contractile proteins in myofilaments, and also the spatial arrangement of myofilaments within a sarcomere. The basic knowledge about X-ray diffraction from muscle was initially established by using bulky isolated whole muscles from frog (e.g., Huxley and Brown, 1967), but brighter X-ray sources, including synchrotron radiation facilities, and more advanced sensitive detectors have made it possible to record X-ray diffraction patterns from wider varieties of muscle specimens with much shorter exposure times. Compared with other techniques, X-ray diffraction can be applied to samples under physiological conditions, and time-resolved measurements are possible (for more detailed explanations for the synchrotron-based X-ray diffraction technique and comparisons with other techniques, refer to Oiwa et al., 2009). In fact, the X-ray diffraction technique has been applied to biopsied specimens of human muscle with congenital myopathies (Ochala et al., 2010; Ochala and Iwamoto, 2013), specimens from transgenic mice with expressed mutations found in human myopathy patients (Ochala et al., 2011, 2013, 2014; Lindqvist et al., 2012, 2013) and rat disease models

(Corpeno et al., 2014). The intense and well-oriented X-rays from the third-generation synchrotron radiation facilities have made it possible to record full 2-D diffraction patterns of *Drosophila* indirect flight muscles (Irving and Maughan, 2000; Dickinson et al., 2005; Iwamoto et al., 2007).

Here we tested several newly developed techniques to record X-ray diffraction patterns from glycerinated *Drosophila* flight muscle specimens, which are too small for ordinary mounting techniques for longer muscle fibers, and the qualities of the obtained diffraction patterns were compared. We applied these techniques combined with electron microscopy analysis to the Mhc^{10}-*Y97* mutant. This mutant is especially suited for studying the role of the myosin motor domain on the general architecture of sarcomeres, and its contributions to the intensities of the myosin-based reflections. The unexpected findings presented here lead to important implications for the interpretation of muscle X-ray diffraction in general.

MATERIALS AND METHODS

SPECIMEN

The strains Mhc^{10} (homozygous myosin null in the indirect flight muscles; Collier et al., 1990) and Mhc^{10}-*Y97* (homozygous myosin null in the indirect flight muscles and homozygous for a transgene expressing headless myosin specifically in these muscles; Cripps et al., 1999) of *D. melanogaster* were verified as to myosin protein content and maintained at San Diego State University. Flies were transferred to SPring-8, and were maintained there for X-ray diffraction studies. The wild type of *D. melanogaster* (Hikone-R strain) was obtained from Ehime University (Iwamoto et al., 2007). Insects other than *Drosophila* were collected at the campus of SPring-8.

For X-ray diffraction studies, the whole thoraces of *Drosophila* adults were glycerinated in a 50% mixture of glycerol and a relaxing solution (for composition see Iwamoto, 2009; Iwamoto et al., 2010) containing phenylmethylsulfoxide and protease inhibitor cocktail (P8340, Sigma-Aldrich, St. Louis, USA), and stored at -20°C in a freezer. The flight muscles of other insects were treated in a similar way. The methods of mounting of *Drosophila* specimens for X-ray recording are detailed in the Results section. Flight muscle fibers of larger insects were mounted as described (Iwamoto et al., 2001, 2010; Iwamoto, 2009).

X-RAY DIFFRACTION RECORDINGS

X-ray diffraction patterns of flight muscle were recorded at the BL45XU small-angle scattering beamline of SPring-8 (Fujisawa et al., 2000). Details of the methods of recording have been described (Iwamoto et al., 2001, 2003; Iwamoto, 2009). Briefly, the specimens were placed in a rigor solution with a composition described previously (Iwamoto, 2000), except for samples from horsefly, which were placed in a relaxing solution (Iwamoto, 2009). In addition, the solution contained 5 mM dithiothreitol to reduce radiation damage. Monochromatized X-ray beams (wavelength, 0.09 or 0.1 nm; flux, 10^{12} photons/s, beam size, 0.3×0.2 mm) were irradiated to the specimen, and the patterns were recorded by using a cooled CCD camera (C4880-50, Hamamatsu Photonics, Hamamatsu, Japan) in combination with an image intensifier (VP5445MOD, Hamamatsu Photonics). The time for single exposure was 1 s. A maximum of 20 exposures were recorded from a single specimen, and the patterns were summed. The background scattering was subtracted by the method described in Iwamoto et al. (2003, 2010).

ELECTRON MICROSCOPY

Indirect flight muscle bundles for electron microscopic observations were dissected at San Diego State University from 2-day-old flies in relaxing solution (Peckham et al., 1990) containing 1% Triton X-100 on ice. After 3 h, the liquid was replaced successively by two washes of fresh relaxing solution containing 50% glycerol and a dissolved Roche protease inhibitor cocktail tablet (aprotinin, leupeptin, EDTA, pefablock). Muscles were stored at −20°C and shipped to Washington State University on ice, where they were fixed with 3% glutaraldehyde, then postfixed with 1% osmium tetroxide in 100 mM phosphate buffer, 10 mM $MgC1_2$; pH 6 (Trombitas and Pollack, 1995). Samples were embedded in Araldite 506. Ultrathin sections (∼20 nm) were cut with an LKB Ultrotome III. Sections were stained with potassium permanganate, and lead citrate, and observed and photographed with a Philips 420 electron microscope.

RESULTS

MOUNTING TECHNIQUES FOR DROSOPHILA FLIGHT MUSCLE

The length of the indirect flight muscle fibers of *D. melanogaster* is only ∼1 mm, and it is very difficult to mount both ends with metal foil clips, as would often be done with longer specimens, while keeping the myofibrils straight (this is required to yield good diffraction patterns). 2-D diffraction patterns from *Drosophila* flight muscles have been recorded from whole live insects by using two configurations.

One is to attach a hollow tube on top of the thorax and irradiate X-rays through it (Irving and Maughan, 2000; Dickinson et al., 2005). By doing so one can obtain diffraction patterns from the dorsal longitudinal muscle (DLM) alone, one of the two antagonistic indirect flight muscles (**Figure 1A**). The other is to glue the whole insect, and irradiate X-rays from the side (**Figure 1B**; Iwamoto et al., 2007), similar to the configuration used for recording diffraction patterns from live bumblebees (Iwamoto and Yagi, 2013). In this configuration, one can simultaneously record diffraction patterns from both of the two antagonistic flight muscles (DLM and dorsoventral muscle, DVM) as well as the jump muscle. In Iwamoto et al. (2007) this configuration was used also for recording diffraction patterns from pupae to study the time course of development of flight muscle architecture.

The drawbacks of such *in vivo* X-ray recording are that (1) there are unwanted materials in the beampath (such as legs, leg muscles, nerves, digestive tracts, etc.) that could compromise the quality of diffraction patterns, and that (2) the solution environment of contractile proteins cannot be changed at will. For these reasons it is desirable to establish techniques to record diffraction patterns from demembranated (glycerinated) flight muscle specimens from *Drosophila*.

Here we tested several techniques to record diffraction patterns from glycerinated specimens, besides the conventional clamping technique. The first one is to use a stainless-steel plate with round holes. The glycerinated thorax was placed in the hole and glued by

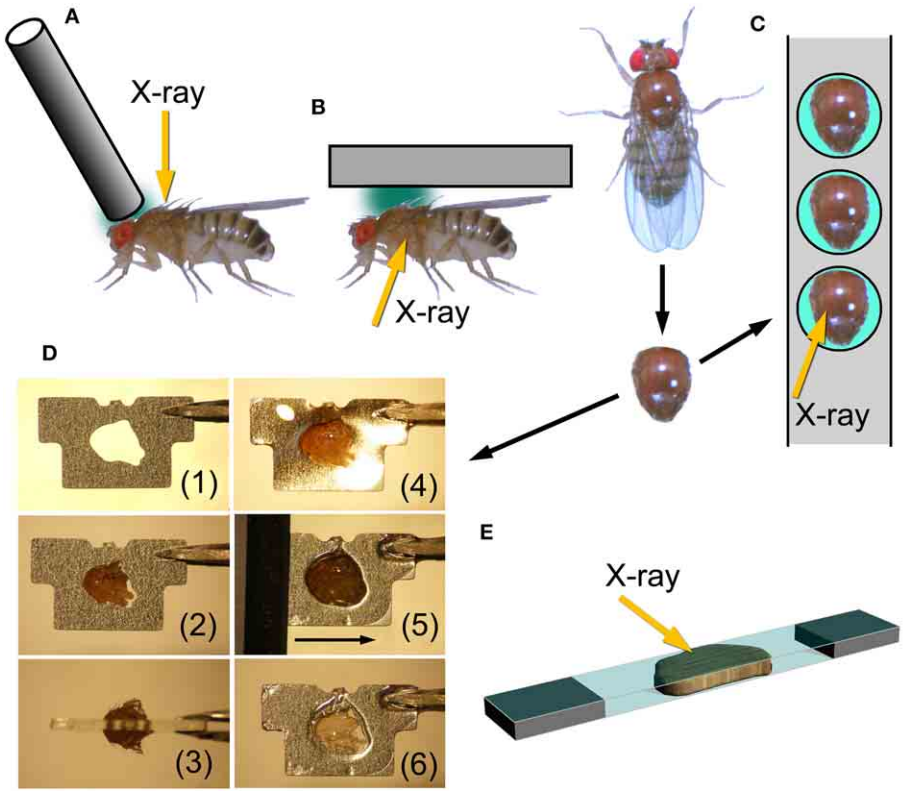

FIGURE 1 | Mounting techniques for *Drosophila* indirect flight muscle. **(A,B)** Methods to record X-ray diffraction patterns from live flies; **(C–E)** methods to record patterns from glycerinated muscle preparations. **(A)**, attaching a metal wire on top of the head and at the anterior end of the thorax and the fly is irradiated with X-rays from the top. This is the method adopted by Irving and Maughan (2000), Dickinson et al. (2005). **(B)**, a fly, glued to a substrate, is irradiated from the side to record patterns from both of the two antagonistic flight muscles (DLM and DVM). This is the configuration used by Iwamoto et al. (2007). **(C)**, gluing an isolated thorax to a stainless-steel plate with round holes. After gluing, unwanted tissues, such as leg muscles and digestive tract, are removed. (**D**), procedure to glue an isolated thorax to a stainless-steel plate with a precision-etched hole and to remove excess parts of the thorax. (1), a plate before mounting; (2) an isolated thorax fitted to the hole; (3) top view; (4) thorax glued to the plate, (5) an ultrasonic-vibrated microtome blade slides along the surface of the plate; (6) finished sample with exposed DLM. **(E)**, sandwiching an isolated flight muscle between two thin plastic films (1.5 μm-thick polyester, Chemplex Industries, Palm City, USA). Incident X-ray beams make a small angle with respect to the film plane.

using a cyanoacrilic resin (**Figure 1C**). After gluing, the legs and other unwanted materials were removed. By irradiating X-rays in the middle of the hole, one can obtain diffraction patterns from DLM alone. The DLM fibers were irradiated from the top of the thorax.

The second technique tested was to fabricate stainless-steel plates (thickness, 0.2 mm) by photo-etching, each with a hole shaped to fit the contour of the thorax. In this method, the orientation of DLM fibers can be precisely fixed with respect to the stainless-steel plate. The thorax was glued so that equal amounts of volume of the thorax stick out of both sides of the plate. After this, the parts of the thorax sticking out of the plate were cut off by using an ultrasonic vibration cutter with microtome blades. This leaves DLM fibers within the thickness of the plate. X-rays were irradiated from the side (**Figure 1D**).

The third technique was to isolate the assembly of 6 indirect flight muscle fibers (both DLM and DVM have 6 flight muscle fibers on each side), and sandwich them with two very thin plastic films (**Figure 1E**). The plastic films had been glued to two pieces of thin plastic plate at both ends, leaving a small gap between them so that the fibers were not crushed. X-ray beams were irradiated so that the beam axis made a small angle with respect to the film plane. By doing so one should be able to eliminate the parasitic scattering resulting from the total reflection from the film surface. However, the fact was that some parasitic scattering was recorded, probably because the film surface was somewhat wavy.

DIFFRACTION PATTERNS RECORDED FROM WILD-TYPE DROSOPHILA FLIGHT MUSCLE

Figure 2 shows some of the diffraction pattern recorded from the indirect flight muscles from wild type and mutant strains of *D. melanogaster*. For wild-type flies, the second technique (using photo-etched stainless steel plates) has so far given the best myofiber orientations (**Figure 2A**). This diffraction pattern was recorded in rigor (in the absence of ATP), and this sample seems to contain a small remnant of DVM as the pattern contains its equatorial reflections. Although there was some problem in data processing, good myofiber orientation was also obtained

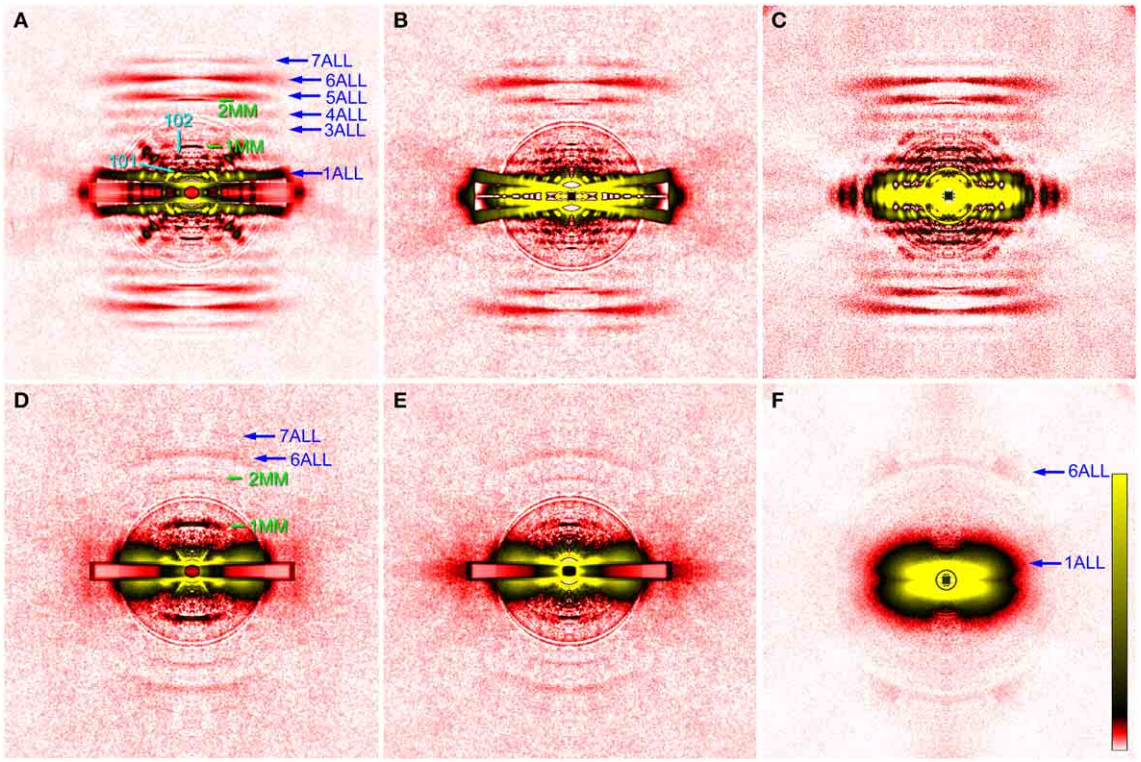

FIGURE 2 | X-ray diffraction patterns from the glycerinated flight muscle (DLM) of wild-type and mutant *Drosophila*. (A–C), wild type; **(D,E)**, headless myosin mutant (*Mhc*^{10}*-Y97*); **(F)** mutant with no myosin heavy chain (*Mhc*^{10}-background line). Patterns in **(A–D)** were recorded from single flies, and the pattern in **(F)** is the sum of data from 9 flies. The mounting techniques used are: **(A)**, 2nd (etched plate); **(B,D)**, 3rd (sandwiching with plastic films); **(C,F)**, 1st (round holes); **(D)**, conventional clamping. The four quadrants of the pattern were folded and the background scattering was subtracted as described by Iwamoto et al. (2003, 2010). The circles around the center are due to the correction of absorption by round aluminum masks to attenuate the intense central parts of the pattern. In (**A,B,D,E**) a rectangular copper mask was also applied to the equator in which the scattering intensity was strongest. The oblique anomalous reflections in **(A)** come from the remnant of DVM. They are observed in four quadrants because the image has been averaged for the four quadrants. The aberration around the equator in **(B)** is generated in the process of background subtraction because of the mismatch of fiber and copper mask orientations. ALL, actin layer line reflection; MM, myosin meridional reflection. The numbers indicate the order or Miller indices of reflections. Note that only actin-based reflections are observed in **(F)**.

with the third technique, i.e., to sandwich the fibers with plastic films (**Figure 2B**). The fiber orientation was worse with the first technique (**Figure 2C**), and the conventional (most labor-intensive) technique of clamping both ends of isolated fibers gave totally unsatisfactory results (data not shown). The recorded diffraction pattern is fundamentally similar to that from flight muscle fibers of different insect species (e.g., Tregear et al., 1998; Bekyarova et al., 2008). The lower-angle layer line reflections are finely lattice-sampled, and unlike in relaxed or activated fibers, the 4th–7th actin layer lines (they have continuous intensities along the layer) are clearly visible, indicating that myosin heads are stereospecifically bound to actin following its periodicity.

As for the innermost reflection spots on the 1st and 2nd layer lines, i.e., the 101 and 102 reflections (cyan arrows in **Figure 2**), the 101 is much more intense than 102, in agreement with that for giant waterbug, *Lethocerus* (Tregear et al., 1998). These reflections are considered to arise from the helical arrangement of troponin complexes around a thick filament, and are known to change their intensities upon stretch activation. Before stretch activation, the 101 is stronger than 102, and vice versa after stretch activation (Tregear et al., 1998; Dickinson et al., 2005; Bekyarova et al., 2008; Iwamoto et al., 2010; Perz-Edwards et al., 2011). This is because a stretch induces stereospecific attachment of myosin heads to the actin target zone located midway between the two neighboring troponin complexes on a thin filament, and these heads negatively interfere with the basic 38.7-nm periodicity of troponin complexes. In rigor, the 101 is intensified again, because excessive myosin binding to the actin target zones restores the 38.7-nm periodicity (Tregear et al., 1998). Together with the reciprocal behavior of these reflections in live flies (Dickinson et al., 2005), the present observations suggest that the numbers of attached myosin heads are similar in *Drosophila* and *Lethocerus* flight muscles, either in active or in rigor states.

The diffraction pattern from the wild-type indirect flight muscle also shows clear myosin meridional reflections based on the 14.5-nm repeat (green arrows in **Figure 2**). The intensity of the 1st meridional reflection is spread along the equator, in contrast to that of other insects which has a sharper peak right on the meridian (Bekyarova et al., 2008; Iwamoto, 2009). Although the peak splitting is not clear, the present observation agrees with the idea

that the thick filaments form a super lattice with a larger lattice constant in *Drosophila* (Squire et al., 2006).

DIFFRACTION PATTERNS RECORDED FROM THE HEADLESS MYOSIN MUTANT

The indirect flight muscles of flies with myosin mutations, either myosin-null or headless, have structural defects (Cripps et al., 1999) and are more fragile than those from wild-type flies. Therefore, slicing with vibrating blades often resulted in unsatisfactory processing. The diffraction patterns from the headless mutant as shown in **Figure 2** were recorded from either clamped (**Figure 2D**) or sandwiched (the 3rd procedure, **Figure 2E**) flight muscle fibers. The two techniques gave equivalent results.

Compared with the wild type, the pattern from the *Mhc*^{10}*-Y97* (headless myosin) flight muscle is much more featureless, indicating that the structure is disorganized. Lattice sampling of layer-line reflections are not recognized. However, the 6th and 7th actin layer line reflections are clearly visible. The arcing of these reflections indicates that actin filaments are not well oriented in this mutant. Although it is not clear from the pattern, equatorial reflections are present as their intensity profiles are shown in **Figure 3** (red). This indicates that the hexagonal lattice arrangement of myofilaments is maintained in this mutant.

Most notable in the pattern from the *Mhc*^{10}*-Y97* indirect flight muscle is the very strong 1st myosin meridional reflection at 14.5 nm^{-1}. The 2nd myosin meridional reflection at 7.2 nm^{-1} is also clearly visible. In the diffraction pattern from the *Mhc*^{10}-background line (missing the entire myosin heavy chain), no meridional reflection was observed at 14.5 nm^{-1} (**Figure 2F**). This pattern was taken by using the first procedure. In this pattern, the strong 1st actin layer line and the weaker 6th actin layer line are observed. The latter is strongly arced, indicating that the actin filament orientation is less organized in the absence of myosin filaments.

To make quantitative comparisons, the integrated intensity of the 1st myosin meridional reflection was normalized to that of the 6th actin layer line reflection, which is often used as an internal standard to compare intensities of various reflections (e.g., Iwamoto, 2009). Its intensity was 76 ± 12% (mean ± S.D., $n = 5$) of that of the 6th actin layer line. Although the patterns were recorded in the absence of ATP, the *Mhc*^{10}*-Y97* myosin cannot form rigor linkage to the thin filaments, and therefore the values should be compared with the values from relaxed wild-type flight muscle fibers. In *Drosophila* it was difficult to obtain an ideally relaxed pattern, probably because of the insufficient supply of ATP due to myosin's high ATPase activity (Swank et al., 2006). Instead, we used flight muscle fibers from a bigger dipteran, *Tabanus trigonus* (a horse fly), to obtain relaxed patterns (**Figure 4**). We recorded patterns from two sets of flight muscle fibers and obtained the intensity ratios of 59 and 64%, which are lower than the values for *Mhc*^{10}*-Y97*. Because of the disorder of actin filament orientations in *Mhc*^{10}*-Y97*, some of scattering intensities may have been lost to the background scattering, and the intensity of the 6th actin layer line may be underestimated. However, it still holds true that the 1st myosin meridional reflection is unexpectedly strong if its major source is the motor domain of the myosin molecule (see Discussion).

ELECTRON MICROSCOPY

The rationale for using the 6th actin layer line reflection as an internal standard is that the *Mhc*^{10}*-Y97* mutant fly retains the same thick-to-thin filament number ratio as in the wild type, in which it is 1:3. To verify this, the cross section of myofibrils of

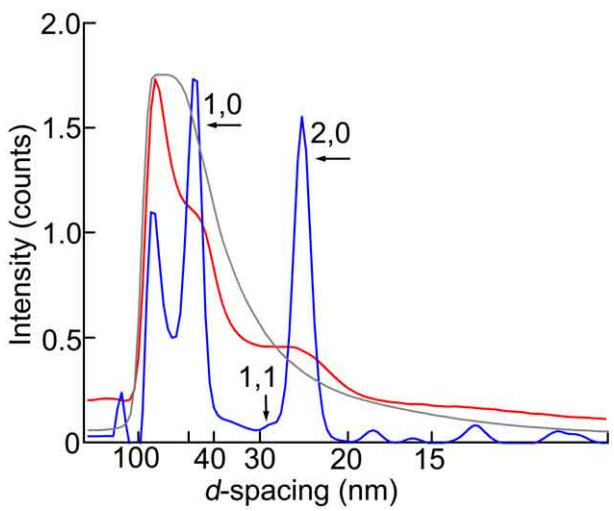

FIGURE 3 | Intensity profiles of the equatorial reflection. Blue, wild type; red, headless myosin mutant (*Mhc*^{10}*-Y97*); gray, mutant with no myosin heavy chain (*Mhc*^{10}-background line). The maximal intensity counts (digitized bits of analog-to-digital converter output) are 2.0 × 10^6 for wild type, 2.0 × 10^5 for *Mhc*^{10}*-Y97*, and 2.8 × 10^7 for the *Mhc*^{10}-background line.

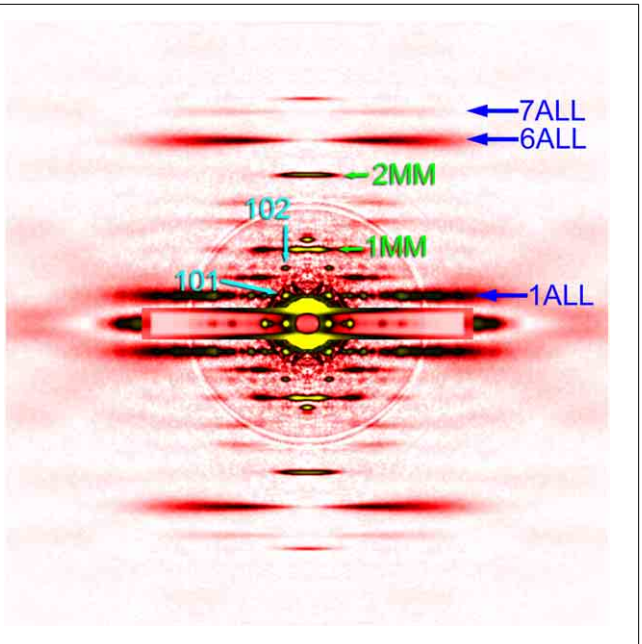

FIGURE 4 | Diffraction pattern from the flight muscle of a horse fly. The pattern was recorded in the presence of ATP (relaxing condition). For labels see legend to **Figure 2**.

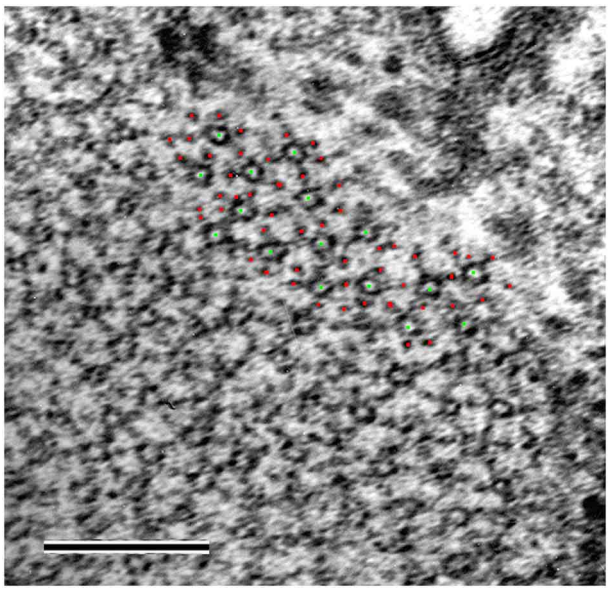

FIGURE 5 | Electron micrograph of a myofibril in transverse orientation from the headless myosin mutant. The green and red dots represent the positions of the thick and thin filaments as recognized by eye. Scale bar, 200 nm.

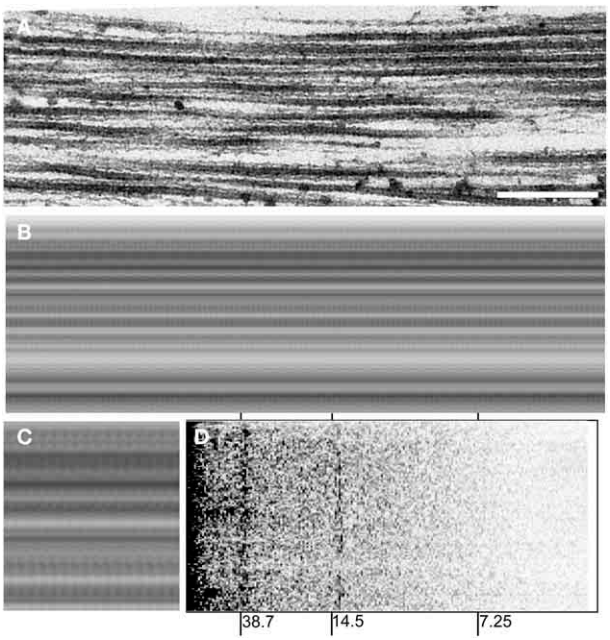

FIGURE 6 | Electron micrograph of a myofibril in longitudinal orientation from the headless myosin mutant. (A), a micrograph before processing. Scale bar, 250 nm. **(B)**, a running-averaged picture of the micrograph in **(A)** obtained by superposing the same picture after translating along the filament axis by multiples of 13.8 nm, which gave the best contrast. The difference between 13.8 nm and the expected 14.5 nm could be due to the shrinkage of the specimen and/or uncertainties of magnification of the electron microscope (the 38.7-nm peak is offset to a similar extent). **(C)**, a 2 × magnified view of a part of **(B)**. **(D)**, power spectrum of the micrograph in **(A)**. Note that peaks (darker) appear at around 14.5 nm and 38.7 nm.

the *Mhc*^{10}*-Y97* flight muscle was observed by electron microscopy (**Figure 5**). Because of the waviness of the myofibrils, clear cross sections of both thick and thin filaments were observed in limited areas. In such an area, the numbers of the recognized thick and thin filaments were 16 (green dots in **Figure 5**) and 51 (red dots), respectively. This is close to the 1:3 ratio. It therefore appears that the thick-to-thin filament ratio is preserved in the *Mhc*^{10}*-Y97* mutant.

The X-ray observation of the strong myosin meridional reflection and the preserved thick-to-thin filament ratio strongly suggest the presence of periodic structures with strong contrast with a 14.5 nm spacing even in the absence of most of the myosin motor domain. We therefore tested whether such periodic structures were visible in the longitudinal sections of myofibrils from the *Mhc*^{10}*-Y97* indirect flight muscle (**Figure 6**).

Figure 6A shows one of the longitudinal sections of the mutant myofibril. The picture in **Figure 6B** is a running-average of the micrograph in **Figure 6A**, calculated by superposing itself multiple times after translating by a fixed distance. By doing so, features are enhanced if its periodicity coincides with the distance of translation. The summed picture in **Figures 6B,C** clearly shows an enhanced feature with a periodicity near 14.5 nm. An alternative way of demonstrating the presence of periodic structures is to calculate a power spectrum of the micrograph, by applying Fourier transformation along the filament axis. The power spectrum calculated from the micrograph in **Figure 6A** clearly shows a peak at ∼14.5 nm along with a strong peak at ∼38.7 nm, which arises from troponin and tropomyosin on the thin filament (**Figure 6D**). These results indicate that there are structures with a 14.5-nm structure that are visible by both X-ray and electron microscopy. If there were intact myosin heads, they would bind to actin target zones (these have a 38.7-nm periodicity) and therefore they would contribute to the 38.7-nm peak, rather than 14.5-nm.

DISCUSSION

In this paper several methods to record X-ray diffraction patterns from glycerinated flight muscle fibers of *Drosophila* are described, and these methods were applied to the wild-type and the *Mhc*^{10}*-Y97* (headless myosin) mutant flies. We have shown that, by the use of intense X-rays generated by the 3rd-generation synchrotron radiation facilities, one can record high-quality 2-dimensional diffraction patterns from glycerinated flight muscle fibers. The most important finding is that intense myosin meridional reflections are recorded from the *Mhc*^{10}*-Y97* mutant flies in which most of the myosin motor domain is missing.

THE BEST MOUNTING METHOD FOR *DROSOPHILA* FLIGHT MUSCLE

For wild-type flies, the best-quality patterns were obtained by the second method, i.e., to glue the thorax to a photo-etched stainless steel plate and to remove excess parts by an ultrasonic-vibrated blade. The merit of this method is that only the DLM remains in the hole with its in-situ length, if the thorax has been glued in a proper position (see **Figure 1D3**) and the blade is moved along the surface of the plate without a gap (the plate is 0.2-mm thick).

In contrast to the two other methods, both sides of the flight muscle fibers are exposed to the surrounding medium, so that this method is most suitable for solution exchange experiments.

This method was successfully applied to wild-type flies, probably because of the physical strength of their flight muscle fibers. Although this method was not successfully applied to the more fragile mutant muscles, it is still a promising mounting method for solution exchange for mutant muscles. Improvements of this method, such as automated controlled blade movements (the blades were moved manually in this work) and/or increasing the physical strength of fibers by soaking in glycerol and slicing at low temperatures, may allow us to apply this method also to mutant flight muscles. The throughput of X-ray recording may be increased by creating stainless-steel strips with multiple photo-etched holes (see **Figure 1C**) instead of just one as in this study.

THE ORIGIN OF THE REFLECTIONS BASED ON A 14.5-nm-SPACING IN THE MUTANT FLY

The most important finding in this study is the strong myosin-based meridional reflections (at 14.5 and 7.2 nm^{-1}) observed in the *Mhc*^{10}*-Y97* mutant, in which most of the motor domain is missing except for a part of the lever arm and the regulatory light chain. The 14.5 nm-spaced features are also evident in electron micrographs (**Figure 6**). The strong myosin meridional reflections are unexpected because it is generally believed that the major source of this reflection is the motor domain of the myosin molecule, while the rod domain may contribute to the 2nd reflection (Huxley et al., 1994; Lombardi et al., 2004).

As mentioned briefly in Results, the intensity of the myosin meridional reflection is compared with that of the 6th actin layer line reflection, which might be underestimated because of the disorder. Indeed, the 6th actin layer line seems to be weaker in the mutant, but it is partly explained by the smaller myofibrillar content in the mutant flight muscle cell as shown by Cripps et al. (1999), **Figure 6C**. On the other hand, the 1st myosin meridional reflection in the mutant pattern is at least as strong as that in the wild type in rigor, despite that its intensity may also be underestimated for the same reason for the 6th actin layer line. Therefore, it still holds true that the 1st myosin meridional reflection is unexpectedly strong.

The question remains whether there are other proteins on the thick filament with a 14.5-nm periodicity. In vertebrate striated muscles, it is known that myosin binding protein C (MyBP-C) has a 42.9-nm periodicity (Rome et al., 1973), and its 3rd-order reflection is expected to overlap with the 1st myosin meridional reflection. MyBP-C is absent from insect flight muscle, but instead, a myosin binding protein flightin has been reported (Vigoreaux et al., 1993). However, the molecular weight of flightin is only 20 kDa and it is unlikely that it contributes significantly to the intensity of the meridional reflection at 14.5 nm^{-1}. Another possibility is the remaining myosin lever arm region containing the regulatory light chain (RLC). The RLC has an N-terminal extension that has been suggested to serve in parallel to the motor domain as a link to the thin filament (Moore et al., 2000; Miller et al., 2011). This is similar to the observation that the essential light chain extension of vertebrates appears to bind to actin within thin filaments (Miller et al., 2005; Lowey et al., 2007). If this extension does not preferentially bind to the actin target zone but simply splays out radially, it could strengthen the 1st myosin meridional reflection to some extent. However, the extension is only 50 residues long and again it is unlikely to contribute significantly to the intensity. In fact, removal of the *Drosophila* RLC extension does not diminish the intensity of the 1st myosin meridional reflection (Farman et al., 2009). Insect muscles are known to contain paramyosin, and it may also contribute to some extent to the 1st myosin meridional reflection. Again, however, the paramyosin content in *Drosophila* flight muscle is small (myosin:paramyosin = 34:1; Vinós et al., 1991), and its structural resemblance to the rod portion of myosin makes it unlikely that paramyosin contributes significantly to the 1st myosin meridional reflection.

From the considerations above, we are currently forced to consider that the strong 14.5 nm-spaced feature arise from the truncated myosin heavy chain and the regulatory light chain. It is generally believed that the rod portions of two myosin heavy chains form a coiled-coil structure to form a dimer, and their periodic clusters of charged residues allow the dimers to assemble into thick filaments with a stagger of 14.5 nm (McLachlan and Karn, 1982). There could be a different extent of deviation from the ideal coiled-coil structure between the charged and non-charged regions, and it could contribute to the intensity of the 1st myosin meridional reflection. The present results could indicate that the contribution of such a structural deviation to the 1st myosin meridional reflection is substantial. Conclusive explanations cannot be given from the present results alone, and further experiments are needed to address this issue. These experiments include the creation of a double mutant with (*Mhc*^{10}*-Y97*) and a knockout of either flightin or RLC or both. It is also important to refine the present method for X-ray diffraction recording to ensure better myofibrillar orientations; it would reduce the ambiguity arising from the poorer filament orientation of actin as compared with myosin.

CONCLUSION

Here we have demonstrated that the flight muscle of *D. melanogaster* can serve as a model to study the causes and effects of myosin myopathies, and their structural consequences can be monitored by X-ray diffraction. This should be applicable to studying models of myosin-based congenital myopathies (Wang et al., 2012). In the particular case of the myosin headless mutation (*Mhc*^{10}*-Y97*), an unexpected observation of the strong feature with a 14.5-nm periodicity prompts us to reinvestigate the origin of the 1st myosin meridional reflection, one of the best-studied X-ray reflections of muscle.

ACKNOWLEDGMENTS

We thank Dr. T. Hikima (RIKEN) for his support at the BL45XU beamline of SPring-8, Dr. Gerald Pollack (University of Washington) and Dr. Karen Hsu (San Diego State University) for helpful discussions and Dr. Henk Granzier (University of Arizona) for access to electron microscopy facilities at Washington State University. The experiments were performed under approval of the SPring-8 Proposal Review Committee

(Proposal Nos. 2009B1274, 2010A1230, 2010B1263, 2011A1242). Supported by Grant-in-Aid for Scientific Research, The Ministry of Education, Culture, Sports, Science and Technology, Japan, No. 23612009 and 26440185 and by United States National Institutes of Health R01 Grants AR43396, GM32443 and HL062881.

REFERENCES

Bekyarova, T. I., Reedy, M. C., Baumann, B. A. J., Tregear, R. T., Ward, A., Krzic, U., et al. (2008). Reverse actin sliding triggers strong myosin binding that moves tropomyosin. *Proc. Natl. Acad. Sci. U.S.A.* 105, 10372–10377. doi: 10.1073/pnas.0709877105

Bernstein, S. I., O'Donnell, P. T., and Cripps, R. M. (1993). Molecular genetic analysis of muscle development, structure, and function in *Drosophila*. *Int. Rev. Cytol.* 143, 63–152. doi: 10.1016/S0074-7696(08)61874-4

Collier, V. L., Kronert, W. A., O'Donnell, P. T., Edwards, K. A., and Bernstein, S. I. (1990). Alternative myosin hinge regions are utilized in a tissue-specific fashion that correlates with muscle contraction speed. *Genes Dev.* 4, 885–895. doi: 10.1101/gad.4.6.885

Corpeno, R., Dworkin, B., Cacciani, N., Salah, H., Bergman, H.-M., Ravara, B., et al. (2014). Time-course analysis of mechanical ventilation-induced diaphragm contractile muscle dysfunction in the rat. *J. Physiol.* 592, 3859–3880. doi: 10.1113/jphysiol.2014.277962

Cripps, R. M., Suggs, J. A., and Bernstein, S. I. (1999). Assembly of thick filaments and myofibrils occurs in the absence of the myosin head. *EMBO J.* 18, 1793–1804. doi: 10.1093/emboj/18.7.1793

Dickinson, M., Farman, G., Frye, M., Bekyarova, T., Gore, D., Maughan, D., et al. (2005). Molecular dynamics of cyclically contracting insect flight muscle *in vivo*. *Nature* 433, 330–333. doi: 10.1038/nature03230

Farman, G. P., Miller, M. S., Reedy, M. C., Soto-Adames, F. N., Vigoreaux, J. O., Maughan, D. W., et al. (2009). Phosphorylation and the N-terminal extension of the regulatory light chain help orient and align the myosin heads in *Drosophila* flight muscle. *J. Struct. Biol.* 168, 240–249. doi: 10.1016/j.jsb.2009.07.020

Fujisawa, T., Inoue, K., Oka, T., Iwamoto, H., Uruga, T., Kumasaka, T., et al. (2000). Small-angle X-ray scattering station at the SPring-8 RIKEN beamline. *J. Appl. Cryst.* 33, 797–800. doi: 10.1107/S002188980000131X

Huxley, H. E., and Brown, W. (1967). The low-angle X-ray diagram of vertebrate striated muscle and its behaviour during contraction and rigor. *J. Mol. Biol.* 30, 383–434. doi: 10.1016/S0022-2836(67)80046-9

Huxley, H. E., Stewart, A., Sosa, H., and Irving, T. (1994). X-ray diffraction measurements of the extensibility of actin and myosin filaments in contracting muscle. *Biophys. J.* 67, 2411–2421. doi: 10.1016/S0006-3495(94)80728-3

Irving, T. C., and Maughan, D. W. (2000). *In vivo* X-ray diffraction of indirect flight muscle from *Drosophila melanogaster*. *Biophys. J.* 78, 2511–2515. doi: 10.1016/S0006-3495(00)76796-8

Iwamoto, H. (2000). Influence of ionic strength on the actomyosin reaction steps in contracting skeletal muscle fibers. *Biophys. J.* 78, 3138–3149. doi: 10.1016/S0006-3495(00)76850-0

Iwamoto, H. (2009). Evidence for unique structural change of the thin filaments upon calcium-activation of insect flight muscle. *J. Mol. Biol.* 390, 99–111. doi: 10.1016/j.jmb.2009.05.002

Iwamoto, H., Inoue, K., Matsuo, T., and Yagi, N. (2007). Flight muscle myofibrillogenesis in the pupal stage of *Drosophila* as examined by X-ray microdiffraction and conventional diffraction. *Proc. Biol. Sci.* 274, 2297–2305. doi: 10.1098/rspb.2007.0607

Iwamoto, H., Inoue, K., and Yagi, N. (2010). Fast X-ray recordings reveal dynamic action of contractile and regulatory proteins in stretch-activated insect flight muscle. *Biophys. J.* 99, 184–192. doi: 10.1016/j.bpj.2010.04.009

Iwamoto, H., Oiwa, K., Suzuki, T., and Fujisawa, T. (2001). X-ray diffraction evidence for the lack of stereospecific protein interactions in highly activated actomyosin complex. *J. Mol. Biol.* 305, 863–874. doi: 10.1006/jmbi.2000.4334

Iwamoto, H., Wakayama, J., Fujisawa, T., and Yagi, N. (2003). Static and dynamic X-ray diffraction recordings from living mammalian and amphibian skeletal muscles. *Biophys. J.* 85, 2492–2506. doi: 10.1016/S0006-3495(03)74672-4

Iwamoto, H., and Yagi, N. (2013). The molecular trigger for high-speed wing beats in a bee. *Science* 341, 1243–1246. doi: 10.1126/science.1237266

Lindqvist, J., Iwamoto, H., Blanco, G., and Ochala, J. (2013). The fraction of strongly bound cross-bridges is increased in mice that carry the myopathy-linked myosin heavy chain mutation MYH4L342Q. *Disease Models Mech.* 6, 834–840. doi: 10.1242/dmm.011155

Lindqvist, J., Pénisson-Besnier, I., Iwamoto, H., Li, M., Yagi, N., and Ochala, J. (2012). A myopathy-related actin mutation increases contractile function. *Acta Neuropathol.* 123, 739–746. doi: 10.1007/s00401-012-0962-z

Lombardi, V., Piazzesi, G., Reconditi, M., Linari, M., Lucii, L., Stewart, A., et al. (2004). X-ray diffraction studies of the contractile mechanism in single muscle fibres. *Phil. Trans. R. Soc. B* 359, 1883–1893. doi: 10.1098/rstb.2004.1557

Lowey, S., Saraswat, L. D., Liu, H., Volkmann, N., and Hanein, D. (2007). Evidence for an interaction between the SH3 domain and the N-terminal extension of the essential light chain in class II myosins. *J. Mol. Biol.* 371, 902–913. doi: 10.1016/j.jmb.2007.05.080

McLachlan, A. D., and Karn, J. (1982). Periodic charge distributions in the myosin rod amino acid sequence match cross-bridge spacings in muscle. *Nature* 299, 226–231. doi: 10.1038/299226a0

Miller, M. S., Farman, G. P., Braddock, J. M., Soto-Adames, F. N., Irving, T. C., Vigoreaux, J. O., et al. (2011). Regulatory light chain phosphorylation and N-terminal extension increase cross-bridge binding and power output in *Drosophila* at *in vivo* myofilament lattice spacing. *Biophys. J.* 100, 1737–1746. doi: 10.1016/j.bpj.2011.02.028

Miller, M. S., Palmer, B. M., Ruch, S., Martin, L. A., Farman, G. P., Wang, Y., et al. (2005). The essential light chain N-terminal extension alters force and fiber kinetics in mouse cardiac muscle. *J. Biol. Chem.* 280, 34427–34434. doi: 10.1074/jbc.M508430200

Moore, J. R., Dickinson, M. H., Vigoreaux, J. O., and Maughan, D. W. (2000). The effect of removing the N-terminal extension of the *Drosophila* myosin regulatory light chain upon flight ability and the contractile dynamics of indirect flight muscle. *Biophys. J.* 78, 1431–1440. doi: 10.1016/S0006-3495(00)76696-3

Ochala, J., Gokhin, D. S., Iwamoto, H., and Fowler, V. M. (2014). Pointed-end capping by tropomodulin modulates actomyosin crossbridge formation in skeletal muscle fibers. *FASEB J.* 28, 408–415. doi: 10.1096/fj.13-239640

Ochala, J., and Iwamoto, H. (2013). Myofilament lattice structure in presence of a skeletal myopathy-related tropomyosin mutation. *J. Muscle Res. Cell Motil.* 34, 171–175. doi: 10.1007/s10974-013-9345-x

Ochala, J., Iwamoto, H., Larsson, L., and Yagi, N. (2010). A myopathy-linked tropomyosin mutation severely alters thin filament conformational changes during activation. *Proc. Natl. Acad. Sci. U.S.A.* 107, 9807–9812. doi: 10.1073/pnas.1001733107

Ochala, J., Iwamoto, H., Ravenscroft, G., Laing, N. G., and Nowak, K. J. (2013). Skeletal and cardiac α-actin isoforms differently modulate myosin cross-bridge formation and myofibre force production. *Hum. Mol. Genet.* 22, 4398–4404. doi: 10.1093/hmg/ddt289

Ochala, J., Lehtokari, V. L., Iwamoto, H., Li, M., Feng, H.-Z., Jin, J.-P., et al. (2011). Disrupted myosin cross-bridge cycling kinetics triggers muscle weakness in nebulin-related myopathy. *FASEB J.* 25, 1903–1913. doi: 10.1096/fj.10-176727

Oiwa, K., Kamimura, S., and Iwamoto, H. (2009). X-ray fiber diffraction studies on flagellar axonemes. *Method Cell Biol.* 91, 89–109. doi: 10.1016/S0091-679X(08)91005-0

Peckham, M., Molloy, J. E., Sparrow, J. C., and White, D. C. (1990). Physiological properties of the dorsal longitudinal flight muscle and the tergal depressor of the trochanter muscle of *Drosophila melanogaster*. *J. Muscle Res. Cell Motil.* 11, 203–215. doi: 10.1007/BF01843574

Perz-Edwards, R. J., Irving, T. C., Baumann, B. A. J., Gore, D., Hutchinson, D. C., Krzic, U., et al. (2011). X-ray diffraction evidence for myosin-troponin connections and tropomyosin movement during stretch activation of insect flight muscle. *Proc. Natl. Acad. Sci. U.S.A.* 108, 120–125. doi: 10.1073/pnas.1014599107

Rome, E., Offer, G., and Pepe, F. A. (1973). X-ray diffraction of muscle labelled with antibody to C-protein. *Nat. New Biol.* 244, 152–154. doi: 10.1038/newbio244152a0

Squire, J. M., Bekyarova, T., Farman, G., Gore, D., Rajkumar, G., Knupp, C., et al. (2006). The myosin filament superlattice in the flight muscles of flies: a-band lattice optimisation for stretch-activation? *J. Mol. Biol.* 361, 823–838. doi: 10.1016/j.jmb.2006.06.072

Swank, D. M., Vishnudas, V. K., and Maughan, D. M. (2006). An exceptionally fast actomyosin reaction powers insect flight muscle. *Proc. Natl. Acad. Sci. U.S.A.* 103, 17543–17547. doi: 10.1073/pnas.0604972103

Tregear, R. T., Edwards, R. J., Irving, T. C., Poole, K. J. V., Reedy, M. C., Schmitz, H., et al. (1998). X-ray diffraction indicates that active cross-bridges bind to actin target zones in insect flight muscle. *Biophys. J.* 74, 1439–1451. doi: 10.1016/S0006-3495(98)77856-7

Trombitas, K., and Pollack, G. H. (1995). Actin filaments in honeybee-flight muscle move collectively. *Cell Motil. Cytoskeleton* 32, 145–150. doi: 10.1002/cm.970320215

Vigoreaux, J. O., Saide, J. D., Valgeirsdottir, K., and Pardue, M. L. (1993). Flightin, a novel myofibrillar protein of *Drosophila* stretch-activated muscles. *J. Cell Biol.* 121, 587–598. doi: 10.1083/jcb.121.3.587

Vinós, J., Domingo, A., Marco, R., and Cervera, M. (1991). Identification and characterization of *Drosophila melanogaster* paramyosin. *J. Mol. Biol.* 220, 687–700. doi: 10.1016/0022-2836(91)90110-R

Wang, Y., Melkani, G. C., Suggs, J. A., Melkani, A., Kronert, W. A., Cammarato, A., et al. (2012). Expression of the inclusion body myopathy 3 mutation in *Drosophila* depresses myosin function and stability and recapitulates muscle inclusions and weakness. *Mol. Biol. Cell* 23, 2057–2065. doi: 10.1091/mbc.E12-02-0120

Conflict of Interest Statement: The authors declare that the research was conducted in the absence of any commercial or financial relationships that could be construed as a potential conflict of interest.

Received: 05 September 2014; accepted: 08 October 2014; published online: 29 October 2014.

*Citation: Iwamoto H, Trombitás K, Yagi N, Suggs JA and Bernstein SI (2014) X-ray diffraction from flight muscle with a headless myosin mutation: implications for interpreting reflection patterns. Front. Physiol. **5**:416. doi: 10.3389/fphys.2014.00416*

This article was submitted to Striated Muscle Physiology, a section of the journal Frontiers in Physiology.

Copyright © 2014 Iwamoto, Trombitás, Yagi, Suggs and Bernstein. This is an open-access article distributed under the terms of the Creative Commons Attribution License (CC BY). The use, distribution or reproduction in other forums is permitted, provided the original author(s) or licensor are credited and that the original publication in this journal is cited, in accordance with accepted academic practice. No use, distribution or reproduction is permitted which does not comply with these terms.

Advantages of publishing in Frontiers

OPEN ACCESS
Articles are free to read, for greatest visibility

COLLABORATIVE PEER-REVIEW
Designed to be rigorous – yet also collaborative, fair and constructive

FAST PUBLICATION
Average 85 days from submission to publication (across all journals)

COPYRIGHT TO AUTHORS
No limit to article distribution and re-use

TRANSPARENT
Editors and reviewers acknowledged by name on published articles

SUPPORT
By our Swiss-based editorial team

IMPACT METRICS
Advanced metrics track your article's impact

GLOBAL SPREAD
5'100'000+ monthly article views and downloads

LOOP RESEARCH NETWORK
Our network increases readership for your article

Frontiers
EPFL Innovation Park, Building I • 1015 Lausanne • Switzerland
Tel +41 21 510 17 00 • Fax +41 21 510 17 01 • info@frontiersin.org
www.frontiersin.org

Find us on